

國立臺灣大學理學院物理學系

博士論文

Department of Physics

College of Science

National Taiwan University

Doctoral Dissertation

二態成長與躍遷模型及其在癌症成長系統及療法開發的應用

Two-state growth with transition model and its application to
cancer growth system and therapy development

The seal of National Taiwan University is a circular emblem. It features a central design with a lamp and open books, surrounded by the university's name in Chinese and English. The text "國立臺灣大學" is at the top, and "NATIONAL TAIWAN UNIVERSITY" is at the bottom. The seal is faintly visible in the background.

胡耿銘

Geng-Ming Hu

指導教授：陳義裕 博士

龐寧寧 博士

Advisors : Yih-Yuh Chen, Ph.D.

Ning-Ning Pang, Ph.D.

中華民國 101 年 6 月

June 2012

致 謝 與 感 言

博士班真是一個漫長的過程，但想到能從文獻中找到靈感，由概念出發建構數學模型來探究其內涵，並找到有趣的詮釋與真實世界系統有所對應，就覺得這些日子確實是做了些有趣的事情。當中最要感謝的當然是龐寧寧老師的悉心指導，讓我能順利的涉足跨領域的題目並且建構相關的模型；以及陳義裕老師在最後的階段的指導跟建議，讓我能順利完成整個論文主題。另也特別感謝我的父母在這段期間對我的包容與絕對支持，讓我能安穩的進行博士班的研究工作。

在這段期間除了老師們的指導外也有一起共同進行研究主題的學弟，一起學習與討論統計分析程式的楷旻；一起看一些統計模型的玉樵；還有最後階段在茫茫文獻跟實驗證據中一起思考跟探索模型應用方向的致遠，有你們一起討論才能讓我更快速且愉悅的完成研究。

另也有許多跟我經歷與分享生活的朋友，601的耿民學長跟智仁學長，鴻隆、琇娟、小龜、雅芬...等等；615的枚樺、旭輝、偉誠、品睿、逸雲...等等；還有銘鍵、小黑、上瑜及許多不及備載的朋友，這段時間有你們在讓我的生活更有趣跟較不孤單阿。

其實還有很多該感謝的人事物，現在回想起來備感溫馨，但版面只有一頁，就此打住好了。

Two-state growth with transition model and its application to cancer growth system and therapy development

Doctoral Dissertation

Geng-Ming Hu

Supervised by

Professors Yih-Yuh Chen and Ning-Ning Pang



Department of Physics

National Taiwan University

June, 2012

摘要

具有異質性的族群是自然界中常見的一種複雜系統，而其中一種讓人感興趣的簡單模型就是僅有兩個子群但彼此會互相競爭且可互相轉換的系統。在本篇的工作中，我們發展了一套描述這樣子的二態成長且具有互相轉換性質系統的數學模型，並且應用這個模型對應到了前列腺癌腫瘤球在治療之下的真實成長數據。

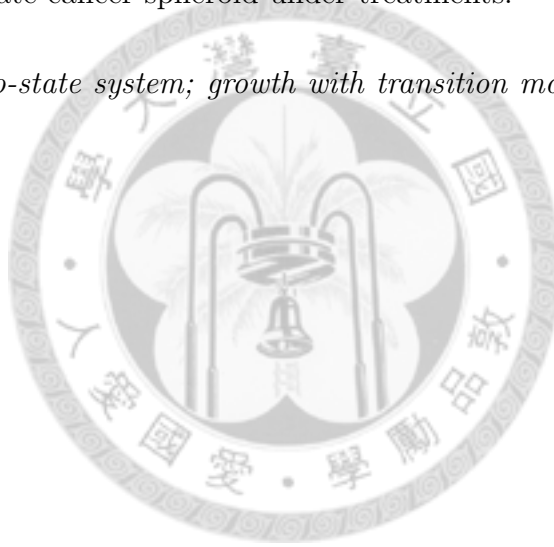
關鍵字：二態系統；成長與躍遷模型；異質性系統；癌症；療法



Abstract

Heterogeneous population is common among complex systems in nature. A simple heterogeneous growth model of interest is one with two states which not only compete with each other but exhibit transition phenomenon. In this work, we develop a mathematical model to describe such a system and apply it to fit the real growth data of the prostate cancer spheroid under treatments.

keywords: two-state system; growth with transition model; heterogeneous system; cancer; therapy



Contents

I	A two-state growth model with transition probability	1
1	Introduction	2
2	Mathematical model of two-state growth with transition probability	6
2.1	The general Growth and transition model	7
2.1.1	The time evolution equation of x_1 and x_2	7
2.1.2	Transforming x_1 and x_2 to x_t and w_1	7
2.1.3	Some simplified cases.	8
2.2	The general two-state growth and transition model with auto/para-crine signaling pathway	10
2.2.1	The auto/para-crine signaling pathway and it mathematical form	10
2.2.2	The nullclines and fixed points in general autocrine transition case	11
2.2.3	Jacobian matrix in general autocrine transition case.	12
2.3	f_i is a constant, the exponential growth model	16
2.3.1	Two-state exponential growth and autocrine transition model	16
2.3.2	The exact solution	16
2.4	When f_i is a linear function- the general logistic growth model . . .	18
2.4.1	A general form of two-state logistic growth and autocrine transition model.	18

2.4.2	The x_t nullcline for the general logistic growth	19
2.4.3	$\tilde{w}_1(x_t)$ in a general logistic growth and autocrine transition model	24
2.4.4	The fixed point formula in general logistic growth and au- tocrine transition model	28
2.4.5	The stability and possible spiral behavior in general logistic growth and autocrine transition model	40
2.5	The classification of logistic growth model.	41
2.6	LH-0 model	42
2.6.1	The exact solution when $r_1 = r_2$	43
2.6.2	The nullclines	44
2.6.3	The fixed point condition	45
2.6.4	The stability of the fixed point	45
2.6.5	The phase portraits of LH-0	45
2.7	LH-A model	45
2.7.1	The nullclines	46
2.7.2	The fixed point condition	48
2.7.3	The stability of fixed point	48
2.7.4	The phase portraits of LH-A	49
2.8	LH-B model	49
2.8.1	The nullclines	50
2.8.2	The fixed point condition	52
2.8.3	The stability of fixed point	53
2.8.4	The phase portraits of LH-B	53
2.9	LH-C model.	53
2.9.1	The nullclines	54
2.9.2	The fixed point condition	57
2.9.3	The stability of fixed point	58
2.9.4	The phase diagram and phase portraits of LH-C	60
2.10	LH-D model.	60

2.10.1	The phase diagram and phase portraits of LH-D	60
3	Conclusion	61
II	An application to cancer growth system and treatment development	62
4	A simple introduction of carcinomatous process	63
5	A heterogeneous cancer growth with autocrine signaling pathway and fitting the growth curves of prostate tumor spheroid	65
5.1	Fitting idea	65
5.2	Result and discussion	68
5.2.1	Some simple properties of this model	68
5.2.2	A comparison of the numerical results and real data from tumor growth with treatments	72
6	IAS treatment simulation by the mathematical model and the planning of optimized therapy.	78
6.1	The clinical prostate cancer therapy of human- IAS (Intermittent Androgen Suppression) therapy	78
7	Conclusion	81
A	Statistical methods to make out sub-state from a whole system.	82
A.1	Least squares method	82
A.2	Maximum likelihood method	84
A.2.1	Maximum Likelihood	84
A.2.2	Logarithmic likelihood ratio test	85
A.3	Numerical simulation method	87

List of Figures

1.1	A imaginal schematic diagram of a multi-phenotypes system. Each node is a phenotype, and the arrow line present the transition relation from one phenotype to another phenotype. Such a multi-phenotype system always construct a complex phenotypes network.	3
1.2	Schematic diagram of the two-state heterogenous system, which is the simplest multi-phenotypes system.	4
2.1	The types of $\tilde{x}_t(w_1)$	35
2.2	The diagram of $\tilde{w}_1(x_t)$ curve without a singular point. (a) and (b) are at the condition $end\ point _{w_1=0} < end\ point _{w_1=1}$. When $\Delta F > 0$, the curve in (a) is S type, and when $\Delta F < 0$, the curve in (b) is Z type. (c) and (d) are at the condition $end\ point _{w_1=0} > end\ point _{w_1=1}$. When $\Delta F > 0$, the curve in (c) is Z type, and when $\Delta F < 0$, the curve in (d) is S type. (e) and (f) are at the condition $end\ point _{w_1=0} = end\ point _{w_1=1}$. They are all S type.	36
2.3	The diagram of $\tilde{w}_1(w_1)$ with a singular point. (a): When $m_w > 0$ and $q_w < 0$, at this condition $\tilde{w}_1(w_1)$ is s band type curve. (b): When $m_w < 0$ and $q_w > 0$, at this condition $\tilde{w}_1(w_1)$ is SC and CS type curve.	37

2.4	The diagram of the three fixed point conditions. The left diagram is the effect of ΔF , and the middle diagram is the effect of $(w_1 - w_1^2)$, the solid line of the right diagram is the effect of $\Delta F(w_1 - w_1^2)$, and the dash line is the total effect of w_1 . We can see there are two types of three fixed point condition: One is S_{q-} , which ΔF has only one root between 0 and 1, and the other is $S_{q\pm}$, which ΔF has two roots between 0 and 1.	38
2.5	The diagram of multiple fixed point condition of ΔF . When it has root between $0 < w_1 < 1$ and $\Delta F(w_1 = 0) < 0$, the system would have three fixed points. This diagram shows the case of ΔF which satisfies these conditions.	39
5.1	Schematic of the two-subpopulation tumor model with transition due to auto/para-crine signaling pathway. x_1 and x_2 are the two subpopulations in a cancer system, each of which follows the logistic growth mode with proliferation r . x_1 has a self-suppressing capacity C_1 . The growth of x_1 is also suppressed by x_2 due to competition. This is characterized by an extra suppressing capacity C_2 of x_2 on x_1 . The heterogeneity coefficient a introduces asymmetry between the two species: State 2 has a self-suppressing capacity aC_2 , and a corresponding suppressing capacity aC_1 from species 1. These two subpopulations have a transition effect due to the autocrine signaling pathway. The strength of the autocrine effect from x_1 to x_2 is k_{12} , and k_{21} is that of x_2 to x_1 , respectively.	67

- 5.2 A series of x_t growth curves with fixed system parameters ($r = 0.3$, $a = 10^6$, $C_1 = 10^4$, $C_2 = 2$) and initial conditions ($x_t(0) = 1, 10, 20, 30$; $w_1(0) = 0.1$), but with different k . (a) $k = 10 > (1 - \frac{1}{a})r$: All curves saturate at 10^4 , the self-suppressing capacity of x_1 , meaning species 1 eventually dominates. (b) $k = 2.5$: As k becomes smaller, the final state of each growth curve depends on the size of the total initial population $x_t(0)$. Species 1 dominates for small $x_t(0)$, but species 2 dominates when $x_t(0)$ exceeds a certain critical size. (The growth curves all saturate at 10^6 .) (c) As k becomes much smaller ($k = 0.1$), the critical $x_t(0)$ size is also larger. When k is large enough, the critical size no longer exists and species 2 dominates the final scene. 70
- 5.3 The growth curves with fixed system parameters and initial conditions ($r = 0.3$, $a = 10^6$, $C_1 = 10^4$, $k = 2.5$, $x_t(0) = 1$, $w_1(0) = 0.01$) but different C_2 . (a) x_t for $C_2 = 1$ (solid), $C_2 = 0.5$ (dashed), and $C_2 = 0.25$ (dash-dot). As C_2 becomes smaller, a delayed phase becomes obvious. (b), (c) and (d) are the growth curves of x_1 , x_2 , and x_t with different C_2 . (b) $C_2 = 1$, (c) $C_2 = 0.5$, and (d) $C_2 = 0.25$, for x_t (bold), x_1 (marked with “+”), and x_2 (marked with “ Δ ”). When C_2 is small, the inhibiting effect to the final dominant state x_1 is more pronounced during transient, and a delayed phase persists until x_2 becomes negligible. 71
- 5.4 Fitting the x_t growth curves with the data from 17AAG treatment of [1]. (a) The numerical results (curves) compared with the actual experimental data (markers). The R square values of them are $R_{1nM}^2 = 0.8030$, $R_{10nM}^2 = 0.8625$, $R_{100nM}^2 = 0.9830$ and $R_{1000nM}^2 = 0.9988$. The fit is best in the high dosage regime. (b) Fitting parameters used in Figure 5.4 (a) as a function of the corresponding dosage. 74

5.5	Fitting the x_t growth curves of data from irradiation treatment. The system parameters are taken as ($r = 0.3$, $C_1 = 10^4$, $C_2 = 2$, $x_t(0) = 1.1$, $w_1(0) = 0.99$). Fitted x_t is for 2 Gy irradiation treatment (solid, $a = 10$, $k = 1.5$), 6 Gy irradiation treatment (dashed, $a = 0.1$, $k = -0.5$), 9 Gy irradiation treatment (dotted, $a = 0.0464$, $k = -2$), and 12 Gy irradiation treatment (dash-dot, $a = 0.0316$, $k = -3.5$). The fit compares favorably well with Fig. 2 of Enmon <i>et al.</i> [3].	75
5.6	Fitting the x_t growth curves of data near the 6 Gy irradiation treatment, using the bistable model with different $x_t(0)$. The system parameters are taken as ($r = 0.3$, $a = 0.1$, $C_1 = 10^4$, $C_2 = 2$, $k = -0.8$, $w_1(0) = 0.99$). Figure 6A corresponds well with the data of 6 Gy treatment in prostate carcinoma spheroids [3].	76
5.7	Fitting the x_t growth curves of 1000 nM 17AAG treatment with different $x_t(0)$, using the bistable model. The system parameters are taken as ($r = 0.3$, $a = 10^6$, $C_1 = 10^4$, $C_2 = 2$, $k = 2.5$, $w_1(0) = 0.01$). . . .	77
1.1	The diagram of $\text{gammq}(a, b)$ with different a . They are decreasing curves from 1 to 0. The curve tends to 0 when b is large, and the tendency is more gentle as a is large. In logarithmic likelihood ratio test, the goodness probability value $q\text{-value} = \text{gammq}(\frac{\nu}{2}, 2R)$. It means the fitting result should be good as the difference of parameter number ν or the logarithmic likelihood ratio R is small.	86
1.2	The diagram showed the concept of transform method. A uniform distribution can be transformed into a non-uniform distribution by non-uniform mapping.	88
1.3	The diagram of the concept of the rejection method. If we have a known distribution $f(x)$, then we can generate a data set with probability density function $g(x)$ by rejecting $\frac{f(x_0)-p(x_0)}{f(x_0)}$ data points when $x = x_0$	91

1.4	The four transformation type of simplex transform. (a) is reflection transform, which is to set a new test point in the reflection point of the highest test point relative the other points. (b) is the transform to set a new test point with reflection and expansion for a scale. (c) is the contraction transform for a point. (D) is the multiple contraction transform. The reflection transform (a) and (b) can help us to find the basin of the surface, and the contraction transform (c) and (d) can help us to see the fine structure of a surface. These four transforms are used to find the local extreme point in a surface.	93
1.5	(a) is the histogram of $maxlik - 3a$, ($\vec{\theta} = (0.6, 10, 0.1, 30, 0.3, 80)$) with linear bin. There is no obvious characteristic in this curve. And (b) is the histogram of the same data set with logarithmic bin. The peak is related to a_i and $\vec{\tau}_i$. It has at least two peaks in the histogram. . . .	99
1.6	(a) is the histogram of $maxlik - 5a$, ($\vec{\theta} = (0.1, 0.1, 0.08, 5, 0.22, 20, 0.15, 200, 0.35, 600)$) with linear bin. There is no obvious characteristic in this curve. And (b) is the histogram of the same data set with logarithmic bin. The peaks are related to a_i and $\vec{\tau}_i$. It has three or four peaks in the histogram.	100
1.7	(a) is the ideal linear bin histogram function of a data set with the probability density function of single exponential component with $\tau = 1$ and $N = 10^5$. It is a decreasing line. And (b) is the ideal histogram function of the same data set with logarithmic bin. There is a peak at $\tau = 1$	102
1.8	(a) is the ideal function compared with the histogram of the data set in “maxlik3a” ($\vec{\theta} = (0.6, 10, 0.1, 30, 0.3, 80)$), and (b) is the guess function compared with the histogram of the data set in “maxlik3a”. We can see the guess function is very close to the ideal function and the histogram of the data set.	105

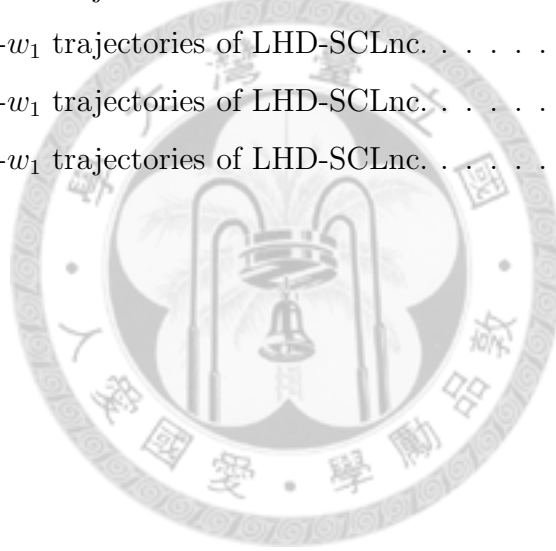
1.9	(a) is the ideal function compared with the histogram of the data set in “ <i>maxlik5a</i> ” ($\vec{\theta} = (0.1, 0.1, 0.08, 5, 0.22, 20, 0.15, 200, 0.35, 600)$), and (b) is the guess function compared with the histogram of the data set in “ <i>maxlik5a</i> ”	108
1.10	The the guess error of testN series data sets, which has the same probability density function with $\vec{\theta} = (0.4, 1, 0.3, 10, 0.3, 100)$ but with different data points number N . We can see in this plot the error of guess and the number of data points N have a power law decaing tendency roughly.	110
1.11	This diagram is the relation of N and error in maxlik2D-32b. We can see it also roughly has a power law decaying relation, as the case of 1-D.	119
2.1	The $x_{tot}-w_1$ trajectories of LH0-LL.	121
2.2	The $x_{tot}-w_1$ trajectories of LH0-LL.	122
2.3	The $x_{tot}-w_1$ trajectories of LH0-LL.	123
2.4	The $x_{tot}-w_1$ trajectories of LH0-LSl.	124
2.5	The $x_{tot}-w_1$ trajectories of LH0-LSl.	125
2.6	The $x_{tot}-w_1$ trajectories of LH0-LSl.	126
2.7	The $x_{tot}-w_1$ trajectories of LH0-LSm.	127
2.8	The $x_{tot}-w_1$ trajectories of LH0-LSm.	128
2.9	The $x_{tot}-w_1$ trajectories of LH0-LSm.	129
2.10	The $x_{tot}-w_1$ trajectories of LH0-LSr.	130
2.11	The $x_{tot}-w_1$ trajectories of LH0-LSr.	131
2.12	The $x_{tot}-w_1$ trajectories of LH0-LSr.	132
2.13	The $x_{tot}-w_1$ trajectories of LHA-H-L.	134
2.14	The $x_{tot}-w_1$ trajectories of LHA-H-L.	135
2.15	The $x_{tot}-w_1$ trajectories of LHA-H-L.	136
2.16	The $x_{tot}-w_1$ trajectories of LHA-H-Sl.	137
2.17	The $x_{tot}-w_1$ trajectories of LHA-H-Sl.	138
2.18	The $x_{tot}-w_1$ trajectories of LHA-H-Sl.	139

2.19	The $x_{tot}-w_1$ trajectories of LHA-H-Sln.	140
2.20	The $x_{tot}-w_1$ trajectories of LHA-H-Sln.	141
2.21	The $x_{tot}-w_1$ trajectories of LHA-H-Sln.	142
2.22	The $x_{tot}-w_1$ trajectories of LHA-H-Sm.	143
2.23	The $x_{tot}-w_1$ trajectories of LHA-H-Sm.	144
2.24	The $x_{tot}-w_1$ trajectories of LHA-H-Sm.	145
2.25	The $x_{tot}-w_1$ trajectories of LHA-H-Smn.	146
2.26	The $x_{tot}-w_1$ trajectories of LHA-H-Smn.	147
2.27	The $x_{tot}-w_1$ trajectories of LHA-H-Smn.	148
2.28	The $x_{tot}-w_1$ trajectories of LHA-H-Sr.	149
2.29	The $x_{tot}-w_1$ trajectories of LHA-H-Sr.	150
2.30	The $x_{tot}-w_1$ trajectories of LHA-H-Sr.	151
2.31	The $x_{tot}-w_1$ trajectories of LHA-H-Srn.	152
2.32	The $x_{tot}-w_1$ trajectories of LHA-H-Srn.	153
2.33	The $x_{tot}-w_1$ trajectories of LHA-H-Srn.	154
2.34	The $x_{tot}-w_1$ trajectories of LHA-H-Zl.	155
2.35	The $x_{tot}-w_1$ trajectories of LHA-H-Zl.	156
2.36	The $x_{tot}-w_1$ trajectories of LHA-H-Zl.	157
2.37	The $x_{tot}-w_1$ trajectories of LHA-H-Zln.	158
2.38	The $x_{tot}-w_1$ trajectories of LHA-H-Zln.	159
2.39	The $x_{tot}-w_1$ trajectories of LHA-H-Zln.	160
2.40	The $x_{tot}-w_1$ trajectories of LHA-H-Zm.	161
2.41	The $x_{tot}-w_1$ trajectories of LHA-H-Zm.	162
2.42	The $x_{tot}-w_1$ trajectories of LHA-H-Zm.	163
2.43	The $x_{tot}-w_1$ trajectories of LHA-H-Zmn.	164
2.44	The $x_{tot}-w_1$ trajectories of LHA-H-Zmn.	165
2.45	The $x_{tot}-w_1$ trajectories of LHA-H-Zmn.	166
2.46	The $x_{tot}-w_1$ trajectories of LHA-H-Zr.	167
2.47	The $x_{tot}-w_1$ trajectories of LHA-H-Zr.	168
2.48	The $x_{tot}-w_1$ trajectories of LHA-H-Zr.	169

2.49	The $x_{tot}-w_1$ trajectories of LHA-H-Zrn.	170
2.50	The $x_{tot}-w_1$ trajectories of LHA-H-Zrn.	171
2.51	The $x_{tot}-w_1$ trajectories of LHA-H-Zrn.	172
2.52	The $x_{tot}-w_1$ trajectories of LHA-Sm-sp.	173
2.53	The $x_{tot}-w_1$ trajectories of LHA-Sm-sp.	174
2.54	The $x_{tot}-w_1$ trajectories of LHA-Sm-sp.	175
2.55	The $x_{tot}-w_1$ trajectories of LHA-Zm-sp.	176
2.56	The $x_{tot}-w_1$ trajectories of LHA-Zm-sp.	177
2.57	The $x_{tot}-w_1$ trajectories of LHA-Zm-sp.	178
2.58	The $x_{tot}-w_1$ trajectories of LHB-HST.	180
2.59	The $x_{tot}-w_1$ trajectories of LHB-HST.	181
2.60	The $x_{tot}-w_1$ trajectories of LHB-HST.	182
2.61	The $x_{tot}-w_1$ trajectories of LHC-U-Sl.	184
2.62	The $x_{tot}-w_1$ trajectories of LHC-U-Sl.	185
2.63	The $x_{tot}-w_1$ trajectories of LHC-U-Sl.	186
2.64	The $x_{tot}-w_1$ trajectories of LHC-U-Sm.	187
2.65	The $x_{tot}-w_1$ trajectories of LHC-U-Sm.	188
2.66	The $x_{tot}-w_1$ trajectories of LHC-U-Sm.	189
2.67	The $x_{tot}-w_1$ trajectories of LHC-U-Sr.	190
2.68	The $x_{tot}-w_1$ trajectories of LHC-U-Sr.	191
2.69	The $x_{tot}-w_1$ trajectories of LHC-U-Sr.	192
2.70	The $x_{tot}-w_1$ trajectories of LHC-S-Sl.	193
2.71	The $x_{tot}-w_1$ trajectories of LHC-S-Sl.	194
2.72	The $x_{tot}-w_1$ trajectories of LHC-S-Sl.	195
2.73	The $x_{tot}-w_1$ trajectories of LHC-S-Sm.	196
2.74	The $x_{tot}-w_1$ trajectories of LHC-S-Sm.	197
2.75	The $x_{tot}-w_1$ trajectories of LHC-S-Sm.	198
2.76	The $x_{tot}-w_1$ trajectories of LHC-S-Sr.	199
2.77	The $x_{tot}-w_1$ trajectories of LHC-S-Sr.	200
2.78	The $x_{tot}-w_1$ trajectories of LHC-S-Sr.	201

2.79	The $x_{tot}-w_1$ trajectories of LHC-P-Sl.	202
2.80	The $x_{tot}-w_1$ trajectories of LHC-P-Sl.	203
2.81	The $x_{tot}-w_1$ trajectories of LHC-P-Sl.	204
2.82	The $x_{tot}-w_1$ trajectories of LHC-P-Sm.	205
2.83	The $x_{tot}-w_1$ trajectories of LHC-P-Sm.	206
2.84	The $x_{tot}-w_1$ trajectories of LHC-P-Sm.	207
2.85	The $x_{tot}-w_1$ trajectories of LHC-P-Sr.	208
2.86	The $x_{tot}-w_1$ trajectories of LHC-P-Sr.	209
2.87	The $x_{tot}-w_1$ trajectories of LHC-P-Sr.	210
2.88	The $x_{tot}-w_1$ trajectories of LHC-U-Zl.	211
2.89	The $x_{tot}-w_1$ trajectories of LHC-U-Zl.	212
2.90	The $x_{tot}-w_1$ trajectories of LHC-U-Zl.	213
2.91	The $x_{tot}-w_1$ trajectories of LHC-U-Zr.	214
2.92	The $x_{tot}-w_1$ trajectories of LHC-U-Zr.	215
2.93	The $x_{tot}-w_1$ trajectories of LHC-U-Zr.	216
2.94	The $x_{tot}-w_1$ trajectories of LHC-S-Zl.	217
2.95	The $x_{tot}-w_1$ trajectories of LHC-S-Zl.	218
2.96	The $x_{tot}-w_1$ trajectories of LHC-S-Zl.	219
2.97	The $x_{tot}-w_1$ trajectories of LHC-S-Zm.	220
2.98	The $x_{tot}-w_1$ trajectories of LHC-S-Zm.	221
2.99	The $x_{tot}-w_1$ trajectories of LHC-S-Zm.	222
2.100	The $x_{tot}-w_1$ trajectories of LHC-S-Zr.	223
2.101	The $x_{tot}-w_1$ trajectories of LHC-S-Zr.	224
2.102	The $x_{tot}-w_1$ trajectories of LHC-S-Zr.	225
2.103	The $x_{tot}-w_1$ trajectories of LHC-PZT.	226
2.104	The $x_{tot}-w_1$ trajectories of LHC-PZT.	227
2.105	The $x_{tot}-w_1$ trajectories of LHC-PZT.	228
2.106	The $x_{tot}-w_1$ trajectories of LHC-UST.	229
2.107	The $x_{tot}-w_1$ trajectories of LHC-UST.	230
2.108	The $x_{tot}-w_1$ trajectories of LHC-UST.	231

2.109	The $x_{tot}-w_1$ trajectories of LHD-SCT.	233
2.110	The $x_{tot}-w_1$ trajectories of LHD-SCT.	234
2.111	The $x_{tot}-w_1$ trajectories of LHD-SCT.	235
2.112	The $x_{tot}-w_1$ trajectories of LHD-SCL.	236
2.113	The $x_{tot}-w_1$ trajectories of LHD-SCL.	237
2.114	The $x_{tot}-w_1$ trajectories of LHD-SCL.	238
2.115	The $x_{tot}-w_1$ trajectories of LHD-CST.	239
2.116	The $x_{tot}-w_1$ trajectories of LHD-CST.	240
2.117	The $x_{tot}-w_1$ trajectories of LHD-CST.	241
2.118	The $x_{tot}-w_1$ trajectories of LHD-CSL.	242
2.119	The $x_{tot}-w_1$ trajectories of LHD-CSL.	243
2.120	The $x_{tot}-w_1$ trajectories of LHD-CSL.	244
2.121	The $x_{tot}-w_1$ trajectories of LHD-SCLnc.	245
2.122	The $x_{tot}-w_1$ trajectories of LHD-SCLnc.	246
2.123	The $x_{tot}-w_1$ trajectories of LHD-SCLnc.	247

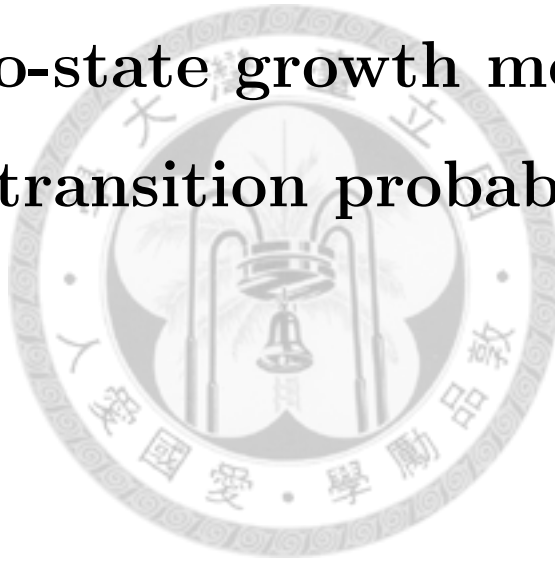


List of Tables

5.1	Parameter values of the cancer system without treatment.	68
1.1	The test results of maxlik-2a.	96
1.2	The test results of maxlik-2b.	96
1.3	The test results of maxlik-2c.	97
1.4	The test results of maxlik-2d.	97
1.5	The error of maxlik2a-2d.	97
1.6	The test results of “maxlik3a”	104
1.7	Logarithmic ratio test result of “maxlik3a”	106
1.8	The test results of “maxlik5a”	107
1.9	Logarithmic ratio test result of “maxlik5a”	109
1.10	Logarithmic ratio test result of “maxlik2D42a-t1”	115
1.11	Logarithmic ratio test result of “maxlik2D42a-t1”	115
1.12	Logarithmic ratio test result of “maxlik2D42a-t2”	116
1.13	Logarithmic ratio test result of “maxlik2D32b-t1”	116
1.14	Logarithmic ratio test result of “maxlik2D32b-t2”	116
1.15	The test results of “maxlik2D42a”	117
1.16	The test results of “maxlik2D32b”	117
1.17	The 2D test results of “maxlik2D42a”	118
1.18	The 2D test results of “maxlik2D32b”	118

Part I

A two-state growth model with transition probability



Chapter 1

Introduction

Life is a complex system; here we talk about such a system: a living individual may have several phenotypes to adapt itself to the various surroundings or to express self-characteristics in some times. As shown in figure 1.1, Such multi-phenotype characteristic and the transition process among them could construct a complex phenotype network with very complex dynamic behaviors. We believe such multi-phenotype system is benefit to the viability of an individual, therefore it should be one of the common system in real-life systems.

If we change the view point from an individual to the population of a species, the multi-phenotype concept shows that the population of a species sometimes can be classified into different sub-populations based on the features associated with a specific phenotype. Using appropriate statistical methods it may be possible to tell apart the various sub-populations and obtain the relative weighting of the sub-populations in a distribution, as is shown in the Appendix A.

The simplest case of heterogeneous systems is one with only two sub-populations, as shown in figure 1.2. For convenience, we may simply treat it as a two-state system, with each state occupying a certain percentage that can vary in time. Despite its simplicity, there are real-life systems which may be treated as such in the lowest order approximation. For example, in human societies, the bi-party political system is not uncommon. And in economy one may wish to roughly distinguish between rich people and poor ones while allowing a transition between the two under certain

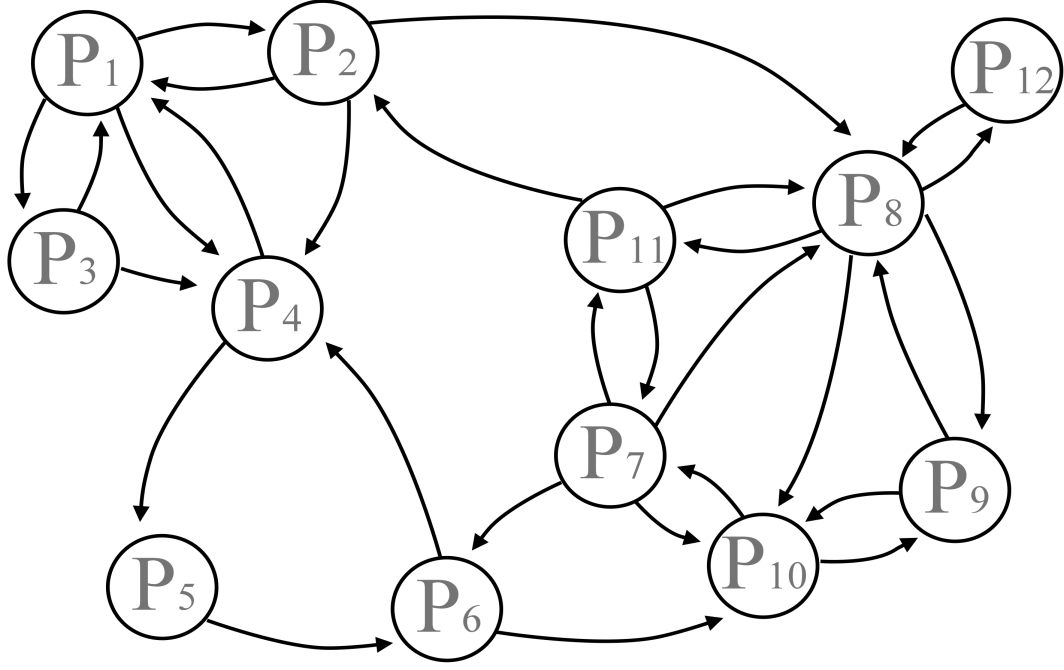


Figure 1.1: A imaginal schematic diagram of a multi-phenotypes system. Each node is a phenotype, and the arrow line present the transition relation from one phenotype to another phenotype. Such a multi-phenotype system always construct a complex phenotypes network.

conditions. As another example, a decision making process may present itself as the simple YES or NO state with some transition probability. Two-state systems are also commonly studied in ecology and in microscopic biology it seems that some cell systems also fit this approximation.

Focusing on some recent researches of heterogeneous system in microscopic biology, Chang *et al.* proposed that the differentiation of mouse haematopoietic progenitor cells is a two sub-populations heterogeneous system [1]. They build a simple two-state growth with transition model to fit their data, each state with the same exponential growth mode and with linear and signaling transition relation. In another



Figure 1.2: Schematic diagram of the two-state heterogeneous system, which is the simplest multi-phenotypes system.

way, Hung *et al.* proposed the cancer attractor hypothesis, which implies cancer system is a multi-phenotype system [2]. They also build a two-state gene circuit model called 2-gene genome network model to described their concept.

In this thesis, we extend the mathematical model of Chang *et al.* [1] to a more general condition. We focus on the two-state heterogeneous system, with emphasis on developing a mathematical model of a two-state growth system which admits a transition between the two states. Basing on the idea of cancer system is one kind of multi-phenotype system, we apply this model to a certain cancer growth system, the prostate cancer. The aim is to fit the actual data obtained from prostate cancer treatments using chemotherapy (17AAG) and radiation therapy [3]. Encouraged by the good agreement between the model and the experimental data, we also use this model to study the optimization of the IAS (Intermittent Androgen Suppression)

time-dependent cancer therapy. It is hoped that new ideas for cancer treatment can be discovered along this line of study.



Chapter 2

Mathematical model of two-state growth with transition probability

A real two-state heterogeneous biological system is always a very complex system, and the characteristics associated with a phenotype may also possess a very high degree of freedom, not to mention that the transition behaviors between each phenotype may be highly nonlinear. On top of this complexity, the dynamic behavior may also be influenced by the surrounding environments and the spatial distribution, or even the period of evolution. To simplify the problem so that a certain progress can be made, we will ignore the spatial distribution and forget about the intrinsic high degree of freedom problem. Thus, we consider a two-state population evolution equation, with the growth of each state contributed by a self-growth term and an inter-transition term. Conceptually, the form looks like

$$\begin{cases} \text{growth rate of state 1} = \text{growth term of state 1} + \text{transition term.} \\ \text{growth rate of state 2} = \text{growth term of state 2} - \text{transition term.} \end{cases} \quad (2.1)$$

2.1 The general Growth and transition model

2.1.1 The time evolution equation of x_1 and x_2

Denoting the population of the two states of interest by x_1 and x_2 , we assume that the mathematical form of the general growth and transition model is

$$\begin{cases} \dot{x}_1 = r_1 f_1(x_1, x_2) x_1 - k_1 x_1 + k_2 x_2 + k S(x_1, x_2), \\ \dot{x}_2 = r_2 f_2(x_1, x_2) x_2 + k_1 x_1 - k_2 x_2 - k S(x_1, x_2), \end{cases} \quad (2.2)$$

where $r_i f_i x_i$ describes the growth of state i with $f_i(x_1, x_2)$ being the normalized average growth frequency function of state i , where $f_i(x_1 = 0, x_2 = 0) = 1$. r_i is the strength constant of growth mode, it also means the cell differentiation strength of state i as $x_1 \sim x_2 \sim 0$. The other terms with parameters k_1 , k_2 , and k are transition terms: the term $-k_1 x_1 + k_2 x_2$ is an assumed linear transition term, which is determined by the intrinsic properties of an individual and its surroundings. The term $k S(x_1, x_2)$ is a signaling term, which simulates a transition effect due to the mean interaction of a sub-population with the whole population; the interaction detail is described via an interaction signaling function $S(x_1, x_2)$.

2.1.2 Transforming x_1 and x_2 to x_t and w_1

From an experimental point of view, the whole population $x_t = x_1 + x_2$ is easier to measure. Thus it is more convenient to compare with the experimental data if we make a variable transformation from the sub-populations x_1 and x_2 to the total population x_t and the weighting of state 1, here denoted by w_1 . The evolution equation of x_t is

$$\begin{aligned} \dot{x}_t &= \dot{x}_1 + \dot{x}_2 \\ &= x_t \{ r_2 f_2 + [r_1 f_1 - r_2 f_2] w_1 \} \\ &= x_t \{ r_2 f_2 + \Delta f w_1 \}. \end{aligned}$$

To get the evolution equation for w_1 , we set $\dot{w}_1 = \dot{w}_1|_g + \dot{w}_1|_T$, where $\dot{w}_1|_g$ is the growth component of \dot{w}_1 , and $\dot{w}_1|_T$ is the transition component of \dot{w}_1 .

The form of $\dot{w}_1|_g$ is

$$\begin{aligned}
\dot{w}_1|_g &= \frac{1}{x_t}(\dot{x}_1 - w_1 \dot{x}_t) \\
&= w_1\{r_1 f_1 - r_2 f_2 - [r_1 f_1 - r_2 f_2] w_1\} \\
&= [r_1 f_1 - r_2 f_2] w_1 w_2 \\
&= [r_1 f_1 - r_2 f_2] (w_1 - w_1^2) \\
&= \Delta f (w_1 - w_1^2),
\end{aligned}$$

where $\Delta f = r_1 f_1 - r_2 f_2$ is the difference of the growth frequency of these two states.

Also, the form of $\dot{w}_1|_T$ is

$$\begin{aligned}
\dot{w}_1|_T &= \frac{1}{x_t}(-k_1 x_1 + k_2 x_2 + kS) \\
&= (-k_1 w_1 + k_2 w_2 + k \frac{S}{x_t}) \\
&= k \frac{S}{x_t} - (k_1 + k_2) w_1 + k_2.
\end{aligned}$$

Therefore, the evolution equation in (x_t, w_1) space is

$$\begin{cases} \dot{x}_t = x_t(r_2 f_2 + \Delta f w_1), \\ \dot{w}_1 = \Delta f (w_1 - w_1^2) + k \frac{S}{x_t} - (k_1 + k_2) w_1 + k_2. \end{cases} \quad (2.3)$$

2.1.3 Some simplified cases.

When transition is not possible, these equations simplify quite a bit, and we can see some characteristics of \dot{x}_t and $\dot{w}_1|_g$ roughly. For later convenience, we list below the

reduced form of the equations.

When $f_1 \neq f_2$ and $r_1 \neq r_2$:

$$\begin{cases} \dot{x}_t = x_t \{r_2 f_2 + \Delta f w_1\} \\ \dot{w}_1 = \Delta f (w_1 - w_1^2) \end{cases} \quad (2.4)$$

This is the most general form.

When $f_1 \neq f_2$ and $r_1 = r_2$:

If $r_1 = r_2 = r$, it means the characteristic time of growth of these two states are the same, and the evolution equations become

$$\begin{cases} \dot{x}_t = r x_t (f_2 + (f_1 - f_2) w_1) \\ \dot{w}_1 = r (f_1 - f_2) (w_1 - w_1^2) \end{cases} \quad (2.5)$$

Under this condition, r can be absorbed into the time variable, meaning that there is only one characteristic time scale for the system.

When $f_1 = f_2$ and $r_1 \neq r_2$:

If $f_1 = f_2 = f$, which means these two states have the same growth form, we have

$$\begin{cases} \dot{x}_t = (r_2 + \Delta r w_1) f x_t \\ \dot{w}_1 = \Delta r f (w_1 - w_1^2) \end{cases} \quad (2.6)$$

where $\Delta r = r_1 - r_2$. The appearance of the same factor f in the two equations means one of the the nullclines of \dot{x}_t ($f(x_t) = 0$) merge with one of the nullclines of \dot{w}_1 .

When $f_1 = f_2$ and $r_1 = r_2$:

The evolution equations become

$$\begin{cases} \dot{x}_t = rf(x_t, w_1)x_t \\ \dot{w}_1 = 0 \end{cases} \quad (2.7)$$

Trivially, then it reduces to a single-component evolution.

2.2 The general two-state growth and transition model with auto/para-crine signaling pathway

2.2.1 The auto/para-crine signaling pathway and its mathematical form

Auto/para-crine is a common signaling pathway. Auto-crine signaling generally refers to signals emitted by an individual which are also received by the same individual or other identical individuals. And if signals are received by other non-identical individuals, then this is para-crine. Following Chang *et al.* [1], we can set the mathematical form of autocrine as w_2x_1 for state 1 and w_1x_2 for state 2. This form means that we assume that an individual would change its identity according to the weighting of these two states in its system. Clearly, this can be viewed as some sort of mean field effect of the autocrine signaling pathway.

The two-state growth and autocrine transition model in x_1 and x_2 space can be written as

$$\begin{cases} \dot{x}_1 = r_1f_1x_1 - k_1x_1 + k_2x_2 - k_{12}w_2x_1 + k_{21}w_1x_2, \\ \dot{x}_2 = r_2f_2x_2 + k_1x_1 - k_2x_2 + k_{12}w_2x_1 - k_{21}w_1x_2. \end{cases} \quad (2.8)$$

Here, k_{12} is the autocrine transition rate strength of x_1 to x_2 , and k_{21} is that of x_2 to

x_1 , respectively. Since the term modeling the autocrine signaling pathway from x_1 to x_2 and from x_2 to x_1 is the same, that is, $w_2x_1 = w_1x_2 = \frac{x_1x_2}{x_t}$, we can follow Chang *et al.*[1] to set an autocrine strength coefficient $k \equiv k_{21} - k_{12}$ to substitute for the two coefficients k_{12} and k_{21} . Then, the growth and transition equations become

$$\begin{cases} \dot{x}_1 = r_1f_1x_1 - k_1x_1 + k_2x_2 + k\frac{x_1x_2}{x_t}, \\ \dot{x}_2 = r_2f_2x_2 + k_1x_1 - k_2x_2 - k\frac{x_1x_2}{x_t}. \end{cases} \quad (2.9)$$

And the corresponding equations in the (x_t, w_1) space is

$$\begin{cases} \dot{x}_t = x_t(r_2f_2 + \Delta f w_1) \\ \dot{w}_1 = (\Delta f + k)(w_1 - w_1^2) - (k_1 + k_2)w_1 + k_2. \end{cases} \quad (2.10)$$

Since both the signaling term and the growth term contribute a factor to the logistic growth term $(w_1 - w_1^2)$ in the \dot{w}_1 equation, the parameter k could be thought of as contributing a step-up or step-down effect to the original Δf . That is, an effective logistic growth factor $\Delta F \equiv \Delta f + k$ has replaced the original Δf .

2.2.2 The nullclines and fixed points in general autocrine transition case

To study the dynamic behavior of this system, it helps to find the nullclines and fixed points in the mathematical model.

The nullclines in general autocrine transition case

The nullcline $\tilde{x}_t(w_1)$ of x_t is found by setting $\dot{x}_t = 0$. Thus, $r_2f_2(x_t, w_1) + \Delta f w_1 = 0$. And when $\dot{w}_1 = 0$, the nullcline for w_1 is $(\Delta f + k)(\tilde{w}_1 - \tilde{w}_1^2) - (k_1 + k_2)w_1 + k_2 = 0$.

If we ignore the transition term ($k_1 = 0$, $k_2 = 0$, and $k = 0$), then the w_1 nullcline is $\tilde{w}_1(w_1) = 0$, $\tilde{w}_1(w_1) = 1$, and $\Delta f = 0$.

Now, if we consider only the growth term and the signaling term while ignoring the linear transition term (by setting $k_1 = 0$ and $k_2 = 0$), the third condition would become $\Delta F = \Delta f + k = 0$. As said before, the signaling term then serves to step-up or -down for the determination of $\tilde{w}_1(w_1)$, and by regulating the parameter k we may change the shape and position of the nullcline and the number of fixed points.

The linear transition term $-(k_1 + k_2)w_1 + k_2$ contributes to \dot{w}_1 in a linear fashion, and its end effect can be seen by examining the limiting cases $w_1 \rightarrow 0$ and $w_1 \rightarrow 1$. This is so because the autocrine and the growth effect in \dot{w}_1 contains the factor $w_1 - w_1^2$, which dictates and eventually w_1 will tend to either 0 or 1. Then, during this late stage of time evolution, the linear transition term becomes a constant depending on the final value of w_1 . Clearly, then, it will change the position or the existence of the fixed points.

The fixed point condition in general autocrine transition case

The fixed points appear where $\tilde{x}_t(w_1)$ and $\tilde{w}_1(w_1)$ cross. They satisfy the combined equations

$$\begin{cases} 0 = r_2 f_2 + \Delta f w_1 \\ 0 = (\Delta f + k)(w_1 - w_1^2) - (k_1 + k_2)w_1 + k_2. \end{cases} \quad (2.11)$$

By simultaneously solving these two equations, we should be able to obtain the value (in principle) of the fixed point components x_t^* and w_1^* .

2.2.3 Jacobian matrix in general autocrine transition case.

From the general form for the two-state growth and autocrine transition model,

$$\begin{cases} \dot{x}_1 = r_1 f_1(x_1, x_2)x_1 - k_1 x_1 + k_2 x_2 + k \frac{x_1 x_2}{x_t} \\ \dot{x}_2 = r_2 f_2(x_1, x_2)x_2 + k_1 x_1 - k_2 x_2 - k \frac{x_1 x_2}{x_t} \end{cases} \quad (2.12)$$

we easily derive the Jacobian matrix in the x_1 and x_2 space as

$$J = \begin{pmatrix} \frac{\partial \dot{x}_1}{\partial x_1} |_f & \frac{\partial \dot{x}_1}{\partial x_2} |_f \\ \frac{\partial \dot{x}_2}{\partial x_1} |_f & \frac{\partial \dot{x}_2}{\partial x_2} |_f \end{pmatrix} = \begin{pmatrix} J_a & J_b \\ J_c & J_c \end{pmatrix},$$

where the matrix elements are

$$\begin{aligned} J_a &= r_1 f_1 + r_1 x_1 \frac{\partial f_1}{\partial x_1} - k_1 + k w_2^2 |_f \\ &= r_1 x_1 \frac{\partial f_1}{\partial x_1} - k_2 \frac{x_2}{x_1} - k(w_1 - w_1^2) |_f \end{aligned}$$

$$J_b = r_1 x_1 \frac{\partial f_1}{\partial x_2} + k_2 + k w_1^2 |_f$$

$$J_c = r_2 x_2 \frac{\partial f_2}{\partial x_1} + k_1 - k w_2^2 |_f$$

$$\begin{aligned}
J_d &= r_2 f_2 + r_2 x_2 \frac{\partial f_2}{\partial x_2} - k_2 - k w_1^2|_f \\
&= r_2 x_2 \frac{\partial f_2}{\partial x_2} - k_1 \frac{x_1}{x_2} + k(w_1 - w_1^2)|_f.
\end{aligned}$$

And the eigenvalues of the Jacobian are

$$\begin{aligned}
\lambda_{1,2} &= \frac{1}{2} (J_a + J_d) \pm \sqrt{(J_a + J_d)^2 - 4(J_a J_d - J_b J_c)} \\
&= \frac{1}{2} (J_a + J_d) \pm \sqrt{(J_a - J_d)^2 + 4J_b J_c} \\
&\equiv \frac{1}{2} (\lambda_a \pm \sqrt{\lambda_b}).
\end{aligned}$$

If $\lambda_a < 0$ and $\text{Det}[J] = (J_a J_d - J_b J_c) > 0$, then the real parts of these two eigenvalue are smaller than 0, and the fixed point would be a sink. And if $\lambda_b < 0$, then the imaginary parts of these two eigenvalues are not 0, and the trajectories would have a spiral form.

These three terms are

$$\begin{aligned}
\lambda_a &= J_a + J_d \\
&= (r_1 x_1 \frac{\partial f_1}{\partial x_1} + r_2 x_2 \frac{\partial f_2}{\partial x_2}) - (k_1 \frac{x_1}{x_2} + k_2 \frac{x_2}{x_1}).
\end{aligned}$$


The term $-(k_1 \frac{x_1}{x_2} + k_2 \frac{x_2}{x_1})$ is always smaller than 0, and if f_i is a decreasing function, then $\frac{\partial f_1}{\partial x_1}$ and $\frac{\partial f_2}{\partial x_2}$ are also always smaller than 0. Therefore, λ_a is always smaller than 0 when f_1 and f_2 are both decreasing functions. It means that the fixed points in these models can only be sinks or saddle points.

Turning to the determinant next:

$$\begin{aligned}
\text{Det}[J] &= J_a J_d - J_b J_c \\
&= \text{Det}[J]_r + \text{Det}[J]_{r,i} + \text{Det}[J]_i \\
&= r_1 r_2 x_1 x_2 \left(\frac{\partial f_1}{\partial x_1} \frac{\partial f_2}{\partial x_2} - \frac{\partial f_1}{\partial x_2} \frac{\partial f_2}{\partial x_1} \right) \\
&\quad - r_1 x_1 \frac{\partial f_1}{\partial x_1} \left(k_1 \frac{w_1}{w_2} - k(w_1 - w_1^2) \right) - r_2 x_2 \frac{\partial f_2}{\partial x_2} \left(k_2 \frac{w_2}{w_1} + k(w_1 - w_1^2) \right) \\
&\quad - r_1 x_1 \frac{\partial f_1}{\partial x_2} (k_1 - k w_2^2) - r_2 x_2 \frac{\partial f_2}{\partial x_1} \left(k_2 \frac{w_2}{w_1} + k w_1^2 \right) \\
&\quad + 0.
\end{aligned}$$

The “interaction term” in $\text{Det}[J]$ is 0.

And the term λ_b is



$$\begin{aligned}
\lambda_b &= (J_a + J_d)^2 - 4\text{Det}[J] \\
&= \lambda_{b,r} \\
&\quad + \lambda_{b,ri} \\
&\quad + \lambda_{b,i} \\
&= \left(r_1 x_1 \frac{\partial f_1}{\partial x_1} - r_2 x_2 \frac{\partial f_2}{\partial x_2} \right)^2 + 4 r_1 r_2 x_1 x_2 \frac{\partial f_1}{\partial x_2} \frac{\partial f_2}{\partial x_1} \\
&\quad + \left(k_1 \frac{x_1}{x_2} + k_2 \frac{x_2}{x_1} \right)^2 \\
&\quad - 2 \left(r_1 x_1 \frac{\partial f_1}{\partial x_1} + r_2 x_2 \frac{\partial f_2}{\partial x_2} \right) \left(k_1 \frac{x_1}{x_2} + k_2 \frac{x_2}{x_1} \right) \\
&\quad - r_1 x_1 \left(\frac{w_1}{w_2} \frac{\partial f_1}{\partial x_1} + \frac{\partial f_1}{\partial x_2} \right) (k_1 - k w_2^2) - r_2 x_2 \left(\frac{w_2}{w_1} \frac{\partial f_2}{\partial x_2} + \frac{\partial f_2}{\partial x_1} \right) (k_2 + k w_1^2).
\end{aligned}$$

If $\lambda_b < 0$, then the system would have a spiral trajectory.

2.3 f_i is a constant, the exponential growth model

When f_i is a constant, it means the growth mode is exponential growth, the population equation is

2.3.1 Two-state exponential growth and autocrine transition model

$$\begin{cases} \dot{x}_1 = r_1 x_1 - k_1 x_1 + k_2 x_2 + k \frac{x_1 x_2}{x_t} \\ \dot{x}_2 = r_2 x_2 + k_1 x_1 - k_2 x_2 - k \frac{x_1 x_2}{x_t} \end{cases} \quad (2.13)$$

and the evolution equation in (x_t, w_1) space is

$$\begin{cases} \dot{x}_t = (r_2 + \Delta r w_1) x_t \\ \dot{w}_1 = (\Delta r + k)(x_t, w_1)(w_1 - w_1^2) - (k_1 + k_2)w_1 + k_2, \end{cases} \quad (2.14)$$

where $\Delta r = r_1 - r_2$ is the difference of the inverse characteristic time.

2.3.2 The exact solution

1. $r_1 = r_2 = r$

When $r_1 = r_2 = r$, the rate equation of x_t is $\dot{x}_t = r x_t$, we can solve it easily, x_t has a simple form of exponential growth with $x_t(t) = x_t(t=0)e^{rt}$.

To solve the exact solution of w_1 , we can set $C = k_2 + k \left(\frac{1 - \frac{k_1}{k} - \frac{k_2}{k}}{2} \right)^2$, and $w'_1 = \sqrt{\frac{k}{C}}(w_1 - \frac{1 - \frac{k_1}{k} - \frac{k_2}{k}}{2})$, then we can obtain

$$\frac{dw'_1}{dt} = \sqrt{kC}(-w_1'^2 + 1)$$

$$\Rightarrow \frac{dw'_1}{(-w_1'^2 + 1)} = \sqrt{kC} dt$$

$$\frac{1}{2} \left(\frac{1}{1+w'_1} + \frac{1}{1-w'_1} \right) dw'_1 = \sqrt{kC} dt$$

$$\int_{w_1'(0)}^{w_1'(t)} \frac{dw_1'}{1+w_1'} - \int_{w_1'(0)}^{w_1'(t)} \frac{dw_1'}{|w_1'-1|} = 2\sqrt{kC} \int dt = 2\sqrt{kC}t.$$

The solution of this equation is $w_1'(t) = \frac{1-u(t)}{1+u(t)}$

where $u(t) = \frac{1-w_1'(0)}{1+w_1'(0)} e^{-2\sqrt{kC}t} = u(0) e^{-2\sqrt{kC}t} = e^{-2\sqrt{kC}t + \ln(u(0))} = e^{-2\tau}$,

and $u(0) = \frac{1-w_1'(0)}{1+w_1'(0)}$, $\tau = \sqrt{kC}t - \ln(u(0))/2$.

Therefore, the solution of w_1 is

$$w_1(\tau) = \begin{cases} w_1(\tau) = \frac{1-\frac{k_1}{k}-\frac{k_2}{k}}{2} + \sqrt{\frac{C}{k}} \tanh(\tau) & \text{if } \frac{1-w_1'(0)}{1+w_1'(0)} > 0 \\ w_1(\tau) = \frac{1-\frac{k_1}{k}-\frac{k_2}{k}}{2} + \sqrt{\frac{C}{k}} \coth(\tau) & \text{if } \frac{1-w_1'(0)}{1+w_1'(0)} < 0 \end{cases} \quad (2.15)$$

The exact solution in τ space is a hyper-tangent function with an intercept. When $t \rightarrow \infty$, $\tanh(\tau) \rightarrow 0$, and w_1 tends to a steady value $w_1(t \rightarrow \infty) \rightarrow \frac{1-\frac{k_1}{k}-\frac{k_2}{k}}{2} + \sqrt{\frac{k_2}{k} + \left(\frac{1-\frac{k_1}{k}-\frac{k_2}{k}}{2}\right)^2}$.

This solution agrees with the result of the previous paper [1], which is a sigmoidal curve.

2. $r_1 \neq r_2$

When $r_1 \neq r_2$, the rate equation of x_t is $\dot{x}_t = (r_2 + \Delta r w_1) x_t$. It is still an exponential-like function. As w_1 converges to a steady value w_1^* , $x_t \propto e^{(r+\Delta r w_1^*)t}$.

And the weighting evolution function is

$$\dot{w}_1 = -[k + (r_1 - r_2)] w_1^2 + [k + (r_1 - r_2) - (k_1 + k_2)] w_1 + k_2.$$

If we set $k' = k + (r_1 - r_2) = k + \Delta r$, then the equation becomes

$$\dot{w}_1 = -k' w_1^2 + (k' - (k_1 + k_2)) w_1 + k_2.$$

It is the same as the case with $r_1 = r_2 = r$ but changing the parameter k into k' . Therefore, the solution is similar with the symmetrical case but changing k to k' . It is also an sigmoidal curve.

2.4 When f_i is a linear function- the general logistic growth model

When f_i is a linear function of x_1 and x_2 , the growth becomes that of a logistical growth model.

2.4.1 A general form of two-state logistic growth and autocrine transition model.

To study the logistic growth model, we first consider the most general linear form for f_i . Thus, we set $f_1(x_1, x_2)$ and $f_2(x_1, x_2)$ as the following form,

$$\begin{cases} f_1 = (1 - \frac{x_1}{C_1} - \frac{x_2}{C_2}), \\ f_2 = (1 - \frac{x_1}{aC_1} - \frac{x_2}{bC_2}), \end{cases} \quad (2.16)$$

where C_1 is the logistic self-suppressing capacity of x_1 . C_2 is the suppressing capacity of x_2 on x_1 , which is due to the competition effect of x_2 on x_1 . Similarly, the logistic self-suppressing capacity of x_2 is bC_2 , and the suppressing capacity of x_2 on x_1 is aC_1 .

Then the evolution equation in (x_t, w_1) space reads

$$\begin{cases} \dot{x}_t = x_t(r_2 + \Delta r w_1) \left(1 - \frac{m_w w_1^2 + (q_w + r_2 a_c 2)w_1 + \frac{r_2}{bC_2}}{r_2 + \Delta r w_1} x_t \right) \\ \dot{w}_1 = (\Delta r (1 - \frac{1}{\Delta r} (m_w w_1 + q_w) x_t) + k)(w_1 - w_1^2) - (k_1 + k_2)w_1 + k_2 \end{cases}$$

,

where the auxiliary parameters are,

$$\begin{aligned}
a_{c1} &= \frac{1}{C_1} - \frac{1}{C_2}, \\
&= -\frac{1}{C_2} \left(1 - \frac{C_2}{C_1}\right) \\
a_{c2} &= \frac{1}{aC_1} - \frac{1}{bC_2}, \\
&= \frac{1}{a}a_{c1} + \frac{\delta}{C_2} \\
&= \frac{1}{C_2} \left(-\frac{1}{a} \left(1 - \frac{C_2}{C_1}\right) + \delta\right) \\
m_w &= r_1 a_{c1} - r_2 a_{c2}, \\
&= \left(r_1 - \frac{r_2}{a}\right) a_{c1} - r_2 \frac{\delta}{C_2} \\
&= \frac{r_2}{C_2} \left(\frac{1}{a} \left(1 - a \frac{r_1}{r_2}\right) \left(1 - \frac{C_2}{C_1}\right) - \delta\right) \\
q_w &= \frac{r_1}{C_2} - \frac{r_2}{bC_2}, \\
&= \left(r_1 - \frac{r_2}{a}\right) \frac{1}{C_2} + r_2 \frac{\delta}{C_2} \\
&= \frac{r_2}{C_2} \left(-\frac{1}{a} \left(1 - a \frac{r_1}{r_2}\right) + \delta\right),
\end{aligned}$$

and $\delta = (\frac{1}{a} - \frac{1}{b})$ is a parameter that breaks the symmetry of the capacity strength.

When $a = b$ ($\delta = 0$), it means the decreasing rates of f_1 and f_2 are in proportion; and if $a = b = 1$ we then have $f_1 = f_2$. If $C_1 = C_2$, it means the decreasing rates of x_1 and x_2 in f_i are the same.

2.4.2 The x_t nullcline for the general logistic growth

We can easily find the x_t nullcline $\tilde{x}_t(w_1)$ and the w_1 nullcline $\tilde{w}_1(w_1)$ via the prescription of Chapter 1. Thus,

$$\begin{aligned}\tilde{x}_t(w_1) &= \frac{r_2 + \Delta r w_1}{m_w w_1^2 + (q_w + r_2 a_{c2}) w_1 + \frac{r_2}{b C_2}} \\ &= \frac{\Delta r}{m_w} \frac{(w_1 - w_A)}{(w_1 - w_B)(w_1 - w_C)}\end{aligned}$$

,

where

$$w_A = \frac{1}{1 - \frac{r_1}{r_2}}$$

$$\begin{aligned}w_B &= \frac{-(q_w + r_2 a_{c2}) + \sqrt{(q_w + r_2 a_{c2})^2 - 4m_w \frac{r_2}{b C_2}}}{2m_w} \\ &= \frac{(\frac{1}{w_b} + \frac{1}{w_c} - 2a\delta) + \sqrt{(\frac{1}{w_b} + \frac{1}{w_c} - 2a\delta)^2 - 4(\frac{1}{w_b} \frac{1}{w_c} - a\delta)(1 - a\delta)}}{2(\frac{1}{w_b} \frac{1}{w_c} - a\delta)}.\end{aligned}$$

$$\begin{aligned}w_C &= \frac{-(q_w + r_2 a_{c2}) - \sqrt{(q_w + r_2 a_{c2})^2 - 4m_w \frac{r_2}{b C_2}}}{2m_w} \\ &= \frac{(\frac{1}{w_b} + \frac{1}{w_c} - 2a\delta) - \sqrt{(\frac{1}{w_b} + \frac{1}{w_c} - 2a\delta)^2 - 4(\frac{1}{w_b} \frac{1}{w_c} - a\delta)(1 - a\delta)}}{2(\frac{1}{w_b} \frac{1}{w_c} - a\delta)}\end{aligned}$$

and

$$\begin{aligned}w_a &= w_A \\ w_b &= \frac{1}{1 - a \frac{r_1}{r_2}} \\ w_c &= \frac{1}{1 - \frac{C_2}{C_1}}\end{aligned}$$

When $\delta = 0$, then $w_B = w_b$, and $w_C = w_c$.

Consider the two “end points” of $\tilde{x}_t(w_1)$ corresponding to $w_1 = 0$ or 1:

$$\tilde{x}_t(w_1 = 0) = \frac{r_2}{\frac{r_2}{bC_2}} = C_{22} = bC_{12}$$

$$\begin{aligned} \tilde{x}_t(w_1 = 1) &= \frac{r_1}{m_w + q_w + r_2 a_{c2} + \frac{r_2}{bC_2}} \\ &= \frac{r_1}{r_1 a_{c1} + q_w + \frac{r_2}{bC_2}} \\ &= \frac{r_1}{r_1 a_{c1} + q_w + \frac{r_2}{bC_2}} \\ &= \frac{r_1}{\frac{r_1}{C_1}} \\ &= C_1. \end{aligned}$$

It is no surprise that the two end points assume the self-suppressing capacity of x_1 and x_2 , and they are all positive values. And we can see that w_A must be smaller than 0 or larger than 1, implying that $\tilde{x}_t(w_1)$ does not intersect with $x_t = 0$. Combining all these facts we see that $\tilde{x}_t(w_1)$ as a function of w_1 is always positive.

The denominator of the expression for $\tilde{x}_t(w_1)$ is a quadratic function of w_1 , and it can be written as

$$\begin{aligned}
& m_w w_1^2 + (q_w + r_2 a_{c2}) w_1 + \frac{r_2}{b C_2} \\
&= \frac{1}{a} \left(\left(\frac{a r_1 - r_2}{C_1} - \frac{a r_1 - \frac{a}{b} r_2}{C_2} \right) w_1^2 + \left(\frac{r_2}{C_1} + \frac{a r_1 - 2 \frac{a}{b} r_2}{C_2} \right) w_1 + \frac{a}{b} \frac{r_2}{C_2} \right) \\
&= \frac{1}{a} \left(((a r_1 - r_2) w_1 + r_2) \left(a_{c1} w_1 + \frac{1}{C_2} \right) \right) - r_2 \frac{\delta}{C_2} (w_1 - 1)^2 \\
&= \frac{a_{c1} (a r_1 - r_2)}{a} \left(\left(w_1 - \frac{1}{(1 - a \frac{r_1}{r_2})} \right) \left(w_1 - \frac{1}{1 - \frac{C_2}{C_1}} \right) \right) - r_2 \frac{\delta}{C_2} (w_1 - 1)^2 \\
&= \frac{r_2}{a C_2} \left(\left(1 - a \frac{r_1}{r_2} \right) \left(1 - \frac{C_2}{C_1} \right) \left(w_1 - \frac{1}{(1 - a \frac{r_1}{r_2})} \right) \left(w_1 - \frac{1}{1 - \frac{C_2}{C_1}} \right) \right) - a \delta (w_1 - 1)^2.
\end{aligned}$$

The first term in the above is always positive, because $(1 - a \frac{r_1}{r_2})(w_1 - \frac{1}{(1 - a \frac{r_1}{r_2})}) < 0$ and $\frac{1}{(1 - \frac{C_2}{C_1})}(w_1 - \frac{1}{(1 - \frac{C_2}{C_1})}) < 0$. And for a fixed parameter a , we see that, as $b \rightarrow \infty$, $\delta \rightarrow \frac{1}{a}$ as its maximum. Under this condition the quadratic function (of the denominator) has a local minimum. But since it has no roots between 0 and 1, w_B and w_C would not lie between 0 and 1, either, implying that $\tilde{x}_t(w_1)$ has no singular points. The discussion above allows one to classify the types of $\tilde{x}_t(w_1)$ through the relation

$$\tilde{x}_t(w_1) \propto \frac{(w_1 - w_A)}{(w_1 - w_B)(w_1 - w_C)}.$$

Fig 2.1 is a diagram showing all the ten types of $\tilde{x}_t(w_1)$ we have classified. Specifically, they are :

(U) is U-shaped curves.

(H1) is a plot of the curve of $\frac{1}{w_1}$ (marked 1), which has the tendency of $\tilde{x}_t(w_1) \rightarrow \infty$ as $w_1 \rightarrow w_B$ or $w_1 \rightarrow w_C$, and $\tilde{x}_t(w_1) \rightarrow 0$ as $w_1 \rightarrow \infty$.

(H2) is a plot of the curve of $\frac{1}{w_1}$ (marked 2), which is similar to H1 but with $x_t = 0$ when $w_1 = w_A$.

(S) is Sigmoidal curve.

(P) is a curve with a peak.

All of these five curves exhibit two tendencies as they approach the bounding points: Either going up (tending to $w_1 = 1$, marked as U) or down (tending to $w_1 = 0$, marked as D). Therefore, we can classify the \tilde{x}_t curves into ten types, which are designated as, UU, DU, UH1, UH2, DH1, DH2, US, DS, UP, and DP, respectively.

Showed in Figure.2.1 show the various types for the case $w_C > w_B$ (we may simply change the index of B and C if $w_B > w_C$).

1. UU

When $w_B < 0 < 1 < w_C < w_A$, the $\tilde{x}_t(w_1)$ is UU type.

2. DU

When $w_A < w_B < 0 < 1 < w_C$, the $\tilde{x}_t(w_1)$ is DU type.

3. DH1

When $w_A, w_B < w_C < 0$, the $\tilde{x}_t(w_1)$ is DH1 type.

4. DH2

When $w_B < w_C < 0 < 1 < w_A$
and $w_B < 0 < 1 < w_A < \frac{w_B + w_C}{2} < w_C$, the $\tilde{x}_t(w_1)$ is DH2 type.

5. UH1

When $1 < w_B < w_A, w_C$, the $\tilde{x}_t(w_1)$ is UH1 type.

6. UH2

When $w_A < 0 < 1 < w_B < w_C$ and $w_B < \frac{w_B + w_C}{2} < w_A < 0 < 1 < w_C$, the $\tilde{x}_t(w_1)$ is UH2 type.

7. US

When $w_B < w_A < 0 < \frac{w_B + w_C}{2} < 1 < w_A < w_C$, the $\tilde{x}_t(w_1)$ is US type.

8. DS

When $w_B < 0 < \frac{w_B + w_C}{2} < 1 < w_A < w_C$, the $\tilde{x}_t(w_1)$ is DS type.

9. UP

When $1 < w_A < w_B < w_C$, the $\tilde{x}_t(w_1)$ is UP type.

10. DP

When $w_B < w_C < w_A < 1$, the $\tilde{x}_t(w_1)$ is DP type.

2.4.3 $\tilde{w}_1(x_t)$ in a general logistic growth and autocrine transition model

By definition, $\tilde{w}_1(x_t)$ corresponds to $\dot{w}_1 = 0$. In a general logistic growth and autocrine transition model, the equation satisfied by $\tilde{w}_1(x_t)$ can be separated into a nonlinear term plus a linear term, thus

$$\begin{aligned} 0 &= ((\Delta r - (m_w \tilde{w}_1 + q_w)x_t) + k)(\tilde{w}_1 - \tilde{w}_1^2) - (k_1 + k_2)\tilde{w}_1 + k_2 \\ &= (\Delta f + k)(\tilde{w}_1 - \tilde{w}_1^2) - (k_1 + k_2)\tilde{w}_1 + k_2 \\ &\equiv \Delta F(\tilde{w}_1 - \tilde{w}_1^2) + [-(k_1 + k_2)\tilde{w}_1 + k_2] \\ &= \text{nonlinear term} + \text{linear term}. \end{aligned}$$

This is a cubic equation which can be analytically solved. However, the analytical form does not permit one to penetrate into the characteristics of $\tilde{w}_1(x_t)$. Therefore we have instead separated $\tilde{w}_1(x_t)$ into two parts, one from the contribution of the nonlinear term and another one from the linear term. It is hoped that this may better capture the characteristics of $\tilde{w}_1(x_t)$.

Explicitly, we arbitrarily set the nonlinear term to be

$$\text{nonlinear term} = \Delta F(\tilde{w}_1 - \tilde{w}_1^2)$$

and the linear term to be

$$\text{linear term} = -(k_1 + k_2)\tilde{w}_1 + k_2.$$

Note that the linear term alone is independent of x_t , so that the $\tilde{w}_1(x_t)$, taking into account the linear term alone, is a straight line.

If we ignore the linear term, then \tilde{w}_1 admits the following solutions: $\tilde{w}_1 = 0$, $\tilde{w}_1 = 1$, and $\Delta F = 0$. And the root of ΔF can be written as a function of $x_t(w_1)$, which is

$x_t = \frac{k+\Delta r}{(m_w w_1 + q_w)}$. This is the reciprocal of a linear function, with a singular point at $m_w w_1 + q_w = 0$. The singular point thus satisfies

$$\begin{aligned} w_1 &= -\frac{q_w}{m_w} = \frac{\frac{(r_1 - \frac{r_2}{b})}{C_2}}{\frac{(r_1 - \frac{r_2}{b})}{C_2} - \frac{(r_1 - \frac{r_2}{a})}{C_1}} \\ &= \frac{(r_1 - \frac{r_2}{b})}{(r_1 - \frac{r_2}{b}) - (r_1 - \frac{r_2}{a}) \frac{C_2}{C_1}}. \end{aligned}$$

We can see that the condition for the existence of the singular point lying in the region of interest $[0, 1]$ is the following:

1. When $r_1 > \frac{r_2}{b}$ and $r_1 < \frac{r_2}{a}$, then $0 < w_1 = -\frac{q_w}{m_w} < 1$.
2. When $r_1 < \frac{r_2}{b}$ and $r_1 > \frac{r_2}{a}$, then we also have $0 < w_1 = -\frac{q_w}{m_w} < 1$.

Therefore, if r_1 is between the two values $\frac{r_2}{a}$ and $\frac{r_2}{b}$, $\tilde{w}_1(x_t)$ would have a singular point.

The two end points of the $\tilde{w}_1(x_t)$ curve are

$$x_t(w_1 = 0) = \frac{k + \Delta r}{(r_1 - \frac{r_2}{b})} C_2,$$

and

$$x_t(w_1 = 1) = \frac{k + \Delta r}{(r_1 - \frac{r_2}{a})} C_1.$$

Quite generally, when $end\ point|_{w_1=0} \geq end\ point|_{w_1=1}$, then $r_1 \frac{a_{c1}}{k+\Delta r} \geq r_2 \frac{a_{c2}}{k+\Delta r}$.

The form of $\tilde{w}_1(x_t)$ can be determined by the condition $\Delta F(x_t = 0) = k + \Delta r$, the end point relation, and the position of the singular point. Figure 2.2 shows the form of $\tilde{w}_1(x_t)$ without a singular point.

We see that, when $end\ point|_{w_1=0} > end\ point|_{w_1=1}$, the curve is of the S type (that is, S-shaped) with the “head” facing left if $\Delta F(x_t = 0) > 0$, and it is of the Z type (Z-shaped) with the head facing right if $\Delta F(x_t = 0) < 0$.

When $end\ point|_{w_1=0} < end\ point|_{w_1=1}$, the curve is of the Z type with the head facing left if $\Delta F(x_t = 0) > 0$, and S type with the head facing right if $\Delta F(x_t = 0) < 0$.

When $end\ point|_{w_1=0} = end\ point|_{w_1=1}$, the curve would be S type with the head facing left if $\Delta F(x_t = 0) > 0$, and S type with the head facing right if $\Delta F(x_t = 0) < 0$.

And if a singular point lies between $0 < w_1 < 1$, then $\tilde{w}_1(x_t)$ consists of two S type curves, or one S type and one C-shaped curve, with possible reversal in order of appearance, that is, S is above C or vice versa. Figure 2.3 shows the form of $\tilde{w}_1(x_t)$ with a singular point.

When $m_w > 0$ and $q_w < 0$, and if $\Delta F > 0$, then $\tilde{w}_1(x_t)$ contains two S type curves with the upper branch having its head facing left. And if $\Delta F < 0$, $\tilde{w}_1(x_t)$ is of the S type curve facing the opposite direction. When $m_w < 0$ and $q_w > 0$, and if $\Delta F > 0$, then $\tilde{w}_1(x_t)$ is an SC type curve, and for $\Delta F < 0$, $\tilde{w}_1(x_t)$ is a CS type curve.

When there is no singular points between $0 < w_1 < 1$, then the $\tilde{w}_1(x_t)$ can be either S type or Z type curve, which depends on the sign of ΔF and $m_w w_1 + q_w$. The sign of m_w , q_w , and $k + \Delta r$ can be used to determine the form of $\tilde{w}_1(x_t)$. Because of this, we now proceed to check the relation between their signs and the original parameters.

1. $m_w = 0$

$$m_w = \frac{r_2}{C_2} \left(\frac{1}{a} (1 - a \frac{r_1}{r_2}) (1 - \frac{C_2}{C_1}) - \delta \right)$$

Therefore, we have: $m_w > 0$ when $a\delta < (1 - a \frac{r_1}{r_2})(1 - \frac{C_2}{C_1})$. Furthermore, when

$r_1 < (\frac{1}{a} - \frac{\delta}{1 - \frac{C_2}{C_1}})r_2$ and $C_1 > C_2$, then $m_w > 0$. And when $r_1 > (\frac{1}{a} + \frac{\delta}{1 - \frac{C_2}{C_1}})r_2$ and $C_1 < C_2$, then $m_w > 0$.

Conversely, when $r_1 > (\frac{1}{a} - \frac{\delta}{1 - \frac{C_2}{C_1}})r_2$ and $C_1 > C_2$, then $m_w < 0$. And when $r_1 < (\frac{1}{a} - \frac{\delta}{1 - \frac{C_2}{C_1}})r_2$ and $C_1 < C_2$, then $m_w < 0$.

2. $q_w = 0$

$$q_w = \frac{r_1}{C_2} - \frac{r_2}{bC_2}$$

Therefore, when $r_1 > \frac{r_2}{b}$, then $q_w > 0$. Also, when $r_1 < \frac{r_2}{b}$ we have instead $q_w < 0$.

3. $m_w + q_w = 0$

$$\begin{aligned} m_w + q_w &= \frac{r_2}{C_2} \left(\frac{1}{a} \left(1 - a \frac{r_1}{r_2} \right) \left(1 - \frac{C_2}{C_1} \right) - \delta \right) + \frac{r_2}{C_2} \left(-\frac{1}{a} \left(1 - a \frac{r_1}{r_2} \right) + \delta \right) \\ &= \frac{r_2}{C_2} \left(\frac{1}{a} \frac{C_2}{C_1} \left(a \frac{r_1}{r_2} - 1 \right) \right) \\ &= \frac{1}{C_1} \left(r_1 - \frac{r_2}{a} \right) \end{aligned}$$

Therefore, when $r_1 > \frac{r_2}{a}$, then $m_w + q_w > 0$. And when $r_1 < \frac{r_2}{a}$, then $m_w + q_w < 0$

2.4.4 The fixed point formula in general logistic growth and autocrine transition model

Substituting x_t nullcline into w_1 nullcline equation, we immediately obtain the condition for the fixed points. Thus,

$$\begin{aligned} 0 &= (k + \Delta r - (m_w w_1^* + q_w) \frac{r_2 + \Delta r w_1^*}{m_w w_1^{*2} + (q_w + r_2 a_{c2}) w_1^* + \frac{r_2}{b C_2}}) (w_1^* - w_1^{*2}) \\ &\quad - (k_1 + k_2) w_1^* + k_2 \\ &= \Delta F(w_1^* - w_1^{*2}) - (k_1 + k_2) w_1^* + k_2. \end{aligned}$$

And the term ΔF is

$$\begin{aligned}
\Delta F &= k + \Delta r - (m_w w_1^* + q_w) \frac{r_2 + \Delta r w_1^*}{m_w w_1^{*2} + (q_w + r_2 a_{c2}) w_1^* + \frac{r_2}{bC_2}} \\
&= k + \Delta r - \frac{(m_w w_1^* + q_w)(r_2 + \Delta r w_1^*)}{m_w w_1^{*2} + (q_w + r_2 a_{c2}) w_1^* + \frac{r_2}{bC_2}} \\
&= k + \Delta r - \Delta r \frac{\frac{r_2}{aC_2}(\frac{1}{w_b w_c} - a\delta) w_1^* + (-\frac{1}{w_b} + a\delta)(w_1^* - w_a)}{\frac{r_2}{aC_2}(\frac{1}{w_b w_c}(w_1^* - w_b)(w_1^* - w_c) - a\delta(w_1^* - 1)^2)} \\
&= k + \Delta r - \Delta r (1 - w_b w_c a\delta) \frac{(w_1^* - \frac{(\frac{1}{w_b} - a\delta)}{(\frac{1}{w_b w_c} - a\delta)})(w_1^* - w_a)}{((w_1^* - w_b)(w_1^* - w_c) - w_b w_c a\delta(w_1^* - 1)^2)}.
\end{aligned}$$

$k + \Delta r$ is a step-up or step-down factor for ΔF and we find that the fixed point equation is a quartic equation. It is not immediately obvious how to solve the roots and see clearly what the solutions physically imply. Likewise, determining the number of roots between 0 and 1 is not straightforward. But from our previous working experience with the discussion of the nullclines, it is illustrative to separate the fixed point equation into $\Delta F(w_1^* - w_1^{*2})$ and $-(k_1 + k_2)w_1^* + k_2$. As shown in Fig. 2.4, the number of fixed points can be determined by the roots and concavity of ΔF when k_1 and k_2 are small.

Figure 2.4 shows a diagram with three fixed points. And Figure 2.5 shows the same picture under different conditions: In one figure the curve concaves upward, while in the other the curve concaves downward. The condition of having three fixed points can be distinguished into two types, one is S_{q-} , for which ΔF has only one root between 0 and 1, and the other is $S_{q\pm}$, which corresponds to ΔF having two roots between 0 and 1.

The denominator of ΔF has no zero point between $0 < w_1 < 1$, therefore it has no singular point. And the numerator of ΔF may have roots between $0 < w_1 < 1$. If it has roots between $0 < w_1 < 1$ and $\Delta F(w_1 = 0) < 0$, then for k_1 and k_2 small, the system has three fixed points.

The following is the simple analysis of this situation. We can set the form of the numerator of ΔF as $Mw_1^2 + Pw_1 + Q$, where

$$\begin{aligned} M &= m_w k, \\ P &= r_2(a_{c2}(k + \Delta r) - m_w) + q_w k, \\ Q &= \frac{r_2}{bC_2}(k + r_1(1 - b)). \end{aligned}$$

In S_{q-} case, we can find the relation from the diagram,

1. $\Delta F(w_1 = 0) < 0$,
2. $\Delta F(w_1 = 1) > 0$.

And for $\Delta F(w_1 = 0) = \frac{r_2}{bC_2}(k + r_1(1 - b)) < 0$, we see that it can be satisfied when $k < (b - 1)r_1$.

When

$$\begin{aligned} \Delta F(w_1 = 1) &= m_w k + (r_2(a_{c2}(k + \Delta r) - m_w) + q_w k) + \frac{r_2}{bC_2}(k + r_1(1 - b)) > 0 \\ &= (k - r_2)(m_w + q_w) + \frac{r_2}{aC_1}(k + \Delta r) > 0 \\ &= (k - r_2)\left(\frac{r_1 - \frac{r_2}{a}}{C_1}\right) + \frac{r_2}{aC_1}(k + \Delta r) > 0 \\ &= \frac{r_1}{aC_1}(ka + (1 - a)r_2), \end{aligned}$$

this condition is satisfied with $k > \frac{a-1}{a}r_2$. Therefore, in the S_{q-} case, the condition

of having three fixed points is

$$(b-1)r_1 > k > \frac{a-1}{a}r_2.$$

But for the $S_{q\pm}$ case, the situation is more complicated. Here, the conditions are

1. $\Delta F(w_1 = 0) > 0$ and $\Delta F(w_1 = 1) > 0$, when it is concave upward, and they are of opposite signs when it is concave downward;

2. the extreme value happens between 0 and 1, that is $0 < \frac{-P}{2M} < 1$;

3. $P^2 - 4MQ > 0$.

The first condition has been calculated in S_{q-} case, whereas the second condition reduces to:

(a) When $\frac{-P}{2M} > 0$, we see that P and M are of opposite signs;

(b) when $\frac{-P}{2M} < 1$, we get $2M + p > 0$ if $M > 0$, and $2M + p < 0$ if $M < 0$.

The discriminant for fixed point bifurcations

Although the fixed point formula is a quartic equation, the special case $a = b$ turns things around because then the parameter $\delta = 0$, implying

$$\Delta F = k + \Delta r - \Delta r \frac{(w_1^* - w_a)}{((w_1^* - w_b))}.$$

That is, the fixed point equation becomes a cubic one, and we can solve the bifurcation condition by considering the associated discriminant. Explicitly, we have

$$\tilde{w}_1(w_1)^3 + na_2\tilde{w}_1(w_1)^2 + na_1\tilde{w}_1(w_1) + na_0 = 0,$$

where

$$\begin{aligned} na_2 &= -\frac{(D_0 - 1)k - D_0(k_1 + k_2) + a_r}{D_0k} \\ na_1 &= -\frac{k - k_1 + (D_0 - 1)k_2 - a_r}{D_0k} \\ na_0 &= -\frac{k_2}{D_0k} \end{aligned}$$

and

$$\begin{aligned} a_r &= (a - 1)r_1 \\ D_0 &= \frac{a_r + \Delta r}{r_2}. \end{aligned}$$

Setting

$$Q = \frac{3na_1 - na_2^2}{9}, R = \frac{9na_1na_2 - 27na_0 - 2na_2^3}{54},$$

we have the discriminant expressed as

$$D = Q^3 + R^2.$$

Developing Q and R as polynomial functions of k ,

$$\begin{aligned} Q &= Q_2 k^2 + Q_1 k + Q_0 \\ R &= R_3 k^3 + R_2 k^2 + R_1 k + R_0, \end{aligned}$$

where

$$Q_2 = \frac{1}{3D_0 k^2} (-3D_0 - (D_0 - 1)^2)$$

$$Q_1 = \frac{1}{3D_0 k^2} (2(D_0 - 1)(D_0(k_1 + k_2) - a_r) + D_0(3k_1 - 3(D_0 - 1)k_2) + 3a_r)$$

$$Q_0 = \frac{1}{3D_0 k^2} (-(D_0(k_1 + k_2) - a_r)^2)$$

$$R_3 = \frac{1}{D_0 k^3} \left(\frac{D_0(D_0 - 1)}{6} + \frac{(D_0 - 1)^3}{27} \right)$$

$$R_2 = \frac{1}{D_0 k^3} \left(-\frac{D_0(D_0 - 1)}{6} \right) k_1 + \left(\frac{D_0(D_0 - 1)^2 - D_0^2}{6} + \frac{D_0^2}{2} \right) k_2 - \frac{D_0(D_0 - 1)a_r + D_0(k_1 + k_2) - a_r}{6} - \frac{(D_0 - 1)^2(D_0(k_1 + k_2) - a_r)}{9}$$

$$R_1 = \frac{1}{D_0 k^3} \left(\frac{D_0(k_1 - (D_0 - 1)k_2 + a_r)(D_0(k_1 + k_2) - a_r)}{6} + \frac{(D_0 - 1)(D_0(k_1 + k_2) - a_r)^2}{9} \right)$$

$$R_0 = \frac{1}{D_0 k^3} \left(-\frac{(D_0(k_1 + k_2) - a_r)^3}{27} \right),$$

and likewise developing D into a polynomial function of k

$$D = D_6 k^6 + D_5 k^5 + D_4 k^4 + D_3 k^3 + D_2 k^2 + D_1 k + D_0,$$

where

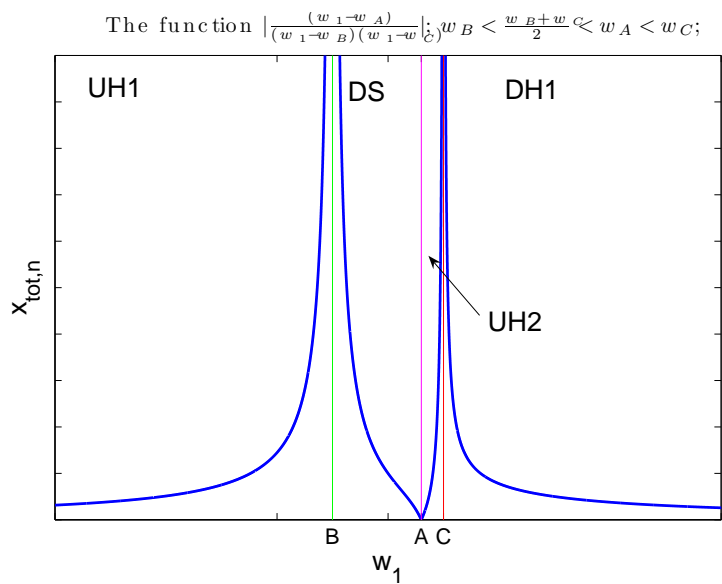
$$\begin{aligned}
D_6 &= Q_2^3 + R_3^2 \\
D_5 &= 3Q_2^2Q_1 + 2R_3R_2 \\
D_4 &= 3Q_2Q_1^2 + 3Q_2^2Q_0 + 2R_3R_1 + R_2^2 \\
D_3 &= Q_1^3 + 6Q_2Q_1Q_0 + 2R_3R_0 + 2R_2R_1 \\
D_2 &= 3Q_2Q_0^2 + 3Q_1^2Q_0 + 2R_2R_0 + R_1^2 \\
D_1 &= 3Q_1Q_0^2 + 2R_1R_0 = 0 \\
D_0 &= Q_0^3 + R_0^2 = 0,
\end{aligned}$$

we can analyze the situation, at least in principle.

When D_1 and D_0 are zero, $\frac{D}{k^2}$ becomes a quartic equation and $D = 0$ can be constructed by four surfaces. The four surfaces divide the space into different regions, with two satisfying the condition $D > 0$. but only the region contains $(b - 1)r_1 > k > \frac{a-1}{a}r_2$. when $k_1 = k_2 = 0$ is the real bifurcation zone.

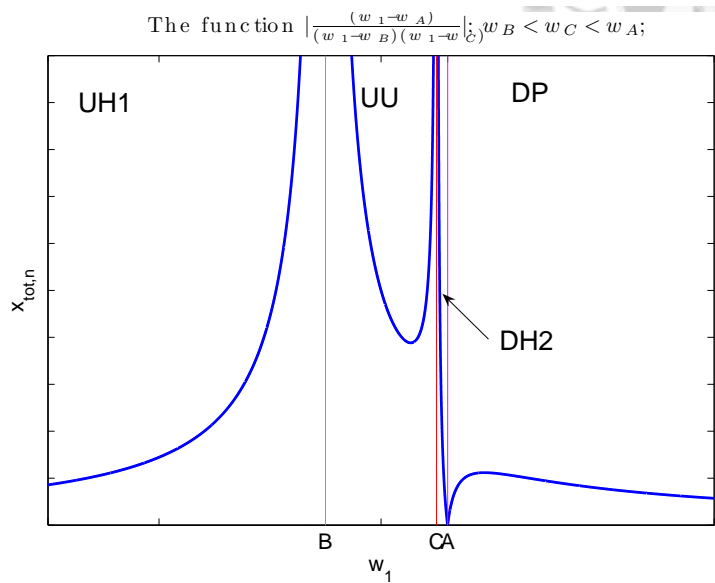
Figure 2.1: The types of $\tilde{x}_t(w_1)$.

(c)



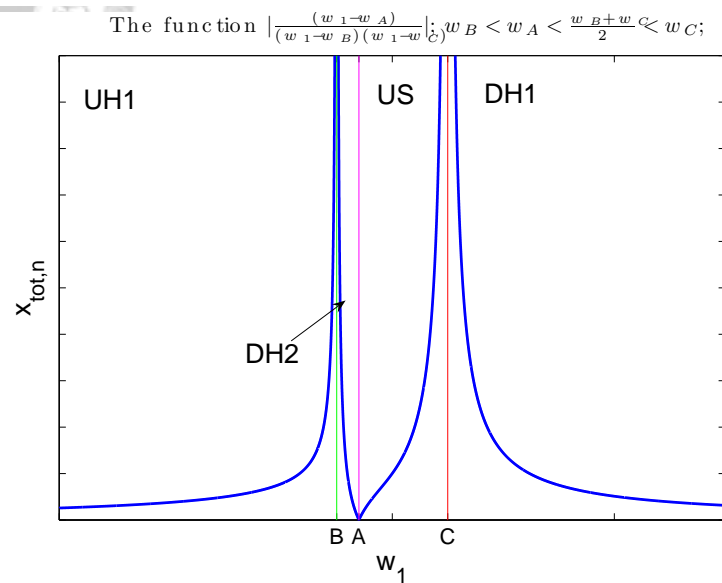
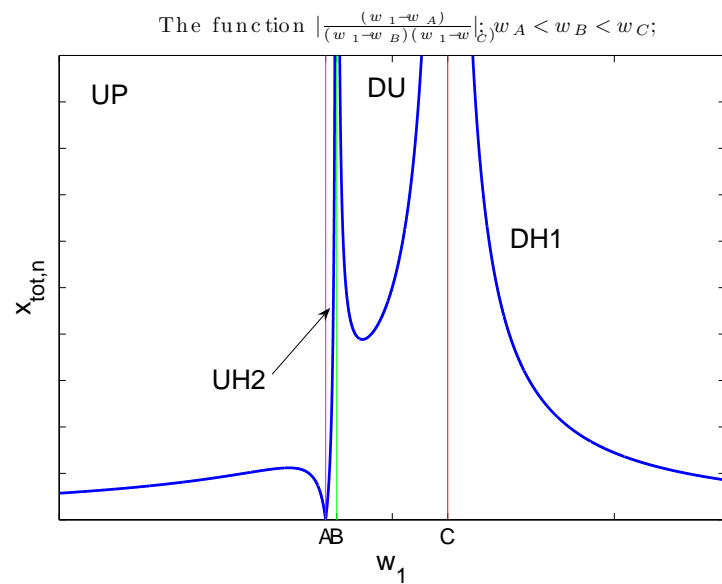
35

(d)



(a)

(b)



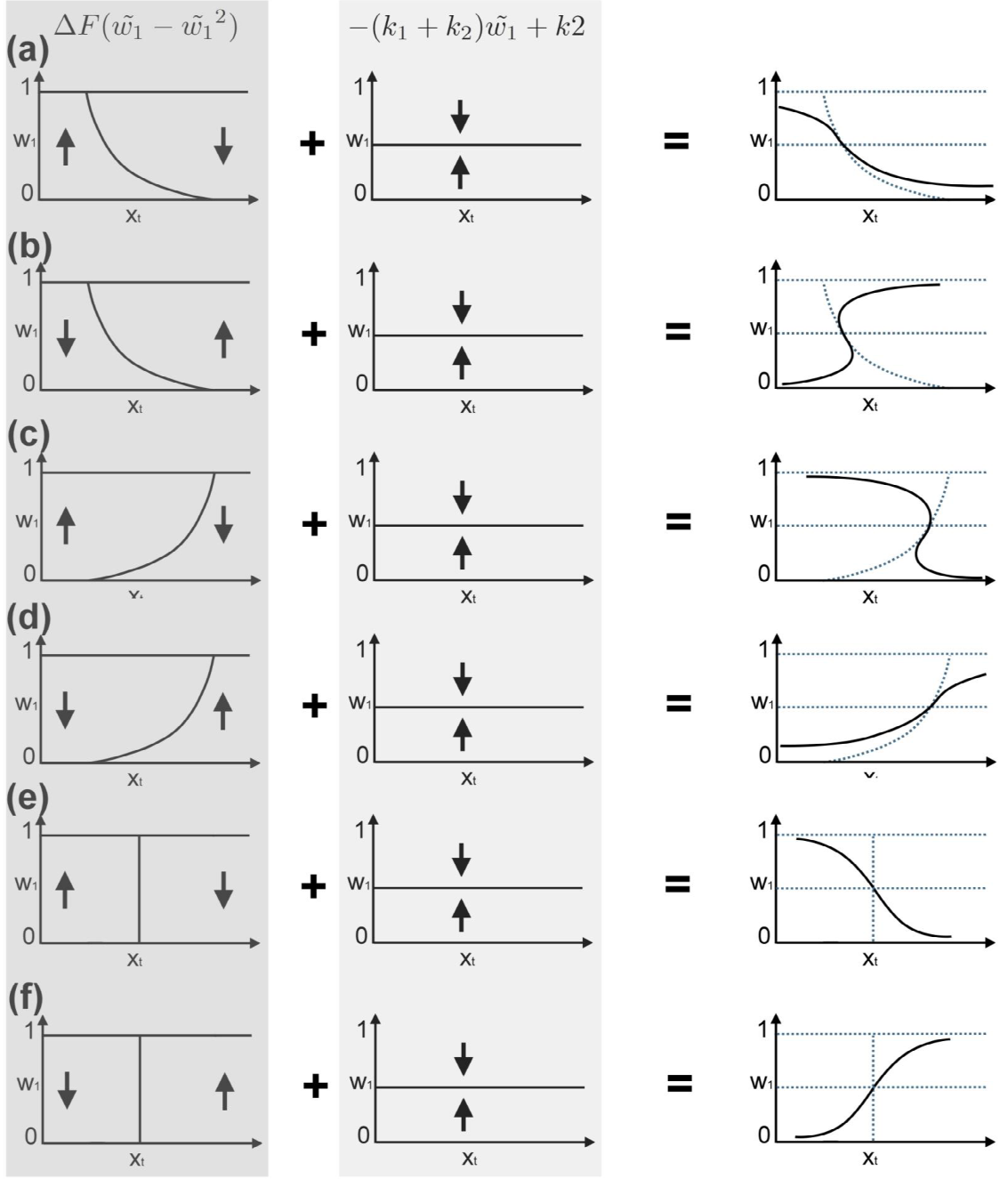
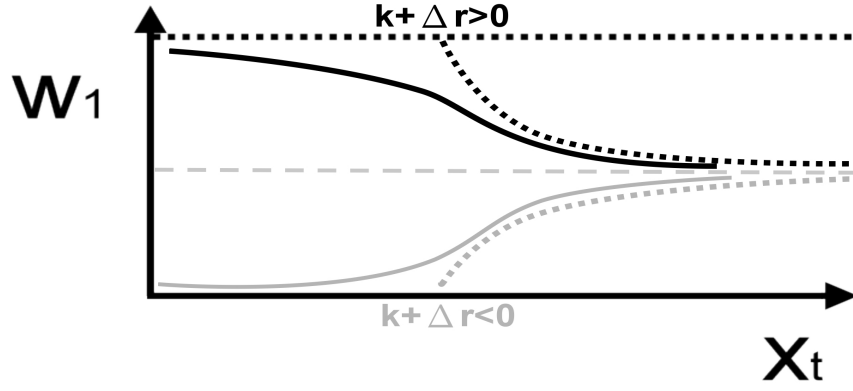


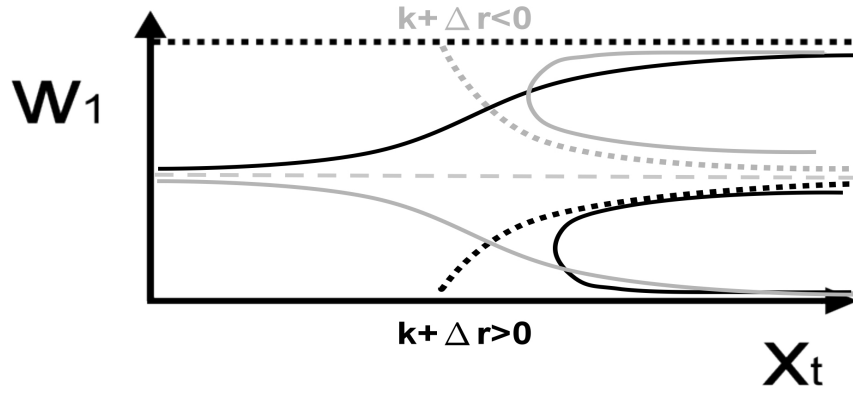
Figure 2.2: The diagram of $\tilde{w}_1(x_t)$ curve without a singular point. (a) and (b) are at the condition $end\ point|_{w_1=0} < end\ point|_{w_1=1}$. When $\Delta F > 0$, the curve in (a) is S type, and when $\Delta F < 0$, the curve in (b) is Z type. (c) and (d) are at the condition $end\ point|_{w_1=0} > end\ point|_{w_1=1}$. When $\Delta F > 0$, the curve in (c) is Z type, and when $\Delta F < 0$, the curve in (d) is S type. (e) and (f) are at the condition $end\ point|_{w_1=0} = end\ point|_{w_1=1}$. They are all S type.

has root, $m_w > 0$; $q_w < 0$



(a)

has root, $m_w < 0$; $q_w > 0$



(b)

Figure 2.3: The diagram of $\tilde{w}_1(w_1)$ with a singular point. (a): When $m_w > 0$ and $q_w < 0$, at this condition $\tilde{w}_1(w_1)$ is s band type curve. (b): When $m_w < 0$ and $q_w > 0$, at this condition $\tilde{w}_1(w_1)$ is SC and CS type curve.

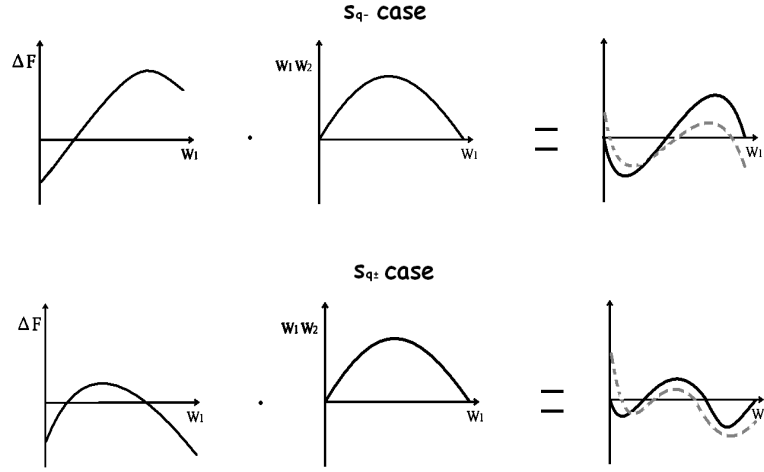


Figure 2.4: The diagram of the three fixed point conditions. The left diagram is the effect of ΔF , and the middle diagram is the effect of $(w_1 - w_1^2)$, the solid line of the right diagram is the effect of $\Delta F(w_1 - w_1^2)$, and the dash line is the total effect of \dot{w}_1 . We can see there are two types of three fixed point condition: One is S_{q-} , which ΔF has only one root between 0 and 1, and the other is $S_{q\pm}$, which ΔF has two roots between 0 and 1.

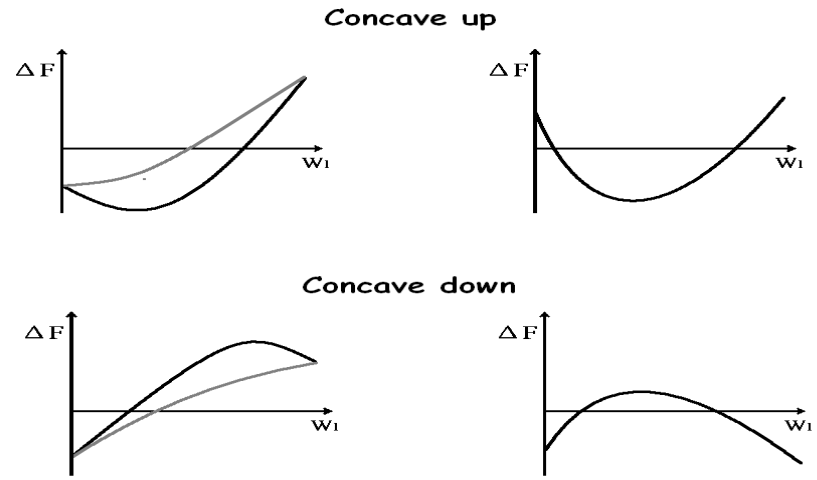


Figure 2.5: The diagram of multiple fixed point condition of ΔF . When it has root between $0 < w_1 < 1$ and $\Delta F(w_1 = 0) < 0$, the system would have three fixed points. This diagram shows the case of ΔF which satisfies these conditions.

2.4.5 The stability and possible spiral behavior in general logistic growth and autocrine transition model

For the general logistic growth and autocrine transition model we have

$$\begin{aligned}\frac{\partial f_1}{\partial x_1} &= -\frac{1}{C_1} \\ \frac{\partial f_1}{\partial x_2} &= -\frac{1}{C_2} \\ \frac{\partial f_2}{\partial x_1} &= -\frac{1}{aC_1} \\ \frac{\partial f_2}{\partial x_2} &= -\frac{1}{bC_2} = -\frac{1}{aC_2} + \frac{\delta}{C_2}.\end{aligned}$$

Substituting these terms into the spiral formula in the general model, we obtain

$$\begin{aligned}\lambda_b &= (J_a + J_d)^2 - 4\text{Det}[J] \\ &= \left(\frac{r_1x_1}{C_1} - \frac{r_2x_2}{aC_2} + r_2x_2\frac{\delta}{C_2}\right)^2 + \frac{4r_1r_2x_1x_2}{aC_1C_2} + \left(k_1\frac{w_1}{w_2} + k_2\frac{w_2}{w_1}\right)^2 \\ &\quad + 2\left(\frac{r_1x_1}{C_1} + \frac{r_2x_2}{aC_2} - r_2x_2\frac{\delta}{C_2}\right)\left(k_1\frac{w_1}{w_2} + k_2\frac{w_2}{w_1}\right) \\ &\quad + r_1x_1\left(\frac{w_1}{w_2}\frac{1}{C_1} + \frac{1}{C_2}\right)(k_1 - kw_2^2) \\ &\quad + \frac{r_2x_2}{a}\left(\frac{w_2}{w_1}\left(\frac{1}{C_2} - a\frac{\delta}{C_2}\right) + \frac{1}{C_1}\right)(k_2 + kw_1^2) \\ &= \lambda_{b,\delta=0} + r_2x_2\frac{\delta}{C_2}\left(r_2x_2\frac{\delta}{C_2} + 2\left(\frac{r_1x_1}{C_1} - \frac{r_2x_2}{aC_2} - \left(k_1\frac{x_1}{x_2} + k_2\frac{x_2}{x_1}\right) - \frac{w_2}{w_1}(k_2 + kw_1^2)\right)\right).\end{aligned}$$

Here, λ_b of the most general case (labelled as Case LH-D in the following) is expressed as the λ_b of the more restricted case (labelled LH-C, with $a = b$) plus some terms involving δ . Because the additional terms form a quadratic function of δ which concaves up, it seems that the system would have no spiral behavior when δ is large.

2.5 The classification of logistic growth model.

Here, we classify five types of the logistic growth model. They are:

1. LH-0

The basic model. f_i is the same and they are depend on the x_t with a suppressing capacity C .

$$\begin{cases} f_1 = (1 - \frac{x_t}{C}) \\ f_2 = (1 - \frac{x_t}{C}) \end{cases} \quad (2.17)$$

2. LH-A

f_i 's are the same, but the suppressing effects from x_1 and x_2 are different. The suppressing capacity of x_1 is C_1 and that of x_2 is C_2 .

$$\begin{cases} f_1 = (1 - \frac{x_1}{C_1} - \frac{x_2}{C_2}) \\ f_2 = (1 - \frac{x_1}{C_1} - \frac{x_2}{C_2}) \end{cases} \quad (2.18)$$

3. LH-B

f_i 's are not the same, but the suppressing effects from x_1 and x_2 are the same. The suppressing capacity in x_1 is C and in x_2 is aC .

$$\begin{cases} f_1 = (1 - \frac{x_t}{C}) \\ f_2 = (1 - \frac{x_t}{aC}) \end{cases} \quad (2.19)$$

4. LH-C

x_1 has a self-suppressing capacity C_1 and a competing suppressing capacity C_2 of x_2 on x_1 . To show the heterogeneity of these two states, a heterogeneity factor a is introduced in the capacity of x_2 . Thus, the self-suppressing capacity of x_2 is aC_2 and the competing suppressing capacity of x_1 on x_2 is aC_1 .

$$\begin{cases} f_1 = (1 - \frac{x_1}{C_1} - \frac{x_2}{C_2}) \\ f_2 = (1 - \frac{1}{a}(\frac{x_1}{C_1} - \frac{x_2}{C_2})) \end{cases} \quad (2.20)$$

5. LH-D

The most general case. The self-suppressing capacity and the competing suppressing capacity in x_1 or x_2 are all independent.

$$\begin{cases} f_1 = (1 - \frac{x_1}{C_1} - \frac{x_2}{C_2}) \\ f_2 = (1 - \frac{x_1}{aC_1} - \frac{x_2}{bC_2}) \end{cases} \quad (2.21)$$

2.6 LH-0 model

When $C_1 = C_2$ and $a = b = 1$, the growth is a simple logistical growth for x_t .

$$f_1 = f_2 = (1 - \frac{x_t}{C})$$

$$\begin{cases} \dot{x}_1 = r_1 x_1 (1 - \frac{x_t}{C}) - k_1 x_1 + k_2 x_2 + k \frac{x_2 x_1}{x_1 + x_2} \\ \dot{x}_2 = r_2 x_2 (1 - \frac{x_t}{C}) + k_1 x_1 - k_2 x_2 - k \frac{x_2 x_1}{x_1 + x_2} \end{cases} \quad (2.22)$$

And the auxiliary parameters are

$$a_{c1} = \frac{1}{C_{11}} - \frac{1}{C_{12}} = 0 ,$$

$$\begin{aligned}
a_{c2} &= \frac{1}{C_{21}} - \frac{1}{C_{22}} = 0, \\
m_w &= r_1 a_{c1} - r_2 a_{c2} = 0, \\
q_w &= \frac{r_1}{C_{12}} - \frac{r_2}{C_{22}} = \frac{\Delta r}{C}, \\
m_w + q_w &= q_w = \frac{\Delta r}{C}.
\end{aligned}$$

Substituting this into the general model equations in the x_t and w_1 space, we obtain

$$\begin{cases} \dot{x}_t = x_t(r_2 + \Delta r w_1)(1 - \frac{x_t}{C}) \\ \dot{w}_1 = (k + \Delta r(1 - \frac{x_t}{C}))(w_1 - w_1^2) - (k_1 + k_2)w_1 + k_2. \end{cases}$$

2.6.1 The exact solution when $r_1 = r_2$

When $r_1 = r_2 = r$, the two formulas can be separated into two independent ones. For instance, \dot{x}_t is a logistical growth differential equation and \dot{w}_1 has the same form of exponential growth and autocrine transition model as $r_1 = r_2$. The exact solution of LH-0 model can be solved easily.

$$\begin{cases} \dot{x}_t = r x_t(1 - \frac{x_t}{C}) \\ \dot{w}_1 = k(w_1 - w_1^2) - (k_1 + k_2)w_1 + k_2 \end{cases}$$

Exact solution of x_t

The evolution equation of x_t is the logistic equation, and the exact solution is

$$x_t = x_t(0) \frac{C e^{rt}}{C + x_t(0)(e^{rt} - 1)}.$$

It has two fixed points at $x_t = 0, C$, and an inflection point at $x_t = \frac{C}{2}$.

Exact solution of w_1

Since \dot{w}_1 of LH-0 is the same as the exponential growth and autocrine transition model, $w_1(t)$ should be the same.

$$w_1(\tau) = \begin{cases} w_1(\tau) = \frac{1 - \frac{k_1}{k} - \frac{k_2}{k}}{2} + \sqrt{\frac{C}{k}} \tanh(\tau) & \text{if } \frac{1 - w_1'(0)}{1 + w_1'(0)} > 0 \\ w_1(\tau) = \frac{1 - \frac{k_1}{k} - \frac{k_2}{k}}{2} + \sqrt{\frac{C}{k}} \coth(\tau) & \text{if } \frac{1 - w_1'(0)}{1 + w_1'(0)} < 0 \end{cases} \quad (2.23)$$

2.6.2 The nullclines

Plugging the auxiliary parameters of LH-0 into the general form of \tilde{x}_t , the \tilde{x}_t in LH-0 is

$$\tilde{x}_t = \frac{r_2 + \Delta r w_1}{\frac{r_2 + \Delta r}{C}} = C.$$

Plugging the auxiliary parameters of LH-0 into the general form of \tilde{w}_1 , the \tilde{w}_1 in LH-0 is

$$0 = (k + \Delta r(1 - \frac{\tilde{x}_t}{C}))(\tilde{w}_1 - \tilde{w}_1^2) - (k_1 + k_2)\tilde{w}_1 + k_2.$$

We can solve this equation to find \tilde{w}_1 :

$$\tilde{w}_1 = \frac{((k + \Delta r(1 - \frac{x_t}{C})) - (k_1 + k_2)) + \sqrt{((k + \Delta r(1 - \frac{x_t}{C})) - (k_1 + k_2))^2 + 4(k + \Delta r(1 - \frac{x_t}{C}))k_2}}{2(k + \Delta r(1 - \frac{x_t}{C}))}.$$

Because \tilde{x}_t is a constant, the two end points have the same value. Therefor, the nullcline must be an S type curve.

When $k + \Delta r > 0$, it would be an S type curve with the head facing left, and when $k + \Delta r < 0$ it would be an S type curve with the head facing right.

2.6.3 The fixed point condition

The fixed point is trivially

$$x_t^* = C, w_1^* = \frac{(k - (k_1 + k_2)) + \sqrt{(k - (k_1 + k_2))^2 + 4kk_2}}{2k}.$$

2.6.4 The stability of the fixed point

In this case it has only one fixed point, and we know $f_1 = f_2 = 1 - \frac{x_t}{C}$ with $\frac{\partial f_1}{\partial x_1} = \frac{\partial f_2}{\partial x_2} = -\frac{1}{C} < 0$. According to the theory for the general model, $J_a + J_d < 0$ and the fixed point must be a sink.

2.6.5 The phase portraits of LH-0

Please see Appendix B.1.

2.7 LH-A model

When $a = b = 1$, the growth forms of x_1 and x_2 are the same, but the suppressing effects from x_1 and x_2 are different. The suppressing capacity of x_1 is C_1 and that of x_2 is C_2 . We abbreviate it as the LH-A model.

$$f_1 = f_2 = 1 - \frac{x_1}{C_1} - \frac{x_2}{C_2},$$

$$\begin{cases} \dot{x}_1 = r_1 x_1 (1 - \frac{x_1}{C_1} - \frac{x_2}{C_2}) - k_1 x_1 + k_2 x_2 + k \frac{x_2 x_1}{x_1 + x_2} \\ \dot{x}_2 = r_2 x_2 (1 - \frac{x_1}{C_1} - \frac{x_2}{C_2}) + k_1 x_1 - k_2 x_2 - k \frac{x_2 x_1}{x_1 + x_2}. \end{cases} \quad (2.24)$$

And the auxiliary parameters are, respectively,

$$a_{c1} = \frac{1}{C_{11}} - \frac{1}{C_{12}} = \frac{1}{C_1} - \frac{1}{C_2} = a_c$$

$$a_{c2} = \frac{1}{C_{21}} - \frac{1}{C_{22}} = \frac{1}{C_1} - \frac{1}{C_2} = a_c$$

$$m_w = r_1 a_{c1} - r_2 a_{c2} = \Delta r a_c$$

$$q_w = \frac{r_1}{C_{12}} - \frac{r_2}{C_{22}} = \frac{\Delta r}{C_2}$$

$$m_w + q_w = \Delta r a_c + \frac{\Delta r}{C_2} = \frac{\Delta r}{C_1}.$$

The rate equations in x_t and w_1 space read

$$\begin{cases} \dot{x}_t = x_t (r_2 + \Delta r w_1) (1 - (a_c w_1 - \frac{1}{C_2}) x_t) \\ \dot{w}_1 = (k + \Delta r (1 - (a_c w_1 - \frac{1}{C_2}) x_t)) (w_1 - w_1^2) - (k_1 + k_2) w_1 + k_2. \end{cases}$$

2.7.1 The nullclines

Substituting the secondary parameters of LH-A into the general form of \tilde{x}_t , the \tilde{x}_t in LH-A is

$$\begin{aligned}
\tilde{x}_t &= \frac{r_2 + \Delta r w_1}{m_w w_1^2 + (q_w + r_2 a_c) w_1 + \frac{r_2}{C_{22}}} \\
&= \frac{r_2 + \Delta r w_1}{\Delta r a_c w_1^2 + (\frac{\Delta r}{C_2} + r_2 a_c) w_1 + \frac{r_2}{C_2}} \\
&= \frac{r_2 + \Delta r w_1}{(r_2 + \Delta r w_1)(a_c w_1 + \frac{1}{C_2})} \\
&= \frac{1}{a_c w_1 + \frac{1}{C_2}}.
\end{aligned}$$

It is the reciprocal of a linear function, and the two end points are $\tilde{x}_t(w_1 = 0) = C_2$ and $\tilde{x}_t(w_1 = 1) = C_1$.

Next, substituting the secondary parameters of LH-A into the general form of \tilde{w}_1 , the \tilde{w}_1 in LH-A is

$$\begin{aligned}
0 &= (\Delta r(1 - \frac{1}{\Delta r}(m_w w_1 + q_w)x_t) + k)(\tilde{w}_1(w_1) - \tilde{w}_1(w_1)^2) - (k_1 + k_2)\tilde{w}_1(w_1) + k_2 \\
&= (\Delta r(1 - \frac{1}{\Delta r}(\Delta r a_c w_1 + \frac{\Delta r}{C_2})x_t) + k)(\tilde{w}_1(w_1) - \tilde{w}_1(w_1)^2) - (k_1 + k_2)\tilde{w}_1(w_1) + k_2 \\
&= (\Delta r(1 - (a_c w_1 + \frac{1}{C_2})x_t) + k)(\tilde{w}_1(w_1) - \tilde{w}_1(w_1)^2) - (k_1 + k_2)\tilde{w}_1(w_1) + k_2.
\end{aligned}$$

The two endpoints of the nonlinear term are $end\ point|_{w_1=0} = \frac{k+\Delta r}{\Delta r}C_2$ and $end\ point|_{w_1=1} = \frac{k+\Delta r}{\Delta r}C_1$. When $C_1 > C_2$, $end\ point|_{w_1=1} > end\ point|_{w_1=0}$; and when $C_1 < C_2$, $end\ point|_{w_1=1} < end\ point|_{w_1=0}$.

And $\Delta F(x_t = 0) = k + \Delta r$, the sign could be determined by k and Δr . Therefore, \tilde{w}_1 in LH-A could be S type curve and Z type curve.

When $k + \Delta r > 0$, $C_1 < C_2$ and it is S type curve with the head facing left.

When $k + \Delta r < 0$, $C_1 < C_2$ and it is Z type curve with the head facing right.

When $k + \Delta r > 0$, $C_1 > C_2$ and it is Z type curve with the head facing left.

When $k + \Delta r < 0$, $C_1 > C_2$ and it is S type curve with the head facing right.

2.7.2 The fixed point condition

In LH-A, if we ignore the transition term $\dot{w}_1|_T$, then \tilde{w}_1 would have to satisfy the condition $\Delta f = (1 - (a_c w_1 + \frac{1}{C_2})x_t) = 0$. It is the same with the condition of \tilde{x}_t . Thus \tilde{w}_1 and \tilde{x}_t coincide.

Because the $\dot{w}_1|_T$ has a zero point at

$$w_1 = \frac{k - (k_1 + k_2) - \frac{k}{|k|} \sqrt{(k - (k_1 + k_2))^2 - 4kk_2}}{2k},$$

we see that if the $\dot{w}_1|_T$ term is included then \tilde{w}_1 and \tilde{x}_t would cross and a fixed point is formed due to the presence of the transition term.

Therefore, in LH-A, it has only one fixed point at (x_t^*, w_1^*) , where

$$w_1^* = \frac{k - (k_1 + k_2) - \frac{k}{|k|} \sqrt{(k - (k_1 + k_2))^2 - 4kk_2}}{2k}$$

and

$$x_t^* = \frac{1}{a_c w_1^* + \frac{1}{C_2}}.$$

2.7.3 The stability of fixed point

In this case it has only one fixed point and we know $f_1 = f_2 = 1 - \frac{x_1}{C_1} - \frac{x_2}{C_2}$, so that

$$\frac{\partial f_1}{\partial x_1} = -\frac{1}{C_1} < 0$$

$$\frac{\partial f_2}{\partial x_2} = -\frac{1}{C_2} < 0.$$

According to the general theory, $J_a + J_d < 0$, the fixed point must be a sink.

To test the spiral behavior, substituting these terms into the general model of λ_b , then we get

$$\begin{aligned}
\lambda_b &= (J_a + J_d)^2 - 4\text{Det}[J] \\
&= \left(\left(\frac{r_1 x_1}{C_1} + \frac{r_2 x_2}{C_2} \right) + \left(k_1 \frac{w_1}{w_2} + k_2 \frac{w_2}{w_1} \right) \right)^2 \\
&\quad + \frac{r_1 x_1}{C_1} \left(\frac{w_1}{w_2} + \frac{C_1}{C_2} \right) (k_1 - k w_2^2) + \frac{r_2 x_2}{C_2} \left(\frac{w_2}{w_1} + \frac{C_2}{C_1} \right) (k_2 + k w_1^2) \\
&= \left(\left(\frac{r_1 x_1}{C_1} + \frac{r_2 x_2}{C_2} \right) + \left(k_1 \frac{w_1}{w_2} + k_2 \frac{w_2}{w_1} \right) \right)^2 \\
&\quad - k x_t \left(\left(\frac{r_1}{C_1} \frac{w_1^2}{w_2} + \frac{C_1}{C_2} \right) (w_2^2 - \frac{k_1}{k}) - \left(\frac{r_2}{C_2} \frac{w_2^2}{w_1} + \frac{C_2}{C_1} \right) (w_1^2 + \frac{k_2}{k}) \right).
\end{aligned}$$

The term λ_b has three parts, $\left(\left(\frac{r_1 x_1}{C_1} + \frac{r_2 x_2}{C_2} \right) + \left(k_1 \frac{w_1}{w_2} + k_2 \frac{w_2}{w_1} \right) \right)^2$, $\left(\frac{w_1}{w_2} + \frac{C_1}{C_2} \right) (k_1 - k w_2^2)$ and $+\frac{r_2 x_2}{C_2} \left(\frac{w_2}{w_1} + \frac{C_2}{C_1} \right) (k_2 + k w_1^2)$.

The first term is a complete square so that it is always greater than 0. The second term is negative if $k > 0$ and $|k|$ is large. And the third term would be negative when $k < 0$ and $|k|$ is large. Therefore, the spiral behavior could be present when the last two terms are negative and large.

2.7.4 The phase portraits of LH-A

Please see Appendix B.2 .

2.8 LH-B model

When $a = b \neq 1$ and $C_1 = C_2 = C$, the suppressing capacity in x_1 is C , and taht in x_2 is aC . It is abbreviated as LH-B. With

$$\begin{aligned} f_1 &= 1 - \frac{x_t}{C} \\ f_2 &= 1 - \frac{x_t}{aC}, \end{aligned}$$

we have

$$\begin{cases} \dot{x}_1 = r_1 x_1 (1 - \frac{x_t}{C}) - k_1 x_1 + k_2 x_2 + k \frac{x_2 x_1}{x_1 + x_2} \\ \dot{x}_2 = r_2 x_2 (1 - \frac{x_t}{aC}) + k_1 x_1 - k_2 x_2 - k \frac{x_2 x_1}{x_1 + x_2} \end{cases} \quad (2.25)$$

and

$$a_{c1} = \frac{1}{C_{11}} - \frac{1}{C_{12}} = 0$$

$$a_{c2} = \frac{1}{C_{21}} - \frac{1}{C_{22}} = 0$$

$$m_w = r_1 a_{c1} - r_2 a_{c2} = 0$$

$$q_w = \frac{r_1}{C_{12}} - \frac{r_2}{C_{22}} = \frac{r_2}{aC} (a \frac{r_1}{r_2} - 1)$$

$$m_w + q_w = \frac{r_2}{aC} (a \frac{r_1}{r_2} - 1).$$

In the x_t and w_1 space, then,

$$\begin{cases} \dot{x}_t = x_t (r_2 + \Delta r w_1) (1 - (\frac{1}{a} \frac{r_2 + (ar_1 - r_2)}{r_2 + \Delta r w_1}) \frac{x_t}{C}) \\ \dot{w}_1 = (k + \Delta r - \frac{1}{a} (ar_1 - r_2) \frac{x_t}{C}) (w_1 - w_1^2) - (k_1 + k_2) w_1 + k_2 \end{cases}$$

2.8.1 The nullclines

Plugging the auxiliary parameters of LH-B into the general form of \tilde{x}_t , the \tilde{x}_t in LH-B is

$$\begin{aligned}
\tilde{x}_t &= \frac{r_2 + \Delta r w_1}{m_w w_1^2 + (q_w + r_2 a_{c2}) w_1 + \frac{r_2}{C_{22}}} \\
&= \frac{r_2 + \Delta r w_1}{(\frac{r_2}{aC} (a \frac{r_1}{r_2} - 1)) w_1 + \frac{r_2}{aC}} \\
&= aC \frac{r_2 + \Delta r w_1}{((ar_1 - r_2)) w_1 + r_2} \\
&= aC \frac{1 + (\frac{r_1}{r_2} - 1) w_1}{(a \frac{r_1}{r_2} - 1) w_1 + 1} \\
&= aC \frac{1 - \frac{r_1}{r_2} w_1 - \frac{1}{1 - \frac{r_1}{r_2}}}{1 - a \frac{r_1}{r_2} w_1 - \frac{1}{1 - a \frac{r_1}{r_2}}} \\
&= \frac{aC w_B}{w_A} \frac{w_1 - w_A}{w_1 - w_B},
\end{aligned}$$

where $w_A = \frac{1}{1 - \frac{r_1}{r_2}}$ and $w_B = \frac{1}{1 - a \frac{r_1}{r_2}}$.

The form of $\frac{w_1 - w_A}{w_1 - w_B}$ behaves like $\frac{w_1 - w_A}{(w_1 - w_B)(w_1 - w_C)}$ as $w_C \rightarrow \infty$, because $m_w = \Delta r (\frac{1}{C_1} - \frac{1}{C_2}) = 0$ and the denominator of \tilde{x}_t has only one root.

According to Fig. 2.1, we see that the $\tilde{x}_t(w_1)$ of LH-B could assume the following forms:

1. DU type : As $w_A < w_B < 0 < 1 < w_C$ and $w_C \rightarrow \infty$, the U curve is hard to show. This happens when $r_1 > r_2$ and $\frac{r_2}{r_1} < a < 1$.

2. UH1 type: As $1 < w_B < w_A$, that is, when $r_1 < r_2$ and $1 < a < \frac{r_2}{r_1}$ the nullcline is UH1 type, and the form is more obvious when $\frac{r_1}{r_2} \rightarrow 0$.

3. UH2 type: As $w_A < 0 < 1 < w_B$, that is, when $r_1 > r_2$ and $ar_1 < r_2$, the nullcline is UH2 type and the form is more obvious when $\frac{r_1}{r_2} \rightarrow \infty$ and $\frac{r_1}{r_2} \rightarrow a$.

4. US type: As $w_B < w_A < 0 < \frac{w_B + w_C}{2}$ and $w_C \rightarrow \infty$, the S type is not easily shown. The form is assumed when $r_1 \gg r_2$ and $\frac{r_2}{r_1} < a < 1$.

5. UP type: As $1 < w_A < w_B$, that is, $r_1 < r_2$, $ar_1 < r_2$, and $a > 1$, the nullcline is UP type and the form becomes more obvious when $\frac{r_1}{r_2} \rightarrow 0$.

Next, substituting the auxiliary parameters of LH-B into the general form of \tilde{w}_1 , the \tilde{w}_1 in LH-B is

$$\begin{aligned} 0 &= (\Delta r - (m_w w_1 + q_w) x_t + k)(\tilde{w}_1 - \tilde{w}_1^2) - (k_1 + k_2) \tilde{w}_1 + k_2 \\ &= (\Delta r - (\frac{1}{a}(ar_1 - r_2)) \frac{x_t}{C} + k)(\tilde{w}_1 - \tilde{w}_1^2) - (k_1 + k_2) \tilde{w}_1 + k_2. \end{aligned}$$

The two endpoints of the growth term are, $end\ point|_{w_1=0} = end\ point|_{w_1=1} = \frac{1}{a} \frac{k+\Delta r}{ar_1-r_2} C_2$. Because the two end points are the same, $\tilde{w}_1(x_t)$ must be an S type curve. And when $k + \Delta r > 0$, it will have its head facing left. But when $k + \Delta r < 0$, the opposite is true.

2.8.2 The fixed point condition

The general fixed point formula is

$$0 = (\Delta r - (m_w w_1^* + q_w) x_t^* + k)(w_1^* - w_1^{*2}) - (k_1 + k_2) w_1^* + k_2,$$

where $x_t^* = \frac{aCw_B}{w_A} \frac{w_1 - w_A}{w_1 - w_B}$. Therefore, in LH-B

$$\begin{aligned} 0 &= (k + \Delta r - (m_w w_1^* + q_w) x_t^*)(w_1^* - w_1^{*2}) - (k_1 + k_2) w_1^* + k_2 \\ &= (k + \Delta r - (\frac{1}{a}(ar_1 - r_2)) \frac{x_t^*}{C})(w_1^* - w_1^{*2}) - (k_1 + k_2) w_1^* + k_2 \\ &= (k + \Delta r + (\frac{r_2}{aw_B} \frac{x_t^*}{C}))(w_1^* - w_1^{*2}) - (k_1 + k_2) w_1^* + k_2 \\ &= (k + \Delta r - \Delta r \frac{w_1 - w_A}{w_1 - w_B})(w_1^* - w_1^{*2}) - (k_1 + k_2) w_1^* + k_2. \end{aligned}$$

It is a cubic equation and there are three roots w_1^* . We therefore expect three fixed points.

Because the bifurcation condition is S_{q-} condition in the general model when $m_w = 0$, we see that there are three fixed points if k_1 and k_2 could be ignored. Also, k must lie between $(a - 1)r_1$ and $\frac{a-1}{a}r_2$.

2.8.3 The stability of fixed point

$$f_1 = 1 - \frac{x_t}{C}$$

$$f_2 = 1 - \frac{x_t}{aC}$$

$$\frac{\partial f_1}{\partial x_1} = -\frac{1}{C} < 0$$

$$\frac{\partial f_2}{\partial x_2} = -\frac{1}{aC} < 0$$

So, with $J_a + J_d < 0$, the general theory says the fixed point must be a sink or a saddle point.

In LH-B, three fixed points can co-exist and it is reasonable to expect it to possess two basins, that is, two sinks near each sides of w_1 and a saddle point in the middle of w_1 .

2.8.4 The phase portraits of LH-B

Please see Appendix B.3.

2.9 LH-C model.

When $a = b \neq 1$ and $C_1 \neq C_2$, the growth becomes a logistic growth form with different capacity of x_1 and x_2 . Also, x_1 has a self suppressing capacity C_1 and a competing suppressing capacity C_2 of x_2 on x_1 . To show the heterogeneity of these two states, a heterogeneity factor a is introduced in the capacity of x_2 . Thus, the self-suppressing capacity of x_2 is aC_2 and the competing suppressing capacity of x_1

on x_2 is aC_1 . It is abbreviated as LH-C. With $f_1 = 1 - \frac{x_1}{C_1} - \frac{x_2}{C_2}$ and $f_2 = 1 - \frac{x_1}{aC_1} - \frac{x_2}{aC_2}$,

we have

$$\begin{cases} \dot{x}_1 = r_1 x_1 (1 - \frac{x_1}{C_1} - \frac{x_2}{C_2}) - k_1 x_1 + k_2 x_2 + k \frac{x_2 x_1}{x_1 + x_2} \\ \dot{x}_2 = r_2 x_2 (1 - \frac{x_1}{aC_1} - \frac{x_2}{aC_2}) + k_1 x_1 - k_2 x_2 - k \frac{x_2 x_1}{x_1 + x_2} \end{cases} \quad (2.26)$$

And the auxiliary parameters are

$$a_{c1} = \frac{1}{C_{11}} - \frac{1}{C_{12}} = a_c$$

$$a_{c2} = \frac{1}{C_{21}} - \frac{1}{C_{22}} = \frac{1}{a} a_c$$

$$m_w = r_1 a_{c1} - r_2 a_{c2} = \frac{1}{a} (ar_1 - r_2) a_c$$

$$q_w = \frac{r_1}{C_{12}} - \frac{r_2}{C_{22}} = \frac{1}{a} (ar_1 - r_2) \frac{1}{C_2}$$

$$m_w + q_w = \frac{r_2}{aC} (a \frac{r_1}{r_2} - 1) = \frac{1}{a} (ar_1 - r_2) (a_c + \frac{1}{C_2}).$$

In the x_t and w_1 space,

$$\begin{cases} \dot{x}_t = x_t (r_2 + \Delta r w_1) (1 - (\frac{1}{a} \frac{r_2 + (ar_1 - r_2) w_1}{r_2 + \Delta r w_1}) (a_c w_1 + \frac{1}{C_2}) x_t) \\ \dot{w}_1 = (k + \Delta r - \frac{1}{a} (ar_1 - r_2) (a_c w_1 + \frac{1}{C_2}) x_t) (w_1 - w_1^2) - (k_1 + k_2) w_1 + k_2 \end{cases}$$

2.9.1 The nullclines

Substituting the auxiliary parameters of LH-C into the general form of \tilde{x}_t , the \tilde{x}_t in LH-C is

$$\begin{aligned}
\tilde{x}_t &= \frac{r_2 + \Delta r w_1}{m_w w_1^2 + (q_w + r_2 a_{c2}) w_1 + \frac{r_2}{C_{22}}} \\
&= \frac{r_2 + \Delta r w_1}{\frac{1}{a}(ar_1 - r_2)a_c w_1^2 + (\frac{1}{a}(ar_1 - r_2)\frac{1}{C_2} + r_2 \frac{1}{a}a_c)w_1 + \frac{r_2}{aC_2}} \\
&= \frac{(r_2 + \Delta f w_1)}{(r_1 - \frac{r_2}{a})a_c w_1 + \frac{r_2}{a})(a_c w_1 + \frac{1}{C_2})} \\
&= -C_2 \frac{w_b w_c}{w_A} \frac{(w_1 - w_A)}{(w_1 - w_b)(w_1 - w_c)},
\end{aligned}$$

where

$$w_A = \frac{1}{1 - \frac{r_1}{r_2}}$$

$$w_b = \frac{1}{1 - a \frac{r_1}{r_2}}$$

$$w_c = \frac{1}{1 - \frac{C_2}{C_1}}.$$

This set has two end points, which are $\tilde{x}_t(w_1 = 0) = aC_2$ and $\tilde{x}_t(w_1 = 1) = C_1$.

According to the general model and from Fig.2.1, we know the curve can be classified into ten types. They are

1. UU type: As $w_b < 0 < 1 < w_c < w_A$, the $\tilde{x}_t(w_1)$ is UU type.
2. DU type: As $w_A < w_b < 0 < 1 < w_c$, the $\tilde{x}_t(w_1)$ is DU type.
3. DH1 type: As $w_A, w_b < w_c < 0$, the $\tilde{x}_t(w_1)$ is DH1 type.
4. DH2 type: As $w_b < w_c < 0 < 1 < w_A$ and $w_b < 0 < 1 < w_A < \frac{w_b + w_c}{2} < w_c$, the $\tilde{x}_t(w_1)$ is DH2 type.
5. UH1 type: As $1 < w_b < w_A, w_c$, the $\tilde{x}_t(w_1)$ is UH1 type.

6. UH2 type: As $w_A < 0 < 1 < w_b < w_c$ and $w_B < \frac{w_B + w_C}{2} < w_A < 0 < 1 < w_C$, the $\tilde{x}_t(w_1)$ is UH2 type.

7. US type: As $w_b < w_A < 0 < \frac{w_b + w_c}{2} < 1 < w_A < w_c$, the $\tilde{x}_t(w_1)$ is US type.

8. DS type: As $w_b < 0 < \frac{w_b + w_c}{2} < 1 < w_A < w_c$, the $\tilde{x}_t(w_1)$ is DS type.

9. UP type: As $1 < w_A < w_b < w_c$, the $\tilde{x}_t(w_1)$ is UP type.

10. DP type: As $w_b < w_c < w_A < 1$, the $\tilde{x}_t(w_1)$ is DP type.

Next, substituting the auxiliary parameters of LH-C into the general form of \tilde{w}_1 , the \tilde{w}_1 in LH-C is

$$\begin{aligned}
0 &= (\Delta r - (m_w w_1 + q_w) x_t + k)(\tilde{w}_1 - \tilde{w}_1^2) - (k_1 + k_2) \tilde{w}_1 + k_2 \\
&= (k + \Delta r - (\frac{1}{a}(ar_1 - r_2)a_c w_1 + \frac{1}{a}(ar_1 - r_2)\frac{1}{C_2})x_t)(\tilde{w}_1 - \tilde{w}_1^2) - (k_1 + k_2) \tilde{w}_1 + k_2 \\
&= (k + \Delta r - (\frac{1}{a}(ar_1 - r_2)(a_c w_1 + \frac{1}{C_2}))x_t)(\tilde{w}_1 - \tilde{w}_1^2) - (k_1 + k_2) \tilde{w}_1 + k_2 \\
&= (k + \Delta r - (\frac{r_2}{a}(a\frac{r_1}{r_1} - 1)a_c(w_1 + \frac{1}{a_c C_2}))x_t)(\tilde{w}_1 - \tilde{w}_1^2) - (k_1 + k_2) \tilde{w}_1 + k_2 \\
&= (k + \Delta r - (\frac{r_2}{a C_2} \frac{1}{w_B w_C}(w_1 - w_C))x_t)(\tilde{w}_1 - \tilde{w}_1^2) - (k_1 + k_2) \tilde{w}_1 + k_2
\end{aligned}$$

The two end points are $end\ point|_{w_1=0} = \frac{k+\Delta r}{r_1-\frac{r_2}{a}}C_2$ and $end\ point|_{w_1=1} = \frac{k+\Delta r}{r_1-\frac{r_2}{a}}C_1$.

Therefore, if $C_1 > C_2$, then $end\ point|_{w_1=1} > end\ point|_{w_1=0}$, or if $C_1 < C_2$, then $end\ point|_{w_1=1} < end\ point|_{w_1=0}$. Thus, \tilde{w}_1 could be S type curve or Z type curve.

When $k + \Delta r > 0$, $C_1 < C_2$, it is a S type curve with the head facing left.

When $k + \Delta r < 0$, $C_1 < C_2$, it is a Z type curve with the head facing right.

When $k + \Delta r > 0$, $C_1 > C_2$, it is a Z type curve with the head facing left.

When $k + \Delta r < 0$, $C_1 > C_2$, it is a S type curve with the head facing right.

2.9.2 The fixed point condition

The general fixed point formula is

$$0 = (\Delta r - (m_w w_1^* + q_w) x_t^* + k) (w_1^* - w_1^{*2}) - (k_1 + k_2) w_1^* + k_2$$

$$\text{where } x_t^* = -C_2 \frac{w_B w_C}{w_A} \frac{(w_1 - w_A)}{(w_1 - w_B)(w_1 - w_C)}.$$

It is a cubic equation for the root w_1^* . Therefore there might exist three fixed points.

Therefore, in LH-C

$$\begin{aligned} 0 &= (k + \Delta r - (m_w w_1^* + q_w) x_t^*) (w_1^* - w_1^{*2}) - (k_1 + k_2) w_1^* + k_2 \\ &= (k + \Delta r - \frac{1}{a} (ar_1 - r_2) (a_c w_1^* + \frac{1}{C_2}) x_t^*) (w_1^* - w_1^{*2}) - (k_1 + k_2) w_1^* + k_2 \\ &= (k + \Delta r - \frac{1}{a} (ar_1 - r_2) (a_c w_1^* + \frac{1}{C_2}) (-C_2 \frac{w_B w_C}{w_A} \frac{(w_1 - w_A)}{(w_1 - w_B)(w_1 - w_C)})) (w_1^* - w_1^{*2}) \\ &\quad - (k_1 + k_2) w_1^* + k_2 \end{aligned}$$

and

$$\begin{aligned} \Delta F &= k + \Delta r - \frac{1}{a} (ar_1 - r_2) \frac{(r_2 + \Delta r w_1) (a_c w_1 + \frac{1}{C_2})}{(a_c w_1 + \frac{1}{C_2}) ((r_1 - \frac{r_2}{a}) w_1 + \frac{r_2}{a})} \\ &= k + \Delta r - \frac{1}{a} (ar_1 - r_2) \frac{(r_2 + \Delta r w_1)}{((r_1 - \frac{r_2}{a}) w_1 + \frac{r_2}{a})} \\ &= k + \Delta r - \Delta r \frac{(w_1 - w_A)}{(w_1 - w_b)}. \end{aligned}$$

In the general model, the bifurcation condition is S_{q-} . Therefore, if k_1 and k_2 could be ignored, it would have three fixed points when k is between $(a - 1)r_1$ and $\frac{a-1}{a}r_2$.

2.9.3 The stability of fixed point

The type of fixed points

$$f_1 = 1 - \frac{x_1}{C_1} - \frac{x_2}{C_2}$$

$$f_2 = 1 - \frac{x_1}{aC_1} - \frac{x_2}{aC_2}$$

$$\frac{\partial f_1}{\partial x_1} = -\frac{1}{C_1} < 0$$

$$\frac{\partial f_2}{\partial x_2} = -\frac{1}{aC_2} < 0$$

According to the general model, $J_a + J_d < 0$, and the fixed points must be a sink or a saddle point.

Similar to LH-B, in LH-C, it could have three fixed points and it is reasonable to see the three fixed points forming two basins with a saddle point in the middle of w_1 .

The spiral behavior of LH-C

In LH-C model,

$$\left\{ \begin{array}{l} \frac{\partial f_1}{\partial x_1} = -\frac{1}{C_1} \\ \frac{\partial f_1}{\partial x_2} = -\frac{1}{C_2} \\ \frac{\partial f_2}{\partial x_1} = -\frac{1}{aC_1} \\ \frac{\partial f_2}{\partial x_2} = -\frac{1}{aC_2} \end{array} \right. \quad (2.27)$$

Substituting these terms into the general model, one yields

$$\begin{aligned}
\lambda_a &= J_a + J_d \\
&= -\left(\frac{r_1 x_1}{C_1} + \frac{r_2 x_2}{C_2} - \left(k_1 \frac{x_1}{x_2} + k_2 \frac{x_2}{x_1}\right)\right) < 0
\end{aligned}$$

$$\begin{aligned}
\text{Det}[J] &= J_a J_d - J_b J_c \\
&= \frac{r_1 x_1}{C_1} \left(k_1 \frac{w_1}{w_2} - k(w_1 - w_1^2)\right) \\
&\quad + \frac{r_2 x_2}{a C_2} k_2 \frac{w_2}{w_1} + k(w_1 - w_1^2) + \frac{r_1 x_1}{C_2} (k_1 - k w_2^2) + \frac{r_2 x_2}{a C_1} \left(k_2 \frac{w_2}{w_1} + k w_1^2\right) \\
&= r_1 x_1 \left(\frac{k_1 \frac{w_1}{w_2} - k(w_1 - w_1^2)}{C_1} + \frac{k_1 - k w_2^2}{C_2}\right) \\
&\quad + r_2 x_2 \left(\frac{k_2 \frac{w_2}{w_1} + k(w_1 - w_1^2)}{a C_2} + \frac{k_2 - k w_1^2}{a C_1}\right)
\end{aligned}$$

$$\begin{aligned}
\lambda_b &= (J_a + J_d)^2 - 4 \text{Det}[J] \\
&= \left(\left(\frac{r_1 x_1}{C_1} + \frac{r_2 x_2}{a C_2}\right) + \left(k_1 \frac{w_1}{w_2} + k_2 \frac{w_2}{w_1}\right)\right)^2 \\
&\quad + \frac{r_1 x_1}{C_1} \left(\frac{w_1}{w_2} + \frac{C_1}{C_2}\right) (k_1 - k w_2^2) + \frac{r_2 x_2}{a C_2} \left(\frac{w_2}{w_1} + \frac{C_2}{C_1}\right) (k_2 + k w_1^2) \\
&= \left(\left(\frac{r_1 x_1}{C_1} + \frac{r_2 x_2}{a C_2}\right) + \left(k_1 \frac{w_1}{w_2} + k_2 \frac{w_2}{w_1}\right)\right)^2 \\
&\quad - k x_t \left(\left(\frac{r_1}{C_1} \frac{w_1^2}{w_2} + \frac{C_1}{C_2}\right) (w_2^2 - \frac{k_1}{k}) - \frac{1}{a} \left(\left(\frac{r_2}{C_2} \frac{w_2^2}{w_1} + \frac{C_2}{C_1}\right) (w_1^2 + \frac{k_2}{k})\right)\right).
\end{aligned}$$

The term λ_b has three parts, $\left(\left(\frac{r_1 x_1}{C_1} + \frac{r_2 x_2}{a C_2}\right) + \left(k_1 \frac{w_1}{w_2} + k_2 \frac{w_2}{w_1}\right)\right)^2$, $\frac{r_1 x_1}{C_1} \left(\frac{w_1}{w_2} + \frac{C_1}{C_2}\right) (k_1 - k w_2^2)$ and $+\frac{r_2 x_2}{a C_2} \left(\frac{w_2}{w_1} + \frac{C_2}{C_1}\right) (k_2 + k w_1^2)$.

The first term is a complete square and always greater than 0. The second term would be negative for $k > 0$ and $|k|$ large, whereas the third term would be negative

when $k < 0$ and $|k|$ large. But from the condition for three fixed points, when $k_1 = k_2 = 0$ we must have $(a - 1)r_1 < k < \frac{(a-1)}{a}r_2$. Thus, the range would be small when k_1 and k_2 deviate slightly from 0. Therefore, to make $\lambda_b < 0$ in the three fixed point case, we must tune the parameters r_1 , r_2 , C_1 , C_2 , and a .

For $k > 0$, we need the second term to become the dominant term. Therefore, $\frac{C_1}{C_2}$ should be large and both $\frac{1}{a}$ and $\frac{k_2}{k}$ should be small. Under this condition, the fixed point with a large w_2 will have a better chance to exhibit spiral trajectories.

For the other case when $k < 0$, we need the third term to become dominant. Therefore, $\frac{C_2}{C_1}$ should be large and $\frac{1}{a}$ should be small. Under this condition, the fixed point with a large w_1 has more chance to exhibit spiral trajectories.

2.9.4 The phase diagram and phase portraits of LH-C

Please see Appendix B.4.

2.10 LH-D model.

LH-D is the most general model and we have shown its mathematical form in the previous section.

2.10.1 The phase diagram and phase portraits of LH-D

Please see Appendix B.5.

Chapter 3

Conclusion

In this part, we discuss the statistical methods to extract the information about the sub-states from a heterogeneous system. We have also discussed a two-state growth with autocrine transition model to study the dynamic behaviors of a two-state heterogeneous population. The analytic work establishes the connection between the system parameters and the characteristics of the phase diagrams. With a complete classification of the possible behavior of the system, we stand a better chance to apply the model to a real-life problem.

In the next part, an application of this model to microscopic biology is presented. Specifically, we will apply the LH-C model to the cancer system. And by adopting appropriate parameters for the model, we will show that the LH-C model corresponds well with the real prostate tumor spheroid growth data under treatments using chemotherapy (17AAG) and radiation therapy. Encouraged by this research result, we also try to develop a new therapy or optimization method using time-dependent treatments, which can be done by tuning the system parameters.

Part II

An application to cancer growth
system and treatment development



Chapter 4

A simple introduction of carcinomatous process

Cancer, a disease of a group of abnormal cells with uncontrolled proliferation, is still one of the main lethal diseases in modern human societies. The origin of the abnormal proliferation cells is the mutation or epigenetic differentiation of normal cells. But the detail carcinomatous mechanism is still not clearly now. A gaining popularity concept of carcinomatous mechanism is the cancer stem cell hypothesis [4], which assumes that a cancer system has at least a subpopulation with high proliferation ability. Recently, Jeffrey et al. also suggest that cancer system is actually one kinds of heterogeneous system [5]. In addition to this are the recent discussions that different sub-populations in a cancer system may transform into other sub-populations by the autocrine signaling pathway [6],[7]. In this regard, these sub-populations thus may be treated as different phenotypes of cancer cells. And this implies that a cancer system may be viewed as a two-state growth with autocrine transition system. The conclusion is that it may be possible to describe a cancer system by the mathematical model discussed in Part I.

In view of the fact that a systematic mathematical model about carcinomatous cell group might help us better understand the cancer system [8], several mathematical models have been proposed [9]. For instance, Garner *et al.* proposed a two-subpopulation model, which has a proliferation and a quiescent subpopulation with a

transition relation [10]. Puri constructed a mathematical model on the regulation of signaling pathway with mutations based on the cancer stem cell hypothesis [11]. Recently, the transition effect between the heterogeneous subpopulations of cancer due to the auto/para-crine signaling pathways have been discussed [6],[7]. Mathematical models on tumorigenesis with the auto/para-crine signaling pathway effect have also been proposed. For example, Bajzer and Vuk-Pavlović proposed a population model in which a single species of cells can interact with a certain growth stimulation activity [12], and Ghosh *et al.* further discussed a model allowing spatial variations [13]. In addition, the mathematical model used to interpret or even give some guidance to the experimental data of cancer treatments has also become a lively discussed topic [14]- [17].



Chapter 5

A heterogeneous cancer growth with autocrine signaling pathway and fitting the growth curves of prostate tumor spheroid

5.1 Fitting idea

According to the concept of cancer stem cell hypothesis, a cancer system should have at least a subpopulation with high proliferation ability. We can set x_1 to be the population of the normal cancer cell state, and x_2 to be that for the high proliferation state. Here, state 2 may be loosely treated as the cancer stem cell state, just to be consistent with the stem cell idea. The obvious difference of the proliferation ability between normal cancer cell state and cancer stem cell state suggests that the heterogeneity factor a should be very large, and the self suppressing capacity of x_2 should be much larger than that for state 1, that is, $aC_2 \gg C_1$. In addition, we will also hypothesize that the state with a high proliferation ability may also have a high ability to consume the resources in the surroundings. This implies that the suppressing ability of state 2 may be much stronger than that of state 1. Thus we

also set $C_2 \ll C_1$. These two hypotheses seem to correspond exactly to the LH-C model, and we use this as a hint on how things should be proceeded.

To simplify the model and to focus on the main characteristics of the real tumor growth data, we assume that the transition effects are all contributed by the autocrine effect, thus we can ignore the k_1 and k_2 parameters. And for convenience, we also set these two states to have the same characteristic growth time, that is $r_1 = r_2$. Here we should notice that although $r_1 = r_2$ means these two states have the same proliferation rate when $x_1 = x_2 = 0$. But since the heterogeneous factor a is very large, when x_1 and x_2 are slightly larger than 0, the proliferation rate would have obvious difference. Therefore the setting is still satisfied with the cancer stem cell hypothesis.

Then we can write the modified LH-C model for the description of the cancer system to be

$$\begin{cases} \dot{x}_1 = r \left(1 - \left(\frac{x_1}{C_1} + \frac{x_2}{C_2} \right) \right) x_1 + k \frac{x_1 x_2}{x_t} \\ \dot{x}_2 = r \left(1 - \frac{1}{a} \left(\frac{x_1}{C_1} + \frac{x_2}{C_2} \right) \right) x_2 - k \frac{x_1 x_2}{x_t}. \end{cases} \quad (5.1)$$

To facilitate the comparison of our model with experimental data, it is more convenient to change the variables from (x_1, x_2) to $(x_t \equiv x_1 + x_2, w_1 \equiv \frac{x_1}{x_t})$. The transformed equations read

$$\begin{cases} \dot{x}_t = r x_t \left(1 - \left[\left(w_1 + \frac{1-w_1}{a} \right) \left(\frac{w_1}{C_1} + \frac{1-w_1}{C_2} \right) \right] x_t \right) \\ \dot{w}_1 = k \left\{ 1 - \frac{r}{k} \left(1 - \frac{1}{a} \right) \left(\frac{w_1}{C_1} + \frac{1-w_1}{C_2} \right) x_t \right\} (w_1 - w_1^2). \end{cases} \quad (5.2)$$

Figure 5.1 shows schematically the conceptual foundation of our model and its relevance to a cancer system. It is a two-subpopulation model, with x_1 being the subpopulation of normal cancer cell state and x_2 the subpopulation of cancer stem cell state. To make the mathematics simple while at the same time capturing the essence of what may be causing the observed behavior, we deliberately assign the

same proliferation rate r to both states, leaving the more general case for later study. Due to competition of the cells in the same cell state, x_1 has a logistic suppressing capacity C_1 . We assume that x_1 and x_2 are competing with each other, and the “suppressing capacity” of x_2 on x_1 is C_2 . (Roughly, this means that the suppression from x_2 on x_1 becomes important when x_2 grows to a value which is of the same order of magnitude of C_2 .)

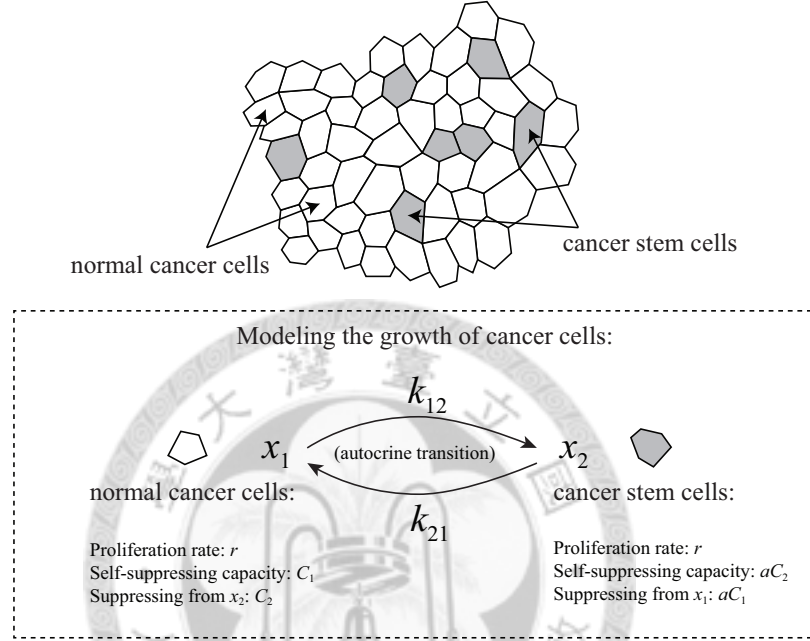


Figure 5.1: Schematic of the two-subpopulation tumor model with transition due to auto/para-crine signaling pathway. x_1 and x_2 are the two subpopulations in a cancer system, each of which follows the logistic growth mode with proliferation r . x_1 has a self-suppressing capacity C_1 . The growth of x_1 is also suppressed by x_2 due to competition. This is characterized by an extra suppressing capacity C_2 of x_2 on x_1 . The heterogeneity coefficient a introduces asymmetry between the two species: State 2 has a self-suppressing capacity aC_2 , and a corresponding suppressing capacity aC_1 from species 1. These two subpopulations have a transition effect due to the autocrine signaling pathway. The strength of the autocrine effect from x_1 to x_2 is k_{12} , and k_{21} is that of x_2 to x_1 , respectively.

Listed in Table 5.1 are the numerical values we have adopted for our model when

a cancer system has not received any treatments. Later we will investigate how the parameters can be modified to better fit the growth curve data of prostate carcinoma spheroid with treatment discussed by Enmon *et al.* [3].

Parameters	Symbols	Values	Unit
Proliferation rate of x_1 and x_2	r	0.3	1/Day
Self carrying capacity of x_1	C_1	10^4	μm^3
Suppressing capacity of x_2 on x_1	C_2	2	μm^3
Heterogeneity coefficient	a	10^6	none
Autocrine strength	k	2.5	1/Day

Table 5.1: Parameter values of the cancer system without treatment.

5.2 Result and discussion

5.2.1 Some simple properties of this model

Because we have adopted a simple model, the interpretation of each of the system parameters in it becomes more transparent. For example, the reciprocal of r is the characteristic time of the system, and it determines the duration of the total growth period. A larger r clearly corresponds to a shorter growth time. But from the mathematical point of view, r can always be absorbed into the time so that its absolute value won't really concern us.

In Part I, we have shown that the autocrine parameter k can be used to regulate the final dominant state. When $k > (a - 1)r$, state 1 dominates the final scene, whereas the opposite is true if $k < (1 - \frac{1}{a})r$. But for an intermediate value of k , that is, when $(1 - \frac{1}{a})r < k < (a - 1)r$, the system goes into a bistable situation, with the final state being dominated by either x_1 or x_2 , depending on the initial conditions. With all the other parameters fixed, Fig. 5.2 shows a series of growth curves for different values of k . Here, we see that the final size of x_t is 10^4 , which is the self suppressing capacity of x_1 , when $k = 10$. (In this sense, then, k can be considered

large in this parameter regime.) But when we tune k to a smaller value, the transition effect may switch the final dominant state, depending on the initial values. If we fix the initial value of w_1 and tune the initial total population x_t , then x_2 will eventually dominate if $x_t(0)$ is larger than a certain critical initial size. The value of the critical size depends on the strength of k in a reciprocal manner: The critical size increases when k decreases. (This can be better seen by looking at the terms inside the curly brackets of Eq.5.2.) As $k < (1 - \frac{1}{a})r$, the final dominant state is always x_2 .

By our construction, $C_1 \gg C_2$, so that typically terms in Eq.5.2 involving C_1 can be ignored when compared with those containing C_2 . And in regards to the role played by the suppressing capacity C_2 , we may say that it provides us with a mechanism to exhibit a “delay” feature that might exist between the initial growth stage and the final settling state. This is so because C_2 acts to suppress the growth of state 1, and whenever state 1 is destined to be the final dominant population, C_2 will simply act to fight against that unavoidable trend. This is particularly true when C_2 is small, because then a small population of species 2 is enough to effectively inhibit the initial growth of species 1. Therefore, it will take some lengthened time for species 1 to grow to a significant percentage in population (via the autocrine parameter k) before the suppressing effect from state 2 can be “quenched.” (At a later time, the effect of C_2 diminishes simply because the population of state 2 is reduced, again, by the autocrine parameter k .) All this is reflected in the duration of time evolution before the system eventually settles down. This aspect is also shown in the form of x_t nullcline, since when $C_1 \gg C_2$ and $a \gg 1$ the x_t nullcline is U type and the growth rate would be slow or even minus when $x_1 \sim x_2$, this is due to the competition effect of x_2 on x_1 . An approximate mathematical form of this property is presented in Appendix C. In Fig. 5.3, we show the growth curves for various values of C_2 when all other parameters and the initial values are fixed. Once again, we note that the delay is more pronounced when C_2 is small.

Finally, we notice that the heterogeneity coefficient a is the key factor deciding which state is the proliferation state. When $a > 1$, x_2 is proliferating subpopulation,

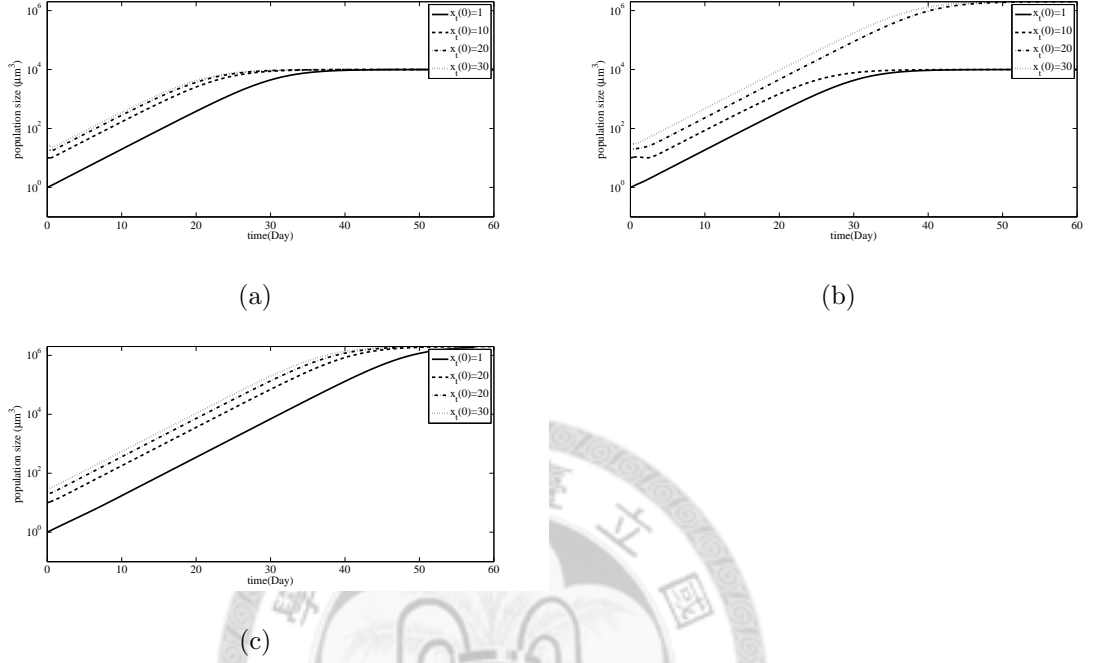


Figure 5.2: A series of x_t growth curves with fixed system parameters ($r = 0.3$, $a = 10^6$, $C_1 = 10^4$, $C_2 = 2$) and initial conditions ($x_t(0) = 1, 10, 20, 30$; $w_1(0) = 0.1$), but with different k . (a) $k = 10 > (1 - \frac{1}{a})r$: All curves saturate at 10^4 , the self-suppressing capacity of x_1 , meaning species 1 eventually dominates. (b) $k = 2.5$: As k becomes smaller, the final state of each growth curve depends on the size of the total initial population $x_t(0)$. Species 1 dominates for small $x_t(0)$, but species 2 dominates when $x_t(0)$ exceeds a certain critical size. (The growth curves all saturate at 10^6 .) (c) As k becomes much smaller ($k = 0.1$), the critical $x_t(0)$ size is also larger. When k is large enough, the critical size no longer exists and species 2 dominates the final scene.

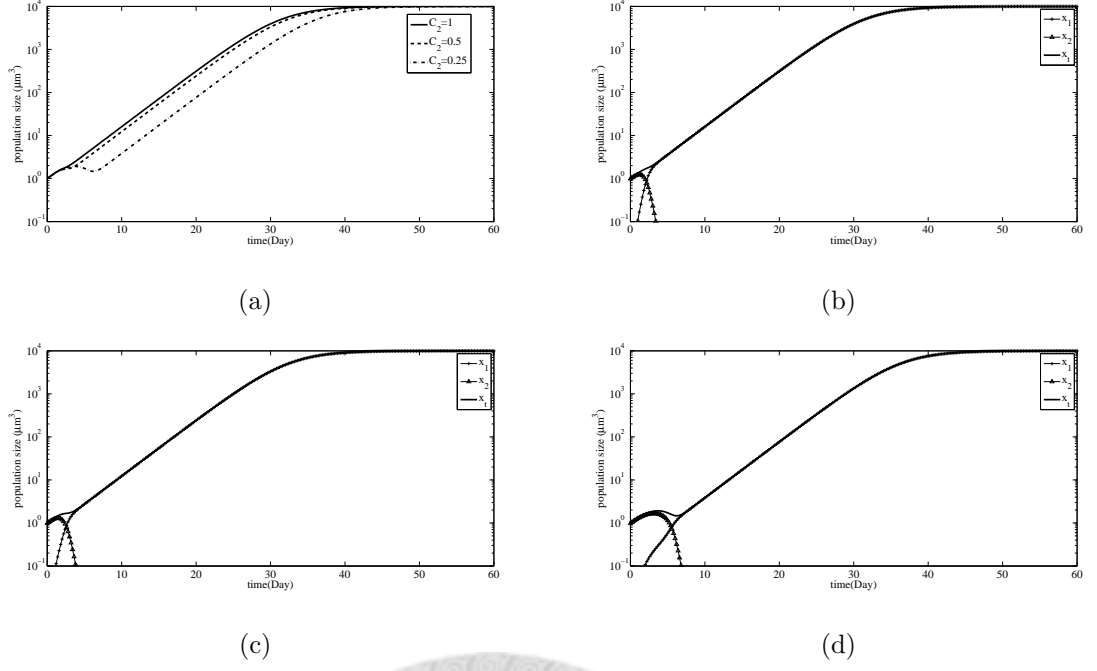


Figure 5.3: The growth curves with fixed system parameters and initial conditions ($r = 0.3$, $a = 10^6$, $C_1 = 10^4$, $k = 2.5$, $x_t(0) = 1$, $w_1(0) = 0.01$) but different C_2 . (a) x_t for $C_2 = 1$ (solid), $C_2 = 0.5$ (dashed), and $C_2 = 0.25$ (dash-dot). As C_2 becomes smaller, a delayed phase becomes obvious. (b), (c) and (d) are the growth curves of x_1 , x_2 , and x_t with different C_2 . (b) $C_2 = 1$, (c) $C_2 = 0.5$, and (d) $C_2 = 0.25$, for x_t (bold), x_1 (marked with “+”), and x_2 (marked with “ Δ ”). When C_2 is small, the inhibiting effect to the final dominant state x_1 is more pronounced during transient, and a delayed phase persists until x_2 becomes negligible.

and the reverse is true when $a < 1$. This is obvious because we have constructed our model so that the roles of x_1 and x_2 are exchanged when a is replaced by $1/a$. However, if we insist on adopting the same parameter regimes for other system parameters but just allow a to be less than unity, then a delayed evolution such as described above is *not* expected to occur, simply because now the associated suppressing capacity of state 1 on state 2 (as characterized by the coefficient aC_1) is not small.

The role of a can also be shown in the structure of x_t nullcline. As $a > 1$, $C_1 > C_2$ and $r_1 = r_2$, the form of x_t nullcline is U type. It means the capacity of x_t decreases

as w_1 assumes a middle value. Then a delayed evolution is expected to occur. But if $a < 1$, $C_1 > C_2$, and $r_1 = r_2$, the form of x_t is UH1 type, in which case the capacity of x_t decreases as $w_1 \rightarrow 0$ and the delayed evolution does not occur.

5.2.2 A comparison of the numerical results and real data from tumor growth with treatments

By associating our system parameters with the various different aspects related to medical treatments on cancer, we are able to fit our numerical results with the experimental data of prostate carcinoma spheroids with treatment of 17-N-Allylamino-17-Demethoxy Geldanamycin and Acute Irradiation [3]. In the following we discuss such possibilities.

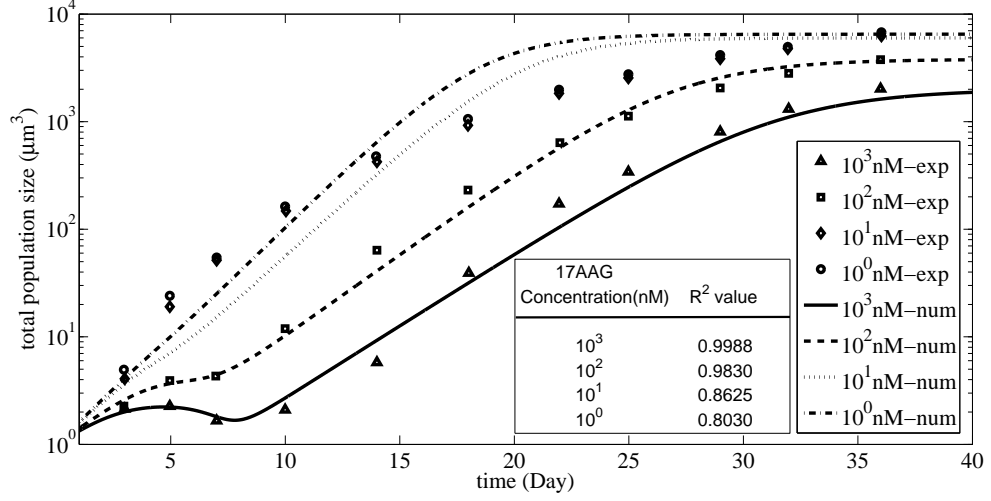
17AAG

17-N-Allylamino-17-Demethoxy-Geldanamycin (17AAG), a geldanamycin analogue, can inhibit the Heat Shock Protein 90 which may provide a mechanism to evade apoptosis of tumor cells [18]. Because 17AAG can inhibit the evading apoptosis mechanism of tumor cells, we naturally associate it with one of the capacity parameters in our model. Specifically, a cancer system receiving this treatment might correspond to having a smaller value of C_2 . From a comparison with the actual treatment data of [1] and our numerical results, we found that the dosage concentration of 17AAG and C_2 seems to have a power law relation. With this in mind, we tentatively choose the treatment function $C_2 = 19.2 \times M^{-0.6}$, where M is the dosage concentration of 17AAG in nM. Since we have no access to the experimental value of w_1 , we simply have to make an educated guess. Now that we are assuming that the effect of 17AAG is to enhance the population of x_1 , we will hypothesize that the initial weighting w_1 is small. To be concrete, we have taken the initial weighting w_1 of a carcinoma spheroids treated by 17AAG to be $w_1(0) = 0.01$. Figure 5.4 shows the comparison between numerical results of our simulation about the 17AAG treatment and the actual experimental data. We have used Fig. 1 of [1] to extract the data and plot them

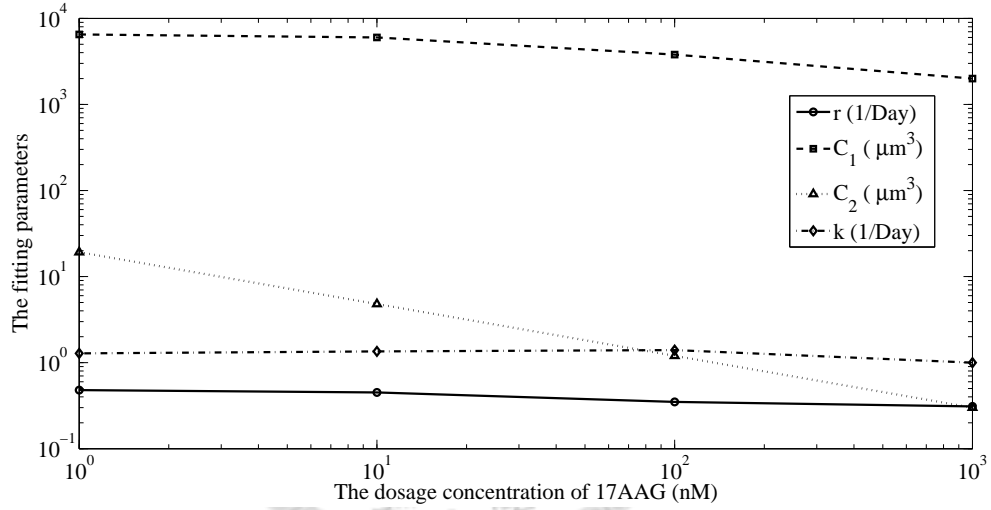
in juxtaposition with our fit. In Fig. 5.4 (a) is shown the numerical fit (curves) and the experimental data of 17AAG treatment (markers). Apparent in this figure, the numerical fit works best in the high dosage regime, whereas the general trend is still captured in the low dosage regime. As good as the numerical fit may be, we must quickly point out that the merit of the present work does not lie in the good fit of the numerical values, but rather in the qualitative features it is capable of explaining for the actual data. Once we know qualitatively what factors can affect the treatment in which way, then a more refined model surpassing the simple logistic growth considered here presumably can be worked out to provide a guidance or even quantitative prediction on how actual treatments should be carried out. Shown in Fig. 5.4 (b) are the fitting parameter values versus the dosage concentration of 17AAG. Here, we see that C_2 changes more rapidly compared with other parameters when we vary the concentration of 17AAG. This suggests that C_2 is probably the most relevant parameter when the concentration of 17AAG is varied.

Irradiation

Irradiation is also a common treatment for cancer, though the underlying mechanism for its success seems more complex. By observing the growth curves with different dosages of irradiation [3], we hypothesize that irradiation treatment might reduce the value of the heterogeneity coefficient a and the autocrine transition effect from x_2 to x_1 . With this hypothesis in mind, we also come up with tentative treatment functions of irradiation for the system parameters a and k . Let D denote the dosage strength of irradiation in units Gy, the treatment functions are taken to be $a = 10^{\frac{6}{D}-2}$ and $k = 2.5 - \frac{D}{2}$, respectively. Since the heterogeneity coefficient is reduced under irradiation treatment, it may imply that the original proliferating subpopulation x_2 is damaged more under the irradiation treatment. Hence we think that the initial weighting of w_1 may be closer to 1. In our simulation, we set the initial weighting to be $w_1(0) = 0.99$. Figure 5.5 shows our simulation results for irradiation treatment. The notable features captured here are the presence of a delayed phase at 6 Gy and the inhibition of the x_t size at 9 Gy and 12 Gy, respectively, which correspond to Fig.



(a)



(b)

Figure 5.4: Fitting the x_t growth curves with the data from 17AAG treatment of [1]. (a) The numerical results (curves) compared with the actual experimental data (markers). The R square values of them are $R_{1nM}^2 = 0.8030$, $R_{10nM}^2 = 0.8625$, $R_{100nM}^2 = 0.9830$ and $R_{1000nM}^2 = 0.9988$. The fit is best in the high dosage regime. (b) Fitting parameters used in Figure 5.4 (a) as a function of the corresponding dosage.

2 of [3].

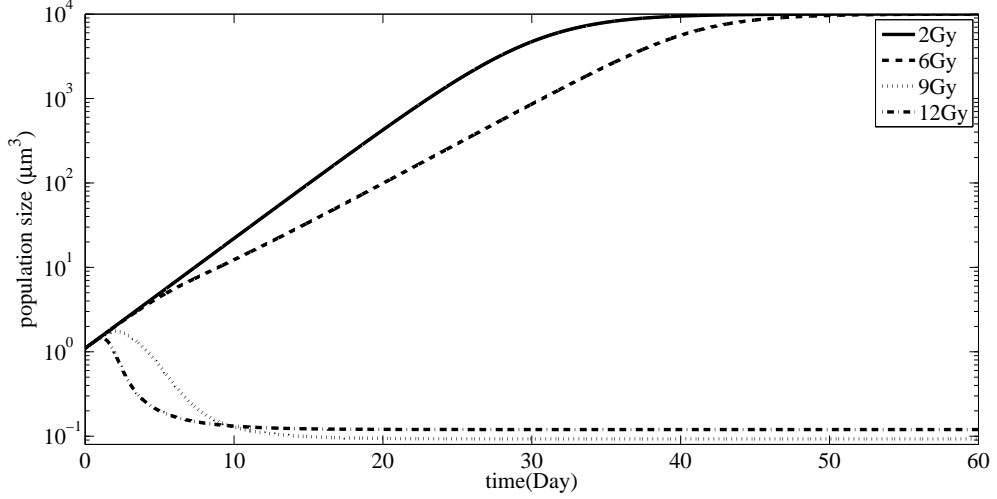


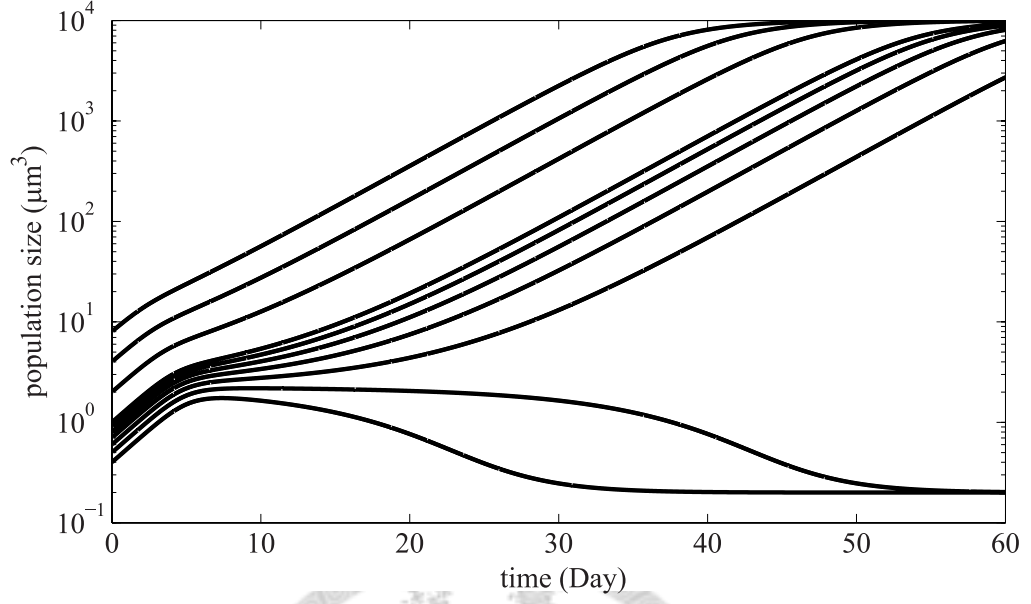
Figure 5.5: Fitting the x_t growth curves of data from irradiation treatment. The system parameters are taken as ($r = 0.3$, $C_1 = 10^4$, $C_2 = 2$, $x_t(0) = 1.1$, $w_1(0) = 0.99$). Fitted x_t is for 2 Gy irradiation treatment (solid, $a = 10$, $k = 1.5$), 6 Gy irradiation treatment (dashed, $a = 0.1$, $k = -0.5$), 9 Gy irradiation treatment (dotted, $a = 0.0464$, $k = -2$), and 12 Gy irradiation treatment (dash-dot, $a = 0.0316$, $k = -3.5$). The fit compares favorably well with Fig. 2 of Enmon *et al.* [3].

Bistable behavior

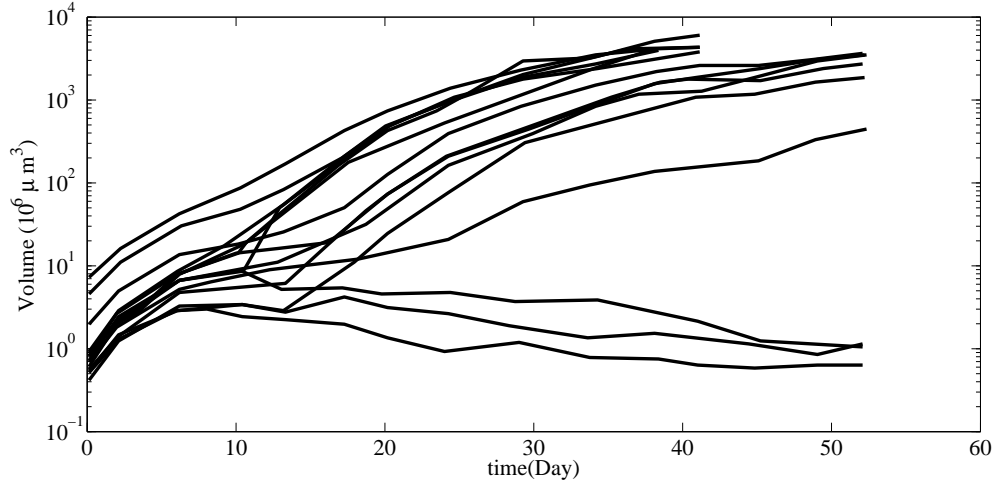
It is interesting to note that the dependence of the bistable behavior on the initial conditions has also been shown in the actual tumor growth data (see Fig. 6A of [3]). In the 6 Gy irradiation treatment, the tumor growth curves have different final states (alive or dead) when the tumor has different initial sizes. This seems to correspond to the existence of a critical $x_t(0)$ in our model.

As a comparison, Fig. 5.6 shows the numerical simulation of the growth curves with different initial $x_t(0)$ in 6 Gy treatment. Here, we see that the behavior of the growth curve has a drastic change when $x_t(0) > 0.6$. In fact, this is due to the fact that the initial value has crossed the critical value. Again, the simulation results shown in the bistable growth curves (Fig. 6A) compare favorably well with those in

the actual 6 Gy treatment in prostate carcinoma spheroids [3].



(a)



(b)

Figure 5.6: Fitting the x_t growth curves of data near the 6 Gy irradiation treatment, using the bistable model with different $x_t(0)$. The system parameters are taken as ($r = 0.3$, $a = 0.1$, $C_1 = 10^4$, $C_2 = 2$, $k = -0.8$, $w_1(0) = 0.99$). Figure 6A corresponds well with the data of 6 Gy treatment in prostate carcinoma spheroids [3].

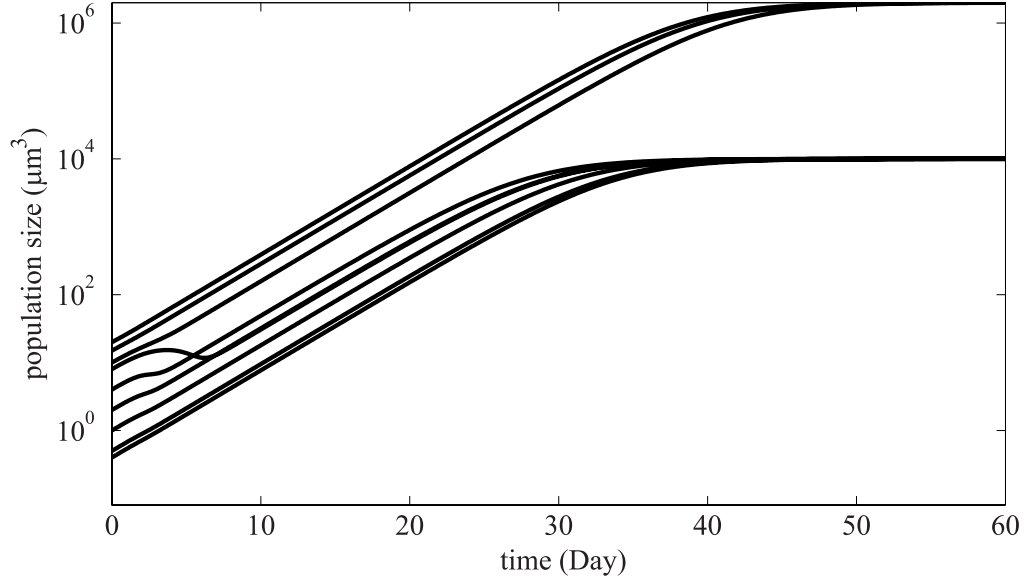


Figure 5.7: Fitting the x_t growth curves of 1000 nM 17AAG treatment with different $x_t(0)$, using the bistable model. The system parameters are taken as ($r = 0.3$, $a = 10^6$, $C_1 = 10^4$, $C_2 = 2$, $k = 2.5$, $w_1(0) = 0.01$).

Finally, another bistable figure when $a \gg 1$ is also shown in Fig. 5.7. It also captures the bistable behavior for the growth curves with different initial total size x_t for the 1000 nM 17AAG treatment (See Fig. 6B of [3]).

Chapter 6

IAS treatment simulation by the mathematical model and the planning of optimized therapy.

6.1 The clinical prostate cancer therapy of human- IAS (Intermittent Androgen Suppression) therapy

In the previous chapter, we showed that the LH-C model of two-state growth with transition probability can describe the growth behaviors of the prostate tumor spheroid in vitro. Here we will apply this model to the clinical prostate cancer therapy of human, and try to provide some suggestions to the optimization of the treatment times.

Due to the sensitivity of androgen to the growth phenotypes of prostate cancer cells [19], hormone therapy is a useful way to inhibit the growth of prostate cancer. The traditional hormone therapy of prostate cancer is the CAS (Continuous Androgen Suppression) therapy, which uses the method of castration [20] or androgen deprivation [21] to inhibit the concentration of androgens. The CAS therapy could inhibit the growth process of prostate in the early period. However, the therapy eventually loses

its efficacy, and the prostate cancer would relapse [19]. The reason of relapse is that prostate cancer cells have two phenotypes, one called the AD (androgen-dependent) state, and the other called the AI (androgen-independent) state. AD cells prefer to live in normal androgen environment, and AI cells prefer to live in an androgen lacking environment. The suppression of androgen would induce the apoptosis of the AD cells and enhance the transition rate of AD to AI [19]. Therefore, the prostate cancer would relapse under CAS therapy when the AD cells are almost fully changed to the AI cells. Basing on this concept, a new time-dependent treatment process, IAS (Intermittent Androgen Suppression) therapy, was developed. By switching on and off the androgen suppression process, the efficacy of cancer suppression could be made better than CAS therapy [22]. The efficacy of the IAS therapy has been confirmed in animals [23] [24] and human [25]. But since this is a time-dependent process, the optimization of the on-off period to obtain the best suppression efficacy is an important research topic.

For this reason, mathematical models are proposed to analyze the characteristics of the time-dependent regulation process [19]. Jackson proposed a basic population model with three variables which are AD, AI, and androgen. This model could get a bifurcation relation about the relapse and suppression of cancer [26],[27]. Guo generalized this population model to 3-D by considering the spatial distribution of prostate cancer cells [28]. Shimada considered the competition effect between the AD and AI cancer cells and showed that the competition effect could make the suppression of cancer more efficiently[29]. Tanka considered the population model with stochastic noise to check the influence of the intrinsic noise in biological system [30]. For finding an effective model to fit the specific patient's data, Hirata proposed a piecewise linear model to fit the clinical data [31].

Although several mathematical models have been proposed to analyze the optimization of on/off periods and fitting the specific patient's data, the optimization method and the personal clinical predication seems to still have room for improvement. Since the LH-C model seems to give a nice description of the growth data of prostate tumor spheroid and the properties of IAS therapy such as having two

states with competition and transition effects also correspond nicely to our model, it is reasonable to test our model against IAS. With this in mind, we have developed a way to study a related phenomenon in our model, hoping that it might also shed some light to IAS.

The idea goes like this. The regulation method corresponds to the on-treatment, and it can change the transition rate of AD to AI. And the effect is reversed when we switch to the off-treatment. By associating the AD state with x_1 , and AI state with x_2 , we assume that changing the concentration of androgen also changes the autocrine transition factor k . Under on-treatment, $k < \frac{r}{a}$, the dominant state is x_2 . And under off-treatment, the normal transition strength $k > (1 - \frac{1}{a})r$, the dominant state is x_1 . When we switch the on/off treatment, the dominant state would change with the switching process. If we can regulate the switching process to keep a balance between the “power” of AD and AI states, the total population x_t might have a smaller suppression capacity due to the competition of x_2 with x_1 , and a delay growth phase may be constructed. Then, for an appropriately chosen time-dependent regulation of k , the delay phase due to the competition of x_2 with x_1 might suppress x_t to the order of C_2 , so that a dynamic suppression of prostate cancer is achieved.

In the preliminary work, we have used this model to describe the growth behavior of IAS therapy, and the initial results look promising because the model seems to exhibit similar features one observed from clinical data. This ongoing project will be further pursued in the future.

Chapter 7

Conclusion

In this part we have touched upon a budding research topic which might turn out quite useful: Specifically, we applied the LH-C model to describe the prostate tumor in vitro and in clinical case, and showed the validity of this application. In vitro case, we described the growth data of prostate tumor spheroid under 17AAG and irradiation treatment successfully. And in clinical case we have made an initial attempt to give suggestions about how the process of the prostate cancer suppression under IAS therapy can be optimized using a dynamical approach. The preliminary simulations have given us some confidence on further pursuing this idea. We hope that we may be able to predict an optimized period of the on-off treatment and compare it with actual clinical data in the near future.

Appendix A

Statistical methods to make out sub-state from a whole system.

To analyze a real heterogeneous system, the first step is to make out the sub-state information from the real experimental data. Since each sub-state may represent a distribution in a specific experimental measurement, the work to make out each sub-state is to make out each sub-distributions from the whole distribution.

For a giving hypothetical mechanism of this system, we may give each sub-state a probability density function in some specific measurements. And the way to fit the real system and the hypothetical mechanism is to decide the appropriate parameters and weighting of each probability density function. In this section we will review two fitting methods. One is the most common fitting method - “Least square method”, and the other is a more general fitting method - “Maximum likelihood method”.

A.1 Least squares method

Least squares method is the most common and well-known fitting method (section 15-1 of [32]). Suppose we have an N -point data, set $\vec{Y} = \sum_{i=1}^N (x_i, y_i)$, where x_i is the index of the data and y_i is the number of data points in the i th interval. A test function $y(\vec{x}|\vec{\theta})$ with corresponding parameters $\vec{\theta}$ can be defined by a testing model, and the test function is expected to predict the characteristics of this data set.

The basic assumption of the method is to suppose the error of each data point follows the same independent Gaussian distribution with standard deviation σ . Therefore, for a given ideal test function, the probability density function p_i of $y_i - y(x_i|\vec{\theta})$ is

$$p_i = \exp\left[-\frac{1}{2}\left(\frac{y_i - y(x_i|\vec{\theta})}{\sigma}\right)^2\right].$$

And P is the probability of generating this data set, which can be written as

$$P = \prod_{i=1}^N (p_i \Delta y) = \prod_{i=1}^N \left\{ \exp\left[-\frac{1}{2}\left(\frac{y_i - y(x_i|\vec{\theta})}{\sigma}\right)^2\right] \Delta y \right\},$$

where Δy is a constant interval.

To find the test function with maximum likelihood, we can maximize P . And maximizing P is equivalent to minimizing $-\log(P)$, which is

$$-\log(P) = \left[\sum_{i=1}^N \frac{[y_i - y(x_i|\vec{\theta})]^2}{2\sigma^2} \right] - N \log(\Delta y)$$

Because N and Δy are constants, it is equivalent to minimizing the sum of the squared errors $S = \sum_{i=1}^N [y_i - y(x_i|\vec{\theta})]^2$.

That is, when we vary the parameters of a test function to find the minimum of S , we expect to find the test function with maximum likelihood. We believe that this is the best fitting result.

Although the least squares method is a convenient test method, it does contain some artificial setting such as setting an artificial bin to get the distribution function,

and the hypothesis of Gaussian random distribution with standard deviation. What this means is that the fitting may be influenced by certain artificial setting.

Another more general fitting method, which has no internal assumption, is the “Maximum likelihood method” reviewed in the next section.

A.2 Maximum likelihood method

Maximum likelihood method is a general and powerful method to analyze random data sets (section 6.5 of [33]). It has less artificial assumptions than the least square method. For a candidate mechanism of a system, we can assume that the system has some kind of probability distribution function. Maximum likelihood method can help us determine the appropriate parameters in the probability distribution function without any artificial assumptions and sorting.

A.2.1 Maximum Likelihood

A conditional probability density function(pdf) with observable \vec{x} and corresponding parameters $\vec{\theta}$ can be described as $p(\vec{x}|\vec{\theta})$, which is the probability of an observable \vec{x} with given parameters $\vec{\theta}$. If we know the probability density function and the corresponding parameters $\vec{\theta}$, we can find the probability with the observable \vec{x} .

But consider a reversed situation. If we have an observable \vec{x} , and a hypothetical probability density function $p(\vec{x}|\vec{\theta})$ to the candidate mechanism is given. Then the likelihood of given parameters $\vec{\theta}$ can be described as the likelihood function $lik(\vec{\theta}|\vec{x})$, which is the probability of the parameters $\vec{\theta}$ with a given observable \vec{x} . For the same \vec{x} and $\vec{\theta}$, quantitatively we have $p(\vec{x}|\vec{\theta}) = lik(\vec{\theta}|\vec{x})$.

For a given data set with N data points $\vec{X} = \vec{x}_1, \vec{x}_2, \vec{x}_3, \dots, \vec{x}_N$, the corresponding likelihood function $Lik(\vec{\theta}|\vec{X})$ can be described according to the concept of conditional probability,

$$Lik(\vec{\theta}|\vec{X}) = lik(\vec{\theta}|\vec{x}_1)lik(\vec{\theta}|\vec{x}_2)lik(\vec{\theta}|\vec{x}_3)\dots lik(\vec{\theta}|\vec{x}_N) = \prod_{i=1}^N lik(\vec{\theta}|\vec{x}_i)$$

$Lik(\vec{\theta}|\vec{X})$ denotes a likelihood for parameters $\vec{\theta}$ with a given data set \vec{X} . For a given \vec{X} , $\vec{\theta}$ can be varied to $\vec{\theta}_{max}$, which corresponds to maximizing the likelihood function. We believe that the probability density function with parameters $\vec{\theta}_{max}$ is the best probability distribution for the data set \vec{X} .

For convenience, we often equivalently maximize the logarithm of the likelihood function, $L(\vec{\theta}|\vec{X}) \equiv \log(Lik(\vec{\theta}|\vec{X})) = \log(\sum_{i=1}^N lik(\vec{\theta}|x_i))$.

A.2.2 Logarithmic likelihood ratio test

It is plausible that the fitting of a data set should be more similar to the original data set as the number of the fitting parameters increases. But in reality the real mechanism behind a system might just have a finite number of parameters. Therefore, we need a method to decide how many parameters, or based on the concept of multi-state probability density function, how many states are enough to fit the data set. And the *logarithmic likelihood ratio test* is a test which can help us decide how many parameters are enough to fit a data set (section 6.2.1 of [33]).

According to the maximum likelihood method, we should find a maximum likelihood value $L(\vec{\theta}_m)$ for a specific test function with m parameters. And we can construct two test functions, one of which has n states and n_2 number of parameters, whereas the other test function has only $n - 1$ states and n_1 number of parameters, with $n_2 > n_1$. Then a quantity R_n , called the logarithmic likelihood ratio can be defined as (section 6.2.1 of [33]), [34].

$$R_n = L_{n_2} - L_{n_1} = \log(Lik(\vec{\theta}_{n_2}|\vec{X})) - \log(Lik(\vec{\theta}_{n_1}|\vec{X})) = \log\left(\frac{Lik(\vec{\theta}_{n_2}|\vec{X})}{Lik(\vec{\theta}_{n_1}|\vec{X})}\right)$$

Then the measure of how good a fitting is can be quantified as a probability value *q-value* which follows the χ^2 distribution. More precisely, *q-value* = $gammq(\frac{\nu}{2}, 2R)$, where $\nu = n_2 - n_1$ is the difference of parameter numbers, and $gammq(a, b)$ is the incomplete Gamma function, which takes the form(section 6.2 of [32])

$$\text{gammq}(a, b) = \frac{1}{\Gamma(a)} \int_b^{\infty} e^{-t} t^{a-1} dt (a > 0).$$

Fig. 1.1 is the curve of $\text{gammq}(a, b)$ with different parameter a . We can see that all curves tend to 0 as b grows. As a becomes larger, the decreasing rate of the curve becomes less abrupt and smoother. Therefore, when R_n is small, which means that there is no obvious change as we add a state, or when ν is small, which means the number of parameters does not change too much as the number of states grows. Under these conditions, the q -value would be closer to 1, and we have more confidence that the number of parameters is enough.

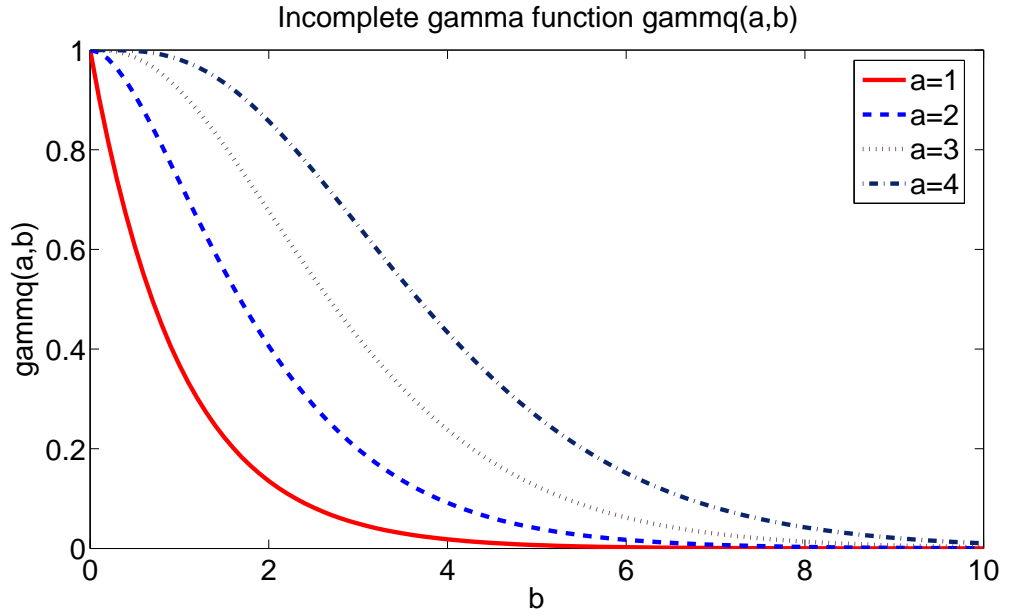


Figure 1.1: The diagram of $\text{gammq}(a, b)$ with different a . They are decreasing curves from 1 to 0. The curve tends to 0 when b is large, and the tendency is more gentle as a is large. In logarithmic likelihood ratio test, the goodness probability value $q\text{-value} = \text{gammq}(\frac{\nu}{2}, 2R)$. It means the fitting result should be good as the difference of parameter number ν or the logarithmic likelihood ratio R is small.

A.3 Numerical simulation method

To approach the test of maximum likelihood method, we generate several 1-D and 2-D non-uniform random number set from multi-state probability density function with different states and lengths as a test data set. Then implement the maximum likelihood method in a numerical program to test this data set. This section shows such an exercise to the test results to verify the capability of maximum likelihood method.

A.3.1 Generation of non-uniform random number

Uniform random numbers between an interval can be easily obtained from the intrinsic pseudo random number generator of many computing program language. It is represented as a long period function with no obvious rules. But the common intrinsic random generator might not be a good generator. In this thesis, we obtain the uniform random numbers from the pseudo random number generating function “*ran(idum)*” recommended in Numerical Recipes (chapter B7 of [35]). It can generate a pseudo random number between 0 and 1 with a long period of about 3.1×10^{18} . This is needed here because the maximum length of the data set which we have tested is 10^7 .

But actually we need a nonuniform random data set to be a test data. This can be done this way: after the uniform random data set is generated, we can generate the nonuniform random number data set by taking some transformation. Here two nonuniform transformation methods are used. They are “Transform method” (section 7.2 of [32]), and “Rejection method” (section 7.3 of [32]).

Transform method

If we have a random variable x with uniform probability density distribution between 0 and 1, the probability density function $p(x)$ is

$$p(x) = \begin{cases} dx & 0 < x < 1 \\ 0 & \text{otherwise.} \end{cases}$$

Now if we want to transform x to another random variable y with probability density distribution $p(y)$, a fundamental transformation relation can be used which is $|p(y)dy| = |p(x)dx|$ or $p(y) = p(x)|\frac{dx}{dy}|$. Fig 1.2 is the diagram of this transform, the probability density function $p(y)$ can be changed as $|\frac{dx}{dy}|$ changes.

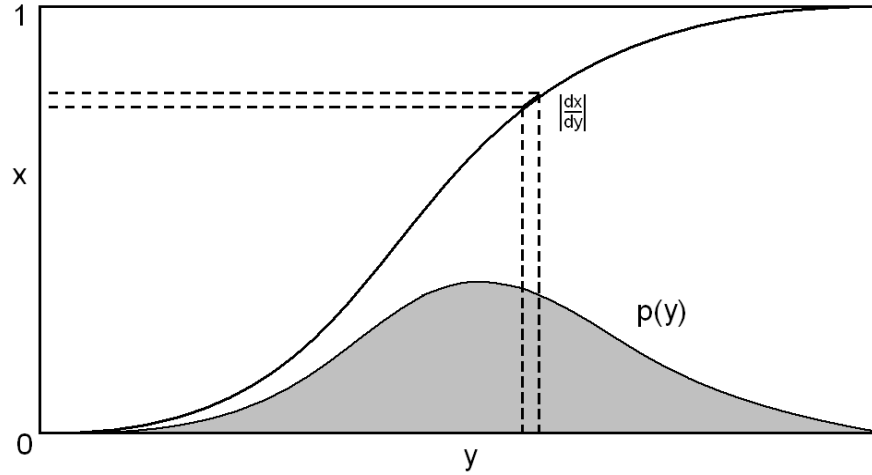


Figure 1.2: The diagram showed the concept of transform method. A uniform distribution can be transformed into a non-uniform distribution by non-uniform mapping.

If we want to find the transfer relation of uniform distribution $p(x)$ to $p(y)$, we need to solve the relation

$$\begin{aligned} p(y) &= \left| \frac{dx}{dy} \right|, \\ p(y)dy &= dx, \text{ where } 0 < x < 1. \end{aligned}$$

Integrating this equation, we have

$$x = F(y) = \int_0^y p(y)dy.$$

And the relation $y(x)$ is

$$y(x) = F^{-1}(x).$$

For example, if we want to transform a single exponential distribution $p(y) = \frac{1}{\tau}e^{-\frac{y}{\tau}}$ from a uniform distribution x , then

$$x = F(y) = \int_0^y \frac{1}{\tau}e^{-\frac{y}{\tau}} = 1 - e^{-\frac{y}{\tau}}.$$

And the inverse function of $F(y)$ is

$$y = F^{-1}(x) = -\tau \ln(1 - x).$$

Therefore we can find the transformation of uniform distribution to a single exponential distribution, which is

$$y = -\tau \ln(1 - x).$$

Since x is a uniform distribution between $(0, 1)$, $1 - x$ is the same distribution of x . Therefore $y = -\tau \ln(x)$.

Here, the 1-D and 2-D data sets with single or multiple exponential components are generated by this transform method.

Transform method is a direct method for generating a nonuniform random distribution from a uniform distribution. But it may not be easy to find the $F^{-1}(x)$ for arbitrary $F(y)$. And another method “Rejection method”, can generate more kinds of nonuniform random numbers but with less precision.

Rejection method

The rejection method is powerful and general technique for random data generating. To approach this method, an known probability density distribution $f(x)$ is generated to cover the probability density distribution $p(x)$, which we want to generate. when we generate a random value x_0 , a part of random number data would be rejected according to a rejection rate $\frac{f(x_0)-p(x_0)}{f(x_0)}$.

Fig1.3 is the diagram of the rejection method, because of the rejection of data points, the probability density function could be modified from $f(x)$ to $p(x)$.

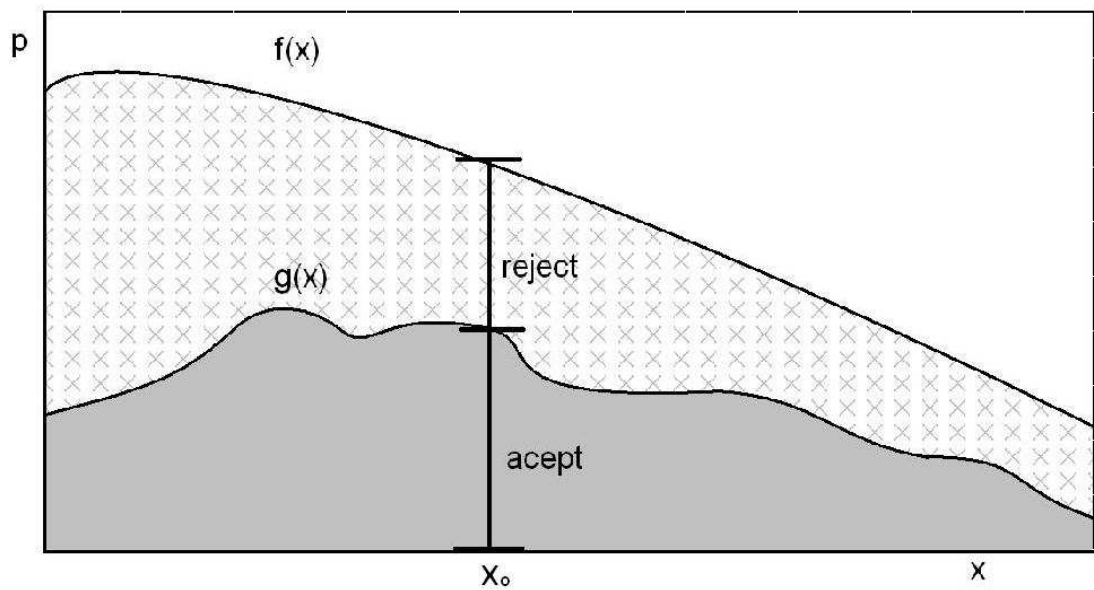


Figure 1.3: The diagram of the concept of the rejection method. If we have a known distribution $f(x)$, then we can generate a data set with probability density function $g(x)$ by rejecting $\frac{f(x_0)-p(x_0)}{f(x_0)}$ data points when $x = x_0$.

Although the rejection method is a powerful method, but because this method rejects many data, it wastes more time to generate a random data set. And the accuracy might be bad when the rejection rate $\frac{f(x_0)-p(x_0)}{f(x_0)}$ is very small. Therefore, all of the the random data points in this thesis are generated by the transform method.

A.3.2 Optimum method

The optimum method here is denoted as the maximization or minimization method. And maximization can be equivalent as minimization if we change the sign of a test value. In the maximum likelihood method, we must maximize the likelihood value of a test function with parameters. In the numerical method, we try to minimize the likelihood value $-Lik(\vec{\theta}|\vec{x})$. The numerical method to minimize the multidimensional variable in my program is “Downhill simplex method” (section 10.5 of [32]).

Downhill means walking forward to the local minimum direction, and simplex is a multiple vertex structure with $M + 1$ vertices in M -dimensional space. For example, in 2-D it is a triangle, and in 3-D it is a tetrahedron ... etc.. The downhill simplex method is a method to vary the structure and the scale of simplex to find the local minimization point.

The evolution rules of simplex are as follows. For a M dimension test function, we can choose $M + 1$ test points arbitrarily to be the initial simplex. Each test point has a minus likelihood value, we would reject the point with the largest minus likelihood value and add a new test point in the reflection point of the rejection point related to the “high dimensional plane”, which is constructed by other test points. If the minus likelihood value of the new test point is smaller than the rejected test point, it means this is a good direction to find a better test point. Then we can expand the distance between the new test points related to the “high dimensional plane” twice

to get another new test point. The diagram of transform is shown in Fig. 1.4 (a) and (b). If we can not find a point with smaller value by these two transforms, it means that this simplex is at a basin. Then we take two kinds of contraction transforms to obtain the finer local structure, which are shown in Fig. 1.4 (c) and (d). When the difference of all test points is smaller than a value ε (in my program $\varepsilon = 10^{-16}$), we believe that the simplex moved to a flat area and the simplex should be in the bottom of a basin, a local minimum point of the test function. Then the minimization process is achieved.

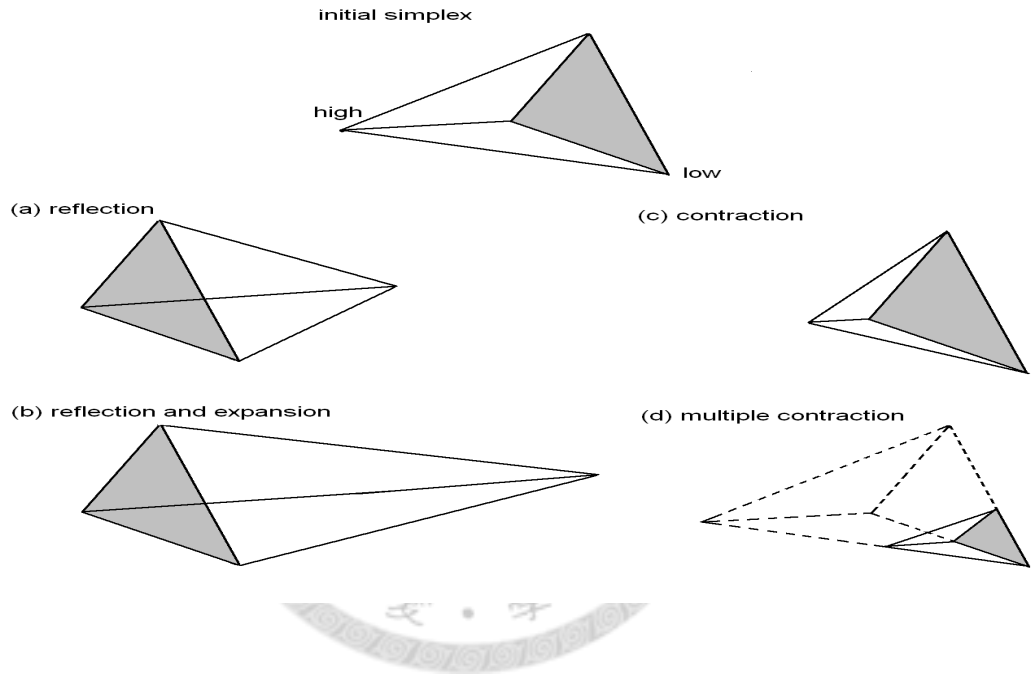


Figure 1.4: The four transformation type of simplex transform. (a) is reflection transform, which is to set a new test point in the reflection point of the highest test point relative the other points. (b) is the transform to set a new test point with reflection and expansion for a scale. (c) is the contraction transform for a point. (D) is the multiple contraction transform. The reflection transform (a) and (b) can help us to find the basin of the surface, and the contraction transform (c) and (d) can help us to see the fine structure of a surface. These four transforms are used to find the local extreme point in a surface.

Since this method can merely find a local minimum point, it is better to take tests several times with different initial tests. After we repeat this method with several different initial simplex, we may find several local minimum points, then we choose the point with a maximum likelihood value.

A.4 Data analysis

In this section we show the numerical result of maximum likelihood method by test is the one-dimensional and two dimensional data set generated by known probability density functions such as one dimensional and two dimensional multiple components exponential functions.

A.4.1 1-D data set

The form of 1-D probability density function is

$$\begin{aligned} p(t) &= \sum_{i=1}^k a_i p_i(t) \\ &= \sum_{i=1}^k \frac{a_i}{\tau_i} e^{-\frac{t}{\tau_i}} \\ &= \sum_{i=1}^k a_i f(\tau_i, t), \end{aligned}$$

where $f(\tau_i, t) = \frac{1}{\tau_i} e^{-\frac{t}{\tau_i}}$ is the normalized single exponential component probability density function with the characteristic time τ_i . a_i is the weighting of the $f(\tau_i, t)$ component and $\sum_{i=1}^k a_i = 1$

We can present this probability density function as the form of likelihood function, $p(t) = p(\vec{\theta}|t) = \text{lik}(t|\vec{\theta})$,

where $\vec{\theta} = (\vec{a}_1, \vec{\tau}_1, \vec{a}_2, \vec{\tau}_2, \vec{a}_3, \vec{\tau}_3 \dots)$.

The sensitivity of maximum likelihood method

It is important to know the sensitivity of this method. In this subsection we would test the sensitivity of this method by a series of two-state random data.

The probability density function of these two-state random data is

$$p_{2s}(t) = a_1 f(\tau_1, t) + a_2 f(\tau_2, t).$$

We have tested 12 random data sets with $\frac{a_2}{a_1} = 1.1, 1.5, 2, 4$ and $\frac{a_2}{a_1} = 1, 1/11, 1/101$. Set $\vec{\theta} = (a_1, \tau_1, a_2, \tau_2)$ and

they are

“maxlik-2aa”, with $\vec{\theta} = (0.5, 1, 0.5, 1.1)$

“maxlik-2ab”, with $\vec{\theta} = (0.9, 1, 0.1, 1.1)$

“maxlik-2ac”, with $\vec{\theta} = (0.99, 1, 0.01, 1.1)$

“maxlik-2ba”, with $\vec{\theta} = (0.5, 1, 0.5, 1.5)$

“maxlik-2bb”, with $\vec{\theta} = (0.9, 1, 0.1, 1.5)$

“maxlik-2bc”, with $\vec{\theta} = (0.99, 1, 0.01, 1.5)$

“maxlik-2ca”, with $\vec{\theta} = (0.5, 1, 0.5, 2)$

“maxlik-2cb”, with $\vec{\theta} = (0.9, 1, 0.1, 2)$

“maxlik-2cc”, with $\vec{\theta} = (0.99, 1, 0.01, 2)$

“maxlik-2da”, with $\vec{\theta} = (0.5, 1, 0.5, 4)$

“maxlik-2db”, with $\vec{\theta} = (0.9, 1, 0.1, 4)$

“maxlik-2dc”, with $\vec{\theta} = (0.99, 1, 0.01, 4)$.

The data points of these data sets are all $N = 10^6$.

maxlik-2a	aa _{ideal}	aa _{guess}	ab _{ideal}	ab _{guess}	ac _{ideal}	ac _{guess}
a_1	0.5	0.9453	0.9	0.5149	0.99	0.5122
τ_1	1	1.0381	1	0.9960	1	0.9850
a_2	0.5	0.0547	0.1	0.4851	0.01	0.4877
τ_2	1.1	1.2773	1.1	1.0200	1.1	1.0180

Table 1.1: The test results of maxlik-2a.

maxlik-2b	ba _{ideal}	ba _{guess}	bb _{ideal}	bb _{guess}	bc _{ideal}	bc _{guess}
a_1	0.5	0.5518	0.9	0.8681	0.99	0.9901
τ_1	1	1.0192	1	0.9872	1	0.9990
a_2	0.5	0.4481	0.1	0.1319	0.01	0.0989
τ_2	1.5	1.5363	1.5	1.4631	1.5	1.4993

Table 1.2: The test results of maxlik-2b.

We test these data sets by the maximum likelihood method with two exponential component probability density function, and the initial test point for all of them is $\vec{\theta} = (0.5, 1, 0.5, 1)$. The following table 1.1 to table 1.4 are the guess results of these 12 data sets and the error is defined as $error_{pi} = \left| \frac{p_{i,ideal} - p_{i,exp}}{p_{i,ideal}} \right|$. Table 1.5 is the average error of each data set.

We can see the average error of τ is in the order 0.01, except the case “maxlik-2a”. It means the fit result is not good as $\frac{\tau_2}{\tau_1} < 1.1$. And the average error becomes larger as $\frac{a_1}{a_2}$ becomes an extreme value. The fit results are not good as $\frac{a_1}{a_2} > 99$ and $\frac{\tau_2}{\tau_1} > 1.5$.

From these test results we can see when the weighting of two states is close, the guess result is more accurate. When $\frac{a_1}{a_2}$ is at the extreme value and the characteristic time τ is too close, the method tends to guess them as the same state. and in extreme weighting and the characteristic time τ being close, τ in the weak state might have a larger error.

maxlik-2c	ca_{ideal}	ca_{guess}	cb_{ideal}	cb_{guess}	cc_{guess}	cc_{guess}
a_1	0.5	0.5142	0.9	0.9005	0.99	0.9936
τ_1	1	1.0103	1	0.9993	1	1.0028
a_2	0.5	0.4858	0.1	0.0995	0.01	0.0006
τ_2	2	2.0204	2	2.0047	2	2.1218

Table 1.3: The test results of maxlik-2c.

maxlik-2d	da_{ideal}	da_{guess}	db_{ideal}	db_{guess}	dc_{ideal}	dc_{guess}
a_1	0.5	0.4991	0.9	0.9007	0.99	0.9889
τ_1	1	0.9974	1	1.0036	1	0.9990
a_2	0.5	0.5009	0.1	0.0993	0.01	0.0111
τ_2	4	3.9930	4	4.0086	4	3.8551

Table 1.4: The test results of maxlik-2d.

error	a	b	c
a	0.4951	1.0889	12.085
b	0.0627	0.0979	2.2228
c	0.04	0.1685	0.2401
d	0.0199	0.0033	0.0371

Table 1.5: The error of maxlik2a-2d.

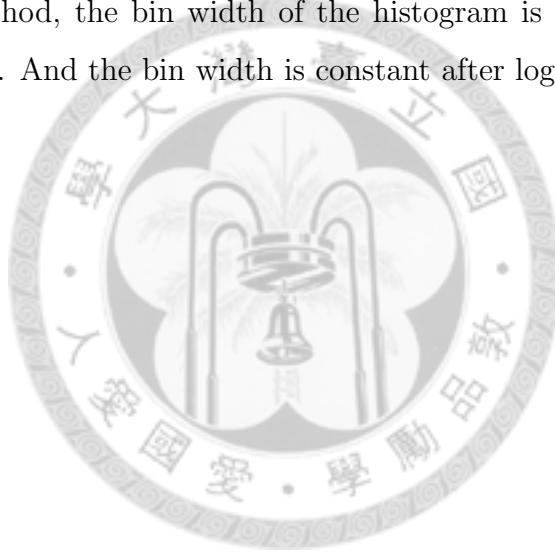
The multi-state data analysis

Here we test two data sets with $N = 10^6$, they are “maxlik3a” and “maxlik5a”, which are generated from the probability density function $p_{3a}(t)$ with three exponential components and $p_{5a}(t)$ with five exponential components, where

$$p_{3a}(t) = 0.6f(10, t) + 0.1f(30, t) + 0.3f(80, t),$$

$$p_{5a}(t) = 0.2f(0.1, t) + 0.08f(5, t) + 0.22f(20, t) + 0.15f(200, t) + 0.35f(600, t)$$

Fig 1.5 (a) and Fig.1.6 (a) are the cumulated histogram of “*maxlik3a*” and “*maxlik5a*”. There are no obvious characteristics in these curves. Another method could see more characteristics is to plot the histogram with a logarithmic bin axis, which is developed by Blatz and Magleby [36], and improved by Sigworth and Sine [37]. In this method, the bin width of the histogram is not constant, but with an exponential scale. And the bin width is constant after logarithmic transformation.



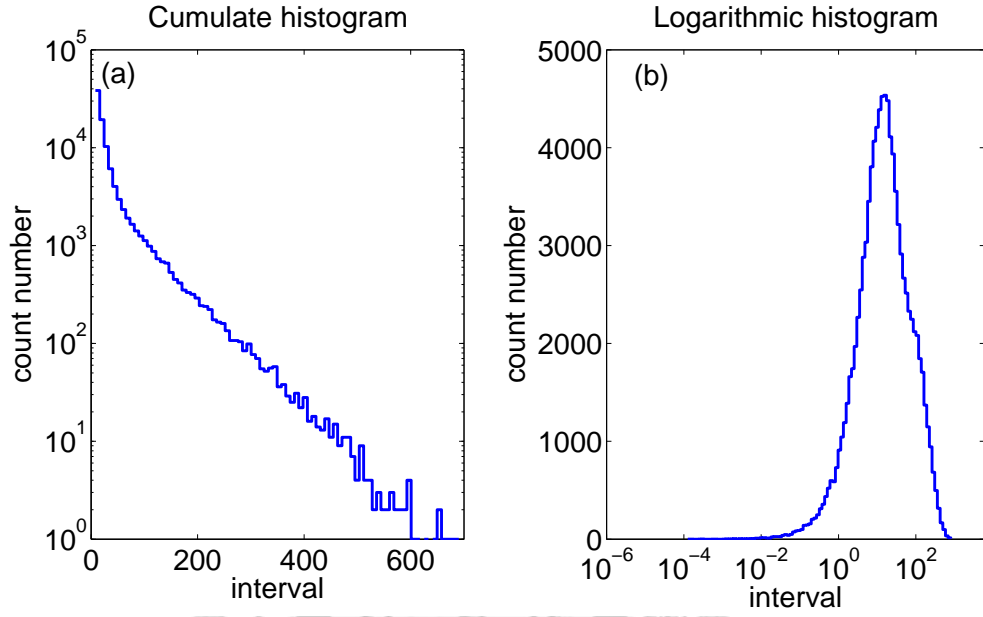


Figure 1.5: (a) is the histogram of $maxlik - 3a$, ($\vec{\theta} = (0.6, 10, 0.1, 30, 0.3, 80)$) with linear bin. There is no obvious characteristic in this curve. And (b) is the histogram of the same data set with logarithmic bin. The peak is related to a_i and $\vec{\tau}_i$. It has at least two peaks in the histogram.

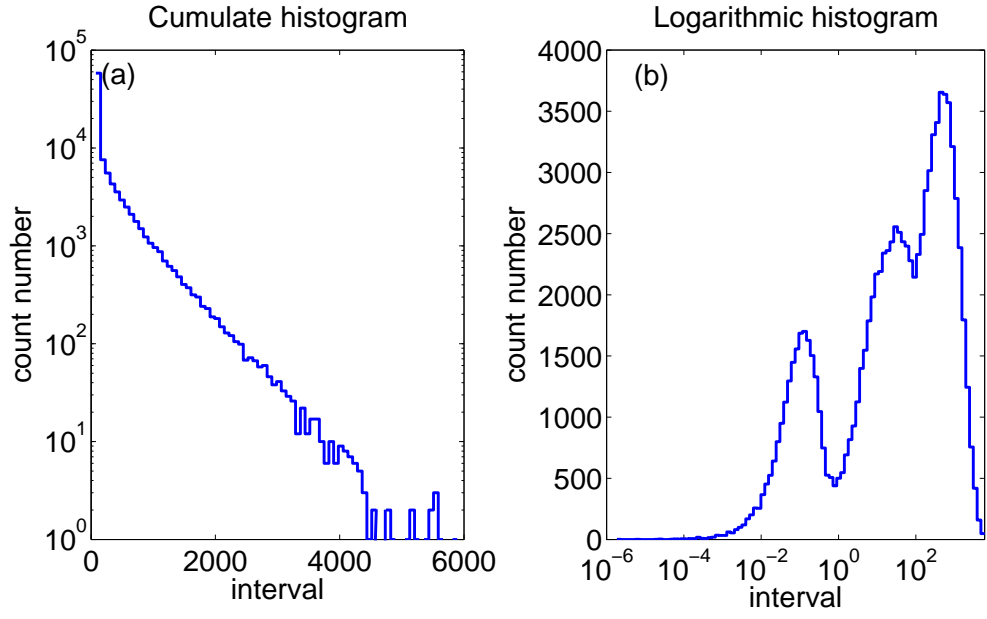
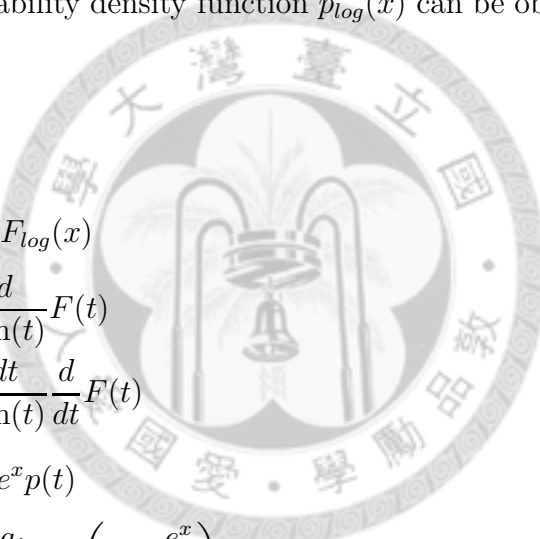


Figure 1.6: (a) is the histogram of $maxlik - 5a$, ($\vec{\theta} = (0.1, 0.1, 0.08, 5, 0.22, 20, 0.15, 200, 0.35, 600)$) with linear bin. There is no obvious characteristic in this curve. And (b) is the histogram of the same data set with logarithmic bin. The peaks are related to a_i and $\vec{\tau}_i$. It has three or four peaks in the histogram.

To describe this method in a mathematical way, we can set $x = \ln(t)$, and the accumulated probability density function with logarithmic transform bin width $F(t)$ can be defined as

$$\begin{aligned}
 F(t') &= \text{Prob}(t < t') \\
 &= \text{Prob}(\ln(t) < \ln(t')) \\
 &= \text{Prob}(x < x') \\
 &\equiv F_{\log}(x').
 \end{aligned}$$

Then the probability density function $p_{\log}(x)$ can be obtained from the derivation of $F_{\log}(x)$.



$$\begin{aligned}
 p_{\log}(x) &= \frac{d}{dx} F_{\log}(x) \\
 &= \frac{d}{d \ln(t)} F(t) \\
 &= \frac{dt}{d \ln(t)} \frac{d}{dt} F(t) \\
 &= \sum_{i=1}^k e^x p(t) \\
 &= \sum_{i=1}^k \frac{a_i}{\tau_i} \exp\left(x - \frac{e^x}{\tau_i}\right)
 \end{aligned}$$

For a single exponential component case,

$$p_{\log}(x)|_{k=1} = \frac{1}{\tau} \exp\left(x - \frac{e^x}{\tau}\right),$$

From

$$\frac{d}{dx} p_{\log}(x) = \frac{(1 - \frac{e^x}{\tau})}{\tau} \exp\left(x - \frac{e^x}{\tau}\right),$$

we can find the extreme point is $x = \ln(\tau_i)$ or $t = \tau_i$.

Figure 1.7 is the ideal diagram of linear bin and logarithmic bin curve of random data with the probability density function $p(t) = e^{-t}$ = single exponential component, with the data number being 100000 .

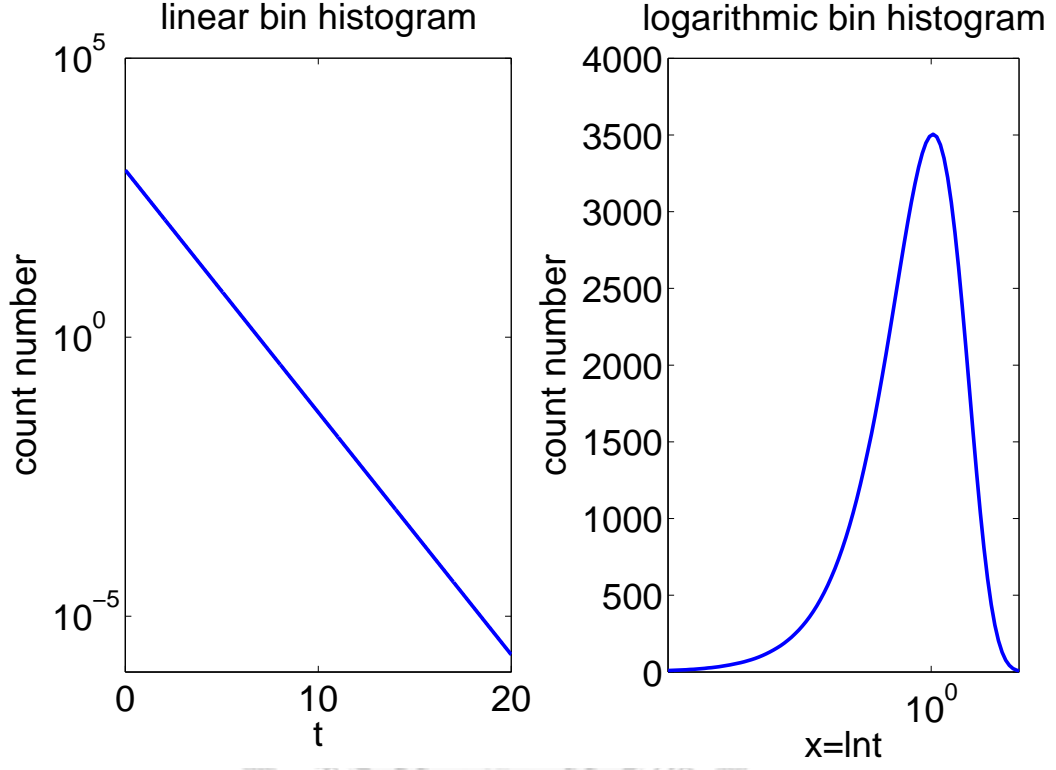


Figure 1.7: (a) is the ideal linear bin histogram function of a data set with the probability density function of single exponential component with $\tau = 1$ and $N = 10^5$. It is a decreasing line. And (b) is the ideal histogram function of the same data set with logarithmic bin. There is a peak at $\tau = 1$

In multiple exponential component case, the probability density function is the superposition of several single exponential component function. Therefore the position of these peaks is related to the characteristic time τ_i , and the height of the peaks is related to the strength of the component a_i .

To compare the histogram with the theoretical function, we need to find the ideal histogram function. It can be found by using the cumulate probability density function,

$$F(t) = \int_t^\infty p(t')dt'$$

and the probability weighting between t_1 and t_2 is $F(t_1) - F(t_2)$.

In logarithmic bin histogram, the bin width in t space is dt , and the interval between t and $t + dt$ can be mapped to t space interval between t and te^{dt} . Therefore, the function of logarithmic bin histogram is

$$LH(t) = F\left(\frac{t}{e^{dt}}\right) - F(t).$$

Fig1.8 (b) and Fig1.9 (b) are the logarithmic bin histograms of *maxlik3a* and *maxlik5a*. We can see that there is a wide peak in the “maxlik3a” histogram and it looks like there are at least two or three peaks mixed in this main peak. And there is three obvious peaks in the “maxlik5a” histogram, but actually there are five exponential components in this probability density function. It might be due to that there is some characteristic times τ_i with the same scale, or the weighting of some components is too small. Although the logarithmic bin histogram have more information than the linear bin histogram, it also needs some experiences to determine the accurate state numbers from the logarithmic bin histogram.

For convenience, in the following test, we will hypothesize that there are three states in “maxlik3a” and five states in “maxlik5a”. And then we can use the maximum

maxlik3a	a_1	τ_1	a_2	τ_2	a_3	τ_3
ideal	0.6	10	0.1	30	0.3	80
1_{guess}	0.3333	10	0.3333	10	0.3333	10
1_{final}	0.6028	9.9996	0.0959	30.105	0.3013	79.939
2_{guess}	0.5	10	0.1667	50	0.3333	100
2_{final}	0.6028	9.9998	0.0995	30.104	0.3012	79.938
3_{guess}	0.6028	9.9998	0.0995	30.104	0.3012	79.938
3_{final}	0.6028	9.9998	0.0959	30.104	0.3012	79.938

Table 1.6: The test results of “maxlik3a”

likelihood method to find better parameters to fit the test data sets. Furthermore, we will check the suggested state number according to the logarithmic likelihood ratio test and compare it with the actual states number.

Table 1.6 is the guess results of “maxlik3a”. We have done testing three times. In the first time, the initial guess is a uniform weighting and the characteristic time($\tau = 10$), which is a bad initial point. In the second time, the initial guess is according to the curve of logarithmic bin histogram. And the third time, the initial guess is the result of second time. We can see that despite the difference of the initial guess, the result is convergeng.

Fig. 1.8. is the ideal and guess function compared with the real logarithmic bin histogram. The difference of them is defined as $\sqrt{F_{ideal(guess)}} - \sqrt{histogram}$ [36]. We can see that the difference of the ideal and guess function has the same scale.

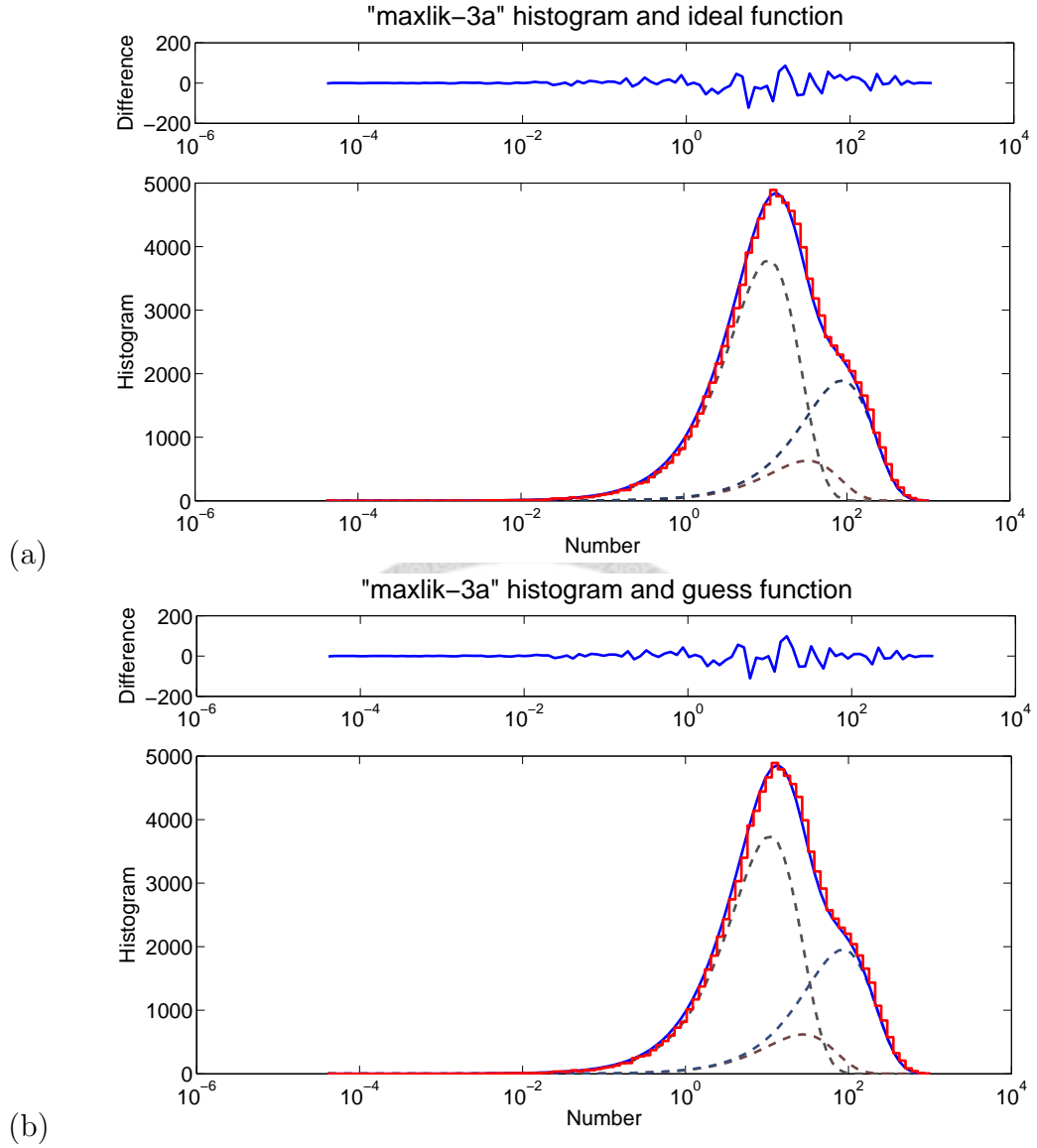


Figure 1.8: (a) is the ideal function compared with the histogram of the data set in “maxlik3a” ($\vec{\theta} = (0.6, 10, 0.1, 30, 0.3, 80)$), and (b) is the guess function compared with the histogram of the data set in “maxlik3a”. We can see the guess function is very close to the ideal function and the histogram of the data set.

states	R	q-value
2	1882276	0
3	179.709	0
4	0.11850	0.7889
5	0.00786	0.9843

Table 1.7: Logarithmic ratio test result of “maxlik3a”

Table 1.7 is the logarithmic likelihood ratio test result of “malik3a”. State number from 1 \sim 5 is tested. We can see the q value has obvious change as state number is 4. Therefore, we have confidence that this data set has three states, because the difference of the maximum likelihood value has no obvious change when the state number changes from 3 to 4.

Table 1.8 is the test result of “maxlik5a”. The initial guess of the first test is a uniform guess with $\tau = 100$. And the initial guess of the second test is according to the hint from the logarithmic bin histogram. And the third test is the result of the second test. We can see despite the difference in the initial guess, the final results are almost the same. And the error is shown in Table 2, where $\Delta a_i = |a_{i,ideal} - a_{i,exp}|$. We can see the results of these tests have converged to the same result.

(maxlike5a)	a_1	τ_1	a_2	τ_2
ideal	0.2	0.1	0.08	5.0
1_{guess}	0.2	10	0.2	10
1_{final}	0.2003	0.1001	0.0790	4.9570
2_{guess}	0.1852	0.1	0.2314	12.0
2_{final}	0.2004	0.1001	0.0790	4.9570
3_{guess}	0.2004	0.1001	0.0790	4.9570
3_{final}	0.200395	0.0993109	0.0820099	4.83924
4_{guess}	0.2	10.0	0.2	10.0
4_{final}	0.200395	0.0993109	0.0820104	4.83928

(maxlike5a)	a_3	τ_3	a_4	τ_4	a_5	τ_5
ideal	0.22	20.0	0.15	200	0.35	600
1_{guess}	0.2	10	0.2	10	0.2	10
1_{final}	0.2210	20.2438	0.1493	200.77	0.3503	600.99
2_{guess}	0.0926	80.0	0.1203	98.0	0.3703	560.0
2_{final}	0.2210	20.2439	0.1493	200.77	0.2210	600.99
3_{guess}	0.2210	20.2439	0.1493	200.77	0.2210	600.99
3_{final}	0.220585	20.6387	0.157138	208.815	0.339870	608.129
4_{guess}	0.2	10.0	0.2	10.0	0.2	10.0
4_{final}	0.220585	20.6388	0.157139	208.816	0.3399	608.130

Table 1.8: The test results of “maxlik5a”

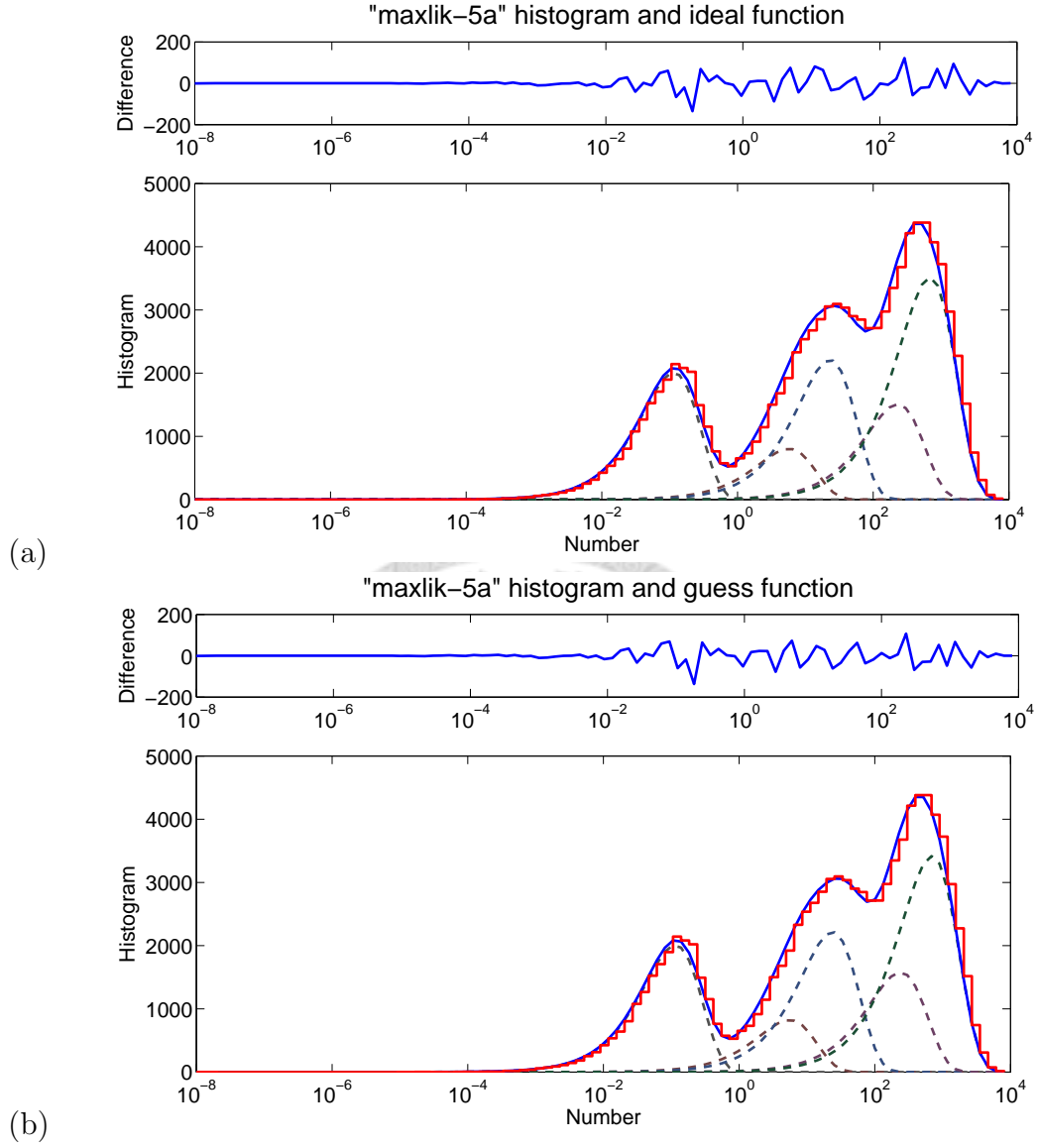


Figure 1.9: (a) is the ideal function compared with the histogram of the data set in “*maxlik5a*” ($\vec{\theta} = (0.1, 0.1, 0.08, 5, 0.22, 20, 0.15, 200, 0.35, 600)$), and (b) is the guess function compared with the histogram of the data set in “*maxlik5a*”

states	R	q-value
2	958389	0.0
3	287088	0.0
4	5775.88	0.0
5	1827.23	0.0
6	1.5×10^{-7}	0.999999
7	3.53×10^{-6}	0.999993

Table 1.9: Logarithmic ratio test result of “maxlik5a”

Further, we will check how many states are enough to fit the data set *maxlike-5a*. Initial guess with state number form 2 \sim 7 is tested, then we take the logarithmic likelihood ratio test for these results. Table 1.9 presents the initial guess state number and q value obtained from the logarithmic likelihood ratio test. The q value is very closed to 1 when the initial guess state is larger than 5, and others tend to 0. The result of the logarithmic likelihood ratio test also supplies more confidence on the maximum likelihood method.

Data set with different N

The error of the guess result and ideal parameters must have high correlation with the number of data points N . To check this concept, we generate a series of three state data set “testN” with different number of data points N from $10^2 \sim 10^7$. The probability density function of *testN* is

$$p_{testN}(t) = 0.4f(1, t) + 0.3f(10, t) + 0.3f(100, t).$$

Fig.1.10 is the relation of mean error and N in *testN* data set series. For each N data point test, five data set are generated. The definition of mean error is the

average of each error of guess parameters. We can see that it has a power law decay tendency roughly.

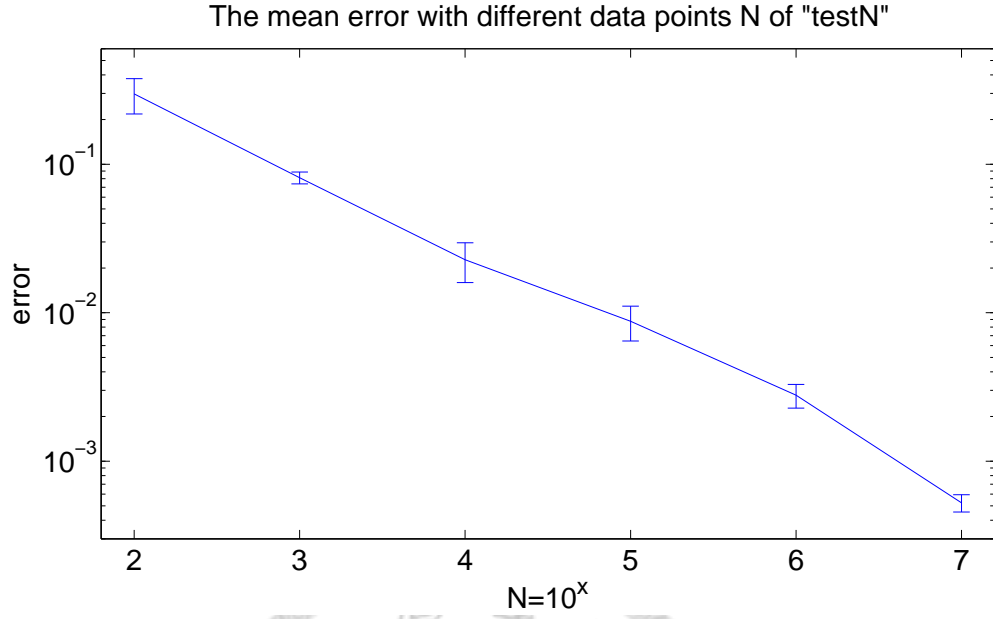


Figure 1.10: The the guess error of testN series data sets, which has the same probability density function with $\vec{\theta} = (0.4, 1, 0.3, 10, 0.3, 100)$ but with different data points number N . We can see in this plot the error of guess and the number of data points N have a power law decaing tendency roughly.

When the data points N are small, the error of the guess result is larger, and the data set might not present the accurate properties of the probability density function. The convergence of the guess results will be broken.

A.4.2 Application of 2-D data analysis

Multivariate random variable data set [34]

In general, we may need to analyze data set with multiple random variables $\hat{X} = (\vec{X}_1, \vec{X}_2, \dots, \vec{X}_N)$, which have a joint probability density function $p(\vec{X}) = p(x_1, x_2, \dots)$. The joint probability density function of multiple random variables is more complicated than the probability density function of single random variable because it may have dependency between the random variables [34]. To discuss the dependency of multiple random variables, for simplicity, a joint probability density function with two random variables will be illustrated here.

Set the joint probability density function with two random variables are $p(\vec{X}) = p(x_1, x_2)$. From the conservation of probability, we have

$$\int_{x_1} \int_{x_2} p(x_1, x_2) dx_1 dx_2 = 1.$$

We can obtain the marginal probability function of x_1 as $p_1(x_1) = \int_{x_2} p(x_1, x_2) dx_2$, and similarly to $p_2(x_2)$.

Furthermore, the conditional probability density function can be written as

$$p(x_2|x_1) = \frac{p(x_1, x_2)}{p_1(x_1)}$$

or

$$p(x_1|x_2) = \frac{p(x_1, x_2)}{p_2(x_2)}.$$

And $p(x_1, x_2)$ can be represented as $p(x_1, x_2) = p_1(x_1)p(x_2|x_1) = p_2(x_2)p(x_1|x_2)$.

But if x_1 and x_2 are independent, then we can write

$$p(x_1, x_2) = p_1(x_1)p_2(x_2).$$

Now if we set the marginal probability density function of x_1 and x_2 was composed by several components of states.

$$p_1(x_1) = \sum_i a_i f_i(x_1|\vec{\theta}_i)$$

and

$$p_2(x_2) = \sum_j b_j f_j(x_2|\vec{\theta}_j),$$

where $f_i(x|\vec{\theta}_i)$ is the normalized state probability density function. And it is evident that $\sum_i a_i = 1$ and $\sum_j b_j = 1$.

For the independent case,

$$p(x_1, x_2) = \sum_i \sum_j V_{ij} f_i(x_1|\vec{\theta}_i) f_j(x_2|\vec{\theta}_j).$$

But if x_1 and x_2 are dependent, the joint probability density function will be different with the independent case. However, we can still expand the joint probability density function with the same basis of the independent case,

$$p(x_1, x_2) = \sum_i \sum_j V_{ij} f_i(x_1|\vec{\theta}_i) f_j(x_2|\vec{\theta}_j).$$

But the weighting V_{ij} is not equal to $a_i b_j$. Furthermore, we can compare the V_{ij} for the dependent and independent cases. The difference of the dependent and independent cases for each basis can be shown. A quantity D is the component dependency defined as [34]

$$D_{ij} = \frac{V_{ij,obs} - V_{ij,ind}}{V_{ij,ind}}.$$

The sign of D_{ij} indicates the enhancement or reduction of the corresponding basis state compared with independent case, and the magnitude of D indicates the strength of variation.

2-D multiple exponential state data analysis

A two-dimensional joint probability density function with each marginal probability density function being multiple exponential component function is used here. The form of joint probability density function $p(t_1, t_2)$ is

$$p(t_1, t_2) = \sum_{i,j=1}^{i,j=k_1,k_2} V_{ij} \frac{1}{\tau_{1,i} \tau_{2,j}} e^{-\frac{t_1}{\tau_{1,i}}} e^{-\frac{t_2}{\tau_{2,j}}}.$$

If t_1 and t_2 are independent, $V_{ij,ind} = a_{1,i} a_{2,j}$, but if they are dependent, the form of V_{ij} is complicated. The only constraint of non-independent V_{ij} of the dependent case is conservation of probability, which is $\sum_{i,j} V_{ij} = 1$.

To test this multiple random variable data set, we can first use the maximum likelihood method to test the marginal probability density function of t_1 and t_2 . Then we can find the guess form of $\sum_i a_i f_i(t|\vec{\theta}_i)$ and $\sum_j b_j f_j(t|\vec{\theta}_j)$ to construct a two dimensional joint probability density function and obtain the weighting V_{ij} . Then we can calculate the component dependency D for each state.

Here we test two data sets “*maxlik2D42a*” and “*maxlik2D32b*”. Each of them

with 10^6 data points. The probability density function of *maxlik2D42a* has 4 exponential components in t_1 and 2 in t_2 . *maxlik2D32b* has 3 exponential components in t_1 and 2 in t_2 . The matrix forms of probability density functions of them are

$$p|_{42b}(t_1, t_2) = \begin{pmatrix} f(20, t_2) & f(250, t_2) \end{pmatrix} \begin{pmatrix} 0.05 & 0.15 & 0.12 & 0.08 \\ 0.1 & 0.2 & 0.18 & 0.12 \end{pmatrix} \begin{pmatrix} f(1, t_1) \\ f(10, t_1) \\ f(50, t_1) \\ f(300, t_1) \end{pmatrix}$$

$$p|_{32b}(t_1, t_2) = \begin{pmatrix} f(30, t_2) & f(120, t_2) \end{pmatrix} \begin{pmatrix} 0.1 & 0.2 & 0.15 \\ 0.2 & 0.2 & 0.15 \end{pmatrix} \begin{pmatrix} f(1, t_1) \\ f(10, t_1) \\ f(100, t_1) \end{pmatrix},$$

where $f(\tau, t)$ is the normalized single exponential probability density function with the characteristic time τ .

For *maxlik2D42a*, the ideal value of V matrix and V_{ind} matrix are

$$V_{42a} = \begin{pmatrix} 0.05 & 0.15 & 0.12 & 0.08 \\ 0.1 & 0.2 & 0.18 & 0.12 \end{pmatrix},$$

and

$$V_{42a,ind} = \begin{pmatrix} 0.06 & 0.14 & 0.12 & 0.08 \\ 0.09 & 0.21 & 0.18 & 0.12 \end{pmatrix}.$$

The ideal dependency of *maxlik2D42a* is

$$D_{42a} = \begin{pmatrix} 0.2 & -0.067 & 0 & 0 \\ -0.1 & 0.05 & 0 & 0 \end{pmatrix}.$$

For *maxlik2D32b*, the ideal value of V matrix and V_{ind} matrix are

Table 1.10: Logarithmic ratio test result of “maxlik2D42a-t1”

maxlik2D42a-t1	R	q-value
2	555787	0
3	63557.8	0
4	10031.4	0
5	2.3E10-7	0.9999
6	7.0E10-8	0.9999

Table 1.11: Logarithmic ratio test result of “maxlik2D42a-t1”

$$V_{32b} = \begin{pmatrix} 0.1 & 0.2 & 0.15 \\ 0.2 & 0.2 & 0.15 \end{pmatrix}$$

and

$$V_{32b,ind} = \begin{pmatrix} 0.135 & 0.18 & 0.135 \\ 0.165 & 0.22 & 0.165 \end{pmatrix}.$$

The ideal dependency of *maxlik2D32b* is

$$D_{32b} = \begin{pmatrix} 0.35 & -0.1 & -0.1 \\ -0.175 & 0.1 & 0.1 \end{pmatrix}.$$

To test these data sets, the first step is to depart the 1-D data sets of t_1 and t_2 as “maxlik2D42a-t1”, “maxlik2D42a-t2” and “maxlik2D32b-t1”, “maxlik2D32b-t2”. Using the 1-D maximum likelihood method and logarithmic likelihood ratio test, we can find the appropriate parameter values of them.

From the logarithmic likelihood ratio test shown in table 1.11, 1.12, 1.13, 1.14, we can decide the state number appropriately. The appropriate state numbers of “maxlik2D42a-t1”, “maxlik2D42a-t2”, “maxlik2D32b-t1”, and “maxlik2D32b-t2” are 4,2,3 and 2 respectively.

maxlik2D42a-t2	R	q-value
2	191663.9	0
3	3.4E10-7	0.99999
4	2.0E10-7	0.99999

Table 1.12: Logarithmic ratio test result of “maxlik2D42a-t2”

maxlik2D32b-t1	R	q-value
2	574614.9	0
3	62611.68	0
4	1.0E10-8	1
5	4.0E10-8	0.9999

Table 1.13: Logarithmic ratio test result of “maxlik2D32b-t1”

With the appropriate state number and using the maximum likelihood method, we can find the appropriate parameters of these marginal probability density functions.

The independent V-matrix can be written as $V_{ij,ind} = a_{1,i}a_{2,j}$

$$V_{ind,42a} = \begin{pmatrix} 0.0603 & 0.1398 & 0.1199 & 0.0798 \\ 0.0906 & 0.2099 & 0.1800 & 0.1197 \end{pmatrix}$$

$$V_{ind,32b} = \begin{pmatrix} 0.1352 & 0.1793 & 0.1358 \\ 0.1650 & 0.2189 & 0.1658 \end{pmatrix}.$$

In another way, we can use the maximum likelihood method for the 2-D system “maxlik2D42a” and “maxlik2D32b”. The initial guess is based on the individual guess

maxlik2D32b-t2	R	q-value
2	43419.3	0
3	3.6E10-8	0.99999
4	7.4E10-7	0.99999

Table 1.14: Logarithmic ratio test result of “maxlik2D32b-t2”

maxlik2D-42a	a_1	τ_1	a_2	τ_2	a_3	τ_3	a_4	τ_4
$t_{1,final}$	0.1509	1.0020	0.3497	10.030	0.3000	50.423	0.1995	300.299
$t_{2,final}$	0.3999	20.045	0.6001	250.18	—	—	—	—

Table 1.15: The test results of “maxlik2D42a”

maxlik2D-32b	a_1	τ_1	a_2	τ_2	a_3	τ_3
$t_{1,final}$	0.3002	1.0005	0.3981	9.9654	0.3016	99.8598
$t_{2,final}$	0.4503	29.985	0.5497	119.83	—	—

Table 1.16: The test results of “maxlik2D32b”

result of t_1 and t_2 and V_{ind} . The following table is the guess result of “maxlik2D42a” and “maxlik2D32b”

We can get the V-matrix of them,

$$V_{42a,guess} = \begin{pmatrix} 0.0501 & 0.1494 & 0.1201 & 0.0801 \\ 0.1008 & 0.2002 & 0.1796 & 0.1193 \end{pmatrix}$$

$$V_{32b,guess} = \begin{pmatrix} 0.0993 & 0.1978 & 0.1498 \\ 0.2009 & 0.2003 & 0.1519 \end{pmatrix}.$$

And the dependency of this system is

$$D_{42a,guess} = \begin{pmatrix} 0.1697 & -0.0684 & 0.0015 & -0.0040 \\ -0.1130 & 0.0460 & 0.0021 & 0.0036 \end{pmatrix}$$

and

$$D_{32b,guess} = \begin{pmatrix} -0.2655 & 0.1032 & 0.1031 \\ 0.2176 & -0.0850 & -0.0838 \end{pmatrix}.$$

From the D matrix, we can find the dependency of these two data sets.

Similarly, we are also interested in the relation between data point and error. The result of N and error test of “maxlik2D-32b” is shown in Fig. 1.11. It also has a power law tendency roughly.

maxlik2D42a	a_{11}	a_{12}	a_{21}	a_{22}	a_{31}	a_{32}	a_{41}	a_{42}
ideal	0.05	0.1	0.15	0.2	0.12	0.18	0.08	0.12
1_{guess}	0.0612	0.0918	0.1429	0.2143	0.1224	0.1632	0.0816	0.1224
1_{final}	0.0501	0.1008	0.1494	0.2002	0.1201	0.1796	0.0801	0.1193

τ_{11}	τ_{12}	τ_{13}	τ_{14}	τ_{21}	τ_{22}
1	10	50	300	20	250
1	10	50	300	20	250
1.002	10.035	50.442	300.31	20.04	250.17

Table 1.17: The 2D test results of “maxlik2D42a”

maxlik2D32b	a_{11}	a_{12}	a_{21}	a_{22}	a_{31}	a_{32}
ideal	0.1	0.2	0.2	0.2	0.15	0.15
1_{guess}	0.1352	0.1650	0.1793	0.2189	0.1358	0.1658
1_{final}	0.0993	0.2009	0.1978	0.2003	0.1498	0.1519

τ_{11}	τ_{12}	τ_{13}	τ_{21}	τ_{22}
1	10	100	30	120
1.0005	9.965	99.860	29.985	119.83
1.0003	9.962	99.805	29.832	119.15

Table 1.18: The 2D test results of “maxlik2D32b”

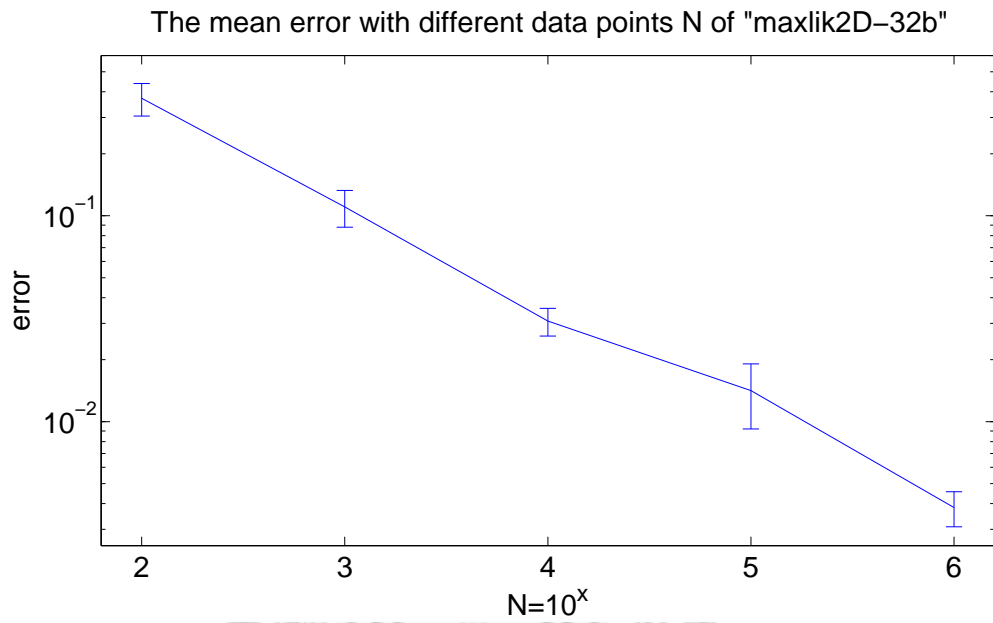


Figure 1.11: This diagram is the relation of N and error in maxlik2D-32b. We can see it also roughly has a power law decaying relation, as the case of 1-D.

Appendix B

The phase portraits of two-state logistic growth and autocrine transition model

B.1 The phase portraits of LH-0

1. \tilde{x}_t and \tilde{w}_1 are straight lines (LH0-LL).

It happens when $r_1 = r_2$. The flow and trajectories are showed in Figure 2.1, Figure 2.2, and Figure 2.3

2. \tilde{x}_t is a straight line \tilde{w}_1 is S type, and they have a cross point at the middle of the S curve (LH0-LSl, LH0-LSm, and LH0-LSr.).

Although S curve could have two forms, one heading to right and the other heading to left, but if we consider the symmetry of w_1 and w_2 , the heading to right case is similar to the heading to left case by changing the parameters from w_1 to w_2 . Therefore, here we show only heading to left case. And the fixed point could be at the left position, the middle position, and the right position. Here we consider these three cases: they are LH0-LSl, LH0-LSm and LH0-LSr.

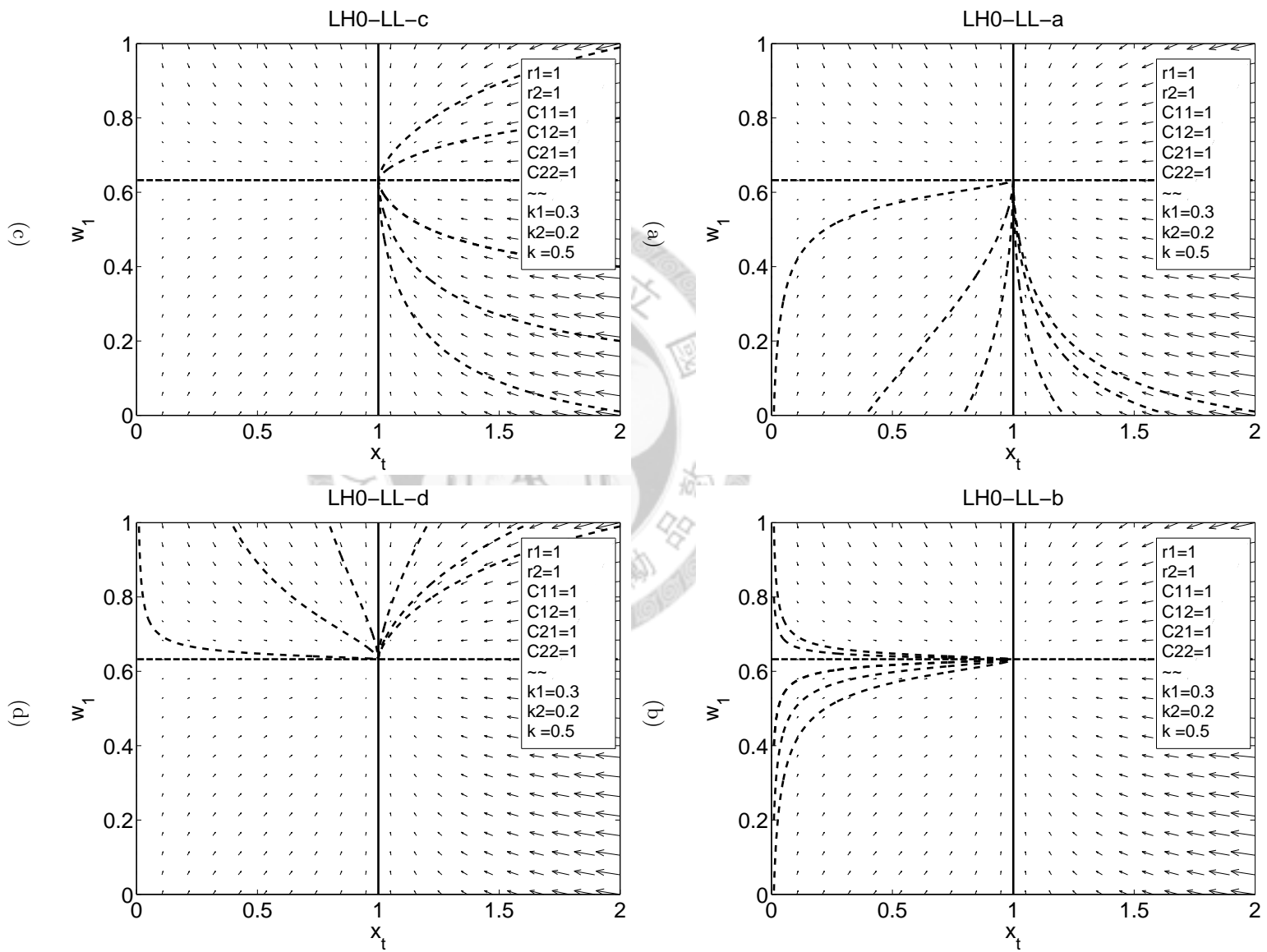


Figure 2.1: The x_{tot} - w_1 trajectories of LH0-LL.

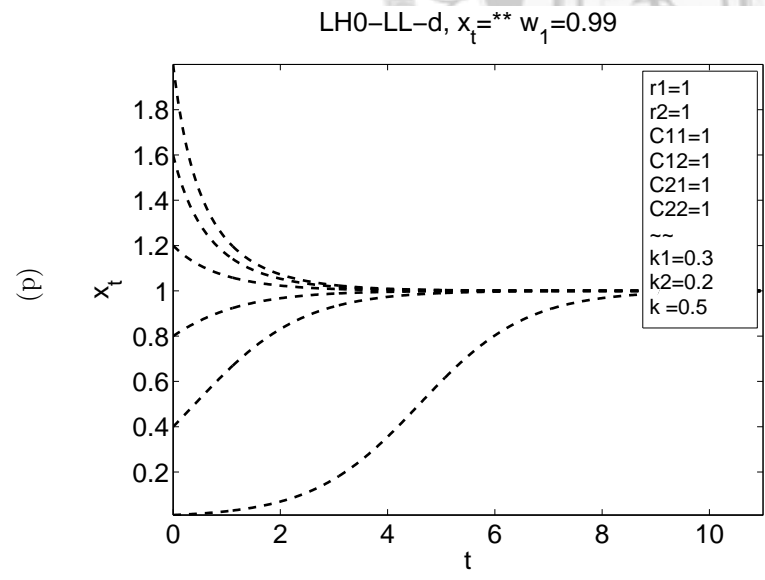
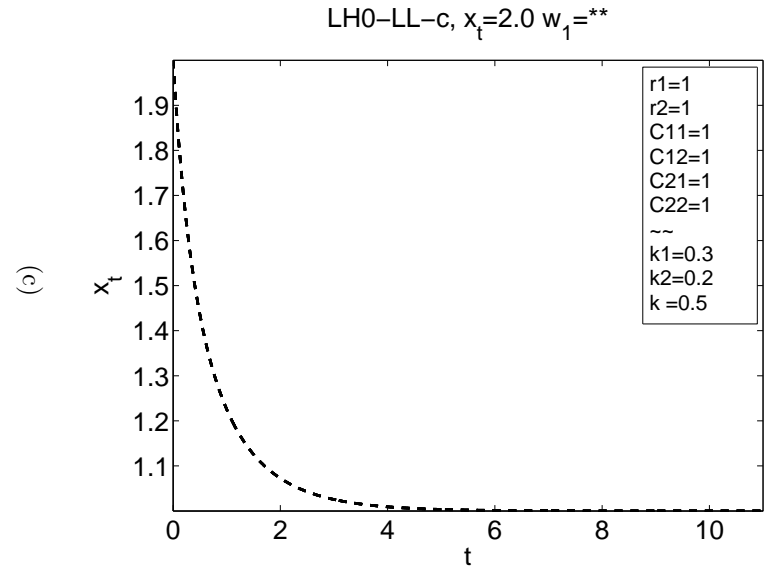
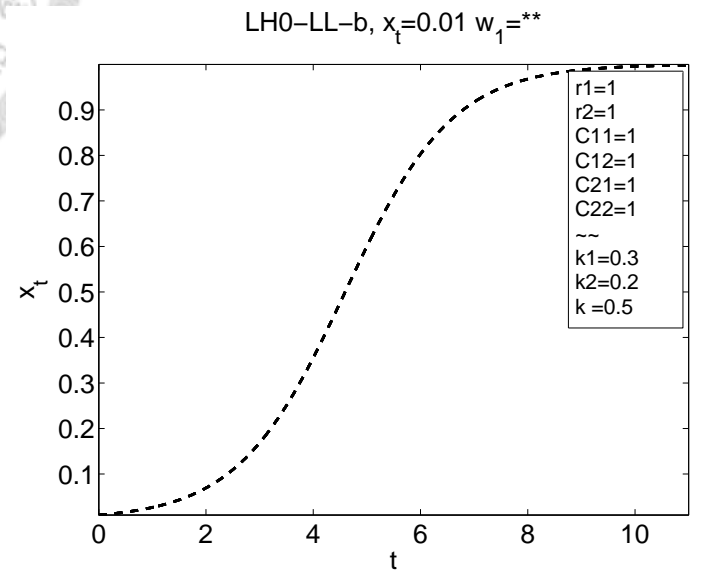
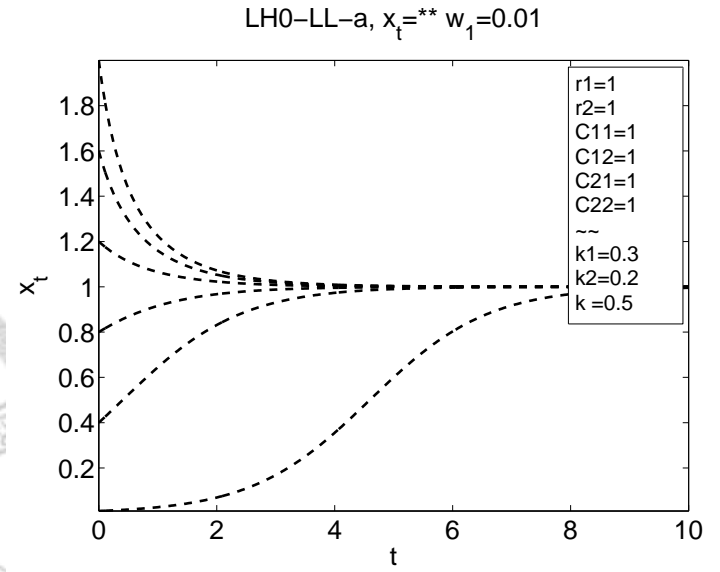


Figure 2.2: The $x_{tot}-w_1$ trajectories of LH0-LL.

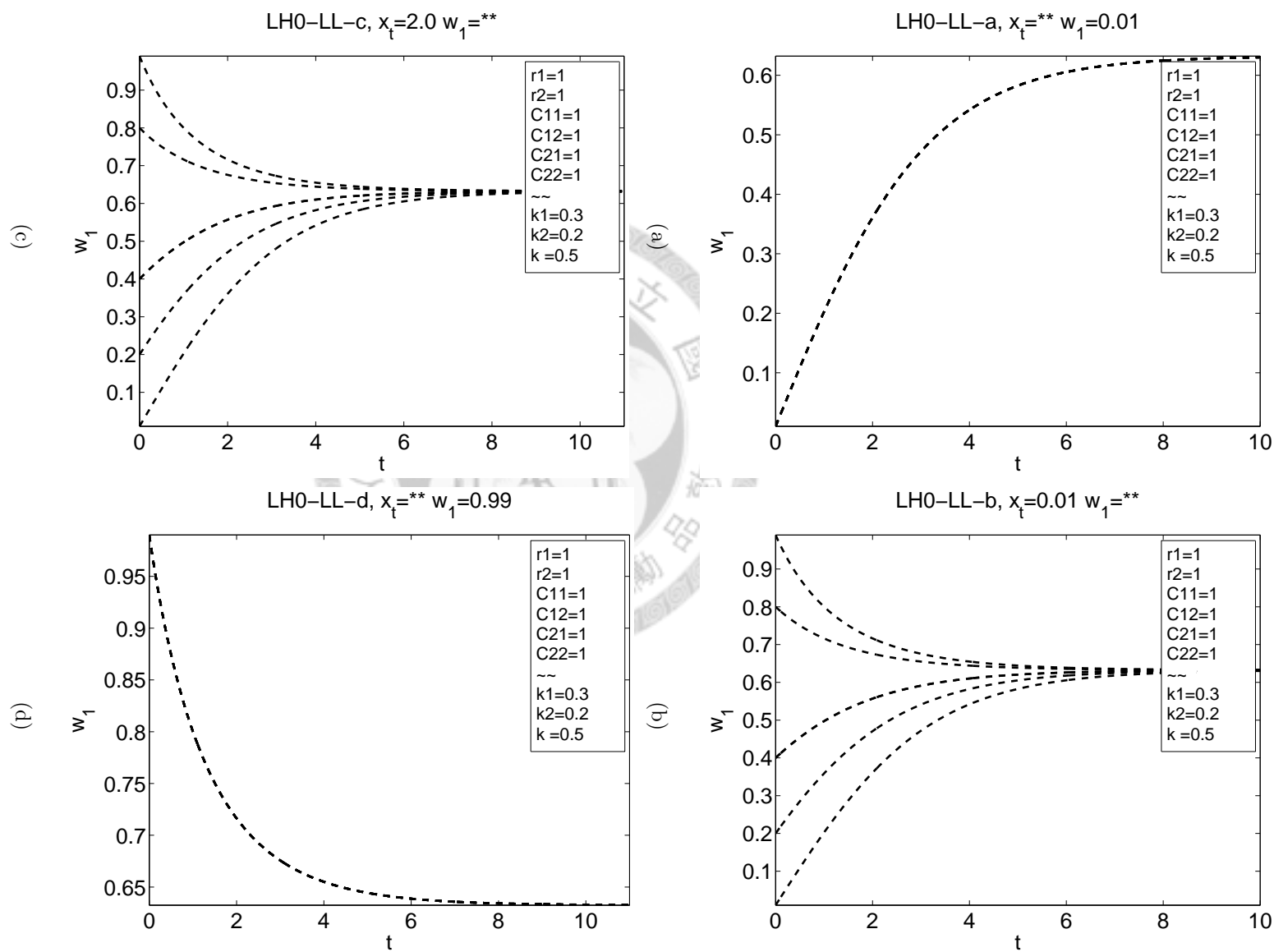


Figure 2.3: The x_{tot} - w_1 trajectories of LH0-LL.

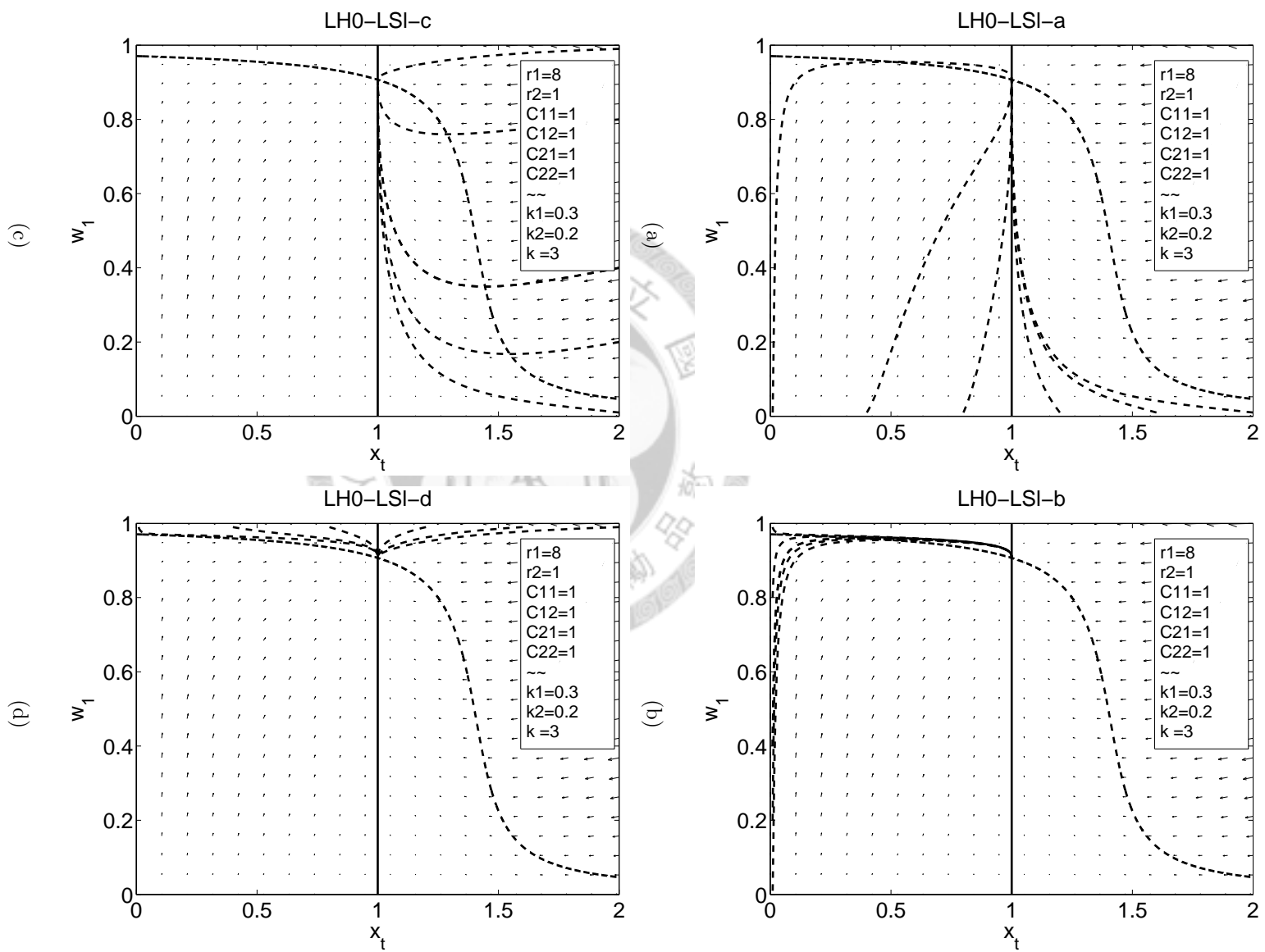


Figure 2.4: The x_{tot} - w_1 trajectories of LH0-LSI.

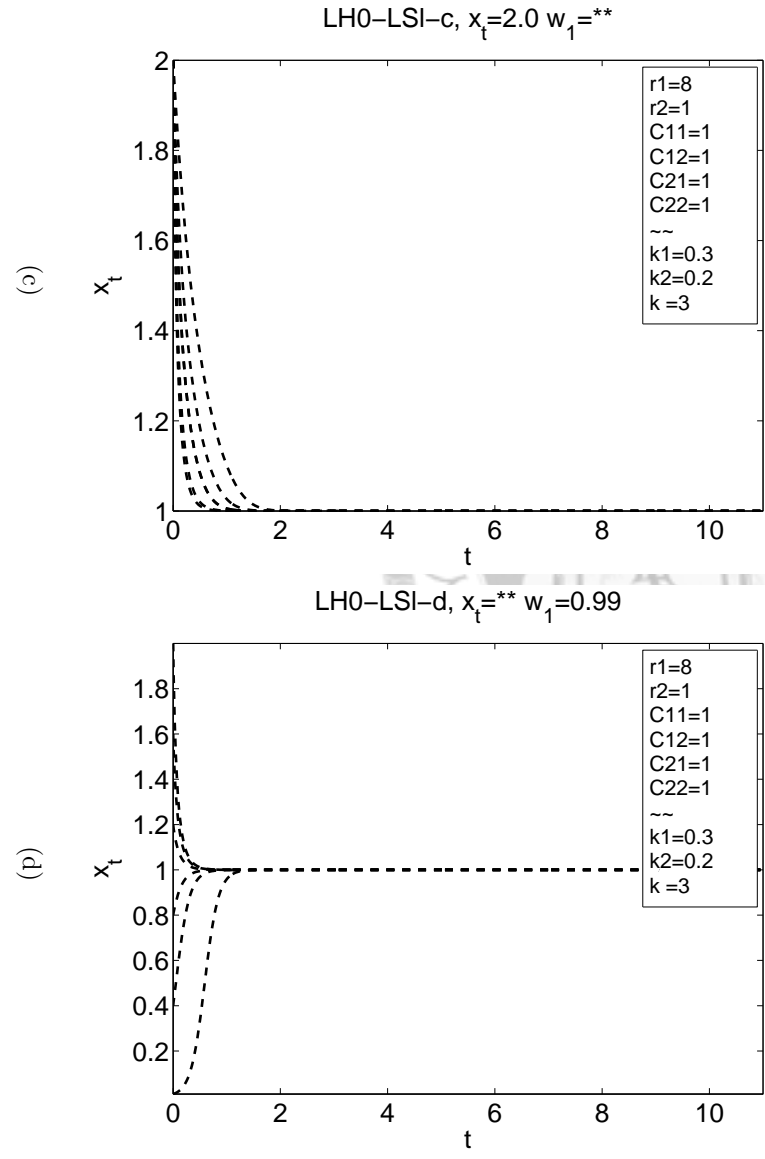
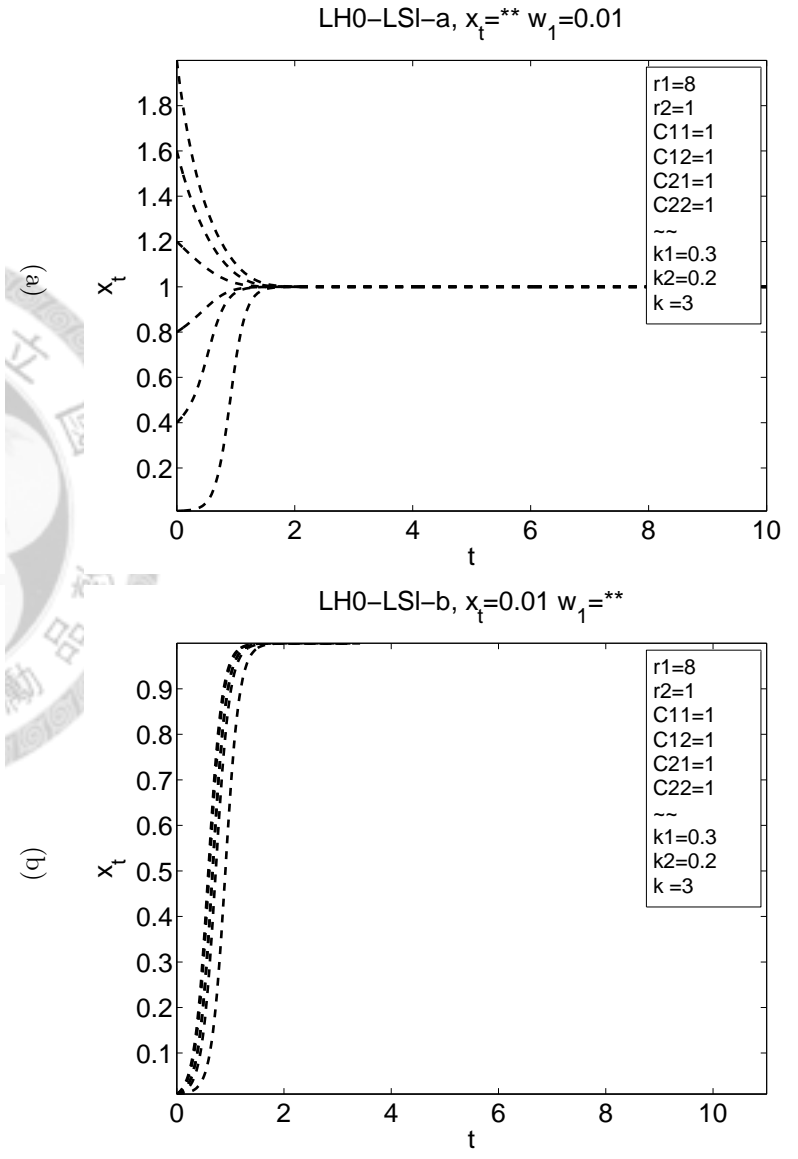


Figure 2.5: The $x_{tot}-w_1$ trajectories of LH0-LSI.

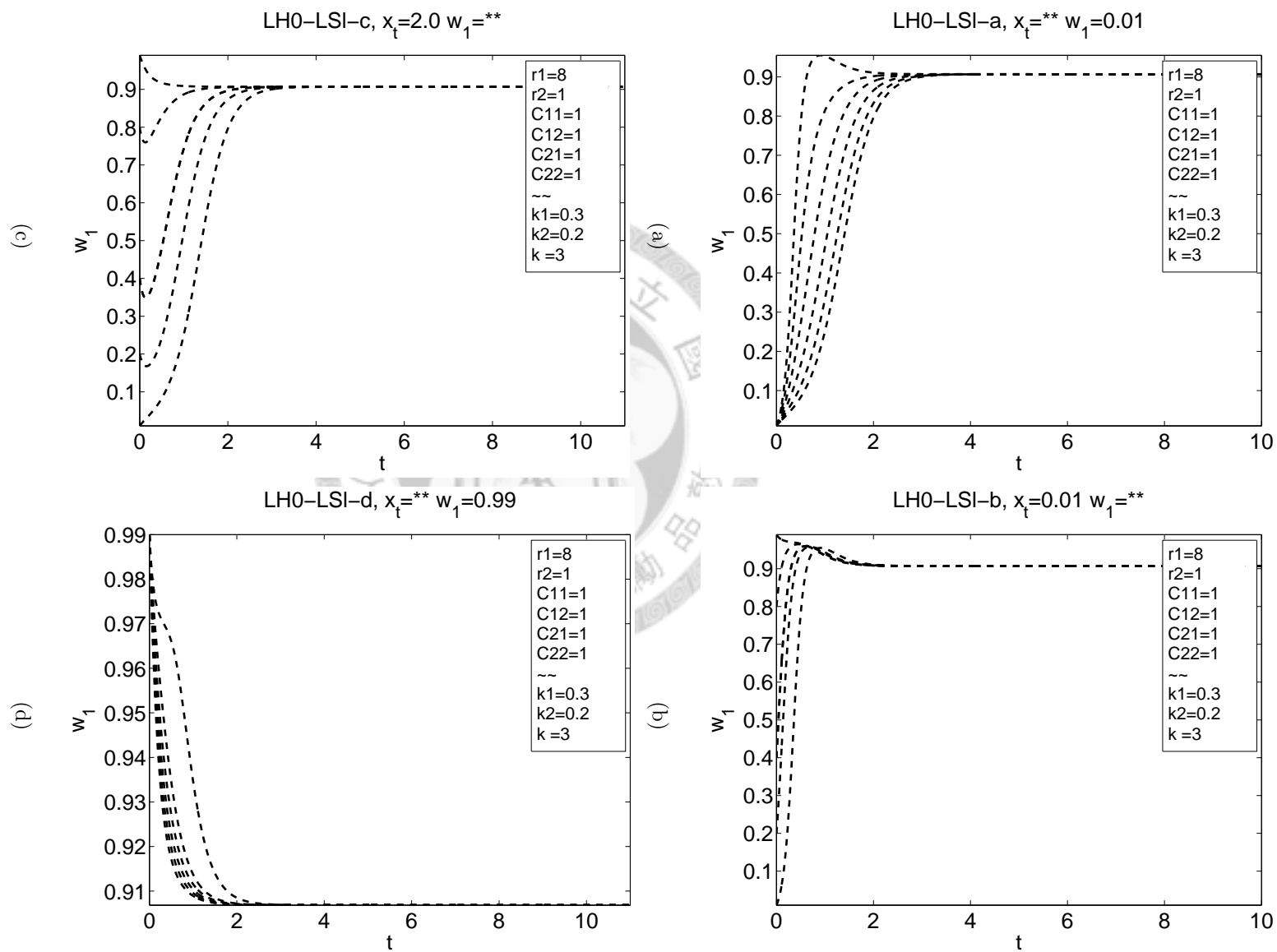


Figure 2.6: The x_{tot} - w_1 trajectories of LH0-LSI.

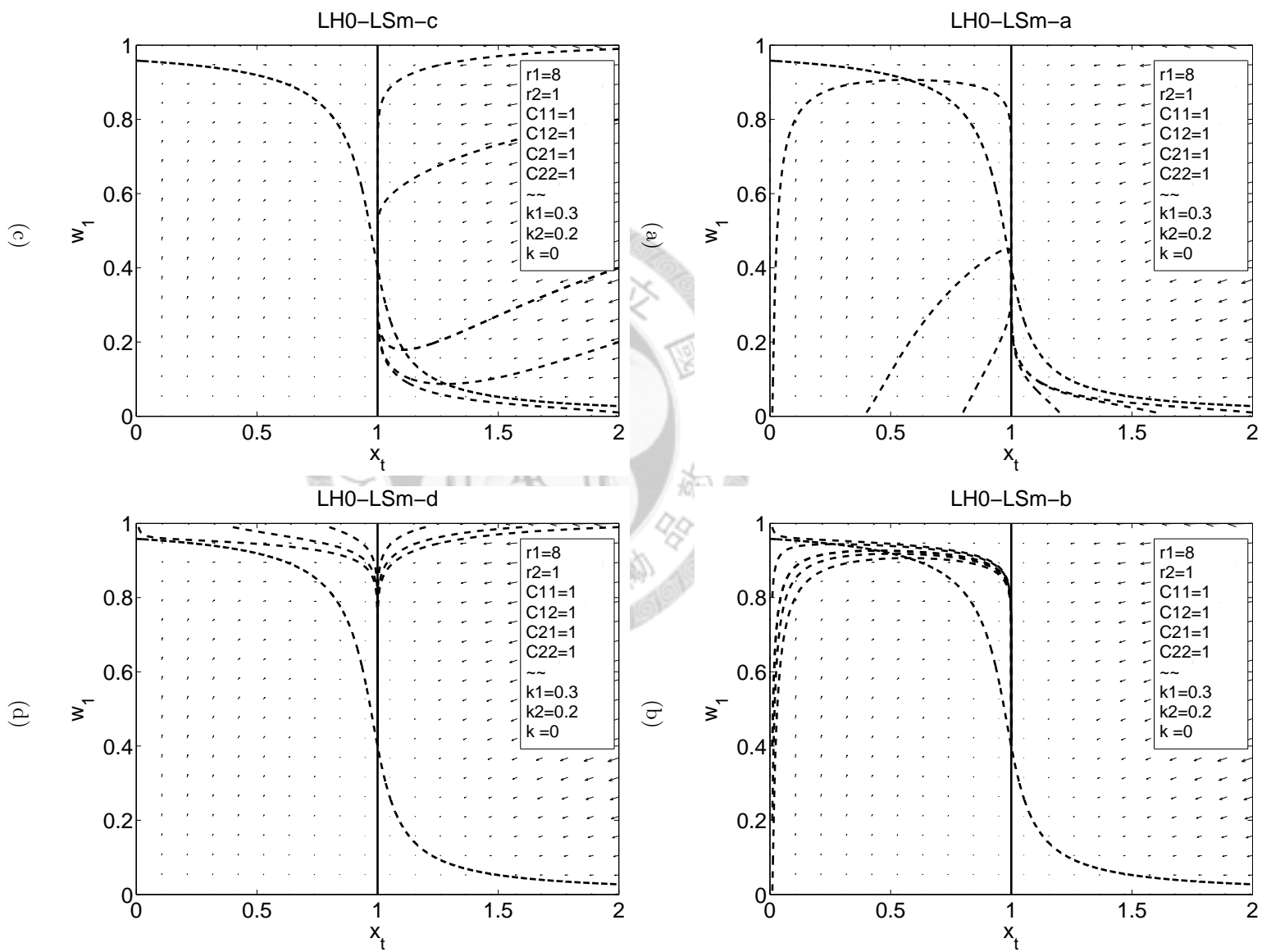


Figure 2.7: The x_{tot} - w_1 trajectories of LH0-LSm.

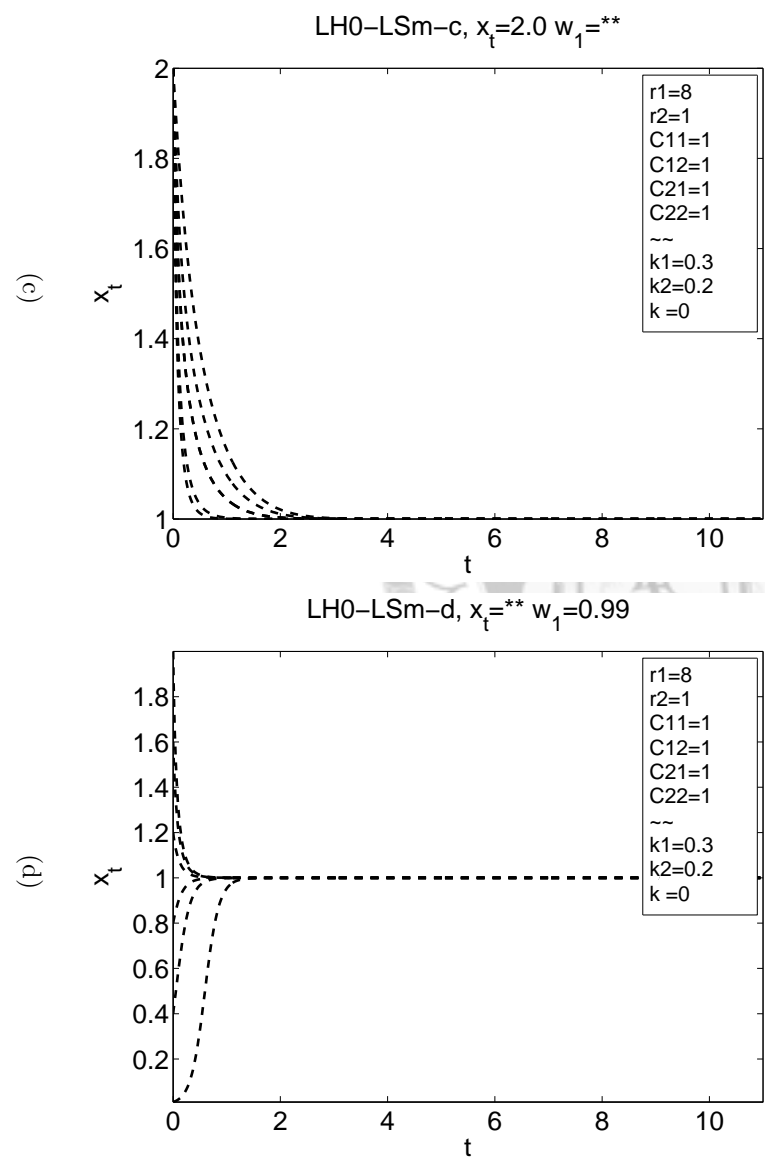
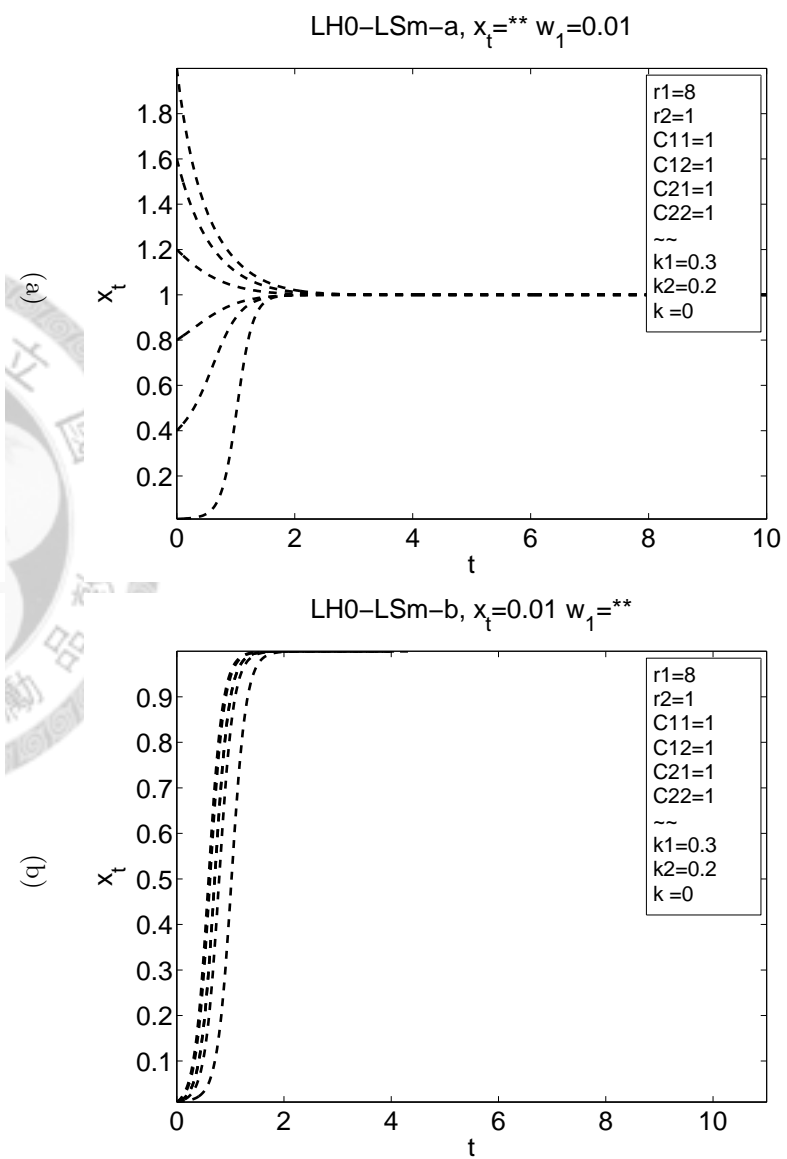


Figure 2.8: The $x_{tot}-w_1$ trajectories of LH0-LSm.

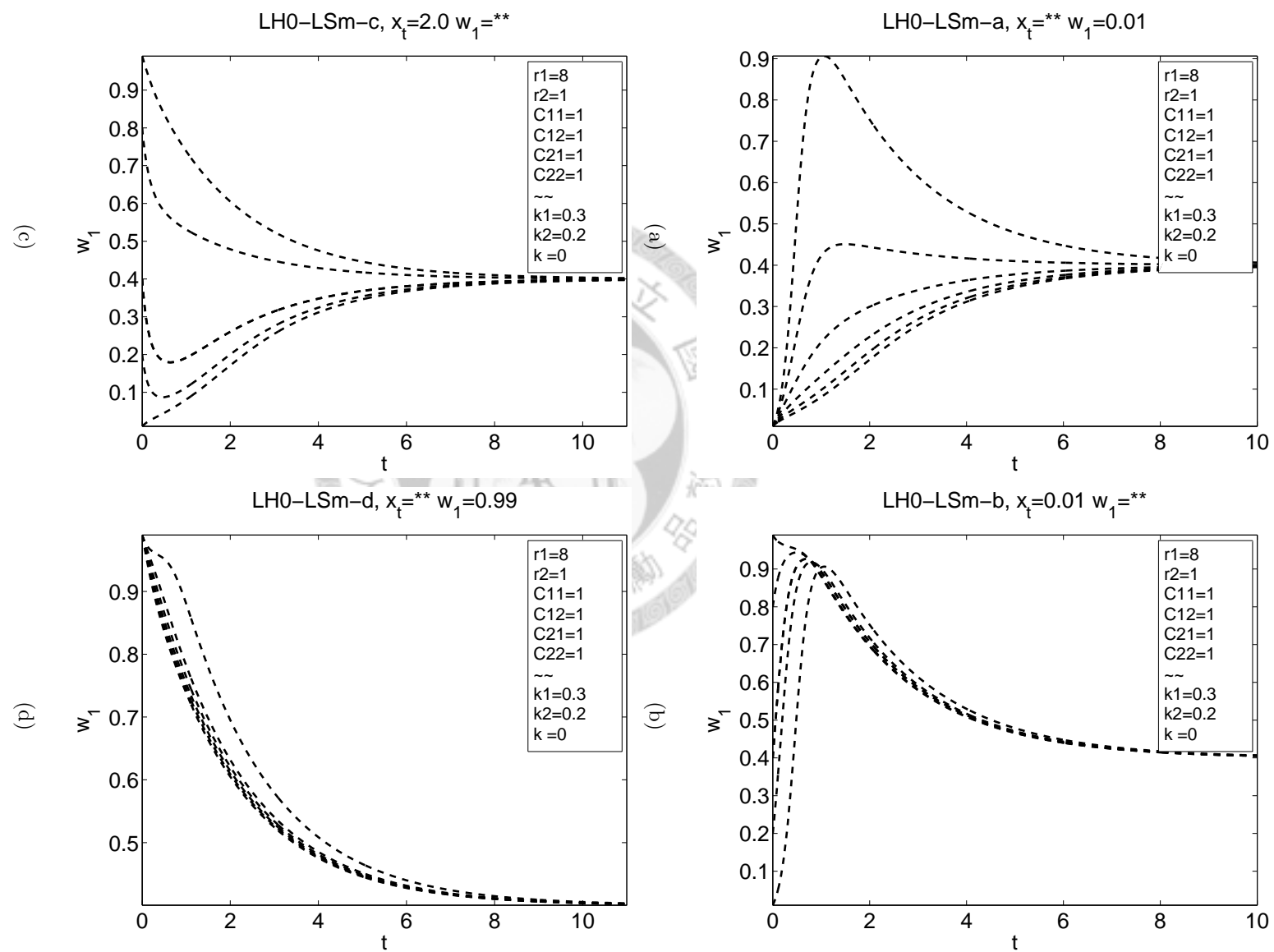


Figure 2.9: The x_{tot} - w_1 trajectories of LH0-LSm.

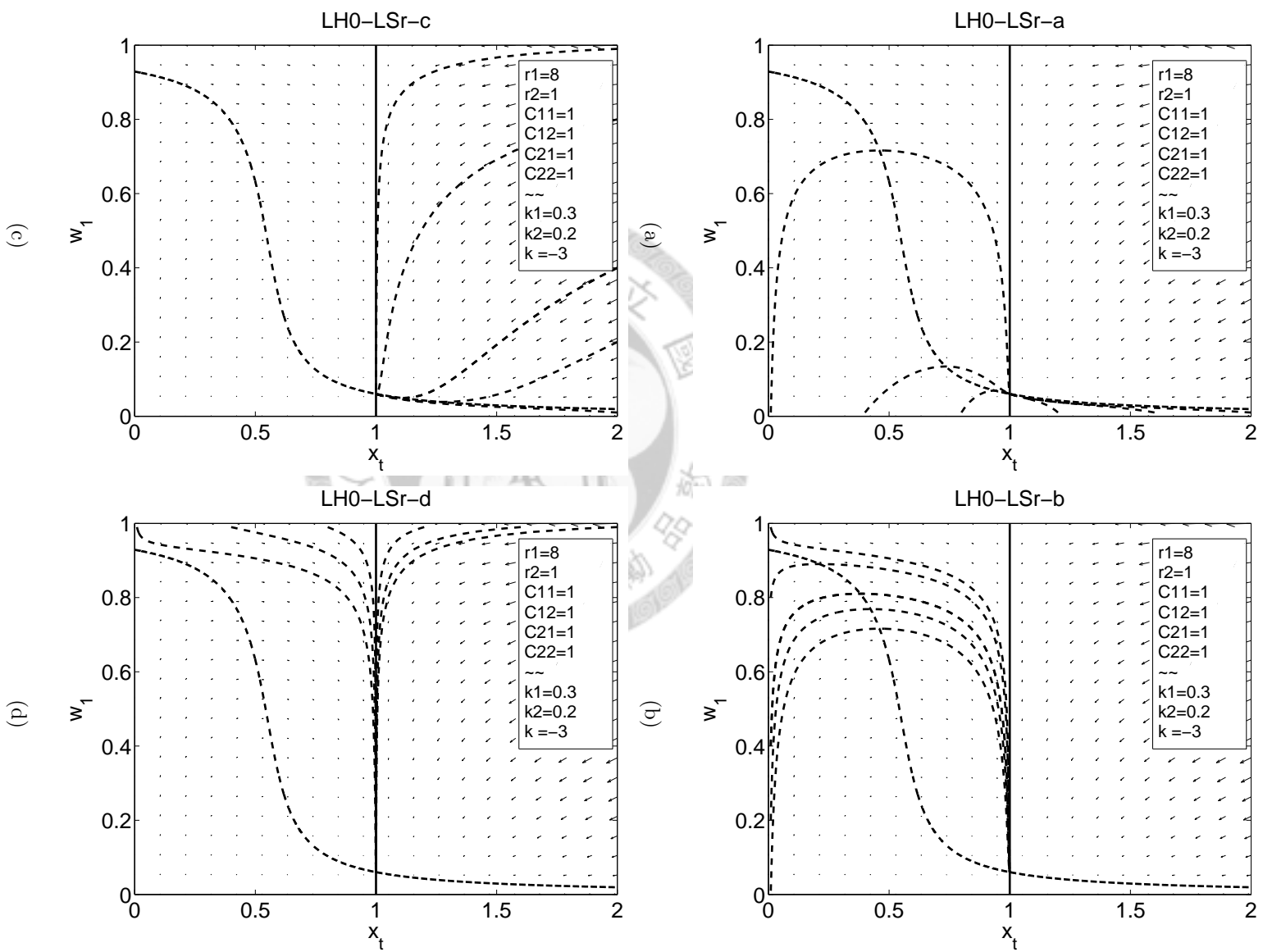


Figure 2.10: The x_{tot} - w_1 trajectories of LH0-LSr.

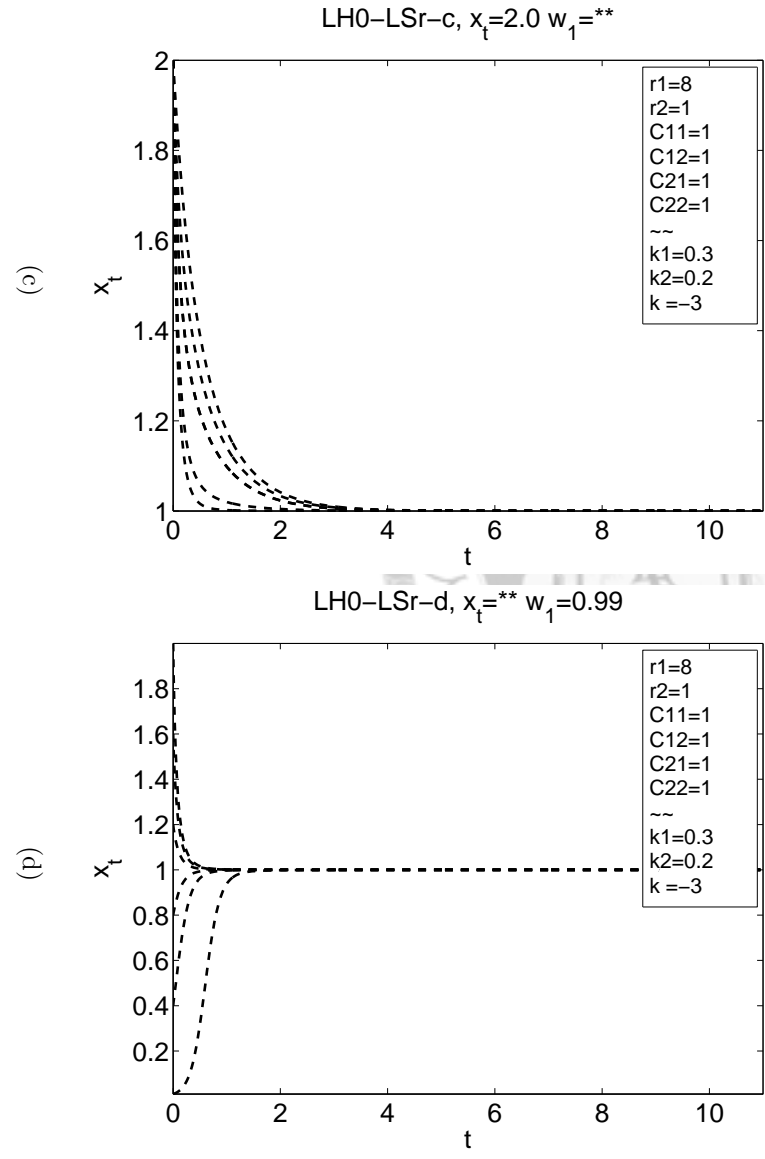
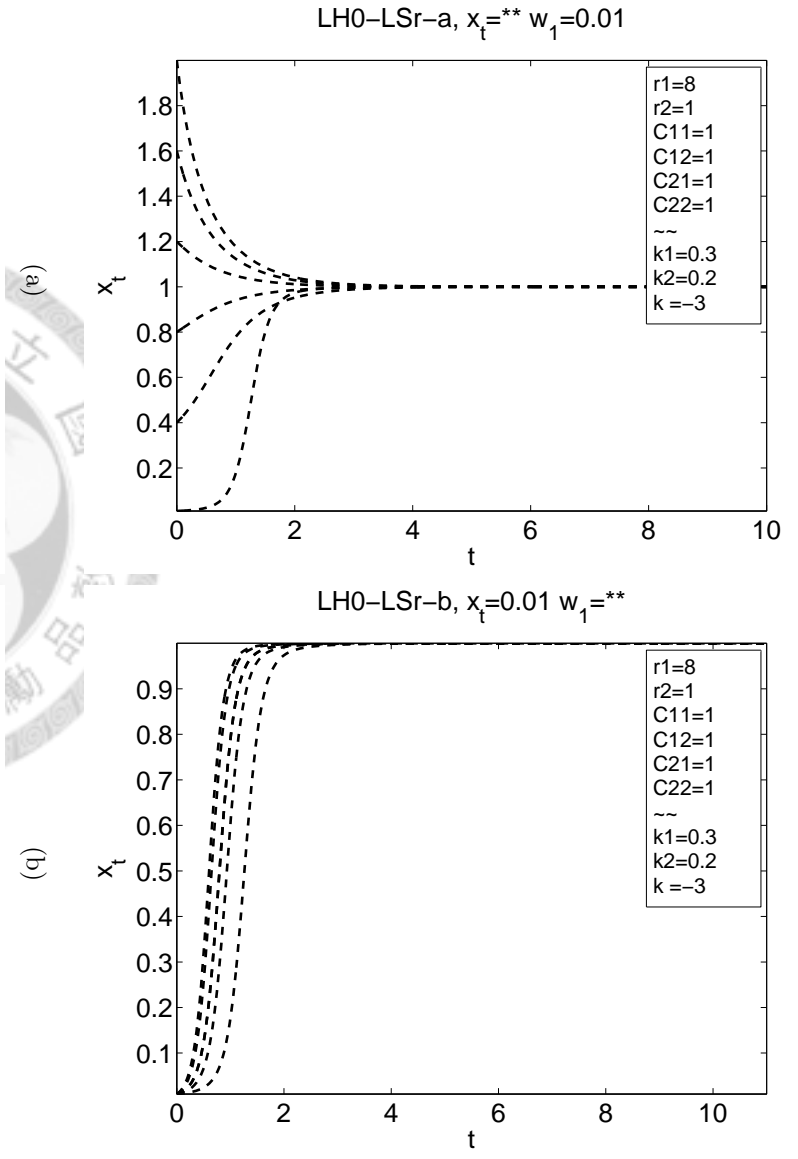


Figure 2.11: The $x_{tot}-w_1$ trajectories of LH0-LSr.

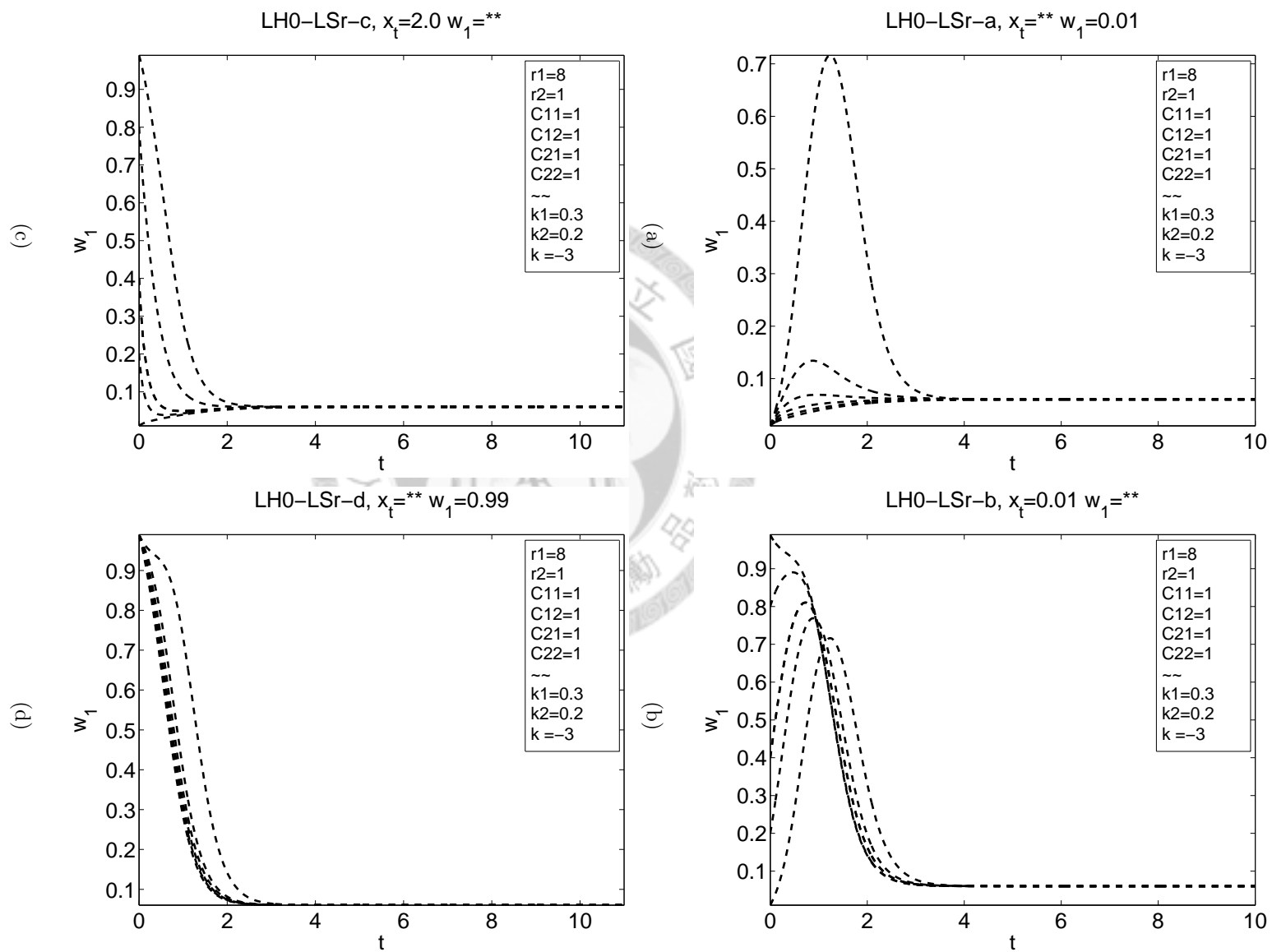


Figure 2.12: The x_{tot} - w_1 trajectories of LH0-LSr.

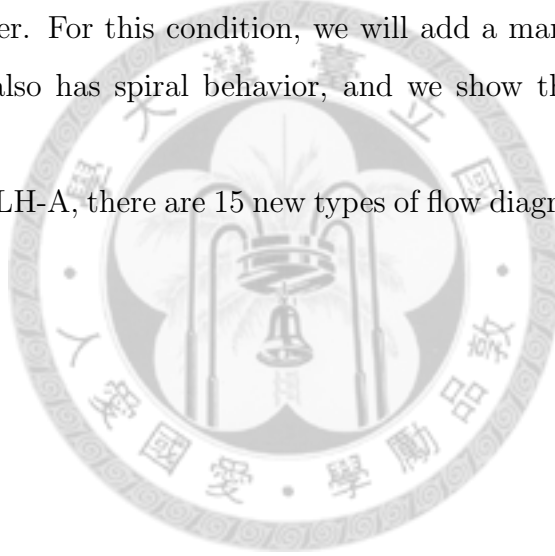
B.2 The phase portraits of LH-A

In LH-A, \tilde{x}_t is an inverse linear function, and from the general \tilde{x}_t form, \tilde{x}_t in LH-A has two types, UH ($C_1 > C_2$) and DH ($C_2 > C_1$).

From the general form of \tilde{w}_1 , it could be S type and Z type curves. In LH-A, if there has no transition effect, \tilde{x}_t and \tilde{w}_1 would merge.

According to these properties and considering the exchange symmetry of w_1 and w_2 , when $C_1 \neq C_2$, several new flow diagrams appear compared with the $C_1 = C_2 = C$ case. When \tilde{w}_1 is S type, the position of fixed point is in left LHA-H-Sl, in middle LHA-H-Sm, and in right LHA-H-Sr. In another way, when \tilde{w}_1 is Z type, it is LHA-H-Zl, LHA-H-Zm, and LHA-H-Zr. When transition term is small, \tilde{x}_t and \tilde{w}_1 will be close to each other. For this condition, we will add a mark “n”. And when $\Delta r = 0$ is LHA-H-L. It also has spiral behavior, and we show them in LHA-H-Sm-sp and LHA-H-Zm-sp

Therefore, in LH-A, there are 15 new types of flow diagrams in the following pages.



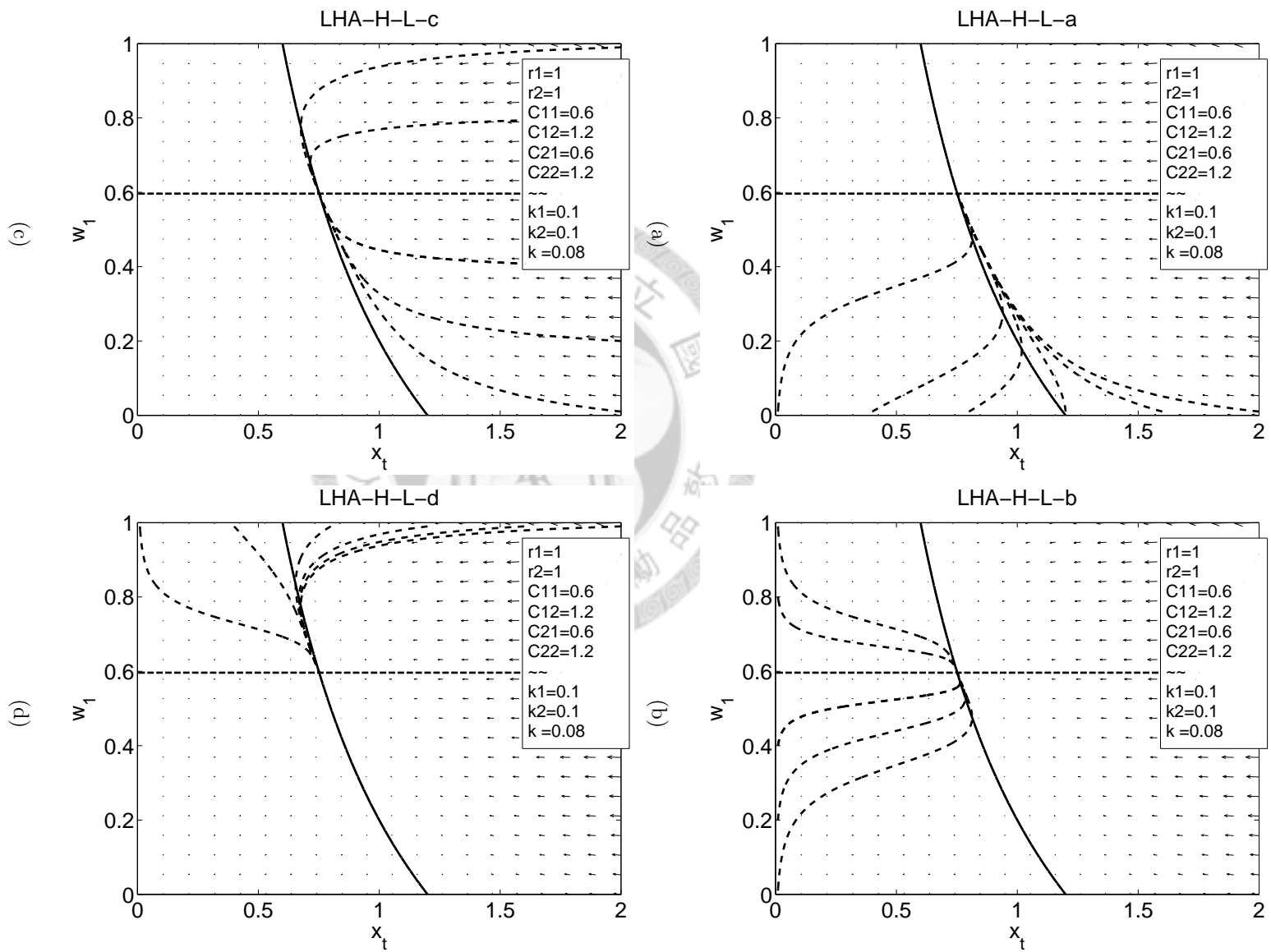
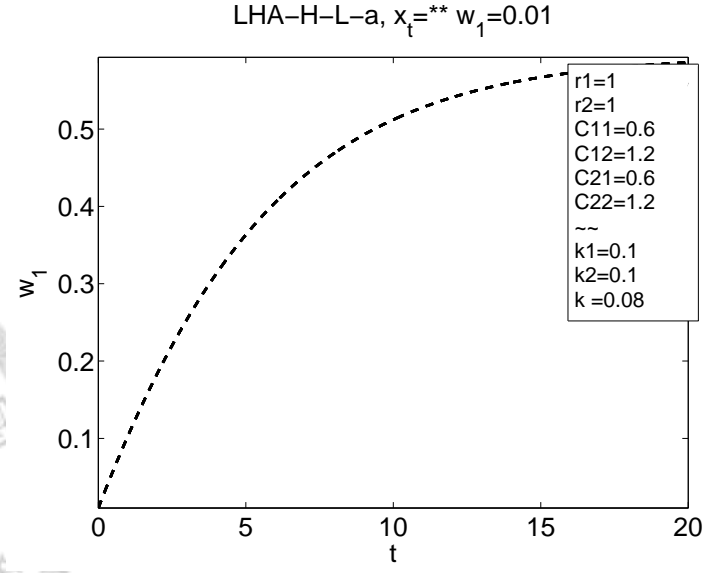
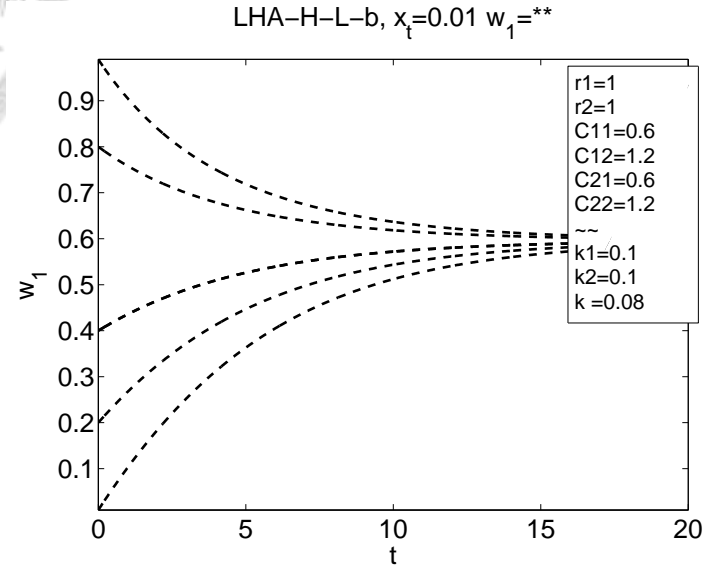


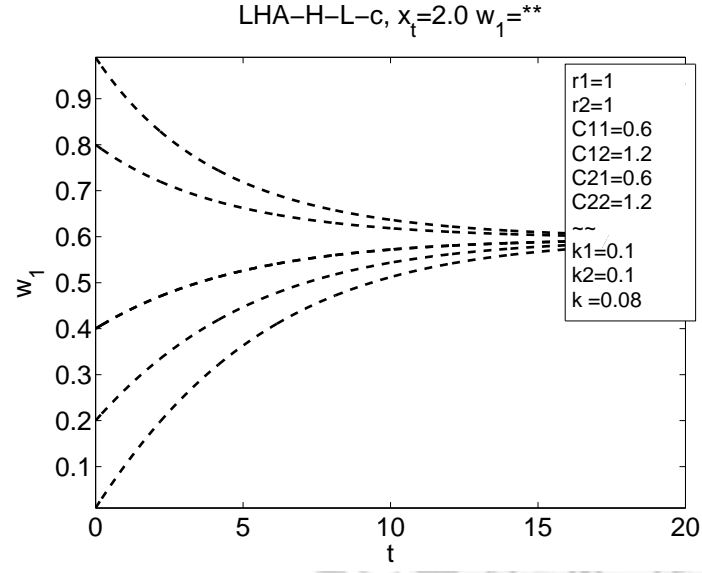
Figure 2.13: The x_{tot} - w_1 trajectories of LHA-H-L.



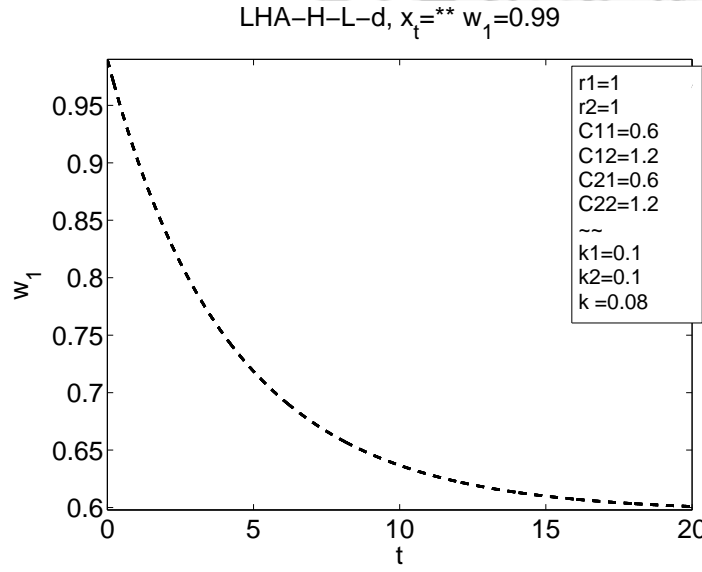
(a)



(b)

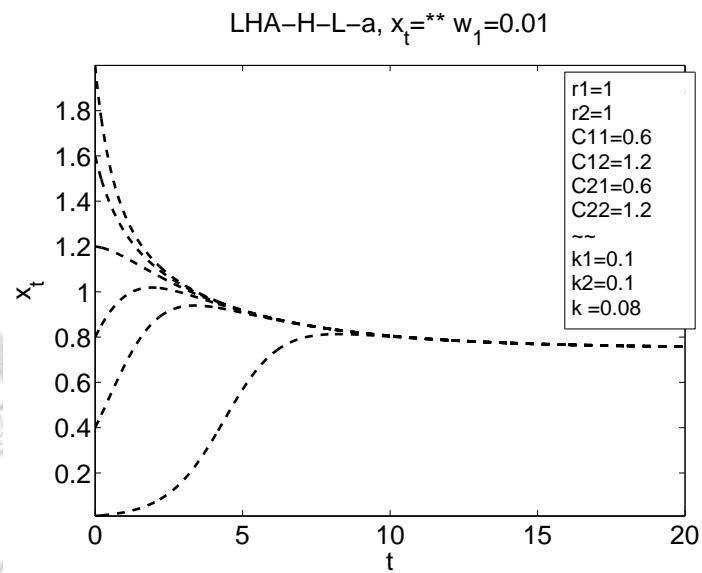


(c)

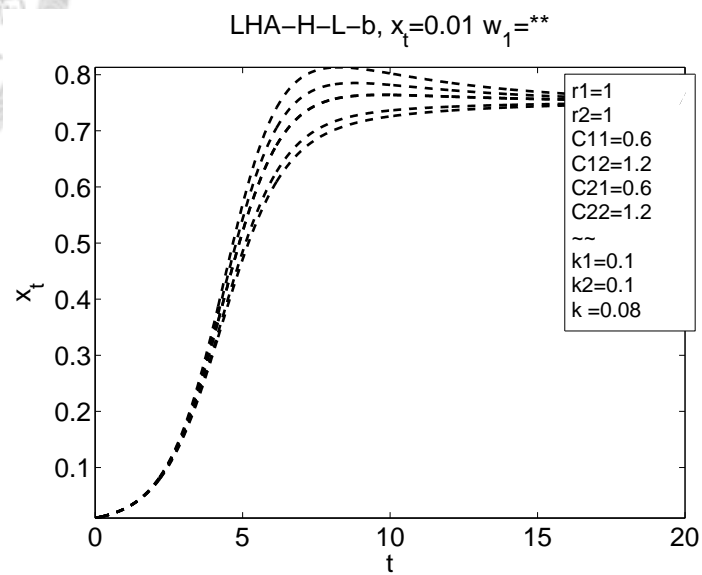


(d)

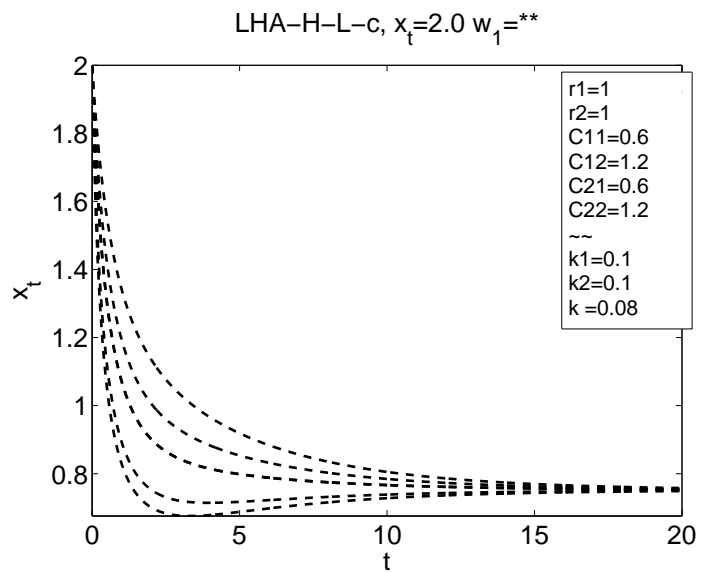
Figure 2.14: The x_{tot} - w_1 trajectories of LHA-H-L.



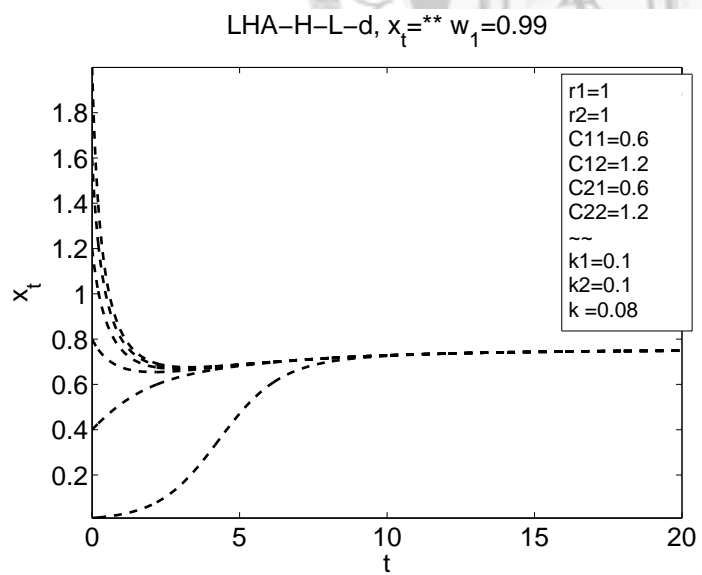
(a)



(b)

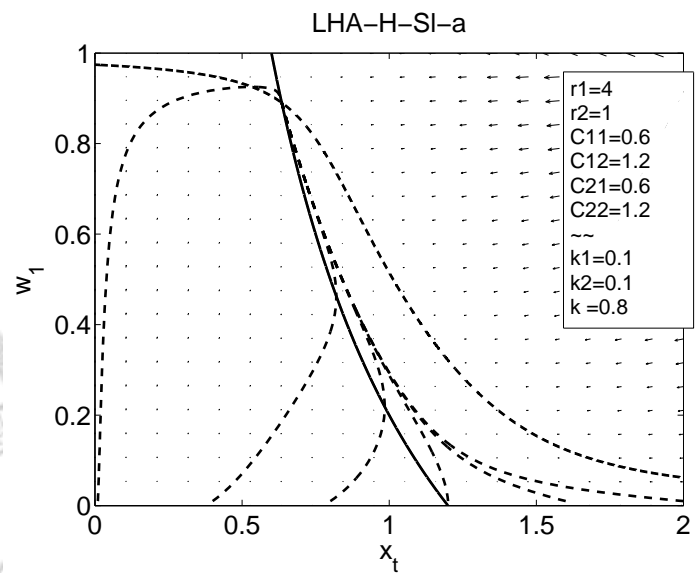


(c)

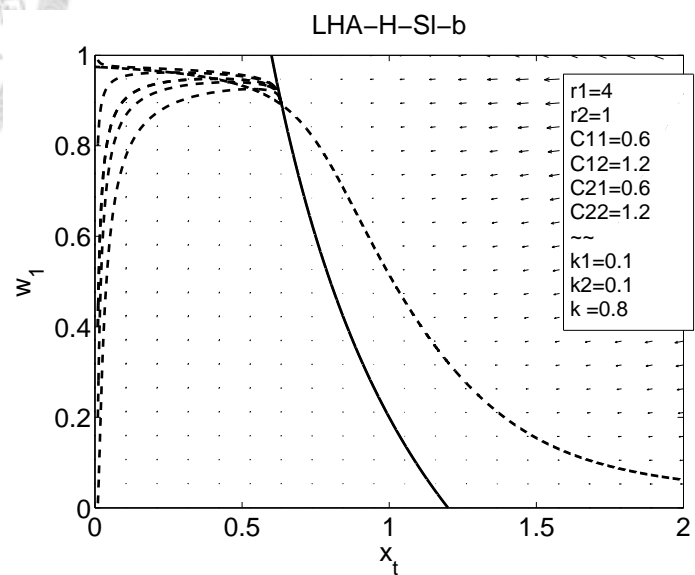


(d)

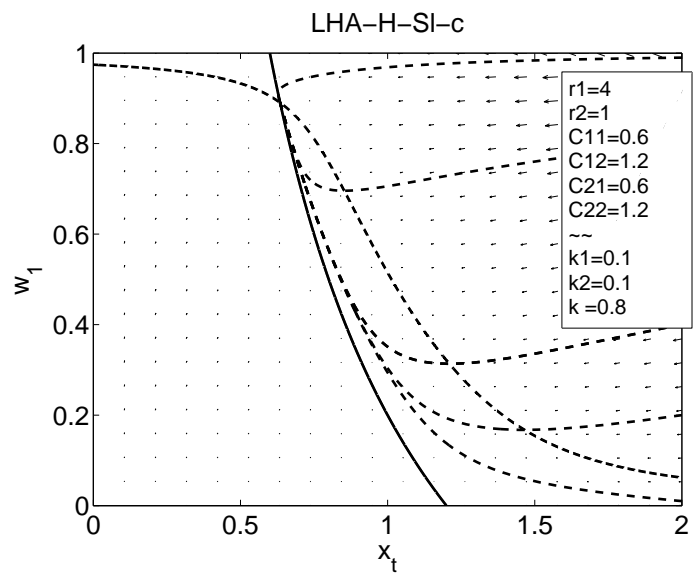
Figure 2.15: The $x_{tot}-w_1$ trajectories of LHA-H-L.



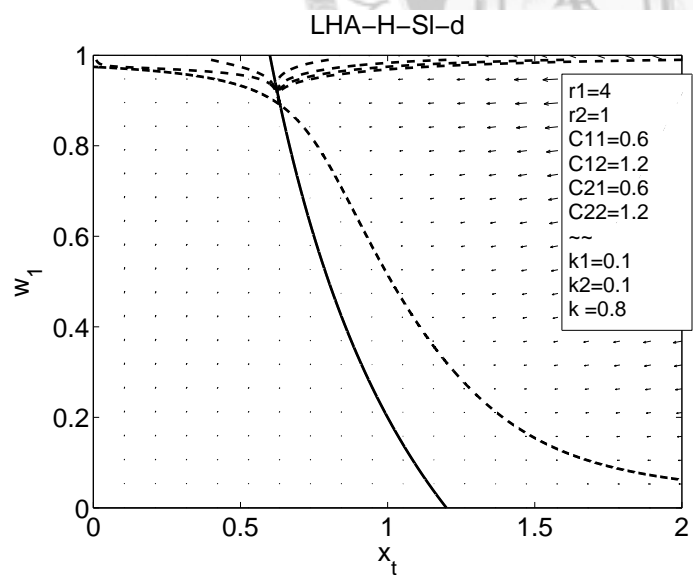
(a)



(b)



(c)



(d)

Figure 2.16: The x_{tot} - w_1 trajectories of LHA-H-SI.

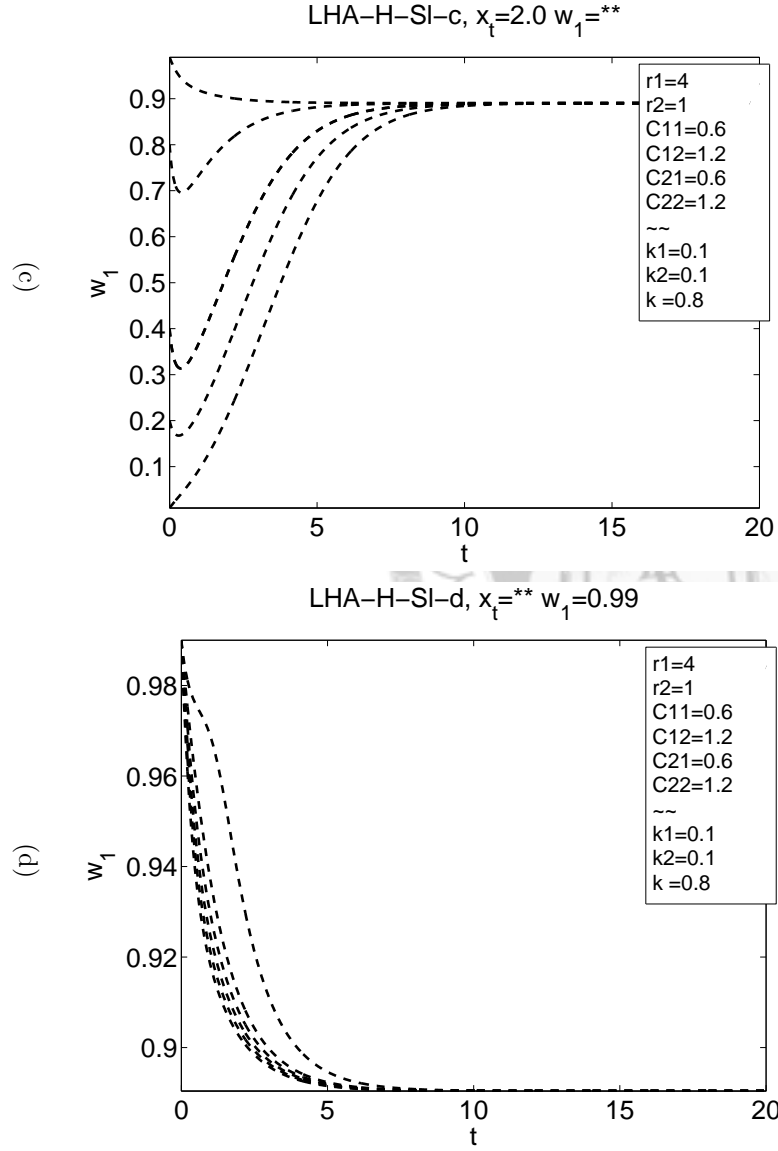
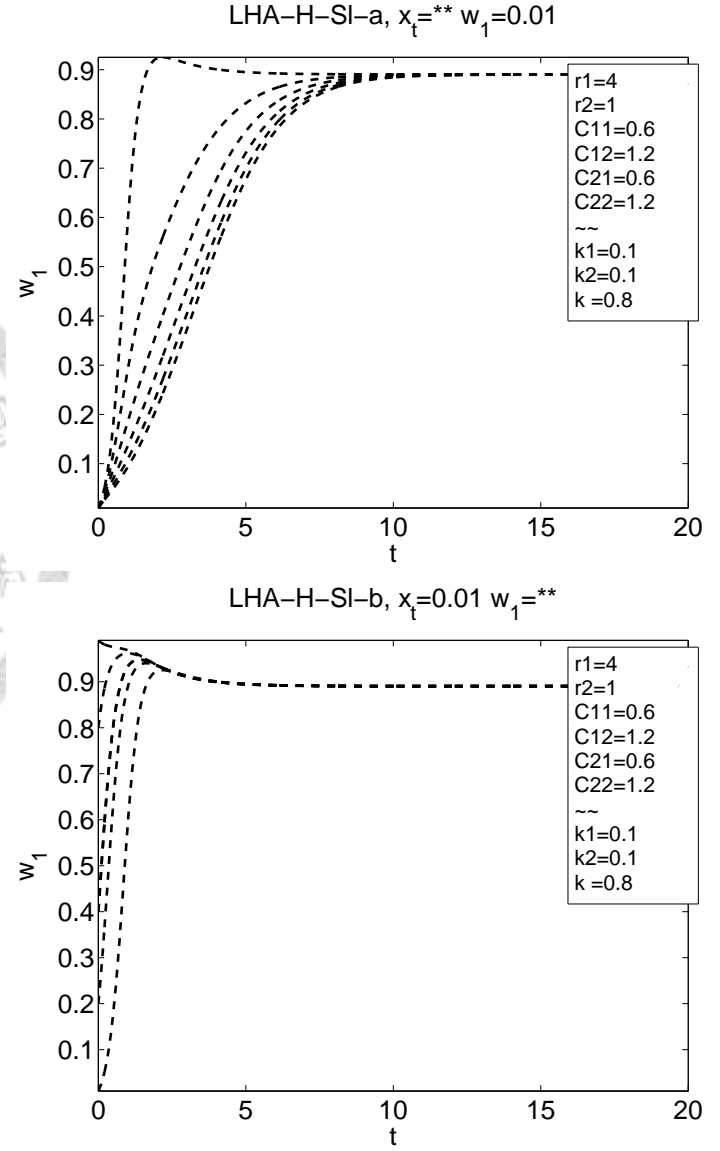
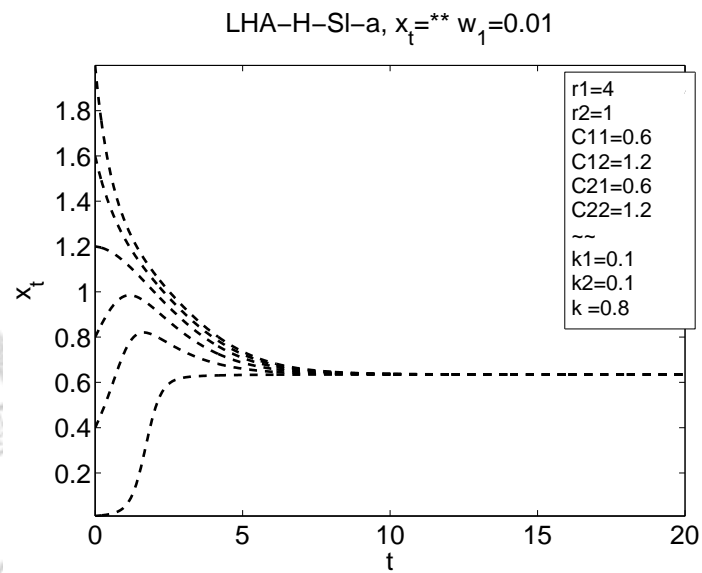
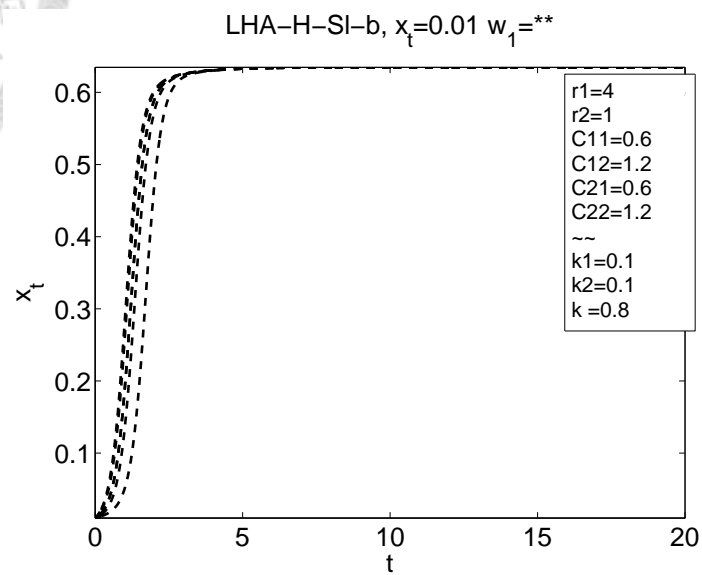


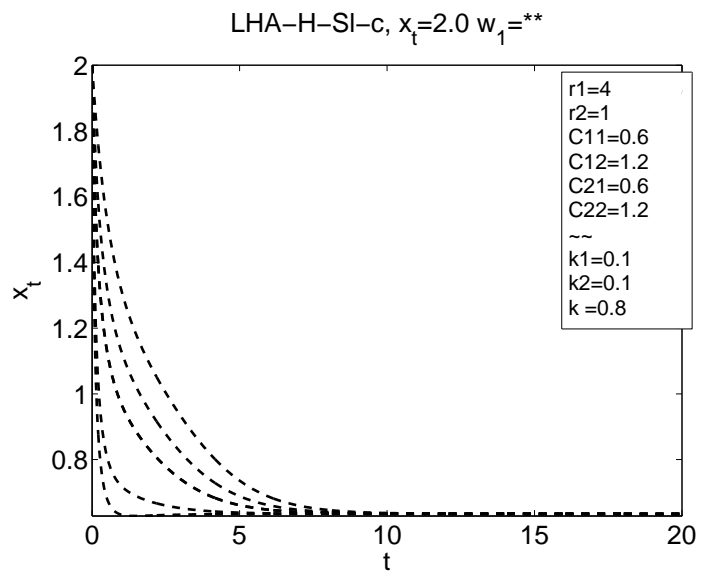
Figure 2.17: The x_{tot} - w_1 trajectories of LHA-H-SI.



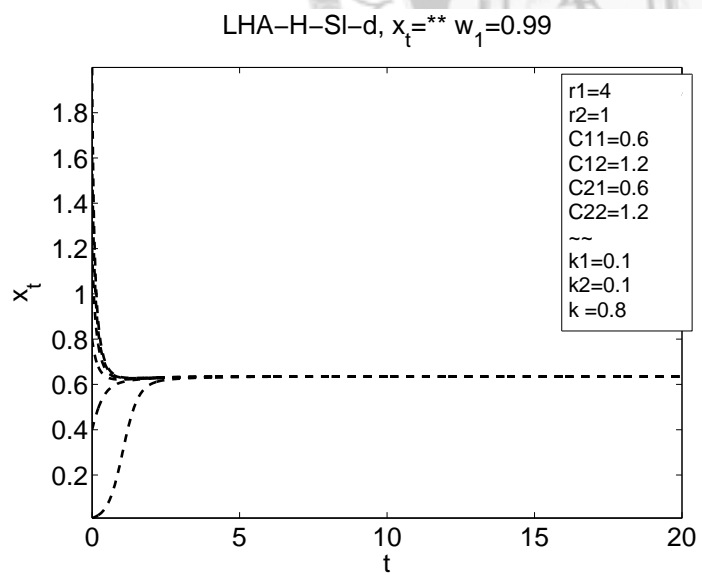
(a)



(b)



(c)



(d)

Figure 2.18: The $x_{tot}-w_1$ trajectories of LHA-H-SI.

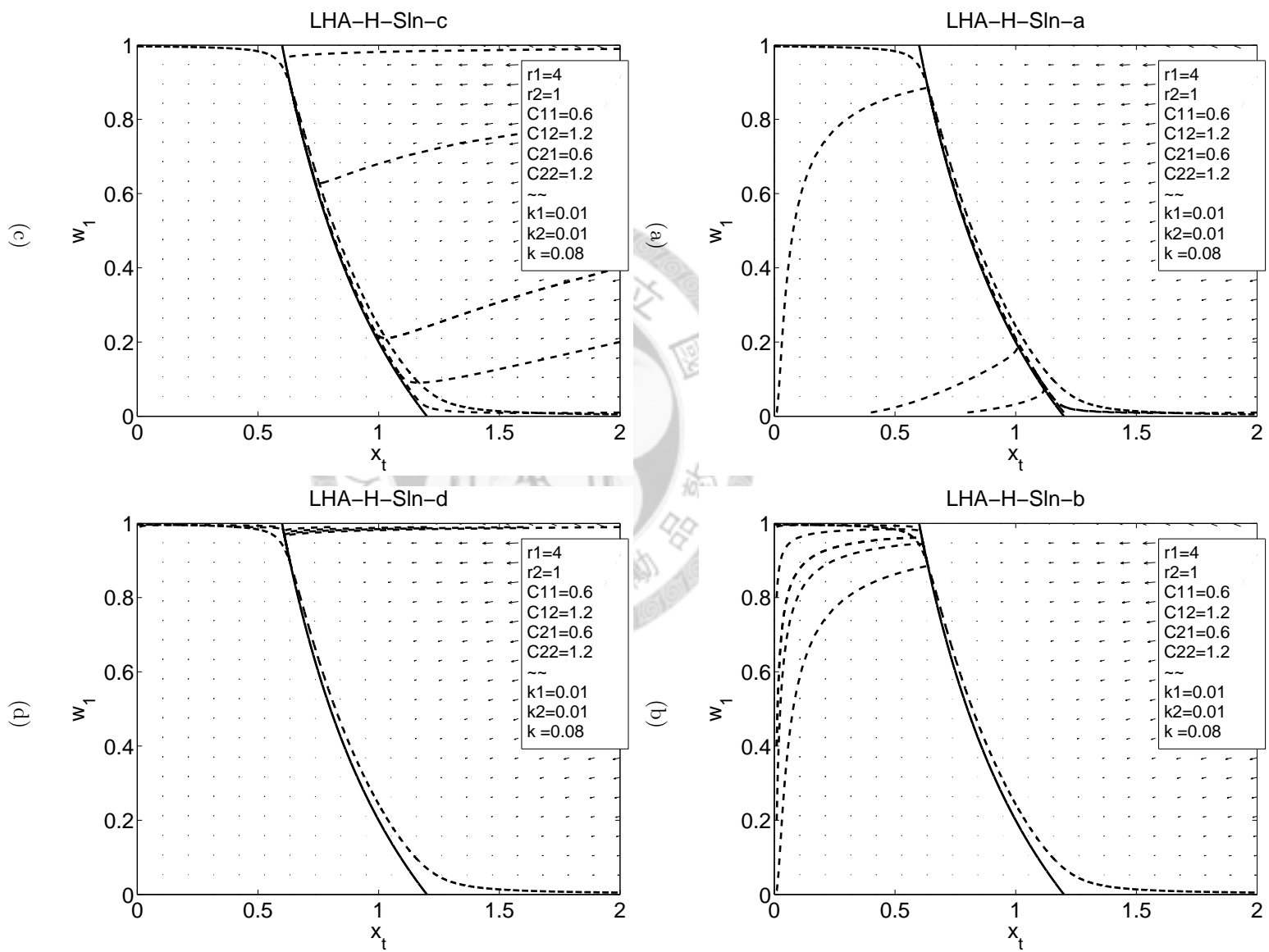


Figure 2.19: The x_{tot} - w_1 trajectories of LHA-H-SIn.

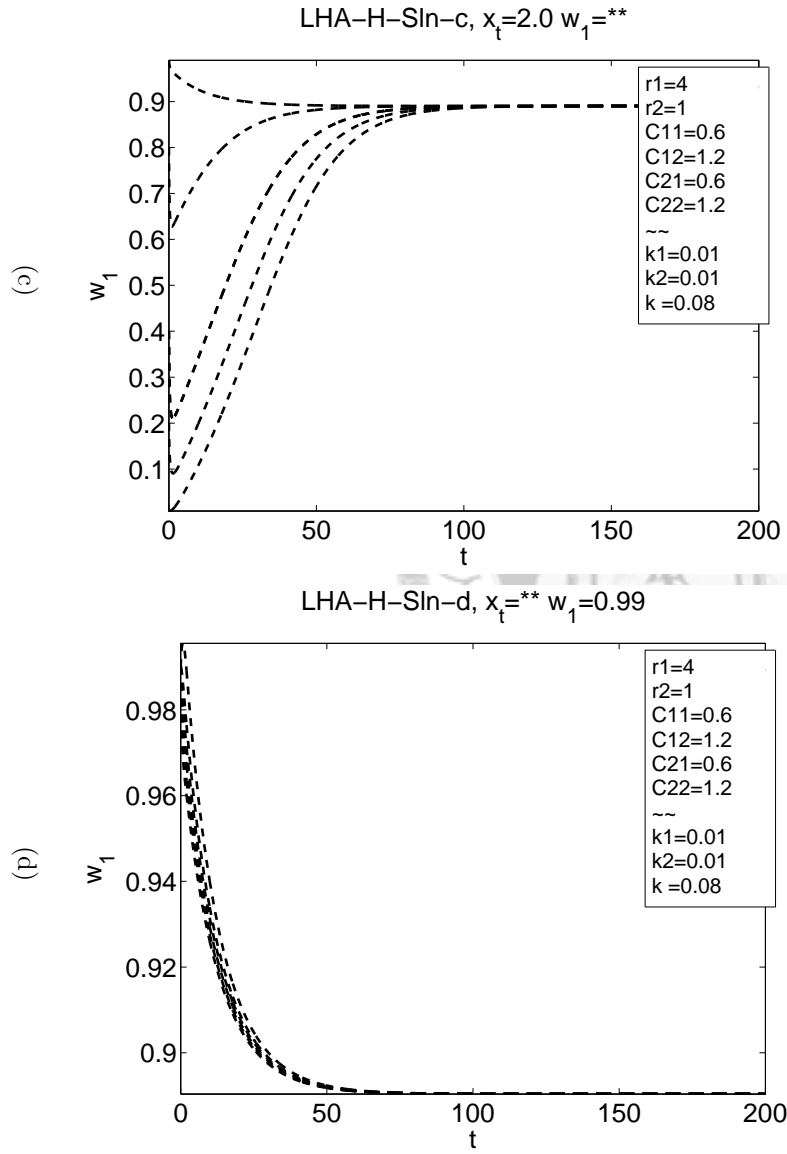
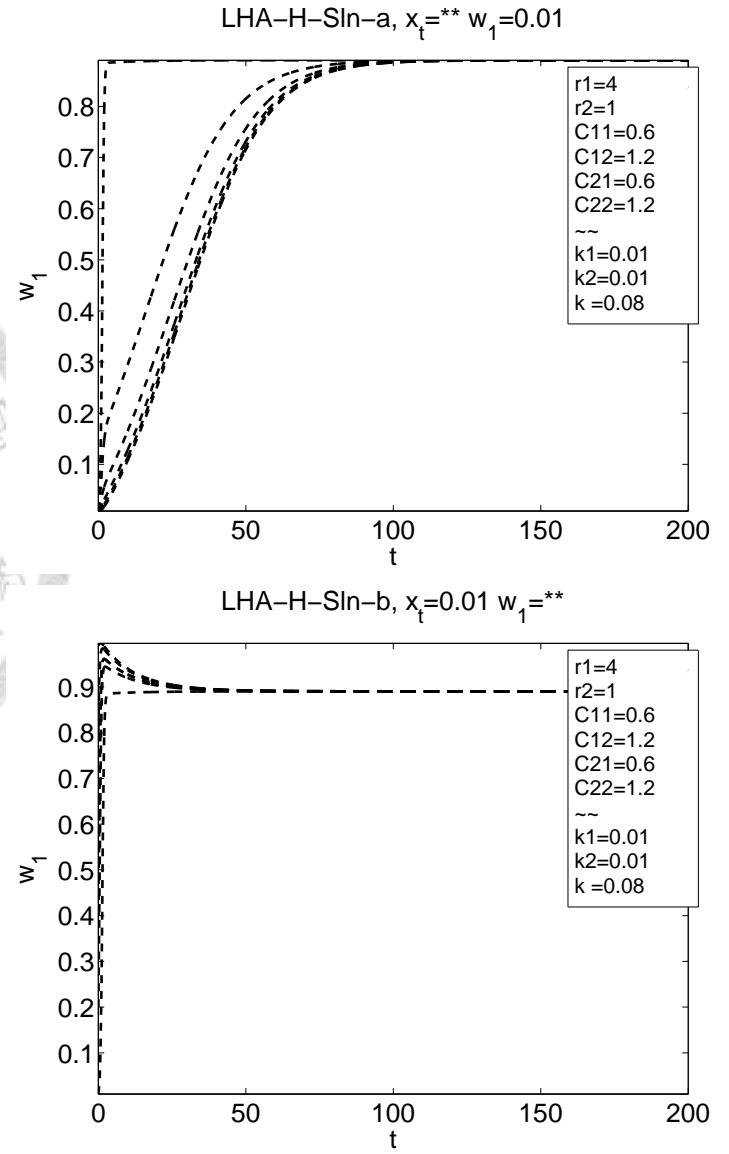


Figure 2.20: The x_{tot} - w_1 trajectories of LHA-H-Sln.

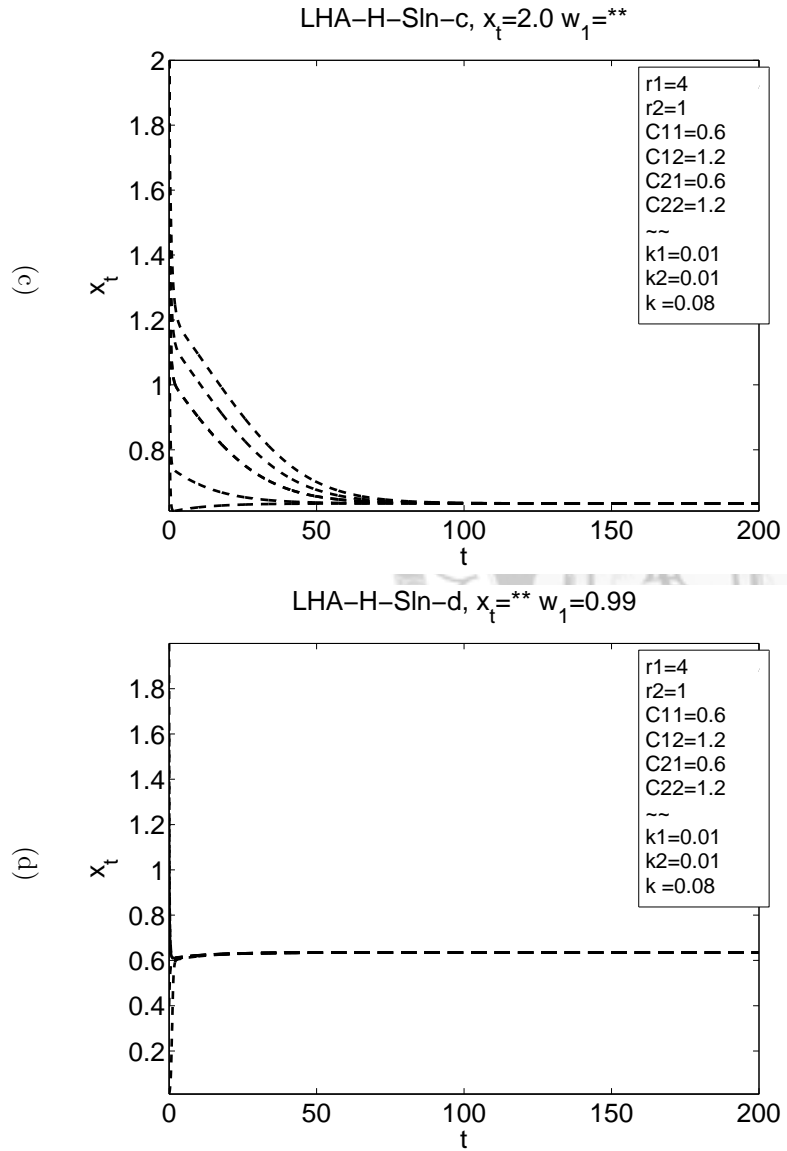
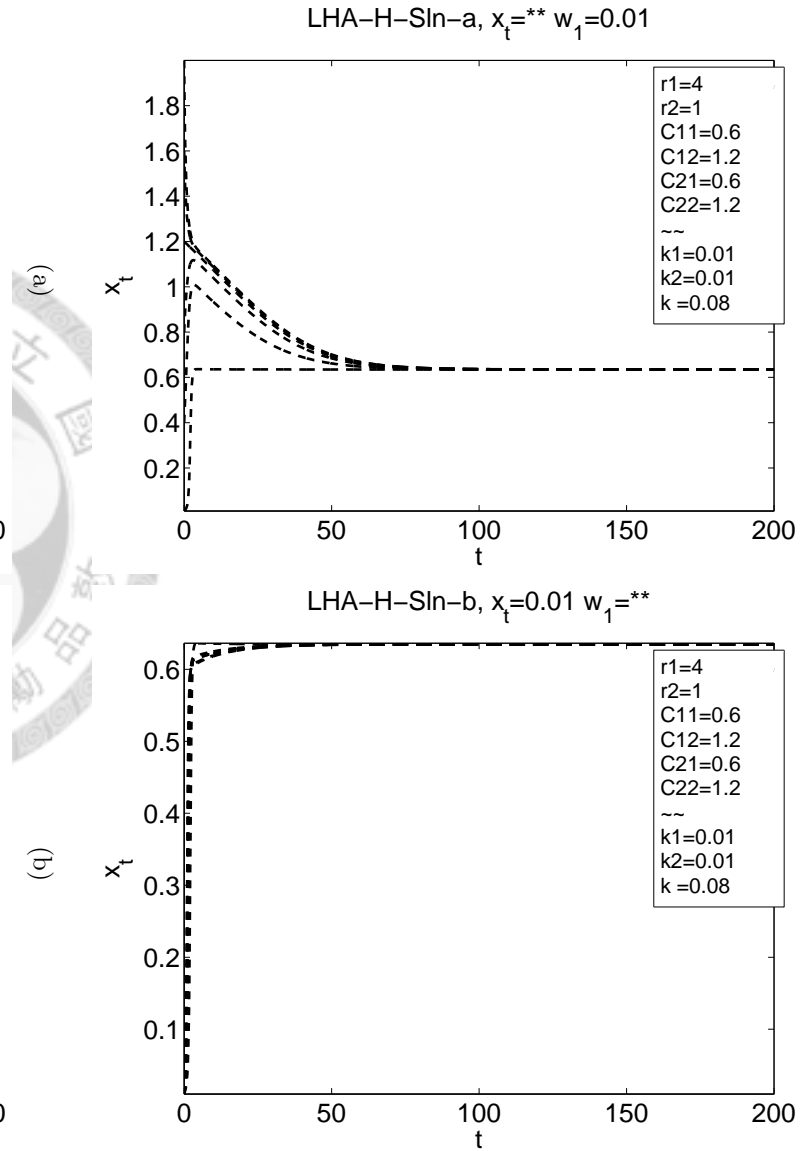


Figure 2.21: The $x_{tot}-w_1$ trajectories of LHA-H-Sln.

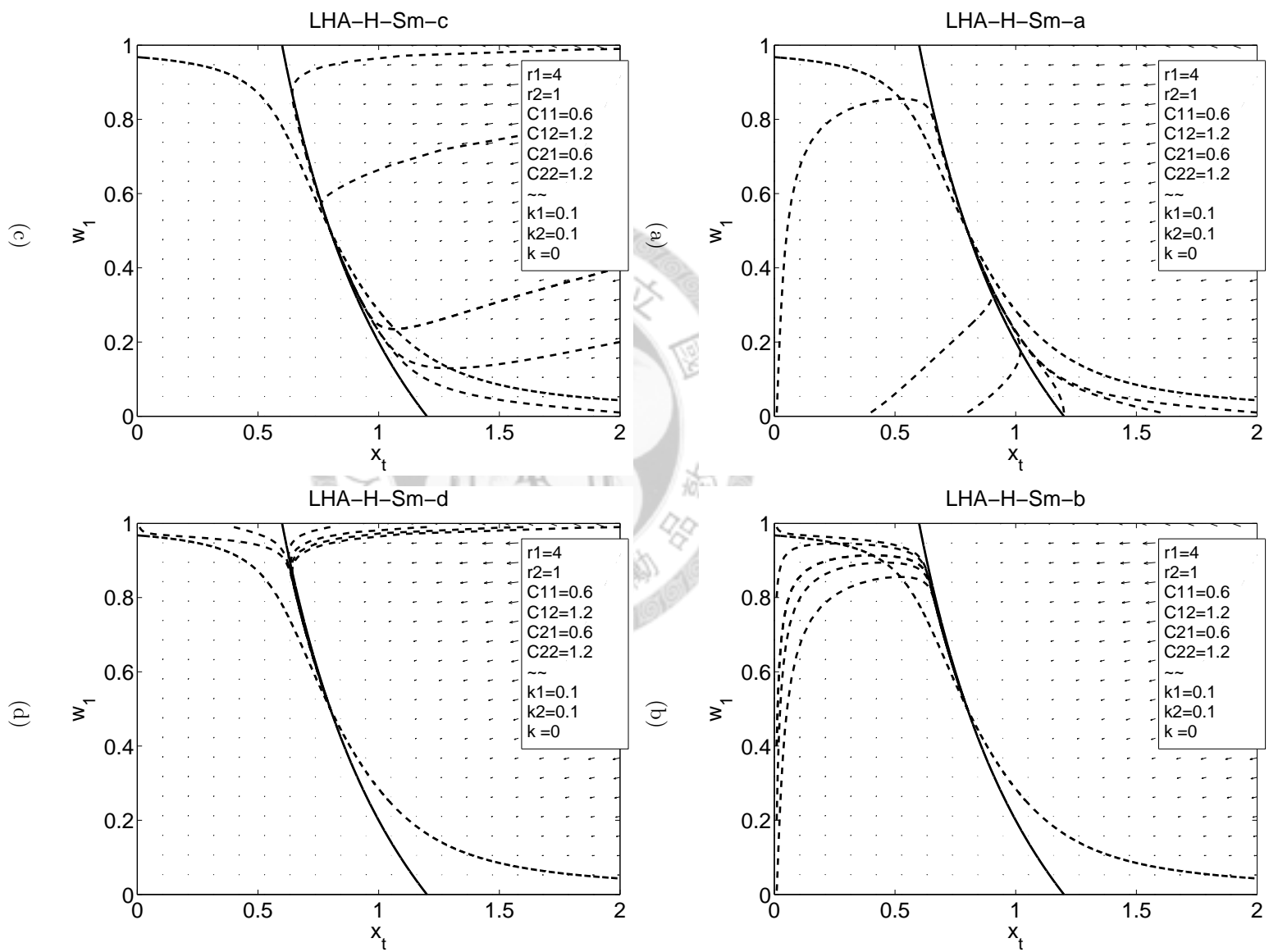


Figure 2.22: The x_{tot} - w_1 trajectories of LHA-H-Sm.

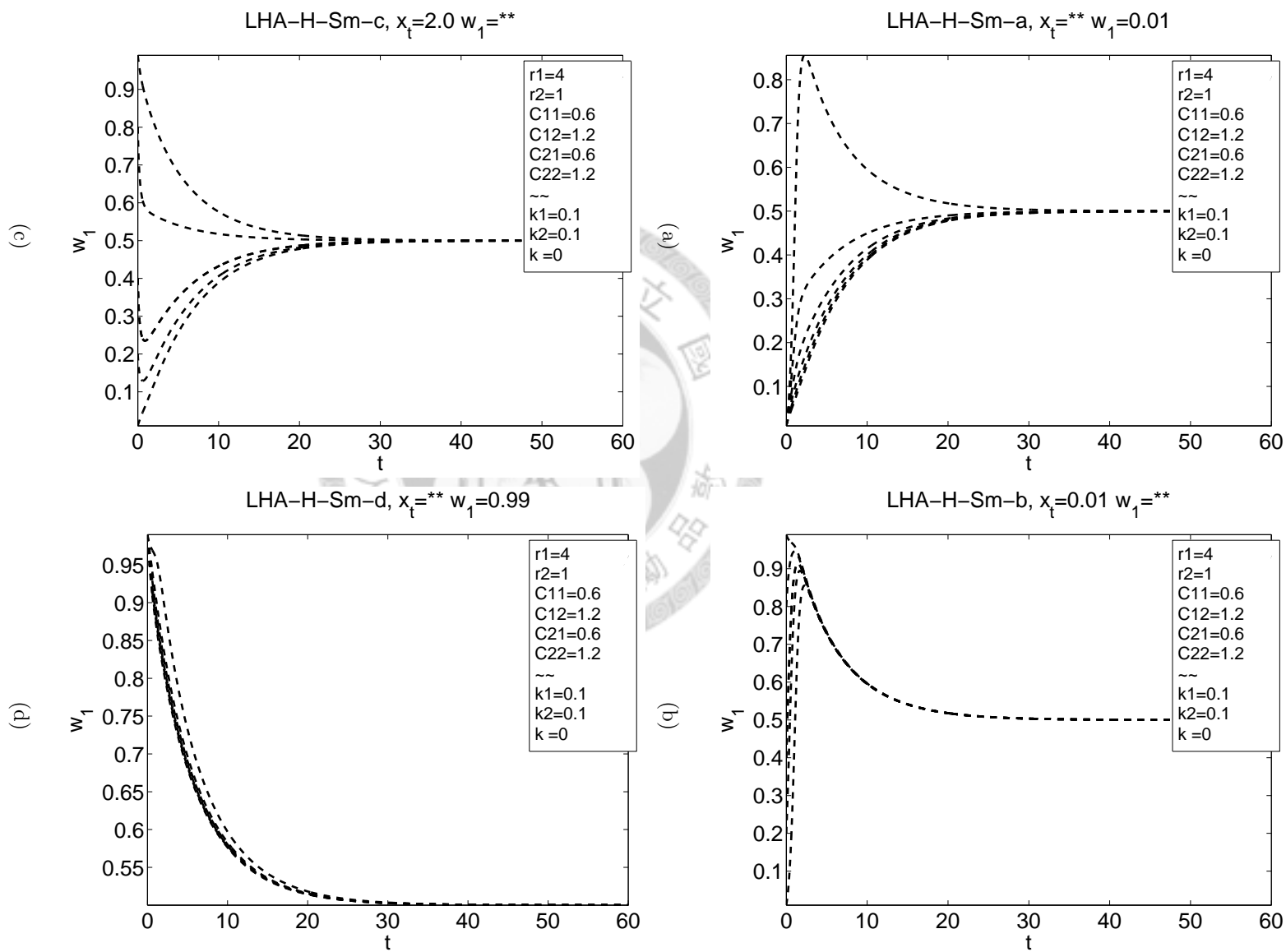
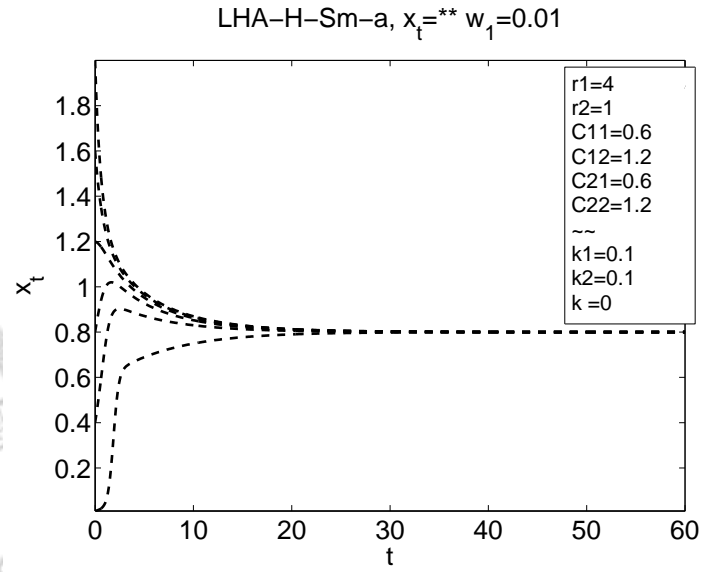
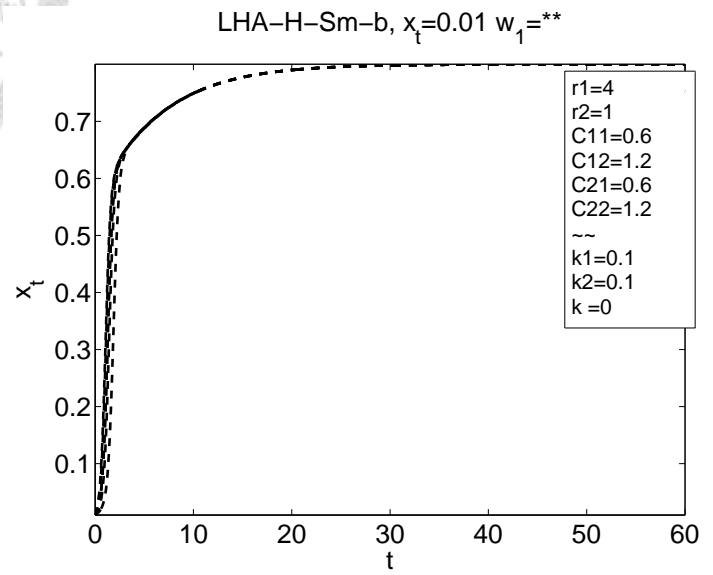


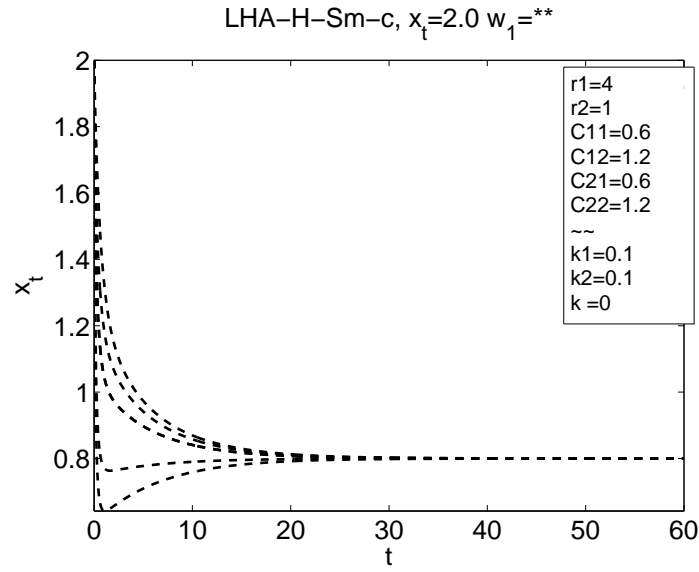
Figure 2.23: The x_{tot} - w_1 trajectories of LHA-H-Sm.



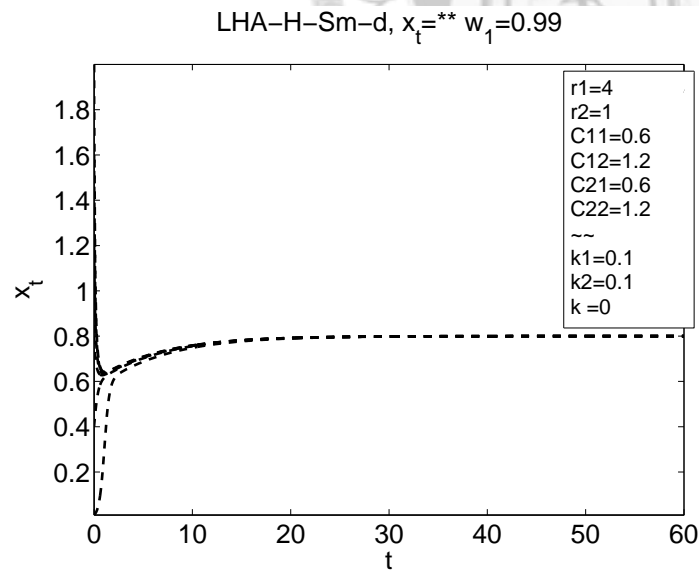
(a)



(b)



(c)



(d)

Figure 2.24: The $x_{tot}-w_1$ trajectories of LHA-H-Sm.

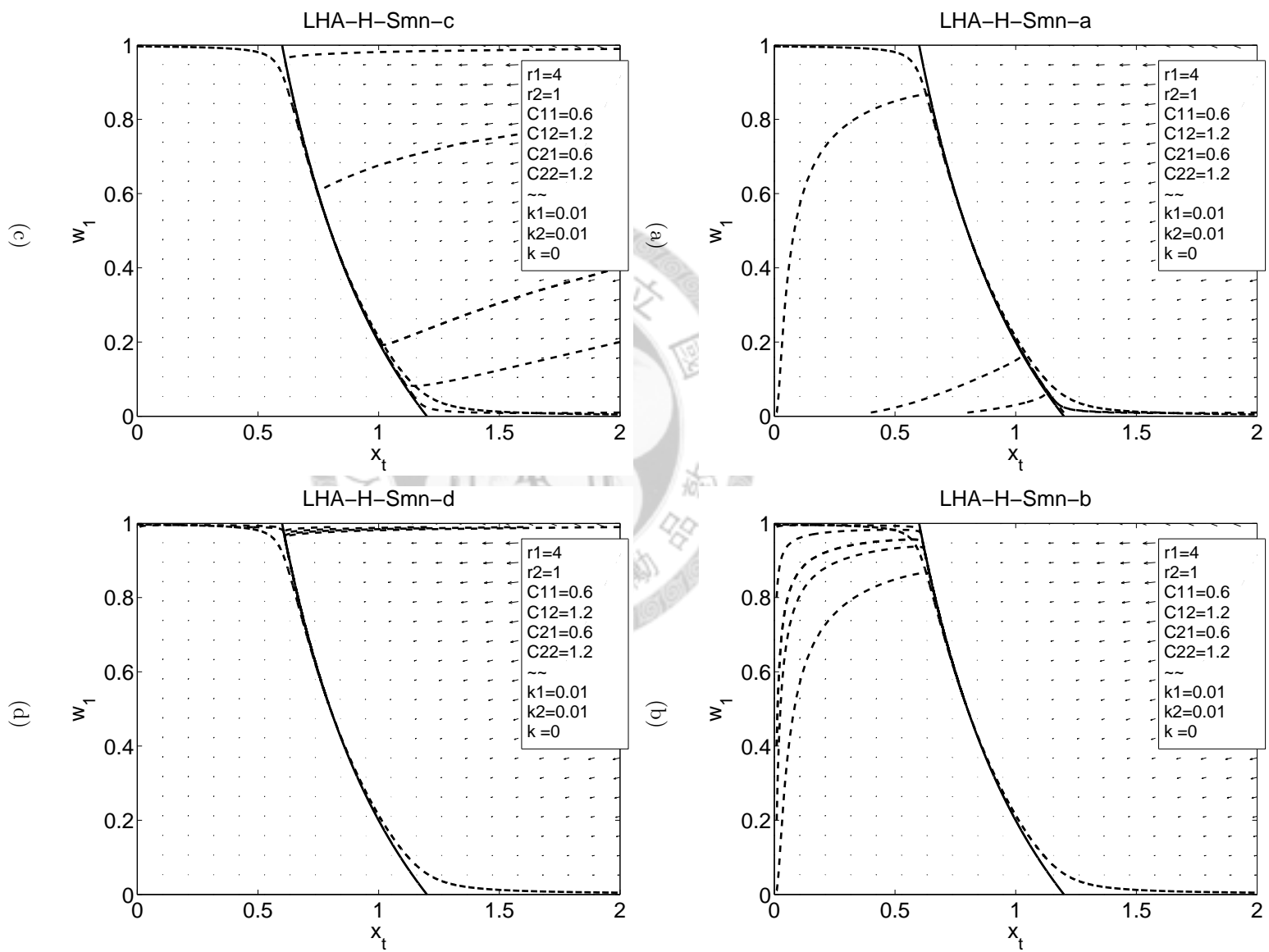


Figure 2.25: The x_{tot} - w_1 trajectories of LHA-H-Smn.

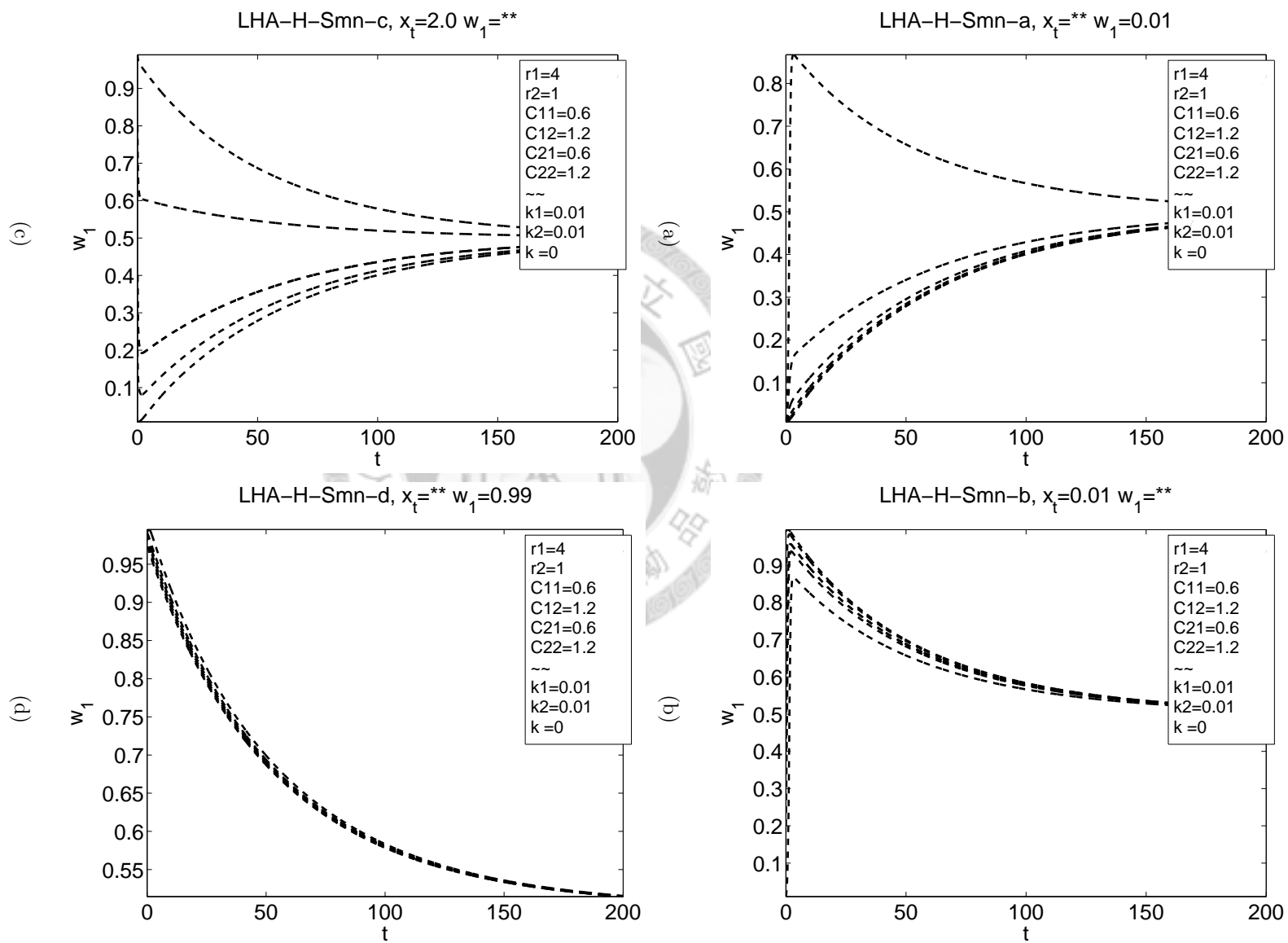
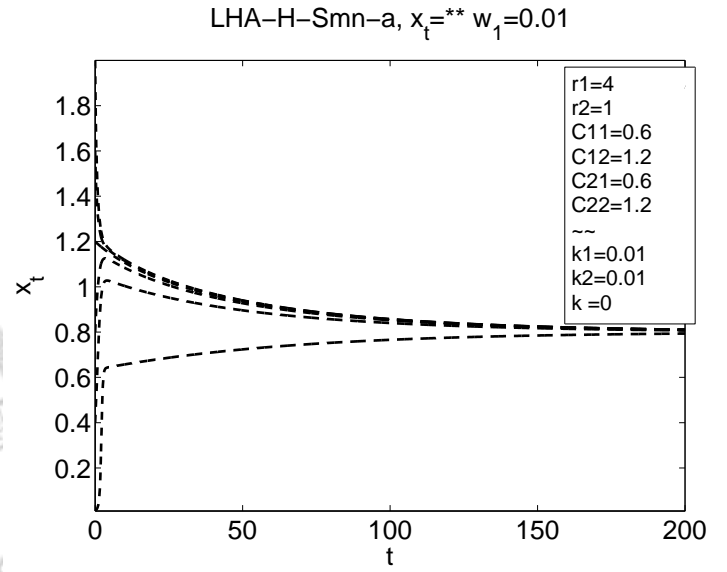
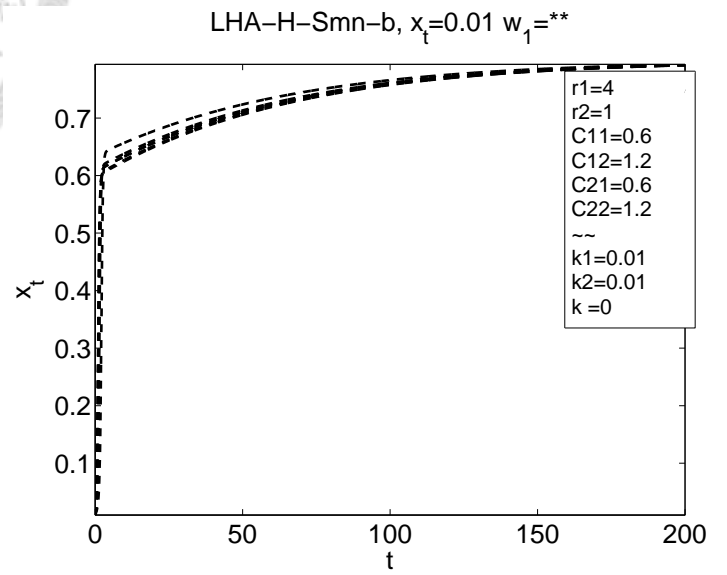


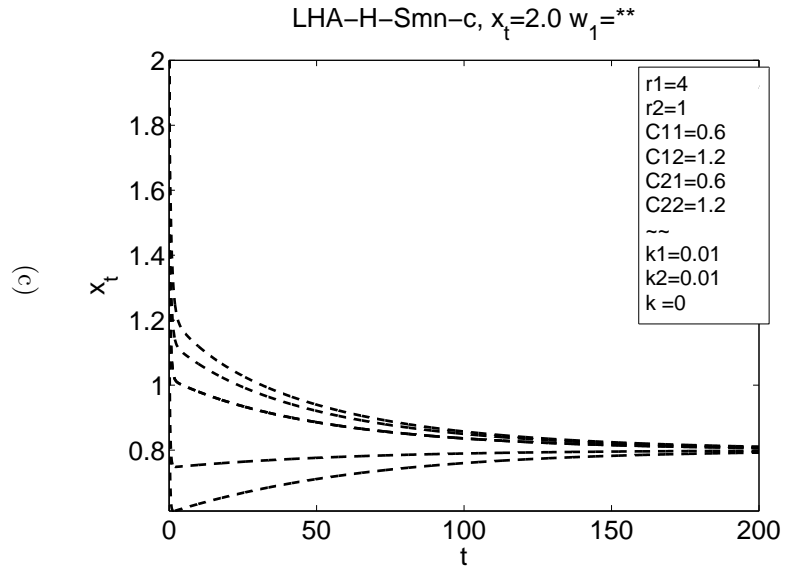
Figure 2.26: The $x_{tot}-w_1$ trajectories of LHA-H-Smn.



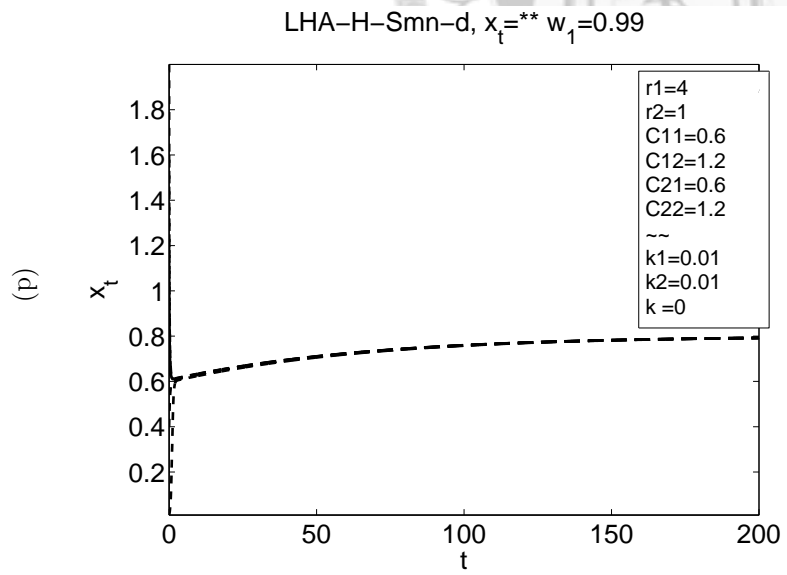
(a)



(b)



(c)



(d)

Figure 2.27: The $x_{tot}-w_1$ trajectories of LHA-H-Smn.

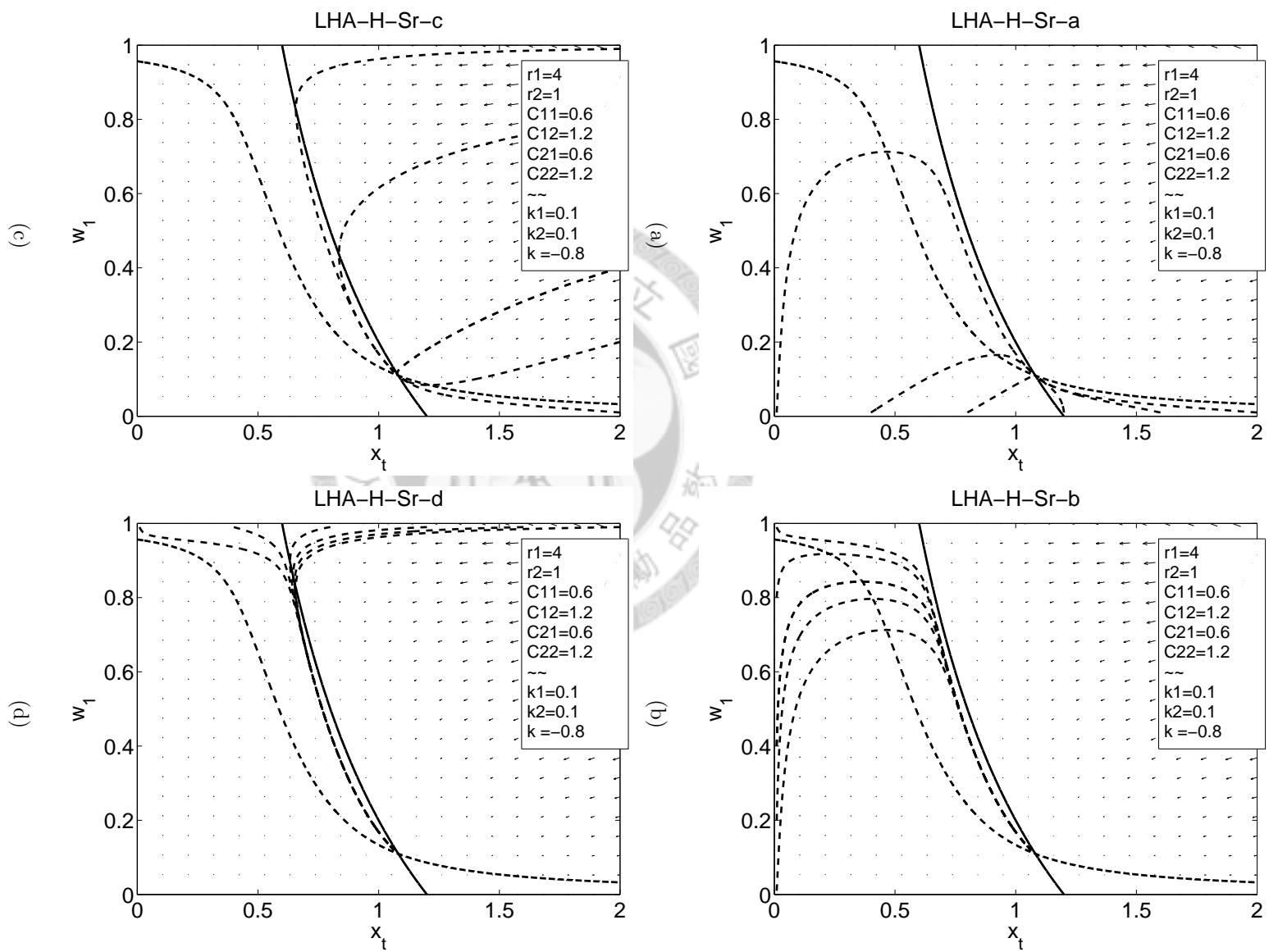
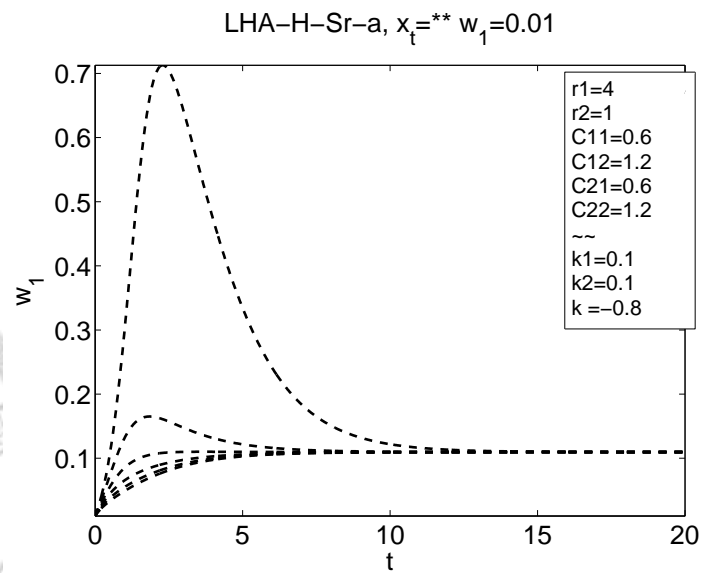
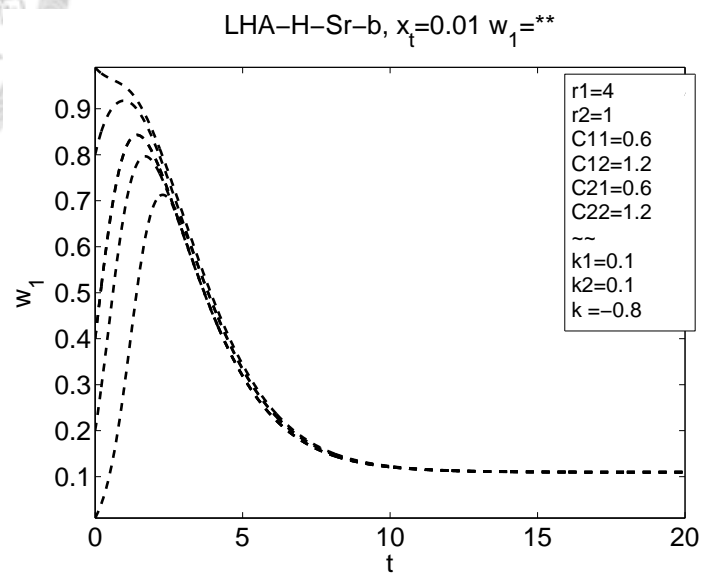


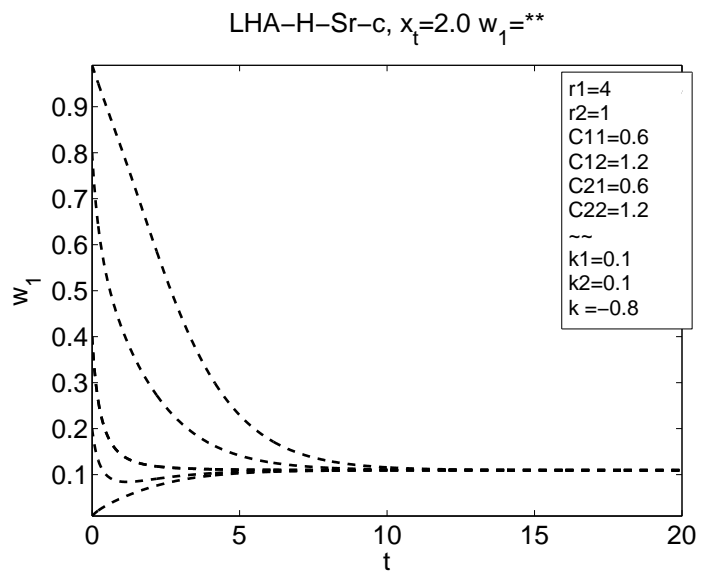
Figure 2.28: The x_{tot} - w_1 trajectories of LHA-H-Sr.



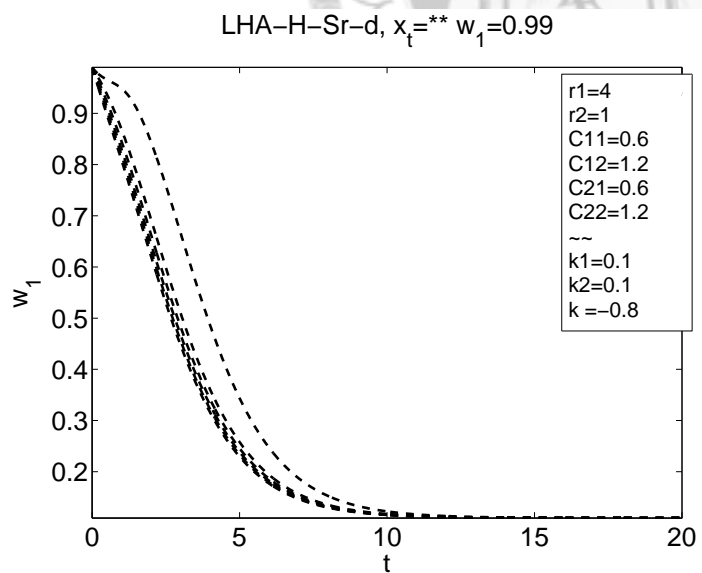
(a)



(b)



(c)



(d)

Figure 2.29: The x_{tot} - w_1 trajectories of LHA-H-Sr.

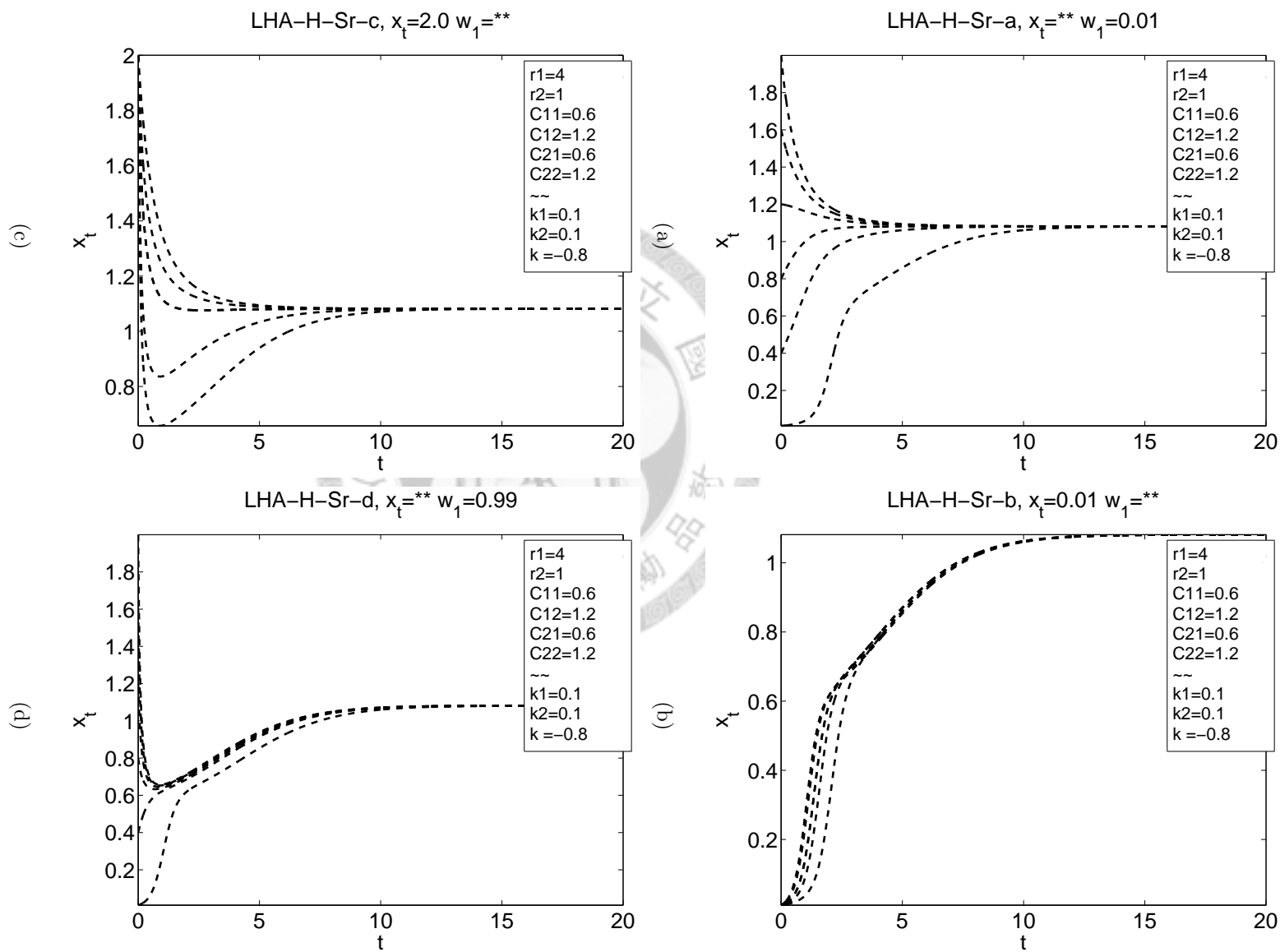


Figure 2.30: The $x_{tot}-w_1$ trajectories of LHA-H-Sr.

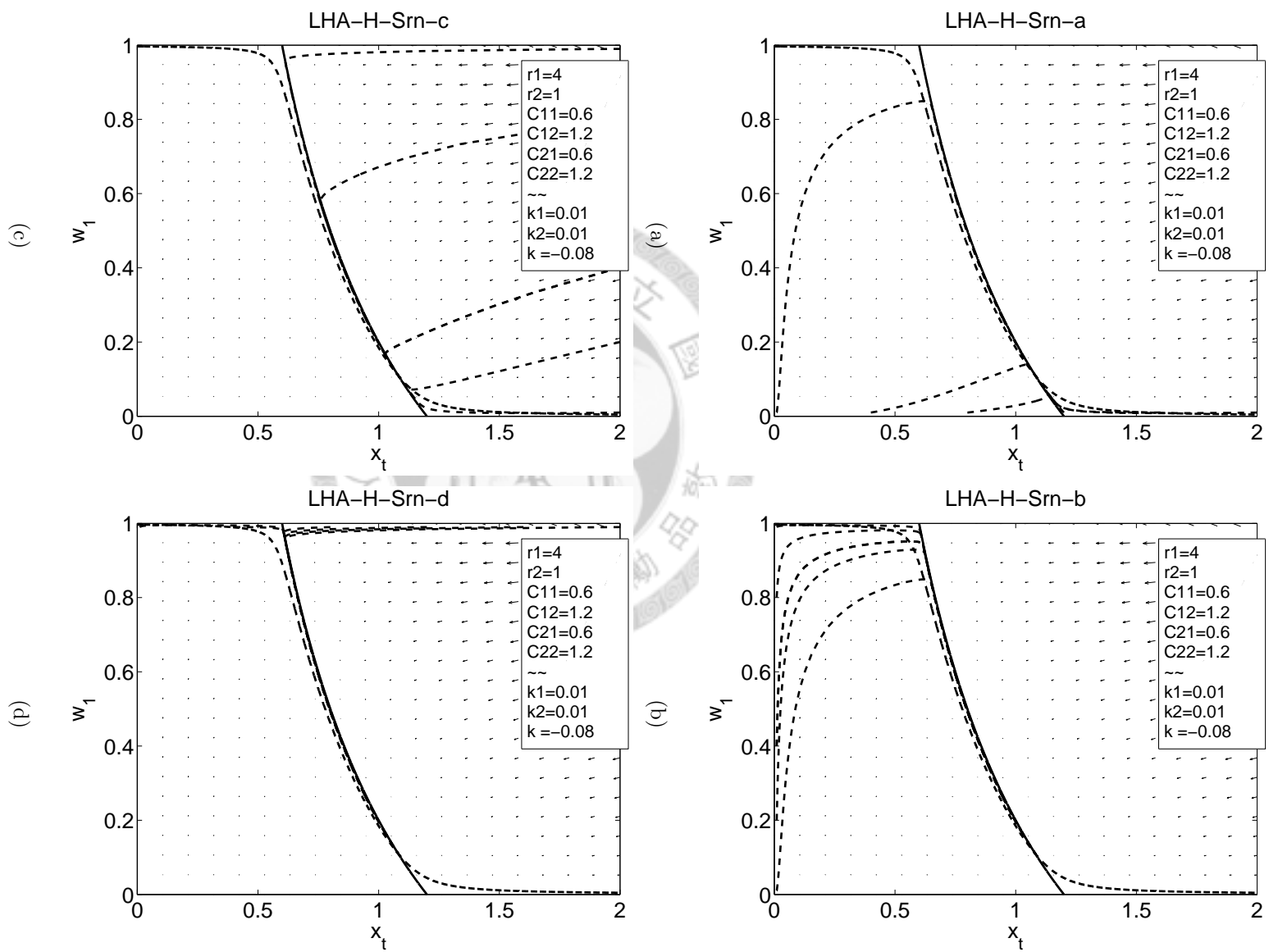


Figure 2.31: The x_{tot} - w_1 trajectories of LHA-H-Srn.

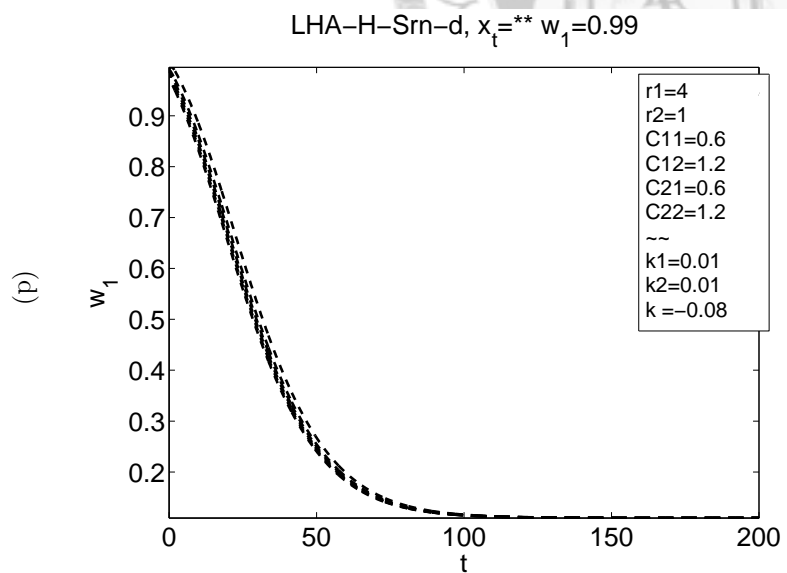
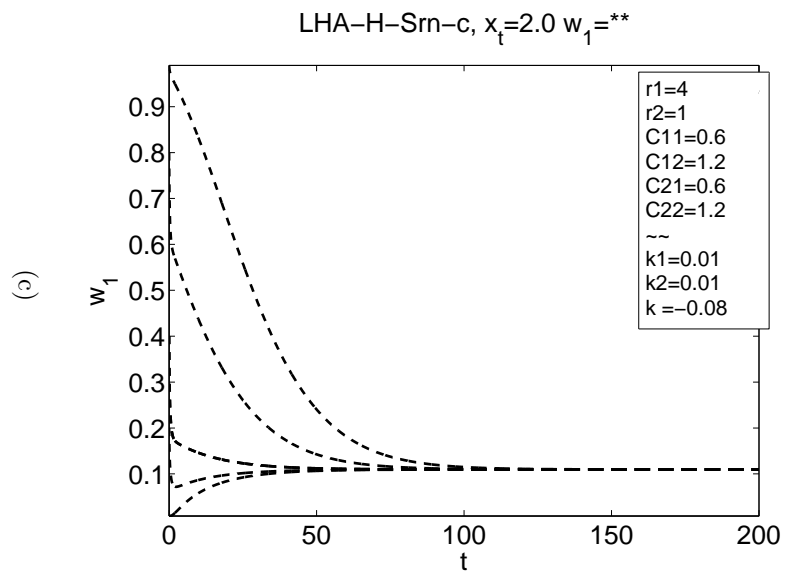
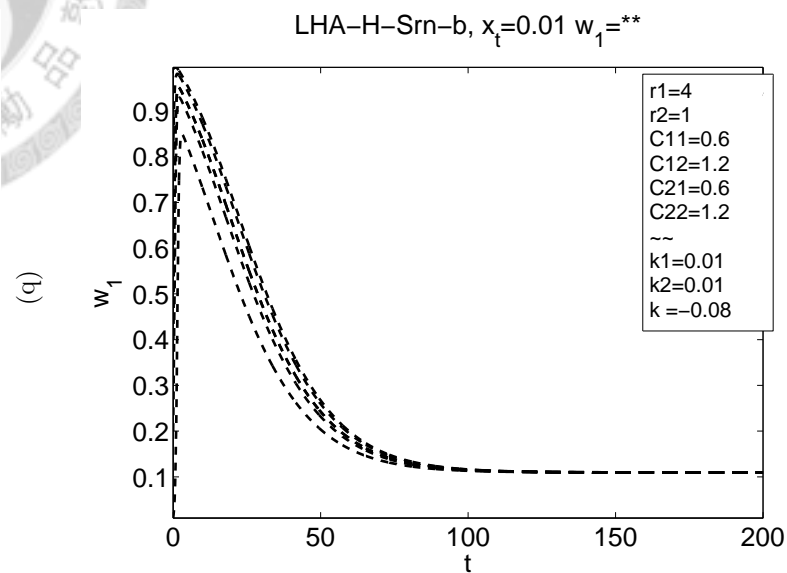
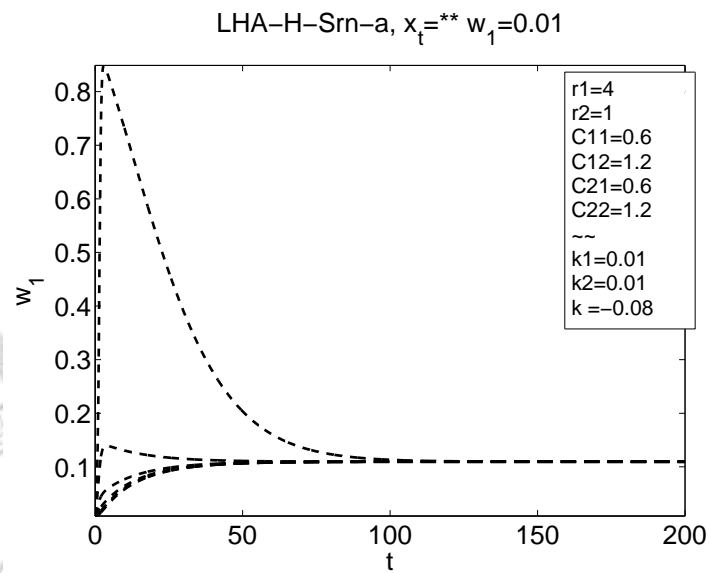
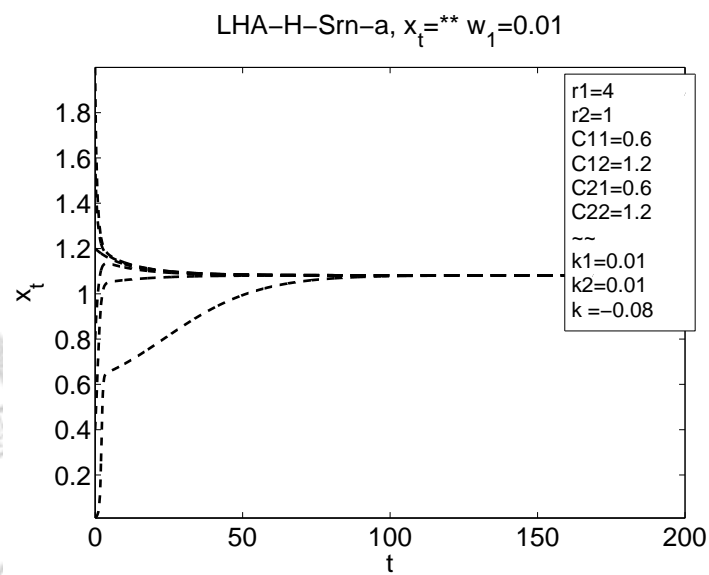
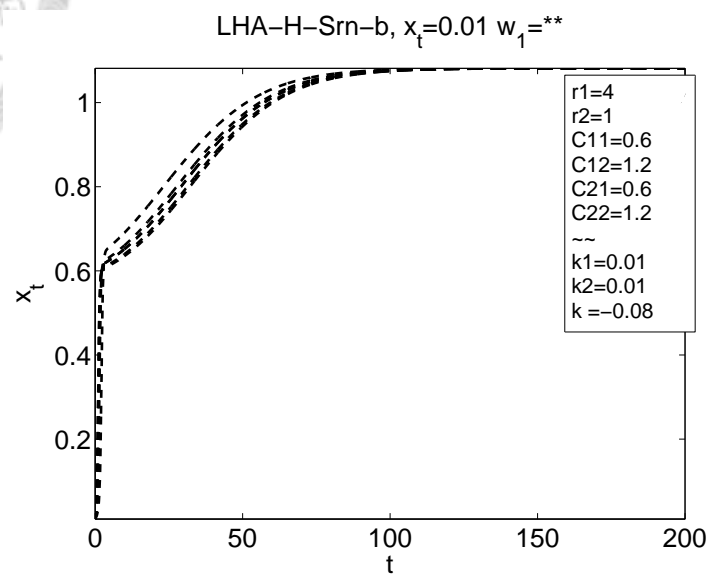


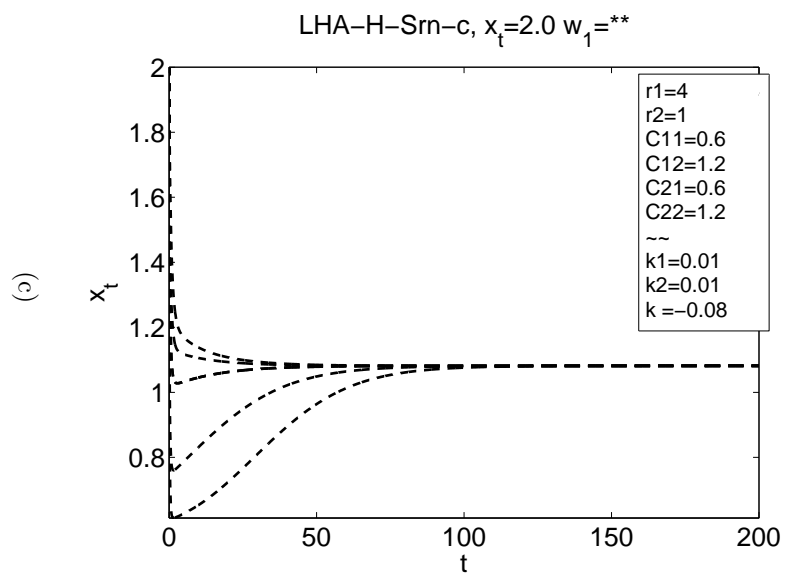
Figure 2.32: The x_{tot} - w_1 trajectories of LHA-H-Srn.



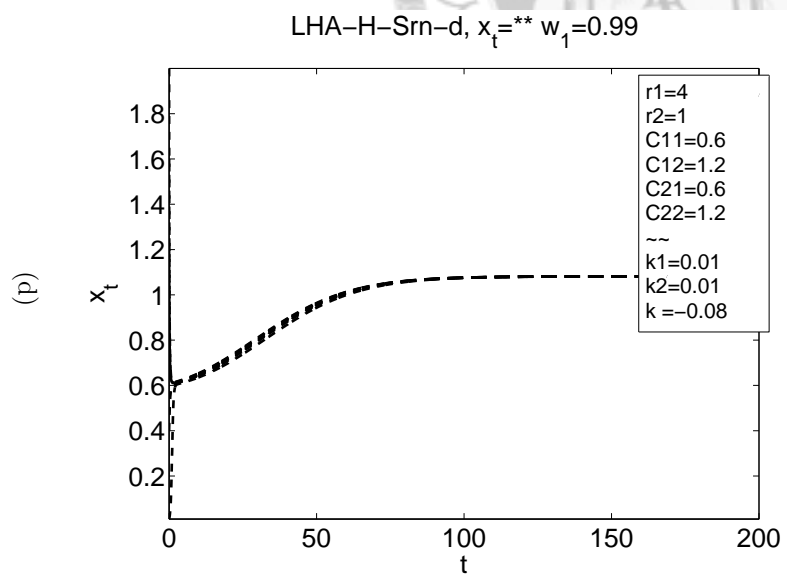
(a)



(b)



(c)



(d)

Figure 2.33: The $x_{tot} w_1$ trajectories of LHA-H-Srn.

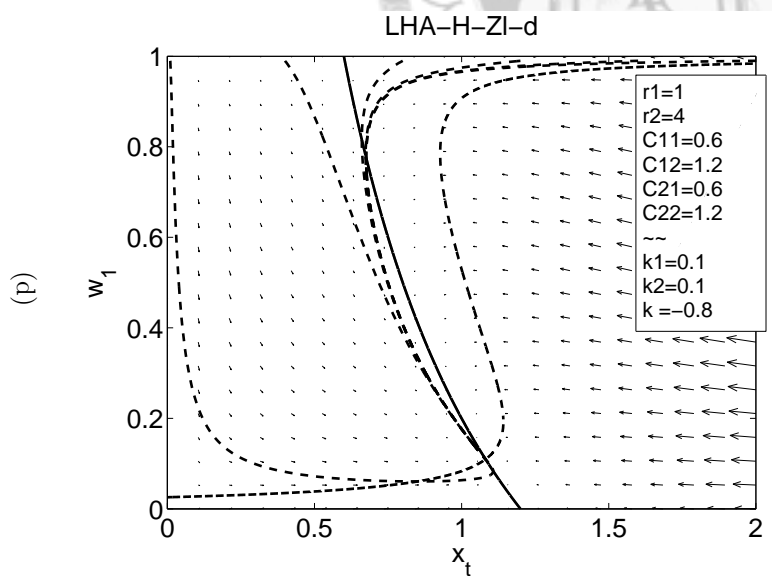
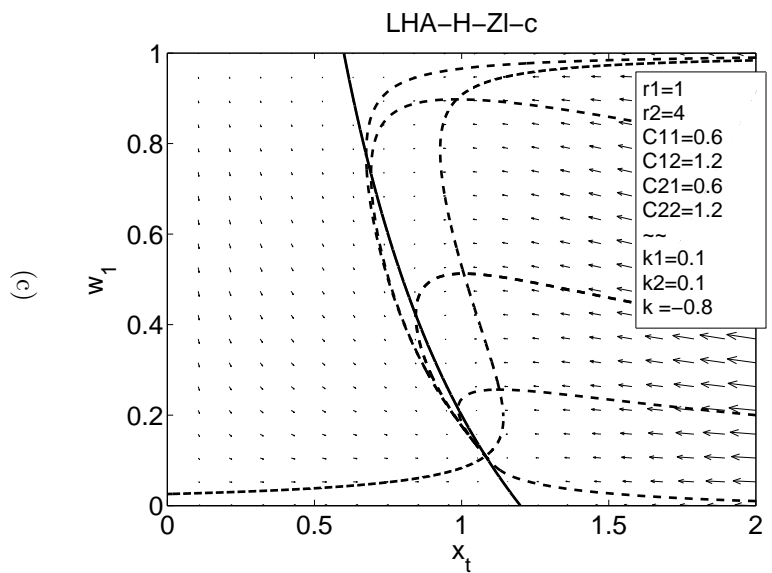
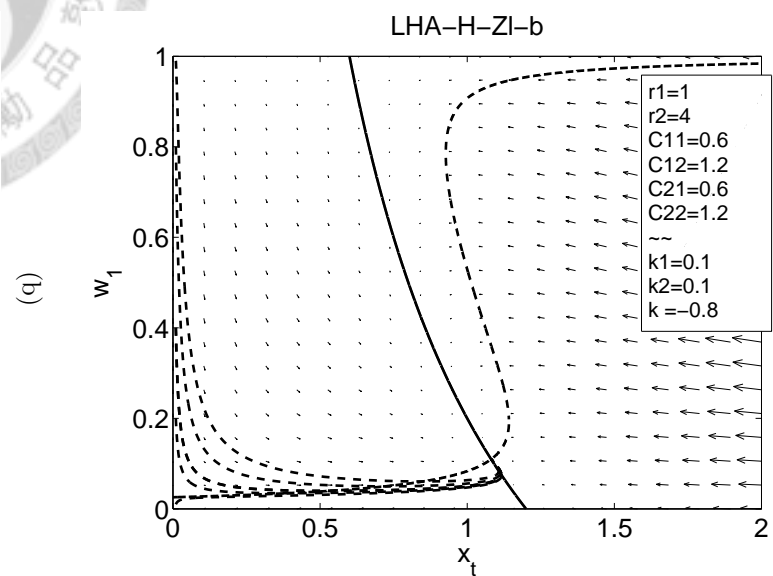
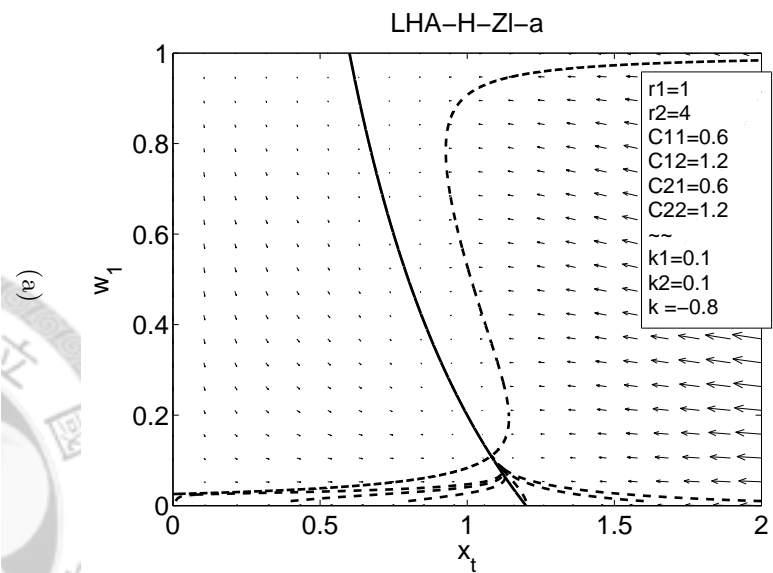


Figure 2.34: The x_{tot} - w_1 trajectories of LHA-H-ZI.

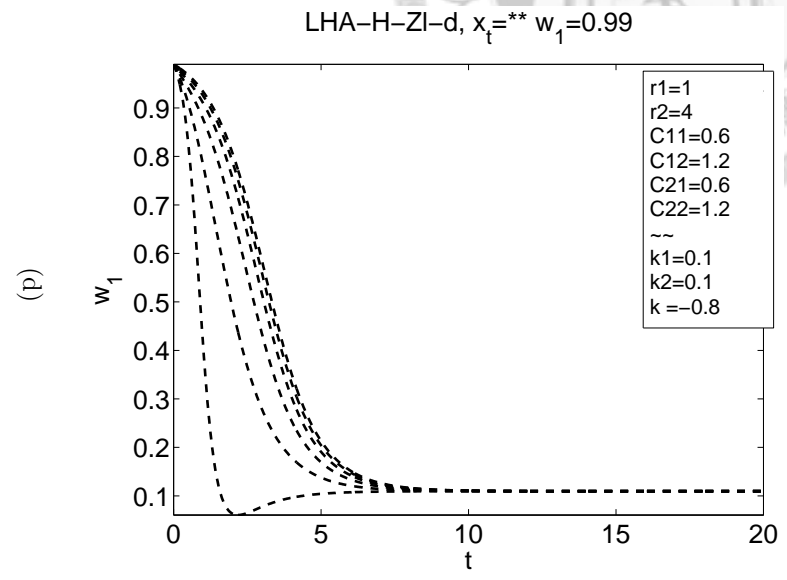
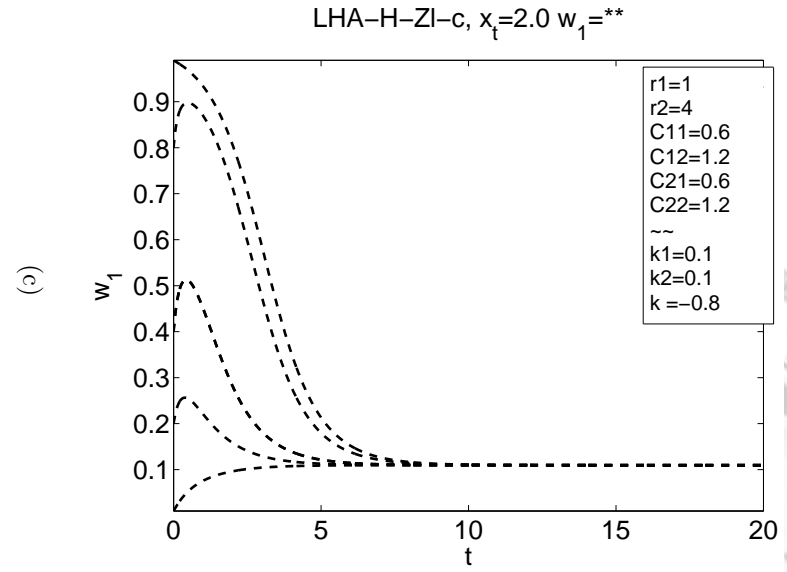
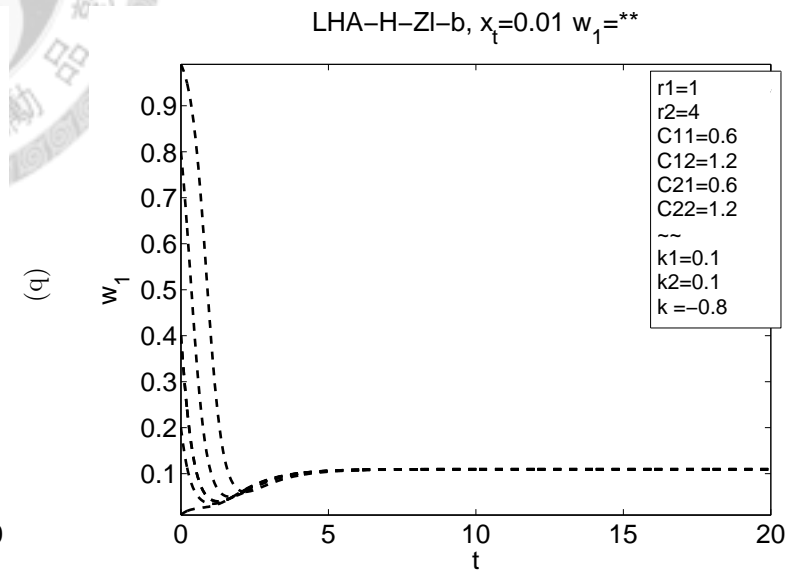
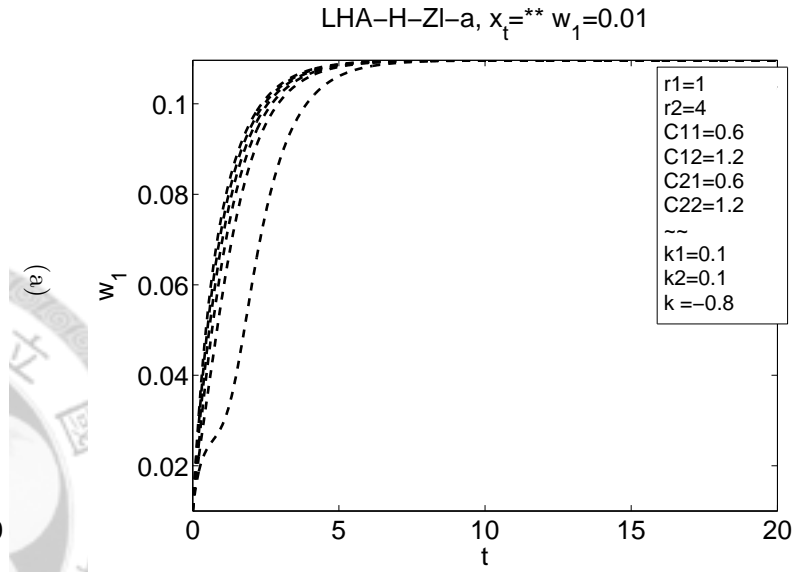


Figure 2.35: The x_{tot} - w_1 trajectories of LHA-H-ZI.

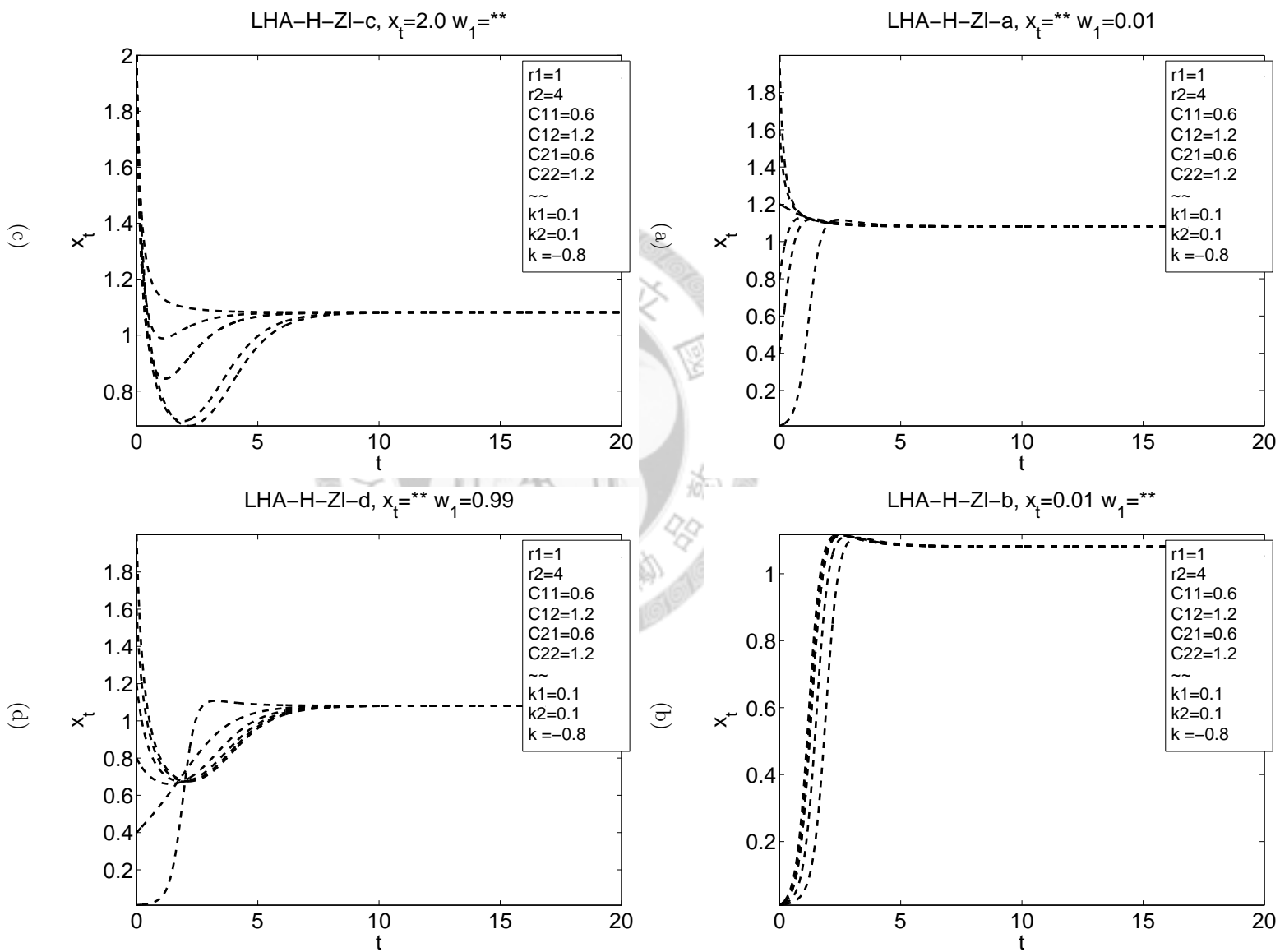


Figure 2.36: The $x_{tot}-w_1$ trajectories of LHA-H-ZI.

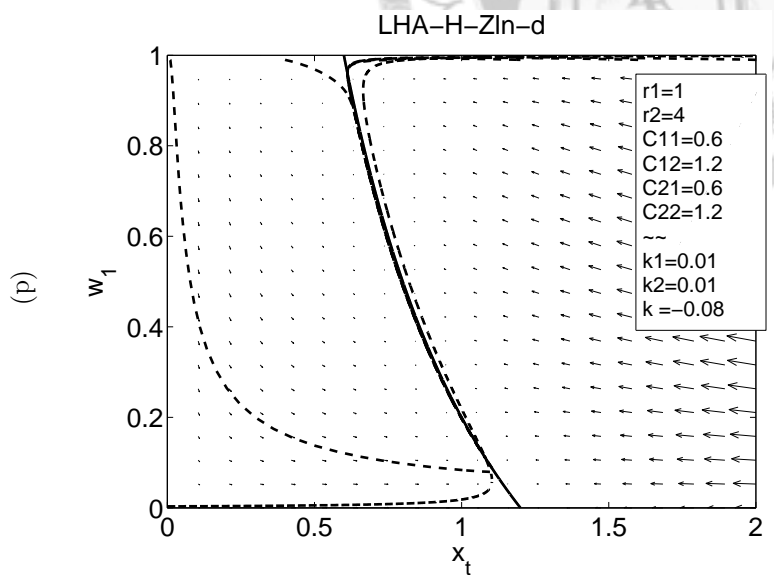
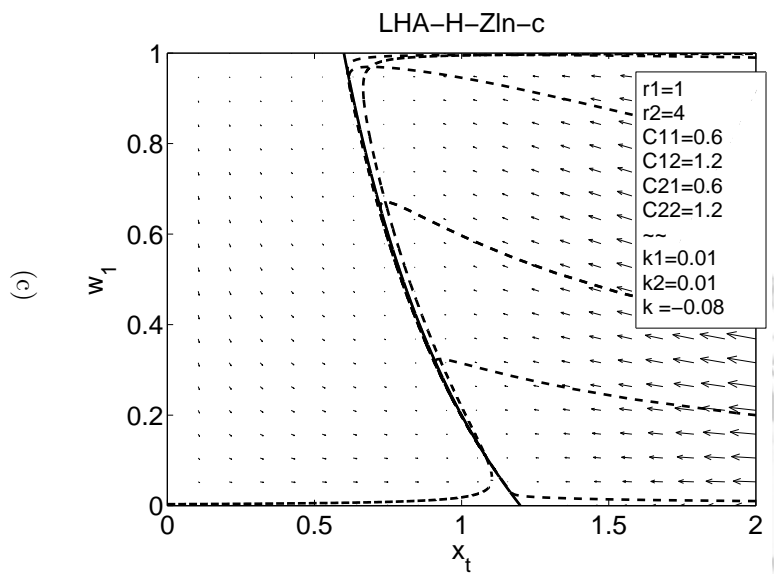
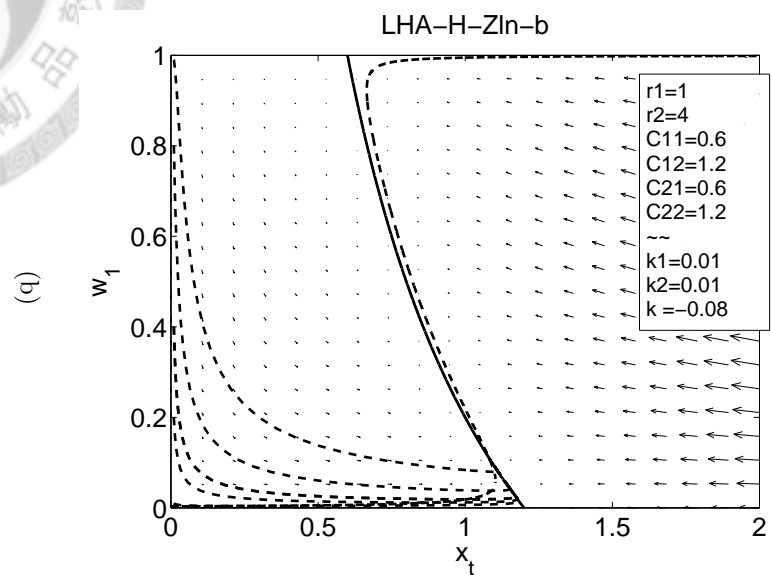
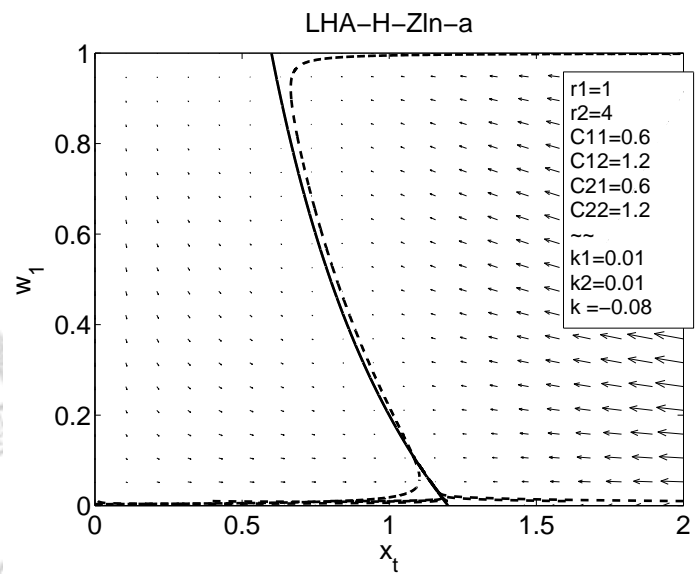


Figure 2.37: The x_{tot} - w_1 trajectories of LHA-H-ZIn.

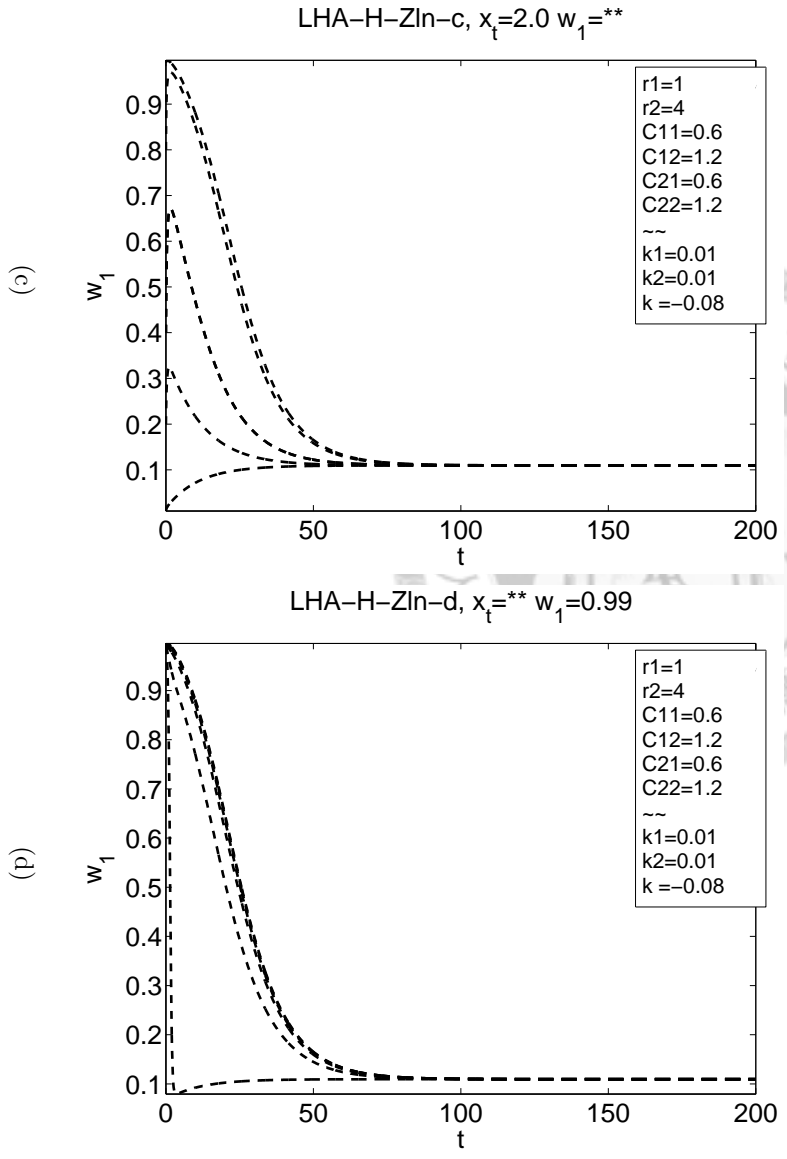
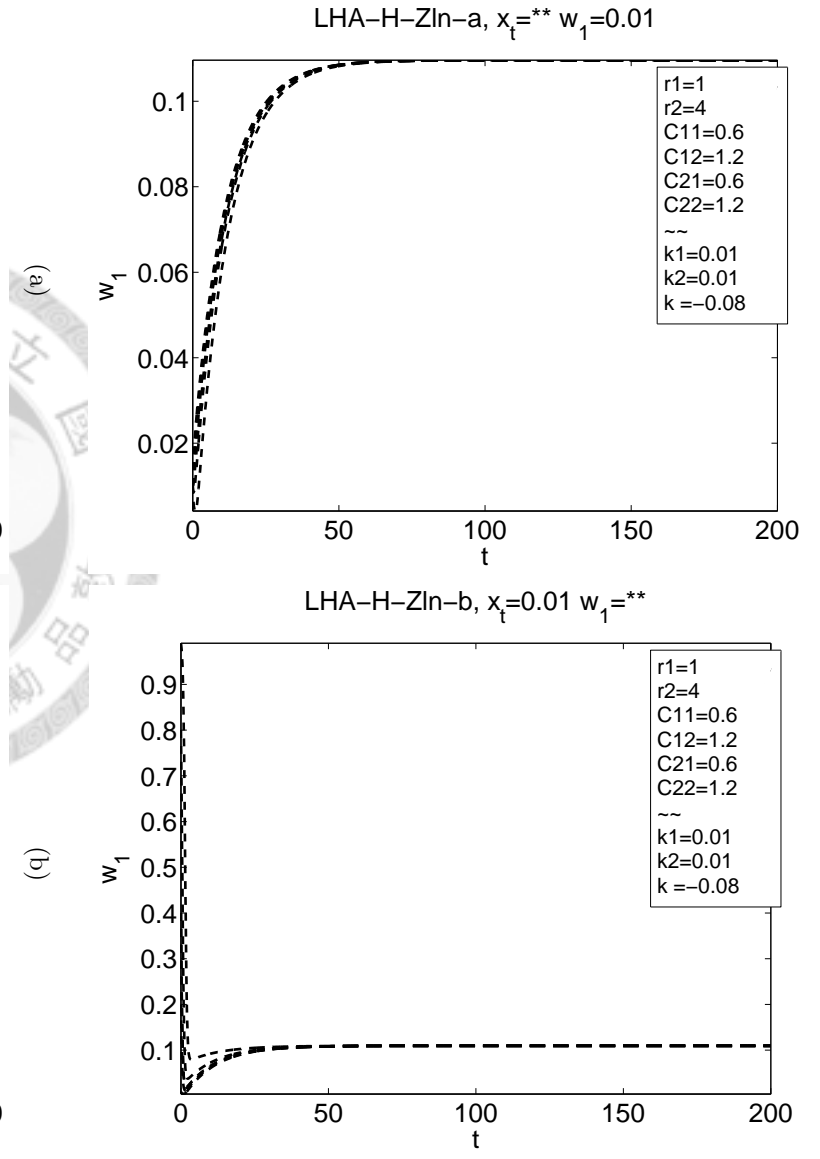


Figure 2.38: The x_{tot} - w_1 trajectories of LHA-H-Zln.

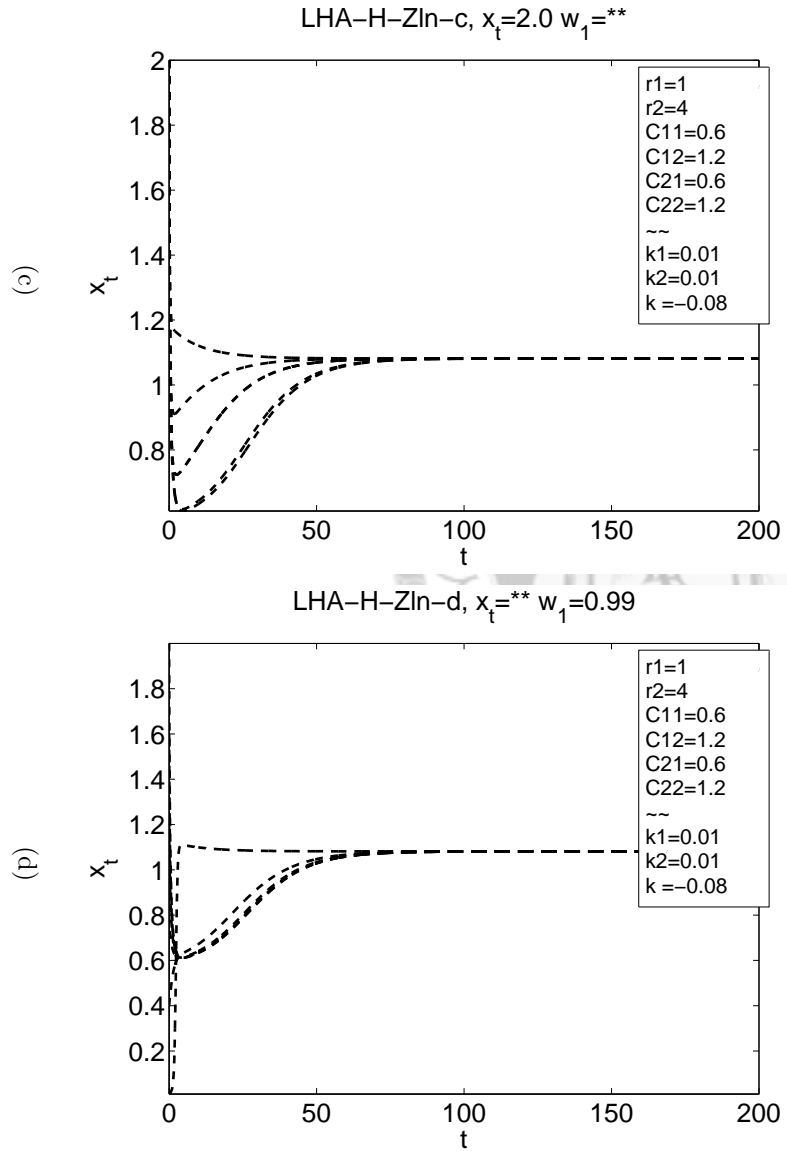
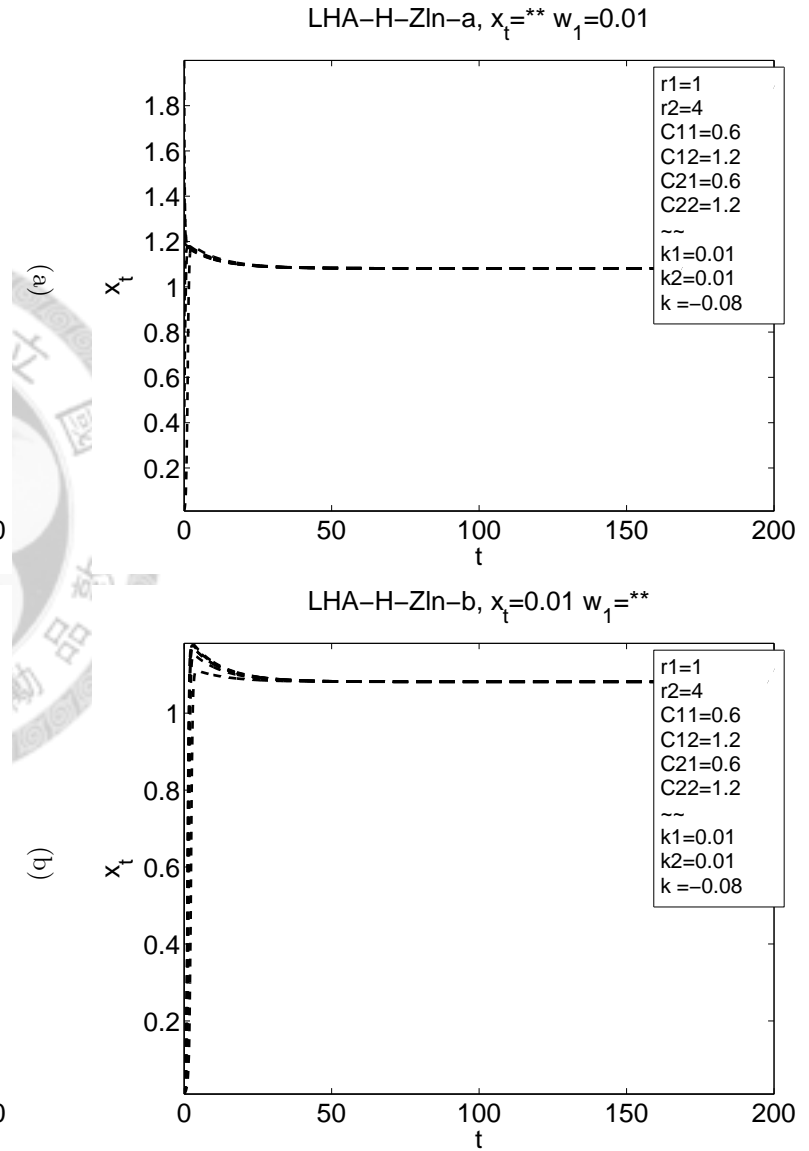


Figure 2.39: The $x_{tot}-w_1$ trajectories of LHA-H-Zln.

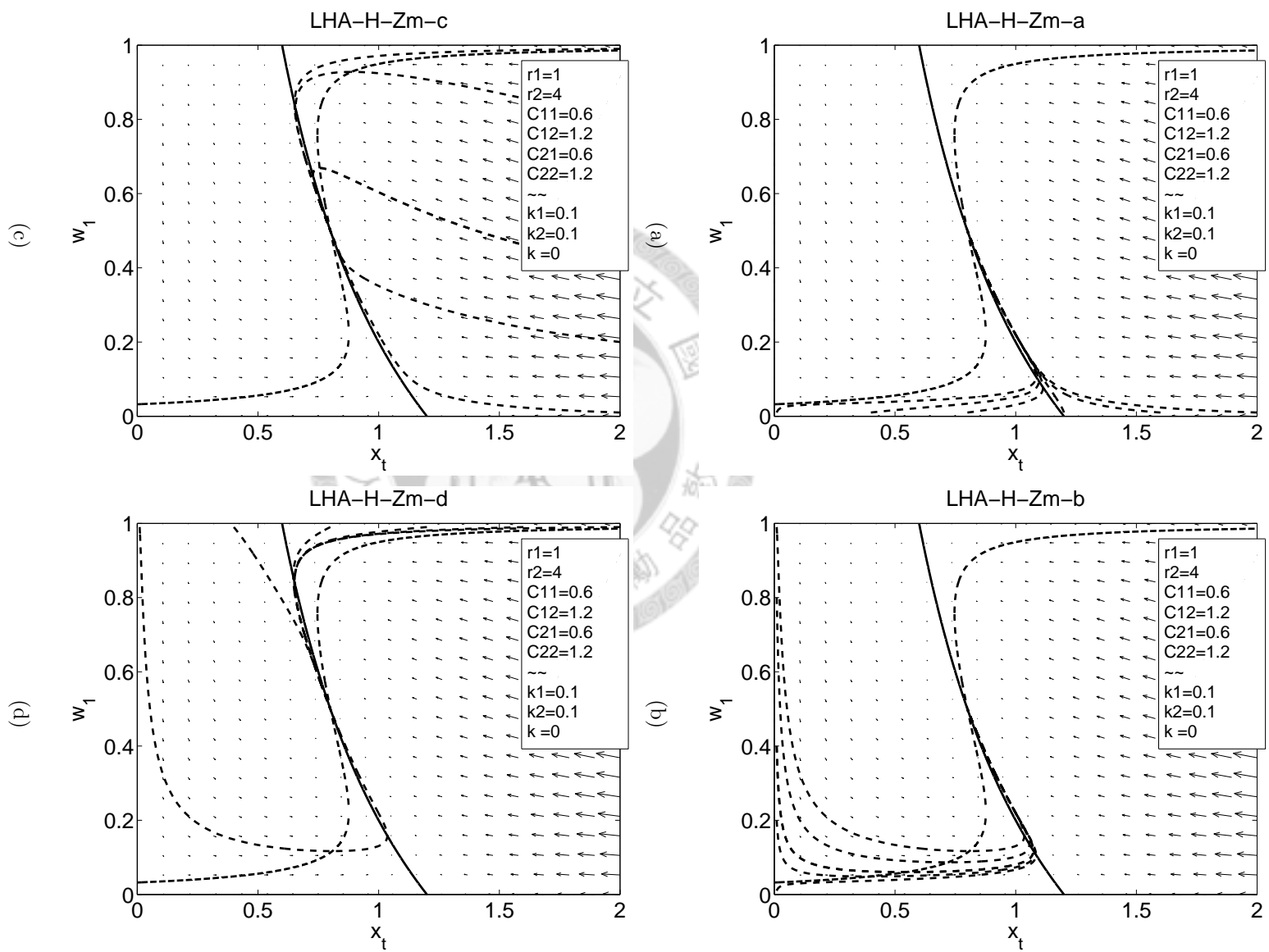


Figure 2.40: The x_{tot} - w_1 trajectories of LHA-H-Zm.

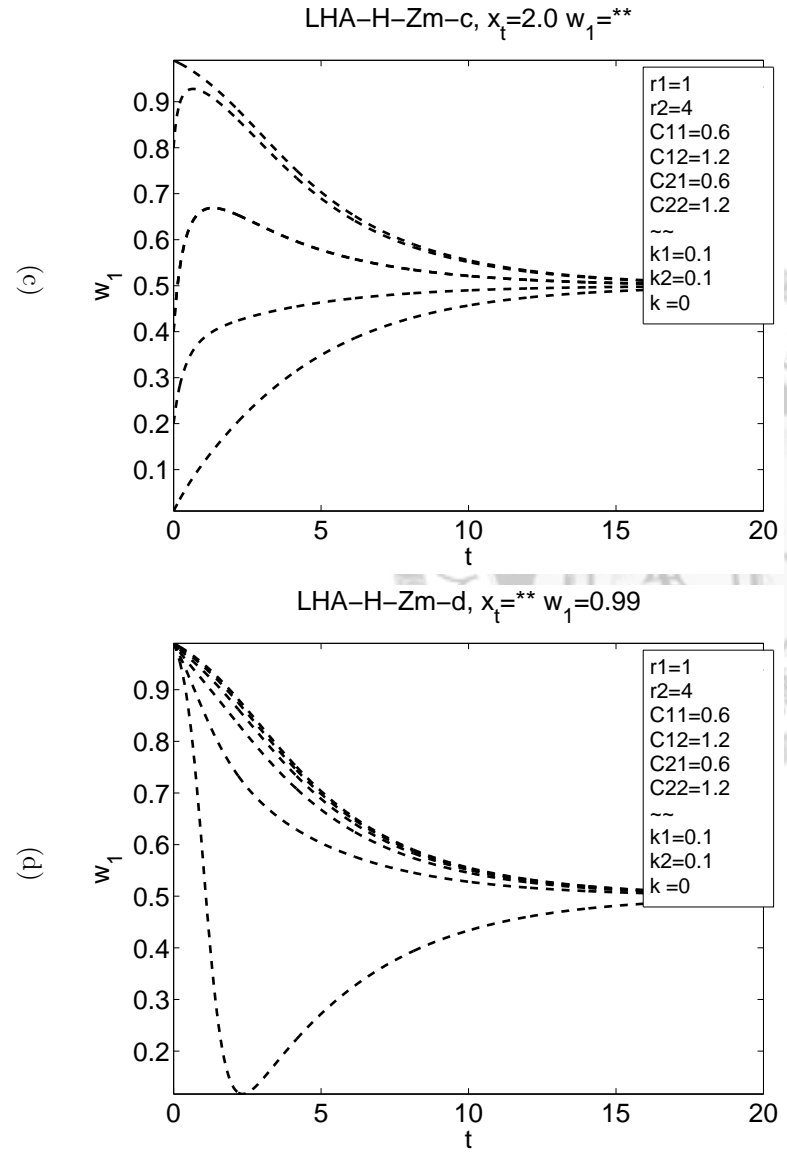
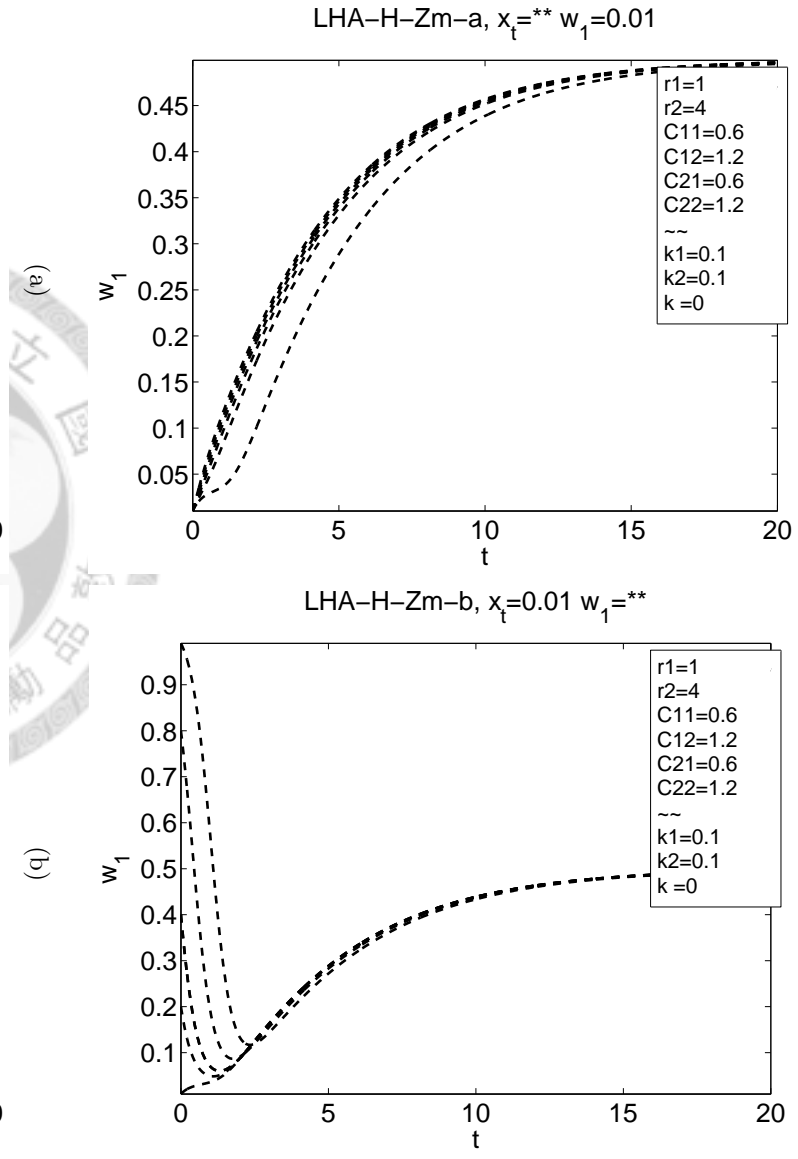


Figure 2.41: The x_{tot} - w_1 trajectories of LHA-H-Zm.

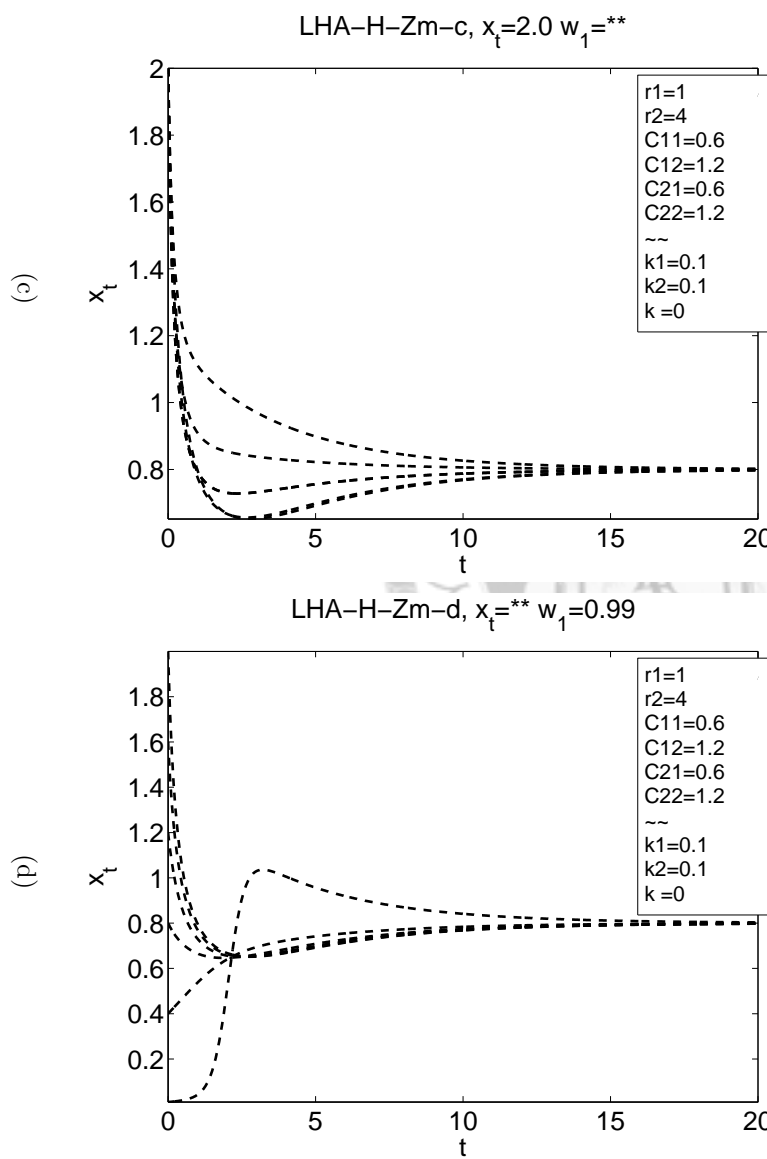
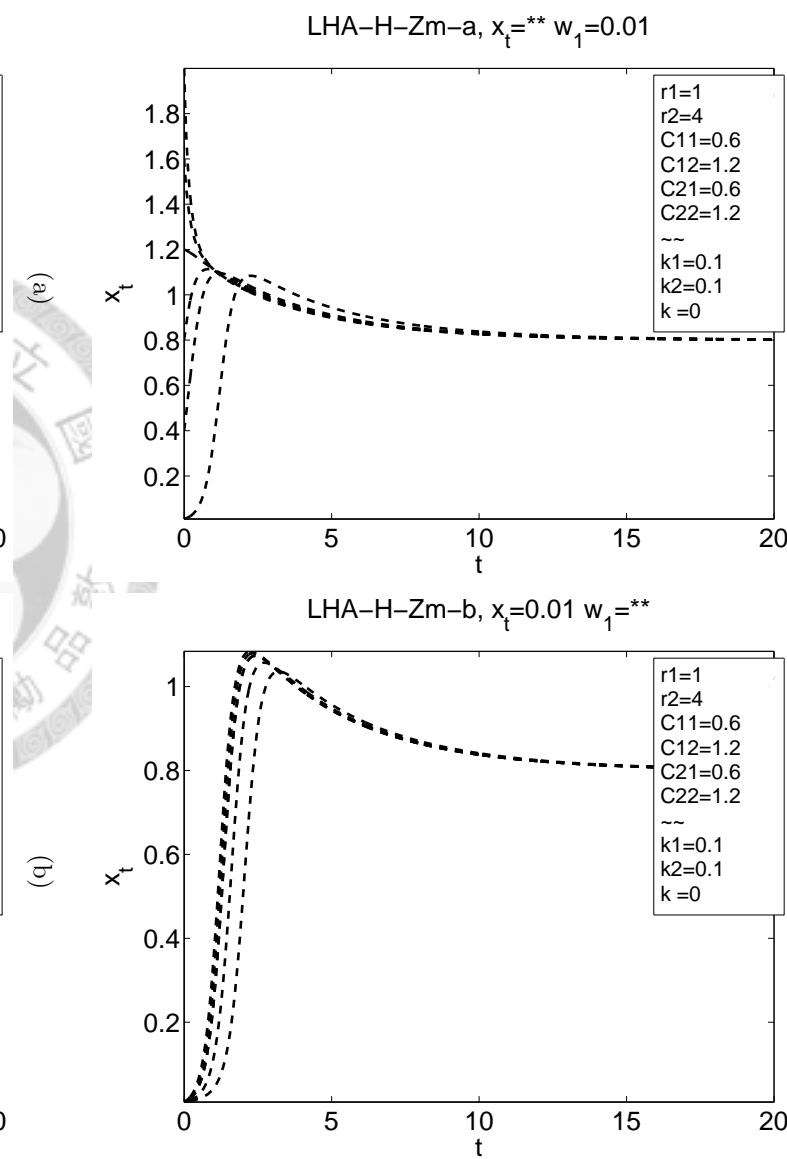


Figure 2.42: The $x_{tot}-w_1$ trajectories of LHA-H-Zm.

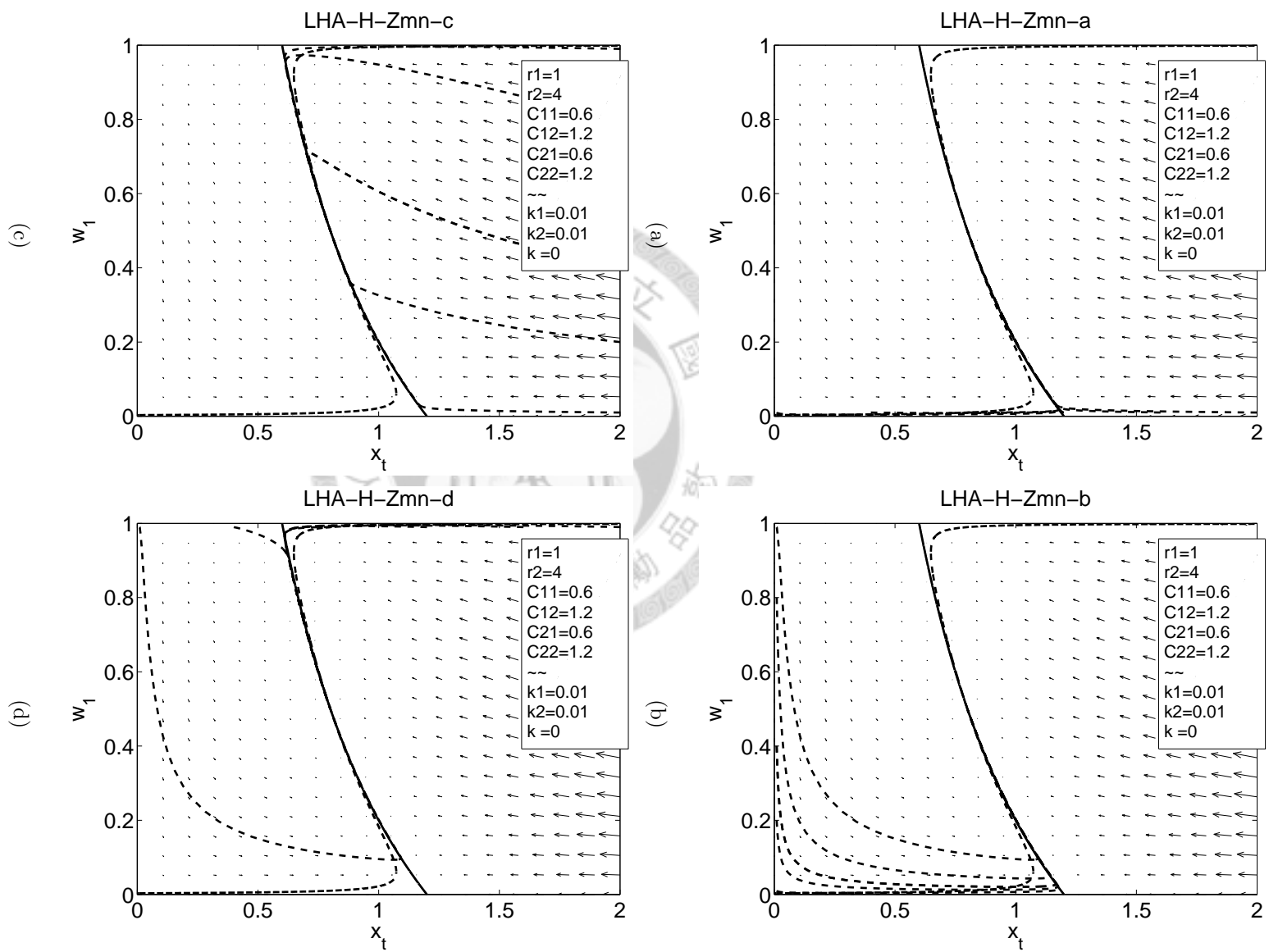


Figure 2.43: The x_{tot} - w_1 trajectories of LHA-H-Zmn.

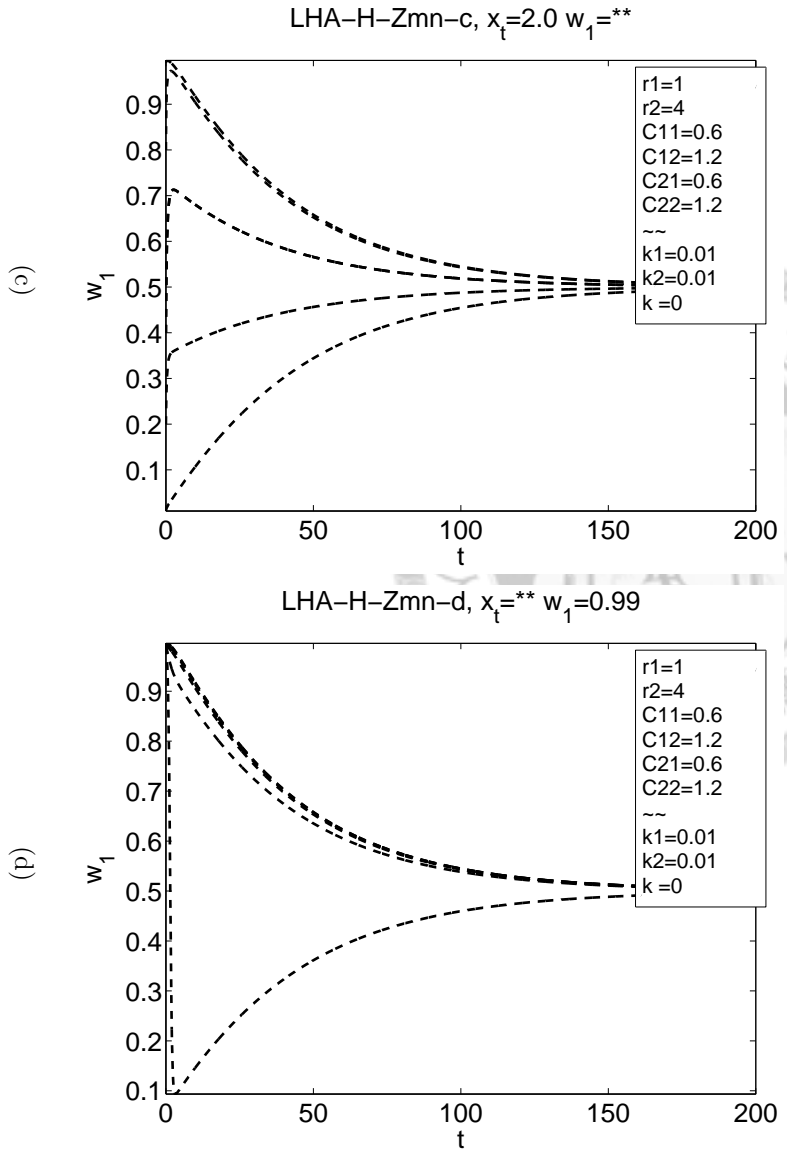
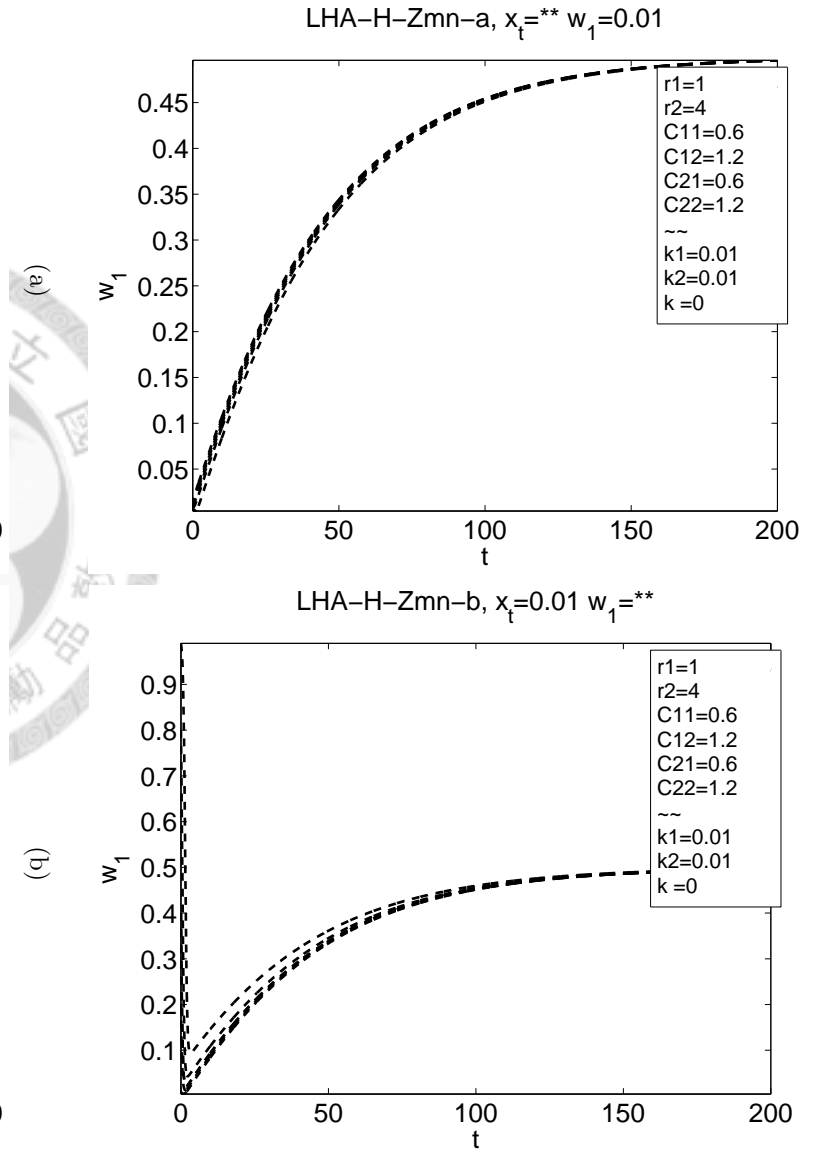


Figure 2.44: The x_{tot} - w_1 trajectories of LHA-H-Zmn.

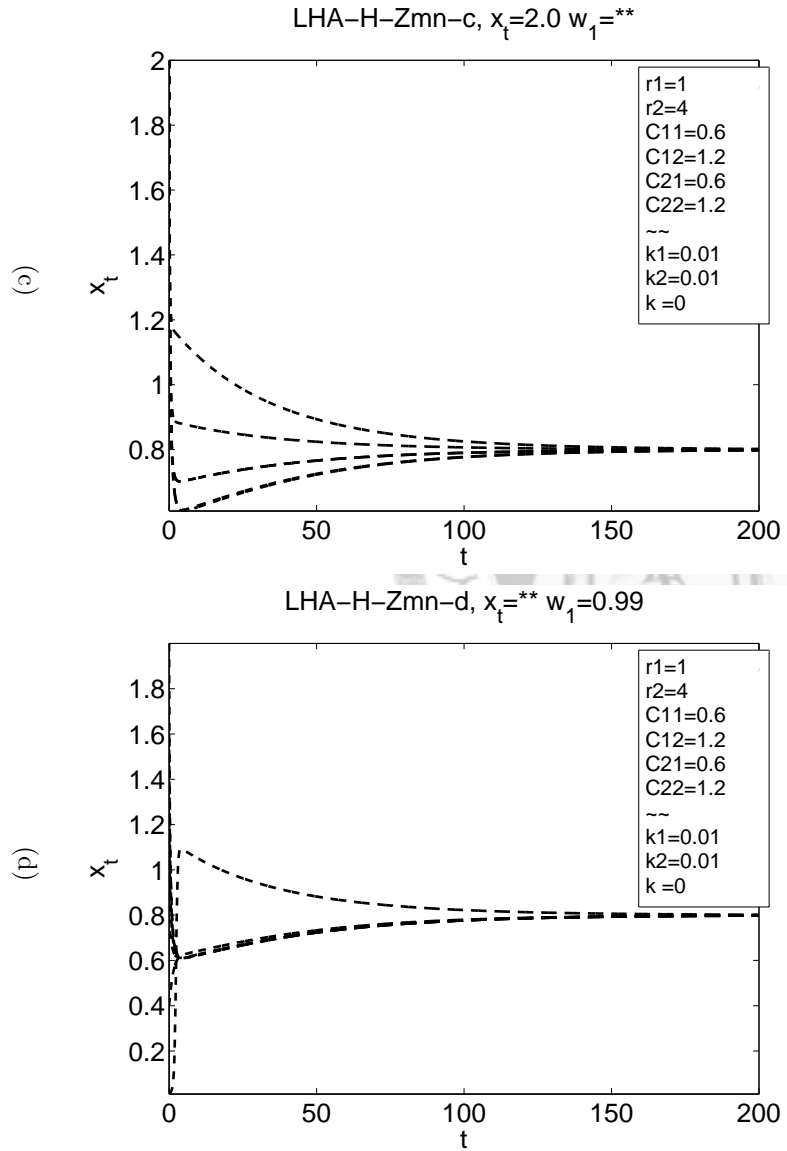
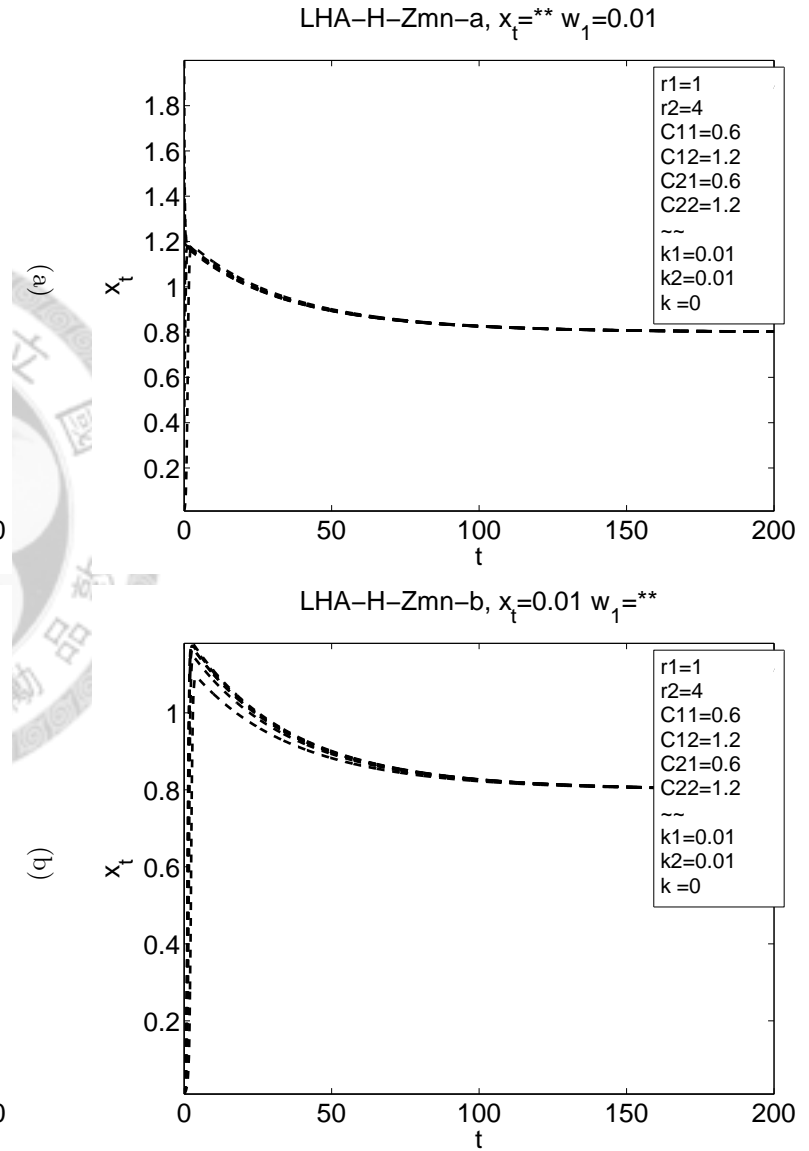


Figure 2.45: The $x_{tot}-w_1$ trajectories of LHA-H-Zmn.

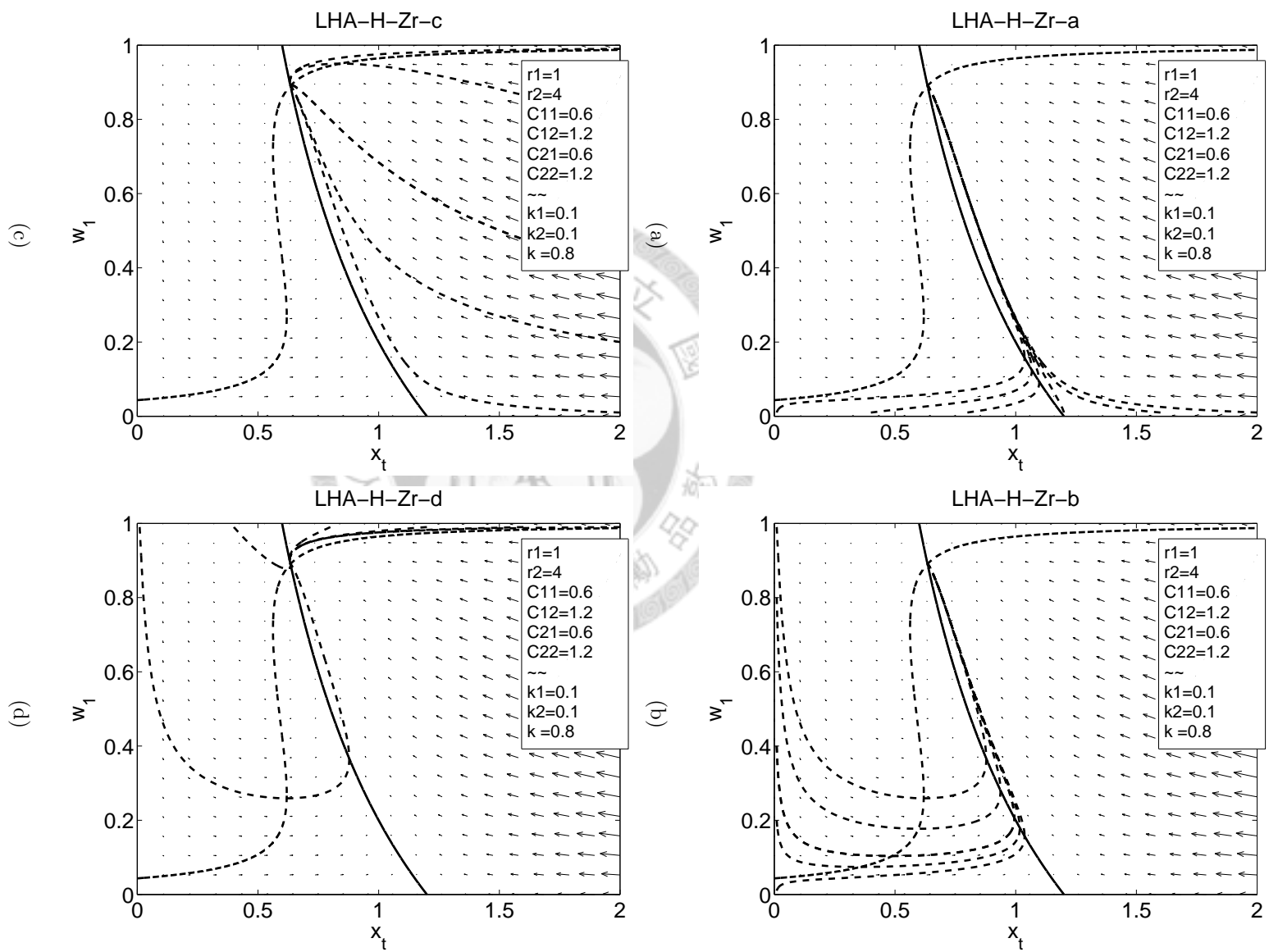


Figure 2.46: The x_{tot} - w_1 trajectories of LHA-H-Zr.

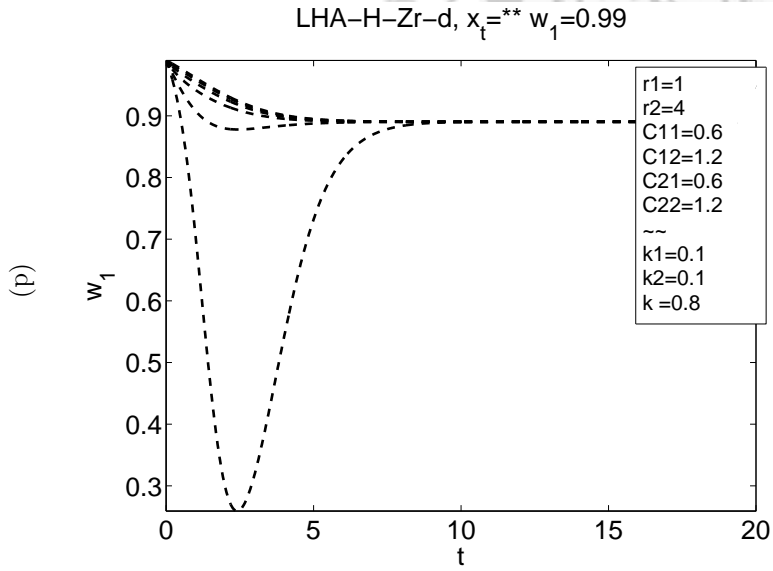
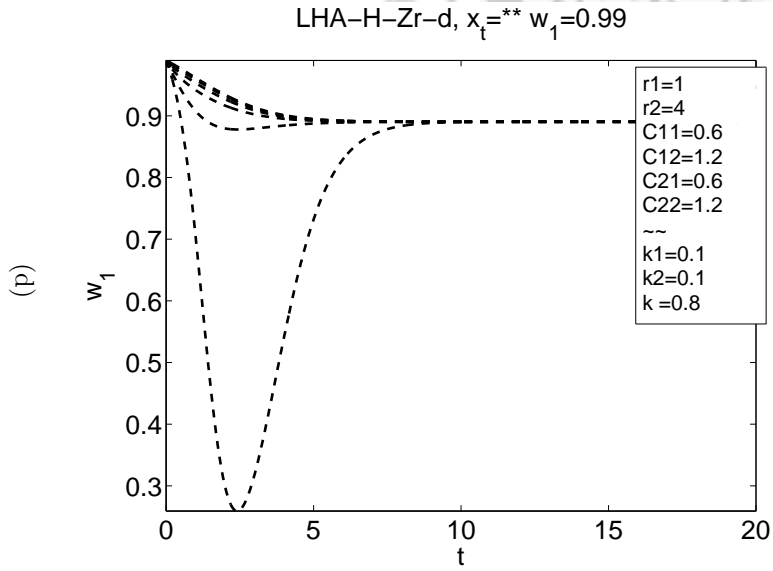
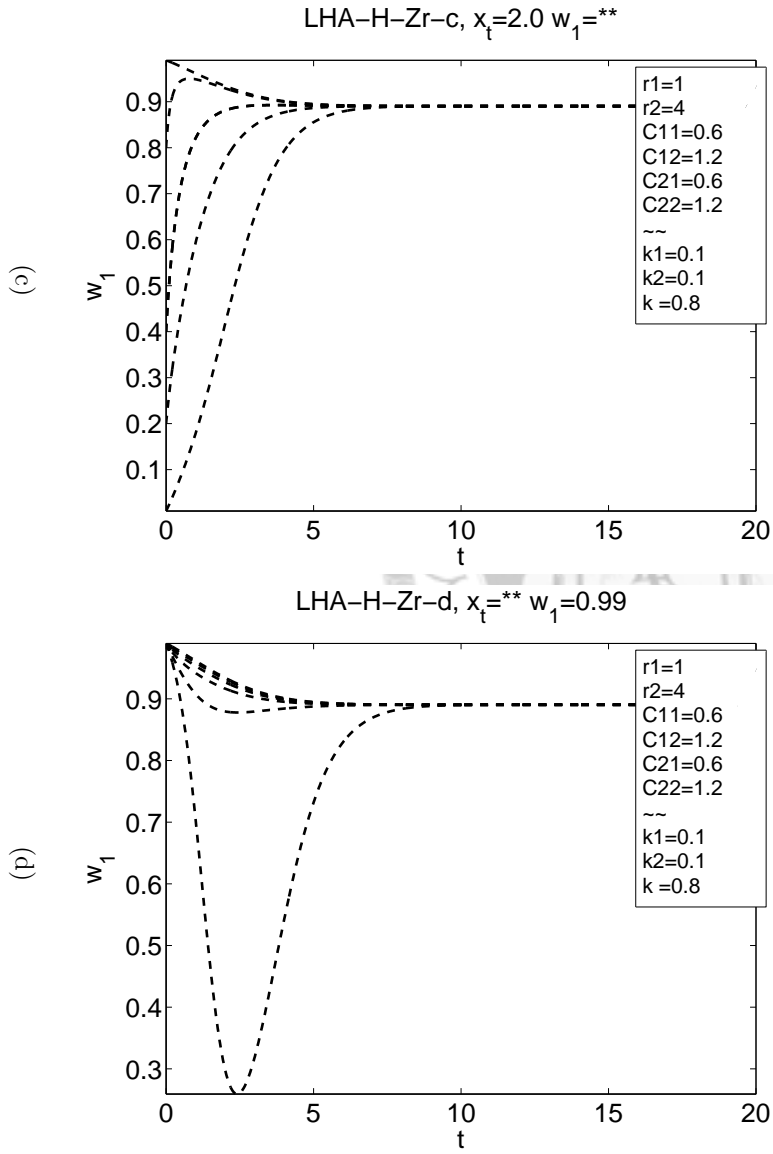
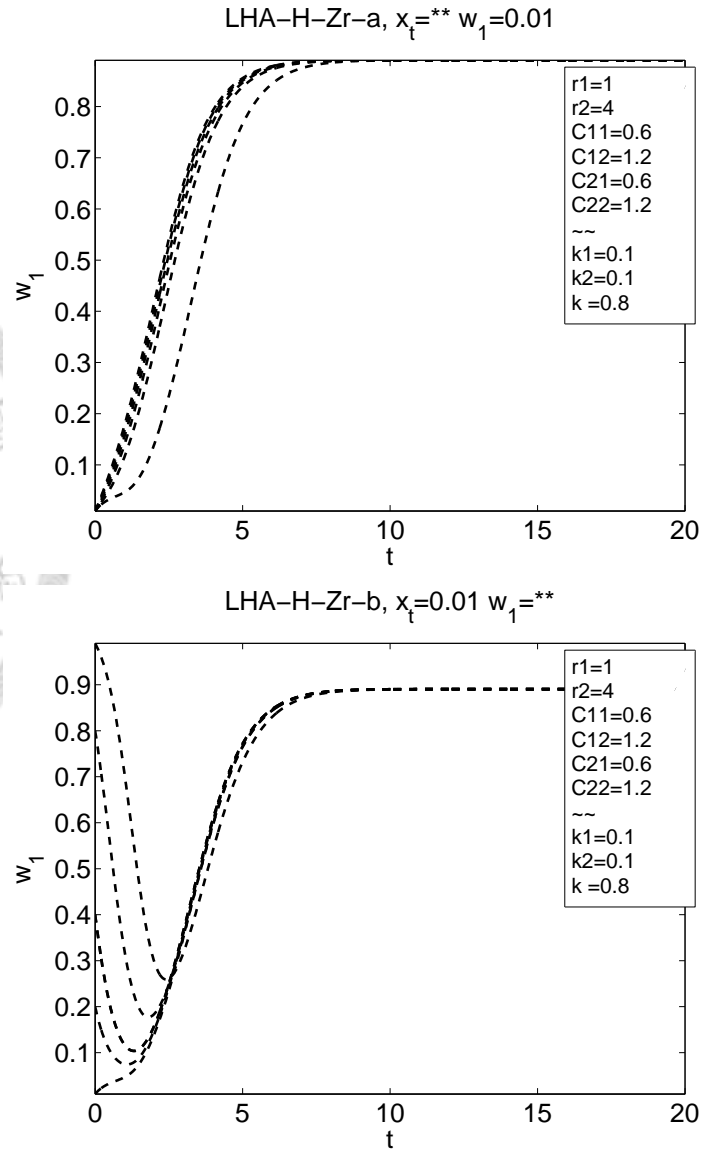
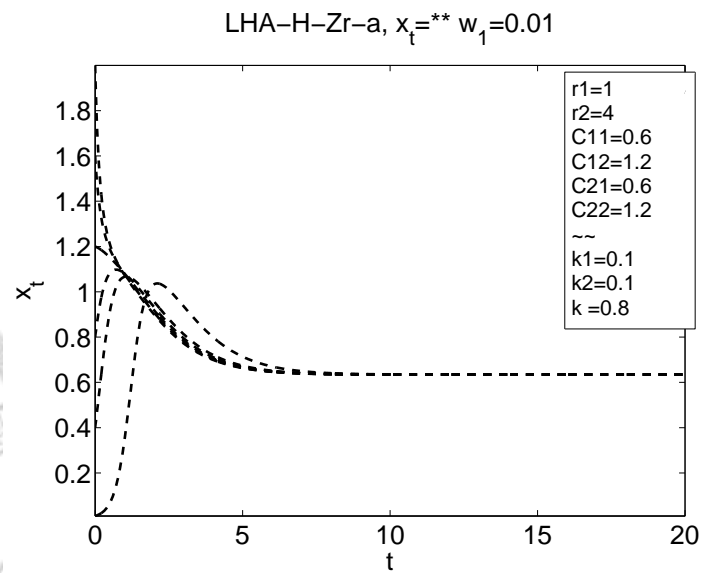
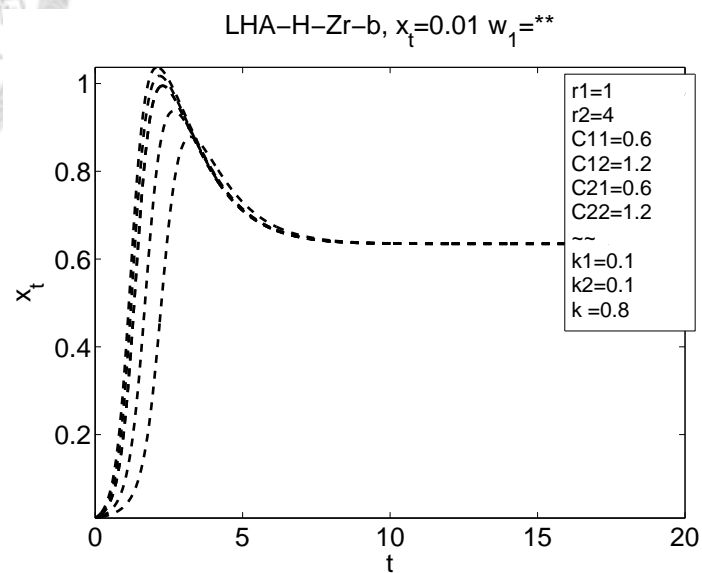


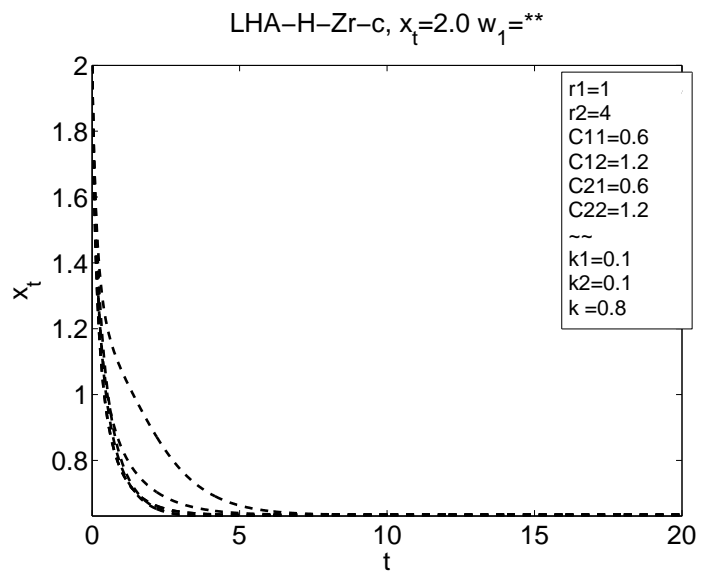
Figure 2.47: The x_{tot} - w_1 trajectories of LHA-H-Zr.



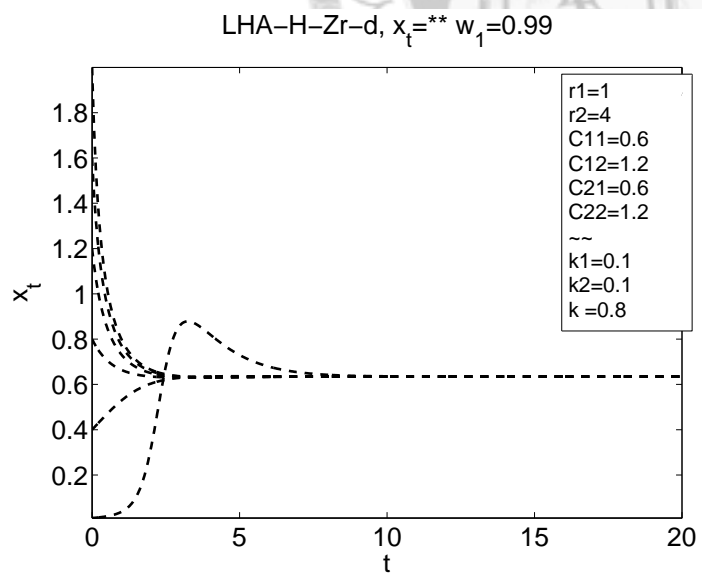
(a)



(b)



(c)



(d)

Figure 2.48: The $x_{tot}-w_1$ trajectories of LHA-H-Zr.

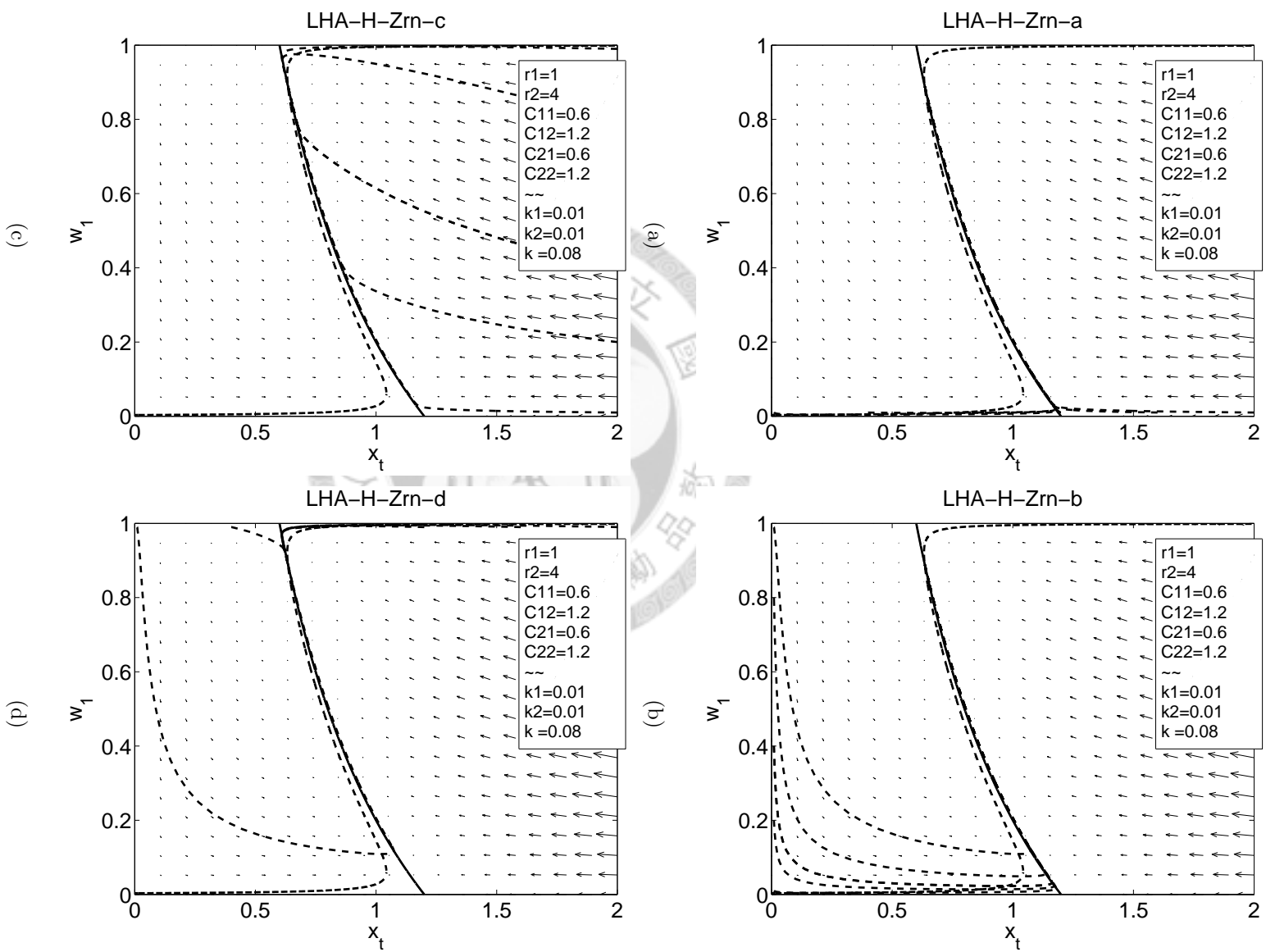


Figure 2.49: The x_{tot} - w_1 trajectories of LHA-H-Zrn.

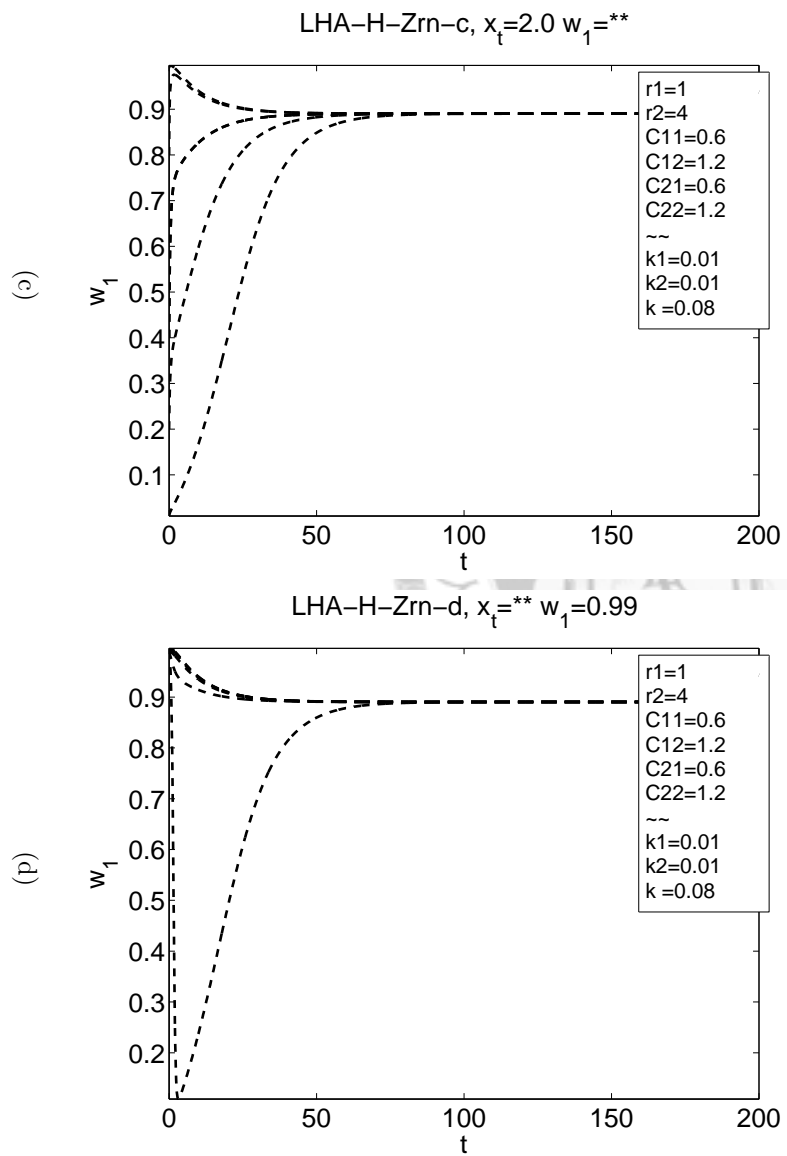
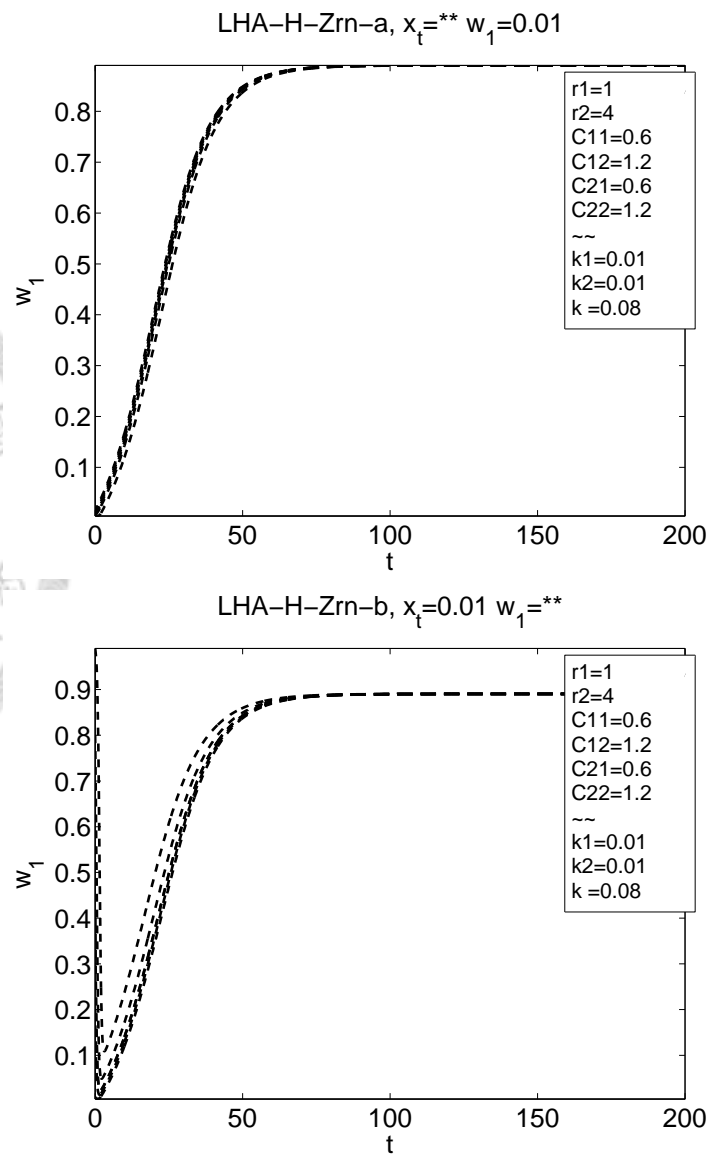


Figure 2.50: The x_{tot} - w_1 trajectories of LHA-H-Zrn.

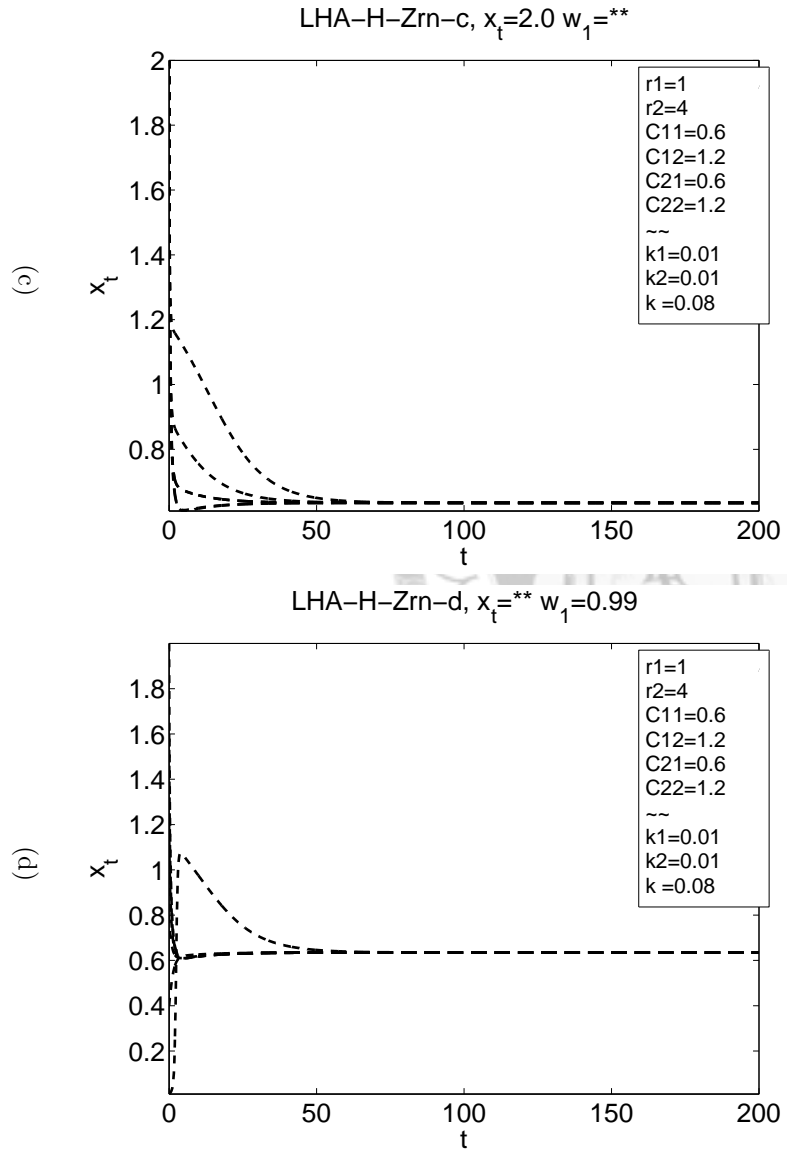
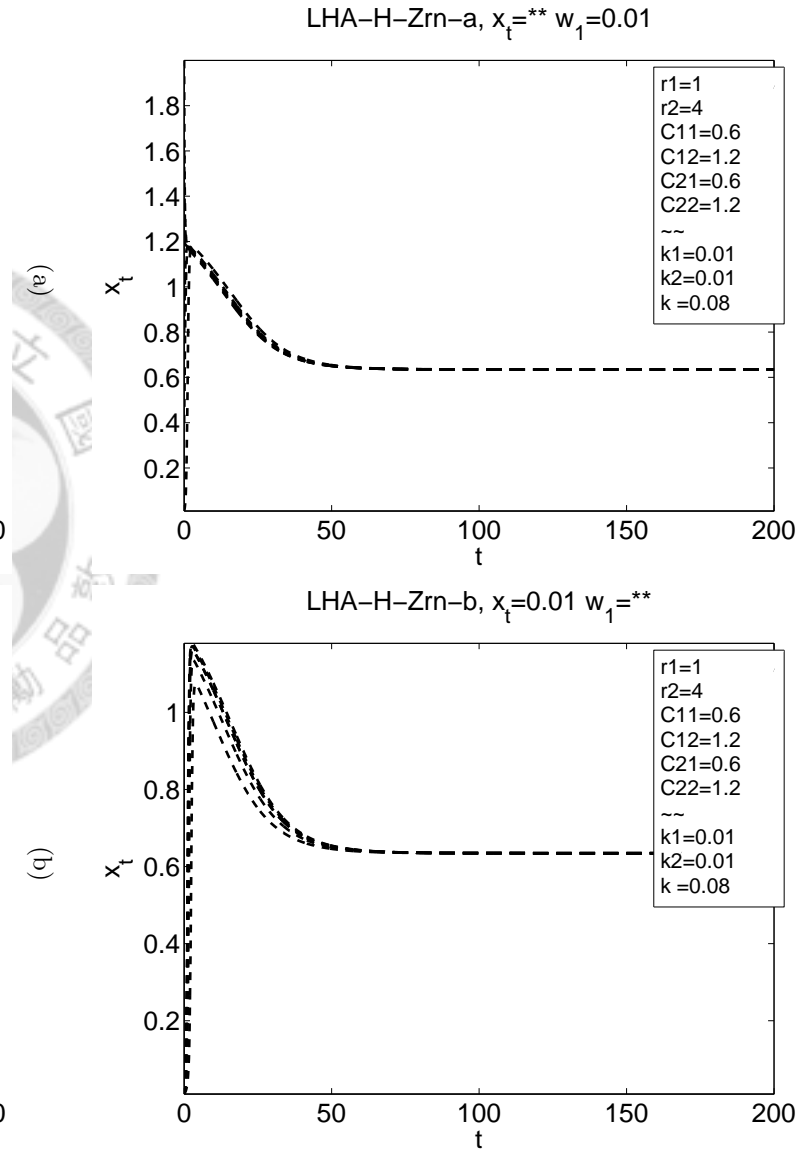


Figure 2.51: The $x_{tot}-w_1$ trajectories of LHA-H-Zrn.

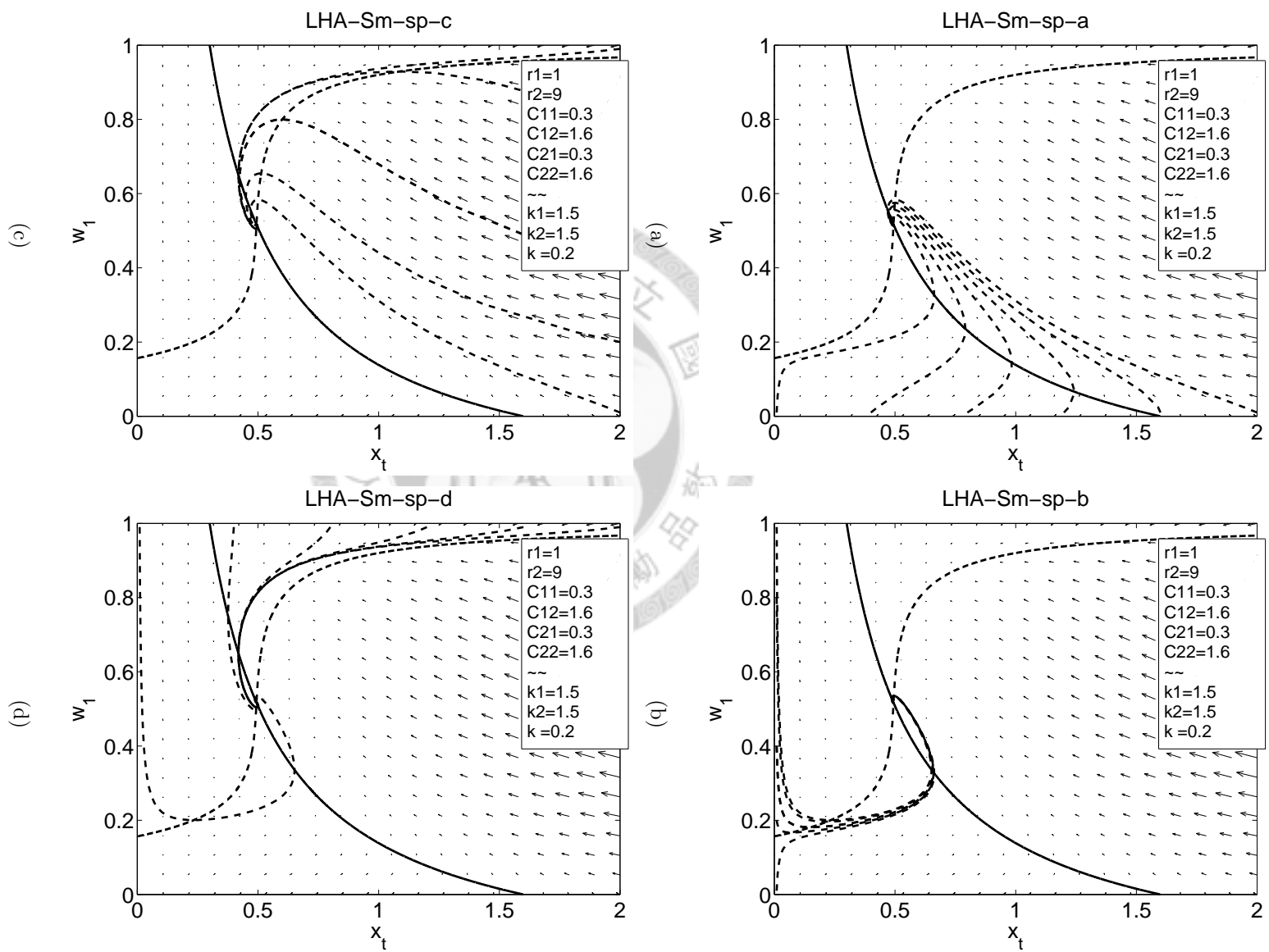
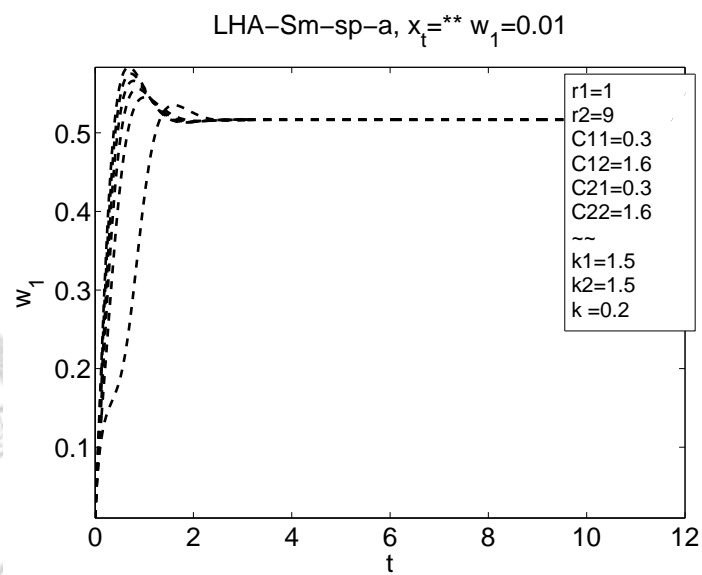
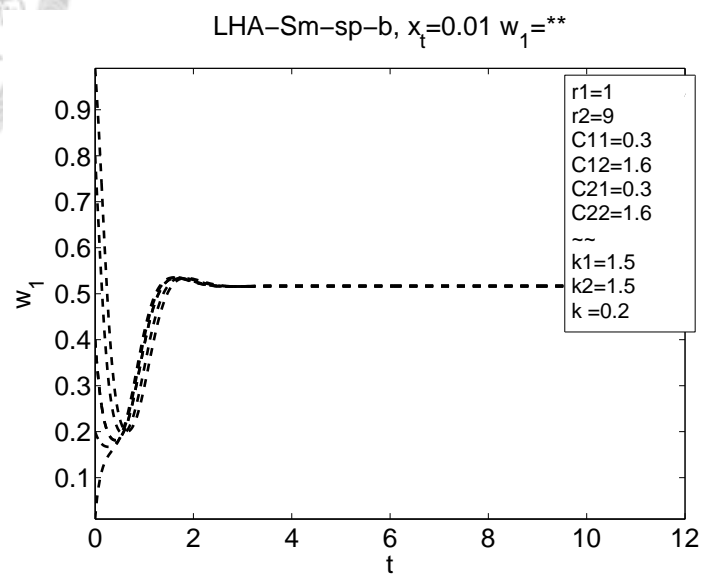


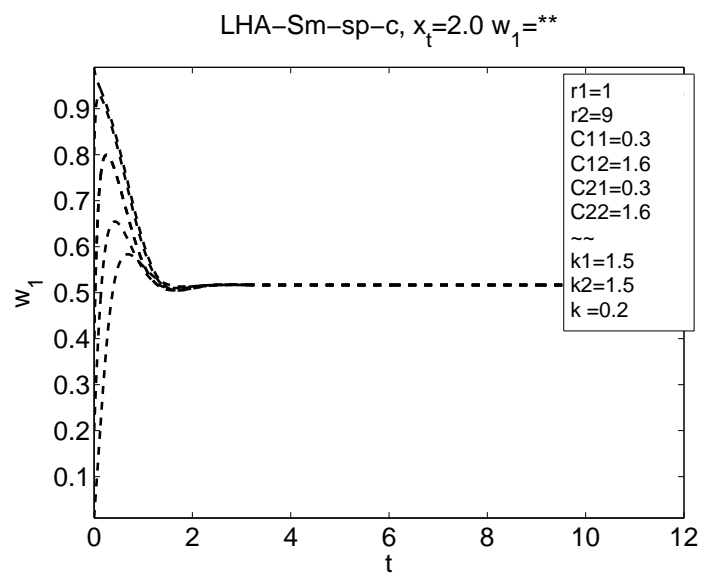
Figure 2.52: The x_{tot} - w_1 trajectories of LHA-Sm-sp.



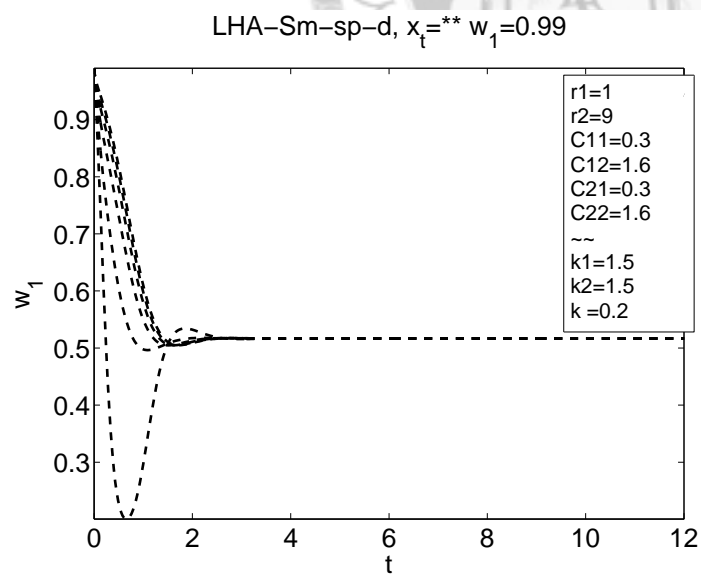
(a)



(b)



(c)



(d)

Figure 2.53: The x_{tot} - w_1 trajectories of LHA-Sm-sp.

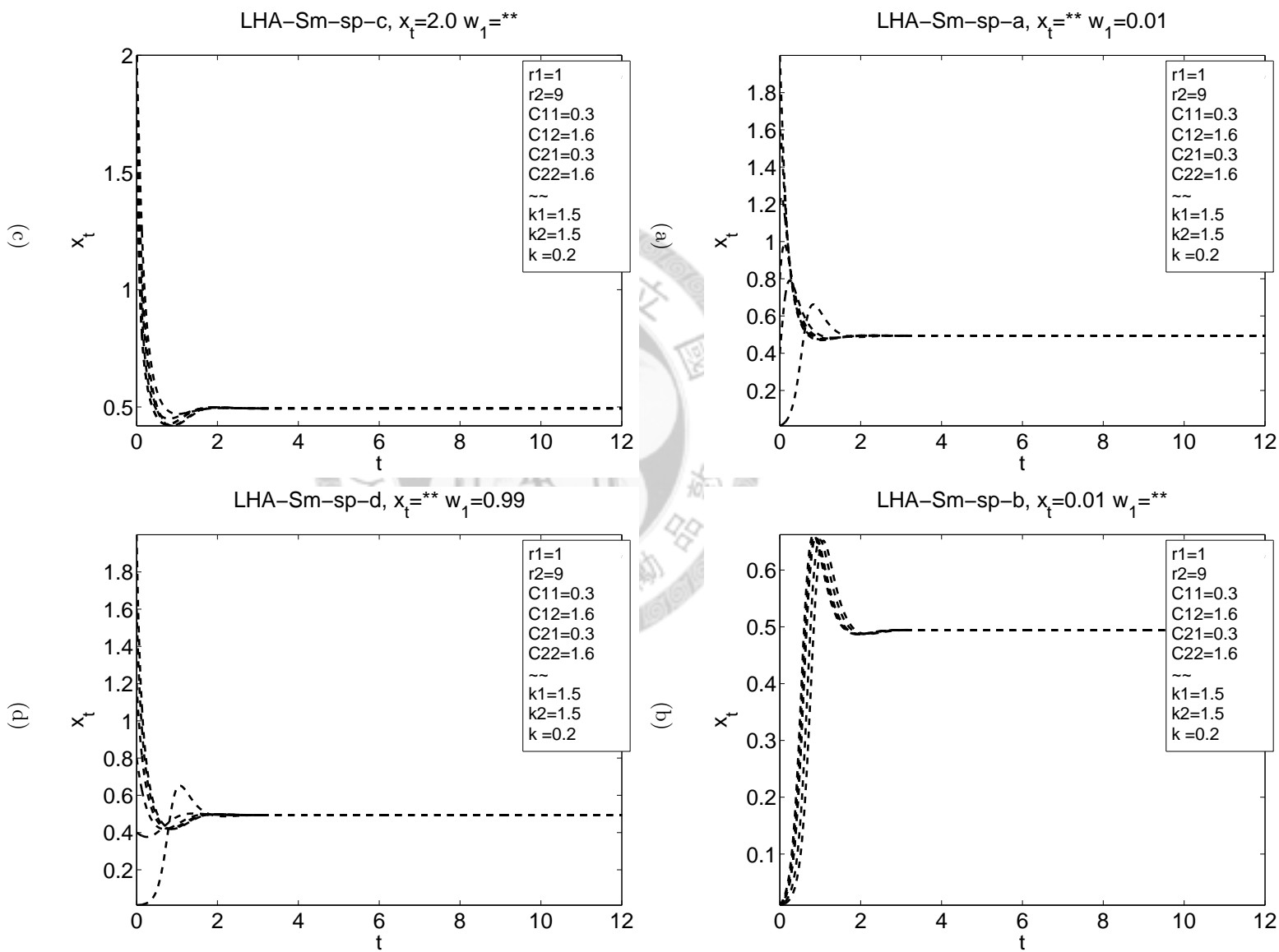


Figure 2.54: The $x_{tot}-w_1$ trajectories of LHA-Sm-sp.

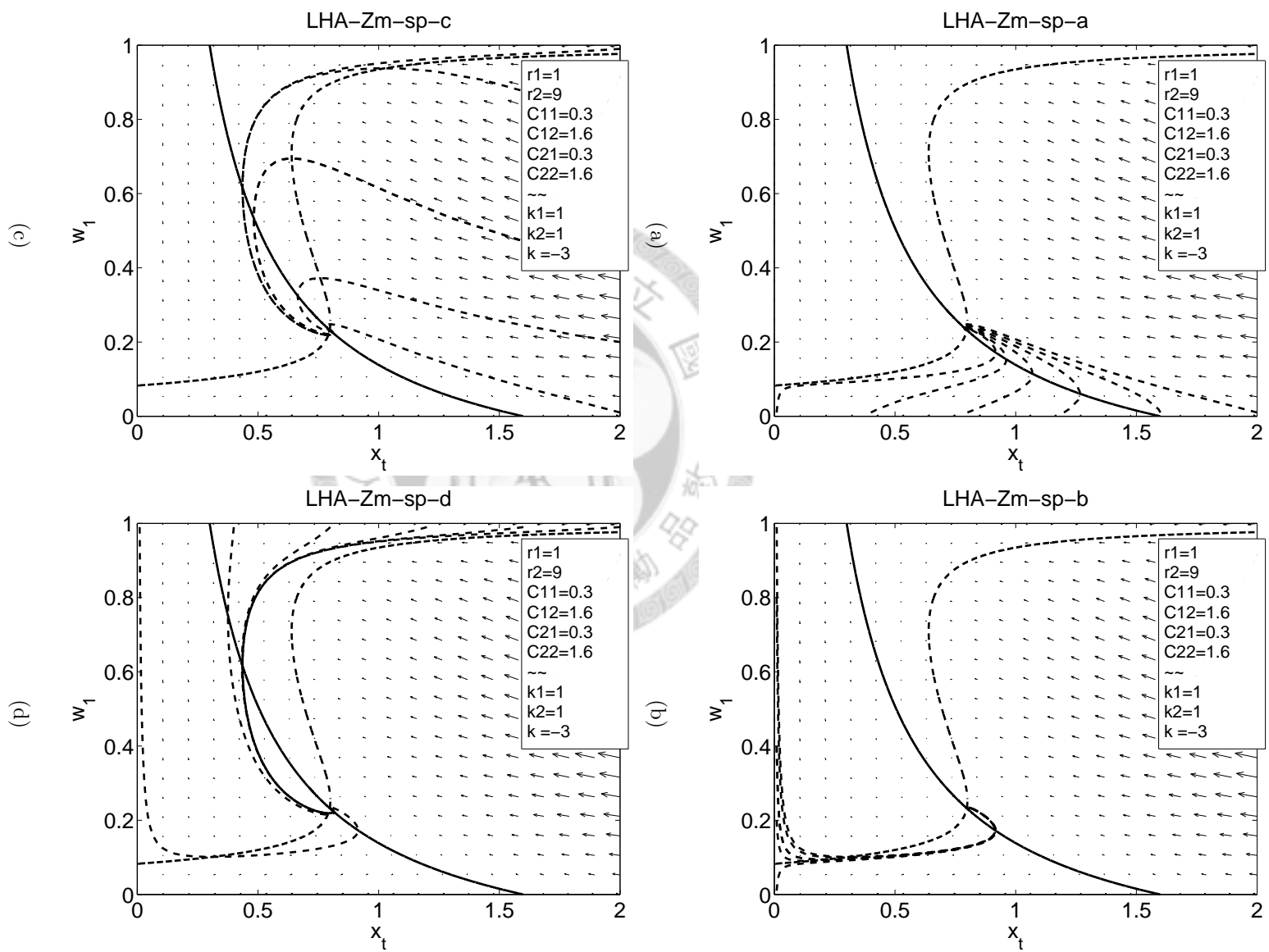


Figure 2.55: The x_{tot} - w_1 trajectories of LHA-Zm-sp.

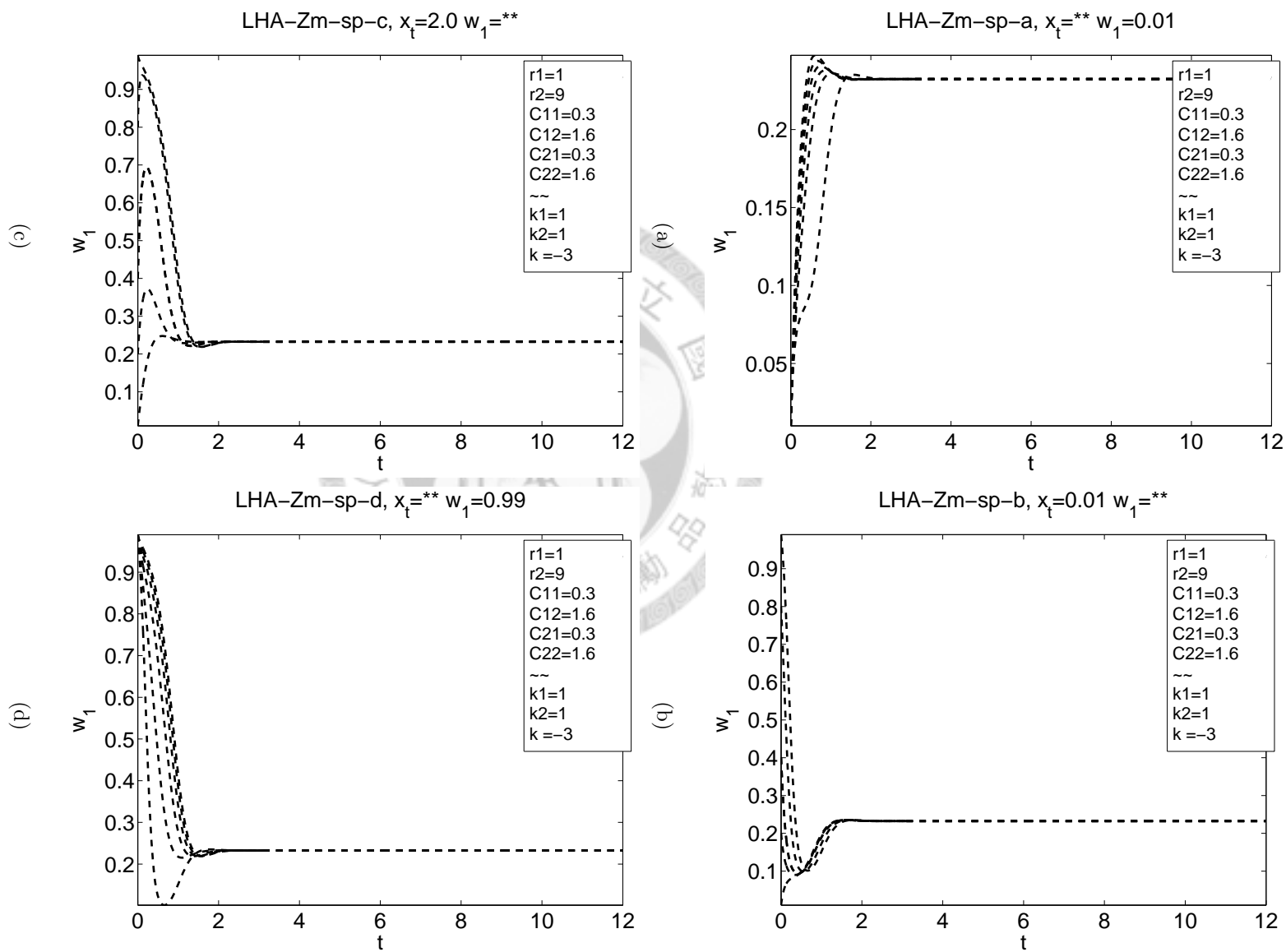


Figure 2.56: The x_{tot} - w_1 trajectories of LHA-Zm-sp.

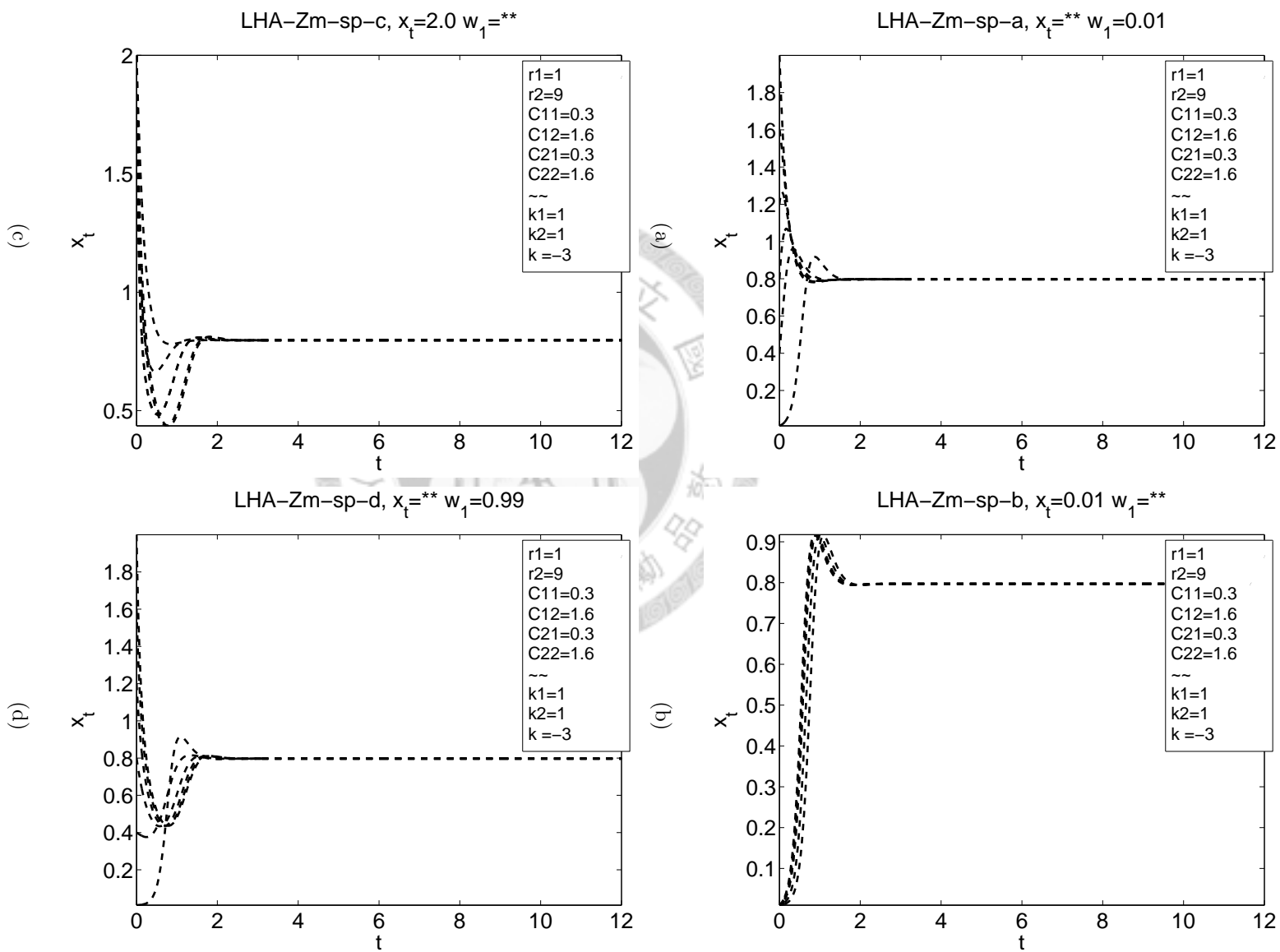


Figure 2.57: The $x_{tot}-w_1$ trajectories of LHA-Zm-sp.

B.3 The phase portraits of LH-B

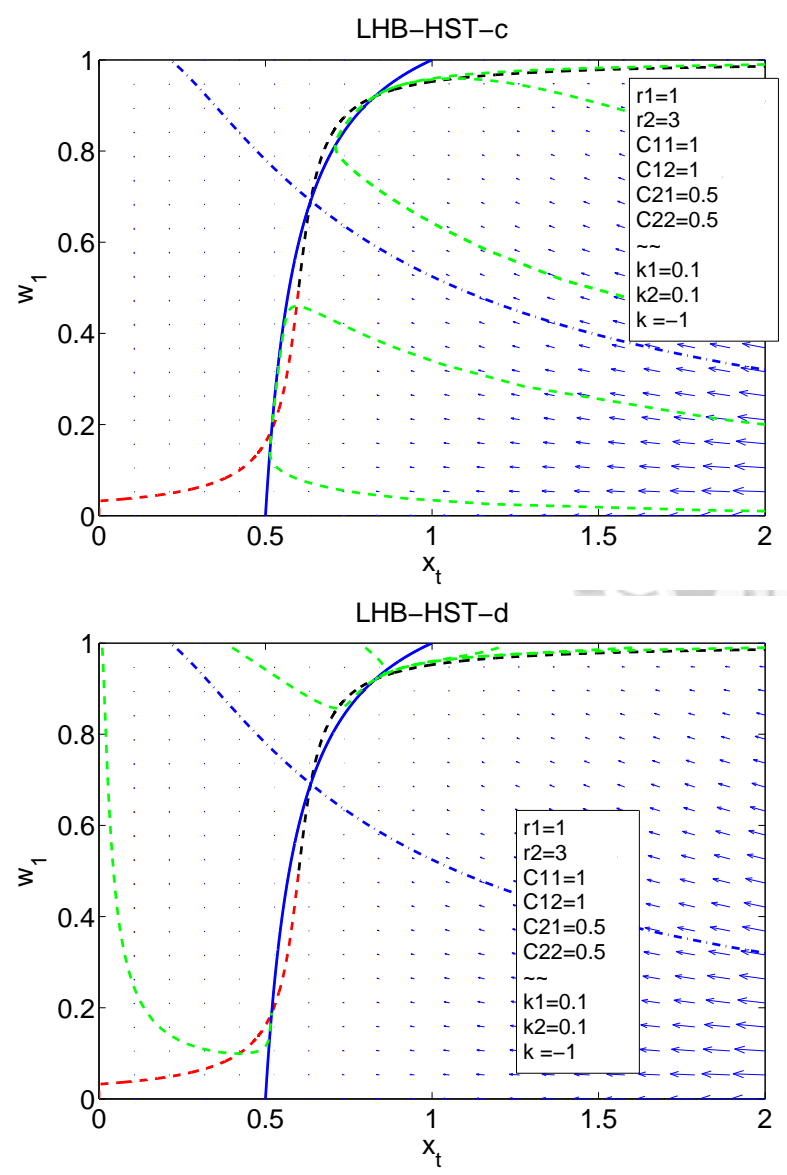
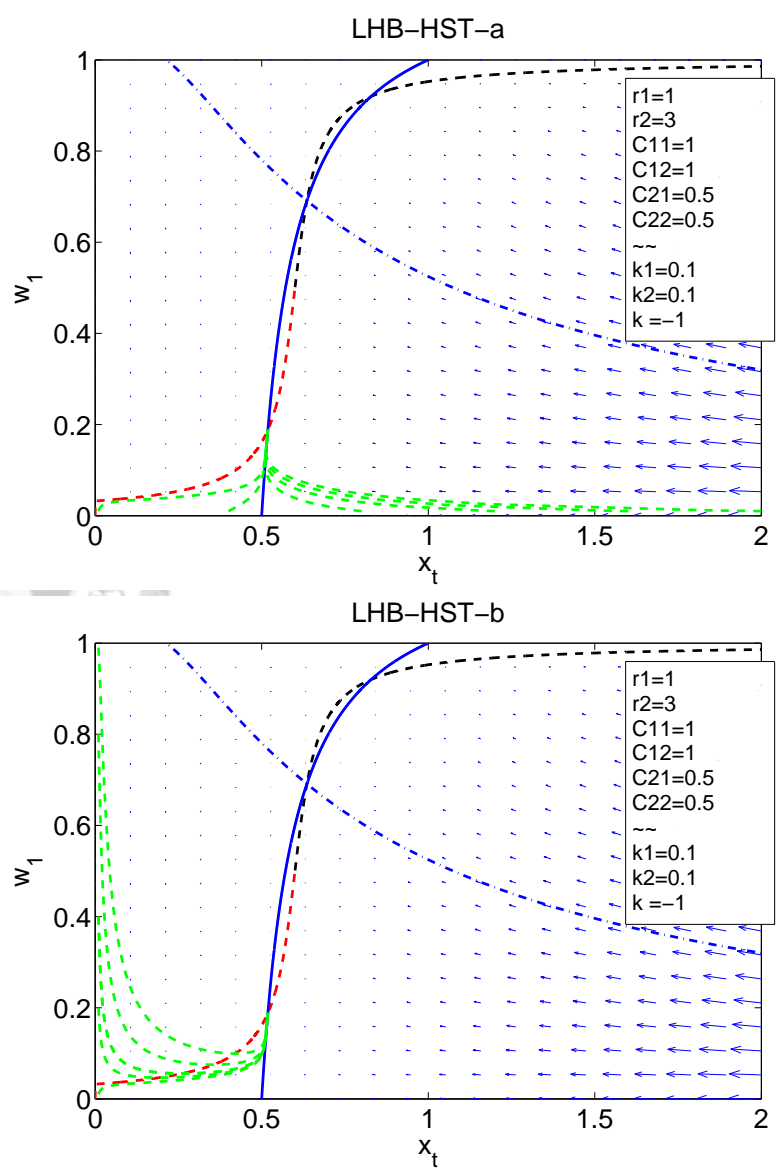
Although LH-B have 5 types of \tilde{x}_t , but because $\frac{1}{w_c} = 0$, all the types of \tilde{x}_t are UH- or DH-like curves. And \tilde{w}_1 is always S type curve.

The most special property of LH-B which is different from LH-0 and LH-A, is it has three fixed points. Here we will show a new phase diagram LHB-HST, which is UH-like for \tilde{x}_t and S type for \tilde{w}_1 with three fixed points.



(a)

(b)



(c)

180

(d)

Figure 2.58: The x_{tot} - w_1 trajectories of LHB-HST.

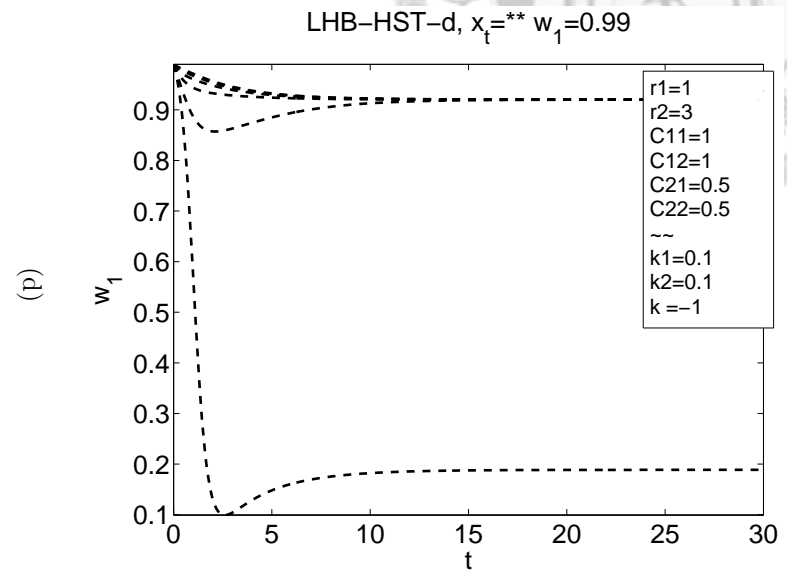
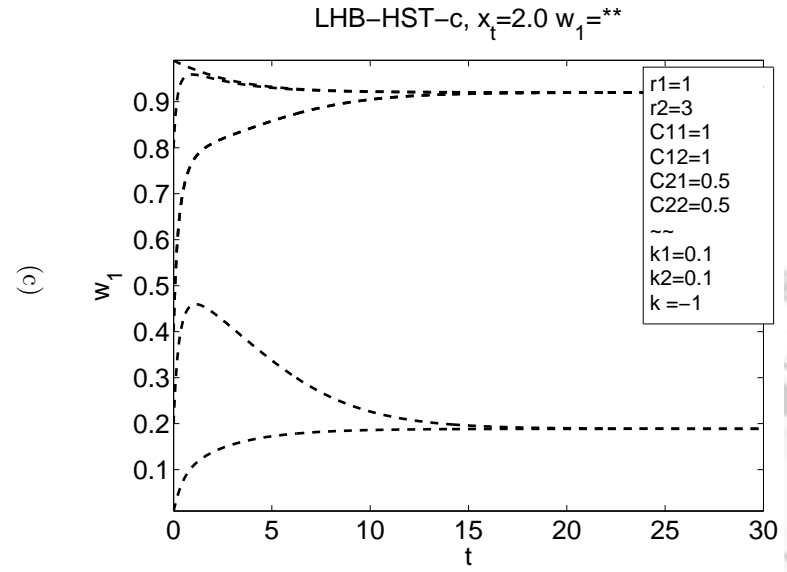
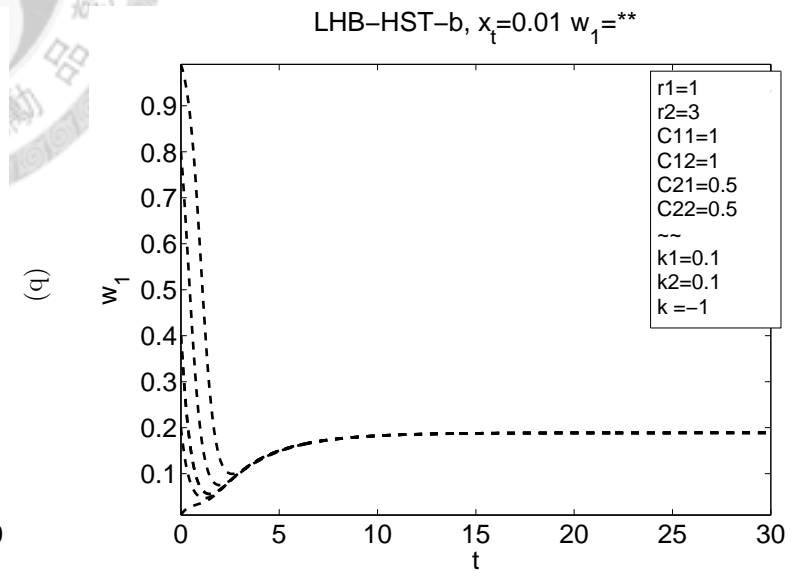
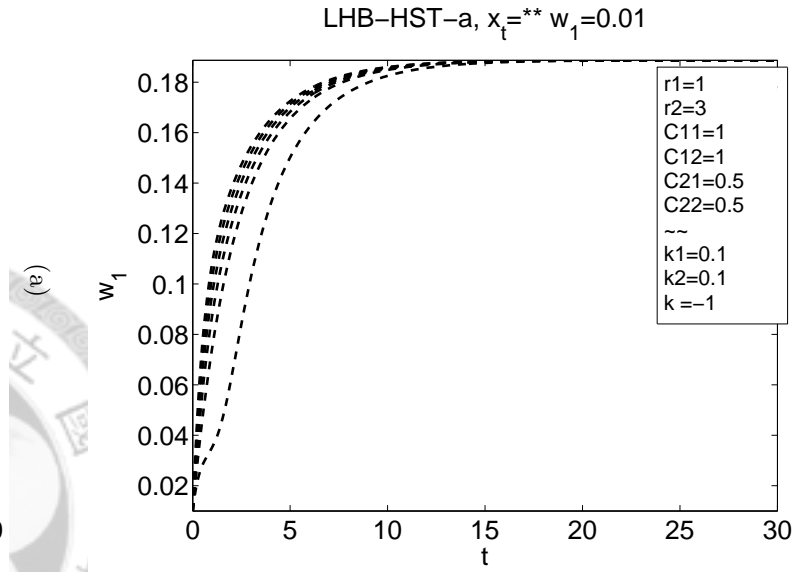
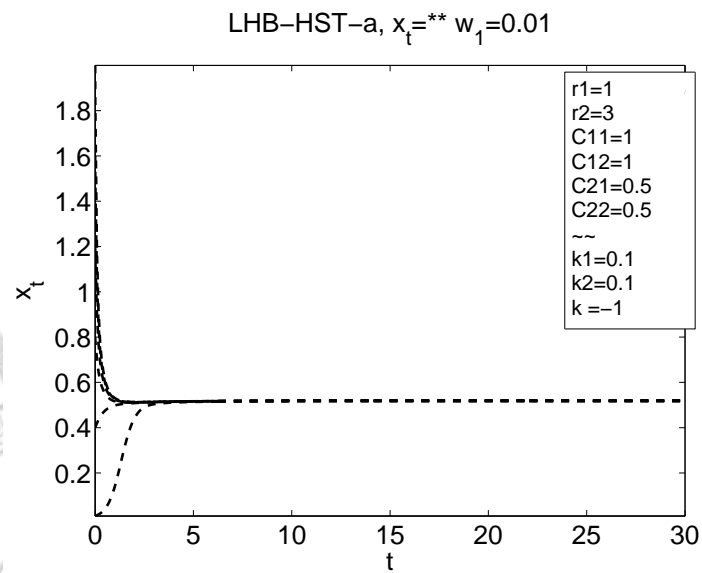
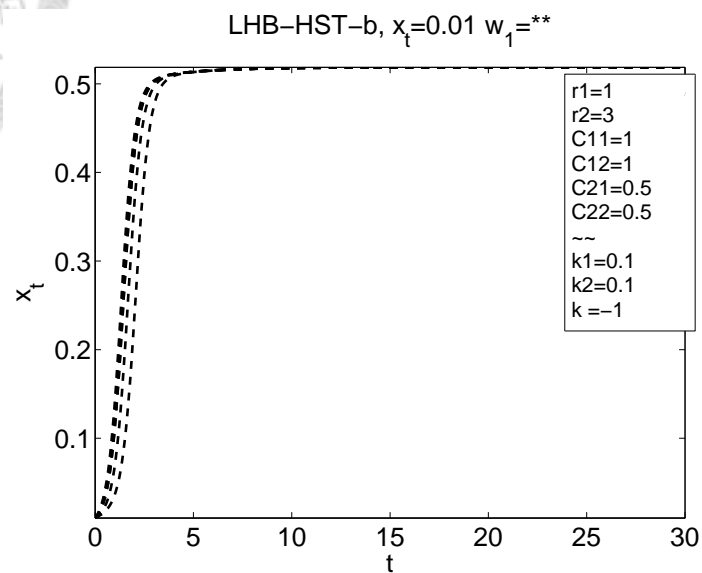


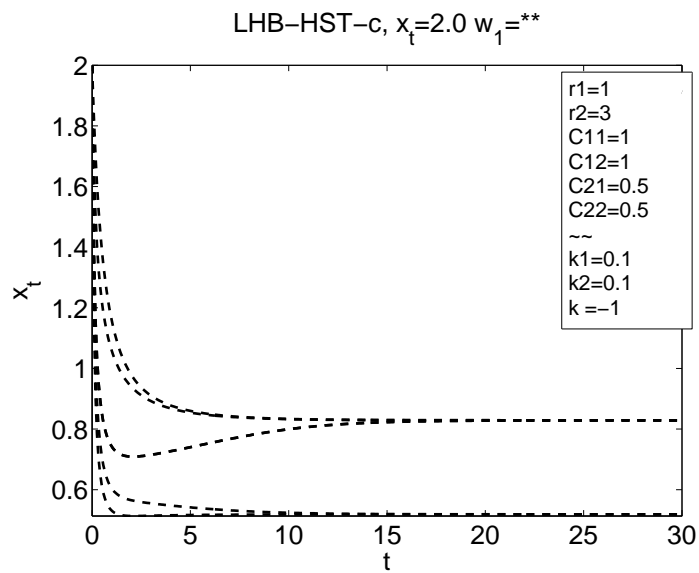
Figure 2.59: The $x_{tot}-w_1$ trajectories of LHB-HST.



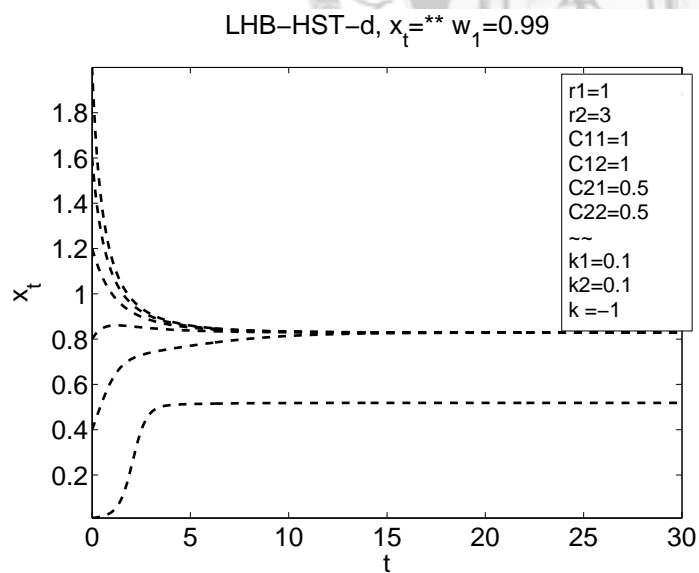
(a)



(b)



(c)



(d)

Figure 2.60: The $x_{tot}-w_1$ trajectories of LHB-HST.

B.4 The phase portraits of LH-C

In LH-C, \tilde{x}_t has 10 classifications, and \tilde{w}_1 can be either S type or Z type curve. It also has three fixed point condition and spiral behavior.

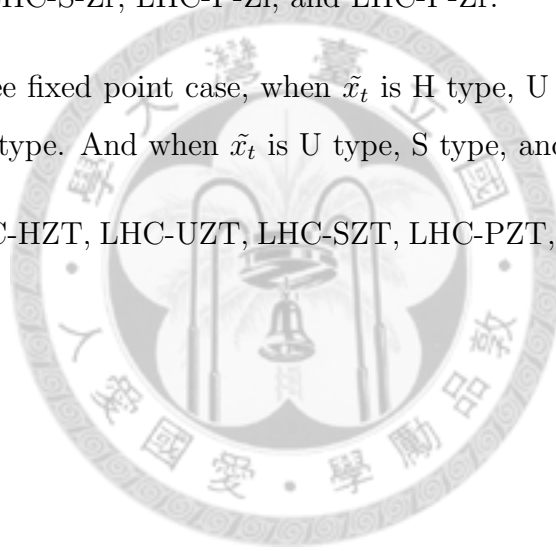
Considering the exchange symmetry of w_1 and w_2 and all other conditions, several new phase diagrams could happen.

1. For the one fixed point case, \tilde{x}_t is U type, S type, and P type, with \tilde{w}_1 being S type and Z type.

The new phase diagrams are LHC-U-Sl, LHC-U-Sm, LHC-U-Sr, LHC-S-Sl, LHC-S-Sm, LHC-S-Sr, LHC-P-Sl, LHC-P-Sm, LHC-P-Sr, LHC-U-Zl, LHC-U-Zr, LHC-S-Zl, LHC-S-Zm, LHC-S-Zr, LHC-P-Zl, and LHC-P-Zr.

2. In the three fixed point case, when \tilde{x}_t is H type, U type, S type, and P type , with \tilde{w}_1 being Z type. And when \tilde{x}_t is U type, S type, and P type , \tilde{w}_1 is S type.

They are LHC-HZT, LHC-UZT, LHC-SZT, LHC-PZT, LHC-UST, LHC-SST, and LHC-PST.



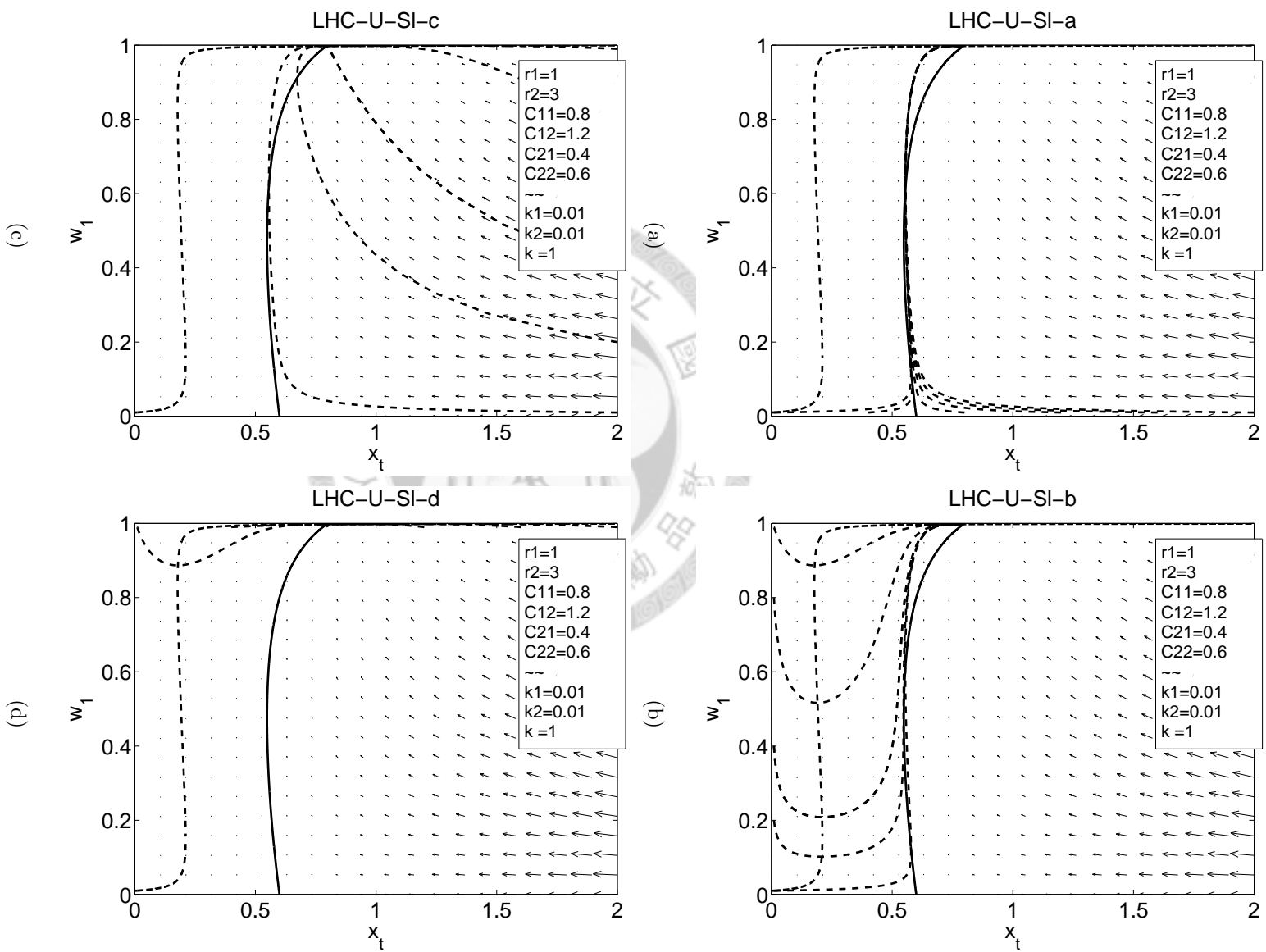


Figure 2.61: The x_{tot} - w_1 trajectories of LHC-U-SI.

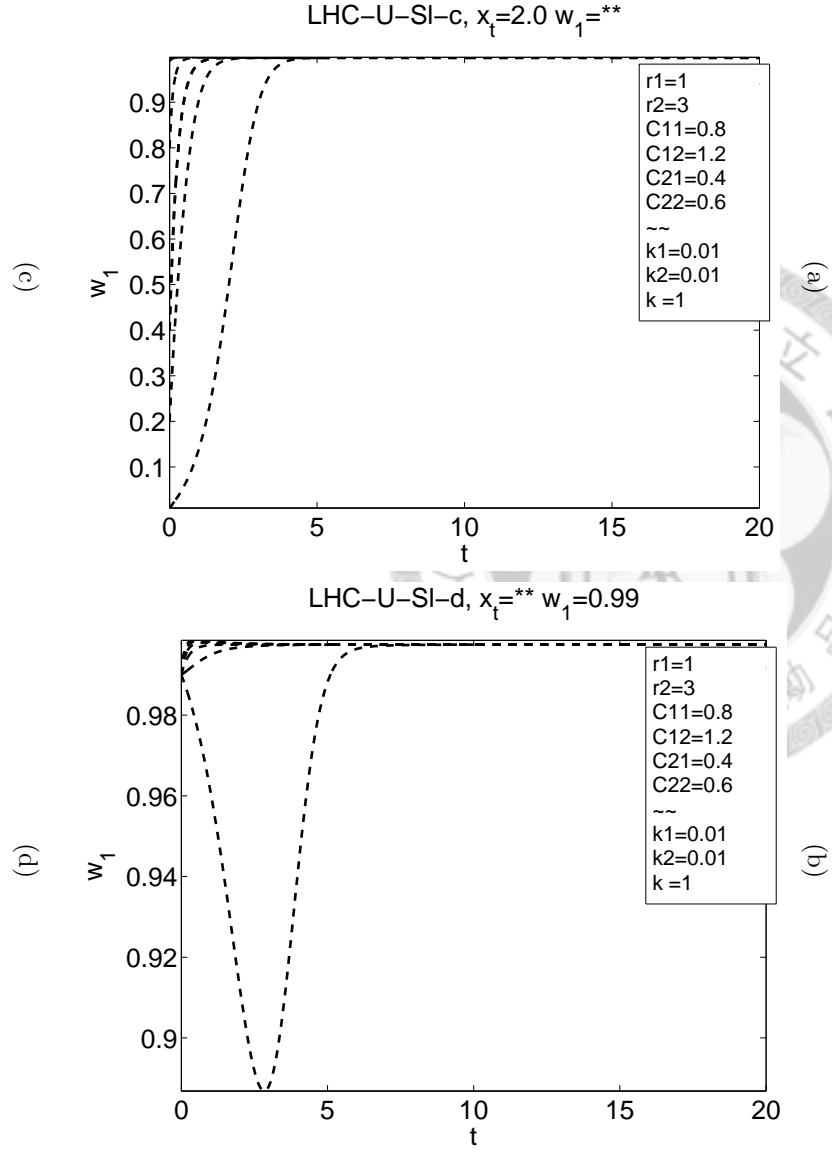
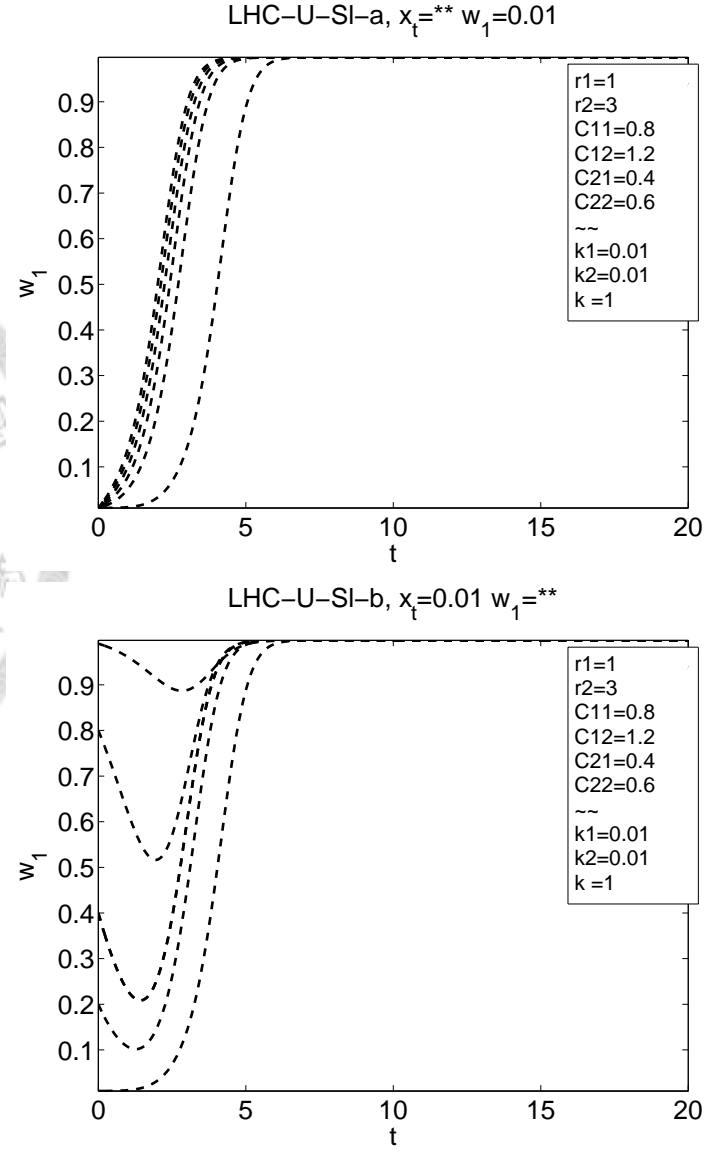


Figure 2.62: The x_{tot} - w_1 trajectories of LHC-U-SI.

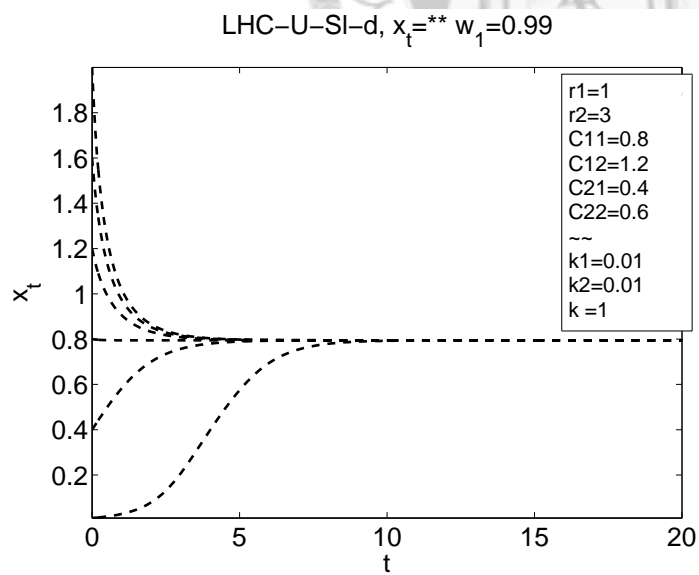
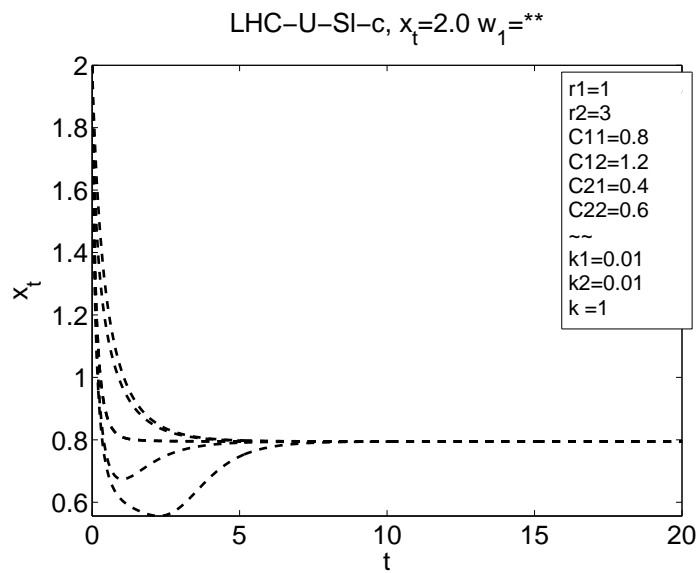
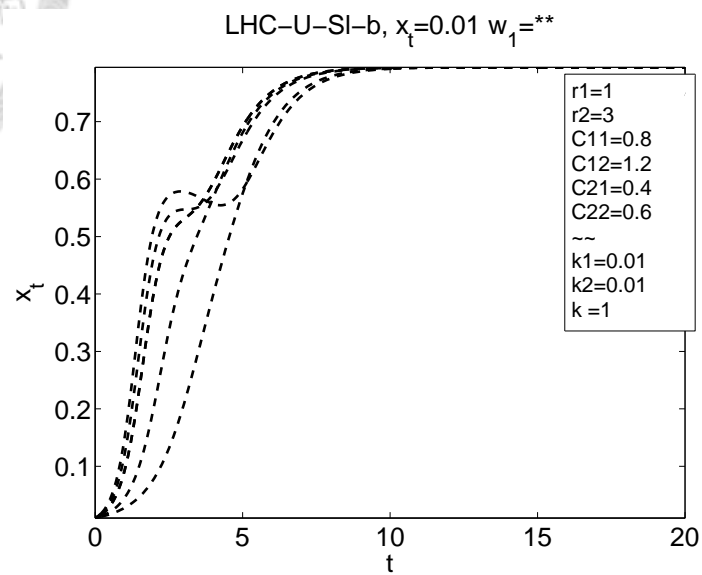
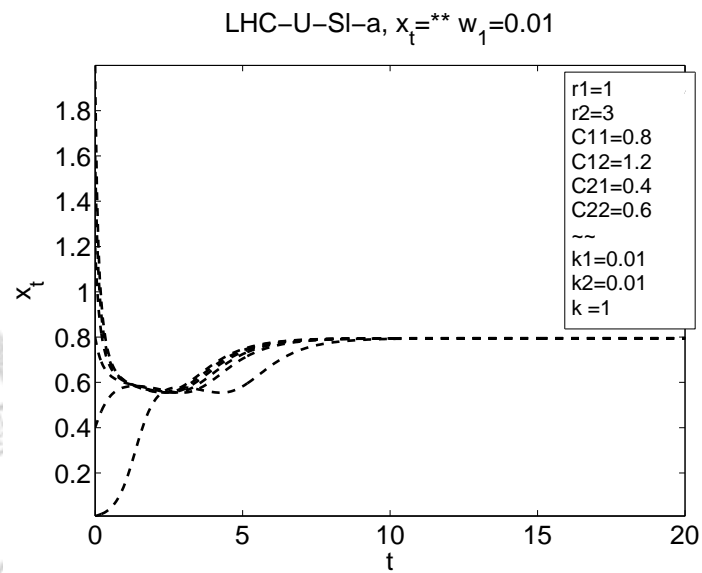


Figure 2.63: The $x_{tot}-w_1$ trajectories of LHC-U-SI.

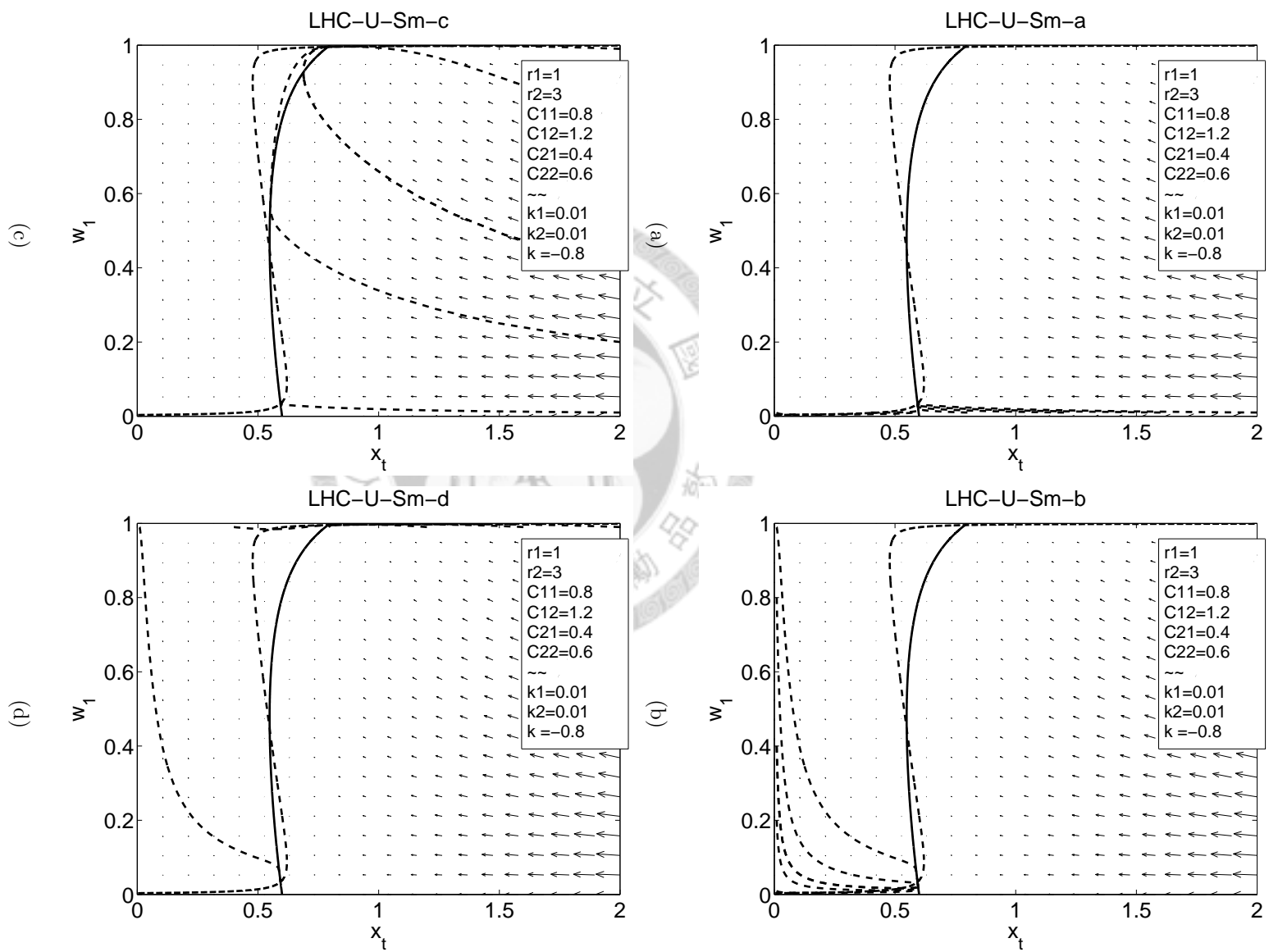


Figure 2.64: The x_{tot} - w_1 trajectories of LHC-U-Sm.

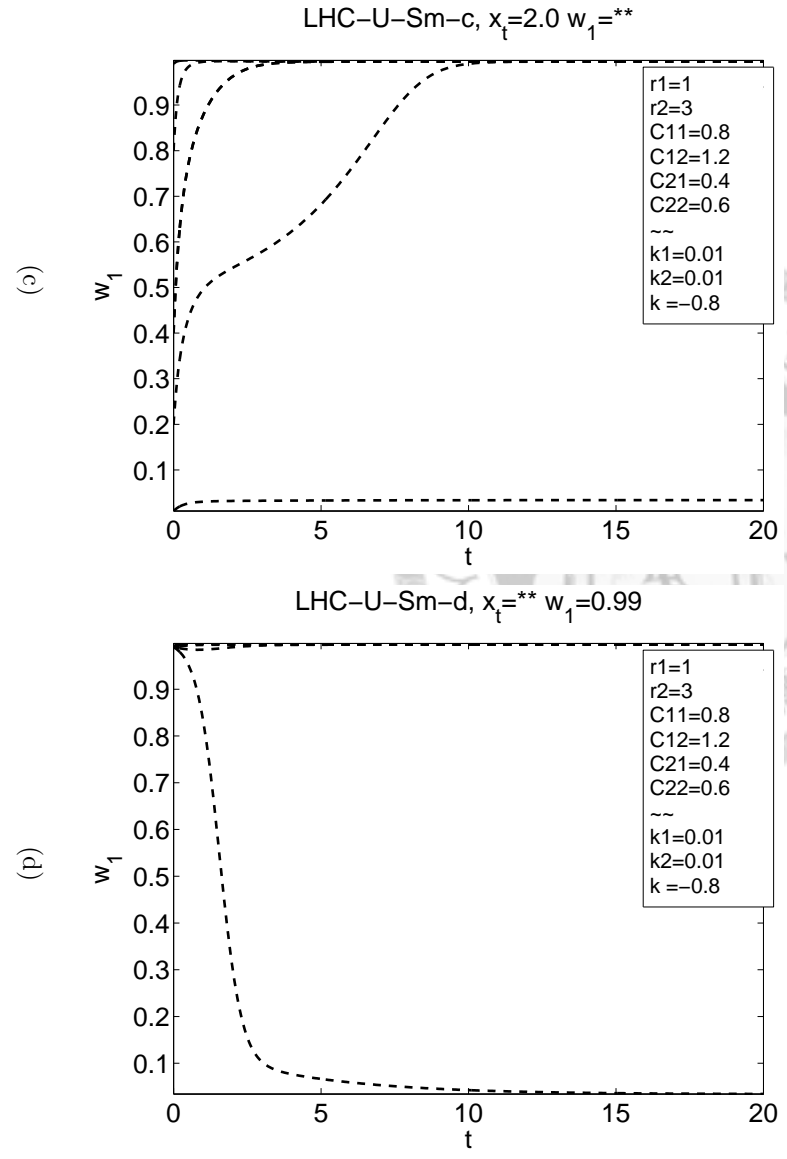
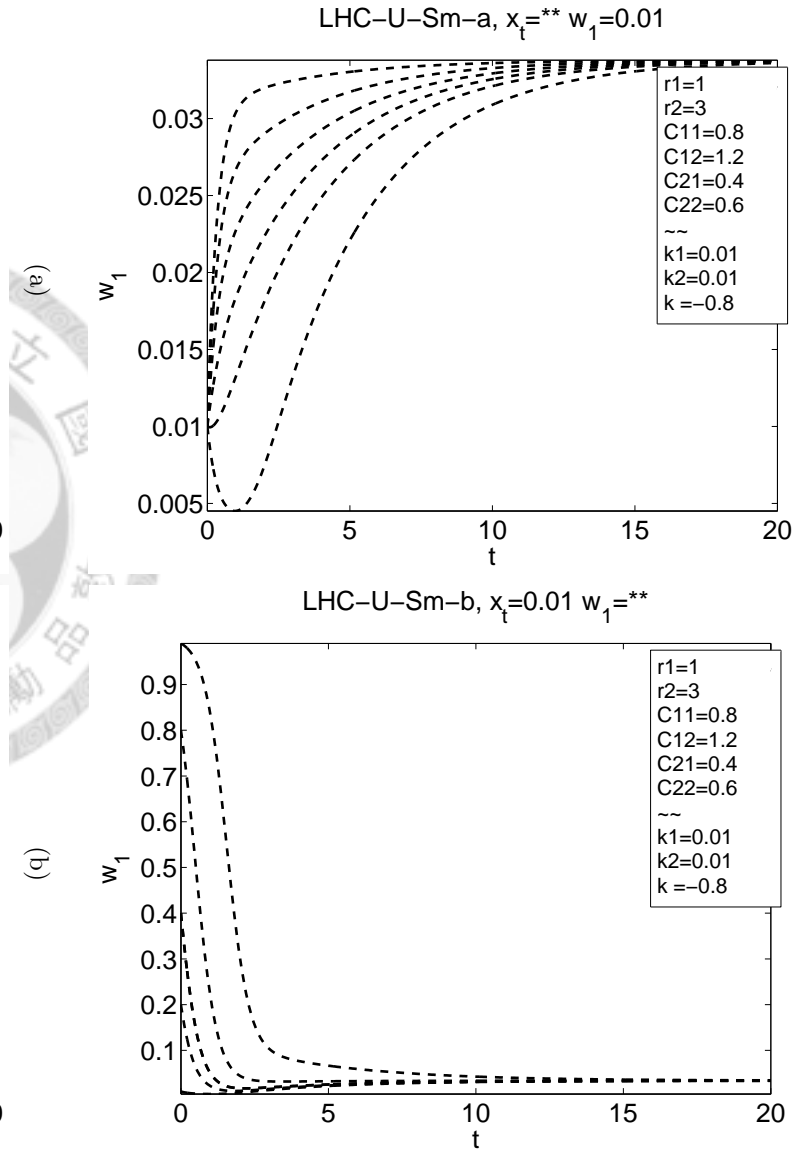


Figure 2.65: The x_{tot} - w_1 trajectories of LHC-U-Sm.

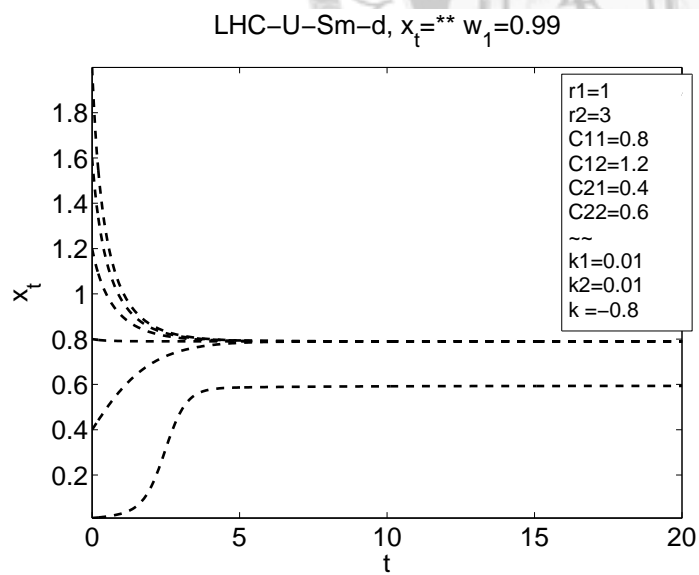
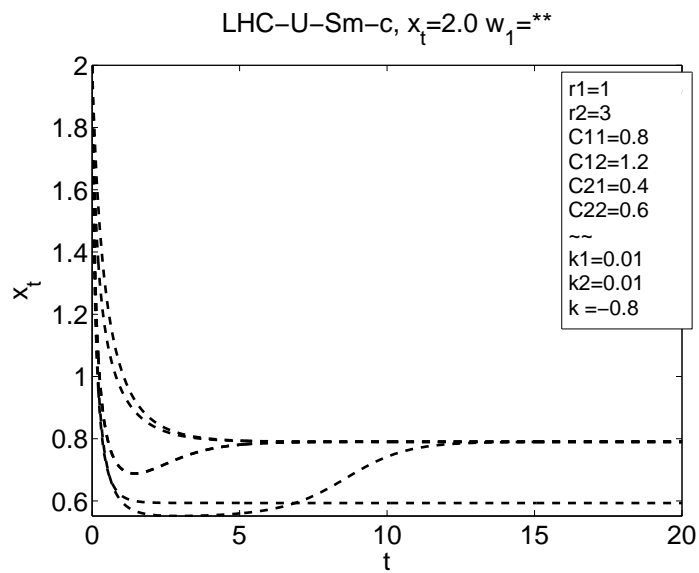
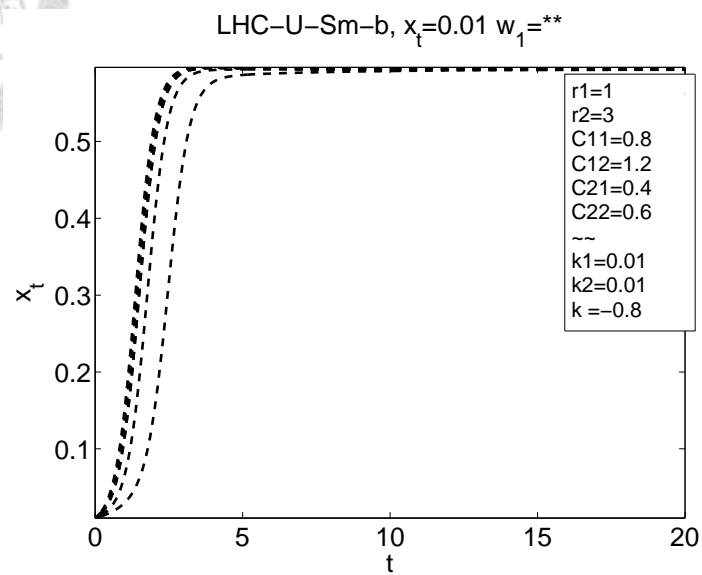
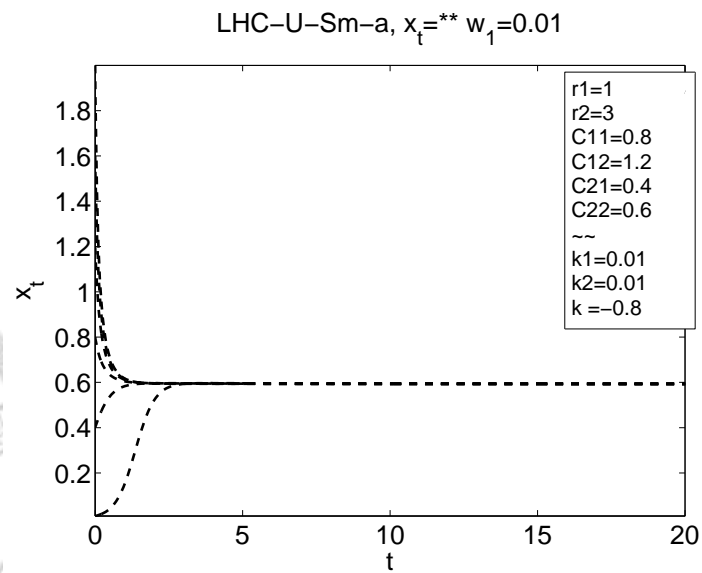


Figure 2.66: The $x_{tot}-w_1$ trajectories of LHC-U-Sm.

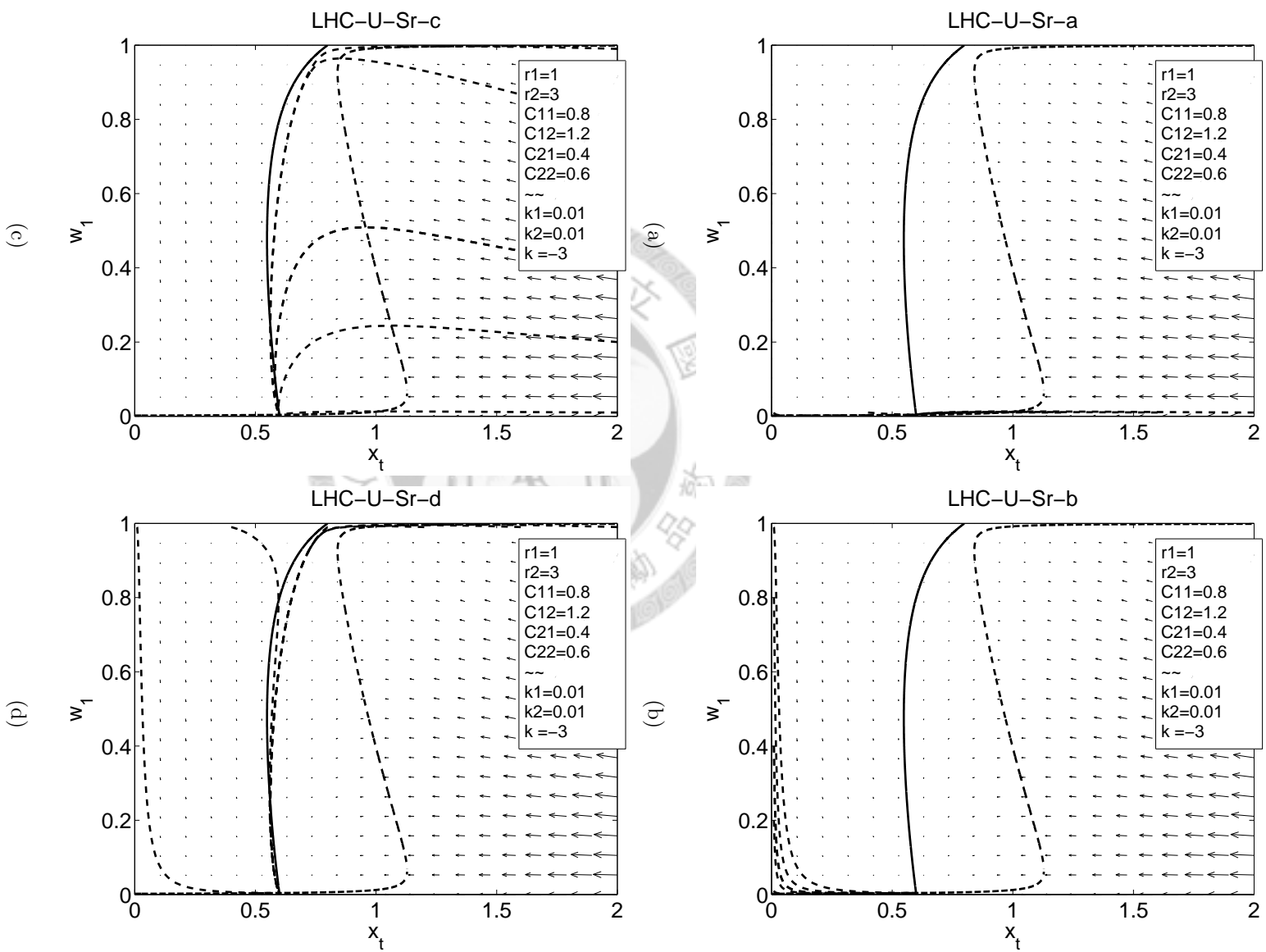


Figure 2.67: The x_{tot} - w_1 trajectories of LHC-U-Sr.

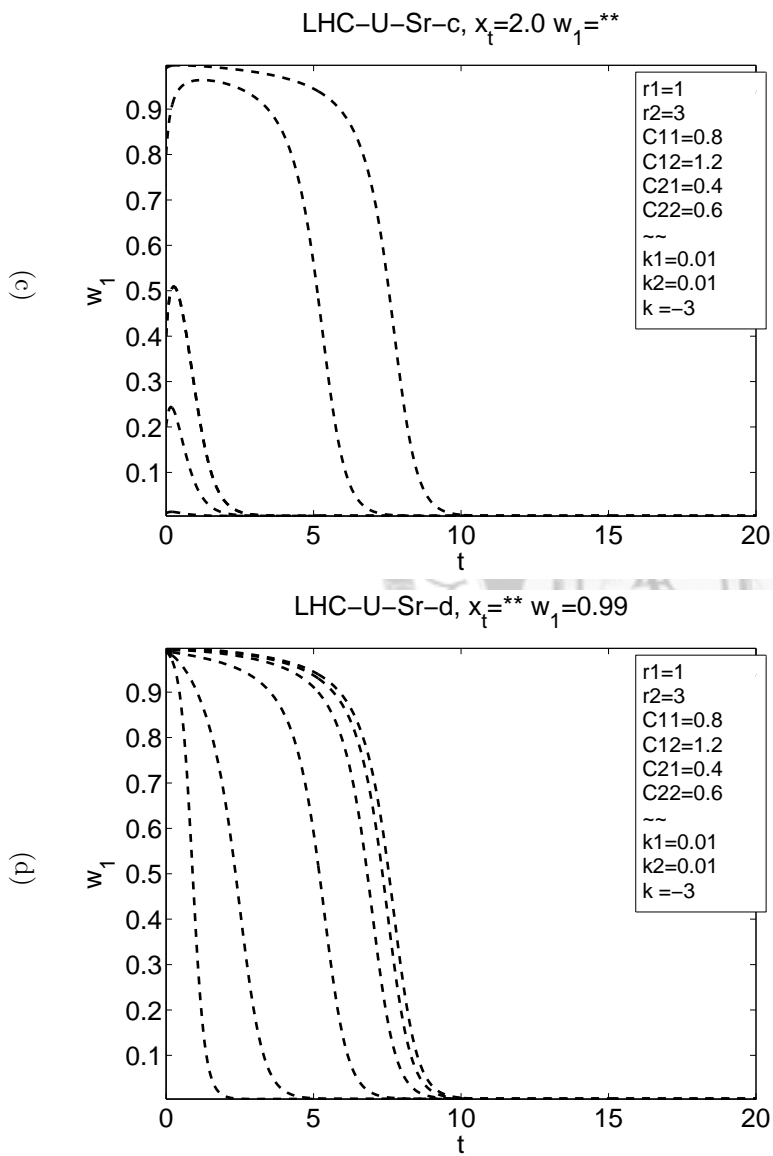
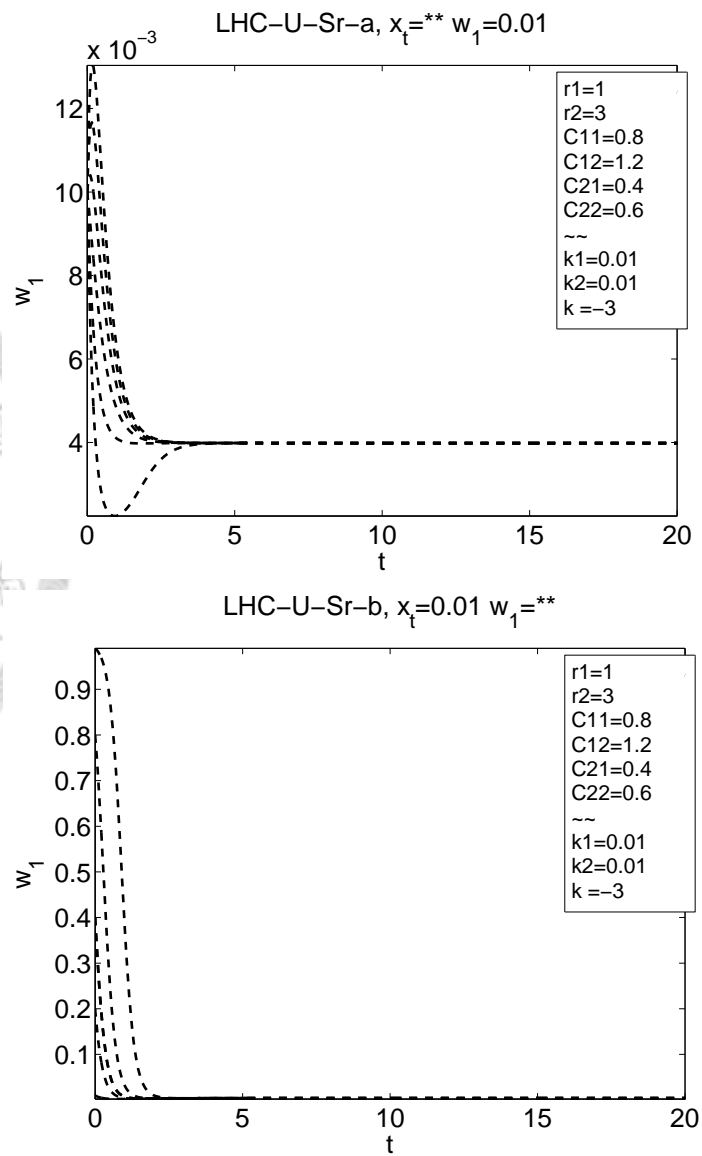
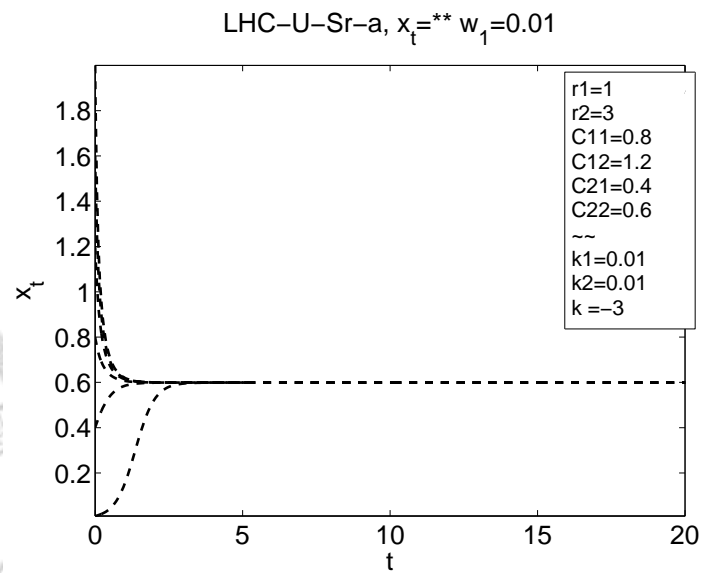
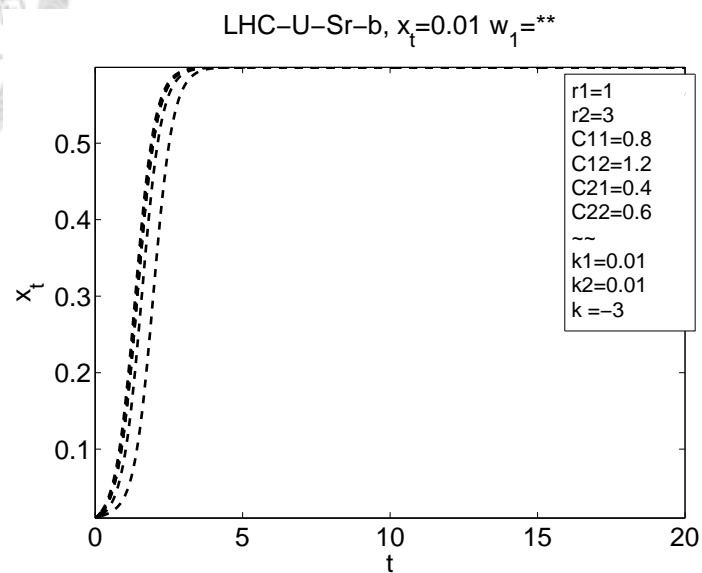


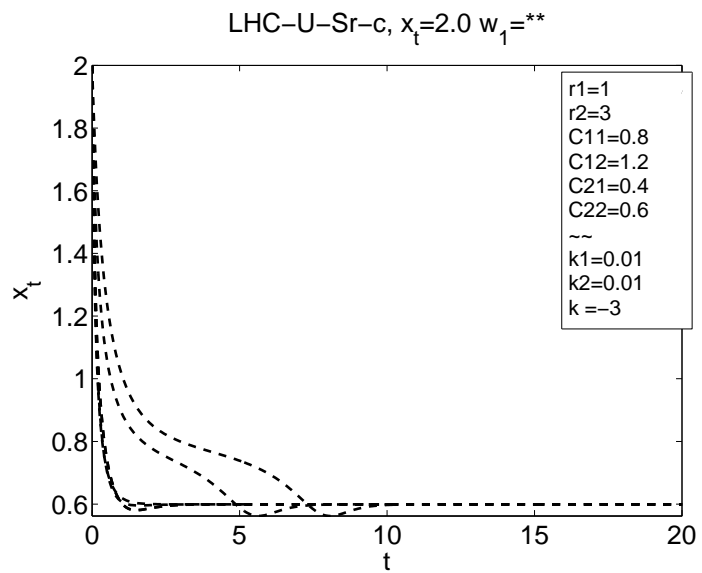
Figure 2.68: The x_{tot} - w_1 trajectories of LHC-U-Sr.



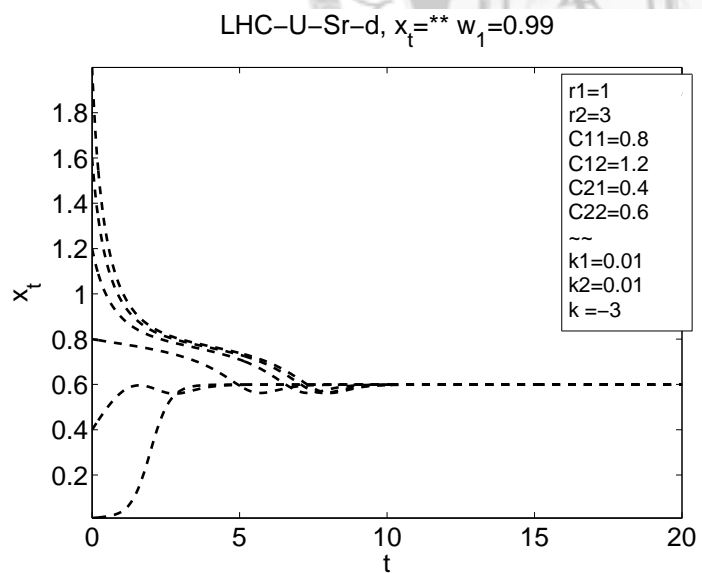
(a)



(b)



(c)



(d)

Figure 2.69: The $x_{tot}-w_1$ trajectories of LHC-U-Sr.

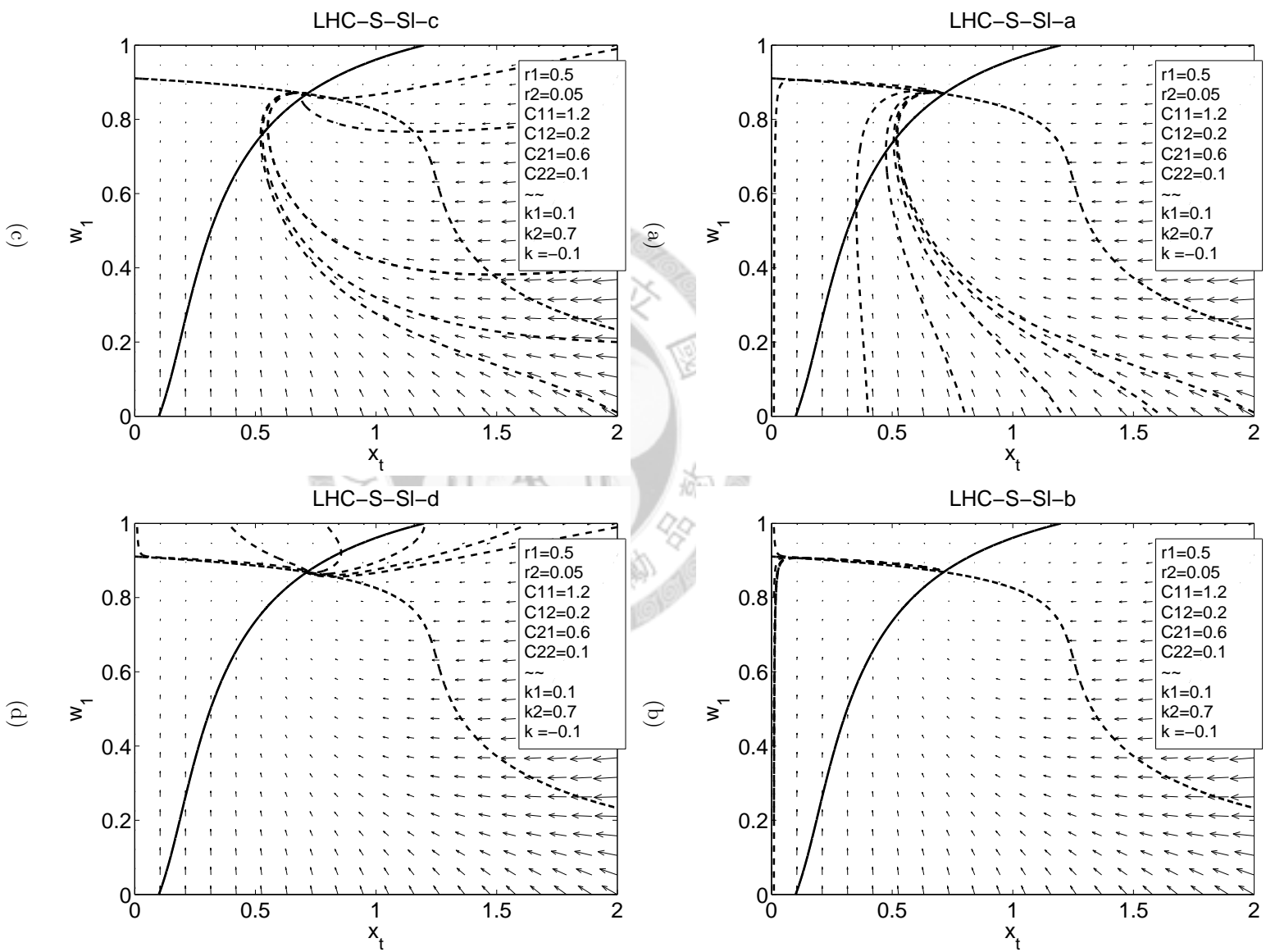


Figure 2.70: The x_{tot} - w_1 trajectories of LHC-S-SI.

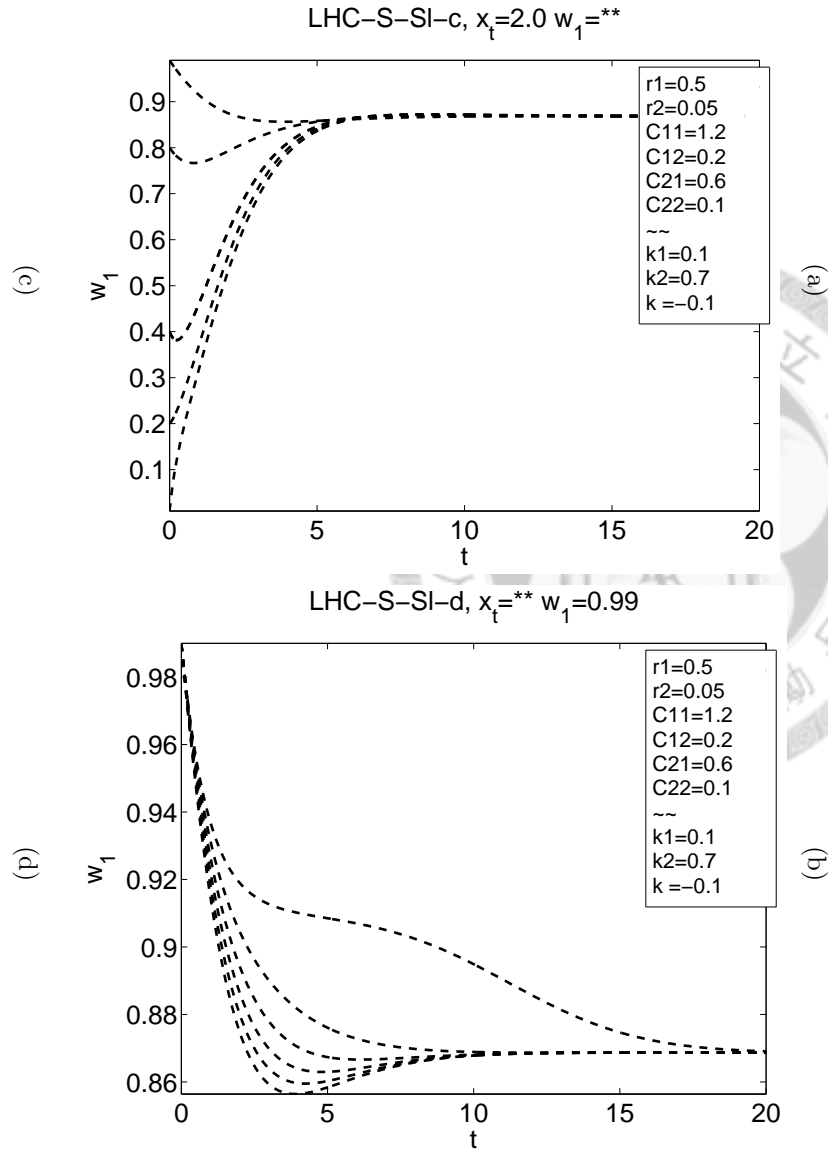
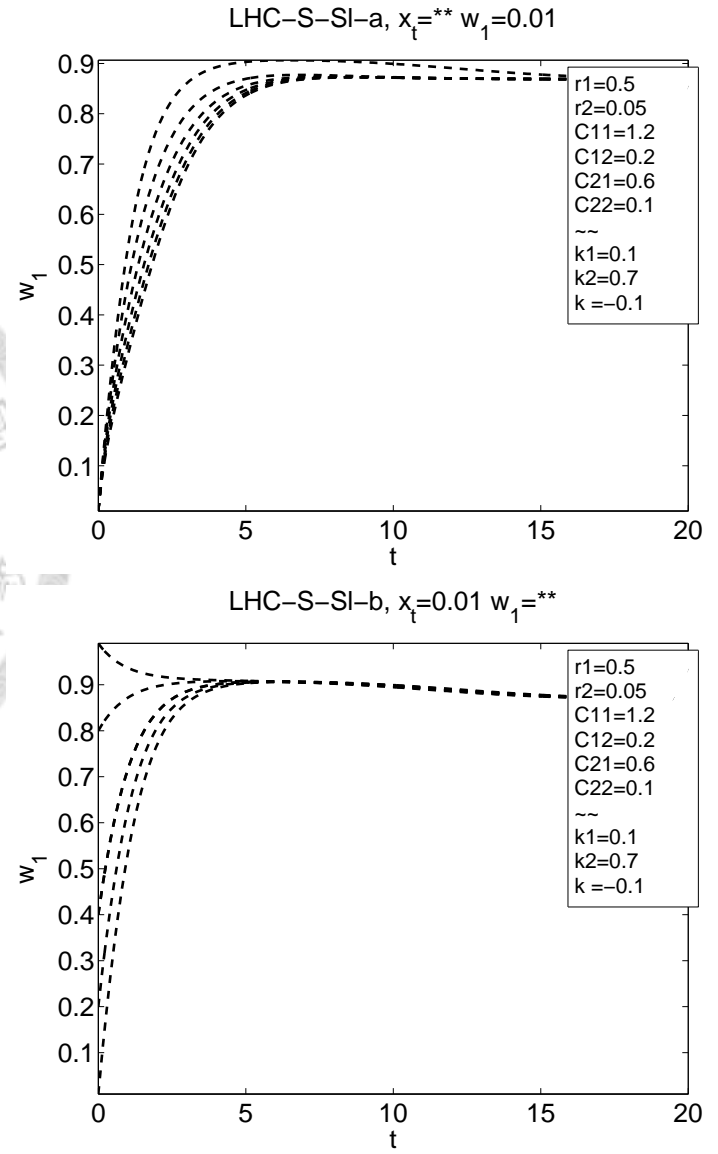
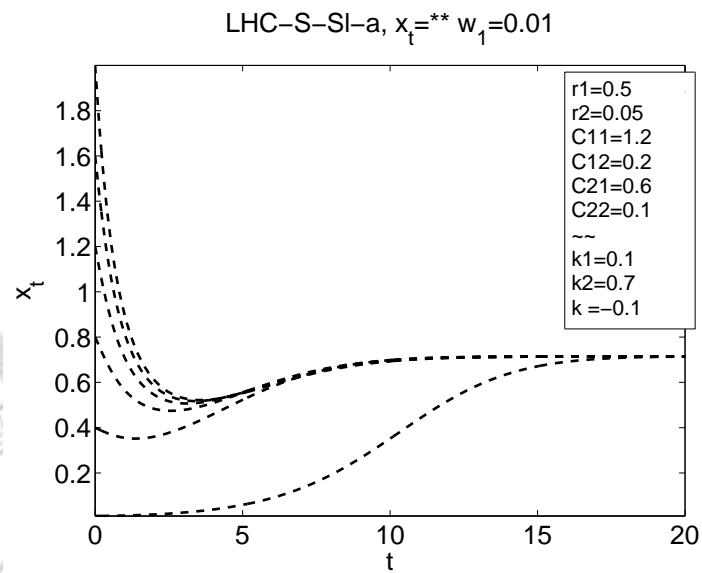
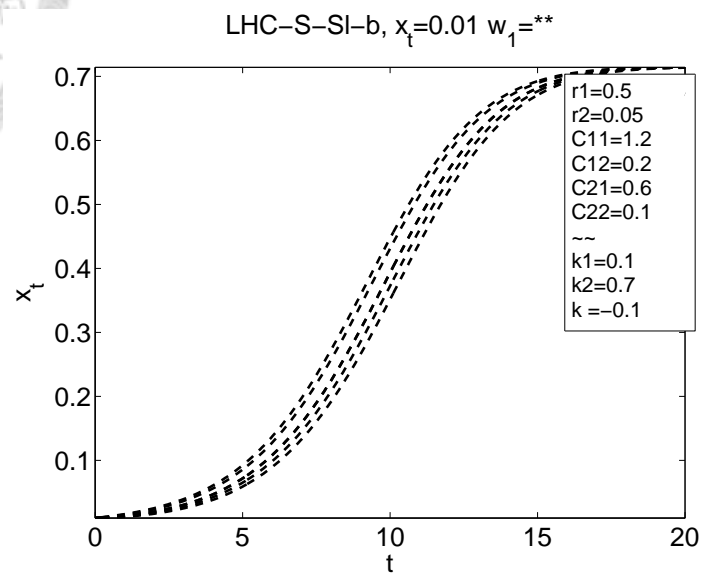


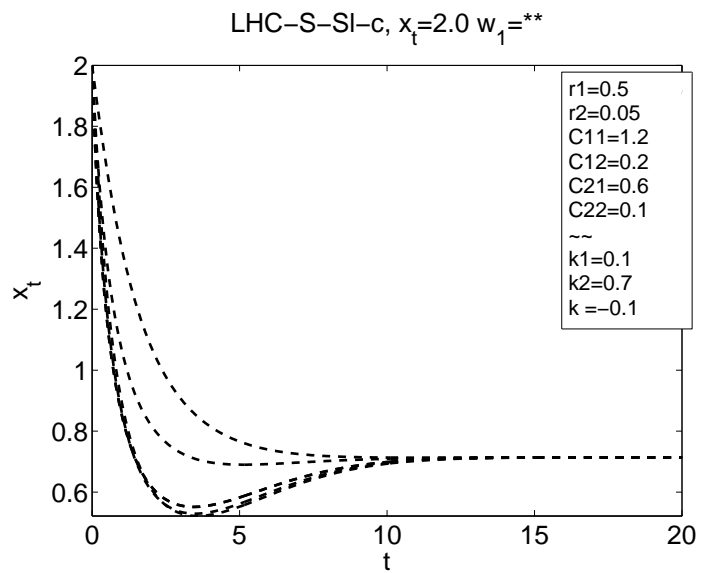
Figure 2.71: The x_{tot} - w_1 trajectories of LHC-S-SI.



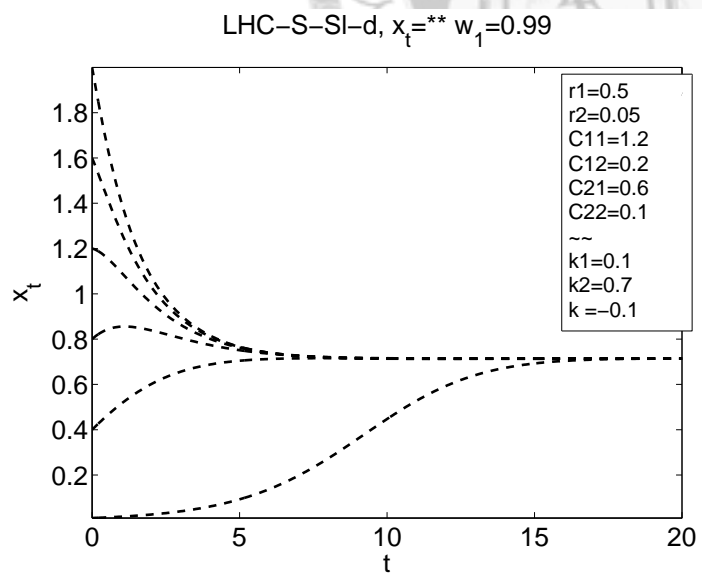
(a)



(b)



(c)



(d)

Figure 2.72: The $x_{tot}-w_1$ trajectories of LHC-S-SI.

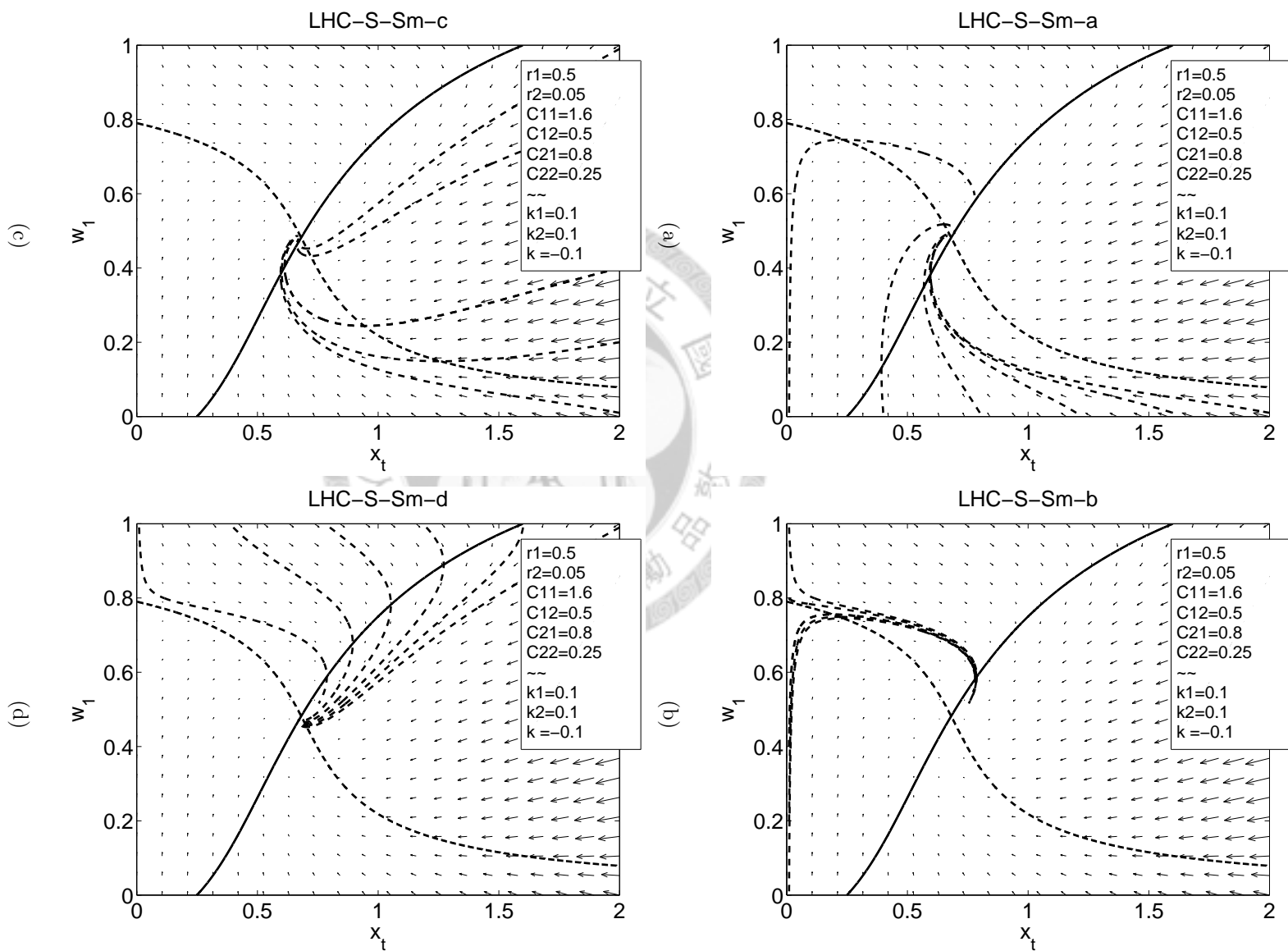
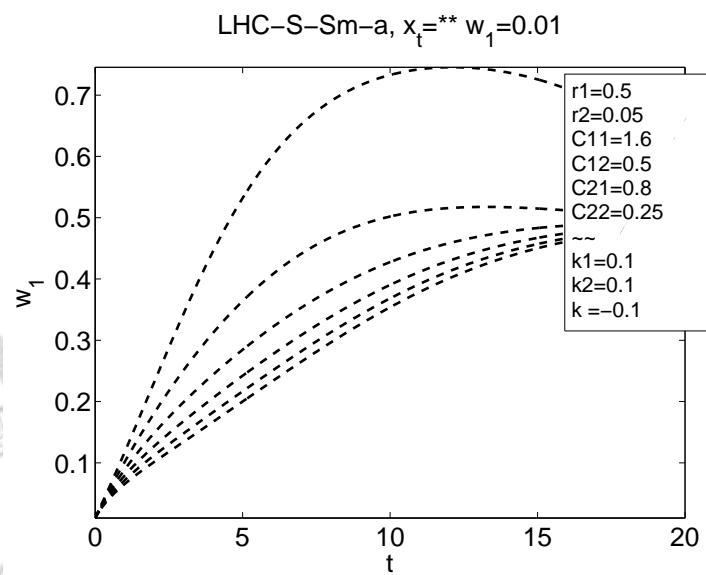
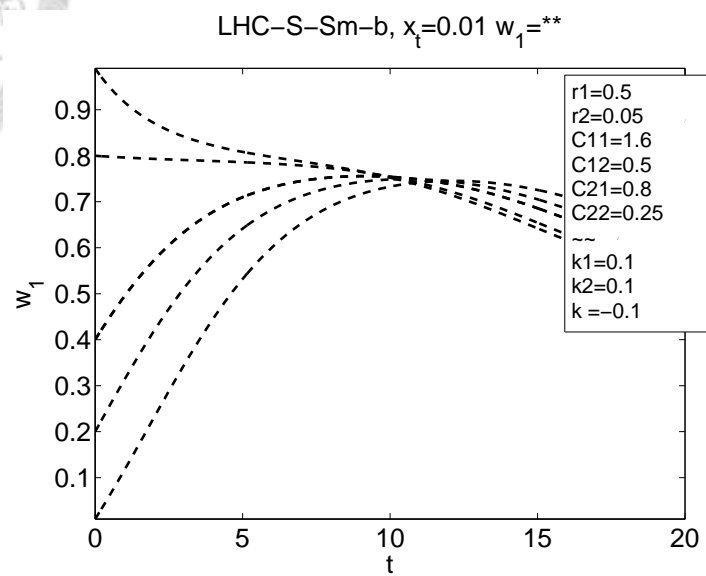


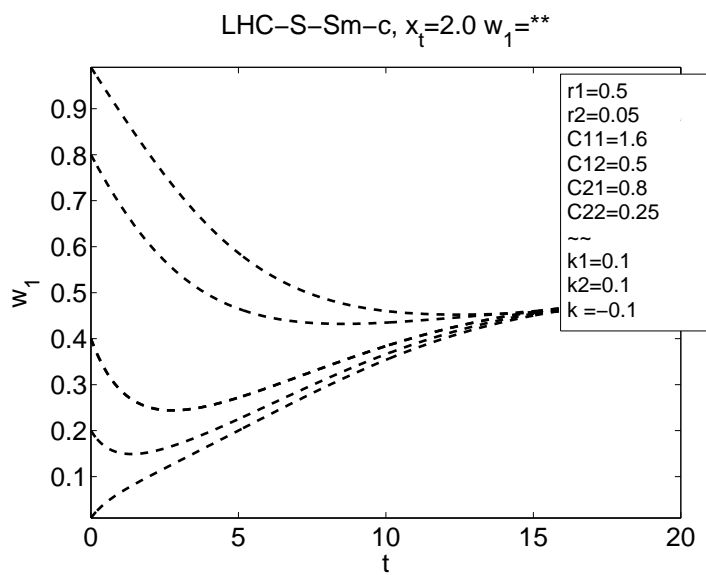
Figure 2.73: The x_{tot} - w_1 trajectories of LHC-S-Sm.



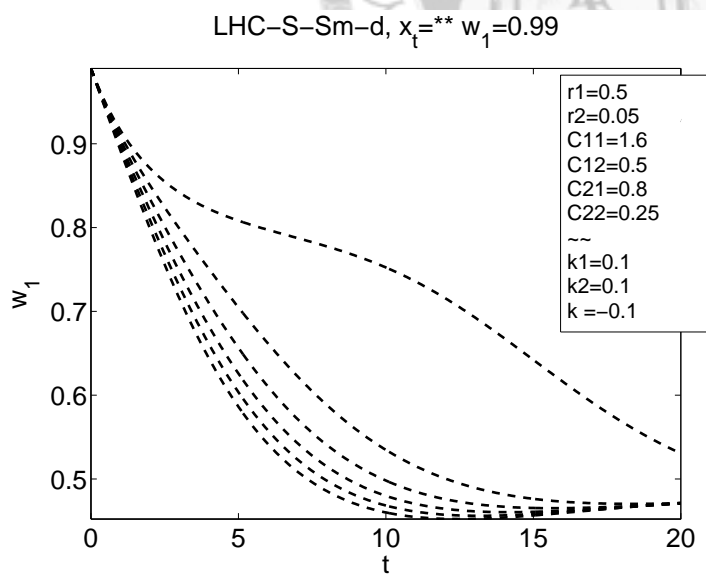
(a)



(b)



(c)



(d)

Figure 2.74: The x_{tot} - w_1 trajectories of LHC-S-Sm.

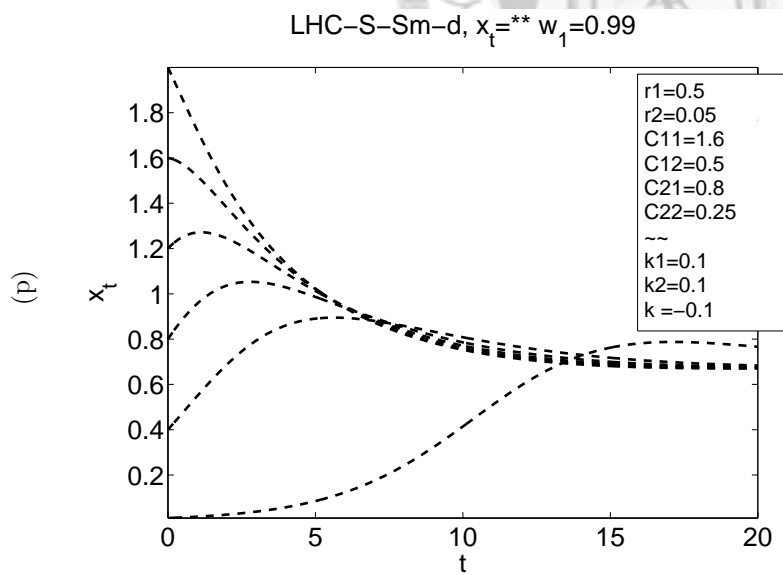
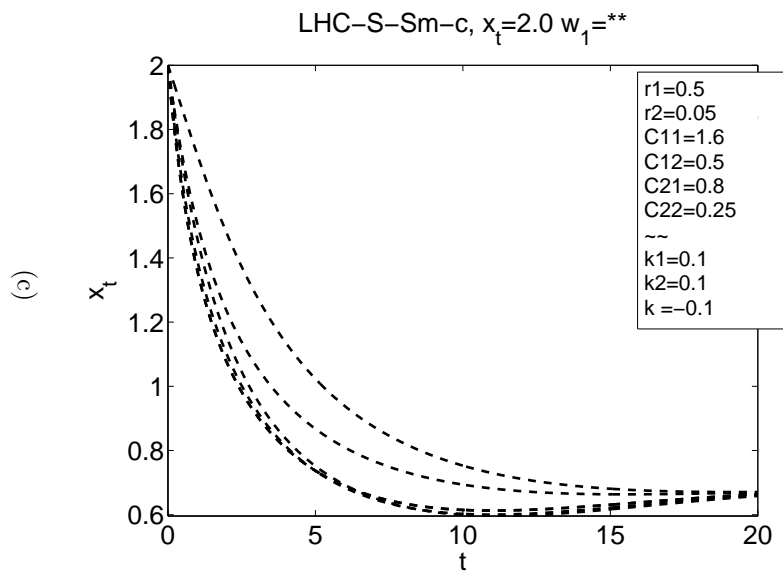
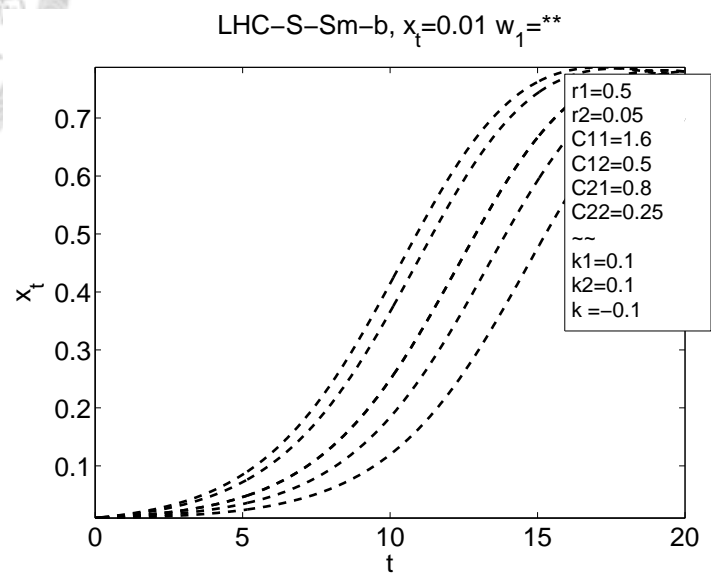
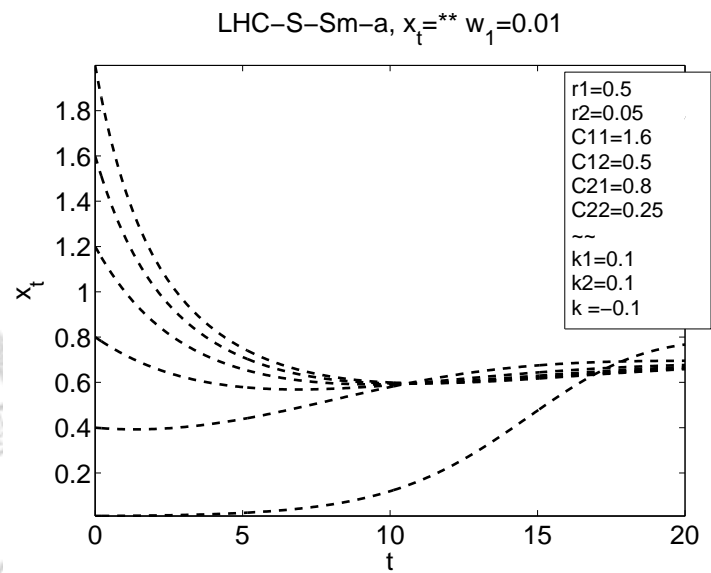


Figure 2.75: The $x_{tot}-w_1$ trajectories of LHC-S-Sm.

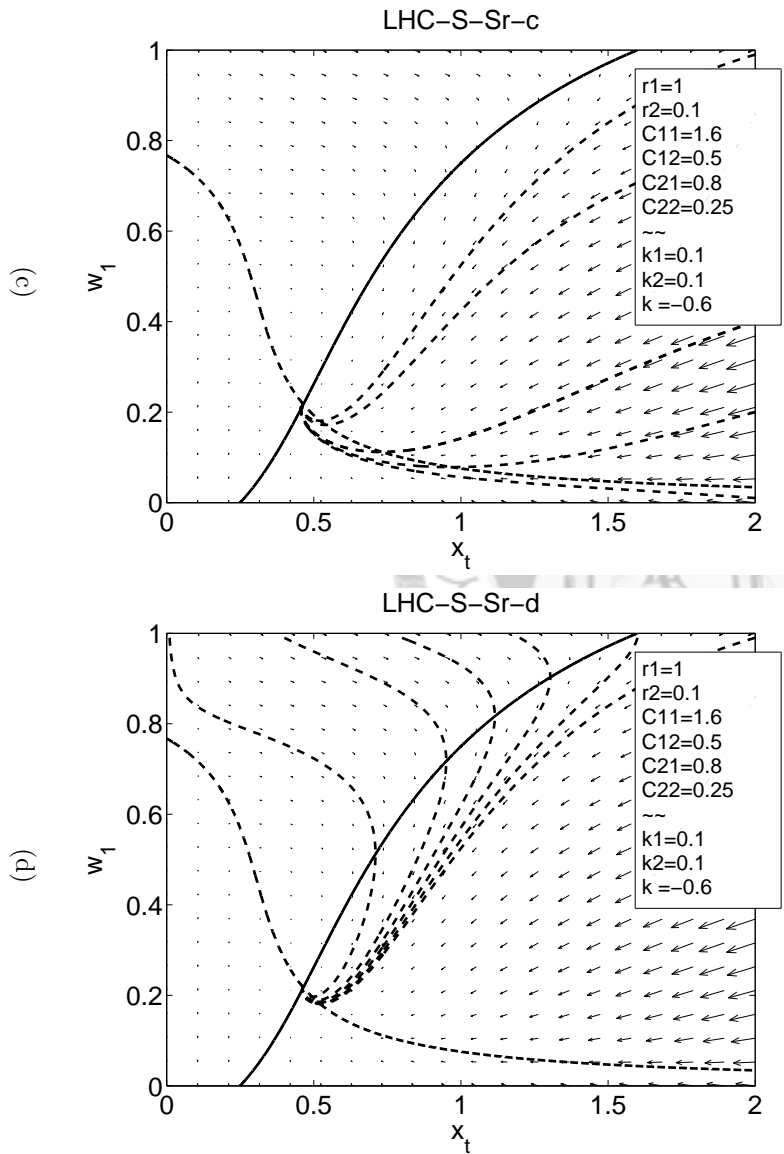
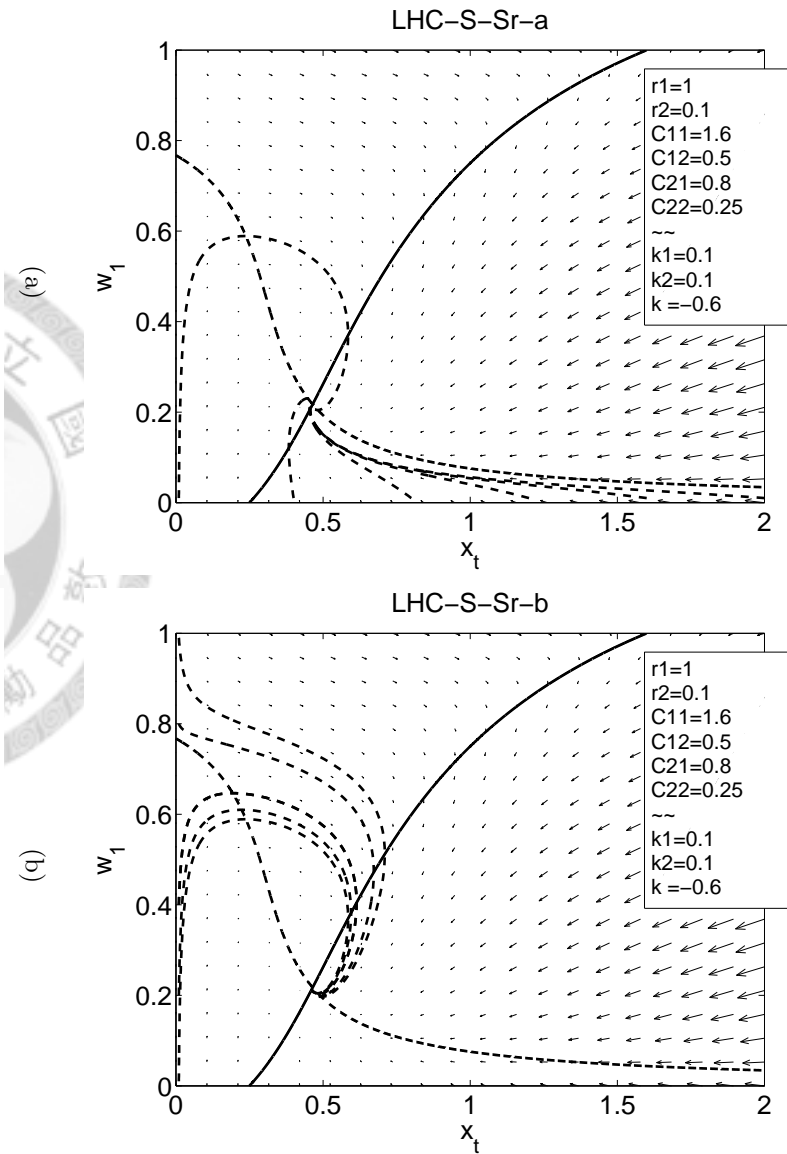
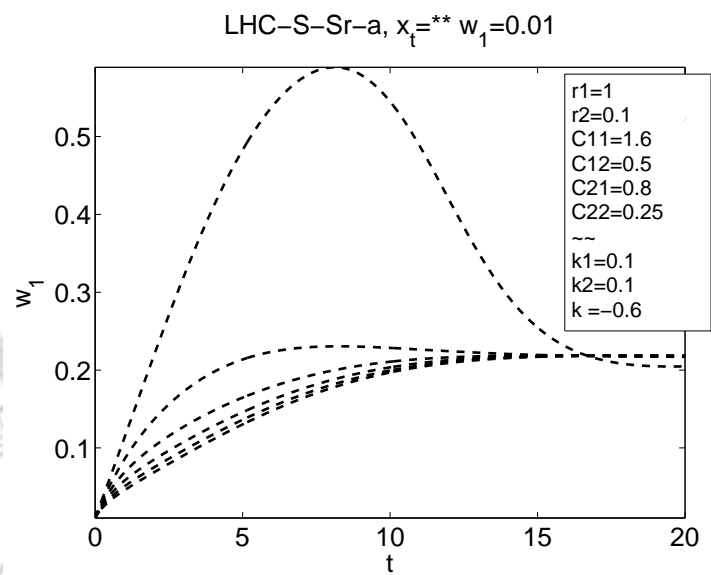
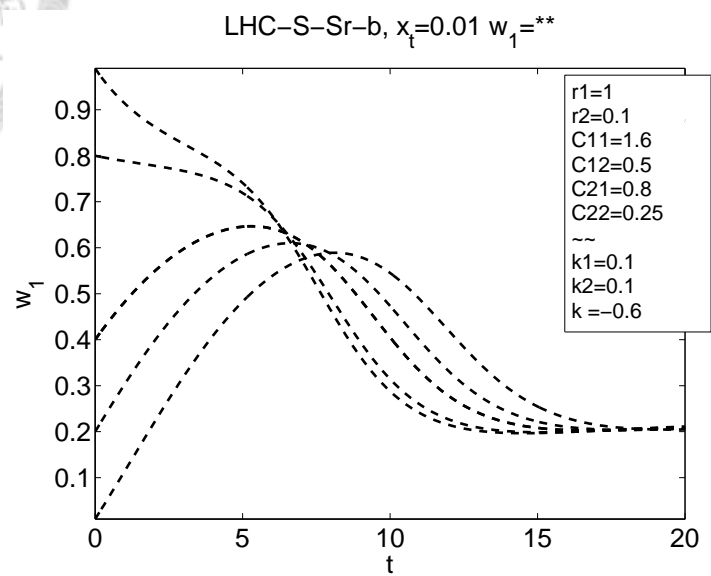


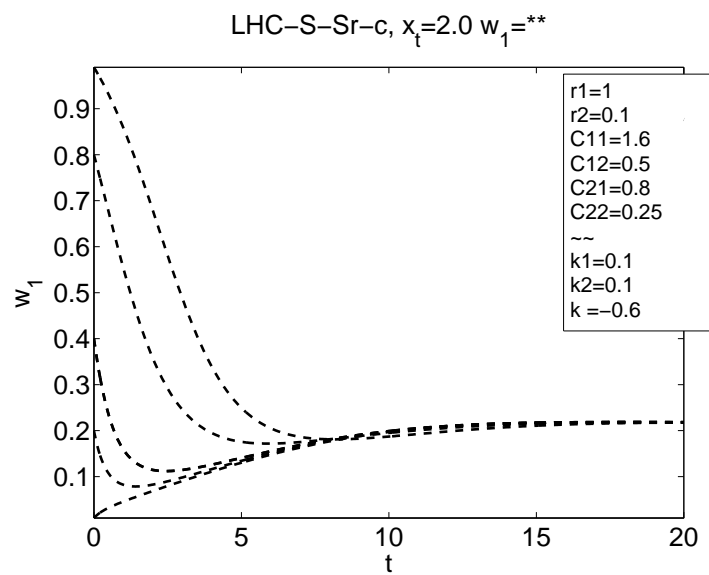
Figure 2.76: The x_{tot} - w_1 trajectories of LHC-S-Sr.



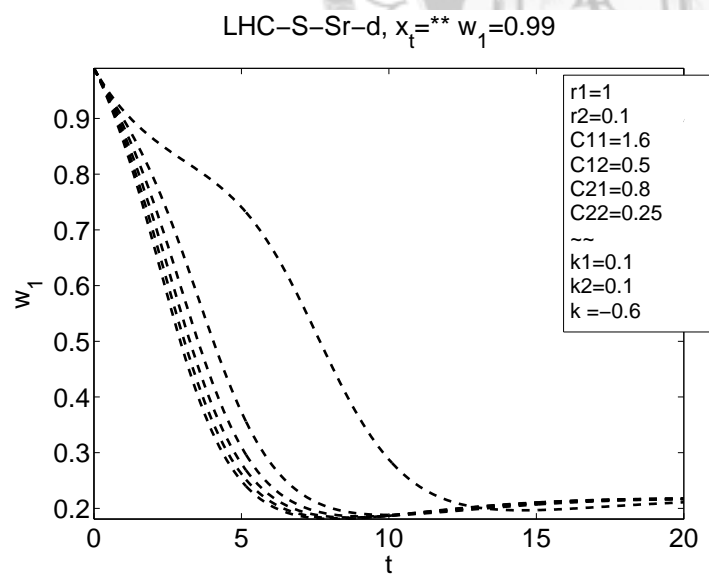
(a)



(b)

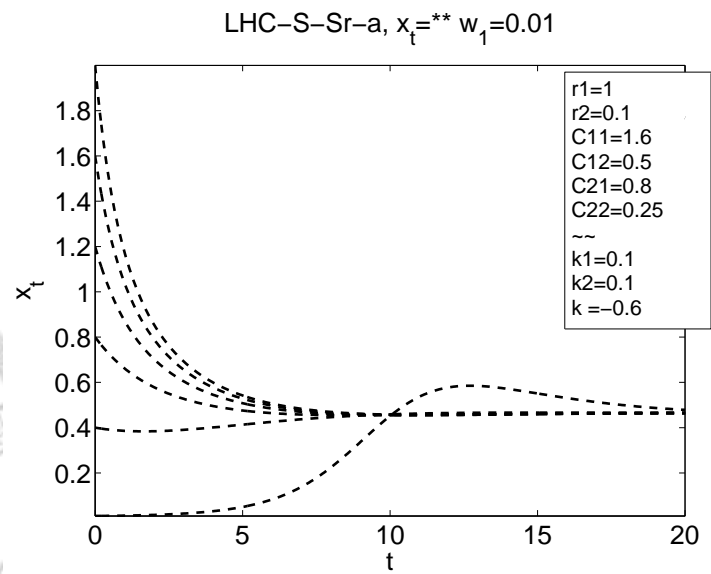


(c)

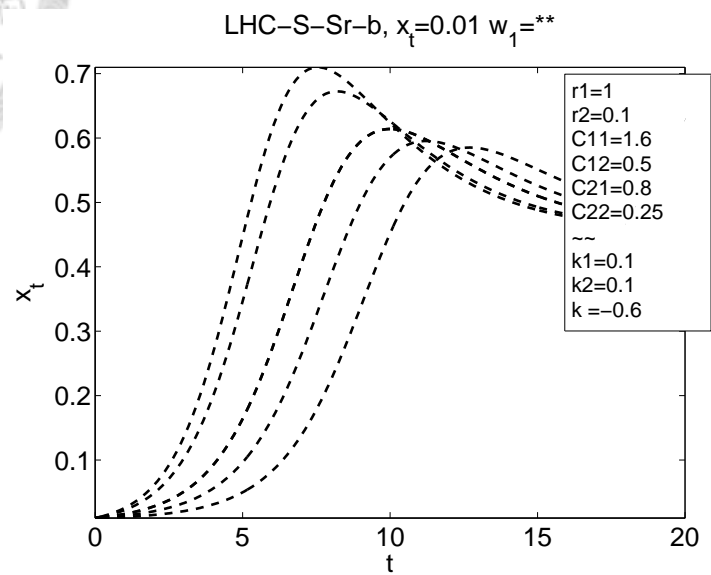


(d)

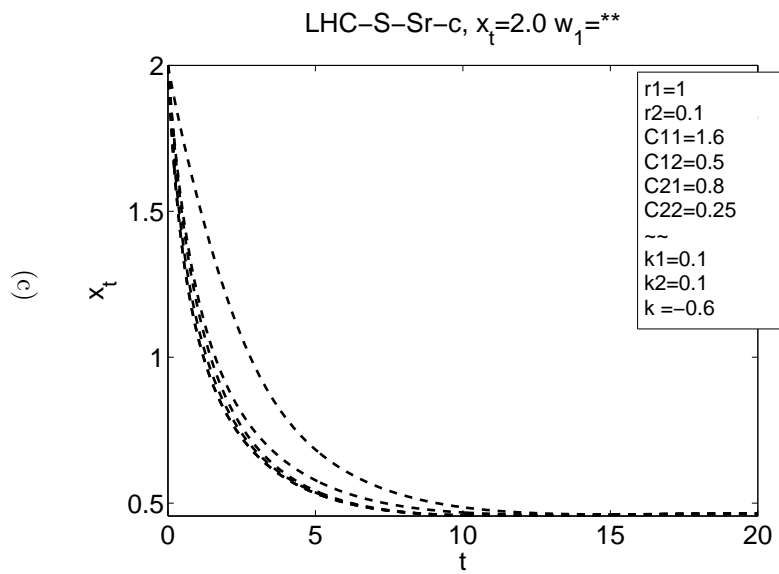
Figure 2.77: The x_{tot} - w_1 trajectories of LHC-S-Sr.



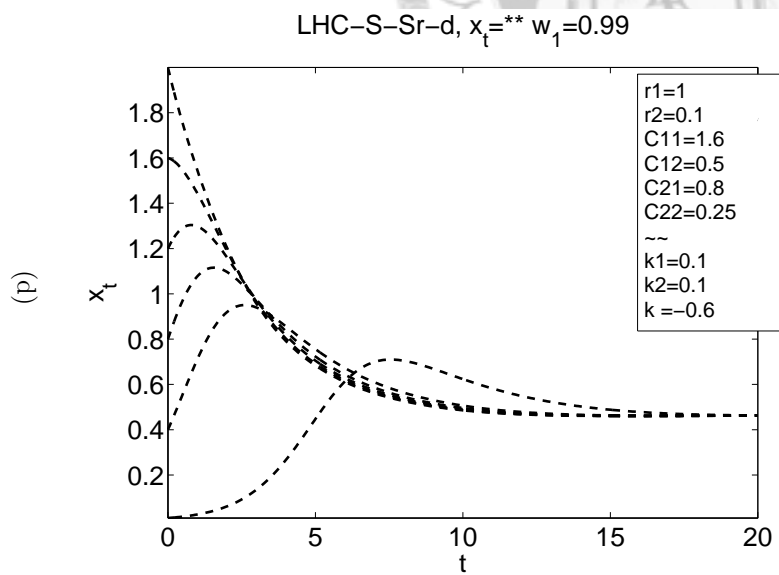
(a)



(b)



(c)



(d)

Figure 2.78: The $x_{tot}-w_1$ trajectories of LHC-S-Sr.

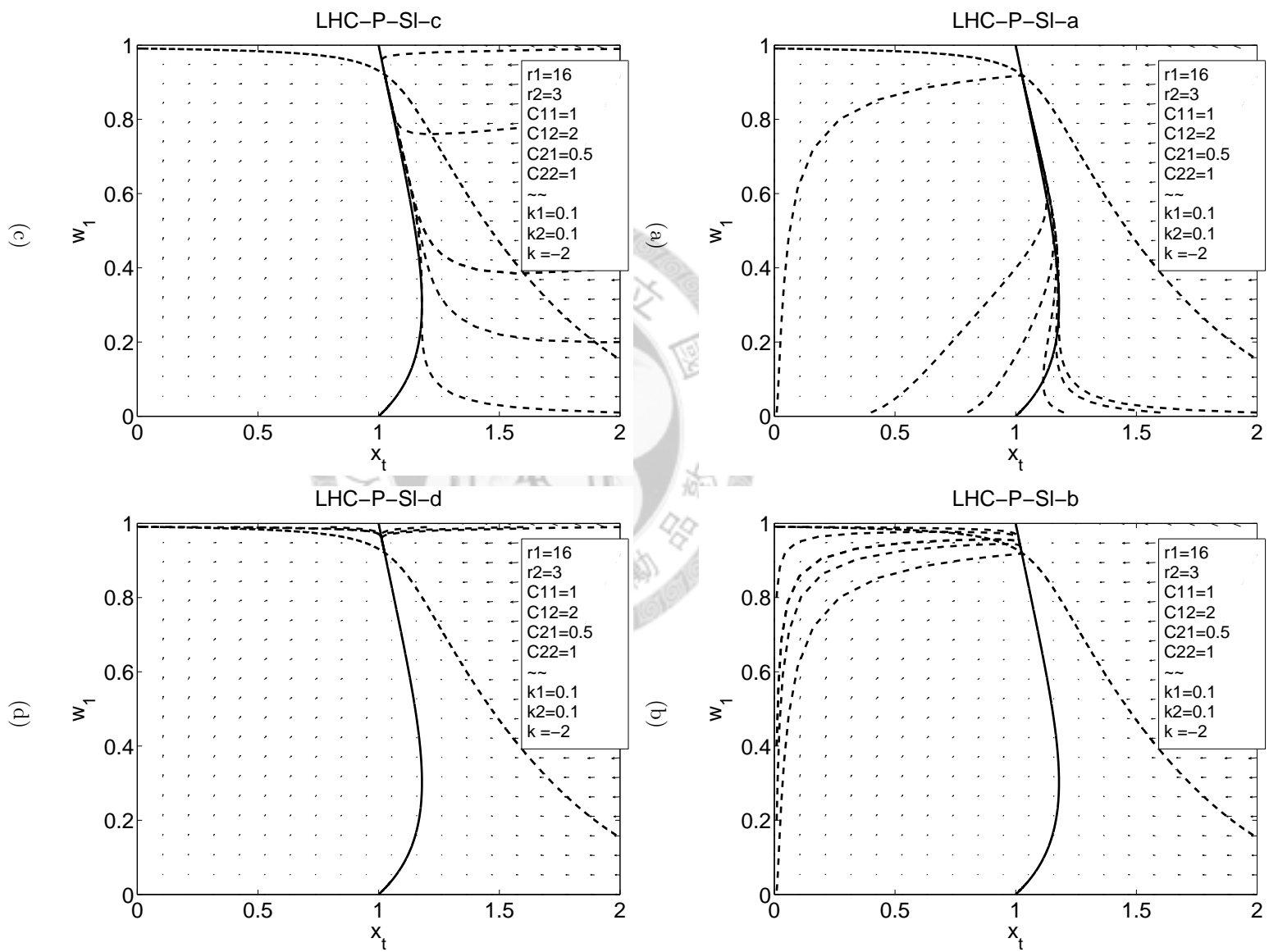


Figure 2.79: The x_{tot} - w_l trajectories of LHC-P-SI.

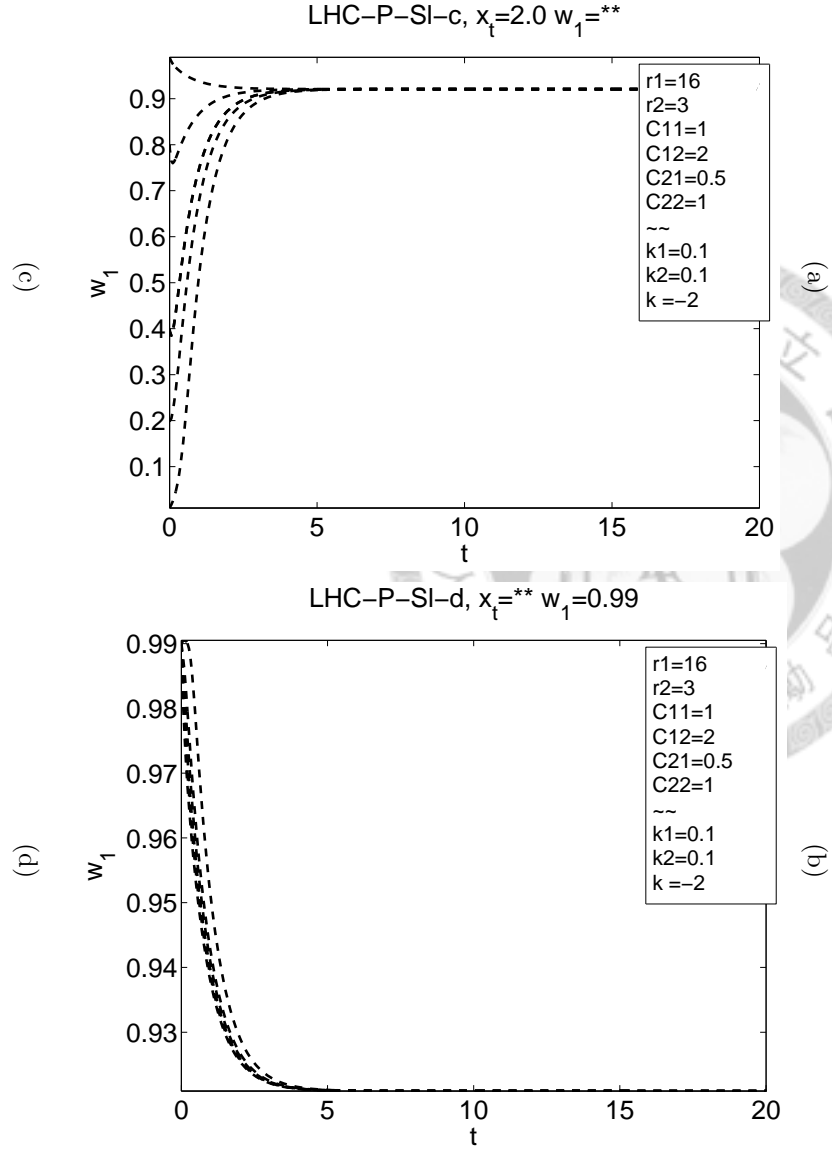
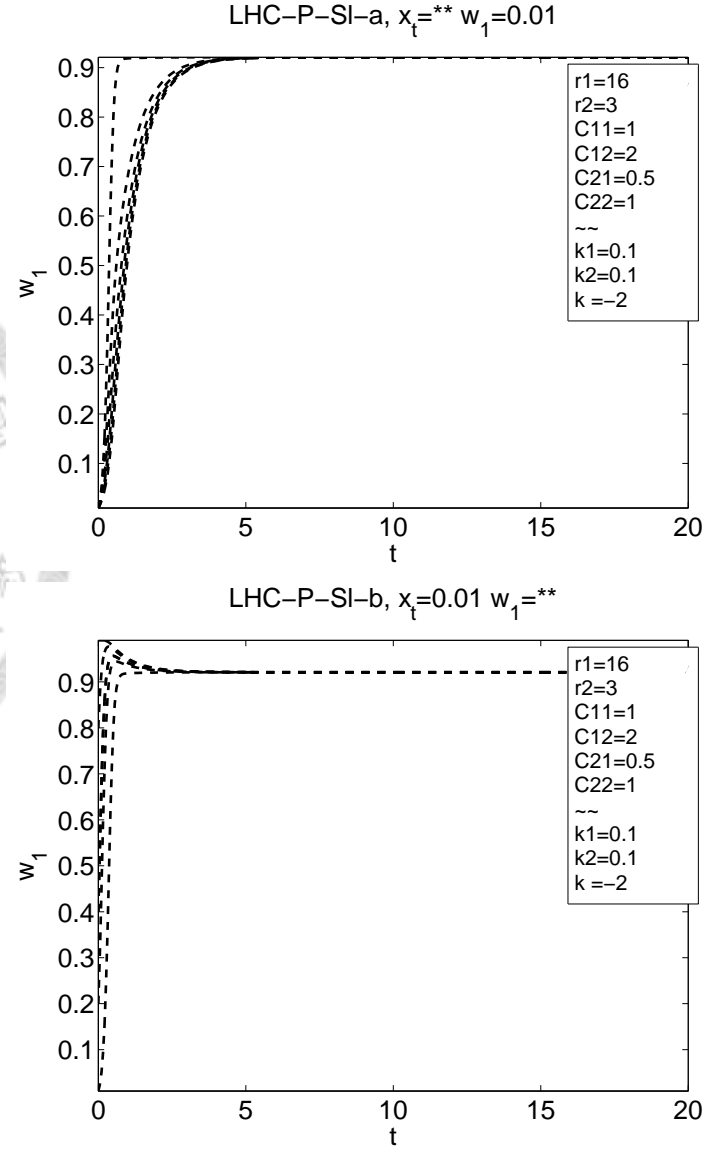
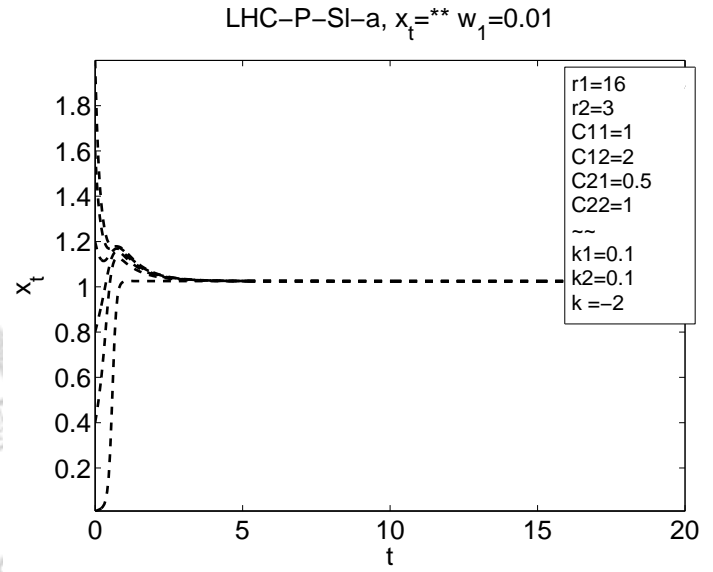
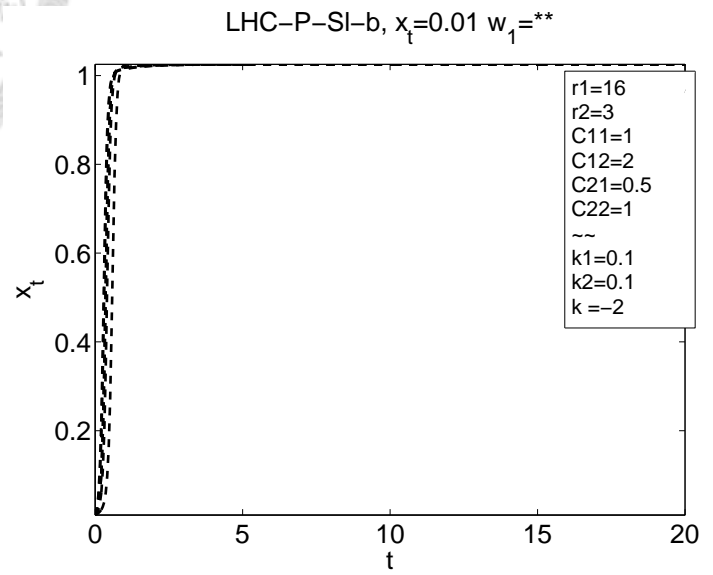


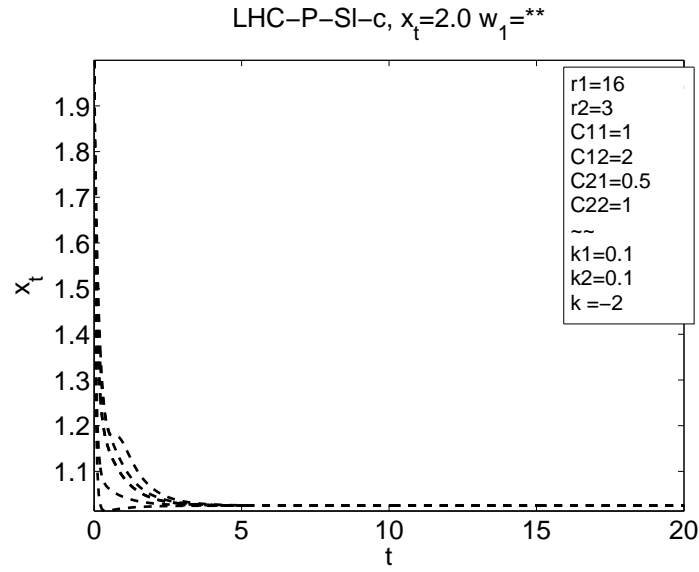
Figure 2.80: The x_{tot} - w_1 trajectories of LHC-P-SI.



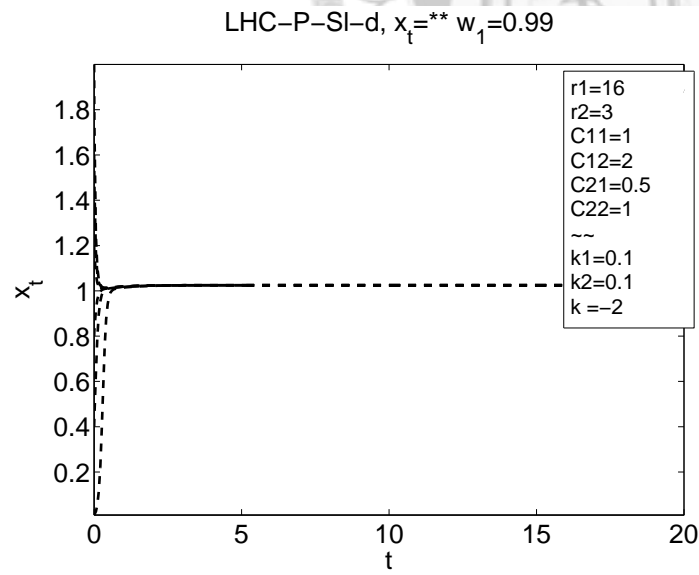
(a)



(b)



(c)



(d)

Figure 2.81: The $x_{tot}-w_1$ trajectories of LHC-P-SI.

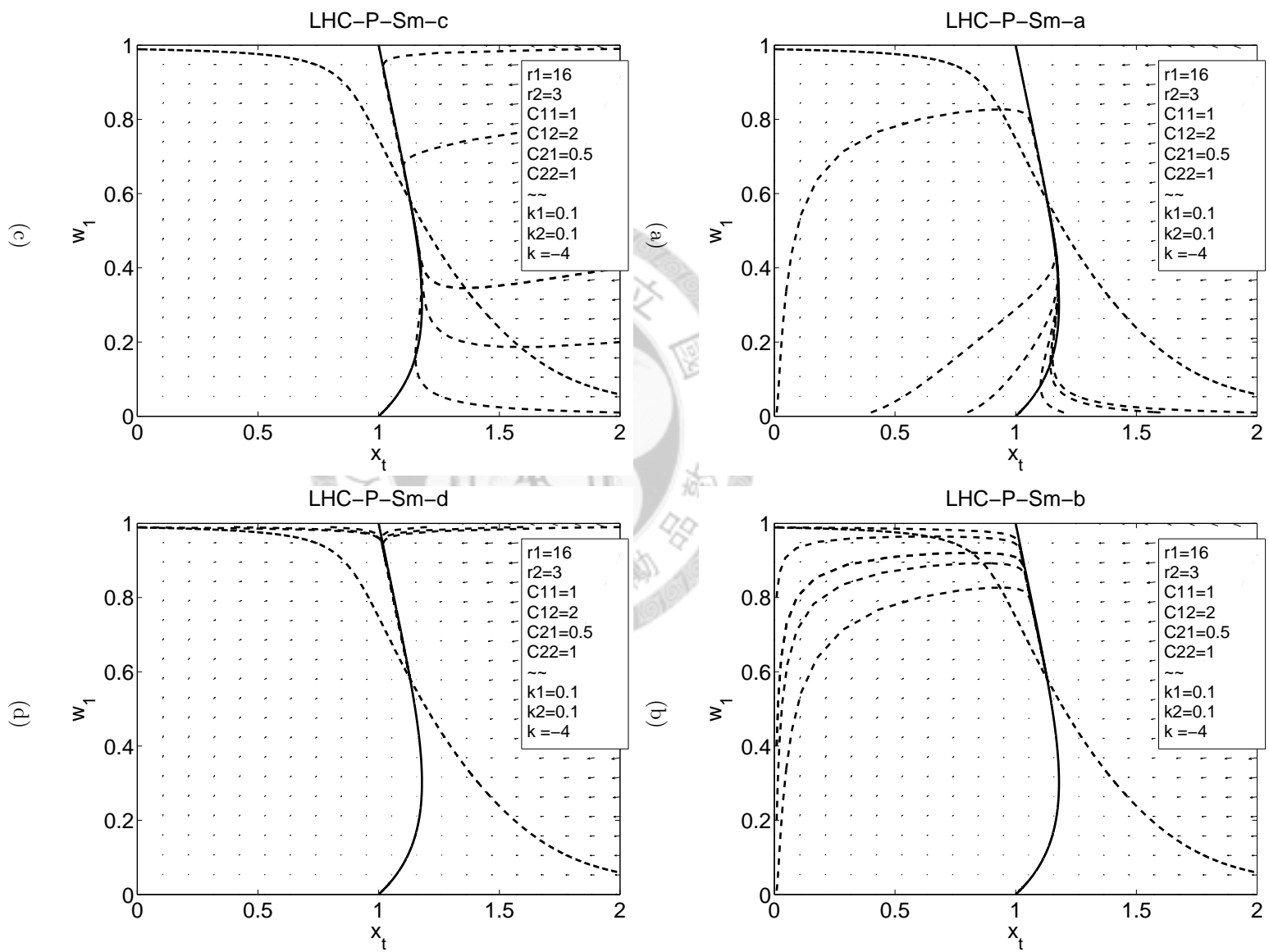


Figure 2.82: The x_{tot} - w_1 trajectories of LHC-P-Sm.

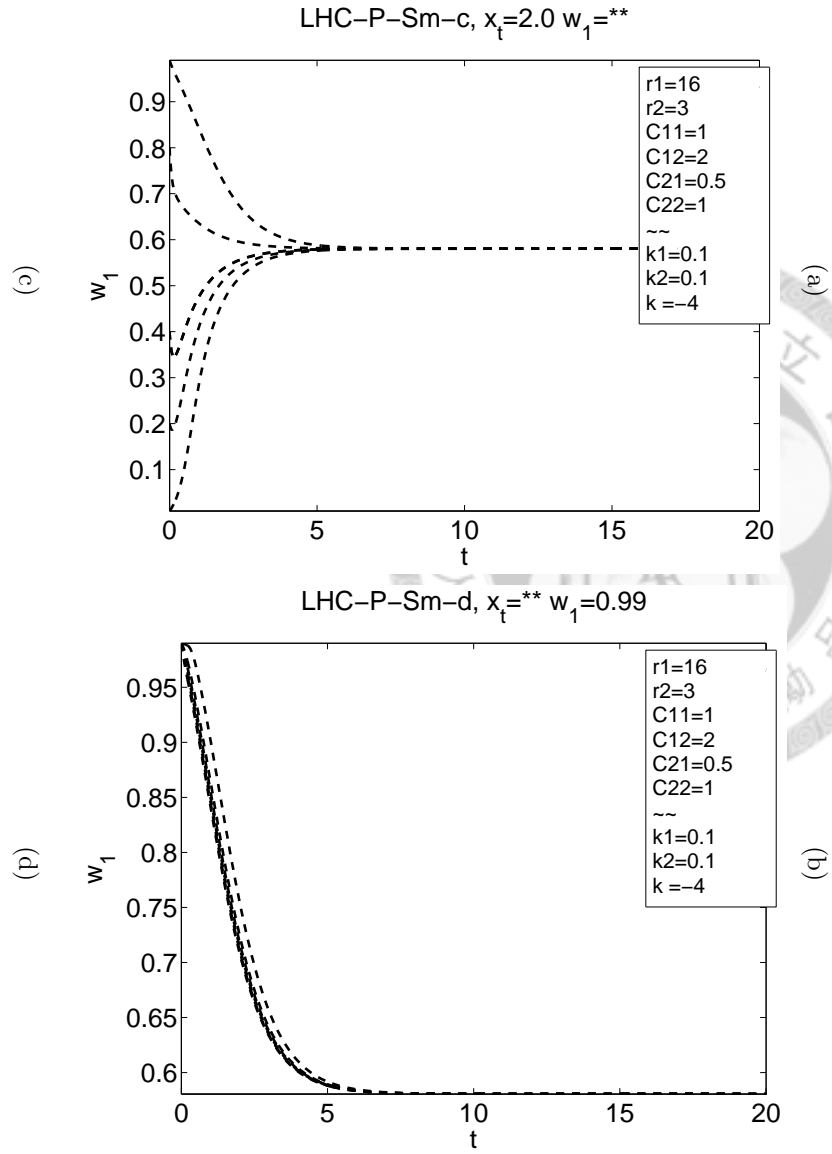
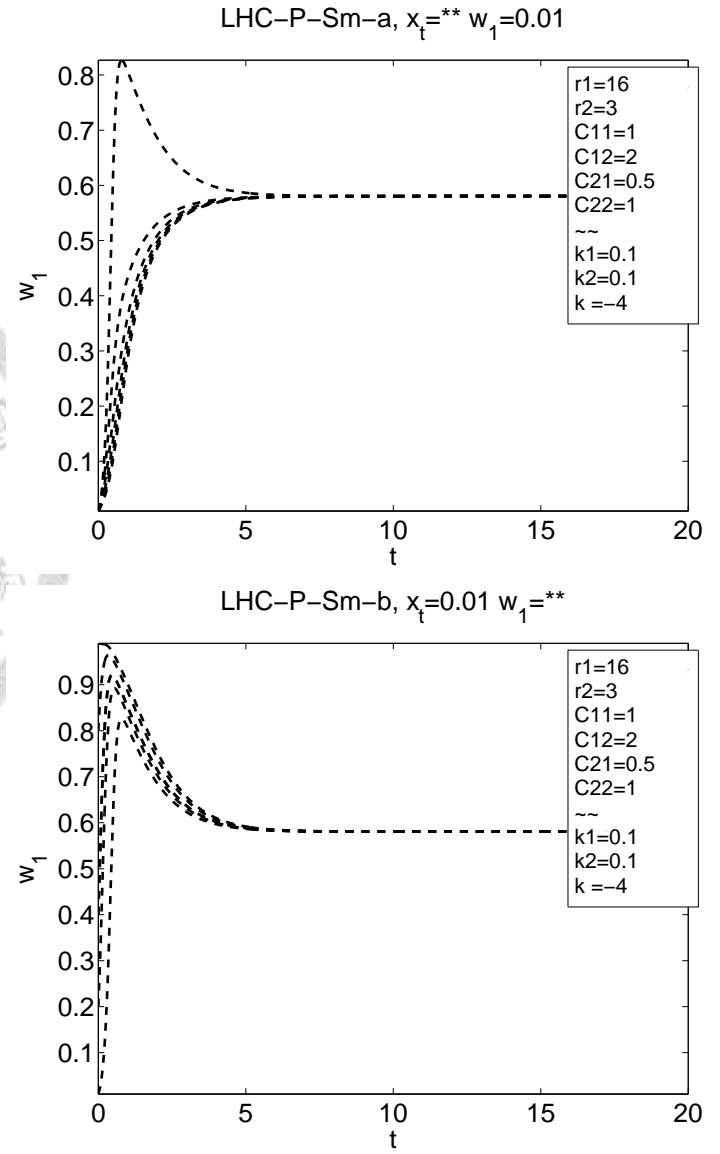


Figure 2.83: The x_{tot} - w_1 trajectories of LHC-P-Sm.

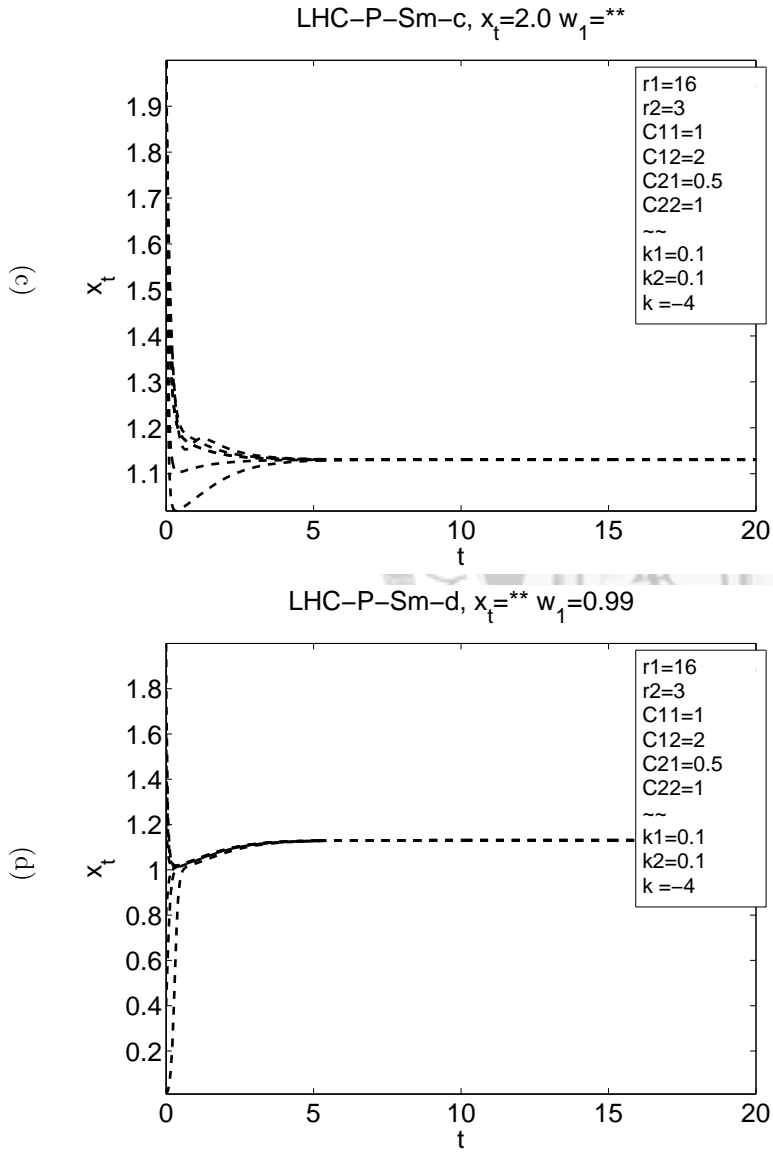
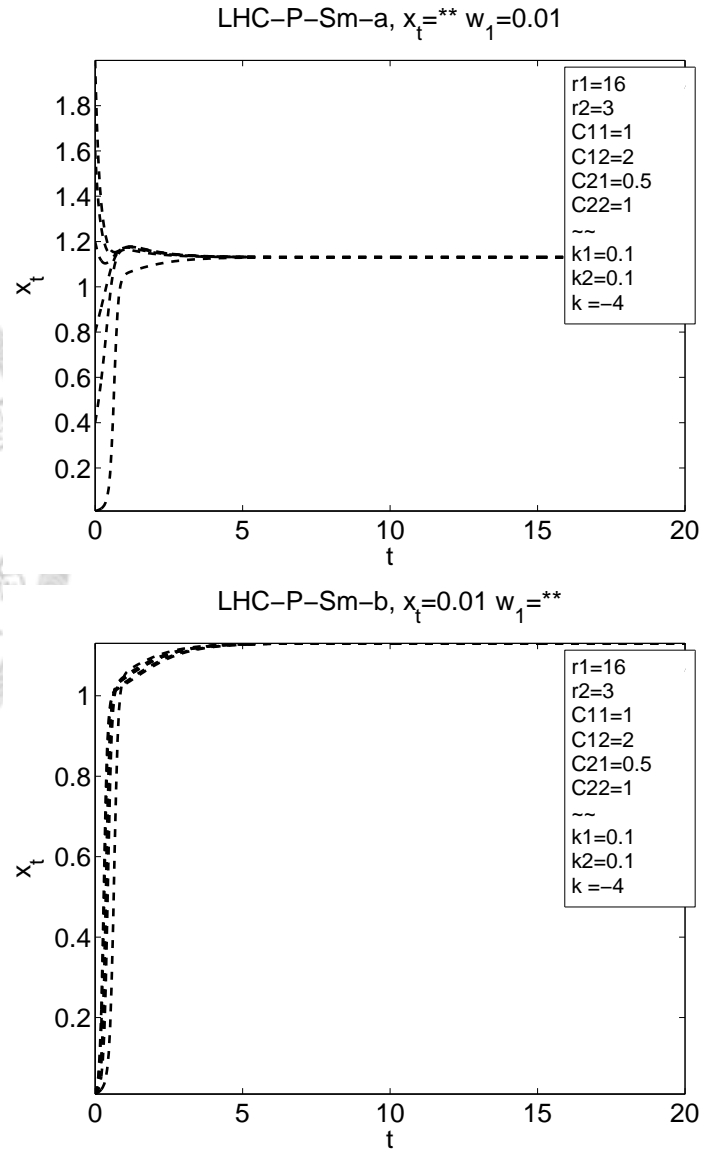
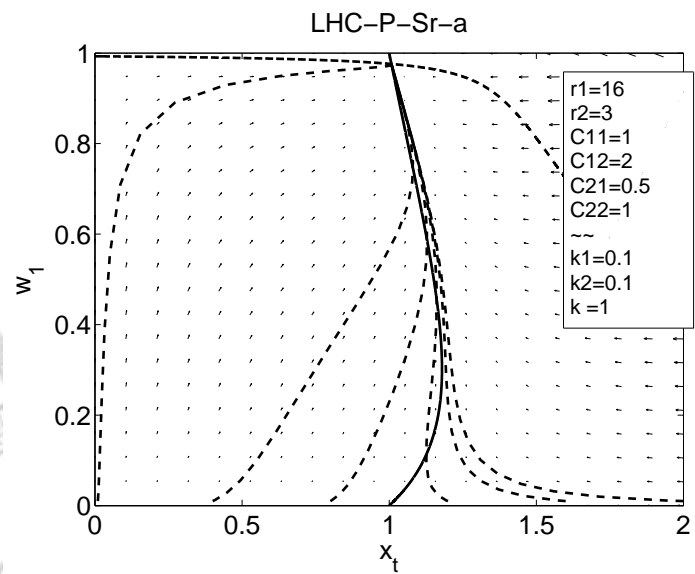
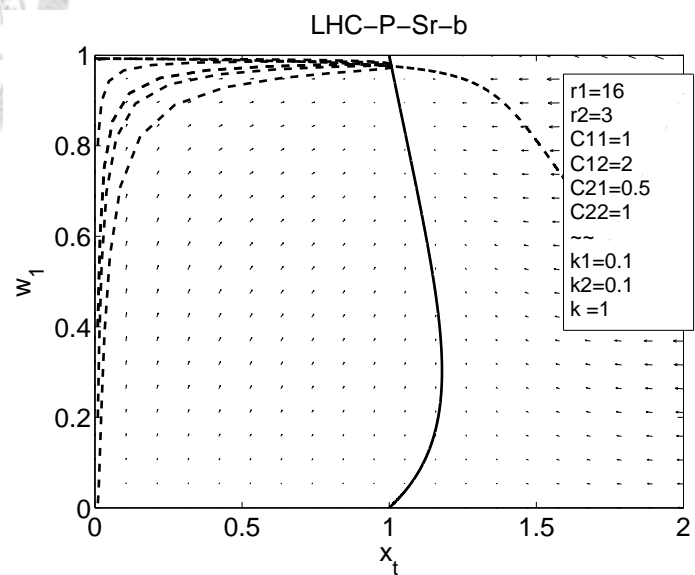


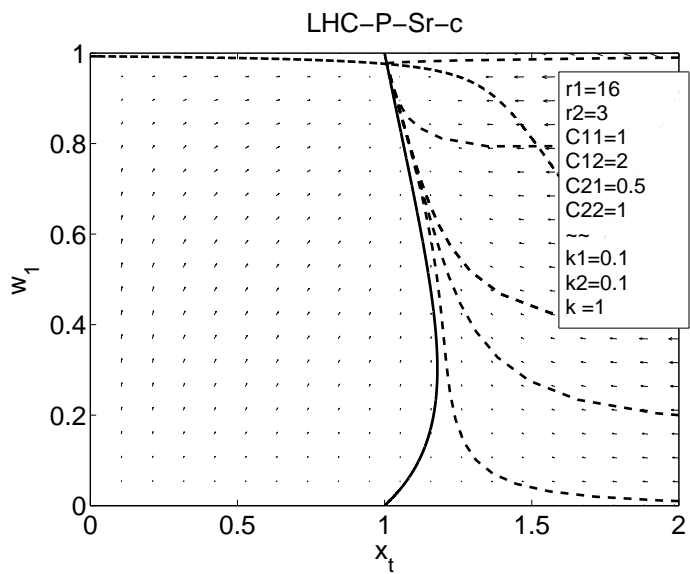
Figure 2.84: The $x_{tot}-w_1$ trajectories of LHC-P-Sm.



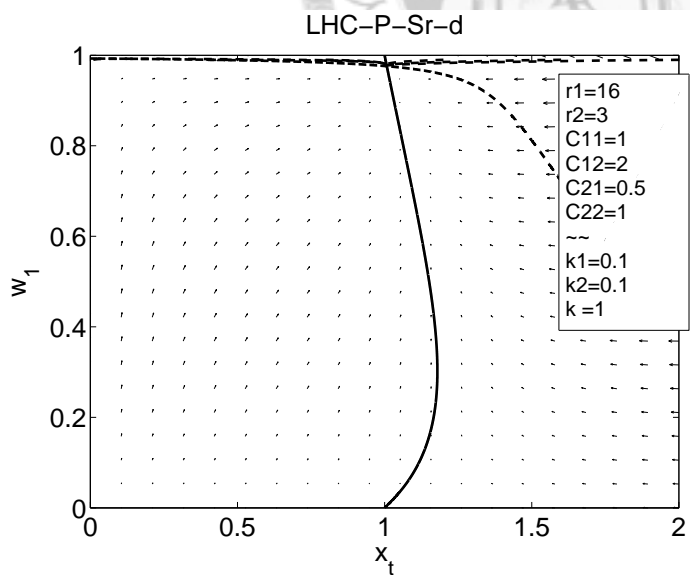
(a)



(b)



(c)



(d)

Figure 2.85: The x_{tot} - w_1 trajectories of LHC-P-Sr.

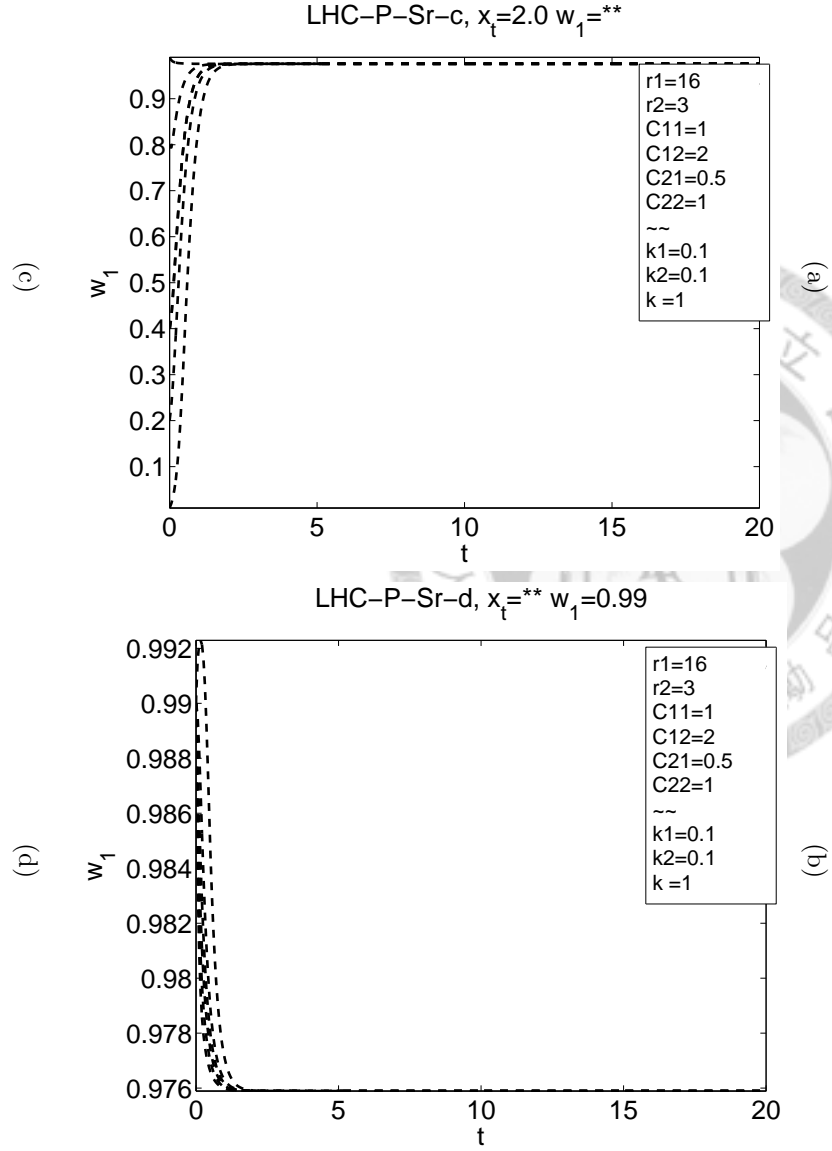
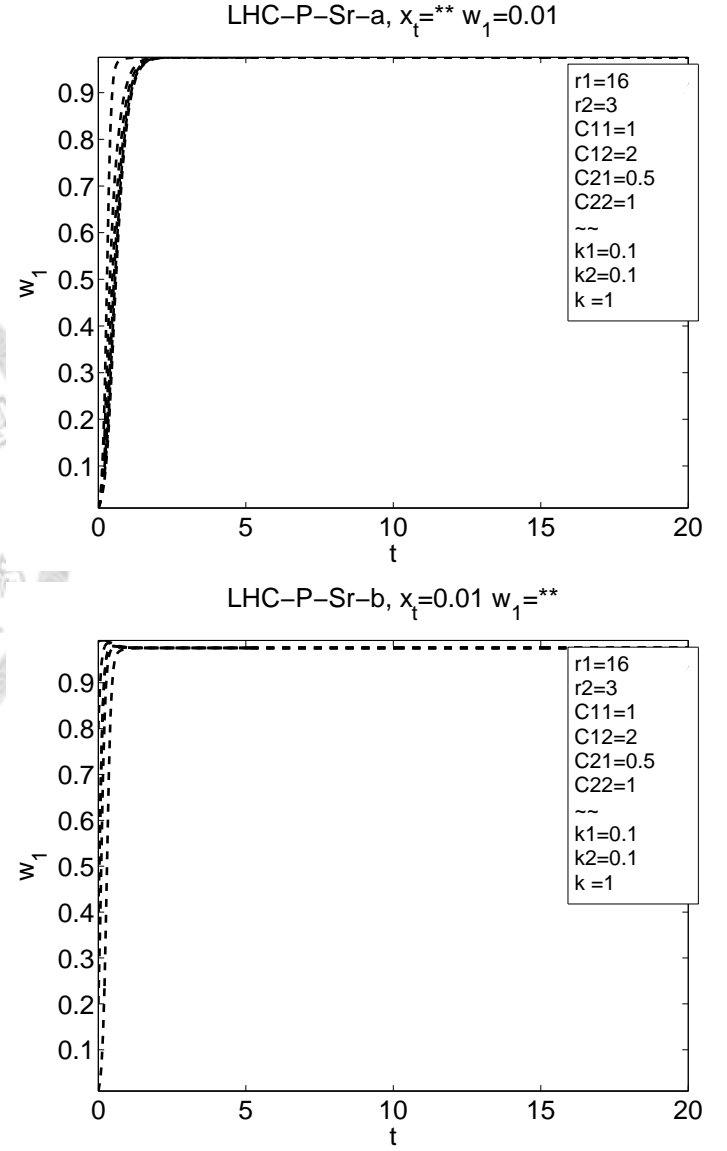
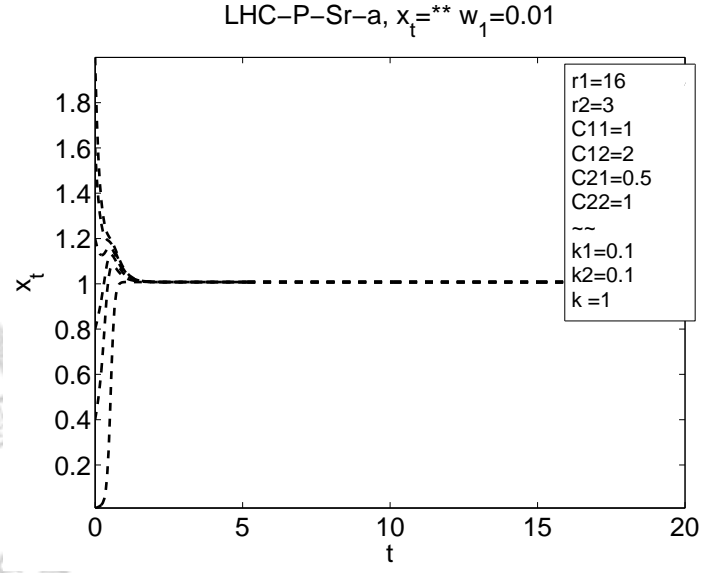
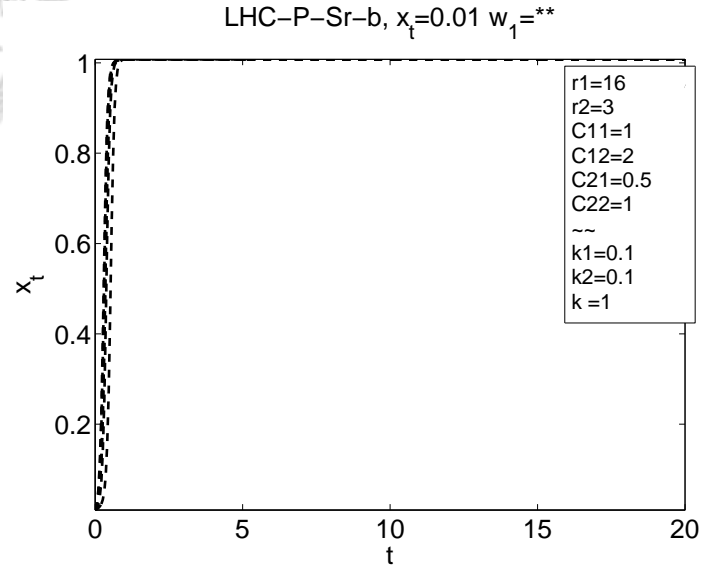


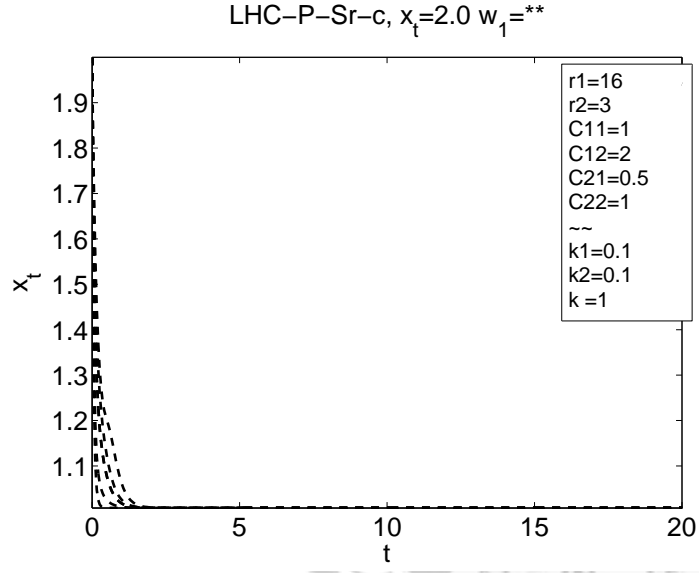
Figure 2.86: The x_{tot} - w_1 trajectories of LHC-P-Sr.



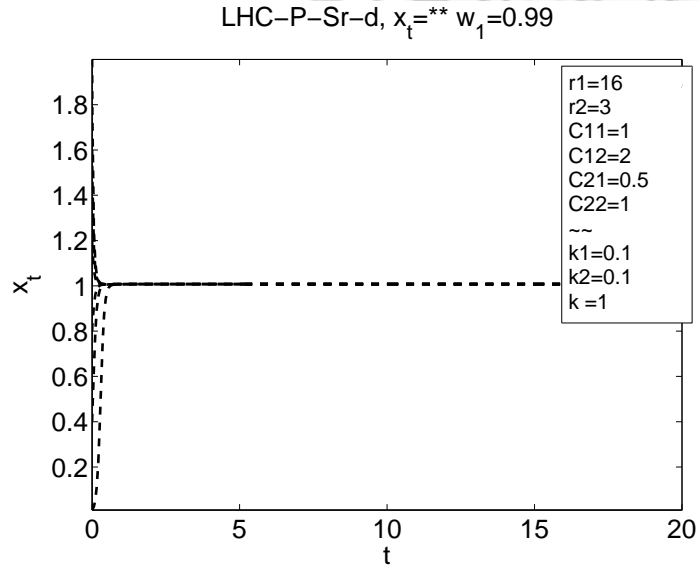
(a)



(b)



(c)



(d)

Figure 2.87: The $x_{tot}-w_1$ trajectories of LHC-P-Sr.

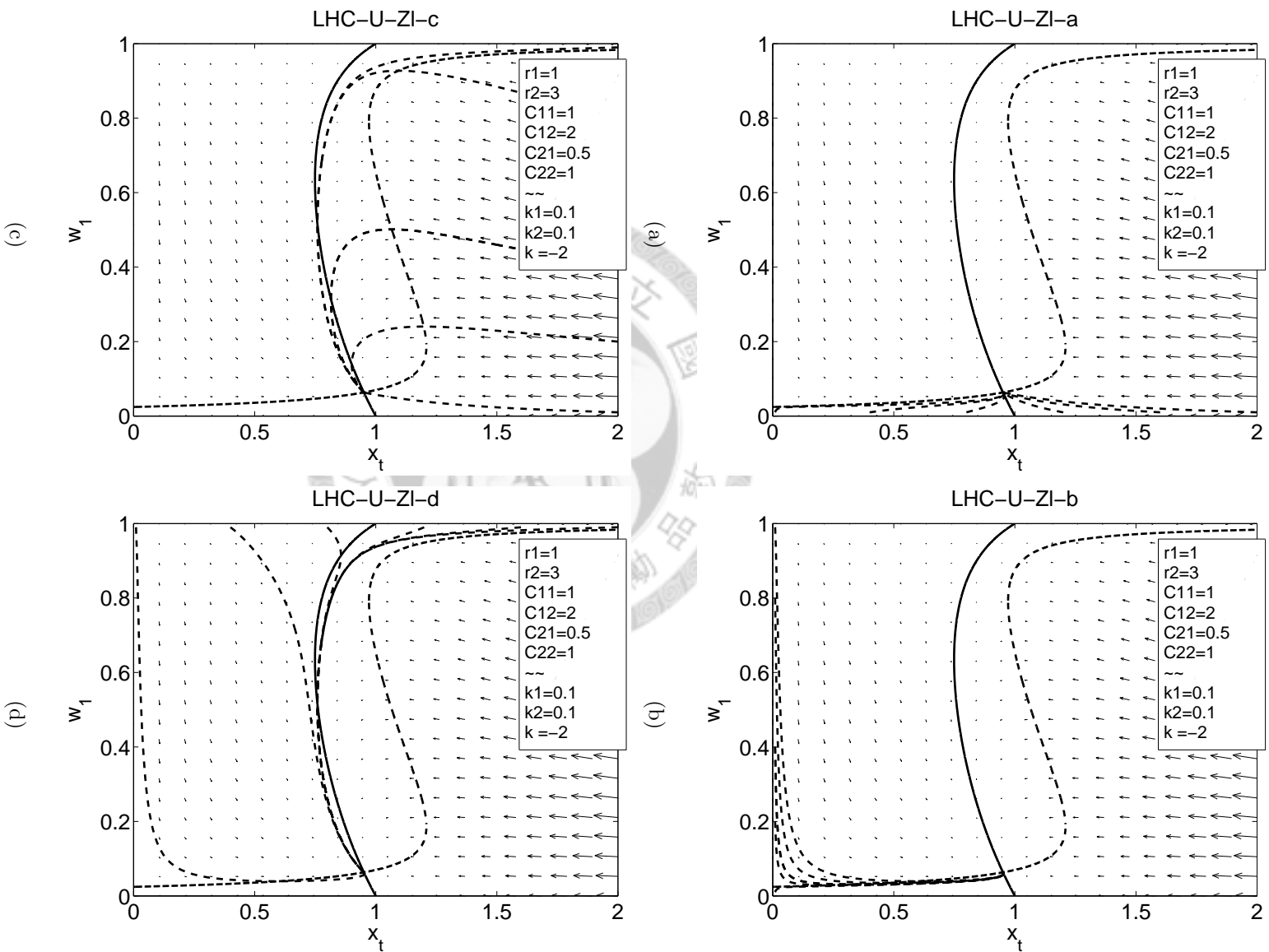


Figure 2.88: The x_{tot} - w_1 trajectories of LHC-U-ZI.

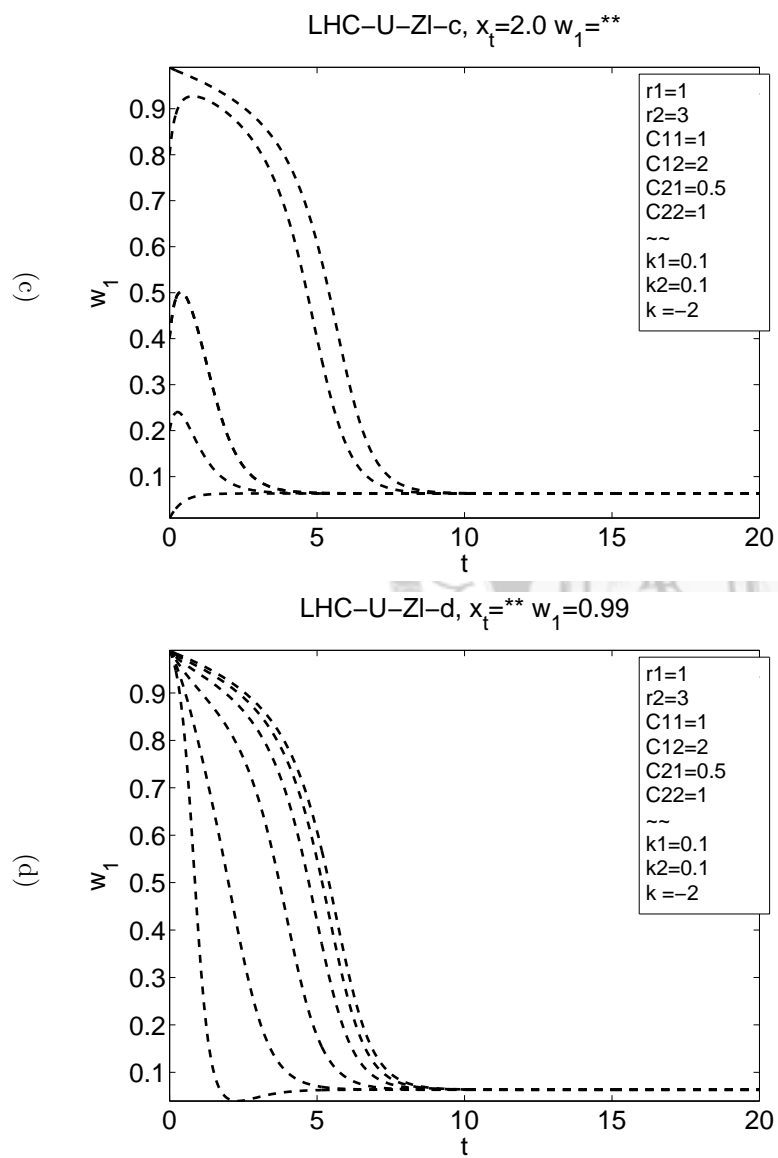
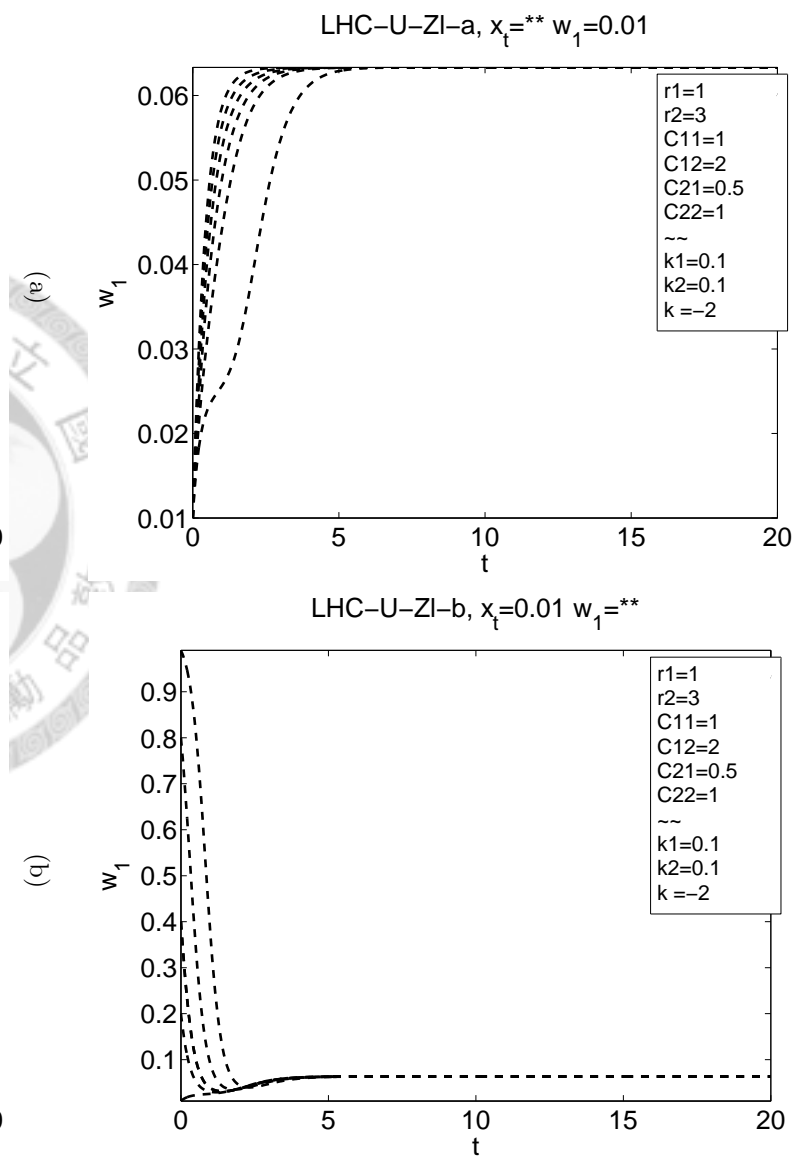
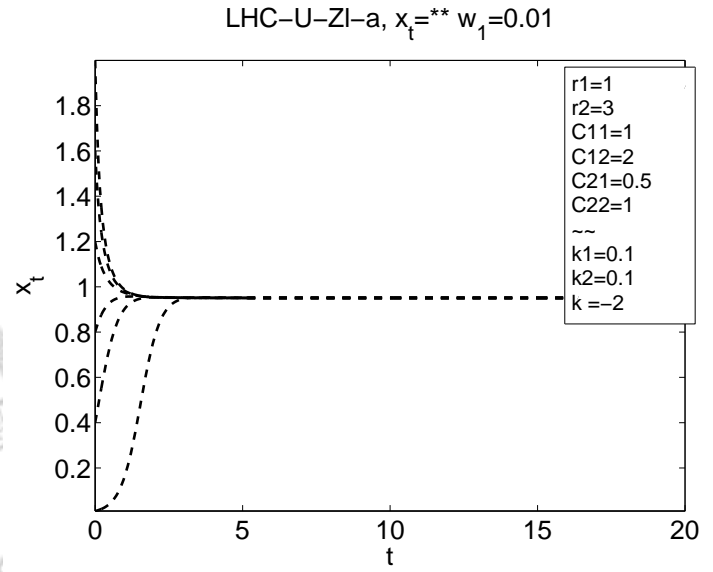
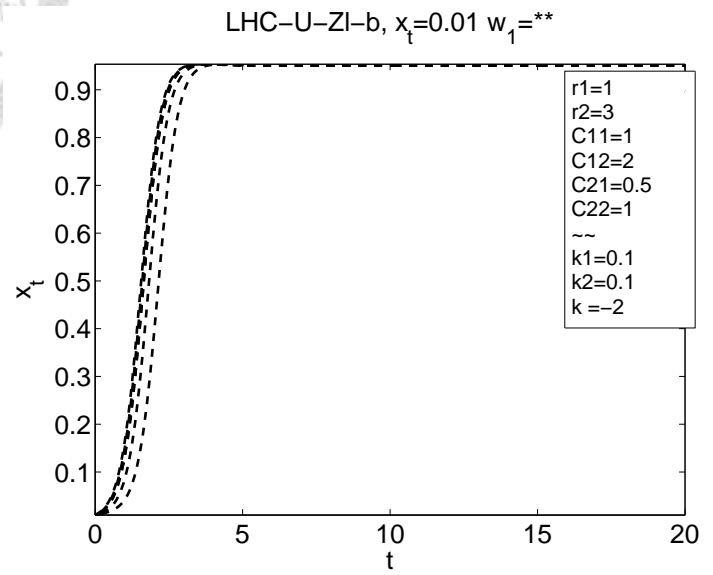


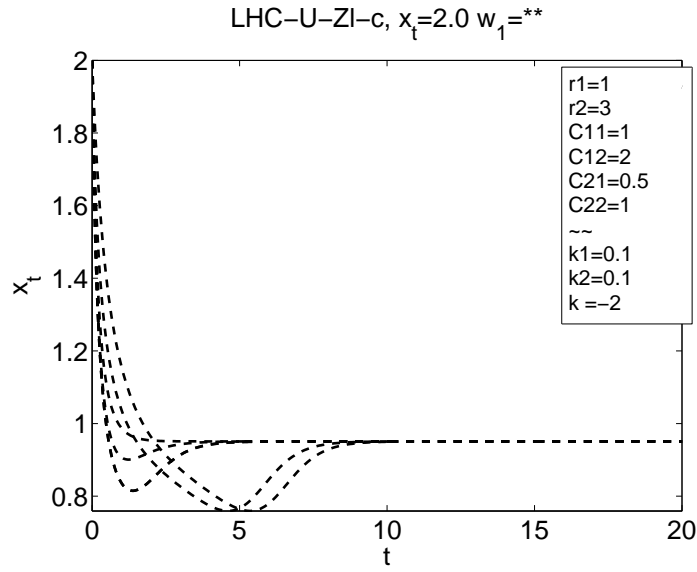
Figure 2.89: The x_{tot} - w_1 trajectories of LHC-U-ZI.



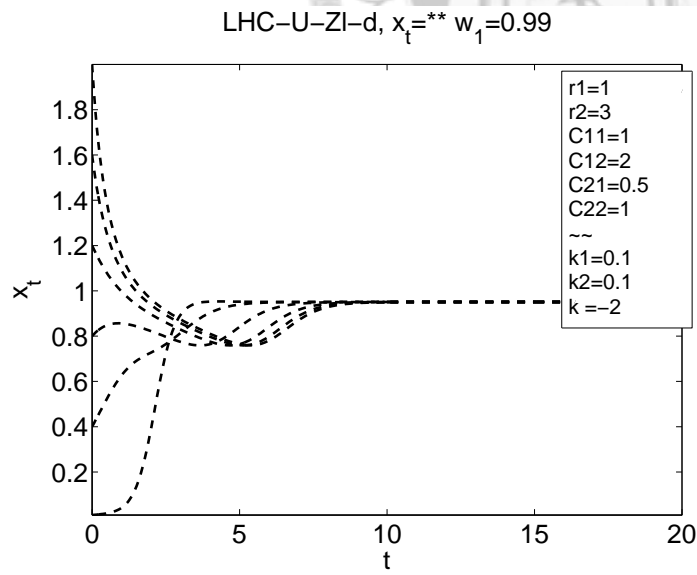
(a)



(b)



(c)



(d)

Figure 2.90: The $x_{tot}-w_1$ trajectories of LHC-U-ZI.

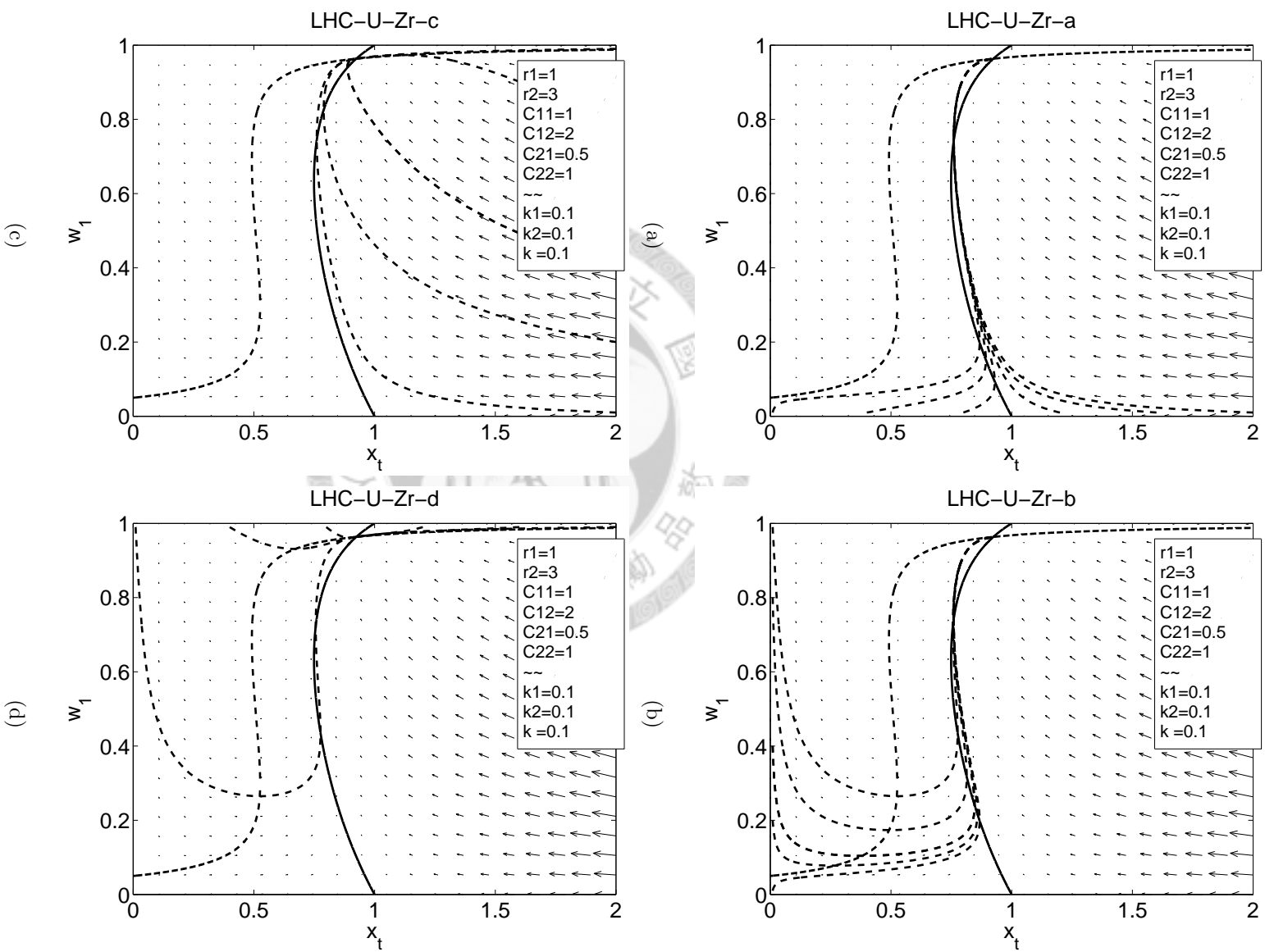
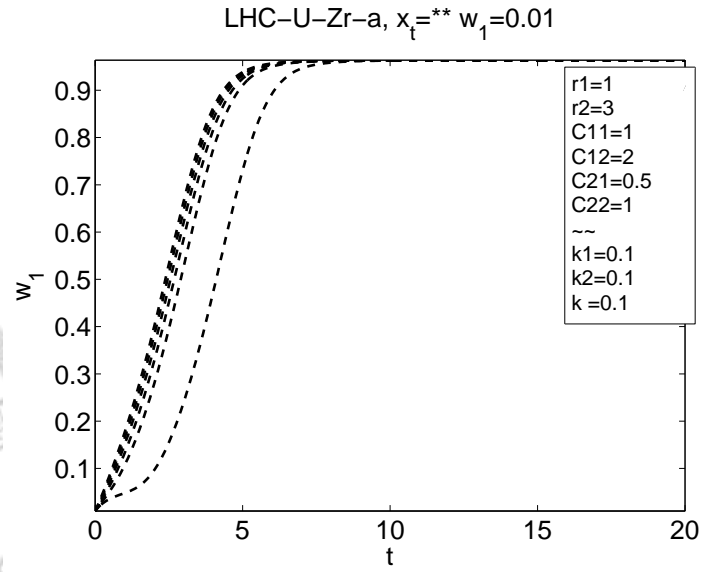
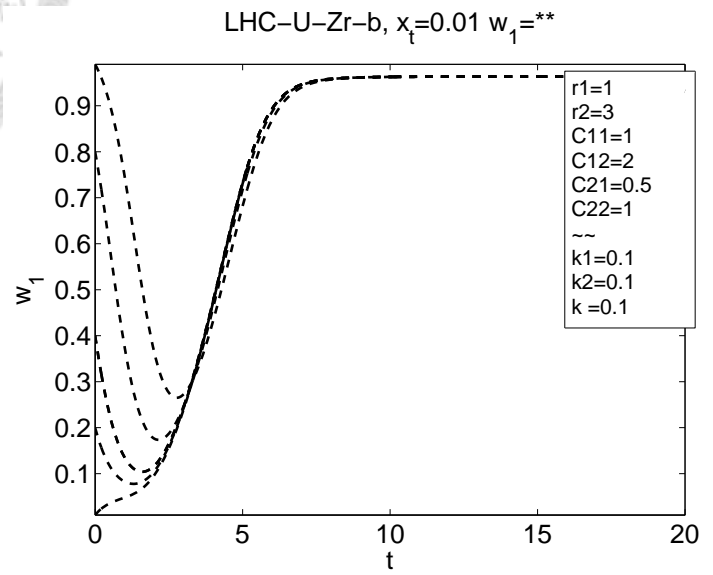


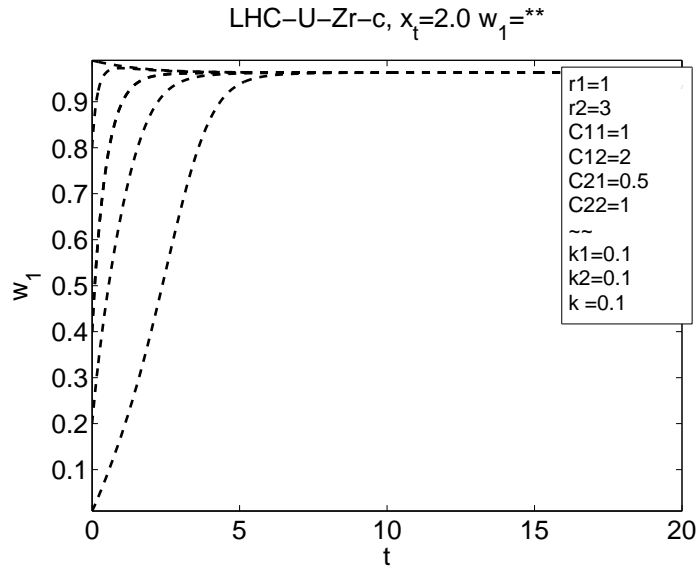
Figure 2.91: The x_{tot} - w_l trajectories of LHC-U-Zr.



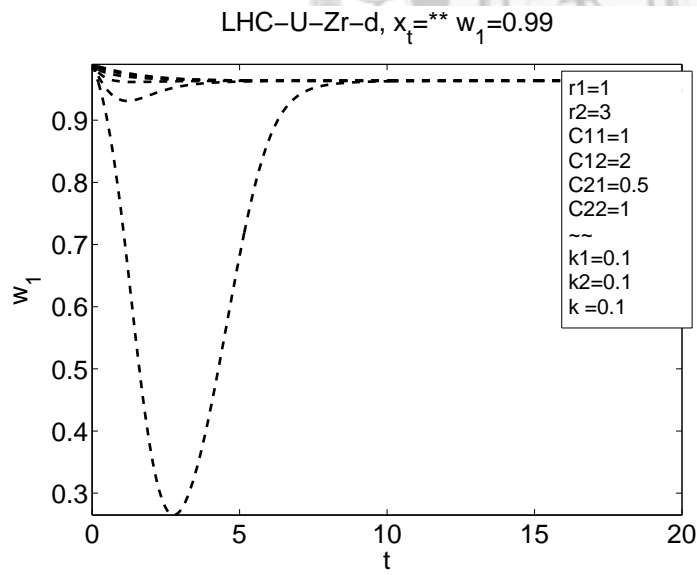
(a)



(b)



(c)



(d)

Figure 2.92: The x_{tot} - w_1 trajectories of LHC-U-Zr.

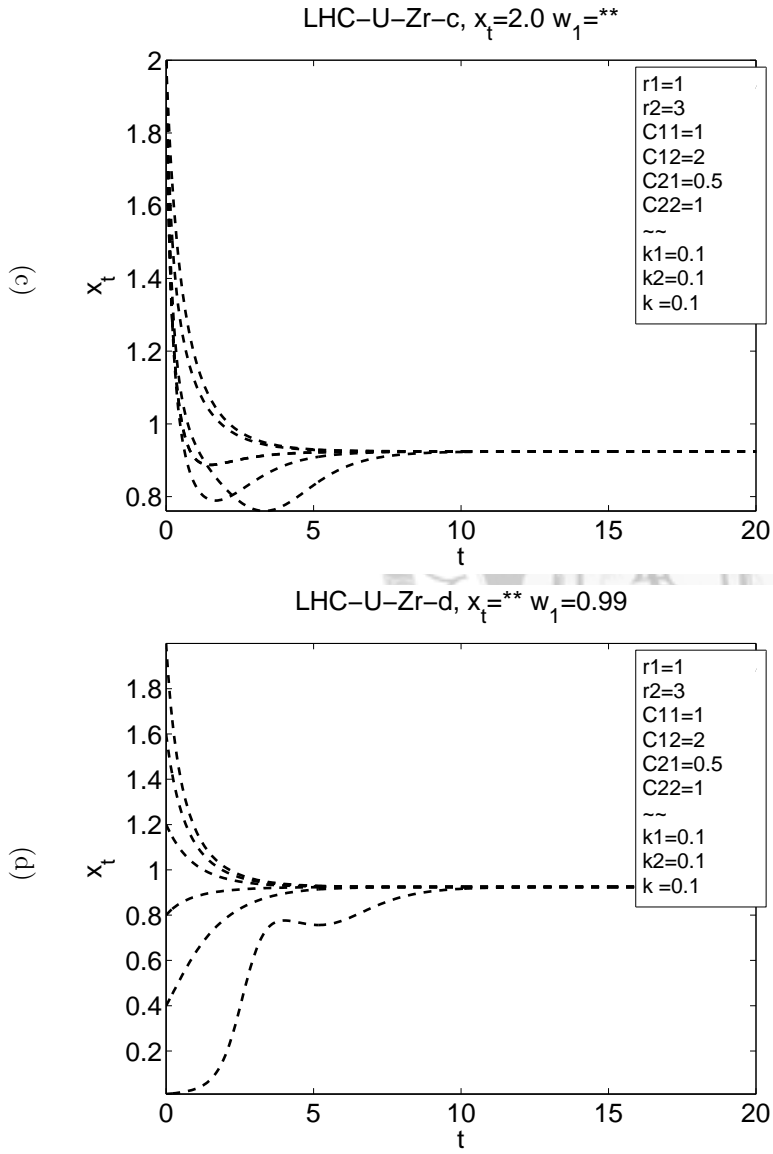
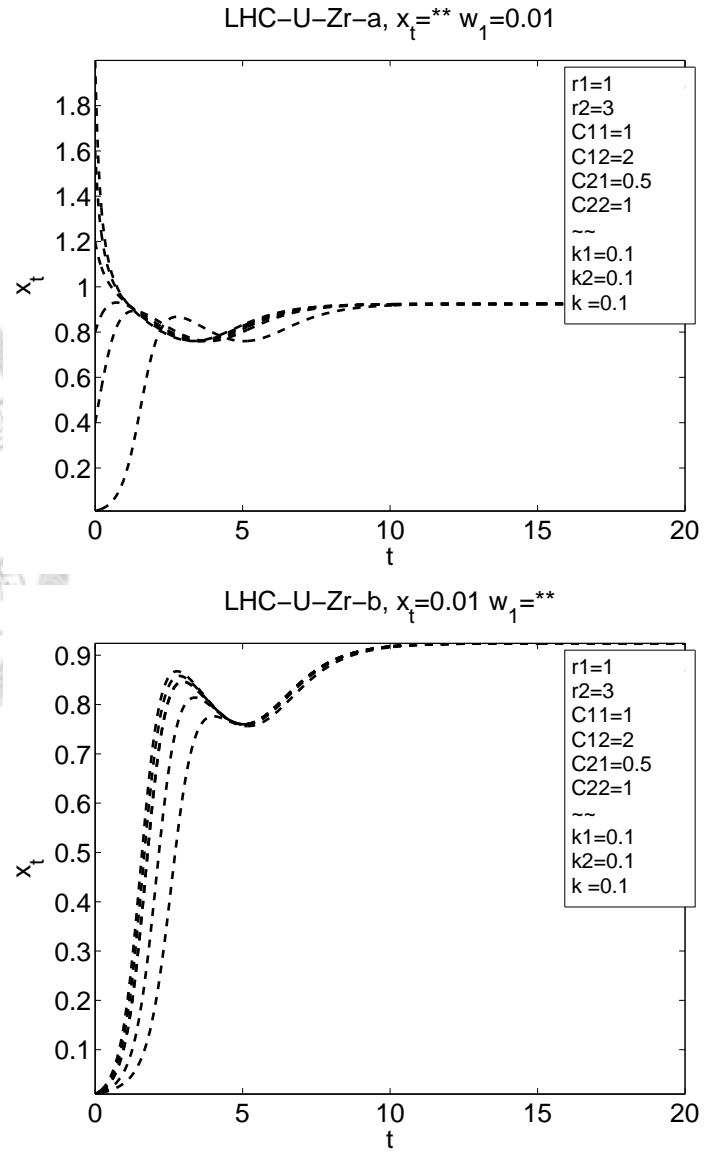


Figure 2.93: The $x_{tot}-w_1$ trajectories of LHC-U-Zr.

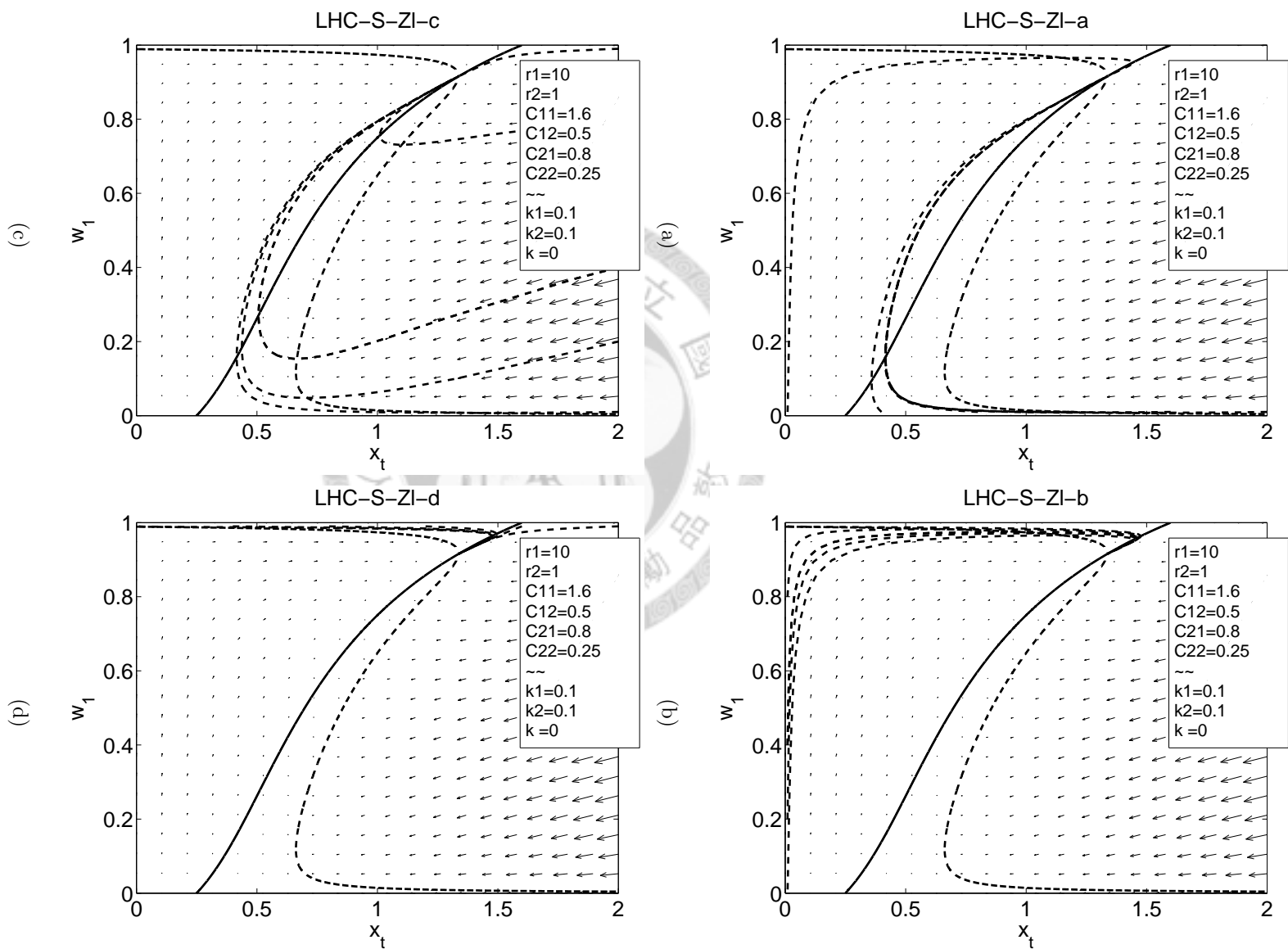


Figure 2.94: The x_t - w_1 trajectories of LHC-S-ZI.

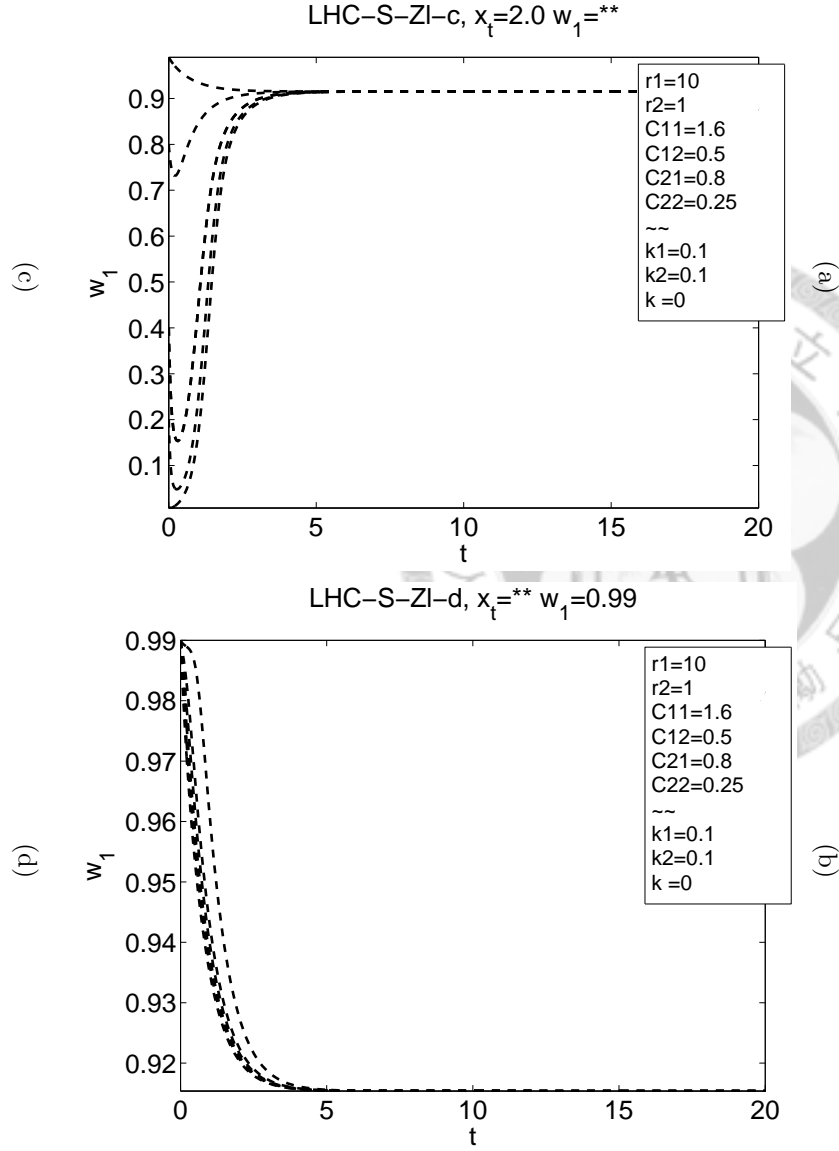
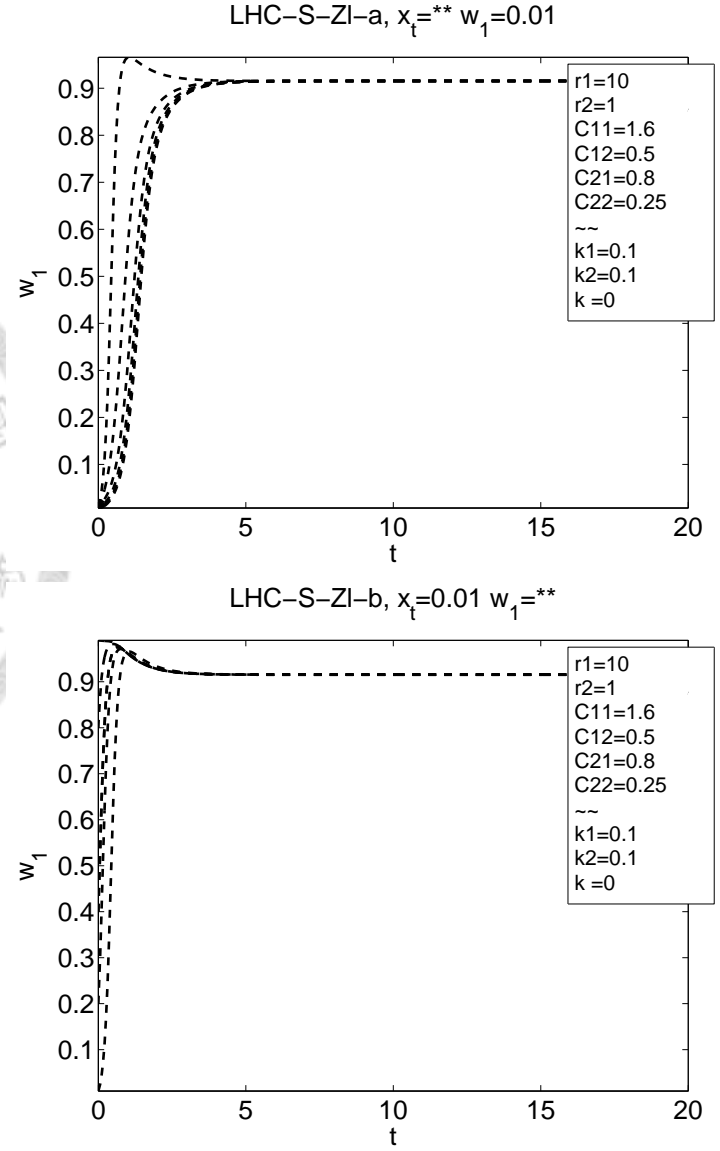


Figure 2.95: The x_{tot} - w_1 trajectories of LHC-S-ZI.

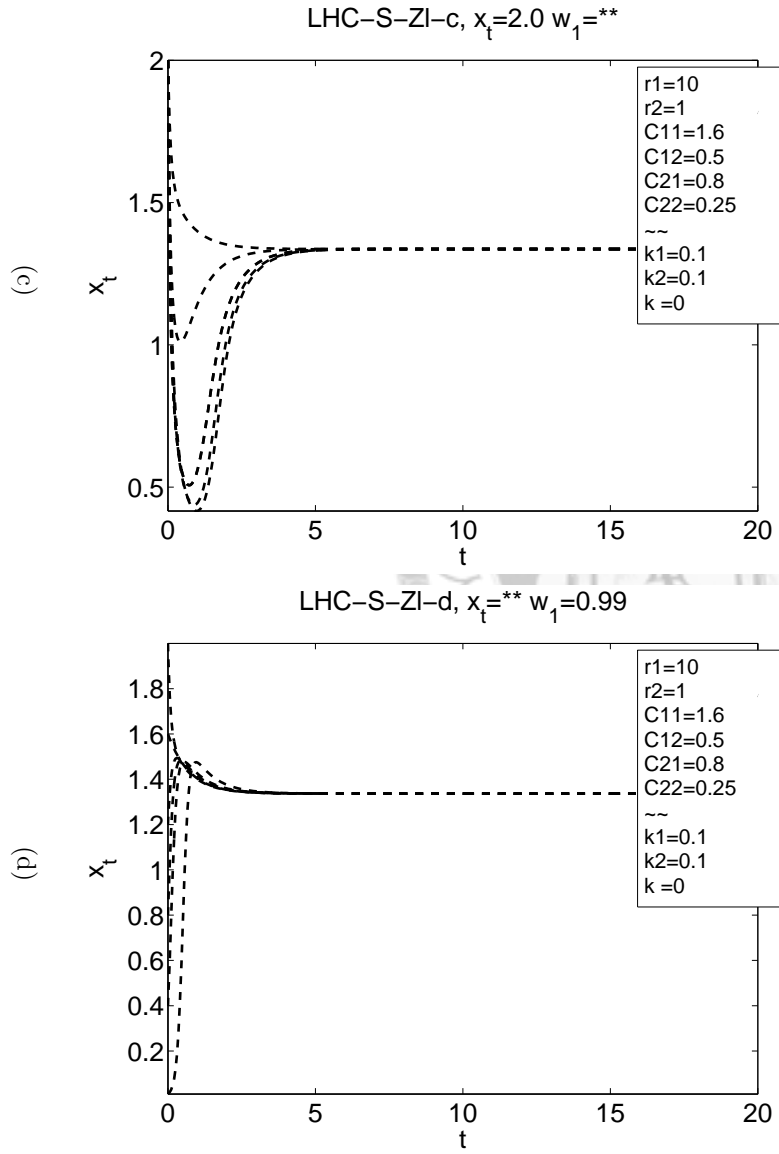
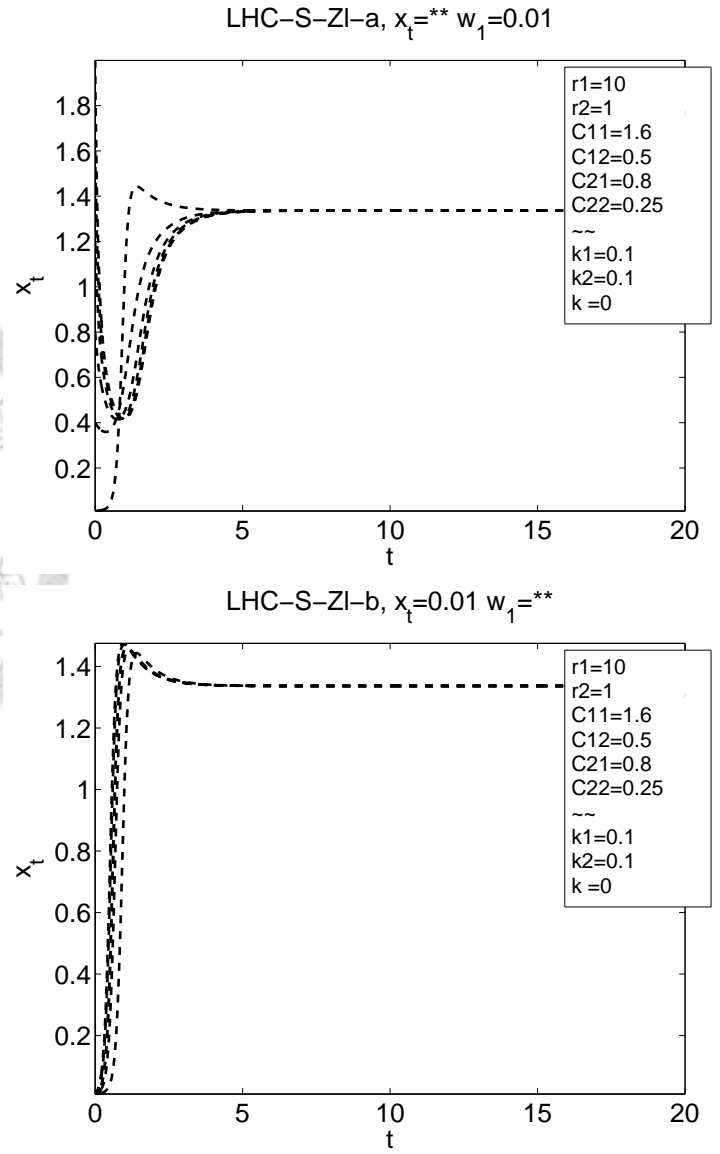


Figure 2.96: The $x_{tot}-w_1$ trajectories of LHC-S-ZI.

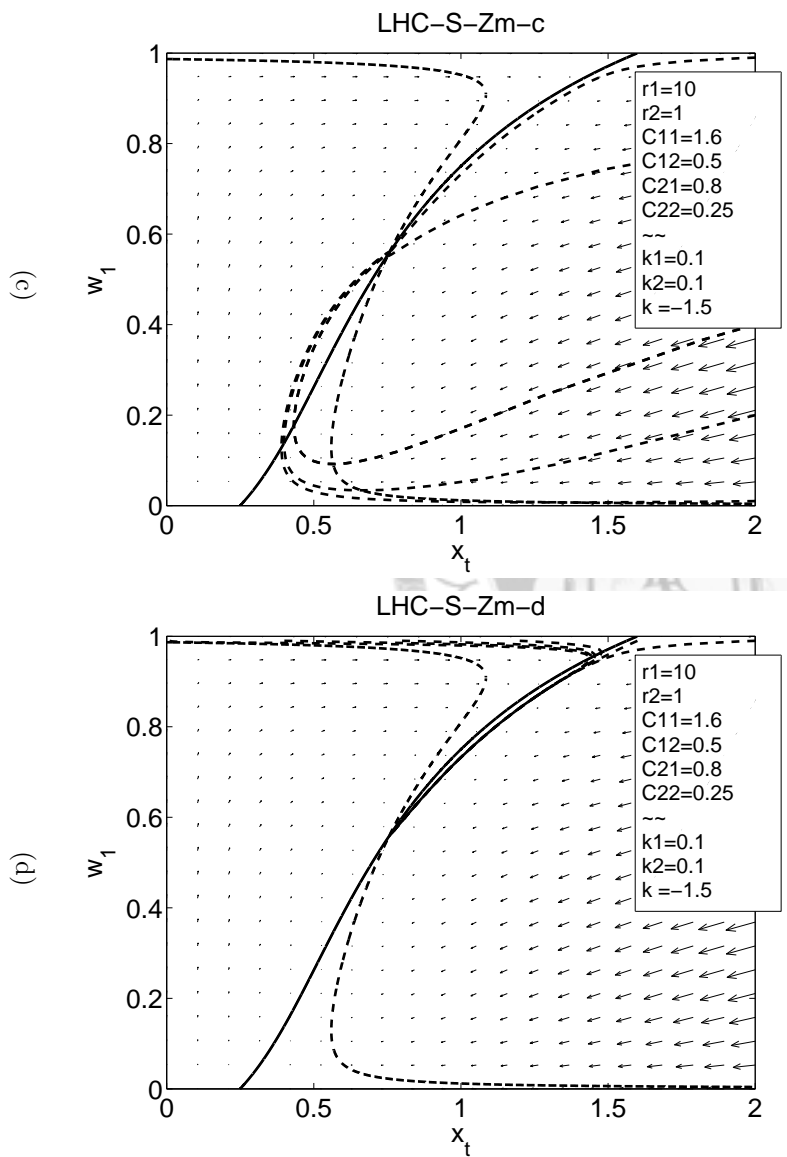
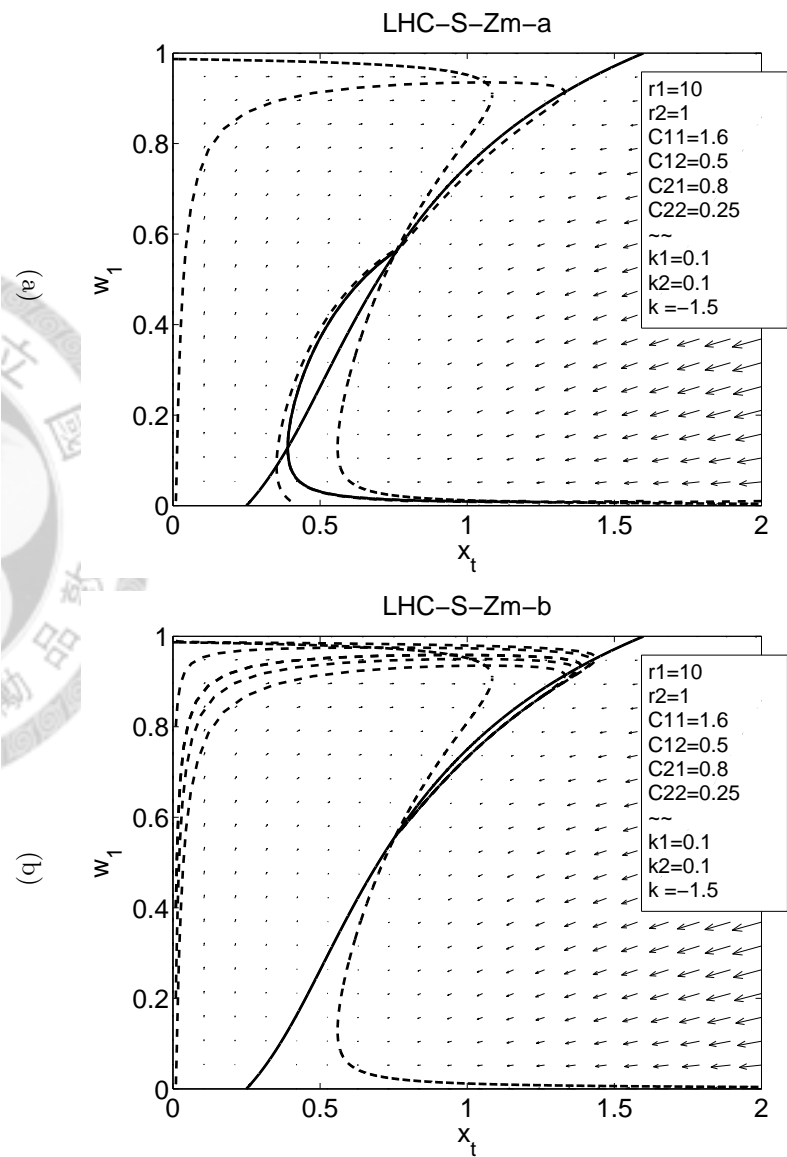


Figure 2.97: The x_{tot} - w_1 trajectories of LHC-S-Zm.

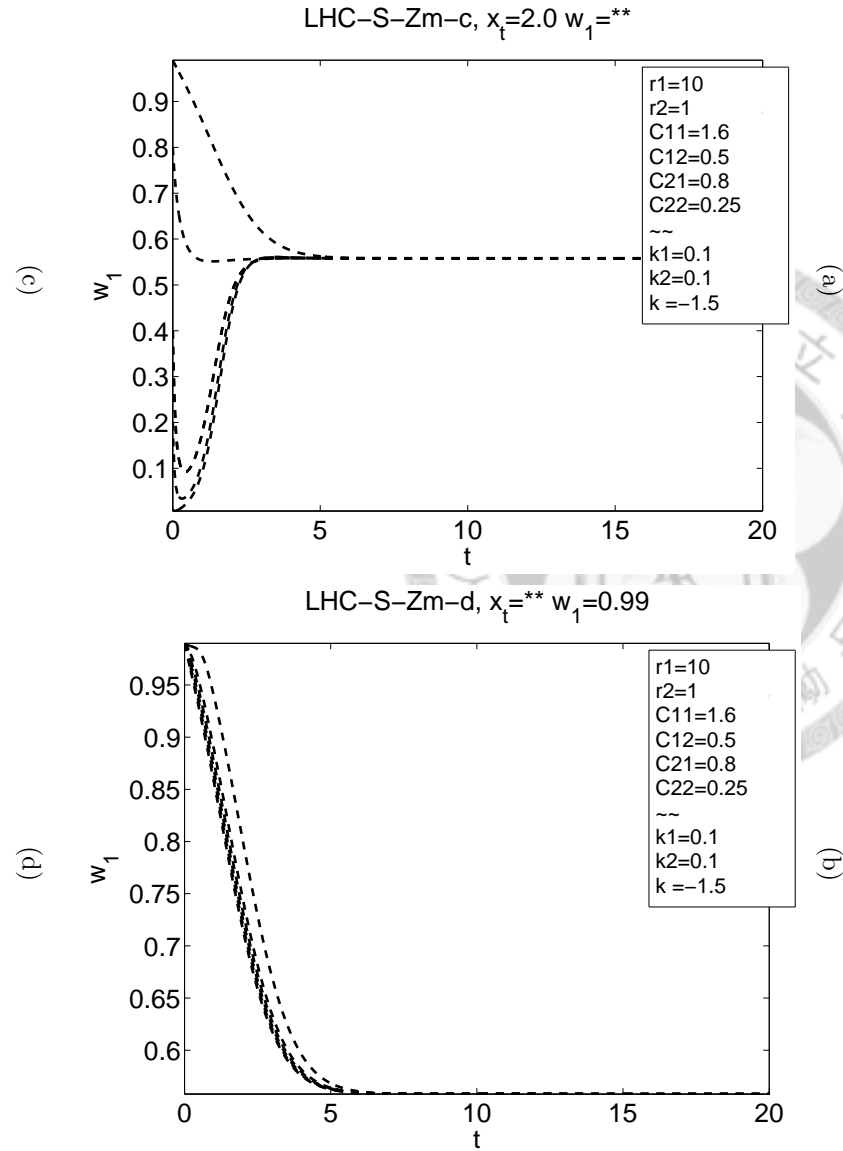
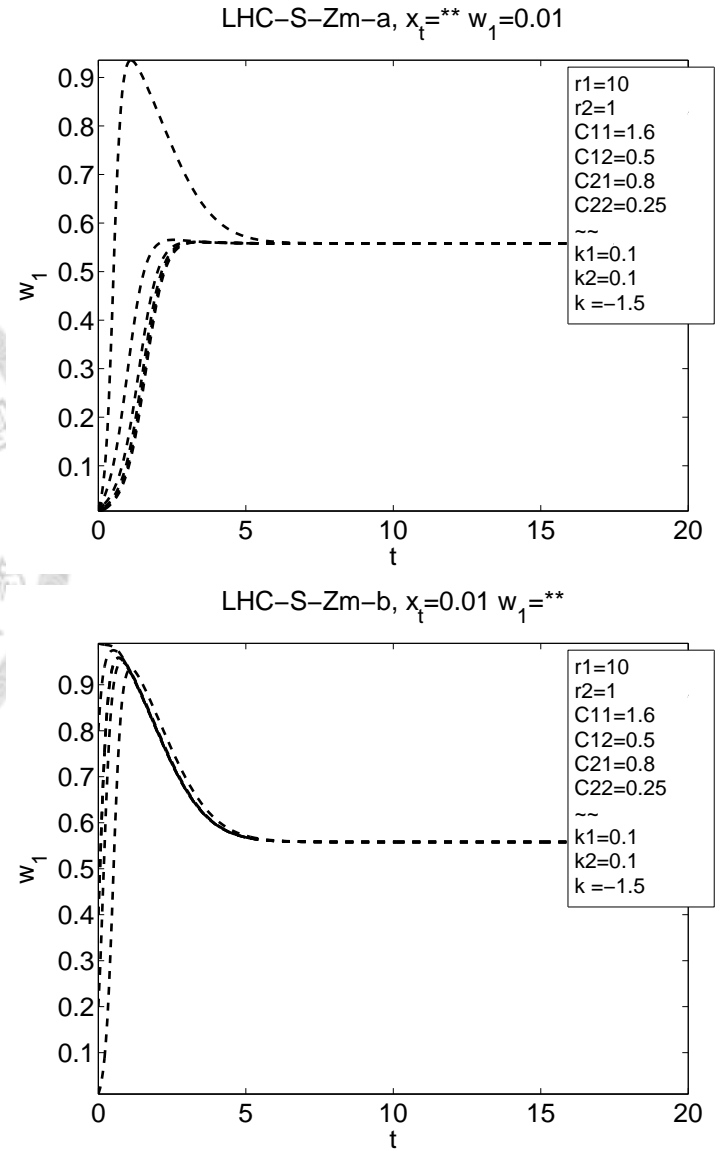


Figure 2.98: The x_{tot} - w_1 trajectories of LHC-S-Zm.

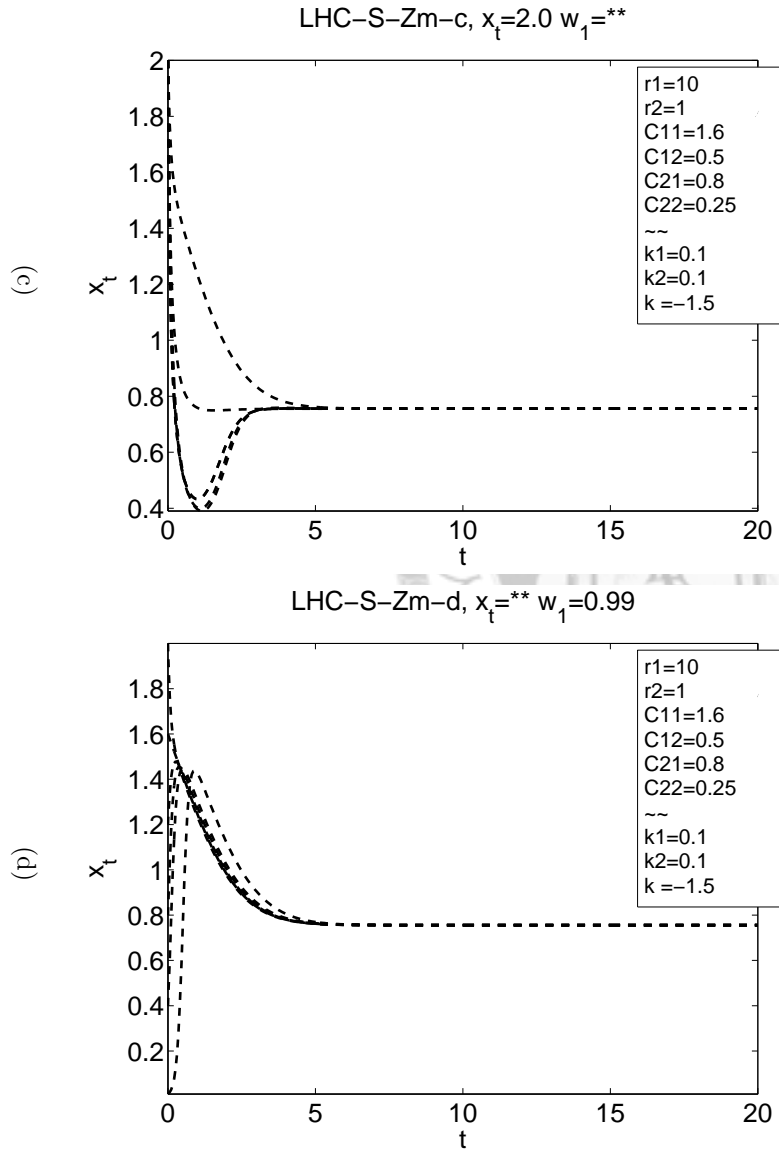
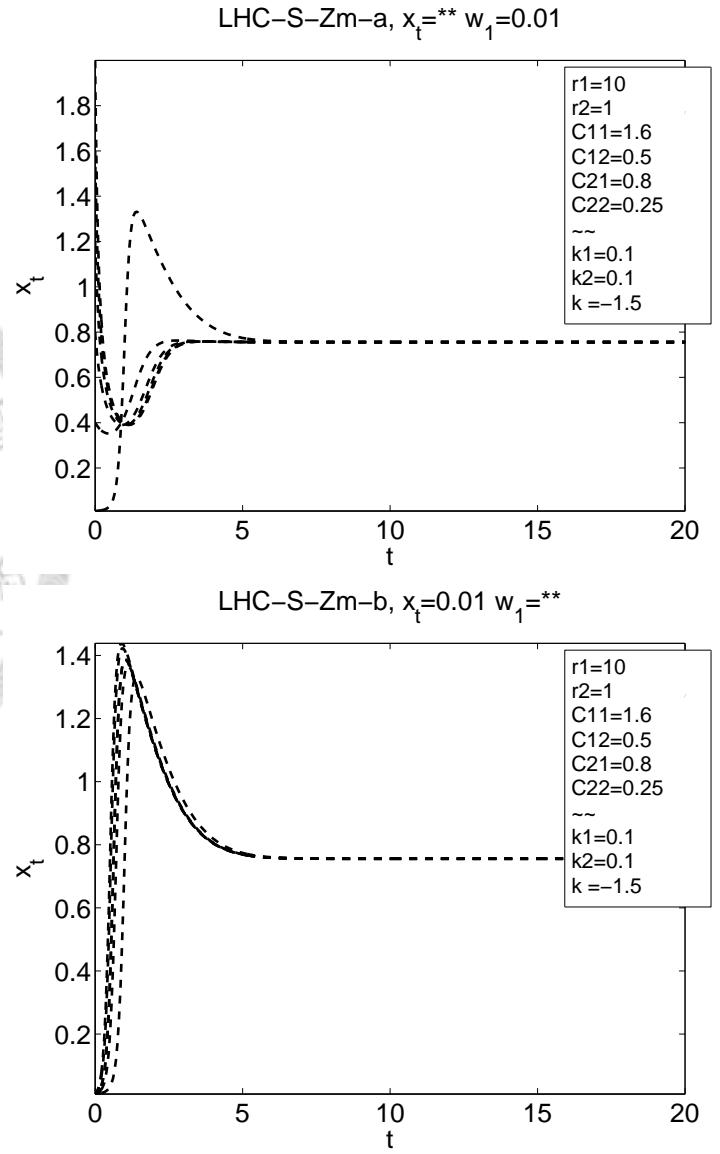


Figure 2.99: The $x_{tot}-w_1$ trajectories of LHC-S-Zm.

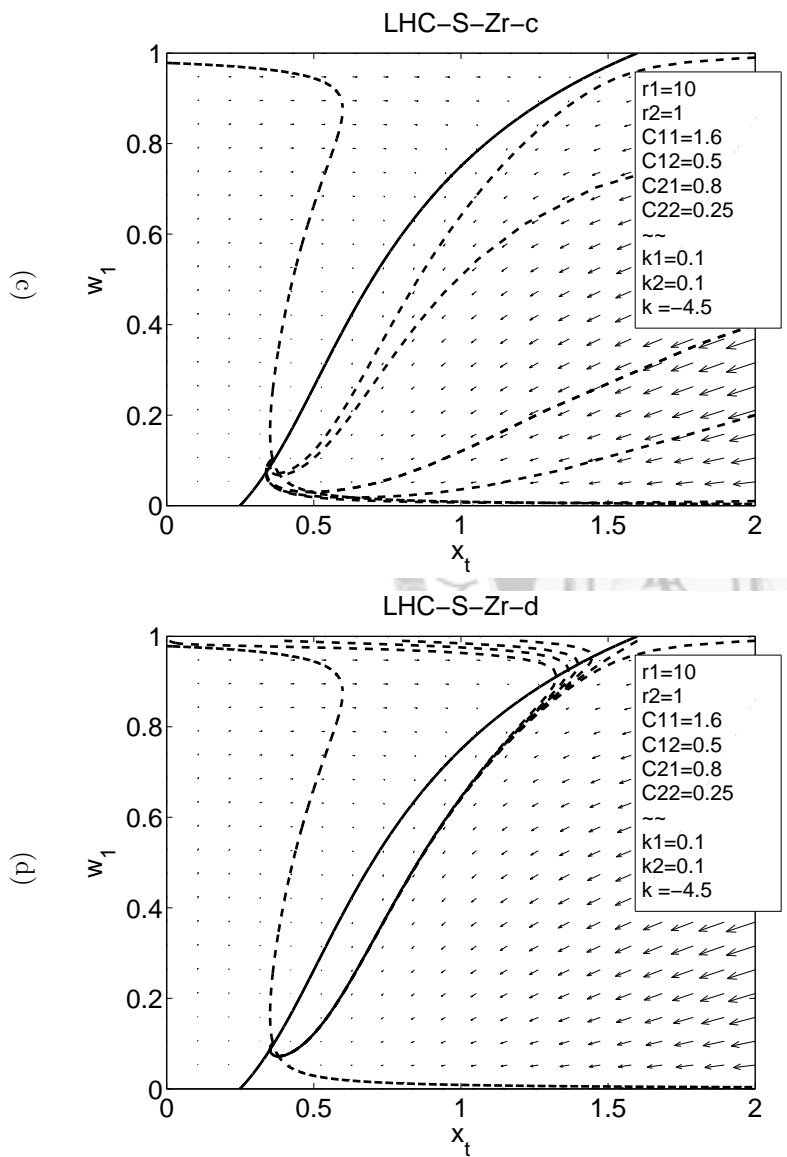
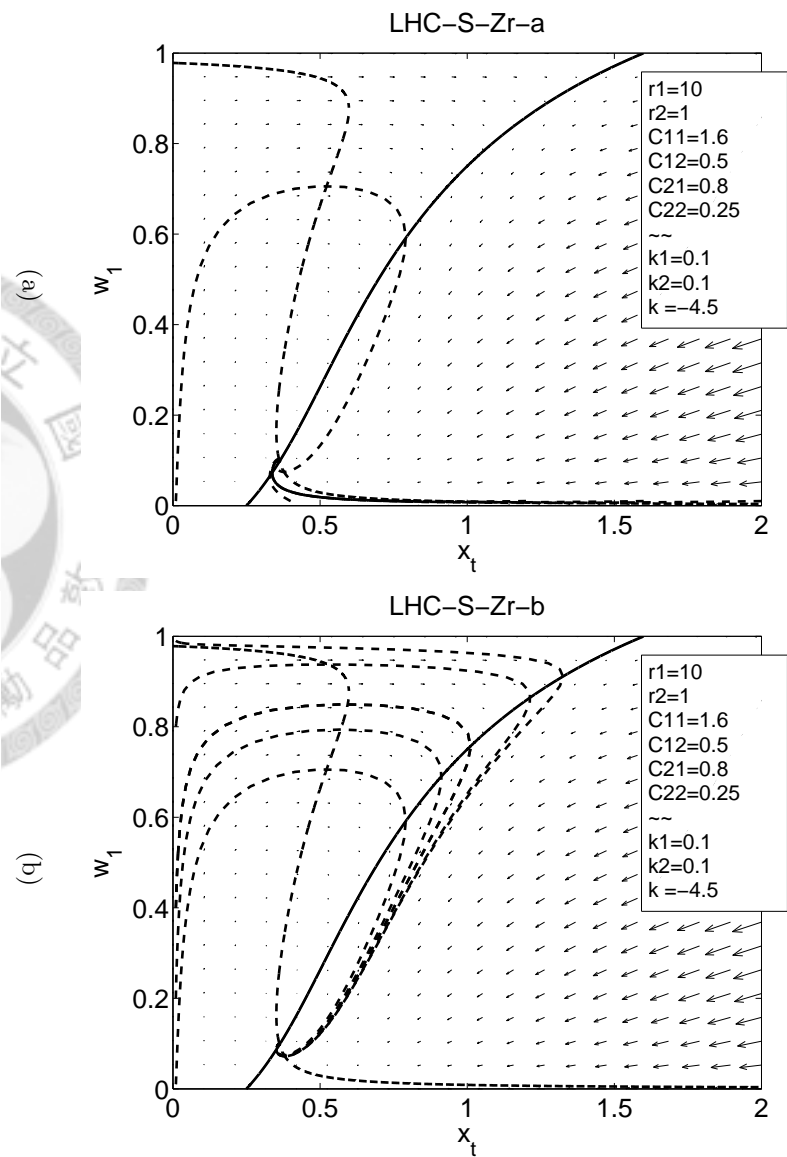


Figure 2.100: The x_{tot} - w_1 trajectories of LHC-S-Zr.

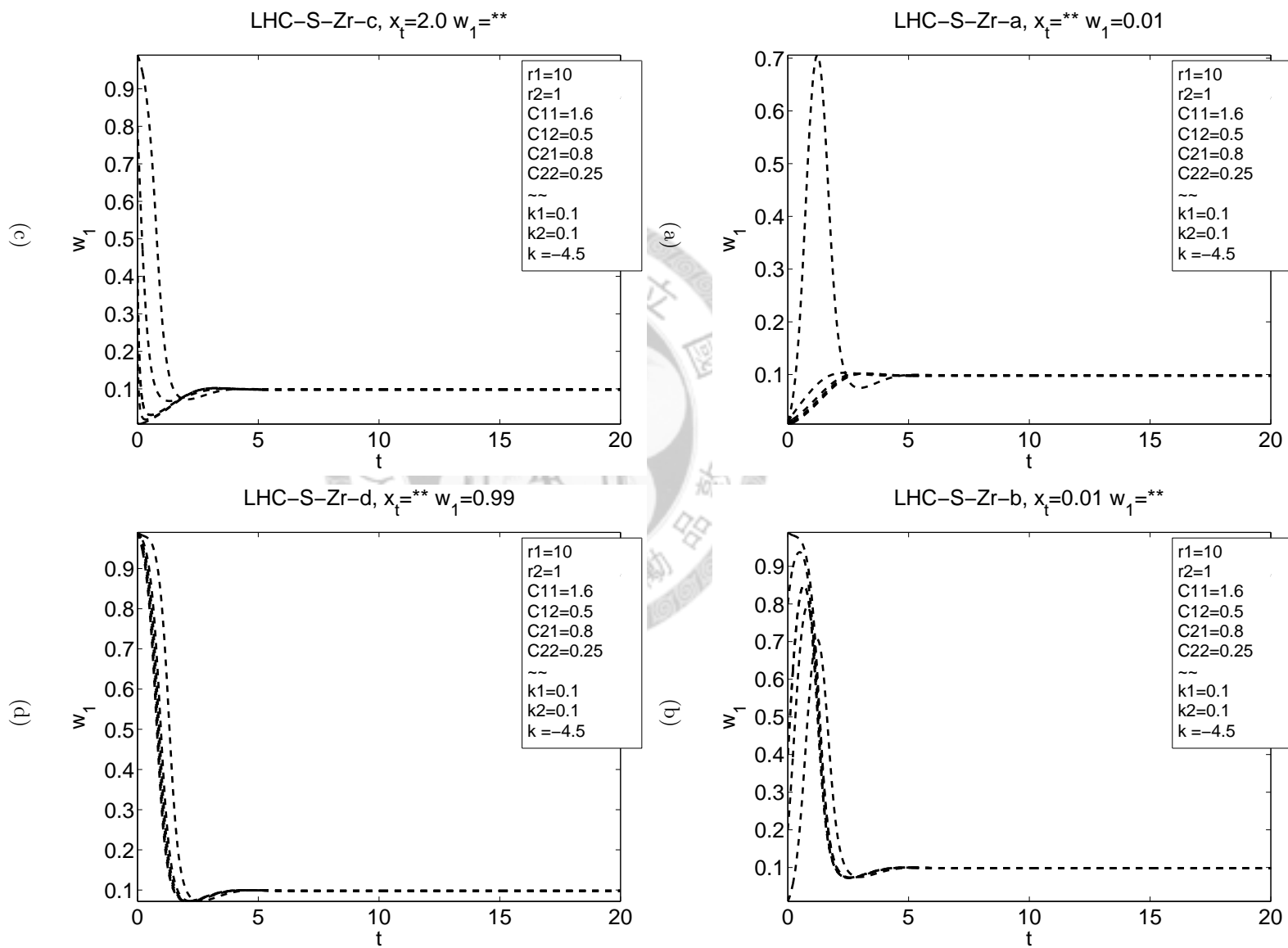


Figure 2.101: The x_{tot} - w_1 trajectories of LHC-S-Zr.

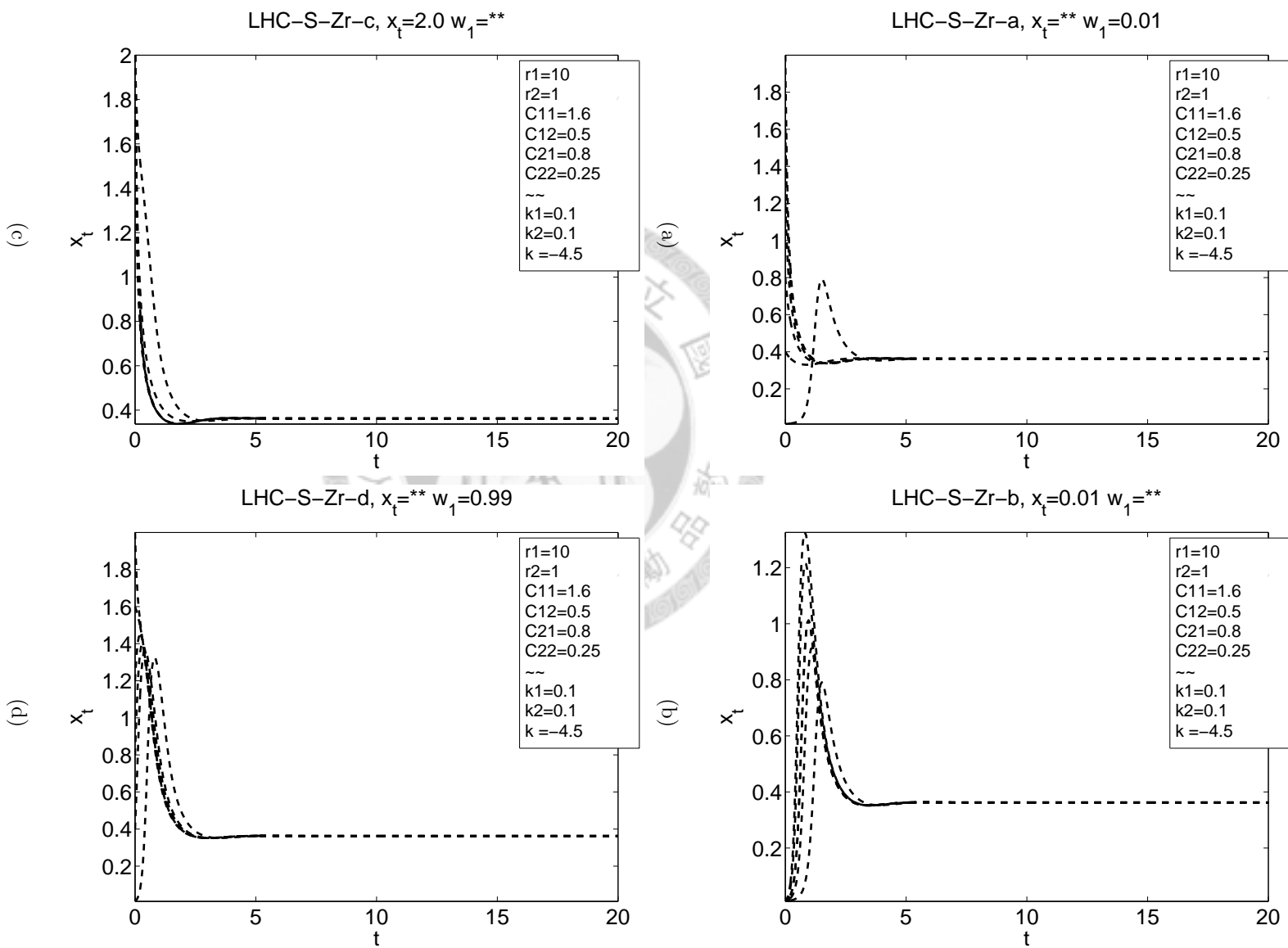


Figure 2.102: The $x_{tot}-w_1$ trajectories of LHC-S-Zr.

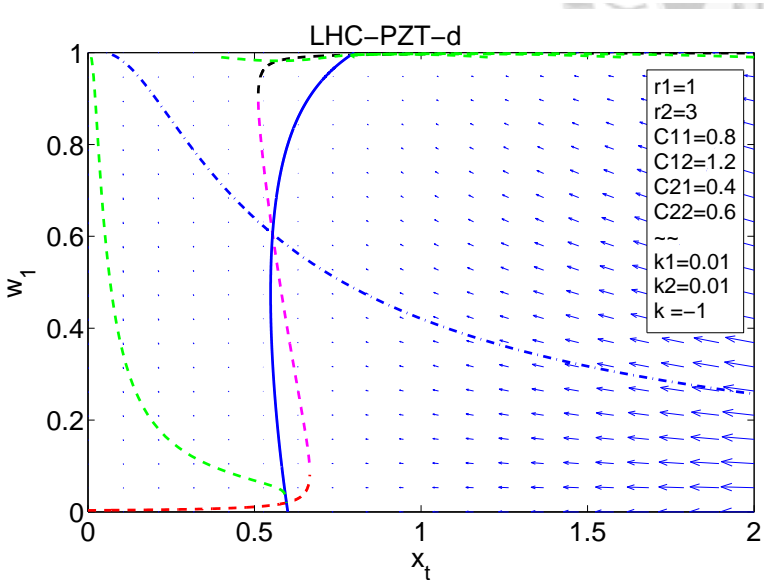
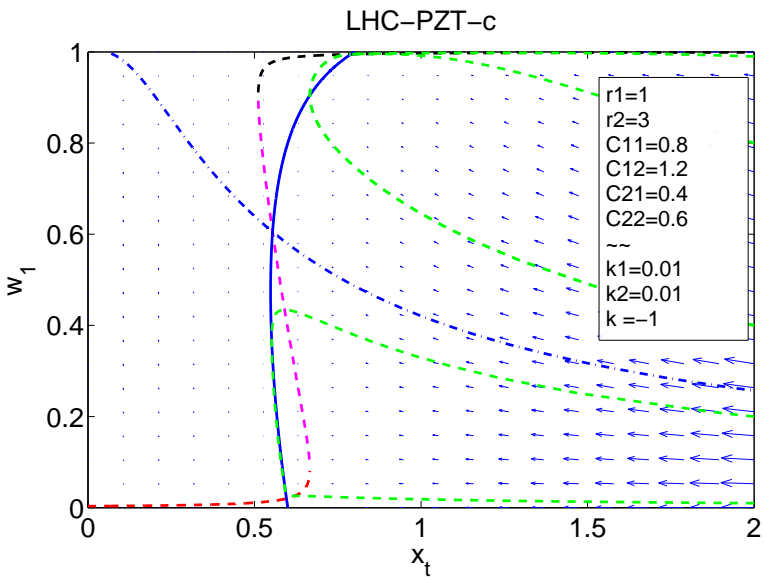
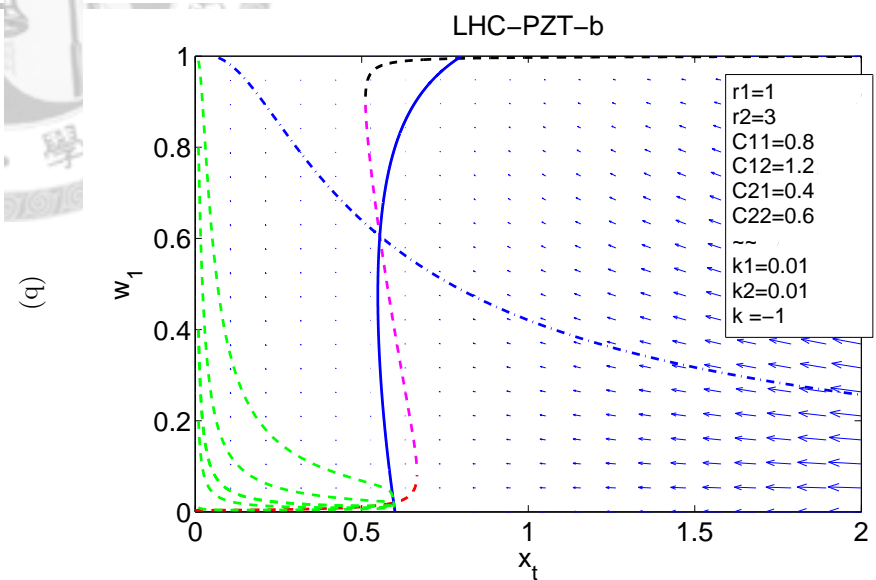
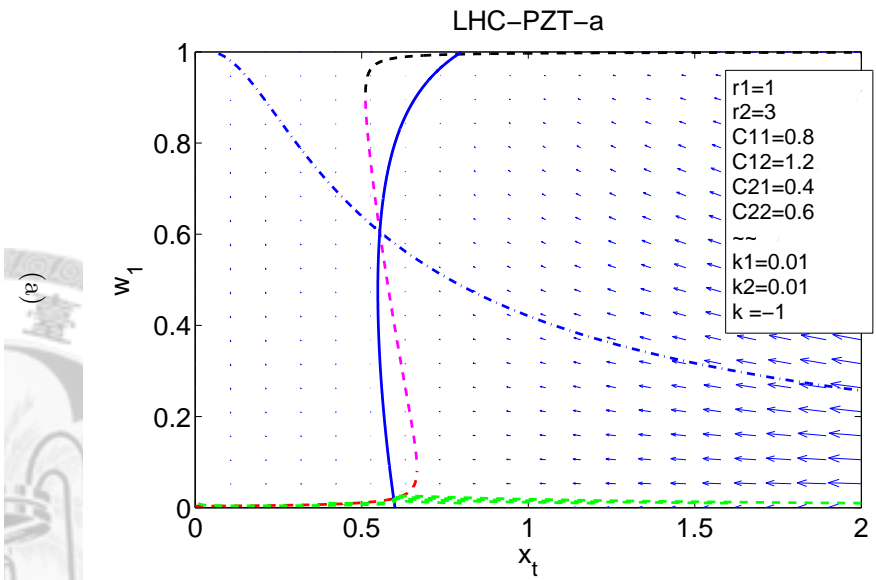
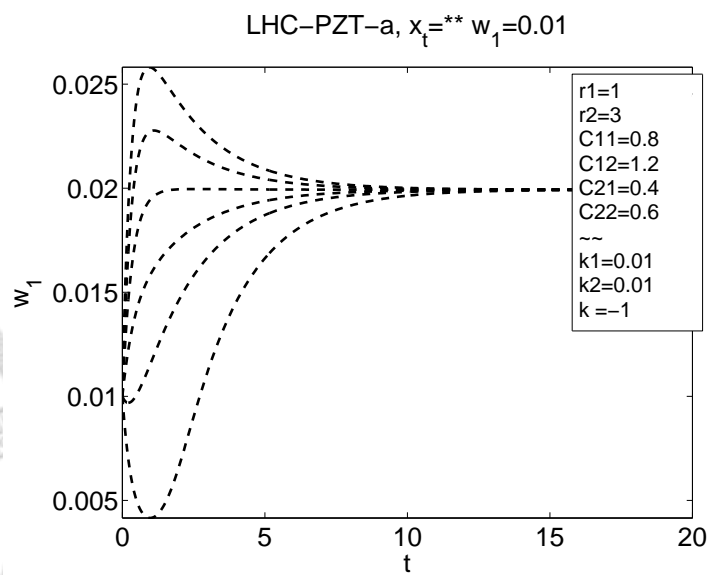


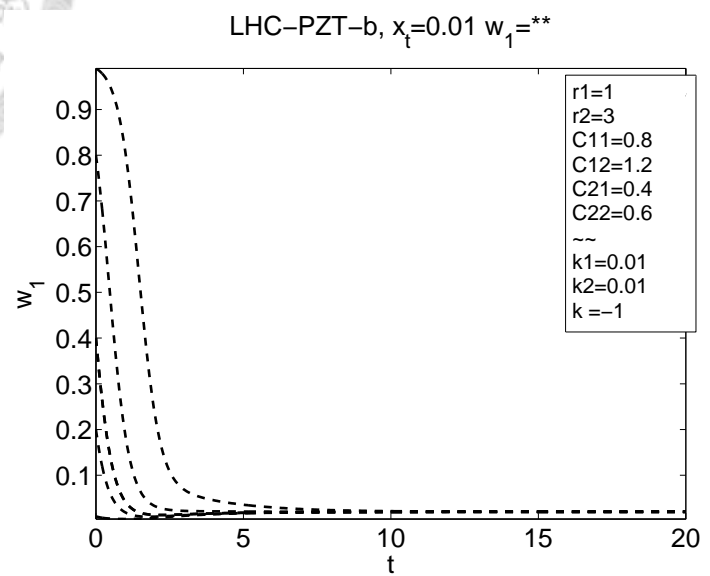
Figure 2.103: The x_{tot} - w_1 trajectories of LHC-PZT.

(c)

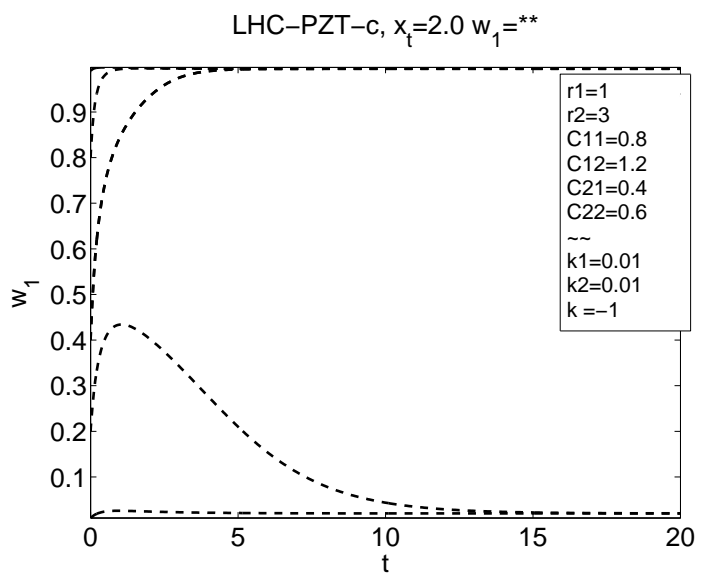
(d)



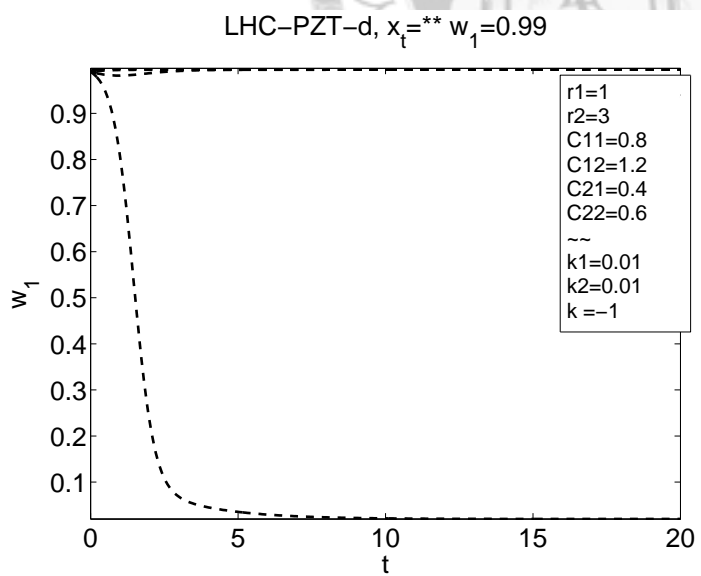
(a)



(b)

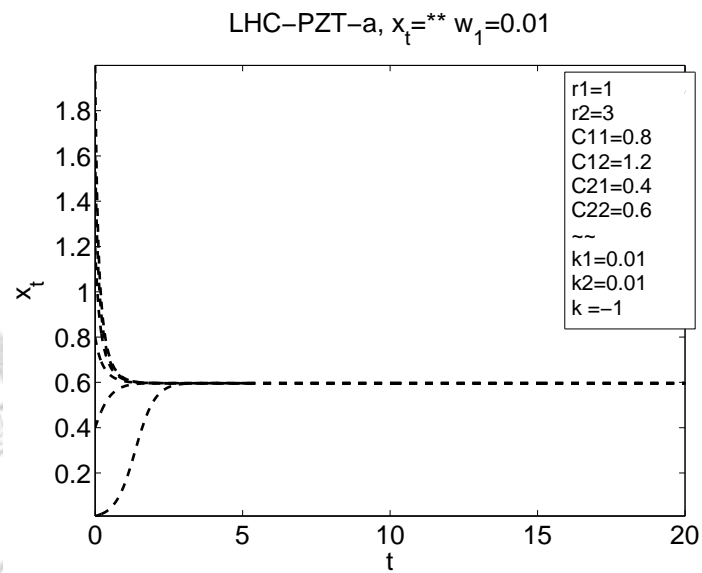


(c)

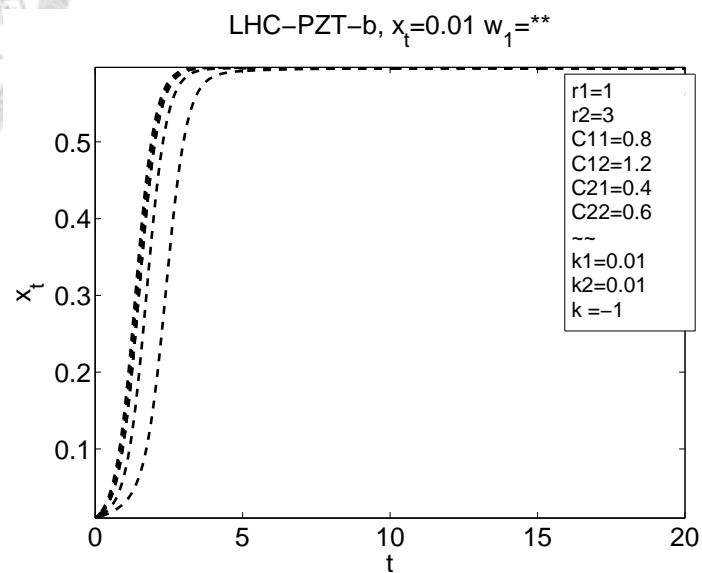


(d)

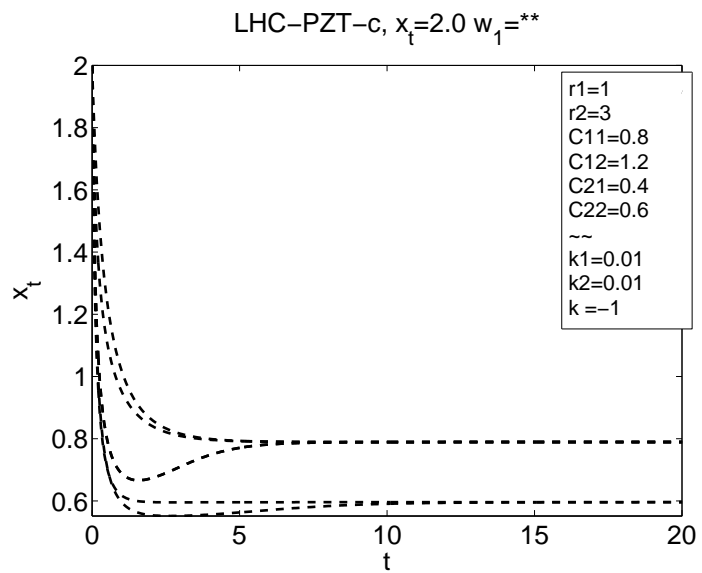
Figure 2.104: The x_{tot} - w_1 trajectories of LHC-PZT.



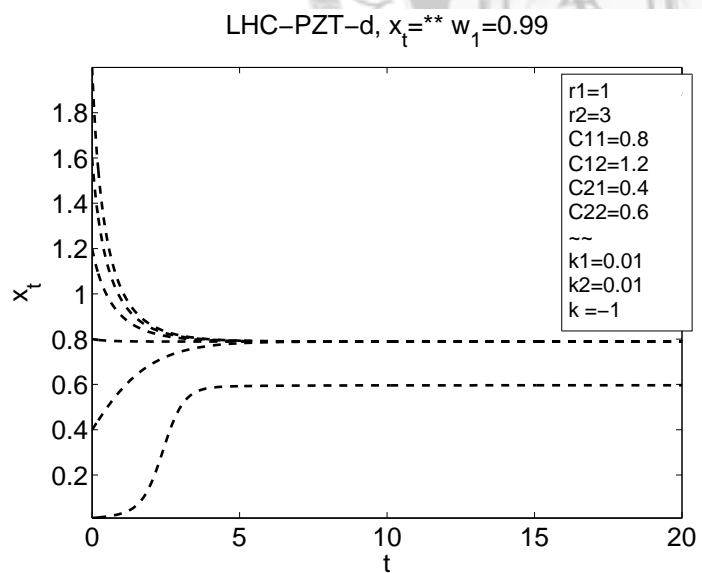
(a)



(b)



(c)



(d)

Figure 2.105: The x_{tot} - w_1 trajectories of LHC-PZT.

(a)

(b)

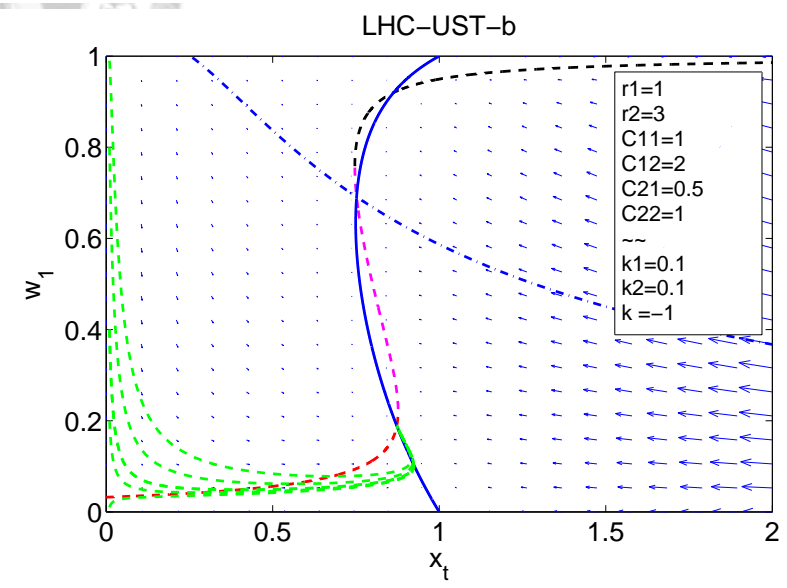
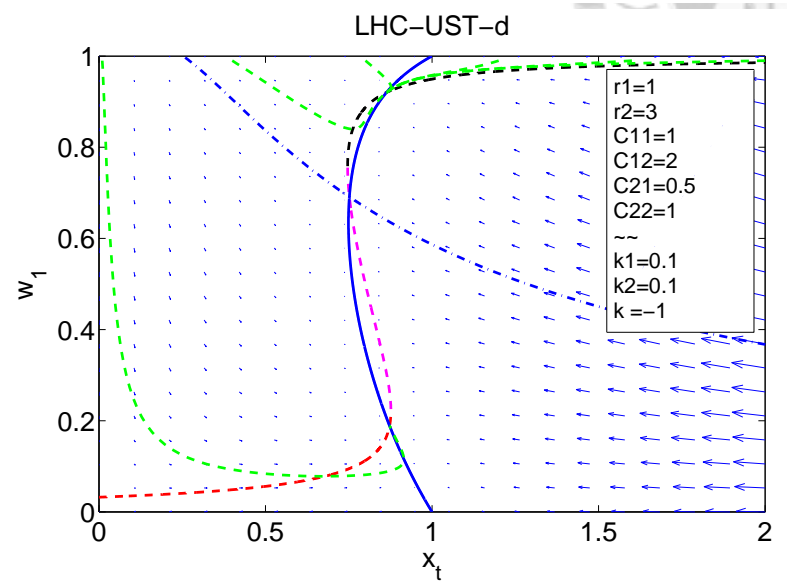
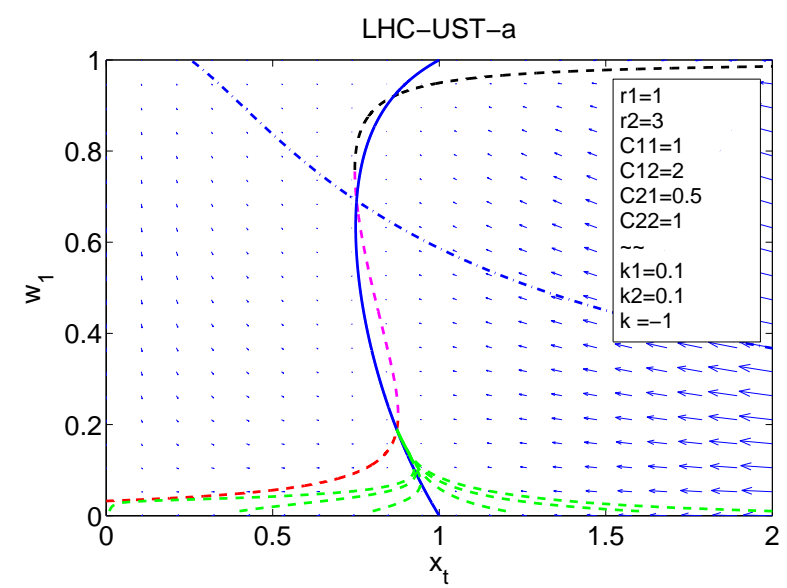
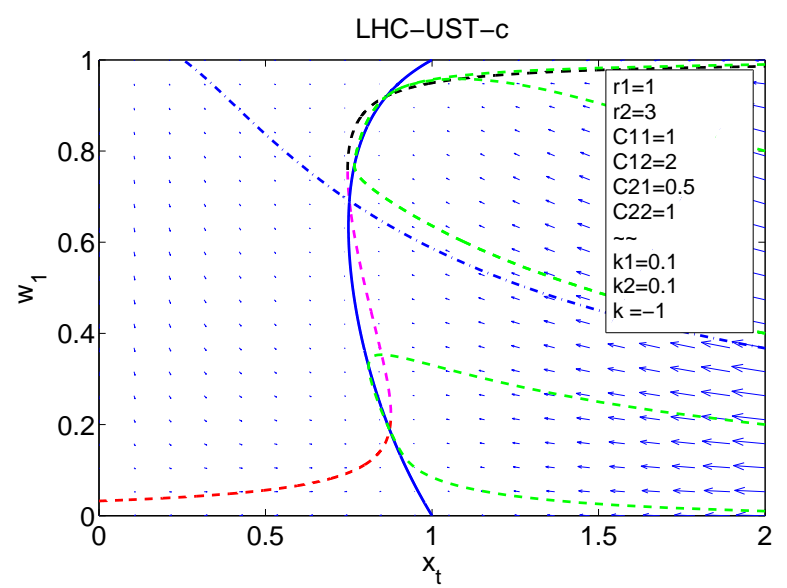


Figure 2.106: The x_{tot} - w_1 trajectories of LHC-UST.

(c)

(d)

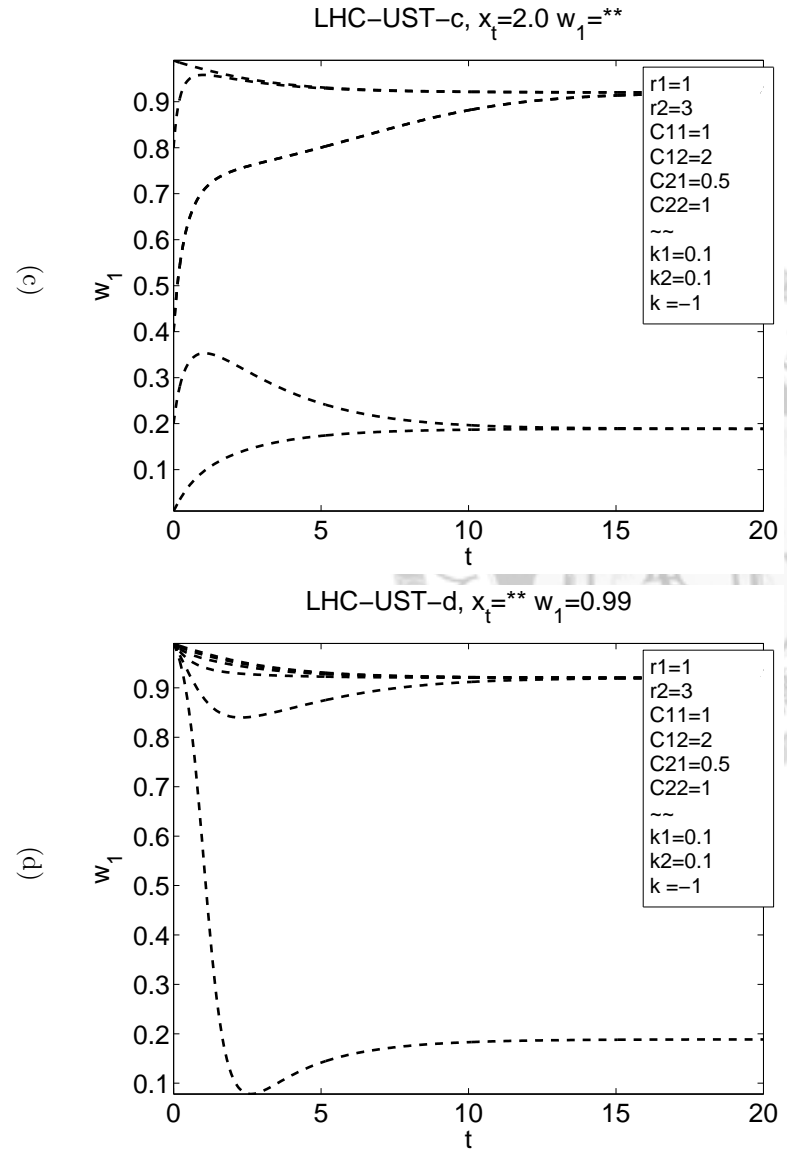
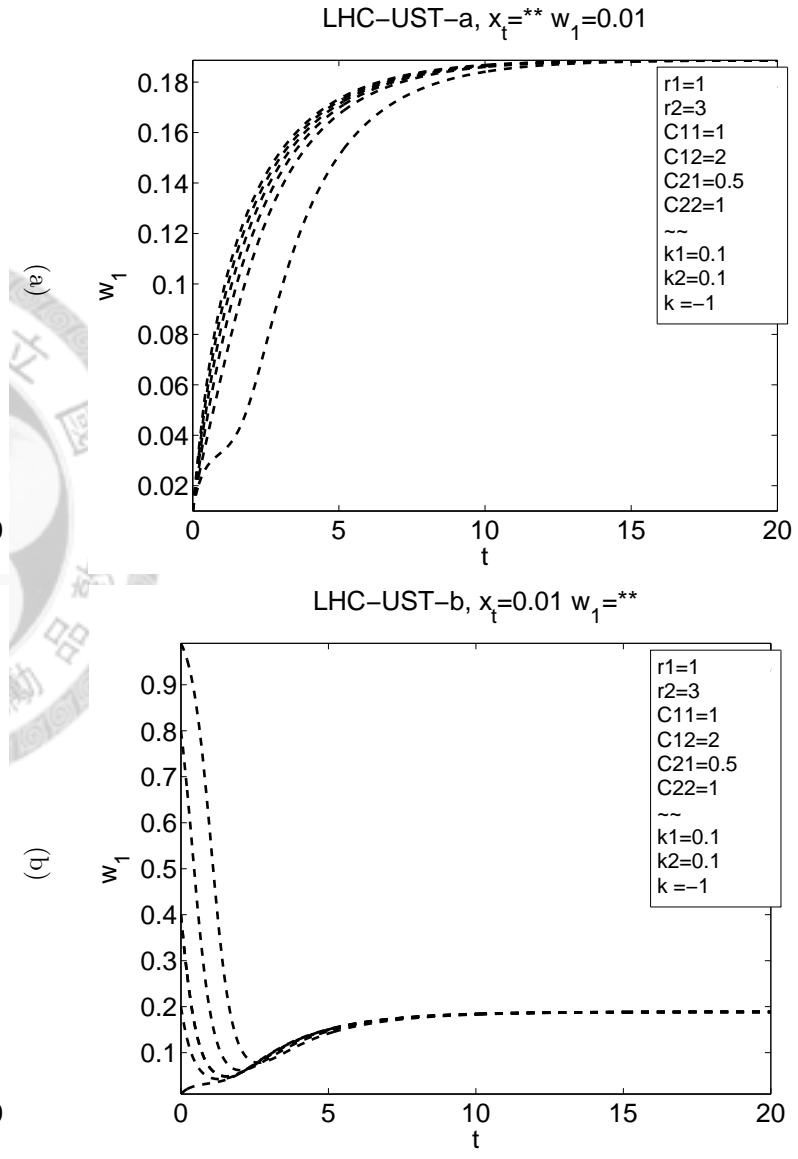
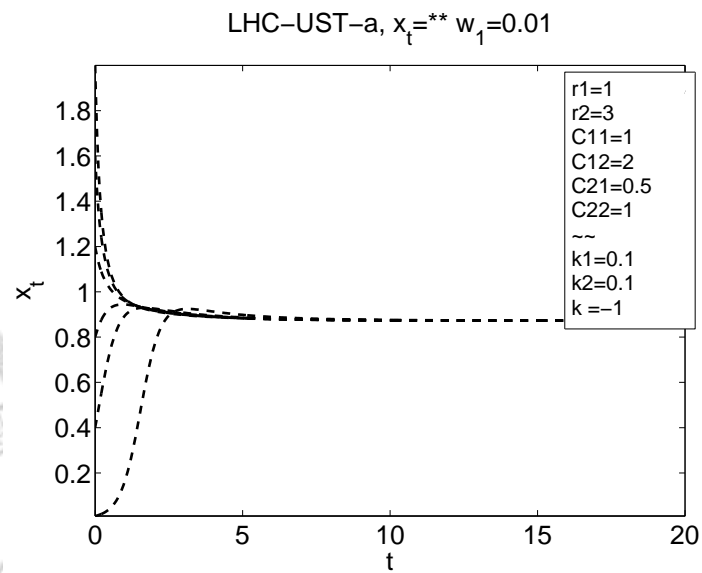
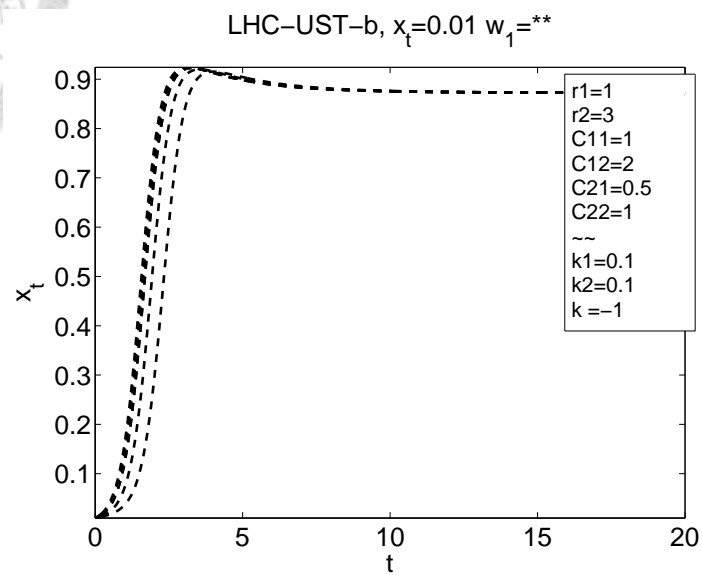


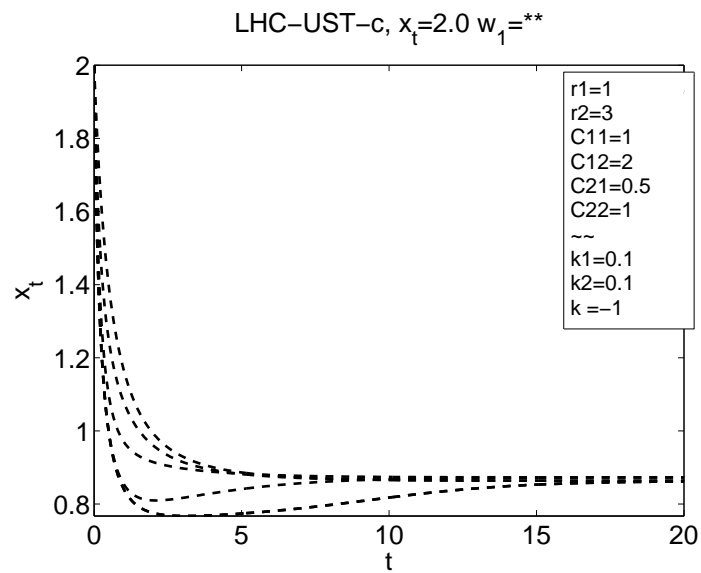
Figure 2.107: The x_{tot} - w_1 trajectories of LHC-UST.



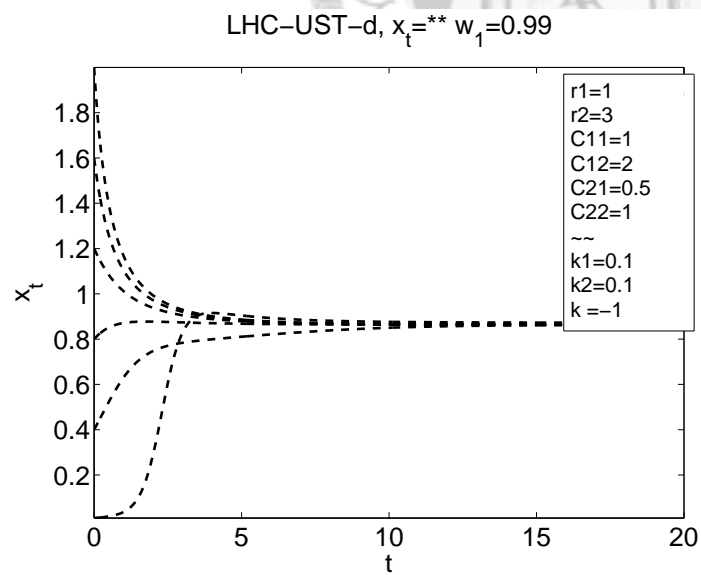
(a)



(b)



(c)



(d)

Figure 2.108: The x_{tot} - w_1 trajectories of LHC-UST.

B.5 The phase portraits of LH-D

In LH-D, the new type of \tilde{w}_1 is SC type, CS type, and S band type. But S band type is similar to S type. Here we show four examples of SC and CS type for \tilde{w}_1 . They are LHD-SCT, LHD-SCL, LHD-SCLnc, LHD-CST, and LHD-CSL.



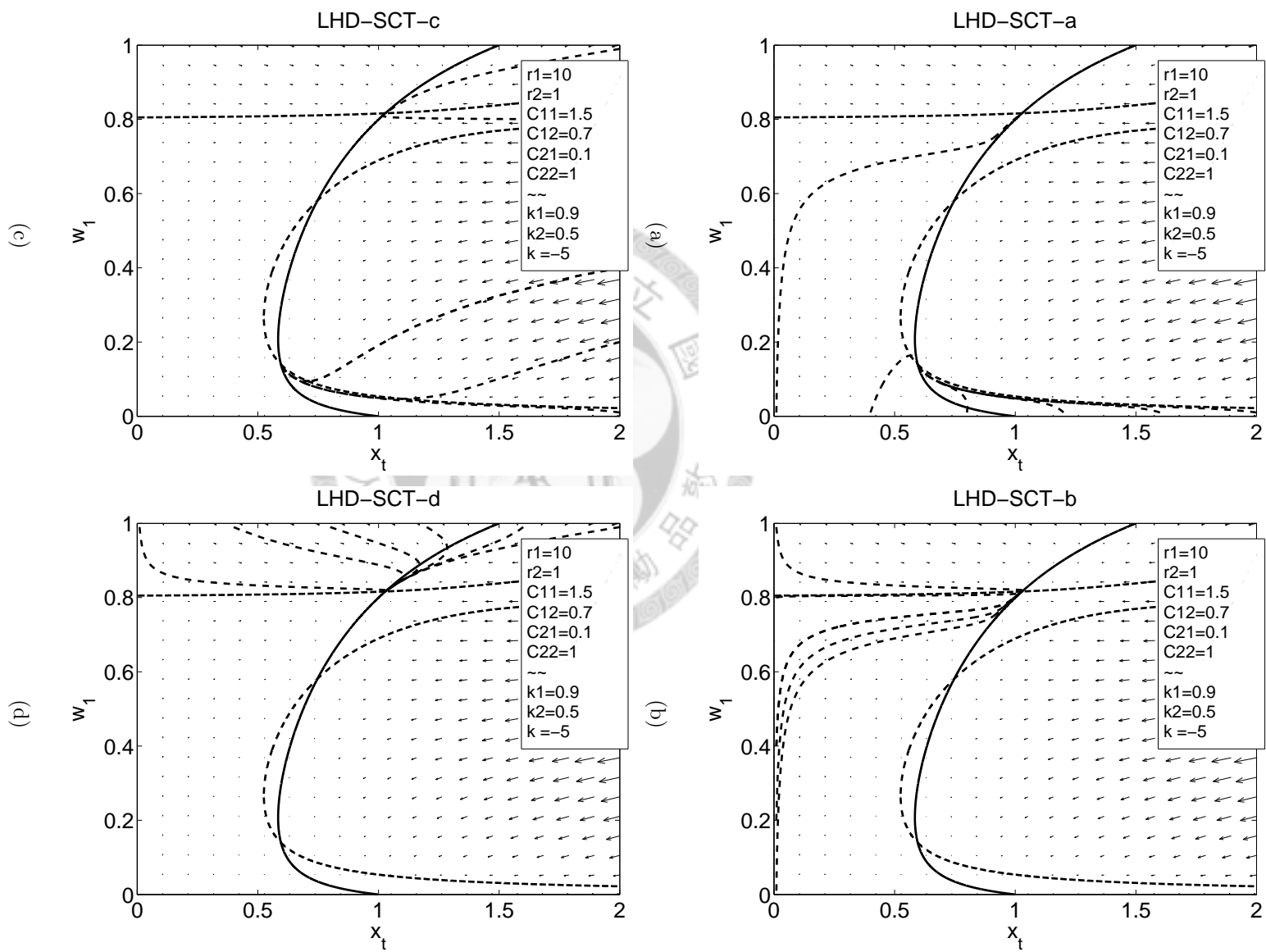


Figure 2.109: The x_{tot} - w_1 trajectories of LHD-SCT.

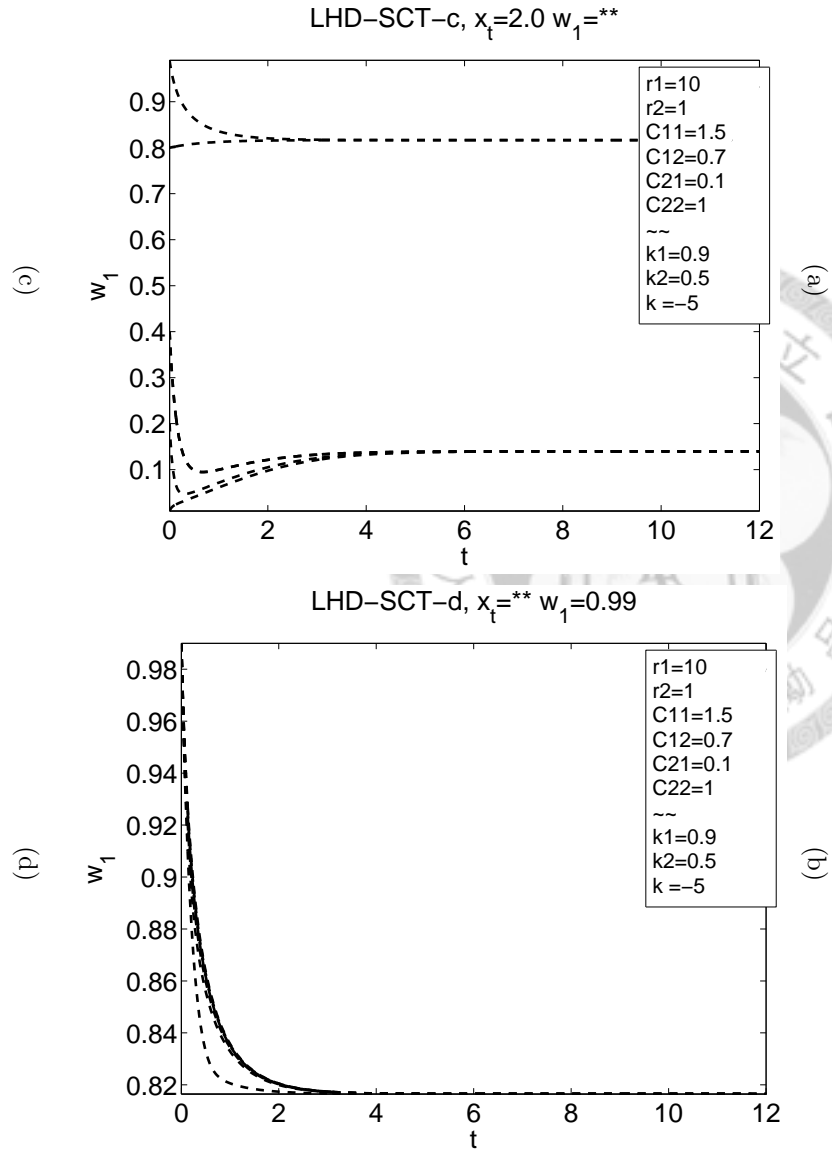
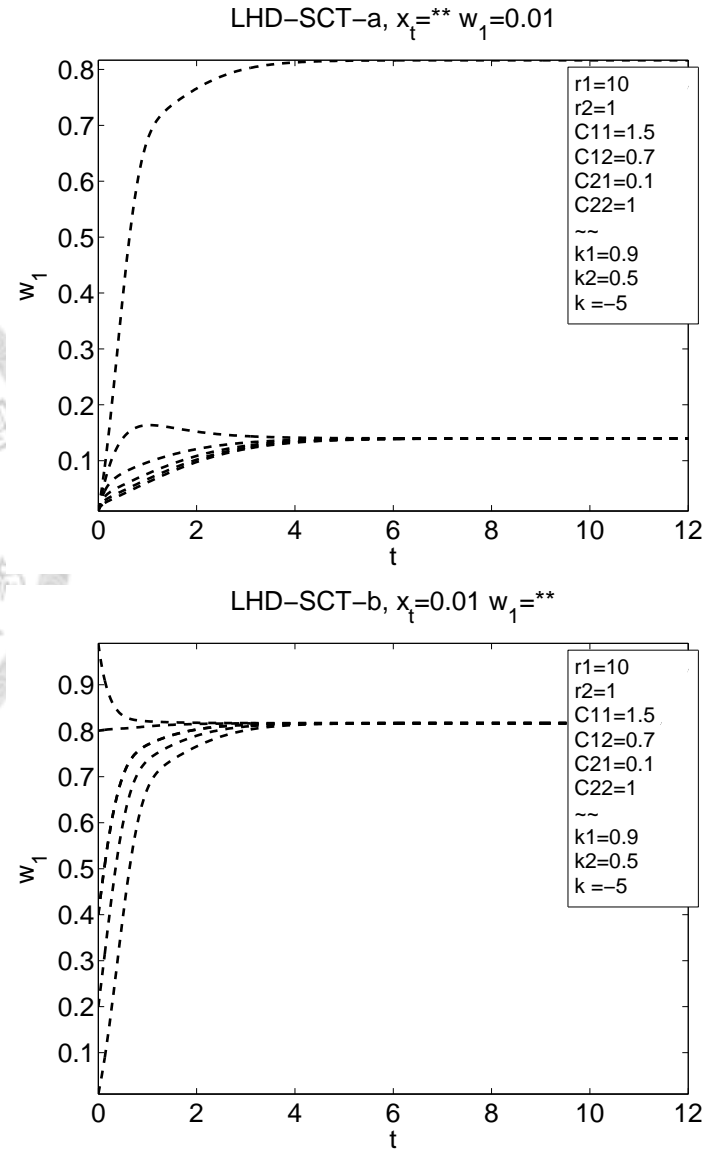
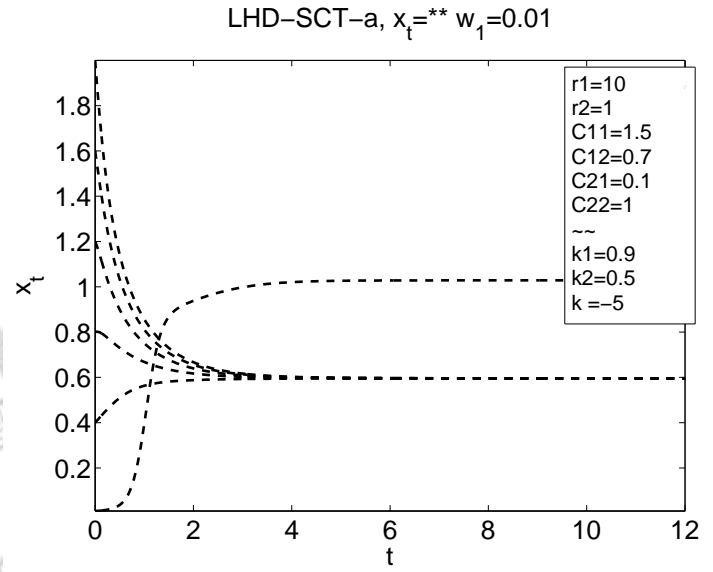
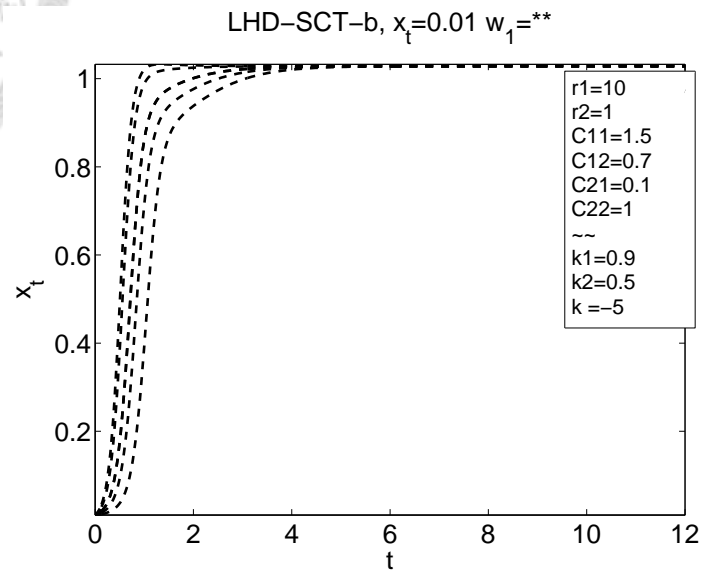


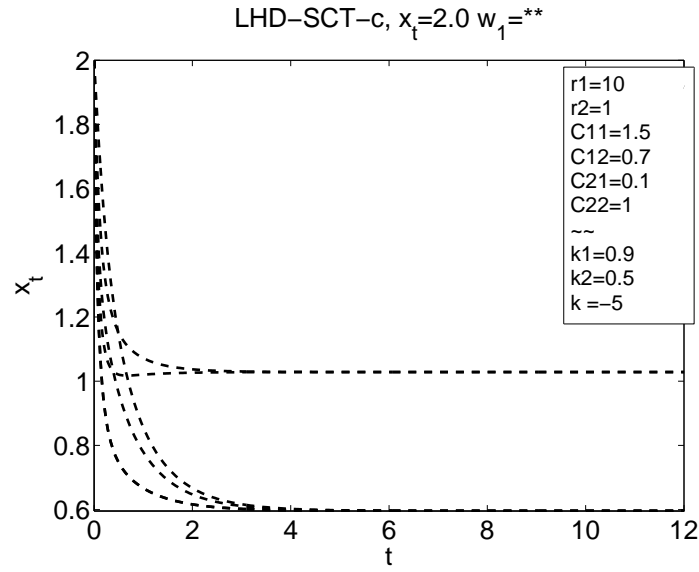
Figure 2.110: The x_{tot} - w_1 trajectories of LHD-SCT.



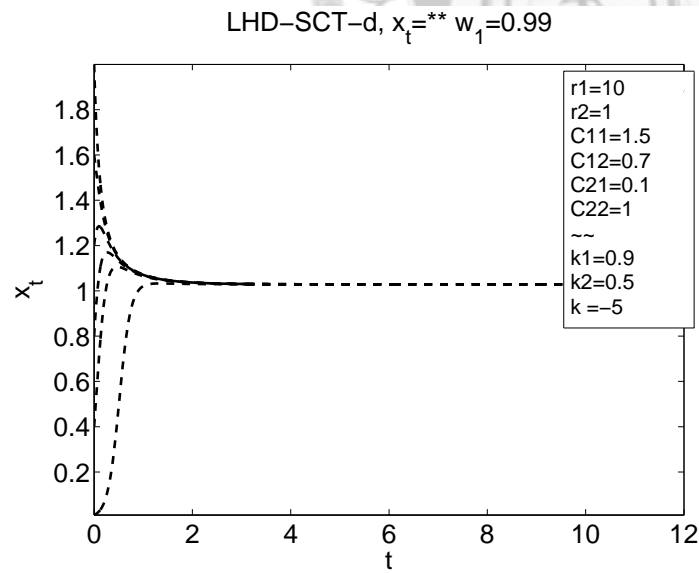
(a)



(b)



(c)



(d)

Figure 2.111: The x_{tot} - w_1 trajectories of LHD-SCT.

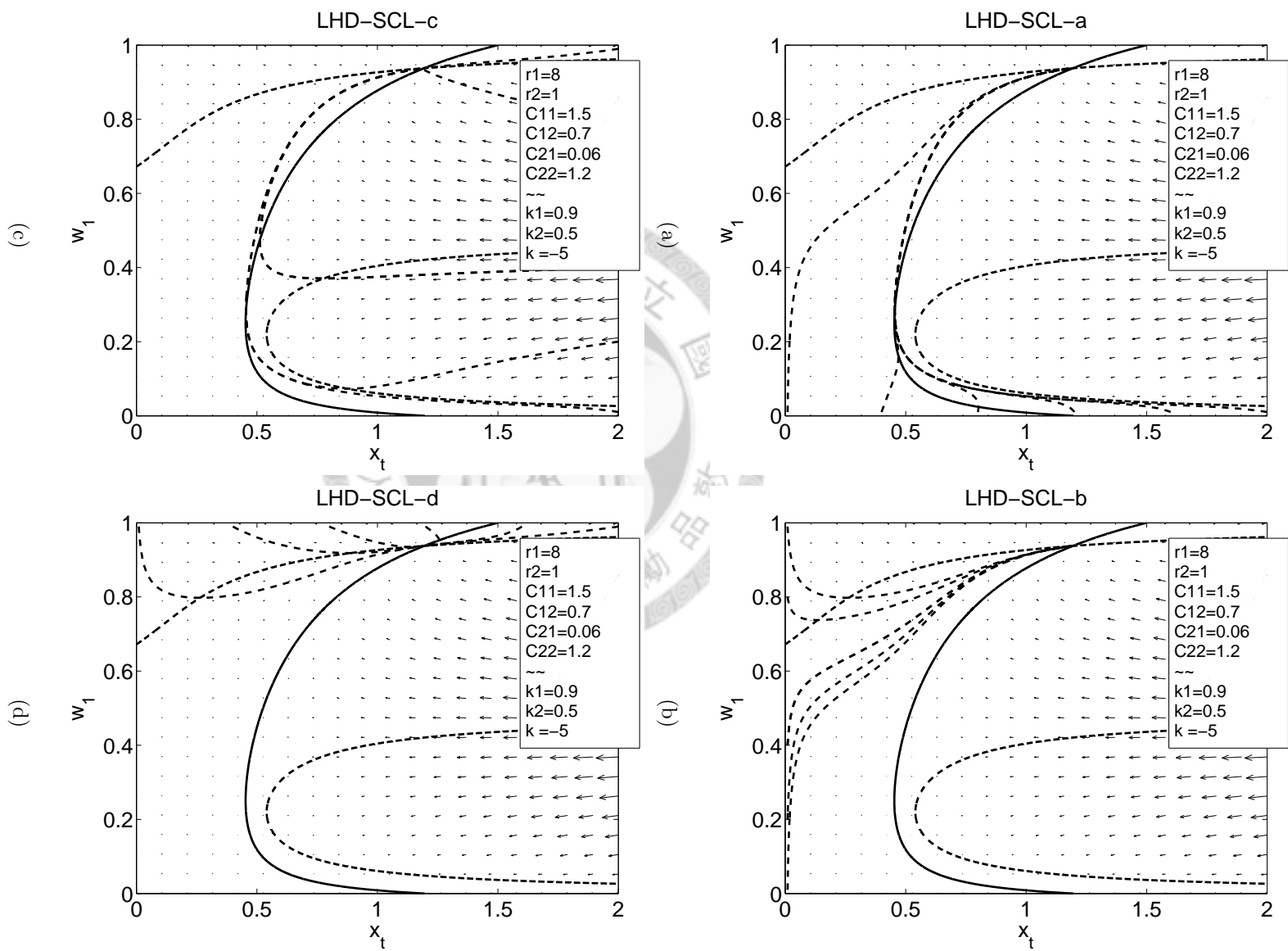


Figure 2.112: The x_{tot} - w_1 trajectories of LHD-SCL.

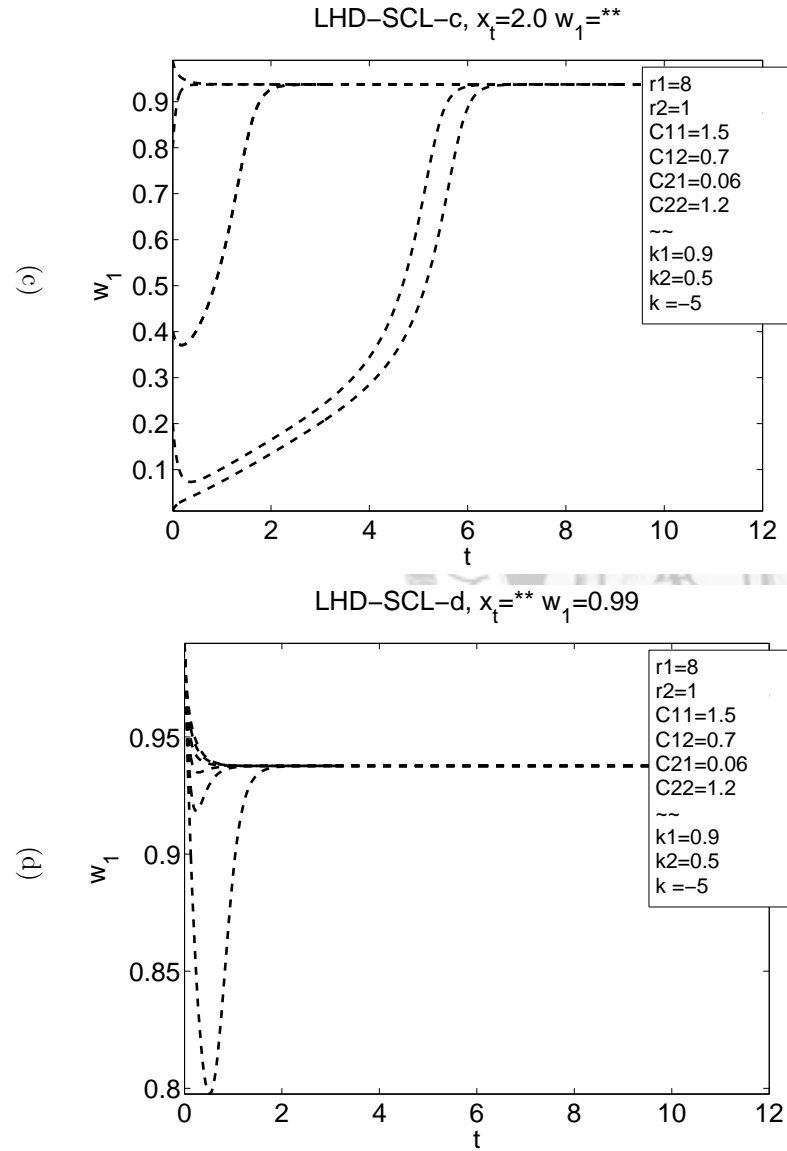
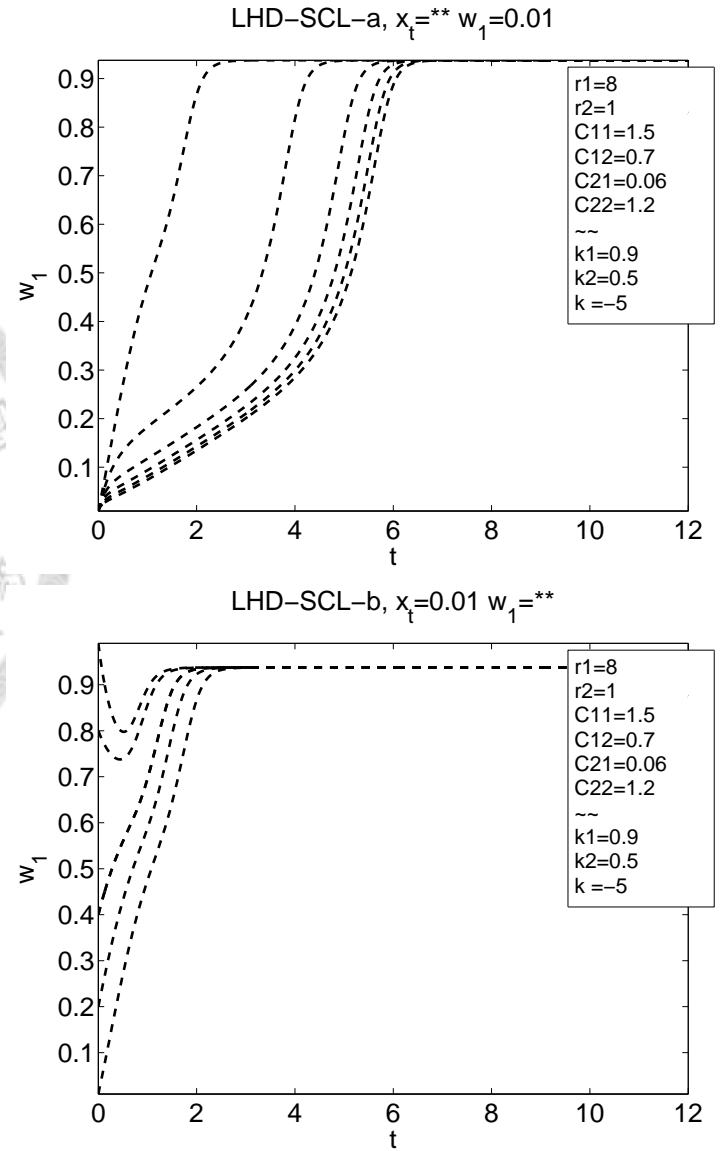


Figure 2.113: The x_{tot} - w_1 trajectories of LHD-SCL.

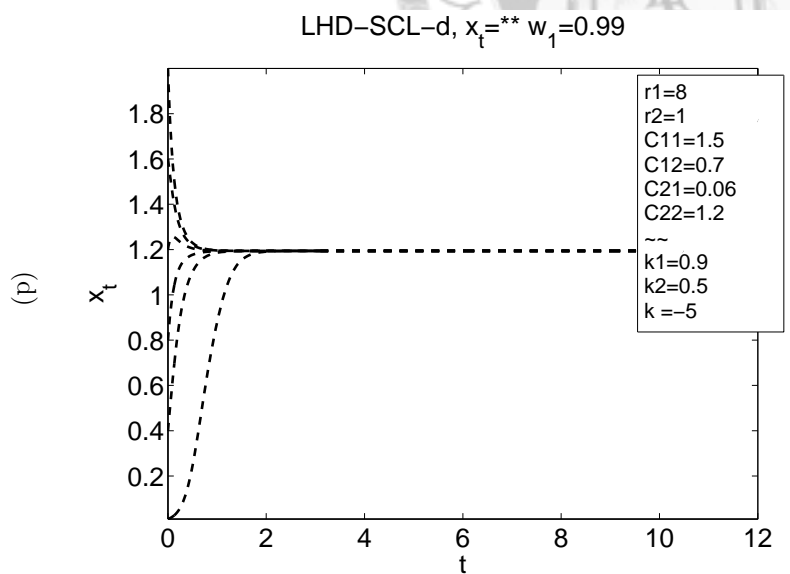
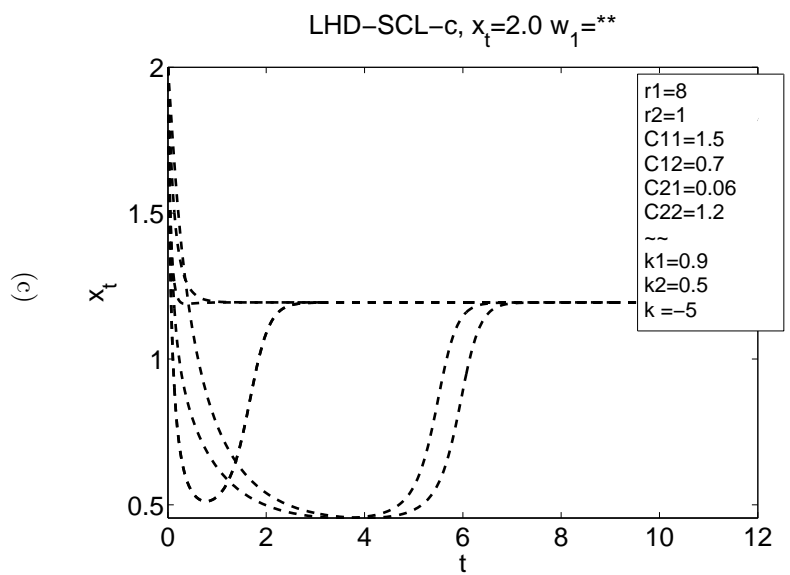
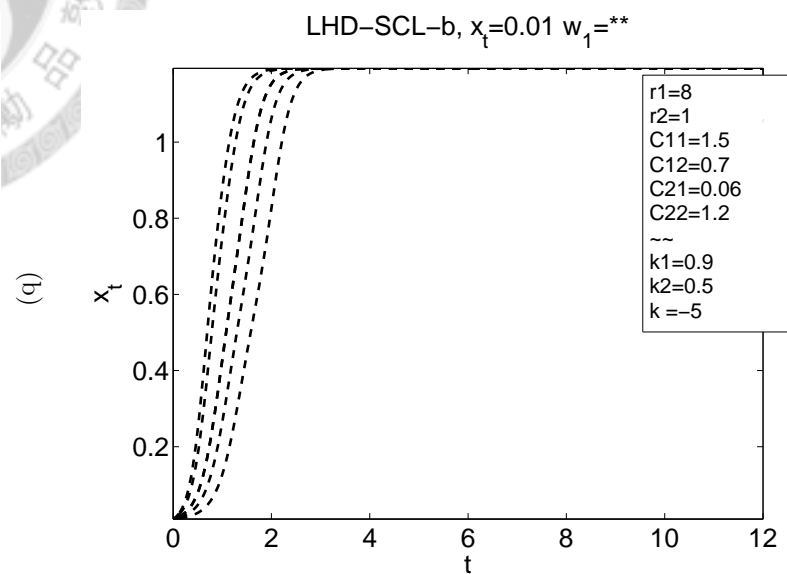
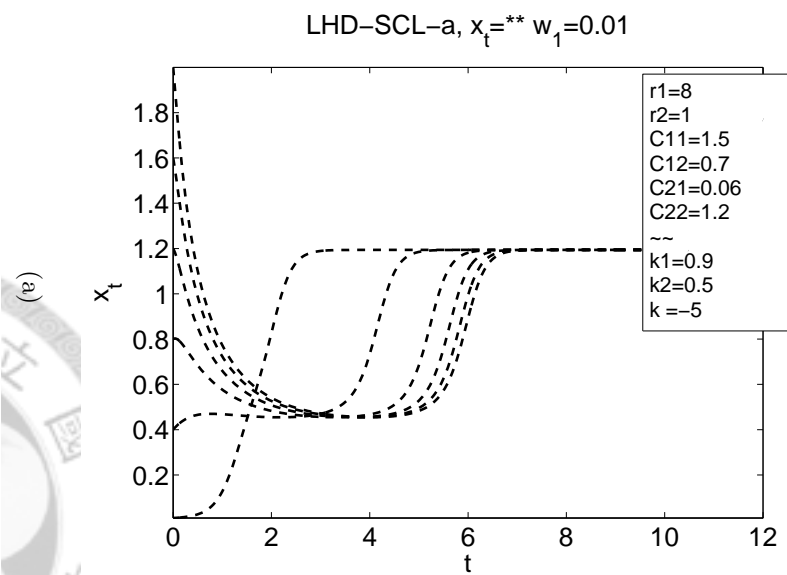


Figure 2.114: The $x_{tot}-w_1$ trajectories of LHD-SCL.

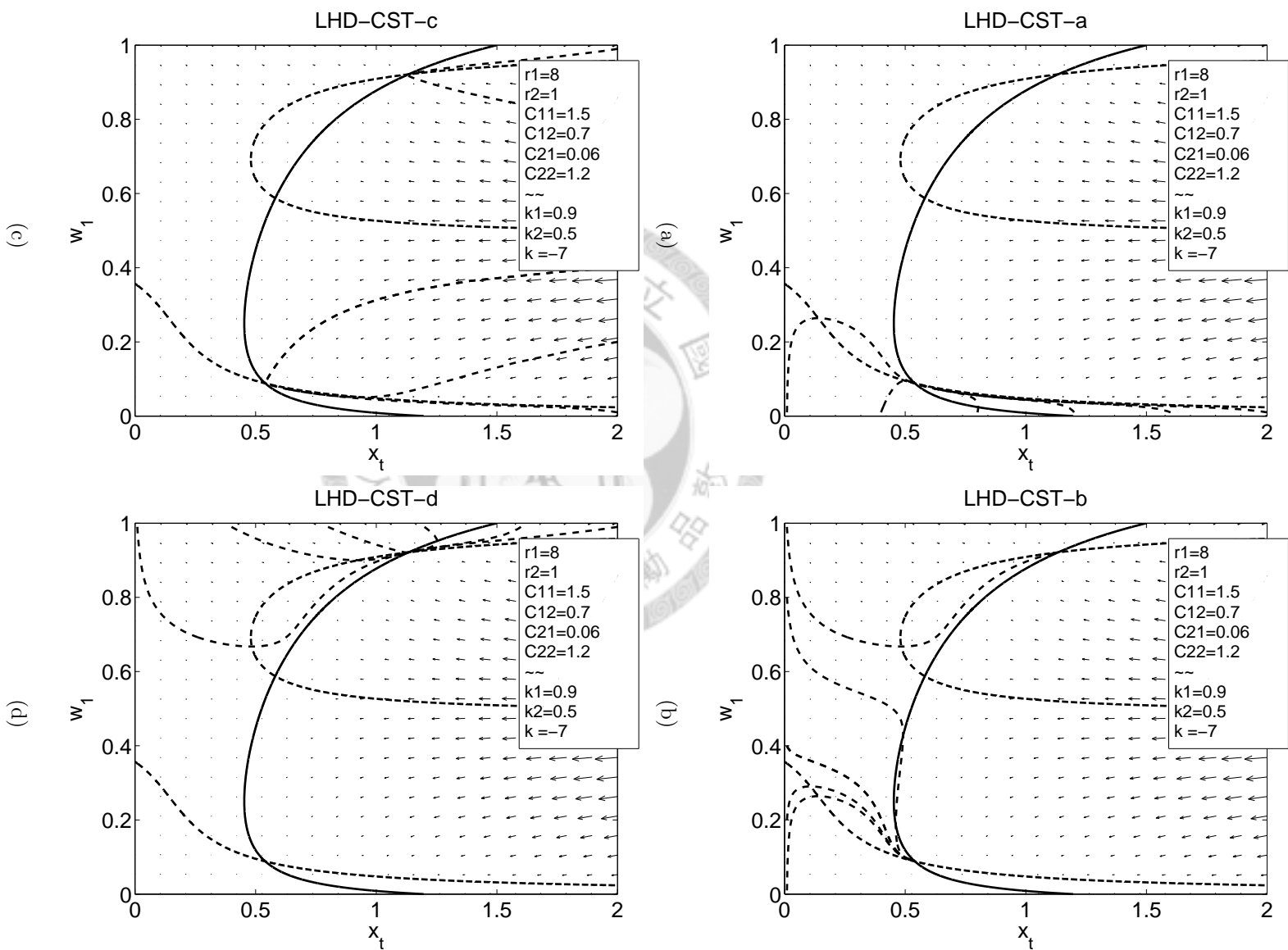
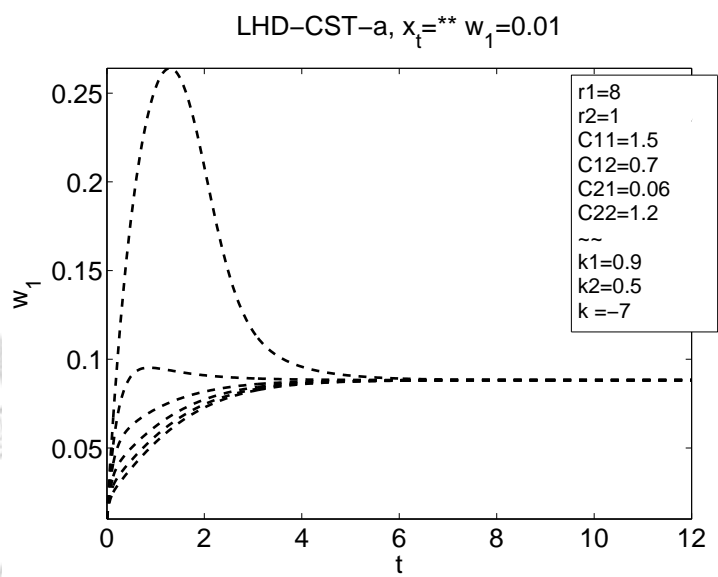
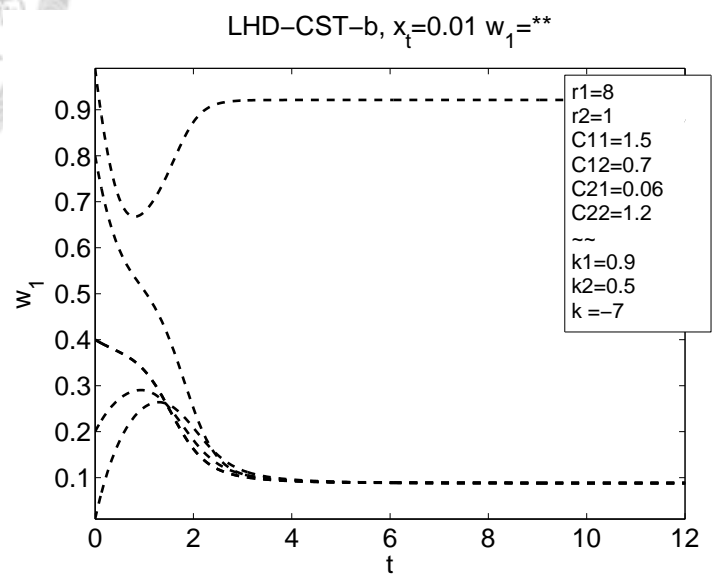


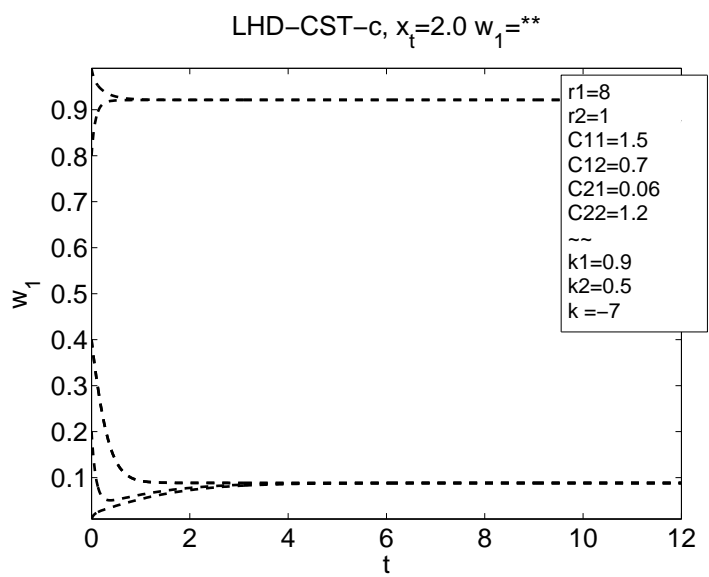
Figure 2.115: The $x_{tot}-w_1$ trajectories of LHD-CST.



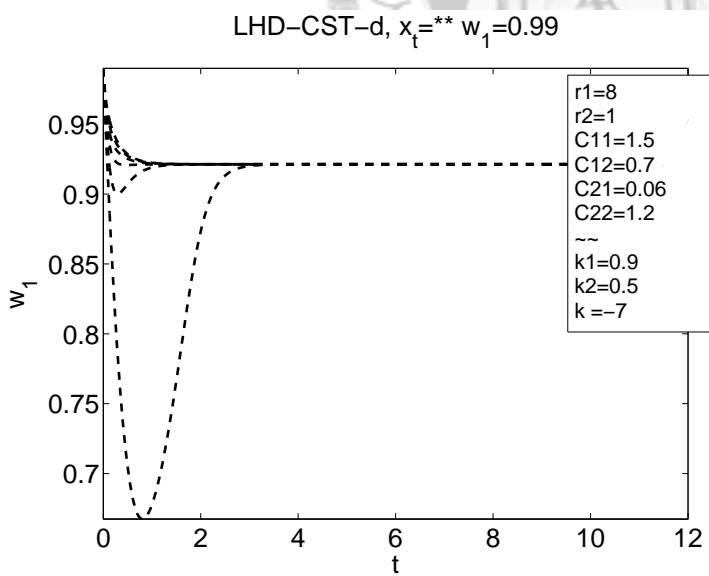
(a)



(b)



(c)



(d)

Figure 2.116: The x_{tot} - w_1 trajectories of LHD-CST.

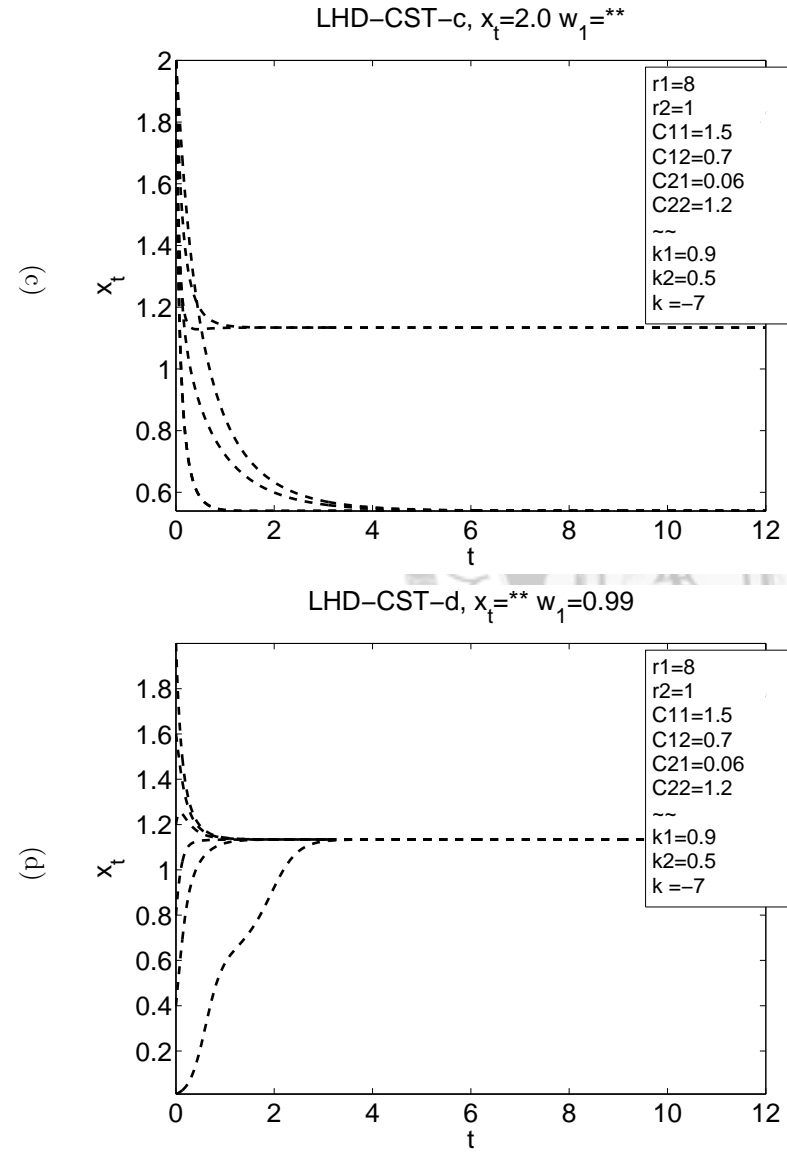
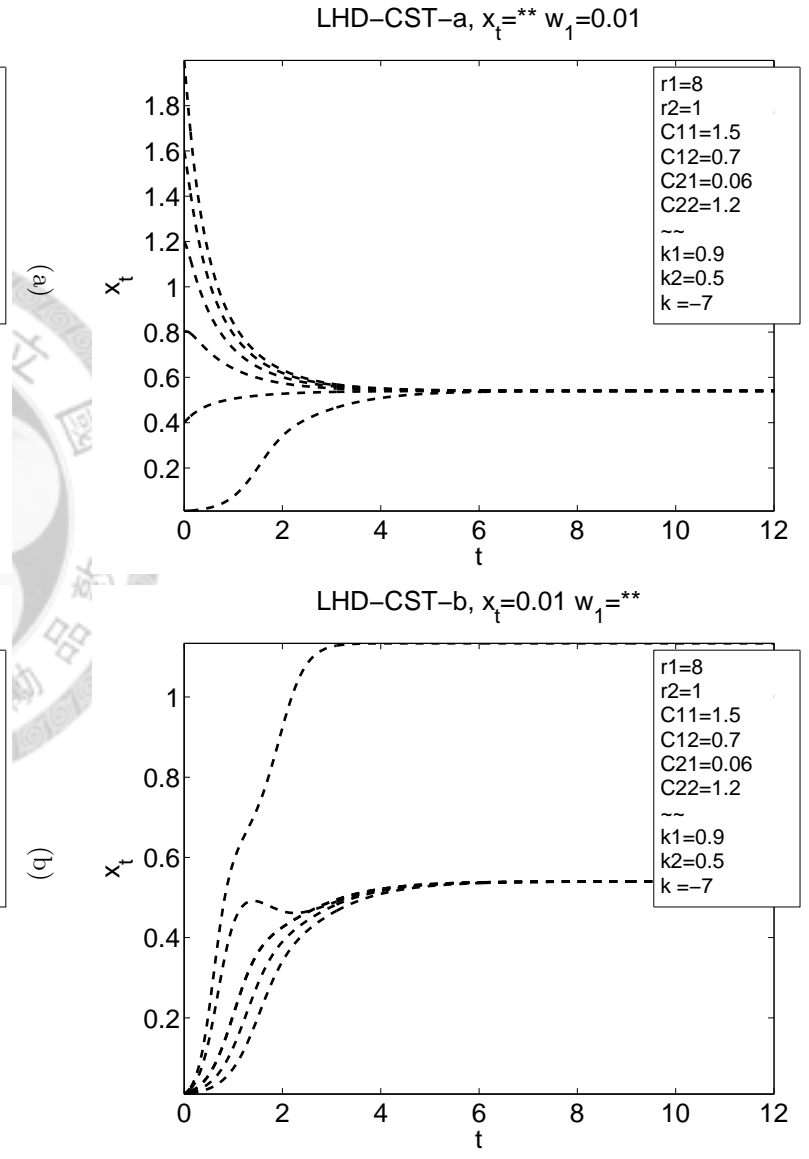


Figure 2.117: The $x_{tot}-w_1$ trajectories of LHD-CST.

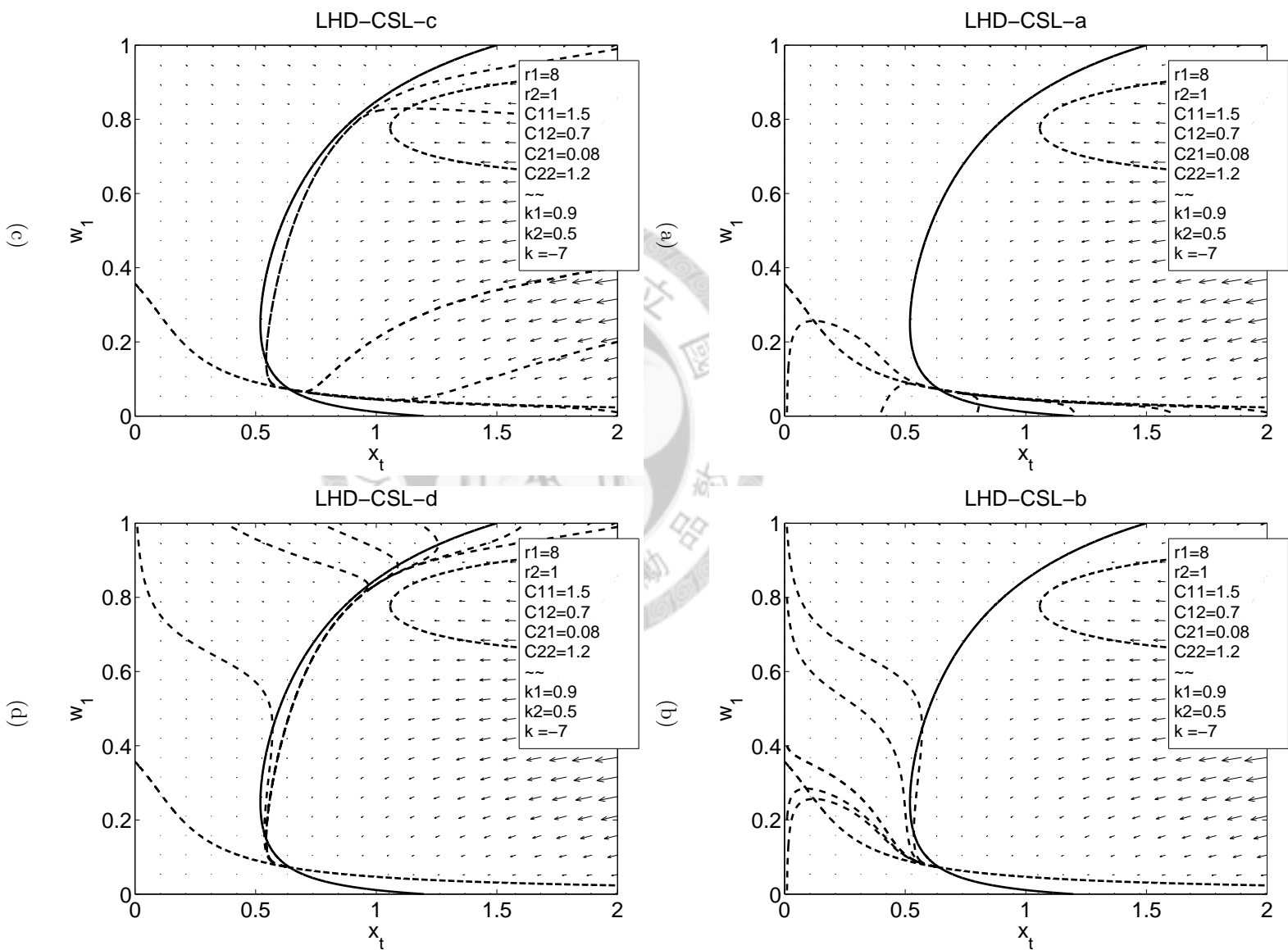


Figure 2.118: The x_{tot} - w_1 trajectories of LHD-CSL.

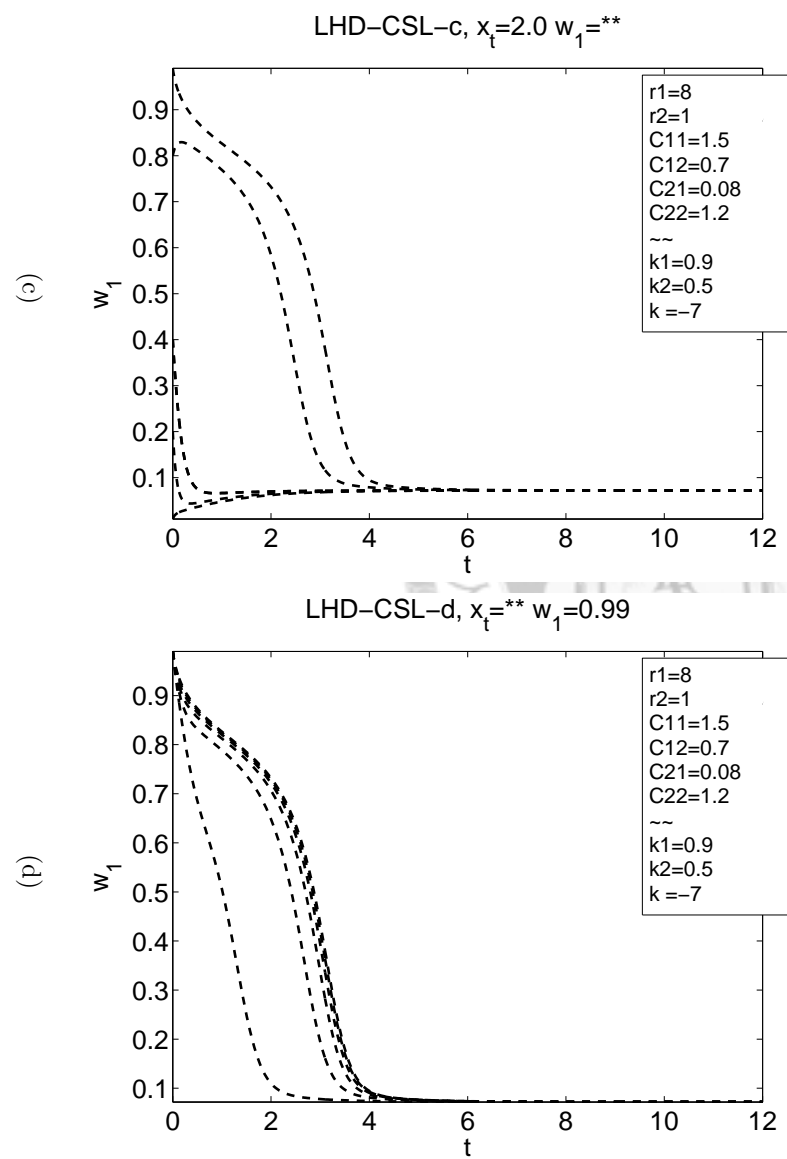
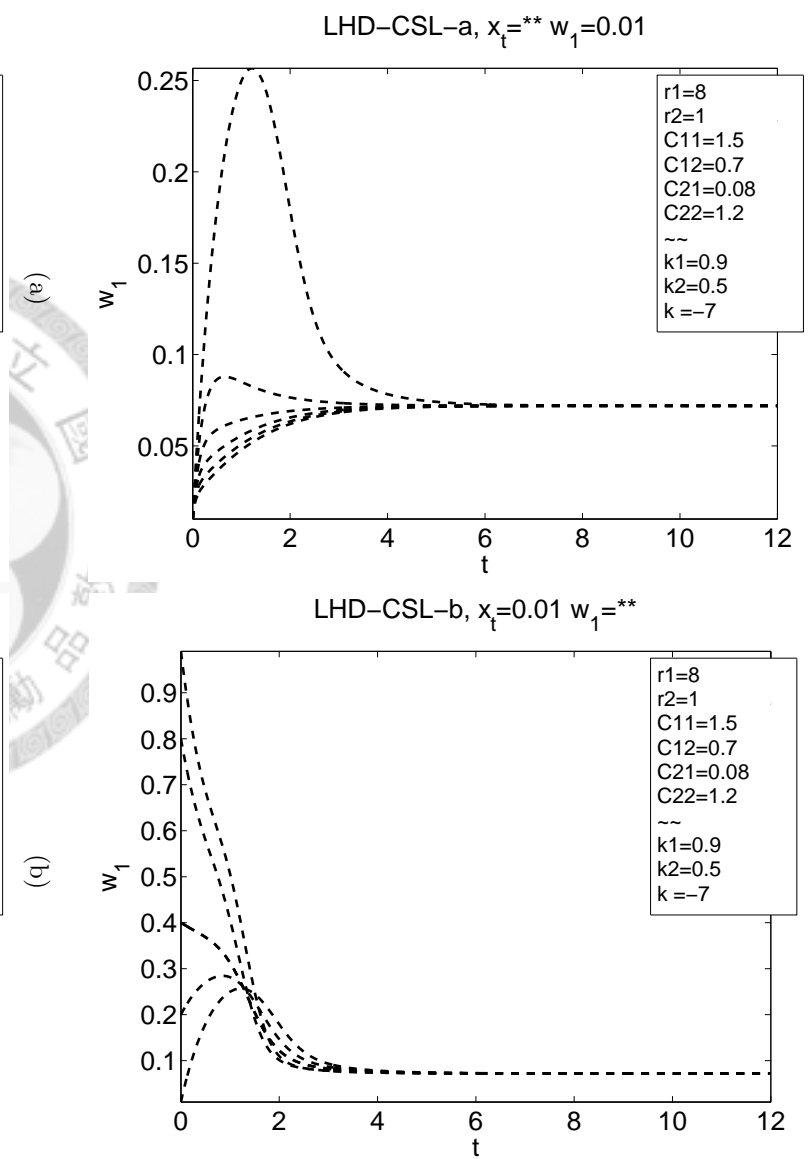
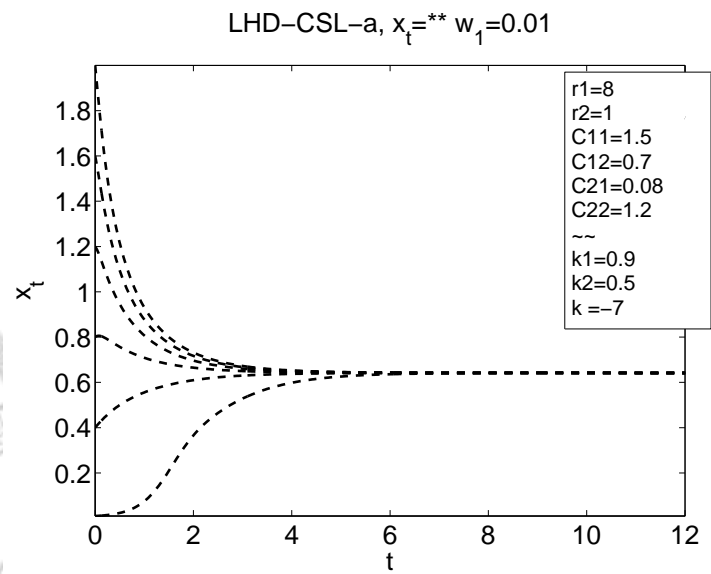
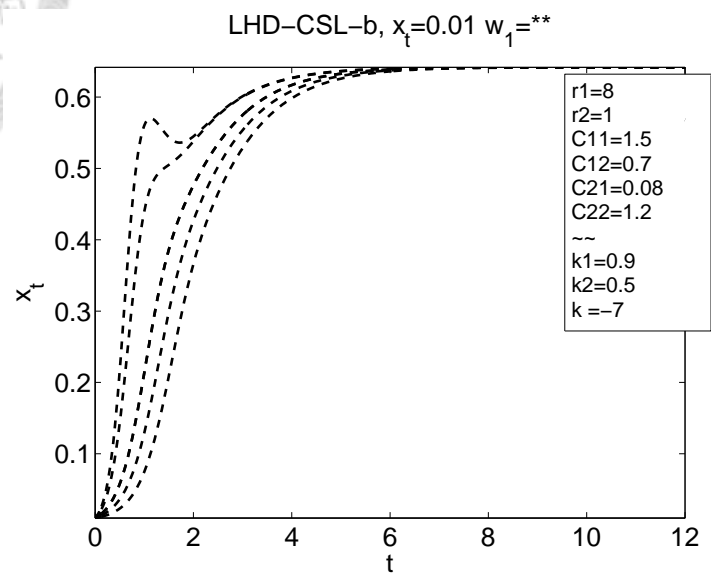


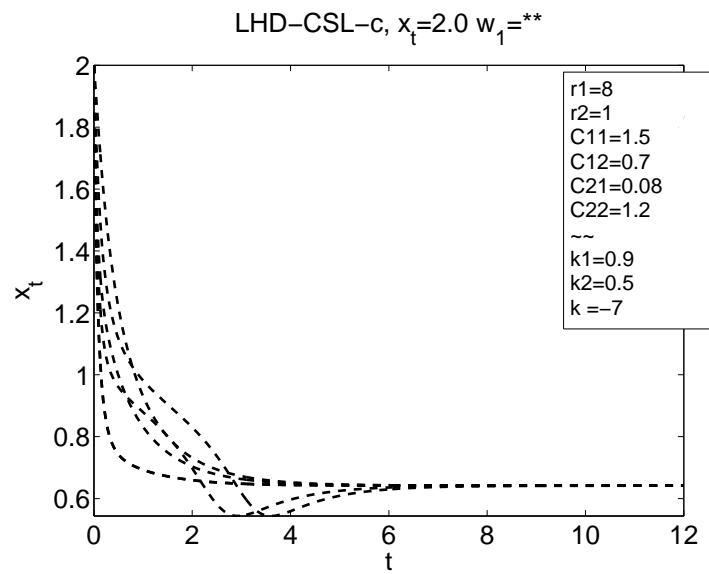
Figure 2.119: The x_{tot} - w_1 trajectories of LHD-CSL.



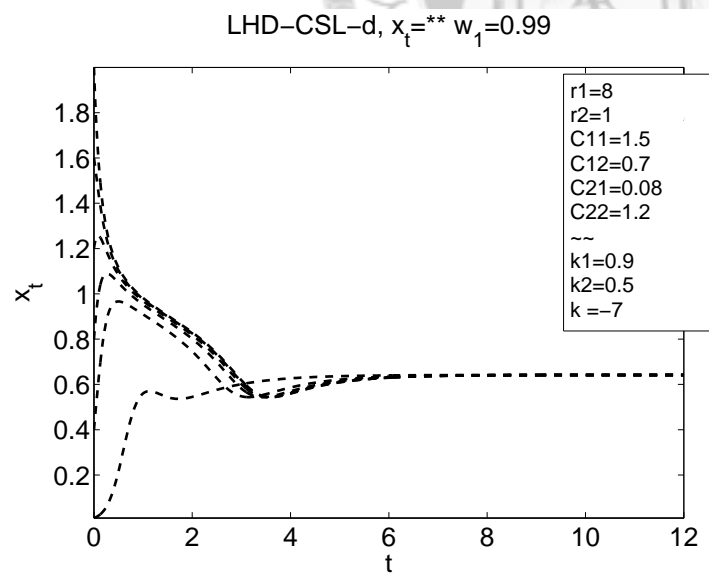
(a)



(b)



(c)



(d)

Figure 2.120: The $x_{tot}-w_1$ trajectories of LHD-CSL.

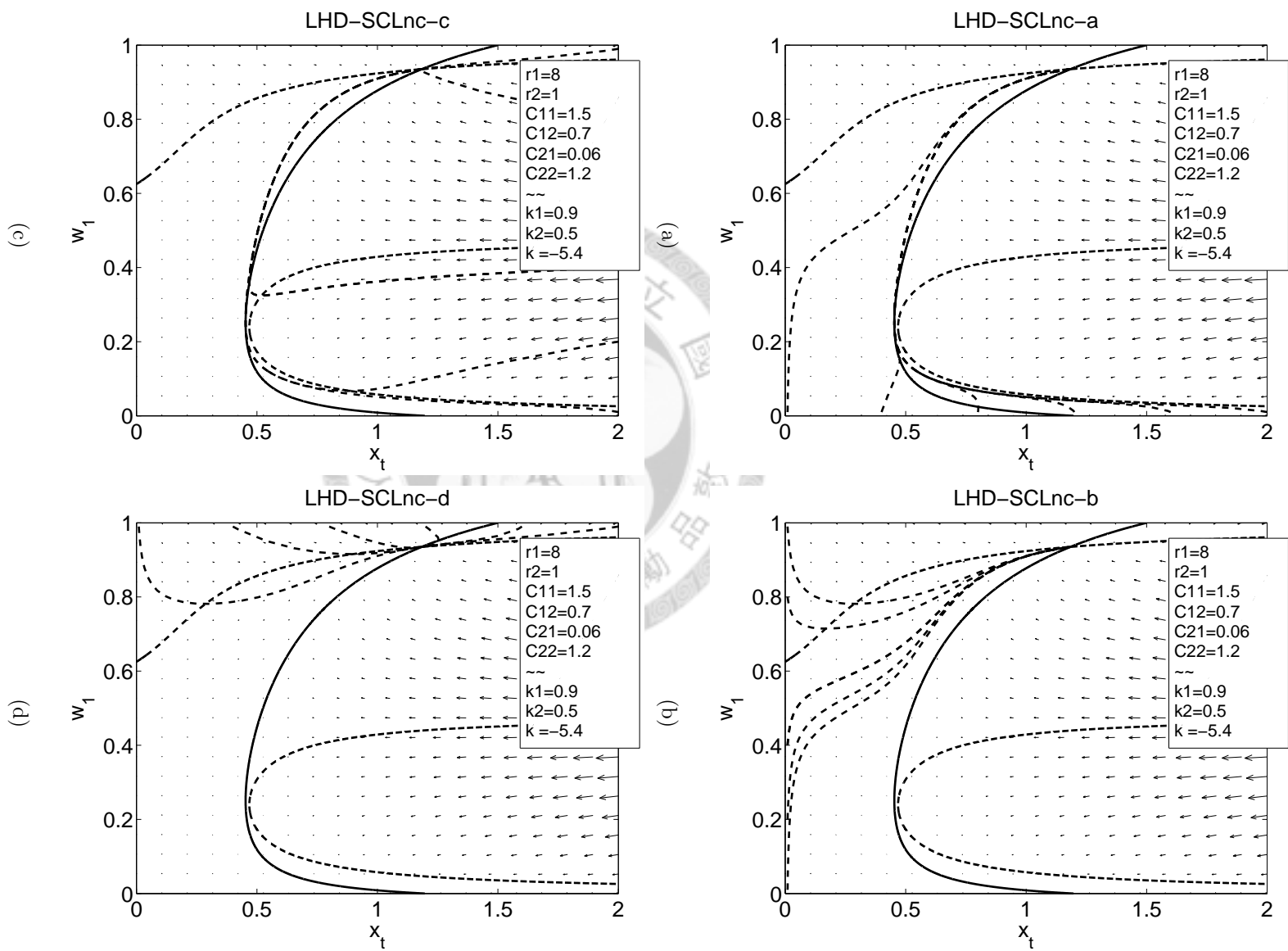


Figure 2.121: The x_{tot} - w_1 trajectories of LHD-SCLnc.

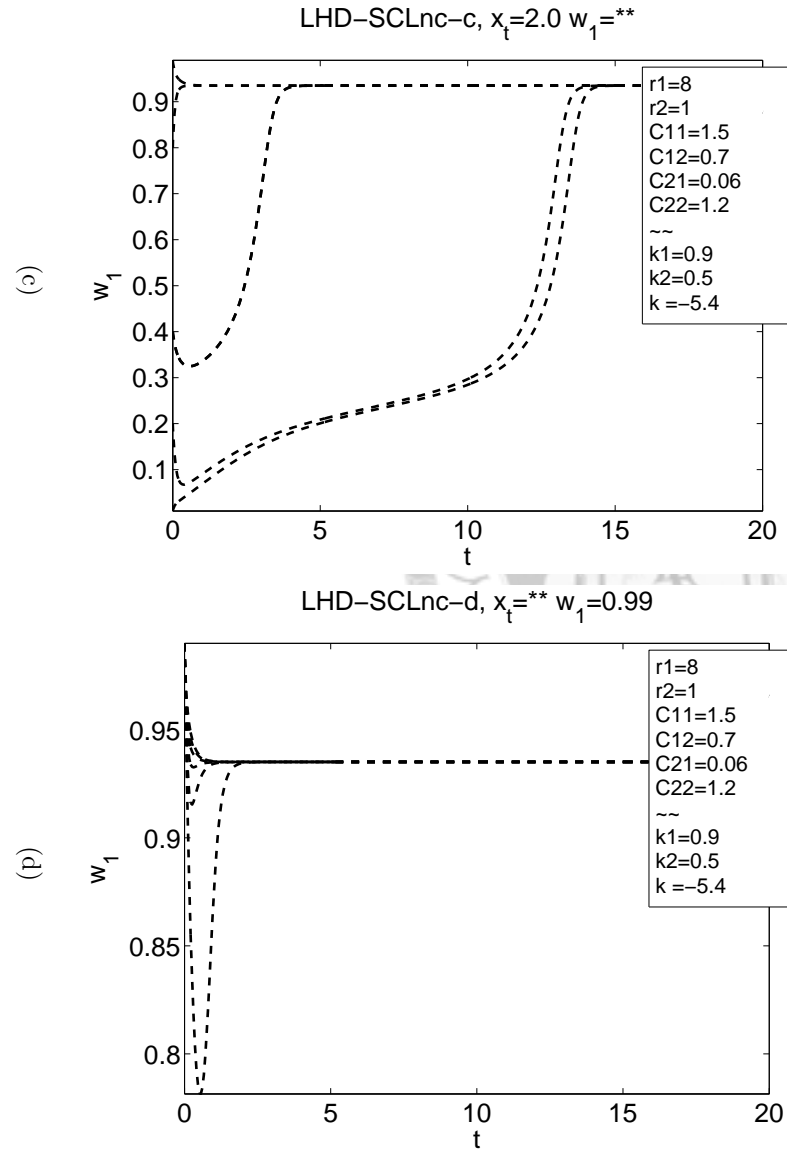
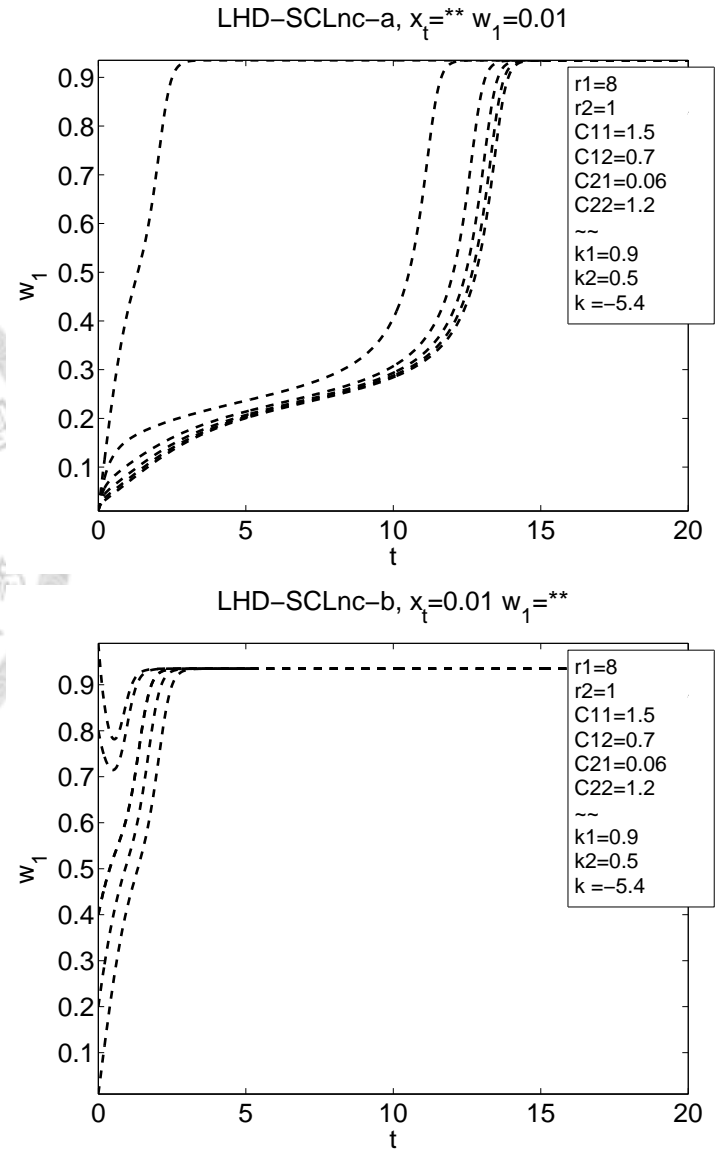


Figure 2.122: The x_{tot} - w_1 trajectories of LHD-SCLnc.

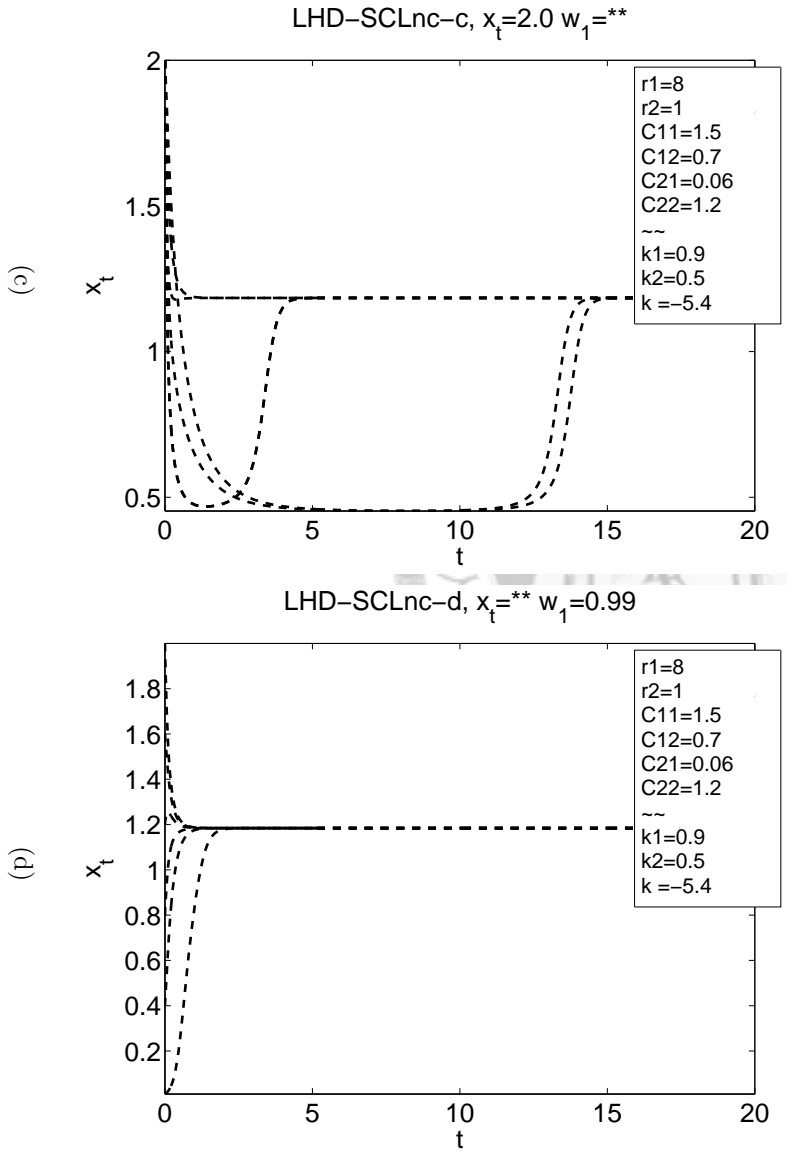
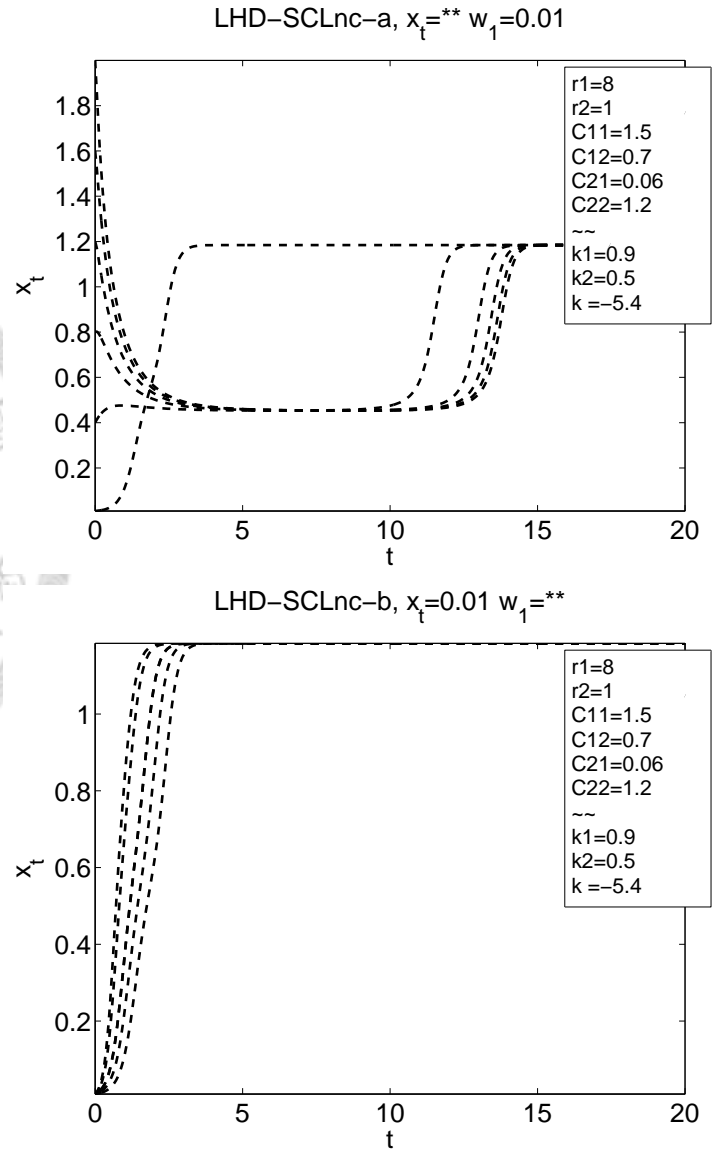


Figure 2.123: The $x_{tot}-w_1$ trajectories of LHD-SCLnc.

Appendix C

Simple analysis of the time evolution of the cancer system model

With the assumption that $a \gg 1$, the governing equation for x_2 takes an especially simple form

$$\dot{x}_2 \approx (r - kw_1) x_2,$$

whereas the equation for x_t is approximated by

$$\dot{x}_t \approx rx_t \left(1 - w_1 \left(\frac{w_1}{C_1} + \frac{1 - w_1}{C_2} \right) x_t \right).$$

In view of the assumption that $C_1 \gg C_2$, one may be tempted to also drop the term w_1/C_1 as well. However, this extra approximation may *not* be legitimate during the late stage of time evolution if state 1 dominates the final scene, because then $w_1 \approx 1$, which renders $(1 - w_1)/C_2$ small.

From the mathematical point of view, it is more convenient to de-dimensionalize

the system. This can be done by the substitution

$$x_j \equiv x'_j C_1, \quad x_t \equiv x'_t C_1$$

$$t \equiv r t',$$

$$k \equiv r k',$$

$$C' \equiv \frac{C_1}{C_2}.$$

The resulting equations then read

$$\frac{dx'_2}{dt'} \approx (1 - k' w_1) x'_2, \tag{C.1}$$

$$\frac{dx'_t}{dt'} \approx x'_t [1 - w_1 (w_1 + C' w_2) x'_t]. \tag{C.2}$$

To give a rough idea of the order of magnitudes of the parameters we will be using, we list below their typical numerical values:

$$x'_1(0) \sim 10^{-6}, \quad x'_2(0) \sim x'_t(0) \sim 10^{-4} \text{ so that } w_1(0) \sim 10^{-2},$$

$$k' \sim 10, \quad C' \sim 10^4.$$

We now discuss the time evolution of the system. To be specific, we will consider the case when state 1 is the minority in the beginning ($w_1 \approx 0$) but later gets to dominate the final stage via two mechanisms: the autocrine signaling pathway (assuming $k > 0$) in the early stage of time evolution, and the familiar logistic type growth. The total population x_t is also assumed small in the beginning.

(1) The very early stage:

With $w_1 \approx 0$ (state 1 being the minority) and $x_t \approx 0$, the governing equations are further simplified to

$$\frac{dx'_2}{dt'} \approx x'_2,$$

$$\frac{dx'_t}{dt'} \approx x'_t,$$

so that the two variables grow exponentially at about the same rate. However, we should *not* assume that x'_1 behaves the same, because it is an even smaller quantity

to begin with so that there is no telling directly from the two approximate equations above if $\dot{x}'_1 = \dot{x}'_t - \dot{x}'_2 \approx x'_1$. In fact, from the rate equation of x_1 we have

$$\begin{aligned}\frac{dx'_1}{dt'} &= [1 + k'w_2 - (x'_1 + C'x'_2)] x'_1 \\ &\approx [1 + k'w_2 - C'x'_2] x'_1 \\ &\approx k'x'_1\end{aligned}$$

for the numerical values we have adopted. Hence, state 1 actually grows much faster than state 2 due to the autocrine transition effect, even though its population is only of the minority in the beginning.

With this in mind, and using a subscript 0 to denote the initial value, we see that

$$w_1 = \frac{x'_1}{x'_t} \approx \frac{x'_{10}}{x'_{t0}} e^{(k'-1)t'},$$

which suggests that, by Eqs.C.1 and C.2, inhibition from w_1 on the growth of x_2 and x_t will quickly manifest itself as time proceeds.

(2) The crossover stage:

When w_1 grows up to the order of $1/k'$, x'_2 begins to feel the suppression in growth. The time τ'_2 it takes for this to happen can be estimated via

$$\frac{x'_{10}}{x'_{t0}} e^{(k'-1)\tau'_2} \sim \frac{1}{k'}.$$

In contrast, for x'_t to begin experiencing any suppression in growth, we need a time τ'_t , which can be estimated from solving

$$\begin{aligned}w_1 &\sim 1/C'x'_2 \sim 1/C'x'_t \\ \implies \frac{x'_{10}}{x'_{t0}} e^{(k'-1)\tau'_t} &\sim \frac{C'}{x'_{t0}} e^{-\tau'_t} \\ \implies \frac{x'_{10}}{C'} e^{k'\tau'_t} &\sim 1.\end{aligned}$$

For our choice of the parameters, it turns out that $\tau'_t \gg \tau'_2$. This means that $(1 - k'w_1)$ in Eq.C.1 will become negative after a time of order τ'_2 , and so afterwards the growth of state 2 not only has been completely suppressed, but the autocrine transition is now

actively converting virtually all of state 2 to state 1. In other words, the population of state 2 decreases rapidly afterwards.

If we denote the variables at the time when state 2 reaches its population maximum by an asterisk “*”, then the scenario described above suggests expanding out $(1 - k'w_1) \approx -\alpha(t' - t'^*)$ for some number α so that, near this crossover region, we have

$$\begin{aligned}\frac{dx'_2}{dt'} &\approx (1 - k'w_1)x'_2 \approx -\alpha(t' - t'^*)x'_2 \\ \implies x'_2 &\approx x'^*_2 e^{-\alpha(t' - t'^*)^2/2}.\end{aligned}$$

Also, because $C'w_2 \gg w_1$ near the crossover region, we may approximate Eq.C.2 as

$$\begin{aligned}\frac{dx'_t}{dt'} &\approx x'_t [1 - w_1(w_1 + C'w_2)x'_t] \\ &\approx x'_t [1 - w_1 C'x'_2] \\ &\approx x'_t \left[1 - \left(\frac{1 + \alpha(t' - t'^*)}{k'} \right) C'x'_2 \right].\end{aligned}$$

Hence, as t' increases from t'^* onward, x'_t reaches an extremum for time t'^* satisfying

$$0 = 1 - \left(\frac{1 + \alpha(t' - t'^*)}{k'} \right) C'x'_2.$$

For $t' - t'^*$ not too large, we may approximate the above by

$$\begin{aligned}0 &= 1 - \left(\frac{1 + \alpha(t' - t'^*)}{k'} \right) C'x'^*_2 e^{-\alpha(t' - t'^*)^2/2} \\ &\approx 1 - \left(\frac{1 + \alpha(t' - t'^*)}{k'} \right) C'x'^*_2 \frac{1}{1 + \alpha(t' - t'^*)^2/2},\end{aligned}$$

which admits the following two solutions:

$$t' - t'^* = \frac{C'x'^*_2}{k'} \pm \sqrt{\left(\frac{C'x'^*_2}{k'} \right)^2 - \frac{2}{\alpha} \left(1 - \frac{C'x'^*_2}{k'} \right)}.$$

This means x'_t actually achieves a local maximum some time after state 2 reaches its maximum; then, as a result of the rapid decrease of state 2, the total population plunges to a local minimum. It is only afterward does the total population begin to pick up again, this time due to the logistic growth of the now-dominant state 1. Such a “hiccup” is apparent in the numerical simulation of Fig. 5.3.

(3) The late stage:

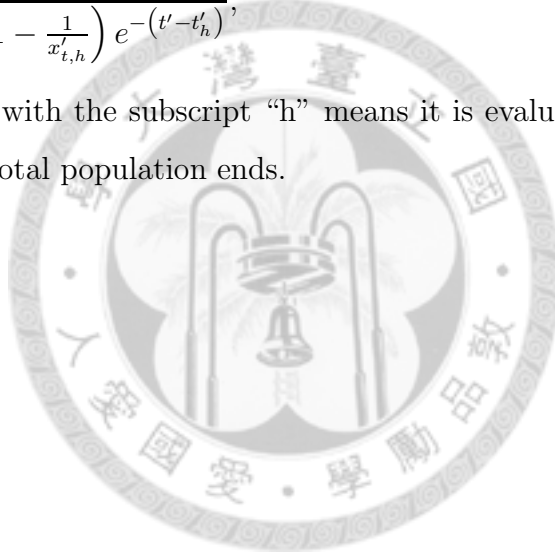
Once the system has passed through the crossover stage, the population of state 2 becomes negligible, and the time evolution of state 1 is basically that of the total population, which follows the simple logistic growth model, because

$$\begin{aligned}\frac{dx'_t}{dt'} &\approx x'_t [1 - w_1 (w_1 + C' w_2) x'_t] \\ &\approx x'_t [1 - 1 \cdot (1 + C' \cdot 0) x'_t] \\ &= x'_t [1 - x'_t].\end{aligned}$$

This equation has the following solution:

$$x'_t \approx \frac{1}{1 - \left(1 - \frac{1}{x'_{t,h}}\right) e^{-(t'-t'_h)}},$$

where a variable with the subscript “h” means it is evaluated at the time when the “hiccup” in the total population ends.



Bibliography

- [1] Chang, H. H., Hemberg, M., Barahona, M., Ingber, D. E., Huang, S.(2008) Transcriptome-wide noise controls lineage choice in mammalian progenitor cells. *Nature*, **453** , 544-548.
- [2] Sui Hung, Ingemar Ernberg, and Stuart Kauffman. (2009) Cancer attractors: A systems view of tumors from a gene network dynamics and developmental perspective. *Semin Cell Dev Biol.* **20(7)**,869-876.
- [3] Enmon, R., Yang, W. H., Ballangrud, A. M., Solit, D. B., Heller, G., Rosen, N., and Scher, H. I. et al. (2003) Combination Treatment with 17-N-Allylamino-17-Demethoxy Geldanamycin and Acute Irradiation Produces Supra-Additive Growth Suppression in Human Prostate Carcinoma Spheroids. *Cancer Res.*, **63** , 8393-8399.
- [4] Reya, T., Morrison, S. J., Clarke, M. F., and Weissman, I. L.(2001) Stem cells, cancer, and cancer stem cells. *Nature* ,**414** , 105-111.
- [5] Jeffrey A. Magee, Elena Piskounova, Sean J. Morrison. (2012) Cancer Stem Cells: Impact, Heterogeneity, and Uncertainty. *CANCER CELL*, **21**, 283-296.
- [6] Gupta, P. B., Chaffer, C. L., and Weinberg, R.A.(2009) Cancer stem cells mirage or reality? *Nat. Med.*. **15**, 1010-1012.
- [7] Grivennikov, S. and Karin, M. (2008) Autocrine IL-6 signaling: a key event in tumorigenesis? *CANCER CELL* , **13** ,7-9.

- [8] Wolkenhauer O, Auffray C, Baltrusch S, Blüthgen N, Byrne H, Cascante M, and Ciliberto A, et al.(2010) Systems Biologists Seek Fuller Integration of Systems Biology Approaches in New Cancer Research Programs. *Cancer Res.*, **70**(1) , 12-13.
- [9] Monika Joanna Piotrowska, Heiko Enderling, Uwe an der Heiden, and Michael C. Mackey. (2008) *Cancer and stem cells*, chapter 2, Nova Science Publishers, Inc.
- [10] Garner, A. L., Lau, Y. Y., Jordan, D. W., Uhler, M. D., and Gilgenbach, R. M.(2006) Implications of a simple mathematical model to cancer cell population dynamics. *Cell Prolif.* , **39**, 15-28.
- [11] Ganguly, R. and Puri, I. K.(2006) Mathematical model for the cancer stem cell hypothesis. *Cell Prolif.*, **39**, 3-14.
- [12] Bajzer Ž., and Vuk-Pavlović S.(2005) Modeling positive regulatory feedbacks in cell-cell interactions. *Biosystems*, **80**, 1-10.
- [13] Ghosh, S., Elankumaran, S., and Puri, I. K.(2011) Mathematical model of the role of intercellular signalling in intercellular cooperation during tumorigenesis. *Cell Prolif.*, **44**, 192-203.
- [14] Swierniak, A., Kimmel, M., and Smieja, J.(2009) Mathematical modeling as a tool for planning anticancer therapy. *Eur. J. Pharmacol.*, **625**, 108-121.
- [15] Tanaka, G., Hirata, Y., Goldenberg, S. L., Bruchovsky, N., and Aihara, K.(2010) Mathematical modelling of prostate cancer growth and its application to hormone therapy. *Philos. Trans. R. Soc. A-Math. Phys. Eng. Sci.*, **368**, 5029-5044.
- [16] Leder, K., Holland, E. C., and Michor, F.(2010) The Therapeutic Implications of Plasticity of the Cancer Stem Cell Phenotype. *PLOS ONE*, **5**, article number: e14366.

- [17] Ganguly, R. and Puri, I. K.(2007) Mathematical model for chemotherapeutic drug efficacy in arresting tumour growth based on the cancer stem cell hypothesis. *Cell Prolif.*, **40**, 338-354.
- [18] Usmani, S. Z., Bon a, R., and Li, Z. H.(2009) 17 AAG for HSP90 Inhibition in Cancer – From Bench to Bedside. *Curr. Mol. Med.*, **9**, 654-664.
- [19] Hirata Y, Tanaka G, Bruchovsky N, Aihara K.(2012) Mathematically modelling and controlling prostate cancer under intermittent hormone therapy. *Asian J Androl.*, **15**, 270-277.
- [20] Huggins, C. and Hodges, C. V.(1941) Studies on prostatic cancer: I. The effect of castration, of estrogen and of androgen injection on serum phosphatases in metastatic carcinoma of the prostate. *Cancer Res.*, **1**, 293-297.
- [21] Chodak, G. W.(2005) Maximum androgen blockade: a clinical update. *Rev. Urol.*, **7**, (Suppl. 5) S13-S17.
- [22] Noble RL.(1977) Hormonal control of growth and progression in tumors of Nb rats and a theory of action. *Cancer Res.*, **37** , 82-94.
- [23] Bruchovsky N., Rennie P.S., Coldman A.J., Goldenberg S.L., To M. et al.(1990) Effects of androgen withdrawal on the stem cell composition of the Shionogi carcinoma. *Cancer Res.*, **50**, 2275-2282.
- [24] Akakura K., Bruchovsky N., Goldenberg S. L., Rennie P. S., Buckley A. R. et al.(1993) Effects of intermittent androgen suppression on androgen-dependent tumors: apoptosis and serum prostate-specific antigen. *Cancer Res.*, **71**, 2782-2790.
- [25] Abrahamsson P.A.(2010) Potential benefits of intermittent androgen suppression therapy in the treatment of prostate cancer: a systematic review of the literature. *Eur Urol*, **57**, 49-59.

- [26] Jackson T.L.(2004) A mathematical investigation of the multiple pathways to recurrent prostate cancer: comparison with experimental data. *Neoplasia*, **6**, 679-704.
- [27] Jackson T.L.(2004) A mathematical model of prostate tumor growth and androgenindependent relapse. *Disc Cont Dyn Syst- Ser. B* , **4**, 187-201.
- [28] Guo Q, Tao Y, Aihara K.(2008) Mathematical modelling of prostate tumor growth under intermittent androgen suppression with partial differential equations. *Int J Bifurcat Chaos* , **18**, 3789-3797.
- [29] Shimada T. , and Aihara K. (2008) A nonlinear model with competition between prostate tumor cells and its application to intermittent androgen suppression therapy of prostate cancer. *Math Biosci* , **214**, 134-139.
- [30] Tanaka G, Hirata Y, Goldenberg SL, Bruchovsky N, Aihara K. (2010) Mathematical modelling of prostate cancer growth and its application to hormone therapy. *Philos Trans R Soc A*, **368**, 5029-44.
- [31] Hirata Y, Bruchovsky N, Aihara K. (2010) Development of a mathematical model that predicts the outcome of hormone therapy for prostate cancer. *J Theor Biol*, **264**, 517-527.
- [32] William H. Press, et al. Numerical recipes in fortran 77. Cambridge [England] ; New York : Cambridge University Press, 1999
- [33] Bert Sakmann and Erwin Neher. Single-Channel Recording. New York : Plenum Press, c1995
- [34] Brad S. Rothberg and Ricardo A. Bello et al (1997). Two-Dimensional Components and Hidden Dependencies Provide Insight into Ion Channel Gating Mechanisms . *Biophys. J.* **72** 2524-2544
- [35] William H. Press, et al. Numerical recipes in fortran 90. Cambridge [England] ; New York : Cambridge University Press, 1996

- [36] A. L. Blatz and K. L. Magleby. (1986) Quantitative description of three modes of activity of fast chloride channels from rat skeletal muscle. *Physiol*, **378(1)**:141-174.
- [37] F. J. Sigworth and S. M. Sine. (1987) Data transformations for improved display and fitting of single-channel dwell time histograms. *Biophys. J.*, **52(6)**:1047-1054.

